Modern Many-Particle Physics
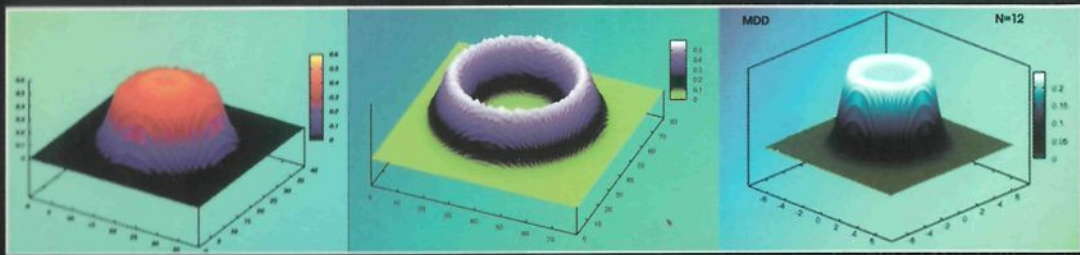

Atomic Gases, Quantum Dots and Quantum Fluids

Enrico Lipparini

This page is intentionally left blank

Modern Many-Particle Physics

Atomic Gases, Quantum Dots and Quantum Fluids

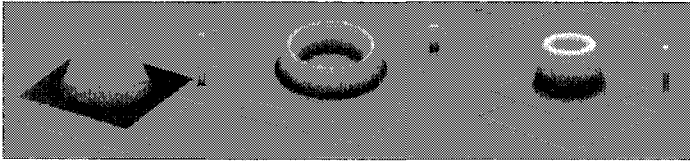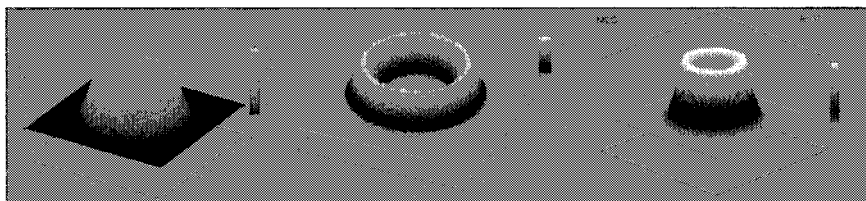# Modern Many-Particle Physics

Atomic Gases, Quantum Dots and Quantum Fluids

Enrico Lipparini
University of Trento, Italy

World Scientific

MODERN MANY-PARTICLE PHYSICS
Atomic Gases, Quantum Dots and Quantum Fluids

Preface

This book is the fruit of my lectures on the Theory of Many Body Systems which I have been teaching for many years in the degree course in Physics at the University of Trento. As often happens, the outline of the book was my students' notes; in particular, the notes of the students of the academic year 1999–2000 which were extremely useful for me. Chapter 6 on the Monte Carlo methods is the work of Francesco Pederiva, a research assistant in our Department. During the course, Francesco, apart from illustrating the method, teaches the students all the computer programmes, continually referred to in the book, by means of practical exercises in our computational laboratory. In particular, he teaches the Hartree–Fock, Brueckner–Hartree–Fock, Kohn-Sham, Diffusion Monte Carlo programmes for the static properties, RPA, and Time-Dependent HF and LSDA for Boson and Fermion finite systems. These programmes are available to anyone who is interested in using them.

The book is directed towards students who have had a conventional course in quantum mechanics and have some basic understanding of condensed matter phenomena. I have often gone into extensive mathematical details, trying to be as clear as possible and I hope that the reader will be able to rederive many of the formulas presented without too much difficulty.

In the book, even though a lot of space is devoted to the description of the homogeneous systems, such as electron gas in different dimensions, quantum wells in intense magnetic field, liquid helium and nuclear matter, the most relevant part is dedicated to the study of finite systems. Particular attention is paid to those systems realized recently in the laboratories throughout the world: metal clusters, quantum dots and the condensates of cold and dilute atoms in magnetic traps. However, some space is also devoted to the more traditional finite systems, like the helium drops and the nuclei. I have tried to treat all these systems in the most unifying way possible, attempting to bring all the analogies to light. My intention was to narrow the gap between the usual undergraduate lecture course and the literature on these systems presented in scientific journals.

It is important to remark that the book takes a "Quantum chemist's" approach to many-body theories. It focuses on methods of getting good numerical approximations to energies and linear response based on approximations to first-principle Hamiltonians. There is another approach to many-body physics that focuses on symmetries and symmetry breaking, quantum field theory and renormalization groups, and aims to extracting the emergent features of the many body systems. This works with "effective" model theories, and does not attempt to do "*ab initio* computations". These two ways of dealing with many-body systems complement each other, and find common ground in the study of atomic gases, metal clusters, quantum dots and quantum Hall effect systems that are the main application of the book.

I am indebted to many of my colleagues in the physical department of Trento for discussions and remarks. Specifically, I'm particular grateful to G. Bachelet, D. M. Brink, S. Giorgini, F. Iachello, W. Leidemann, R. Leonardi, F. Pederiva, G. Orlandini, S. Stringari, M. Traini, G. Viliani and A. Vitturi. Many aspects of the book were clarified during my stays in Barcelona, in Paris and in Palma de Mallorca where I had the occasion to discuss many subjects with M. Barranco, A. Emperador, M. Pi, X. Campi, N. Van Giai, D. Vautherin, Ll. Serra and A. Puente, and during the frequent visits to our department by my friends A. Richter and K. Takayanagi.

Thanks are also due to Irene Diamond for the English translation of the book.

The book has cost me a great investment in time, which recently has kept me from other research projects and, above all, from my family. The book is dedicated to my wife, Giovanna, and to my children, Fiorenza, Filippo and Luigi. Filippo has been of enormous help in editing the figures.

Enrico Lipparini   January 2003.

Contents

PART 1

<center>Chapter 1</center>

Independent-Particle Model

1.1 Introduction

The main purpose of many body theory in non-relativistic quantum mechanics is the study of the properties of the solutions of Schrödinger's equation with Hamiltonian

$$H = \sum_{i=1}^{N} \left(\frac{p_i^2}{2m} + v_{\text{ext}}(\mathbf{r}_i) \right) + \sum_{i<j=1}^{N} v(\mathbf{r}_{ij}), \qquad (1.1)$$

which describes a system composed of N identical particles, which interact with an external field through a one-body potential $v_{\text{ext}}(\mathbf{r}_i)$, and among themselves through a two-body potential $v(\mathbf{r}_{ij})$.

The simplest model case is when the Hamiltonian contains only one-body terms, and is referred to as the independent-particle model:

$$H_0 = \sum_{i=1}^{N} \left(\frac{p_i^2}{2m} + v_{\text{ext}}(\mathbf{r}_i) \right). \qquad (1.2)$$

In this approximation the eigenfunctions of H_0 may be written as the product of single-particle wavefunctions, each of which satisfies the equation ($\hbar = 1$)

$$\left(-\frac{\nabla^2}{2m} + v_{\text{ext}}(\mathbf{r}) \right) \varphi_k(\mathbf{r}, \sigma) = \varepsilon_k \varphi_k(\mathbf{r}, \sigma), \qquad (1.3)$$

where k indicates the set of quantum numbers that characterize the single-particle state, and $\mathbf{r}$ and σ are the position and spin variables, respectively. A further variable is introduced in nuclear physics — the isospin τ. In what follows we will indicate as x the variable set $\mathbf{r}$, σ and τ. For example, for electrons in a central external field,

$$\varphi_k(x) = \varphi_{n,\ell,m}(\mathbf{r})\chi_{m_s}(\sigma). \qquad (1.4)$$

<center>1</center>

Here $\chi_{m_s}(\sigma)$ is the spinor which satisfies the equations

$$s^2\chi_{m_s}(\sigma) = \frac{3}{4}\chi_{m_s}(\sigma), \qquad s_z\chi_{m_s}(\sigma) = m_s\chi_{m_s}(\sigma)\,, \tag{1.5}$$

with $s^2 = s_x^2 + s_y^2 + s_z^2$, $s_{x,y,z} = \frac{1}{2}\sigma_{x,y,z}$ and $\sigma_{x,y,z}$ are the Pauli matrices; the spinor has components

$$\chi_{\frac{1}{2}}(1) = \chi_{-\frac{1}{2}}(-1) = 1, \qquad \chi_{\frac{1}{2}}(-1) = \chi_{-\frac{1}{2}}(1) = 0\,. \tag{1.6}$$

The wavefunctions φ_k constitute a complete set which fulfills the conditions:

$$\int \varphi_k^*(x)\varphi_\ell(x)dx \equiv \sum_\sigma \int \varphi_k^*(\mathbf{r},\sigma)\varphi_\ell(\mathbf{r},\sigma)d\mathbf{r} = \delta_{k,\ell}\,, \tag{1.7}$$

where we assumed that the single-particle energies ϵ_k are discrete (in the case of continuum values, the Kronecker's symbol is to be replaced by the Dirac's delta function).

An eigenfunction of H_0 with eigenvalue E is therefore written as

$$\psi(x_1,\ldots,x_N) = \prod_{i=1}^{N} \varphi_{k_i}(x_i)\,, \tag{1.8}$$

with

$$E = \sum_{i=1}^{N} \varepsilon_{k_i}\,. \tag{1.9}$$

However, the solution expressed as a product of single-particle wavefunctions should satisfy the symmetry or antisymmetry requisite under particle exchange, depending on whether we have a system of Bosons or Fermions, respectively.

1.2   Bosons

Symmetric wavefunctions under the exchange of the x coordinates of any two particles, are obtained by considering all possible permutations P of N objects, and taking the following linear combination:

$$\psi_B(x_1,\ldots,x_N) = \sqrt{\frac{n_1! n_2! \cdots}{N!}} \sum_P P \prod_{i=1}^{N} \varphi_{k_i}(x_i)\,. \tag{1.10}$$

The coefficients n_i which appear in the normalization constant of equation (1.10) represent the number of times the wavefunction φ_{k_i} appears in the product $\Pi_{i=1}^N \varphi_{k_i}$ and thus the average occupation number of state φ_{k_i}. Therefore, such number may be larger than 1, thanks to the Boson nature of the particles.

The ground state of a system of N Bosons is obtained by occupying N times the lowest-energy state φ_{k_1}:

$$\psi_B(x_1, \ldots, x_N) = \varphi_{k_1}(x_1) \cdots \varphi_{k_1}(x_N). \tag{1.11}$$

This situation, which is characterized by a macroscopic occupation of only one single-particle state, is known as Bose-Einstein condensation and has been realized experimentally by cooling, by means of laser techniques and evaporation of hotter atoms, a diluted alkali atom gas in a magnetic trap (Anderson et al. 1995; Davis et al. 1995; Bradley et al. 1995). However, a realistic description of this phenomenon demands for the solution of the many body problem with the two-body interaction included in the Hamiltonian (1.1). This description will be presented in the forthcoming chapters.

1.3 Fermions

In the case of a system of N Fermions, starting from the product functions of equation (1.8), we obtain a fully antisymmetric wavefunction under the exchange of the coordinates of two particles with the following combination:

$$\psi_F(x_1, \ldots, x_N) = \frac{1}{\sqrt{N!}} \sum_P (-1)^P P \prod_{i=1}^N \varphi_{k_i}(x_i). \tag{1.12}$$

In equation (1.12), the factor $(-1)^P$ is equal to 1 if the permutation is an even one. In the case of Fermions, the occupation number of a single-particle state φ_{k_i} is either 0 or 1, otherwise the function (1.12) vanishes identically (Pauli exclusion principle). This can be seen very easily by putting the wavefunction (1.12) in determinant form (Slater determinant):

$$\psi_F(x_1, \ldots, x_N) = \frac{1}{\sqrt{N!}} \det \begin{vmatrix} \varphi_{k_1}(x_1) & \varphi_{k_1}(x_2) & \cdots & \varphi_{k_1}(x_N) \\ \varphi_{k_2}(x_1) & \varphi_{k_2}(x_2) & \cdots & \varphi_{k_2}(x_N) \\ \vdots & \vdots & \ddots & \vdots \\ \varphi_{k_N}(x_1) & \varphi_{k_N}(x_2) & \cdots & \varphi_{k_N}(x_N) \end{vmatrix}. \tag{1.13}$$

The determinant is zero if two rows are equal (i.e. if two sets of quantum numbers are equal) and changes its sign under the exchange of two columns (i.e. the coordinates of two particles).

In the independent-particle model, the ground state for a system of N Fermions is obtained by occupying the N lowest-energy single-particle states characterized by the sets of quantum numbers $k_1, k_2, \ldots, k_N$. The highest-energy occupied state defines the Fermi level, and its energy defines the Fermi energy.

For example, if we consider a single-particle Hamiltonian for a three-dimensional

harmonic oscillator:

$$H_0 = \sum_{i=1}^{N} \left(\frac{p_i^2}{2m} + \frac{m\omega_0^2 r_i^2}{2} \right), \qquad (1.14)$$

the single-particle spectrum is given by ($\hbar = 1$):

$$\epsilon_{nl} = \left(N + \frac{3}{2} \right) \omega_0 \quad \text{with } N = 2(n-1) + l,$$

where $N = 0, 1, 2, \ldots, l = N, N-2, \ldots, 0$ or 1. We have that up to $l = 3$, in order of increasing energy, the orbitals and their degeneracy $[2(2l+1)]$ that for fixed values of n and l determines the number of particles that can be accommodated in the orbital without violating the Pauli principle (we have $2l+1$ different values of m, and for each m value two possible values of m_s), are reported in the following Table.

<div align="center">TABLE 1.1</div>

N	E	n	l	Orbital	Degeneracy
3	$(9/2)\omega_0$	$\begin{cases} 1 \\ 2 \end{cases}$	$\begin{matrix} 3 \\ 1 \end{matrix}$	$\begin{matrix} 1f \\ 2p \end{matrix}$	$14 + 6$
2	$(7/2)\omega_0$	$\begin{cases} 1 \\ 2 \end{cases}$	$\begin{matrix} 2 \\ 0 \end{matrix}$	$\begin{matrix} 1d \\ 2s \end{matrix}$	$10 + 2$
1	$(5/2)\omega_0$	1	1	$1p$	6
0	$(3/2)\omega_0$	1	0	$1s$	2

Thus, if we have 8 particles then the Fermi level coincides with the $1p$ orbital, and the Fermi energy is $5/2\omega_0$. The ground state of the independent-particle model is the Slater determinant of the 8×8 matrix built up by means of the single-particle wavefunctions characterized by the sets of quantum numbers (n, l, m, m_s):

$$(1,0,0,1/2), \ (1,0,0,-1/2), \ (1,1,1,1/2), \ (1,1,1,-1/2),$$
$$(1,1,0,1/2), \ (1,1,0,-1/2), \ (1,1,-1,1/2), \ (1,1,-1,-1/2).$$

Finally, the ground state energy is $E_0^F = [2(3/2) + 6(5/2)]\omega_0 = 18\omega_0$.

The same system, but now made up of Bosons, has the ground state wavefunction ($a = \sqrt{m\omega_0}$):

$$\psi(r_1, \ldots, r_8) = \varphi_{1s}(r_1)\varphi_{1s}(r_2) \cdots \varphi_{1s}(r_8)$$

$$= (2\pi^{-1/4}a^{3/2})^8 \exp\left(-1/2a^2 \sum_{i=1}^{8} r_i^2 \right) \qquad (1.15)$$

to which corresponds the energy $E_0^B = 8(3/2)\omega_0 = 12\omega_0$.

The excited states of the Fermion system are obtained from the ground state in the following way: one-particle–one-hole $(1p - 1h)$ states are obtained by occupying $N - 1$ single-particle states below the Fermi level and 1 state above the Fermi level. In the following we will indicate such state as $|i^{-1}m\rangle$, where φ_i is the unoccupied

state below the Fermi level (hole), and φ_m is the occupied state above the Fermi level (particle). The wavefunction of the state $|i^{-1}m\rangle$, is the Slater determinant obtained by substituting the row characterized by the set of quantum numbers i, by the row characterized by the set of quantum numbers m. Its energy is given by $E_0 + \epsilon_m - \epsilon_i$, where E_0 is the ground state energy and ϵ_m, ϵ_i are the energies of the single-particle states φ_m and φ_i.

Two-particle–two-hole states $(2p - 2h)$ are obtained by occupying $N - 2$ single-particle states below the Fermi level and two single-particle states above the Fermi level, and are indicated by $|i^{-1}j^{-1}mn\rangle$, which means the Slater determinant obtained from the ground state by substituting the two rows i and j by the rows m and n. The energy of state $|i^{-1}j^{-1}mn\rangle$ is given by $E_0 + \epsilon_m + \epsilon_n - \epsilon_i - \epsilon_j$. In the same way it is possible to build up three-particle–three-hole states, and so on. In the following, we will always indicate hole states by the letters i, j, k, l, and particle states by the letters m, n, p, q.

In the Boson system case, in order to build 1-particle–1-hole states, or two-particle–two-hole ones, one proceeds in the same way, but starting from the ground state of the Boson condensate of (1.11), where all particles occupy the same lowest-energy state. For example, to set up a $1p - 1h$ state it is enough to replace a single-particle wavefunction φ_{k_1}, by a wavefunction corresponding to a higher-energy state, and then to symmetrize the product wavefunction so obtained.

Note that, since the above N-particle states are a complete set of eigenstates of H_0, a sum of Slater determinants (symmetric products) forms the general element of the many-Fermion (Boson) Hilbert space when the effects of the interaction are included in the theory.

1.4 Matrix Elements of One-Body Operators

By the term one-body operator we mean an operator of the kind

$$F_1 = \sum_{i=1}^{N} f(x_i), \qquad (1.16)$$

where f is a function of the variables x. In what follows we will evaluate the matrix elements of such operators between N-particle states in the independent-particle model. In general, we have

$$\langle \phi | F_1 | \psi \rangle = \int \phi^*(x_1, \ldots, x_N) \sum_{i=1}^{N} f(x_i) \psi(x_1, \ldots, x_N) dx_1 \cdots dx_N$$

$$= N \int \phi^*(x_1, \ldots, x_N) f(x_1) \psi(x_1, \ldots, x_N) dx_1 \cdots dx_N, \qquad (1.17)$$

where ϕ and ψ are two N-particle states and in the last passage we exploited the symmetry or antisymmetry property of the two wavefunctions. By writing

down explicitly, for both Fermions and Bosons, the wavefunctions ϕ and ψ as products of single-particle wavefunctions [see Eqs. (1.10–1.13)], it is easily seen that the matrix element (1.17) vanishes if ϕ and ψ differ by more than one pair of single-particle states. The only two possibilities are then: 1) $\phi = \psi$, i.e. the same single-particle states are occupied in the two wavefunctions; 2) the same $N-1$ single-particle states are occupied in ϕ and ψ, while the N-th state of ϕ is φ_i and that of ψ is φ_m ($m \neq i$). By taking ϕ to be the ground state ($|\phi\rangle = |0\rangle$) and specializing to Fermions, in the first case we obtain

$$\langle 0|F_1|0\rangle = \sum_{s=1}^{N} \int \varphi_{i_s}^*(x)f(x)\varphi_{i_s}(x)dx , \tag{1.18}$$

and in the second case:

$$\langle 0|F_1|i^{-1}m\rangle = \int \varphi_i^*(x)f(x)\varphi_m(x)dx . \tag{1.19}$$

Equations (1.18) and (1.19) are easily obtained by employing in (1.17) the expansion of the determinant (1.13) according to the elements of the first column.

In the Boson case, where the ground state is a single-particle state φ_{i_1} which is N-fold occupied, we obtain

$$\langle 0|F_1|0\rangle = N \int \varphi_{i_1}^*(x)f(x)\varphi_{i_1}(x)dx \tag{1.20}$$

and

$$\langle 0|F_1|i_1^{-1}m\rangle = \sqrt{N} \int \varphi_{i_1}^*(x)f(x)\varphi_m(x) \tag{1.21}$$

where we have made use of

$$|i_1^{-1}m\rangle = \frac{1}{\sqrt{N}} \sum_P P\varphi_m(x_1)\varphi_{i_1}(x_2)\varphi_{i_1}(x_3)\cdots\varphi_{i_1}(x_N) . \tag{1.22}$$

As an example of the mean value of a one-body operator, let us compute the mean square radius of a system of N Fermions in a three-dimensional harmonic potential. The mean square radius is defined as $\langle r^2\rangle = \langle 0|\frac{1}{N}\sum_{i=1}^{N} r_i^2|0\rangle$, and by (1.18), we have

$$\langle r^2\rangle = \frac{1}{N} \sum_{n,l,m,m_s} \langle n,l|r^2|n,l\rangle , \tag{1.23}$$

where $\langle n,l|r^2|n,l\rangle = \int R_{n,l}^2 r^2 dr$. To evaluate the matrix element $\langle n,l|r^2|n,l\rangle$, it is convenient to use the virial theorem:

$$\langle n,l|\frac{p^2}{2m}|n,l\rangle = \langle n,l|\frac{m\omega_0^2 r^2}{2}|n,l\rangle = \frac{1}{2}\epsilon_{n,l} = \frac{1}{2}\left[2(n-1)+l+\frac{3}{2}\right]\omega_0 . \tag{1.24}$$

Using equations (1.23) and (1.24), we finally obtain

$$\langle r^2 \rangle = \frac{2}{Nm\omega_0} \sum_{n,l} (2l+1) \left[2(n-1) + l + \frac{3}{2} \right]. \qquad (1.25)$$

In the Boson case, since in the ground state only the $1s$ state is occupied, which has degeneracy N [instead of $2(2l+1)$], we have

$$\langle r^2 \rangle = \frac{3}{2m\omega_0}, \qquad (1.26)$$

independent of the number of particles.

Note that the virial theorem can be considered as a consequence of the identity

$$0 = \langle 0|[H,F]|0 \rangle, \qquad (1.27)$$

if we use the harmonic oscillator Hamiltonian for H, and the operator

$$F = \sum_{i=1}^{N} \mathbf{r}_i \cdot \nabla_{\mathbf{r}_i}$$

for F.

1.5   Matrix Elements of Two-Body Operators

By the term two-body operator we mean an operator of the following type

$$F_2 = \sum_{i<j=1}^{N} f(x_i, x_j), \qquad (1.28)$$

with $f(x_i, x_j) = f(x_j, x_i)$.

A particular case of two-body operator is the two-body interaction

$$F_2 = \sum_{i<j=1}^{N} v(r_{i,j})$$

with $r_{i,j} = |\mathbf{r}_i - \mathbf{r}_j|$. We are interested in evaluating the matrix elements

$$\langle \phi | F_2 | \psi \rangle = \int \phi^*(x_1, \ldots, x_N) \sum_{i<j=1}^{N} f(x_i, x_j) \psi(x_1, \ldots, x_N) dx_1 \cdots dx_N$$

$$= \frac{N(N-1)}{2} \int \phi^*(x_1, \ldots, x_N) f(x_1, x_2) \psi(x_1, \ldots, x_N) dx_1 \cdots dx_N. \qquad (1.29)$$

If we take state ϕ as the ground state $|0\rangle$, it is easily realized that in this case there exist only three non-vanishing matrix elements, and more precisely $\langle 0|F_2|0 \rangle$, $\langle 0|F_2|i^{-1}, m \rangle$ and $\langle 0|F_2|i^{-1}, k^{-1}, m, n \rangle$. As in the case of one-body operator, in this case as well the calculation is different for Boson and Fermions.

Bosons

When $\phi = \psi = |0\rangle$, from equations (1.11) and (1.29), and taking into account the normalization of the single-particle wavefunctions, we obtain immediately

$$\langle 0|F_2|0\rangle = \frac{N(N-1)}{2} \int \varphi_{i_1}^*(x_1)\varphi_{i_1}^*(x_2)f(x_1,x_2)\varphi_{i_1}(x_1)\varphi_{i_1}(x_2)dx_1 dx_2 \,. \quad (1.30)$$

When $\phi = |0\rangle$ and $\psi = |i_1^{-1}m\rangle$, using equation (1.22), we have

$$\langle 0|F_2|i_1^{-1}m\rangle = \sqrt{N}(N-1) \int \varphi_{i_1}^*(x_1)\varphi_{i_1}^*(x_2)f(x_1,x_2)\varphi_m(x_1)\varphi_{i_1}(x_2)dx_1 dx_2 \,. \quad (1.31)$$

Finally, if $\phi = |0\rangle$ and $\psi = |i_1^{-1}i_1^{-1}mn\rangle$ then using

$$|i_1^{-1}i_1^{-1}mn\rangle = \frac{1}{\sqrt{N(N-1)}} \sum_P P\varphi_m(x_1)\varphi_n(x_2)\varphi_{i_1}(x_3)\cdots\varphi_{i_1}(x_N) \,, \quad (1.32)$$

we easily obtain

$$\langle 0|F_2|i_1^{-1}i_1^{-1}mn\rangle$$

$$= \sqrt{N(N-1)} \int \varphi_{i_1}^*(x_1)\varphi_{i_1}^*(x_2)f(x_1,x_2)\varphi_m(x_1)\varphi_n(x_2)dx_1 dx_2 \,. \quad (1.33)$$

Fermions

In the Fermion case, we use the representation of the wavefunctions as Slater determinants, and expanding with respect to the two first columns:

$$\Phi(x_1,\ldots,x_N) = \frac{1}{\sqrt{N!}} \begin{vmatrix} \varphi_{i_1}(x_1) & \varphi_{i_1}(x_2) & \varphi_{i_1}(x_3) & \cdots & \varphi_{i_1}(x_N) \\ \varphi_{i_2}(x_1) & \varphi_{i_2}(x_2) & \varphi_{i_2}(x_3) & \cdots & \varphi_{i_2}(x_N) \\ \varphi_{i_3}(x_1) & \varphi_{i_3}(x_2) & \varphi_{i_3}(x_3) & \cdots & \varphi_{i_3}(x_N) \\ \vdots & \vdots & \vdots & \ddots & \vdots \\ \varphi_{i_N}(x_1) & \varphi_{i_N}(x_2) & \varphi_{i_N}(x_3) & \cdots & \varphi_{i_N}(x_N) \end{vmatrix}$$

$$= \frac{1}{\sqrt{N!}} \sum_{i_s<i_t}^N [\varphi_{i_s}(x_1)\varphi_{i_t}(x_2)-\varphi_{i_s}(x_2)\varphi_{i_t}(x_1)]M_{\{i_k\}\neq i_s,i_t}^{N-2}(x_3,\ldots,x_N) \,,$$

where $M_{\{i_k\}\neq i_s,i_t}^{N-2}(x_3,\ldots,x_N)$ means the minor of order $N-2$ which depends on the space variables $x_3,\ldots,x_N$, from which the first and second columns, as well as the i_s-th and i_t-th rows, have been removed. Hence it depends on a set of quantum numbers $\{i_k\}$ which are all different from i_s and i_t. In order to avoid cumbersome notation, we will write $\mathcal{M}(x_3,\ldots,x_N)$ instead of $M_{\{i_k\}\neq i_s,i_t}^{N-2}(x_3,\ldots,x_N)$. Let us

now compute the matrix element:

$$
\langle\phi|F_2|\psi\rangle = \frac{N(N-1)}{2N!}\sum_{i_s<i_t}^{N}\sum_{i_{\tilde{s}}<i_{\tilde{t}}}^{N}\int\phi^*(x_1,x_2,i_s,i_t)\mathcal{M}^*(x_3,\ldots,x_N)f(x_1,x_2)
$$

$$
\times\psi(x_1,x_2,i_{\tilde{s}},i_{\tilde{t}})\tilde{\mathcal{M}}(x_3,\ldots,x_N)dx_1\cdots dx_N\,, \tag{1.34}
$$

where $\phi(x_1,x_2,i_s,i_t)=\varphi_{i_s}(x_1)\varphi_{i_t}(x_2)-\varphi_{i_s}(x_2)\varphi_{i_t}(x_1)$ and similar for ψ. Starting from equation (1.34), it is easily seen that the only non-vanishing matrix elements are, as mentioned, $\langle0|F_2|0\rangle$, $\langle0|F_2|i^{-1},m\rangle$, $\langle0|F_2|i^{-1},k^{-1},m,n\rangle$. One finally obtains:

$$
\langle0|F_2|0\rangle = \frac{1}{2}\sum_{i_s,i_t}^{N}\int\varphi_{i_s}^*(x_1)\varphi_{i_t}^*(x_2)f(x_1,x_2)
$$

$$
\times[\varphi_{i_s}(x_1)\varphi_{i_t}(x_2)-\varphi_{i_s}(x_2)\varphi_{i_t}(x_1)]dx_1dx_2\,, \tag{1.35}
$$

$$
\langle0|F_2|i^{-1},m\rangle = \sum_{i_t}^{N}\int\varphi_i^*(x_1)\varphi_{i_t}^*(x_2)f(x_1,x_2)
$$

$$
\times[\varphi_m(x_1)\varphi_{i_t}(x_2)-\varphi_m(x_2)\varphi_{i_t}(x_1)]dx_1dx_2\,, \tag{1.36}
$$

$$
\langle0|F_2|i^{-1},j^{-1},m,n\rangle = \int\varphi_i^*(x_1)\varphi_j^*(x_2)f(x_1,x_2)
$$

$$
\times[\varphi_m(x_1)\varphi_n(x_2)-\varphi_m(x_2)\varphi_n(x_1)]dx_1dx_2\,. \tag{1.37}
$$

Note the presence of the exchange term $x_1\to x_2$ and $x_2\to x_1$, which is proper to Fermions since it originates from the antisymmetrization of the wavefunction.

1.6 Density Matrices

Generally speaking, the one-body and two-body properties of a many-body system are embodied in the one-body and two-body density matrices, respectively. The one-body density matrix is defined as

$$
\rho^{(1)}(x_1,x_1') = N\int\phi_0^*(x_1,x_2,\ldots,x_N)\phi_0(x_1',x_2,\ldots,x_N)dx_2\cdots dx_N\,, \tag{1.38}
$$

and the two-body one as

$$
\rho^{(2)}(x_1,x_2,x_1',x_2') = N(N-1)\int\phi_0^*(x_1,x_2,x_3,\ldots,x_N)
$$

$$
\times\phi_0(x_1',x_2',x_3,\ldots,x_N)dx_3\cdots dx_N\,. \tag{1.39}
$$

The following properties hold:

$$\int \rho^{(2)}(x, x_2, x', x_2)dx_2 = (N-1)\rho^{(1)}(x, x'), \qquad (1.40)$$

$$\int \rho^{(1)}(x, x)dx = N. \qquad (1.41)$$

The diagonal part of the one-body density matrix (when $x = x'$) is related to the particle density $\rho(\mathbf{r})$:

$$\rho(\mathbf{r}) = \sum_\sigma \rho^{(1)}(\mathbf{r}, \sigma, \mathbf{r}, \sigma). \qquad (1.42)$$

while the non-diagonal part is related to the momentum distribution $n(\mathbf{p})$:

$$n(\mathbf{p}) = \frac{1}{(2\pi)^3} \sum_\sigma \int \rho^{(1)}(\mathbf{r}, \sigma, \mathbf{r}', \sigma)e^{i\mathbf{p}\cdot(\mathbf{r}-\mathbf{r}')}d\mathbf{r}d\mathbf{r}'. \qquad (1.43)$$

The densities $\rho^{(1)}$ and $\rho^{(2)}$ can be used in order to calculate the mean values of one-body and two-body operators in the ground state:

$$\langle 0| \sum_i f(x_i)|0\rangle = \int \rho^{(1)}(x, x)f(x)dx, \qquad (1.44)$$

$$\langle 0| \sum_{i<j} f(x_i, x_j)|0\rangle = \frac{1}{2} \int \rho^{(2)}(x_1, x_2, x_1, x_2)f(x_1, x_2)dx_1dx_2. \qquad (1.45)$$

In the case when the ground state is that of the independent-particle model, we obtain

$$\rho_B^{(1)}(x_1, x_1') = N\varphi_{i_1}^*(x_1)\varphi_{i_1}(x_1'), \qquad (1.46)$$

$$\rho_B^{(2)}(x_1, x_2, x_1', x_2') = N(N-1)[\varphi_{i_1}^*(x_1)\varphi_{i_1}^*(x_2)\varphi_{i_1}(x_1')\varphi_{i_1}(x_2')], \qquad (1.47)$$

for Bosons (φ_{i_1} is the lowest-energy single-particle state), and

$$\rho_F^{(1)}(x_1, x_1') = \sum_{i=1}^{N} \varphi_i^*(x_1)\varphi_i(x_1'), \qquad (1.48)$$

$$\rho_F^{(2)}(x_1, x_2, x_1', x_2') = \rho_F^{(1)}(x_1, x_1')\rho_F^{(1)}(x_2, x_2') - \rho_F^{(1)}(x_1, x_2')\rho_F^{(1)}(x_2, x_1'), \qquad (1.49)$$

for Fermions. Note that the following property holds for Slater determinants:

$$\int \rho_{SD}^{(1)}(x, x')\rho_{SD}^{(1)}(x', x'')dx' = \rho_{SD}^{(1)}(x, x''). \qquad (1.50)$$

As an example of the calculation of density matrices, let us compute $\rho^{(1)}$ for a system of Fermions in a spherical one-body potential, so that the single-particle wavefunctions can be written in the form $\varphi_i = R_{n,l}Y_{l,m}\chi_{m_s}$. Let us carry out the

calculation for a system with N such that the $2(2l + 1)$ degenerate states of each level n, l are completely occupied (closed-shell system). By using the properties:

$$\sum_m Y_{lm}(\vartheta, \varphi) Y_{lm}(\vartheta', \varphi') = \frac{2l + 1}{4\pi} P_l(u) , \qquad (1.51)$$

where the $P_l(u)$ are the Legendre polynomials and $u = \cos(\theta - \theta')$, and

$$\sum_{m_s} \chi^*_{m_s}(\sigma) \chi_{m_s}(\sigma') = \delta_{\sigma,\sigma'} , \qquad (1.52)$$

we have

$$\rho^{(1)}(\mathbf{r}, \sigma, \mathbf{r}', \sigma') = \frac{1}{4\pi} \sum_{n,l} (2l + 1) R_{n,l}(r) R_{n,l}(r') P_l(u) \delta_{\sigma,\sigma'} . \qquad (1.53)$$

Therefore, the density is written as

$$\rho(\mathbf{r}) = \sum_\sigma \rho^{(1)}(\mathbf{r}, \sigma, \mathbf{r}, \sigma) = 2 \sum_{n,l} \frac{2l + 1}{4\pi} |R_{n,l}(r)|^2 , \qquad (1.54)$$

and it is spherical.

1.7 The Ideal Bose Gas Confined in a Harmonic Potential

The non-interacting Bose gas confined in a magnetic trap is described by (1.3) taking

$$v_{\text{ext}}(\mathbf{r}) = \frac{1}{2} m(\omega_x^2 x^2 + \omega_y^2 y^2 + \omega_z^2 z^2) . \qquad (1.55)$$

This potential exactly reproduces all possible experimental situations. The single-particle energies for this potential are given by

$$\epsilon_{n_x n_y n_z} = \left(n_x + \frac{1}{2}\right) \omega_x + \left(n_y + \frac{1}{2}\right) \omega_y + \left(n_z + \frac{1}{2}\right) \omega_z , \qquad (1.56)$$

where the n_x, n_y, n_z are non-negative integers and the single-particle wavefunction is given by

$$\varphi_{n_x n_y n_z}(x, y, z) = \phi_{n_x}(x) \phi_{n_y}(y) \phi_{n_z}(z) , \qquad (1.57)$$

with

$$\phi_{n_x}(x) = (m\omega_x/\pi)^{1/4} (1/\sqrt{2^{n_x} n_x!}) e^{\frac{-m\omega_x}{2} x^2} H_{n_x}(x\sqrt{m\omega_x}) ,$$

where H_{n_x} are the Hermite polynomials, and similarly for the functions depending on y and z.

In the ground state, at zero temperature, all the Bosons occupy the state $(n_x, n_y, n_z) = (0, 0, 0)$ at the energy $\epsilon(0, 0, 0) \equiv \epsilon_0$ and with the wavefunction

$$\phi_0 = \left(\frac{m\bar{\omega}}{\pi}\right)^{3/4} e^{-m/2(\omega_x x^2 + \omega_y y^2 + \omega_z z^2)},$$

where we have defined $\bar{\omega} = (\omega_x \omega_y \omega_z)^{1/3}$, and one has the Bose–Einstein condensate at zero temperature. One also talks about condensate at finite temperature, when there is a macroscopic occupation of state ϵ_0. As temperature is increased, a critical temperature is reached at which the lowest-energy state is no longer macroscopically occupied.

In the following we calculate, in the limit of large number N of Bosons, the critical temperature T_c at which phase transition takes place, as well as the temperature dependence of the depopulation of the condensate state.

The Boson distribution function at temperature T is given by Bose statistics:

$$n_{n_x, n_y, n_z} = \frac{1}{e^{[\beta(\epsilon_{n_x, n_y, n_z} - \mu)]} - 1}, \tag{1.58}$$

where $\beta = 1/KT$ (K is Boltzmann's constant) and μ is the chemical potential, which is determined by the condition that the summation of the number of occupied states coincides with the total number of Bosons:

$$N = \sum_{n_x, n_y, n_z} n_{n_x, n_y, n_z}. \tag{1.59}$$

Once N is fixed, let us find the condition that must be fulfilled by the chemical potential of the confined gas in order that there is a macroscopic occupation of state ϵ_0. The occupation n_0 of this state is given by

$$n_0 = \frac{1}{e^{-\beta\mu} e^{\beta(\frac{\omega_x}{2} + \frac{\omega_y}{2} + \frac{\omega_z}{2})} - 1}, \tag{1.60}$$

which shows that there is condensation when

$$\mu = \mu_c = \left(\frac{\omega_x}{2} + \frac{\omega_y}{2} + \frac{\omega_z}{2}\right) + \alpha, \tag{1.61}$$

with $\alpha \to 0$ when $N \to \infty$. Due to confinement, this condition differs from the one for homogeneous ideal gas in which case condensation takes place in the limit $\mu \to 0$.

Now we can calculate the number of Bosons outside the condensate $N - N_0$, by using for the chemical potential its limiting value for which Bose–Einstein condensation takes place, in (1.58) and (1.59):

$$N - N_0 = \sum_{n_x, n_y, n_z \neq 0, 0, 0} \frac{1}{e^{[\beta(\omega_x n_x + \omega_y n_y + \omega_z n_z)]} - 1}. \tag{1.62}$$

In order to compute expression (1.62) we replace the summation $\sum_{n_x, n_y, n_z}$ by the integral $\int dn_x dn_y dn_z$. This approximation turns out to be a good one if

$KT \gg \omega_x, \omega_y, \omega_z$ and the main contribution to the summation comes from states whose energy is much higher than $\omega_x, \omega_y, \omega_z$. In this case, we obtain

$$N - N_0 \simeq \int_0^\infty \frac{dn_x dn_y dn_z}{e^{[\beta(\omega_x n_x + \omega_y n_y + \omega_z n_z)]} - 1}, \tag{1.63}$$

and thus

$$N - N_0 \simeq \left(\frac{KT}{\bar{\omega}}\right)^3 \zeta(3), \tag{1.64}$$

where $\zeta(n)$ is the Riemann function. The temperature dependence of the condensate depopulation, T^3, is different from the homogeneous gas case, where the law is $T^{3/2}$. The critical temperature for the transition to the condensate is obtained from equation (1.64) by putting $N_0 = 0$. We find

$$KT_c \simeq 0.94\bar{\omega}N^{1/3}. \tag{1.65}$$

For temperatures higher than T_c the chemical potential is smaller than μ_c and depends on N and the population of the lowest-energy state is no longer of the order of N. Note that the thermodynamic limit for confined systems is obtained by taking $N \to \infty$ and $\bar{\omega} \to 0$ while keeping the product $N\bar{\omega}^3$ constant. With this definition, T_c is well defined in the thermodynamic limit.

If we insert the expression of T_c in the equation for $N - N_0$ we obtain the T-dependence of the condensate fraction for $T \leq T_c$:

$$\frac{N_0}{N} = 1 - \left(\frac{T}{T_c}\right)^3. \tag{1.66}$$

For the magnetic traps that are realized nowadays, for which $\bar{\omega}/K$ is of the order of a few nanokelvin, and for N values in the range 10^3 to 10^7, the critical temperature turns out to be of the order of tens or a few hundred nanokelvin. Such low temperatures are realized by means of laser cooling and evaporation techniques.

The effects of interaction on the critical temperature and on the behavior of the condensate depopulation, are discussed in detail by Dalfovo et al. (1999).

1.8   The Fermi Gas

The non-interacting Fermi gas is obtained from equation (1.3) by putting $v_{\text{ext}} = 0$ and imposing periodicity conditions to the plane-wave-like solutions:

$$\varphi_i(x) = \frac{1}{\sqrt{V}} e^{i\mathbf{k}\cdot\mathbf{r}} \chi_{m_s}(\sigma), \quad i \equiv k_x, k_y, k_z, m_s, \tag{1.67}$$

at the boundaries of a cube having volume V and side L:

$$e^{ik_x(x+L)} = e^{ik_x x}, \qquad e^{ik_y(y+L)} = e^{ik_y y}, \qquad e^{ik_z(z+L)} = e^{ik_z z}. \tag{1.68}$$

Therefore, the particle momentum **k** can only take on the values

$$k_\alpha = \frac{2\pi}{L} n_\alpha \qquad (\alpha = x, y, z) \, , \tag{1.69}$$

where n_x, n_y, n_z are positive and negative integers, including zero. In general, if D is the dimensionality of the problem, with $D = 3, 2, 1$, then we will have $V = L^D$ and $\mathbf{k} = \frac{2\pi}{L}(n_x, n_y)$ for $D = 2$ and $k_x = \frac{2\pi}{L} n_x$ for $D = 1$.

The single-particle energies are given by

$$\epsilon_\mathbf{k} = \frac{k^2}{2m} \, . \tag{1.70}$$

In the $V \to \infty$ limit, the allowed values **n** in momentum space become closely spaced, and since their density is given by $dn = L^D/(2\pi)^D d\mathbf{k}$, we can write

$$\sum_{n_x, n_y, n_z, m_s} \longrightarrow \frac{L^D}{(2\pi)^D} \sum_{m_s} \int d\mathbf{k} \, . \tag{1.71}$$

Therefore, the ground state is set up by filling a sphere ($3D$), or a circle ($2D$), or a segment ($1D$), with radius k_F, within which the single-particle states are all occupied, and outside which are all unoccupied. The Fermi energy, i.e. the energy on the Fermi surface, boundary or extremum is given by $\epsilon_F = k_F^2/2m$. The value of k_F is connected to the density $\rho = N/L^D$. In order to find such relationship, let us calculate the number N of particles using equation (1.71):

$$N = \sum_{n_x, n_y, n_z, m_s}^{N} = \frac{L^D}{(2\pi)^D} \sum_{m_s} \int n_\mathbf{k} d\mathbf{k} \, , \tag{1.72}$$

where $n_\mathbf{k}$ is the ground state distribution:

$$n_\mathbf{k} = \begin{cases} 1 & \text{if } k \leq k_F \\ 0 & \text{if } k > k_F \end{cases} . \tag{1.73}$$

For the densities $\rho = N/L^D$, we obtain

$$\rho^{3D} = \frac{k_F^3}{3\pi^2}, \qquad \rho^{2D} = \frac{k_F^2}{2\pi}, \qquad \rho^{1D} = \frac{2k_F}{\pi} \, . \tag{1.74}$$

The energy per particle of the Fermi gas is given by

$$\frac{E}{N} = \frac{1}{N} \sum_i \epsilon_i = \frac{2}{N} \frac{L^D}{(2\pi)^D} \int n_\mathbf{k} \frac{k^2}{2m} d\mathbf{k} \, . \tag{1.75}$$

From equation (1.75), we obtain

$$\frac{E}{N} = \frac{D}{D+2} \frac{k_F^2}{2m} \, . \tag{1.76}$$

If we add a particle to the system, we have the ground state energy of a system with $N + 1$ particles if the added particle is put in the available state of lowest energy, i.e. on the Fermi surface. The system's chemical potential μ, defined by

$$\mu = E(N + 1) - E(N) = \left(\frac{\partial E}{\partial N}\right)_V, \qquad (1.77)$$

is therefore given by $\mu = \epsilon_F$.

The energy of the system may be written as a function of volume $V = L^D$, from which it is possible to write down the pressure P defined as

$$P = -\frac{\partial E}{\partial V} = \rho^2 \frac{\partial E/N}{\partial \rho}. \qquad (1.78)$$

Moreover, the compressibility K is given by

$$\frac{1}{K} = -V\frac{\partial P}{\partial V} = \rho^2 \left(\rho\frac{\partial^2 E/N}{\partial \rho^2} + 2\frac{\partial E/N}{\partial \rho}\right), \qquad (1.79)$$

and is connected to the sound velocity v by

$$v^2 = \frac{1}{Km\rho}. \qquad (1.80)$$

For the Fermi gas in three dimensions, for example, one obtains $\frac{1}{K} = \frac{1}{9\pi^2}k_F^5$.

The one-body density matrix is given by

$$\rho^{(1)}(\mathbf{r}, \sigma, \mathbf{r}', \sigma') = \sum_i \varphi_i^*(\mathbf{r}, \sigma)\varphi_i(\mathbf{r}', \sigma') = \delta_{\sigma,\sigma'} \frac{1}{(2\pi)^D} \int n_\mathbf{k} e^{-i\mathbf{k}\cdot(\mathbf{r}-\mathbf{r}')} d\mathbf{k}. \quad (1.81)$$

The calculation of the integral leads to

$$\rho^{(1)}(\mathbf{r}, \sigma, \mathbf{r}', \sigma') = \delta_{\sigma,\sigma'} \frac{k_F^3}{2\pi^2} \frac{C(k_F \mid \mathbf{r} - \mathbf{r}' \mid)}{k_F \mid \mathbf{r} - \mathbf{r}' \mid} \qquad \text{(in } 3D\text{)}, \qquad (1.82)$$

$$\rho^{(1)}(\mathbf{r}, \sigma, \mathbf{r}', \sigma') = \delta_{\sigma,\sigma'} \frac{k_F^2}{2\pi} \frac{J_1(k_F \mid \mathbf{r} - \mathbf{r}' \mid)}{k_F \mid \mathbf{r} - \mathbf{r}' \mid} \qquad \text{(in } 2D\text{)}, \qquad (1.83)$$

$$\rho^{(1)}(x, \sigma, x', \sigma') = \delta_{\sigma,\sigma'} \frac{1}{\pi} \frac{\sin(k_F(x - x'))}{k_F(x - x')} \qquad \text{(in } 1D\text{)}, \qquad (1.84)$$

where $C(x) = \frac{\sin x - x\cos x}{x^2}$ and J_1 is the Bessel function. Putting $\mathbf{r} = \mathbf{r}'$ and $\sigma = \sigma'$ in the previous equations and summing over σ, one re-obtains the diagonal density of (1.74).

By using equation (1.49), let us now calculate the diagonal part of the two-body density matrix $\rho_F^{(2)}(x_1, x_2, x_1, x_2)$ in the three-dimensional case taken as an

example. We obtain

$$
\rho_{SD}^{(2)}(\mathbf{r}_1, \sigma_1, \mathbf{r}_2, \sigma_2, \mathbf{r}_1, \sigma_1, \mathbf{r}_2, \sigma_2) = \frac{k_F^6}{36\pi^4} \left[1 - 9\delta_{\sigma_1, \sigma_2} \left(\frac{C(k_F \mid \mathbf{r}_1 - \mathbf{r}_2 \mid)}{k_F \mid \mathbf{r}_1 - \mathbf{r}_2 \mid} \right)^2 \right]
$$

$$
\equiv \frac{k_F^6}{36\pi^4} g_{\sigma_1, \sigma_2}(\mathbf{r}_1 - \mathbf{r}_2), \tag{1.85}
$$

where we have introduced the pair correlation function

$$
g_{\sigma_1, \sigma_2}(\mathbf{r}) = 1 - 9\delta_{\sigma_1, \sigma_2} \left(\frac{C(k_F \mid \mathbf{r}_1 - \mathbf{r}_2 \mid)}{k_F \mid \mathbf{r}_1 - \mathbf{r}_2 \mid} \right)^2. \tag{1.86}
$$

The function g is proportional to the probability of finding two particles at distance $r = |\mathbf{r}_1 - \mathbf{r}_2|$ apart, with spin variables σ_1 and σ_2.

If we are interested in the probability that two particles are at a distance r apart, irrespective of the spin, we should calculate

$$
\sum_{\sigma_1, \sigma_2} g_{\sigma_1, \sigma_2} = 4 - 18 \left(\frac{C(k_F r)}{k_F r} \right)^2. \tag{1.87}
$$

If, on the other hand, we are interested in the probability that two particles with the same spin variables are at a distance r apart, we should calculate

$$
\sum_{\sigma_1 = \sigma_2} g_{\sigma_1, \sigma_2} = 2 - 18 \left(\frac{C(k_F r)}{k_F r} \right)^2. \tag{1.88}
$$

Finally, for the probability that two particles with opposite spin are at a distance r apart, we have

$$
\sum_{\sigma_1 \neq \sigma_2} g_{\sigma_1, \sigma_2} = 2. \tag{1.89}
$$
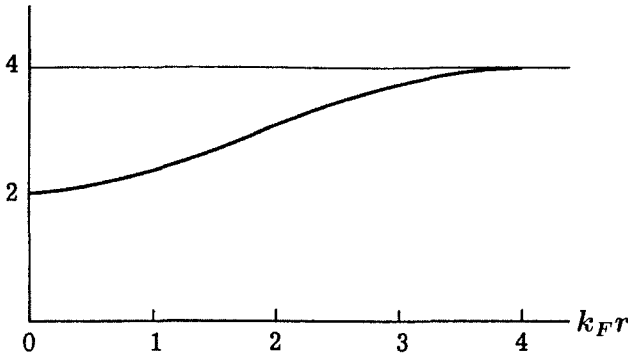
Fig. 1.1   Pair correlation function $\sum_{\sigma_1, \sigma_2} g_{\sigma_1, \sigma_2}$ of Eq. (1.87).
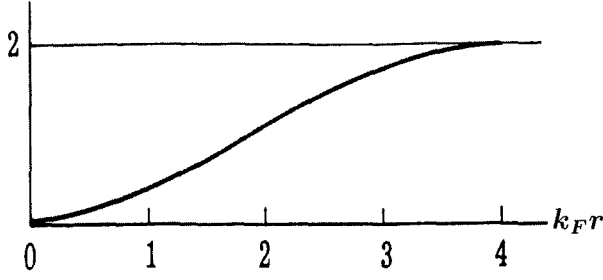
Fig. 1.2   Pair correlation function $\sum_{\sigma_1 = \sigma_2} g_{\sigma_1, \sigma_2}$ of Eq. (1.88).
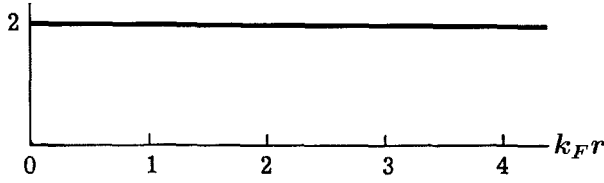
Fig. 1.3   Pair correlation function $\sum_{\sigma_1 \neq \sigma_2} g_{\sigma_1, \sigma_2}$ of Eq. (1.89).

The above three probabilities are plotted as a function of r in Figs. 1.1–1.3. The fact that the probability in (1.88) tends to zero for $r \to 0$ is a consequence of the antisymmetrization of the wavefunction and of the presence of an exchange term in $\rho_F^{(2)}$. The Pauli principle prevents the two particles with the same spin from being at the same place ($r = 0$). When the two particles have opposite spins like in (1.89), they become distinguishable and the Pauli principle does not operate, so that the probability is independent of r like in the classical case. The situation described by equation (1.87) is intermediate between the two previous ones, and results from the co-presence in $\rho_F^{(2)}$ of both symmetric and antisymmetric components under the exchange of $\mathbf{r_1} \to \mathbf{r_2}$.

1.8.1   *Excited states*

The excited states of the Fermi gas, for example, the one-particle–one-hole ($1p-1h$) state $|i^{-1}, m\rangle$, obtained by operating on the ground state with the density operator

$$\hat{\rho} = \sum_{i=1}^{N} e^{i \mathbf{q} \cdot \mathbf{r}_i} , \qquad (1.90)$$

are set up by annihilating an occupied hole state with momentum $| \mathbf{p} | < k_F$ in the ground state, and creating a particle state with momentum $| \mathbf{p} + \mathbf{q} | > k_F$. This can be easily seen from equation (1.19), which yields a non-zero result only under these conditions. Moreover, since the matrix element $\int \varphi_m^*(\mathbf{r}, \sigma) e^{i \mathbf{q} \cdot \mathbf{r}} \varphi_i(\mathbf{r}, \sigma) d\mathbf{r}$ between

plane-wave states is equal to 1, the dynamic form factor defined as

$$S(\mathbf{q}, \omega) = \sum_{n \neq 0} |\langle 0|\hat{\rho}|n\rangle|^2 \delta(\omega - \omega_{n0}) \tag{1.91}$$

in the Fermi gas may be written as

$$S(\mathbf{q}, \omega) = 2 \sum_{p < k_F, |\mathbf{p}+\mathbf{q}| > k_F} \delta(\omega - \omega_{\mathbf{pq}}), \tag{1.92}$$

where

$$\omega_{\mathbf{pq}} = \frac{(\mathbf{p}+\mathbf{q})^2}{2m} - \frac{p^2}{2m} = \frac{q^2}{2m} + \frac{\mathbf{p}\cdot\mathbf{q}}{m}, \tag{1.93}$$

and the factor 2 takes into account the summation on the spin index. In this way, the calculation of $S(\mathbf{q}, \omega)$ is reduced to a simple integration over the region in momentum space such that $p < k_F$ and $|\mathbf{p} + \mathbf{q}| > k_F$, from which one-particle–one-hole pairs with total momentum $\mathbf{q}$ may be excited. This region, in the $D = 3$ case that we took as an example, corresponds to the shaded area in Fig. 1.4, which is bounded by the Fermi sphere and by the sphere obtained by shifting S_F by the quantity $-\mathbf{q}$. Even without carrying out any calculation, it is clear that the excitation spectrum for the one-particle–one-hole states with momentum $\mathbf{q}$ will consist in a continuum between the following limits

$$0 \leq \omega_{\mathbf{pq}} \leq \frac{q^2}{2m} + \frac{qk_F}{m}, \qquad \text{for } q \leq 2k_F,$$

$$\frac{q^2}{2m} - \frac{qk_F}{m} \leq \omega_{\mathbf{pq}} \leq \frac{q^2}{2m} + \frac{qk_F}{m}, \qquad \text{for } q \geq 2k_F, \tag{1.94}$$
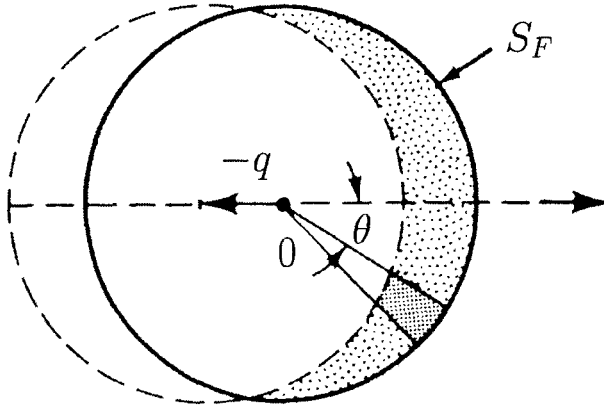
Fig. 1.4   Region in momentum space from which the $1p - 1h$ states with momentum q may be excited.
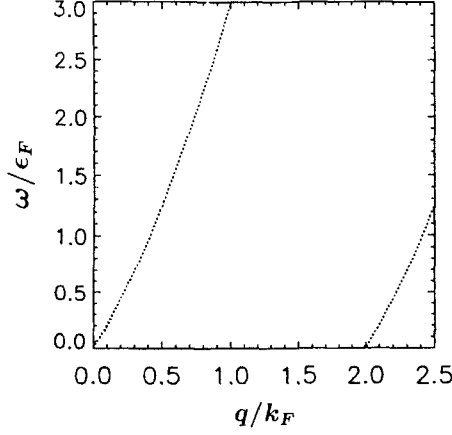
Fig. 1.5   Excitation spectrum of the $1p - 1h$ states as a function of q, in the $2D$ and $3D$ cases.

in the $D = 3$ and $D = 2$ cases, while in the $1D$ case the limits are

$$-\frac{q^2}{2m} + \frac{qk_F}{m} \leq \omega_{\mathbf{pq}} \leq \frac{q^2}{2m} + \frac{qk_F}{m}, \qquad \text{for } q \leq 2k_F,$$

$$\frac{q^2}{2m} - \frac{qk_F}{m} \leq \omega_{\mathbf{pq}} \leq \frac{q^2}{2m} + \frac{qk_F}{m}, \qquad \text{for } q \geq 2k_F. \tag{1.95}$$

The above-allowed energies correspond to the areas within the dotted lines in Figs. 1.5 and 1.6. Outside these zones the dynamic form factor vanishes. This behavior is characteristic of non-interacting systems and does not hold in the presence of interaction. Notice the relevance of dimensionality in determining the single-particle spectrum. The relevant feature of the one-dimensional spectrum, as compared to two and three dimensions, is that the one-particle–one-hole excitations are forbidden in a large part of the low-energy phase space, i.e. the one that lies below the dashed line ABC in Fig. 1.6.

The explicit calculation of $S(\mathbf{q}, \omega)$ is very simple in the case where q is much smaller than k_F. In fact, in this limit the regions in momentum space from which the $1p - 1h$ states can be excited, are very thin. Taking as an example the three-dimensional case, the number of states in the elementary volume having polar angles between θ and $\theta + d\theta$ can be written as

$$dn = \frac{V}{(2\pi)^3} 2\pi k_F^2 q \cos\theta \sin\theta d\theta, \tag{1.96}$$

and that the excitation energy for the pair is approximately given by

$$\omega_{\mathbf{pq}} = q v_F \cos\theta, \tag{1.97}$$
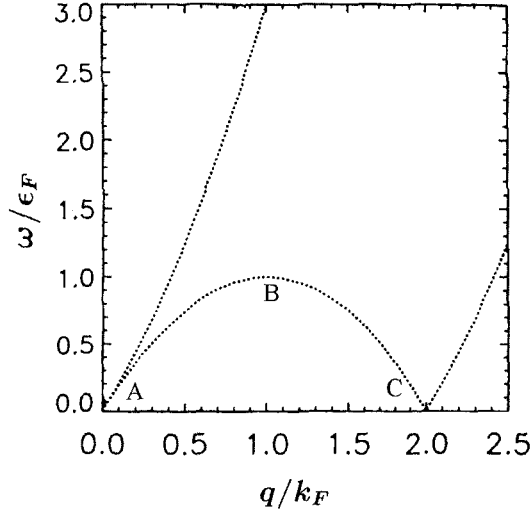
Fig. 1.6   Excitation spectrum of the $1p - 1h$ states as a function of q, in the $1D$ case.

where $v_F = k_F/m$ is the Fermi velocity. Replacing the summation in (1.92) by an integration on θ, and using the property

$$\delta(cx - x_0) = \delta\left(x - \frac{x_0}{c}\right)/|c|\,,$$

one finds

$$S_{3D}(\mathbf{q}, \omega) = V\frac{m^2\omega}{2\pi^2 q}, \qquad \text{for } \omega < qv_F\,,$$

$$S_{3D}(\mathbf{q}, \omega) = 0, \qquad\qquad \text{for } \omega > qv_F\,. \tag{1.98}$$

Note that for all q values $S(\mathbf{q}, \omega)$ goes to zero when $\omega \to 0$. This behavior stems from the Pauli principle which limits the number of low-energy excitations.

Finally, let us calculate the static form factor

$$S(\mathbf{q}) = \frac{1}{N}\int d\omega S(\mathbf{q}, \omega) = \frac{2}{N}\sum_{p<k_F, |\mathbf{p}+\mathbf{q}|>k_F} 1\,, \tag{1.99}$$

which is proportional to the area of the shaded region in Fig. 1.4. A simple calculation yields:

$$(3D): \qquad S(\mathbf{q}) = \begin{cases} \dfrac{3q}{4k_F} - \dfrac{q^3}{16k_F^3} & \text{if } q < 2k_F \\[2mm] 1 & \text{if } q \geq 2k_F \end{cases}, \tag{1.100}$$

$$(\text{2D}): \quad S(\mathbf{q}) = \begin{cases} \dfrac{2}{\pi}\sin^{-1}\left(\dfrac{q}{2k_F}\right) + \dfrac{q}{\pi k_F}\sqrt{1 - \left(\dfrac{q}{2k_F}\right)^2} & \text{if } q < 2k_F \\ 1 & \text{if } q \geq 2k_F \end{cases} , \qquad (1.101)$$

$$(\text{1D}): \qquad\qquad S(\mathbf{q}) = \begin{cases} \dfrac{q}{2k_F} & \text{if } q < 2k_F \\ 1 & \text{if } q \geq 2k_F \end{cases} . \qquad (1.102)$$

1.8.2 Polarized Fermi gas

The Fermi gas may be (partially) spin-polarized, the polarization being defined by

$$\xi = \frac{\rho_+ - \rho_-}{\rho}, \qquad (1.103)$$

where $\rho_\pm$ are the electron densities with up and down spin, respectively. Using equation (1.103) together with

$$\rho = (\rho_+ + \rho_-), \qquad (1.104)$$

one may write

$$\rho_\pm = \frac{\rho}{2}(1 \pm \xi). \qquad (1.105)$$

Here, $\xi = 0$ means that the system is unpolarized, while $\xi = 1$ means that the Fermi gas is completely polarized.

Using

$$N_+ = \sum_{n_x, n_y, n_z, m_s = 1/2}^{N_+} = \frac{L^D}{(2\pi)^D} \int n_{\mathbf{k}}^+ d\mathbf{k}, \qquad (1.106)$$

where $n_{\mathbf{k}}^+$ is the distribution: $n_{\mathbf{k}}^+ = 1$ for $k < k_F^+$ and $n_{\mathbf{k}}^+ = 0$ for $k > k_F^+$, and analogously for N_-, we obtain:

$$k_F^\pm(3D) = [3\pi^2 \rho(1 \pm \xi)]^{1/3},$$

$$k_F^\pm(2D) = [2\pi\rho(1 \pm \xi)]^{1/2}, \qquad (1.107)$$

$$k_F^\pm(1D) = \frac{\pi\rho}{2}(1 \pm \xi).$$

If we now use the generalization of equation (1.75), it is easy to obtain the energy of the polarized Fermi gas:

$$\frac{E^{3D}}{N} = \frac{3}{20m}(3\pi^2\rho)^{2/3}[(1+\xi)^{5/3} + (1-\xi)^{5/3}],$$

$$\frac{E^{2D}}{N} = \frac{\pi\rho}{2m}(1+\xi^2),$$

$$\frac{E^{1D}}{N} = \frac{\pi^2\rho^2}{48m}[(1+\xi)^3 + (1-\xi)^3].$$

(1.108)

It is interesting to remark that the above formulae hold also in the case of isospin polarization that occurs in asymmetric nuclear matter. In this case N_+ and N_- represent the number of neutrons N and protons Z, respectively, and $k_F^{\pm}$ are the Fermi momenta of neutrons and protons. The polarization ξ is given by $\frac{N-Z}{A}$, where A is the mass number, and formulae (1.108), expanded at the lowest order in ξ, yield the symmetry energy of nuclear matter (see for example the book by Bohr and Mottelson).

As an application of the obtained formulas, let us calculate the spin susceptibility of the Fermi gas. To this purpose, let us put the Fermi gas in a magnetic field **B** in the direction of the z-axis. The total energy per particle of the system is given by

$$\frac{E}{N} = \frac{E_T(\rho,\xi)}{N} + \mu_0 B\xi,$$

(1.109)

where $E_T(\rho,\xi)/N$ are the kinetic energies per particle of equation (1.108), μ_0 is Bohr's magneton $e\hbar/2mc$, and the Fermions interact with the magnetic field via the interaction Hamiltonian

$$\mu_0 \mathbf{B} \cdot \sigma.$$

The polarization ξ is obtained by requiring that the variation of the energy (1.109) with respect to ξ is zero. The magnetic susceptibility χ_σ is given by

$$\chi_\sigma = \frac{\langle \sum_i \sigma_z^i \rangle}{B} = \frac{\xi\rho L^D}{B}.$$

(1.110)

For example, in the case of a two-dimensional gas we obtain $\xi = -m\mu_0 B/\pi\rho$ and

$$\frac{\chi_\sigma}{N} = -\frac{m\mu_0}{\pi\rho} = -\frac{\mu_0}{\epsilon_F}.$$

(1.111)

1.9   Finite Temperature and Quasiparticles

By definition the ground state of the system is the zero-temperature state. If the system temperature is increased, the system is automatically excited. In the limit of low temperatures, the number of allowed excited states for the Fermion system is strongly reduced by the Pauli exclusion principle. At (low) temperature T, only those single-particle states whose energy differs from the Fermi energy ϵ_F by KT (where K is Boltzmann's constant) are affected by a temperature change.

It is convenient to describe the structure of these excited states in terms of the changes of their occupation numbers as compared to those in the ground state. If we refer to the unoccupied hole states with $\epsilon < \epsilon_F$ and occupied particle states with $\epsilon > \epsilon_F$, as the quasiparticle states, it is possible to describe the statistical properties of the degenerate Fermi gas in terms of these elementary excitations. In fact, the creation of an excited state through the excitation of a given number of particles across the Fermi surface S_F, is equivalent to the creation of the same number of particles outside S_F and of holes inside S_F. The excitation energy of the Fermi gas at equilibrium at temperature T is characterized by the quantity

$$\delta n_{\mathbf{k}} = n_{\mathbf{k}}(T, \mu) - n_{\mathbf{k}}(0, \mu), \tag{1.112}$$

which measures how much the quasiparticle distribution function has been changed with respect to its value in the ground state, which is given by (1.73). The excitation of a particle with momentum $k' > k_F$ corresponds to $\delta n_{\mathbf{k}} = \delta_{\mathbf{k}, \mathbf{k}'}$, and the excitation of a hole with momentum $k' < k_F$ corresponds to $\delta n_{\mathbf{k}} = -\delta_{\mathbf{k}, \mathbf{k}'}$. Note that, since in an isolated system the number of particles is conserved, the number of excited particles must equal that of excited holes, which entails

$$\sum_{\mathbf{k}} \delta n_{\mathbf{k}} = 0. \tag{1.113}$$

For a non-interacting system, the excitation energy is given by

$$E - E_0 = \sum_{\mathbf{k}} \frac{k^2}{2m} \delta n_{\mathbf{k}}, \tag{1.114}$$

where E_0 is the ground state energy. In equation (1.112), the quasiparticle distribution function at temperature T is given by

$$n_{\mathbf{k}} = \frac{1}{1 + \exp[\beta(\epsilon_{\mathbf{k}} - \mu)]}, \tag{1.115}$$

where $\beta = 1/KT$ and μ is the chemical potential, which for a non-interacting system and in the limit of low temperature is equal to the Fermi energy. A simple calculation (see Huang 1963) yields for the excitation energy:

$$E - E_0 = \frac{\pi^2}{4\epsilon_F} N(KT)^2, \tag{1.116}$$

and for the specific heat:

$$C_v = \left(\frac{\partial E}{\partial T}\right)_N = \frac{\pi^2}{2\epsilon_F} NK^2 T. \tag{1.117}$$

The quasiparticles introduced above, are the low-energy elementary excitations for the degenerate Fermi systems. In the limit of low energy the quantum states of the degenerate Fermi liquids, which in nature are realized by liquid ^{3}He (above 4 m $^{\circ}$K), by the conduction electrons of non-superconducting metals and in nuclear

matter, may be described in terms of such elementary excitations. The theory of these states in terms of quasiparticles was established in 1956 by Landau. A detailed description of this theory is found in the book by Pines and Nozières; in the following we report only its main steps.

The basic hypothesis of the Landau theory is that the dynamic and thermodynamic properties of a Fermi liquid can be traced back to those of a gas of elementary excitations near the Fermi surface: i.e. the quasiparticles. The theory studies the effect of the deviations $\delta n(\mathbf{k}, \mathbf{r})$ of the local distribution function $n(\mathbf{k}, \mathbf{r})$, which provides the quasiparticle distribution in a unitary volume centered at $\mathbf{r}$, with respect to the equilibrium distribution $n_{\mathbf{k}}^0$, which is assumed to have the same form as that of a non-interacting Fermion gas. Therefore, the concept of Fermi surface is still valid, and in order that the idea of quasiparticle makes sense, the deviations $\delta n(\mathbf{k}, \mathbf{r})$ must be appreciably large only for values $k \simeq k_F$. Stated otherwise, the energy ω and the momentum q associated to the quasiparticles should be much smaller than the Fermi energy and momentum.

The deviations $\delta n(\mathbf{k}, \mathbf{r})$ produce changes in the quasiparticle gas energy which, to second order in $\delta n(\mathbf{k}, \mathbf{r})$, are written in the form

$$E(n(\mathbf{k}, \mathbf{r})) - E_0 = \int \delta E(\mathbf{r}) dr$$
$$\delta E(\mathbf{r}) = \sum_{\mathbf{k}} \epsilon_{\mathbf{k}} \delta n(\mathbf{k}, \mathbf{r}) + \frac{1}{2} \sum_{\mathbf{k}, \mathbf{k}'} f_{\mathbf{k}, \mathbf{k}'} \delta n(\mathbf{k}, \mathbf{r}) \delta n(\mathbf{k}', \mathbf{r}) , \tag{1.118}$$

where ϵ and f are the first and second functional derivatives of the energy with respect to the quasiparticle distribution. They have the respective meanings of the energy associated with a single quasiparticle excitation and interaction energy between quasiparticles. By means of $\epsilon_{\mathbf{k}}$ it is possible to define the group velocity of quasiparticles $\mathbf{v}_{\mathbf{k}} = \nabla_{\mathbf{k}} \epsilon_{\mathbf{k}}$ and hence their effective mass is introduced via $\mathbf{v}_{\mathbf{k}} = \mathbf{k}/m^*$.

The basic equation for the dynamics of the quasiparticles is the transport equation of the type similar to the Boltzmann equation for the deviations of the distribution function $n(\mathbf{k}, \mathbf{r}, t)$, which gives the probability of finding a quasiparticle located at $\mathbf{r}$ with momentum $\mathbf{k}$ at time t:

$$\frac{\partial}{\partial t} \delta n(\mathbf{k}, \mathbf{r}, t) + \mathbf{v}_{\mathbf{k}} \cdot \nabla_{\mathbf{r}} \delta n(\mathbf{k}, \mathbf{r}, t)$$
$$- \nabla_{\mathbf{k}} n_{\mathbf{k}}^0 \cdot \sum_{\mathbf{k}'} f_{\mathbf{k}, \mathbf{k}'} \nabla_{\mathbf{r}} \delta n(\mathbf{k}', \mathbf{r}, t) = I(\delta n)_{\text{coll}} . \tag{1.119}$$

With respect to the usual Boltzmann equation, the novel features of the Landau equation are the effective quasiparticle mass which appears in $\mathbf{v}_{\mathbf{k}} = \mathbf{k}/m^*$ and, most of all, the external force term $\nabla_{\mathbf{k}} n_{\mathbf{k}}^0 \cdot F_{\text{ext}}$ which in the case of Eq. (1.119) has the form

$$F_{\text{ext}} = \sum_{\mathbf{k}'} f_{\mathbf{k}, \mathbf{k}'} \nabla_{\mathbf{r}} \delta n(\mathbf{k}', \mathbf{r}, t) ,$$

and is not a force external to the system but rather is produced by the other quasiparticles. This term must be computed in a self-consistent way since it depends on δn. The external force in the Landau equation is characterized by the function $f_{\mathbf{k},\mathbf{k}'}$. The force acting on the quasiparticle with momentum $\mathbf{k}$, is due to all other quasiparticles with momentum $\mathbf{k}'$. It is assumed that $f_{\mathbf{k},\mathbf{k}'}$ is continuous as $\mathbf{k}$ or $\mathbf{k}'$ cross the Fermi surface. Since the whole theory is valid in the neighborhood of the Fermi surface, what is needed in practice is only the values of f on the Fermi surface, so that $f_{\mathbf{k},\mathbf{k}'}$ depends only on the directions of $\mathbf{k}$ and $\mathbf{k}'$ and on the spins of the two quasiparticles. It is convenient to introduce spin-symmetric ($f^s_{\mathbf{k},\mathbf{k}'}$) and spin-antisymmetric ($f^a_{\mathbf{k},\mathbf{k}'}$) components of the quasiparticle interaction by means of the following equations

$$f^{\uparrow\uparrow}_{\mathbf{k},\mathbf{k}'} = f^s_{\mathbf{k},\mathbf{k}'} + f^a_{\mathbf{k},\mathbf{k}'}, \quad f^{\uparrow\downarrow}_{\mathbf{k},\mathbf{k}'} = f^s_{\mathbf{k},\mathbf{k}'} - f^a_{\mathbf{k},\mathbf{k}'}. \tag{1.120}$$

Moreover, if the system is isotropic the f depend only on the angle θ between the directions $\mathbf{k}$ and $\mathbf{k}'$, and may be expanded in series of Legendre polynomials:

$$f^{s,a}_{\mathbf{k},\mathbf{k}'} = \sum_{l=0}^{\infty} f^{s,a}_l P_l(\cos\theta). \tag{1.121}$$

The coefficients $f^{s,a}_l$ fix the interaction. Finally, it is opportune to put these coefficients in terms of dimensionless coefficients:

$$\nu(0) f^{s,a}_l = F^{s,a}_l, \tag{1.122}$$

where

$$\nu(0) = \sum_{\mathbf{k}} \delta(\epsilon_{\mathbf{k}} - \epsilon_F) = \frac{V m^* k_F}{\pi^2} \tag{1.123}$$

is the quasiparticle density of states at the Fermi surface. In equation (1.119), the term $I(\delta n)_{\text{coll}}$ accounts for the changes $\delta n(\mathbf{k}, \mathbf{r}, t)$ due to quasiparticle collisions. These collisions are similar to those between molecules in the normal kinetic theory of gases. Their importance is evaluated qualitatively by the collision time τ, i.e. the time elapsed between two collisions. This depends on the nature of the particle interaction and on temperature T. At low temperature, which is the case we are interested in, collisions are quenched by the Pauli principle; there are few of them and τ is large. It can be shown that its behavior is approximately T^{-2}. Therefore, collisions play a role only in phenomena characterized by low frequency ω such that $\omega\tau \ll 1$ (e.g. viscosity, thermal conduction, etc.). This regime is referred to as the hydrodynamic or classical regime. In the opposite limit, $\omega\tau \gg 1$, the frequency is so high that the system can undergo many oscillation periods without any collision. In this case the collision term can be neglected and the system is said to be in the elastic regime. In this regime, the interaction plays a crucial role. To study these two regimes, it is possible to change the temperature and, consequently, τ.

The Landau theory has been very successful especially because it can explain a large number of physical phenomena with a very small number of parameters in the

interaction $F_l^{s,a}$. For example, for a systematic description of the dynamic properties of ^{3}He, only four parameters are needed (F_0^s and F_1^s for the spin-symmetric quantities, and F_0^a and F_1^a for the spin-antisymmetric ones). These parameters can be connected to quantities known from experiments, as we will discuss briefly in the following.

First we should remember that by integrating the distribution function $n(\mathbf{k}, \mathbf{r}, t)$ in momentum space we obtain the quasiparticle spatial density:

$$\rho(\mathbf{r}, t) = \sum_{\mathbf{k}} n(\mathbf{k}, \mathbf{r}, t) = \frac{V}{(2\pi)^3} \int n(\mathbf{k}, \mathbf{r}, t) d\mathbf{k},$$

while by integrating it in coordinate space we obtain the momentum density $n(\mathbf{k}, t) = \int n(\mathbf{k}, \mathbf{r}, t) d\mathbf{r}$. By integrating the Landau equations in momentum space we have

$$\frac{\partial}{\partial t} \rho(\mathbf{r}, t) + \nabla_{\mathbf{r}} \left[\sum_{\mathbf{k}} \left(\delta n(\mathbf{k}, \mathbf{r}, t) - \frac{\partial n_{\mathbf{k}}^0}{\partial \epsilon_{\mathbf{k}}} \sum_{\mathbf{k}'} f_{\mathbf{k}, \mathbf{k}'} \delta n(\mathbf{k}', \mathbf{r}, t) \right) \cdot \mathbf{v}_{\mathbf{k}} \right]$$

$$= \sum_{\mathbf{k}} I(\delta n(\mathbf{k}, \mathbf{r}, t))_{\text{coll}}, \tag{1.124}$$

where we have used $\nabla_{\mathbf{k}} n_{\mathbf{k}}^0 = \mathbf{v}_{\mathbf{k}} \frac{\partial n_{\mathbf{k}}^0}{\partial \epsilon_{\mathbf{k}}}$. Equation (1.124) yields the continuity equation

$$\frac{\partial}{\partial t} \rho(\mathbf{r}, t) + \nabla_{\mathbf{r}} \mathbf{J}(\mathbf{r}, t) = 0, \tag{1.125}$$

with

$$\mathbf{J}(\mathbf{r}, t) = \sum_{\mathbf{k}} \left[\delta n(\mathbf{k}, \mathbf{r}, t) - \frac{\partial n_{\mathbf{k}}^0}{\partial \epsilon_{\mathbf{k}}} \sum_{\mathbf{k}'} f_{\mathbf{k}, \mathbf{k}'} \delta n(\mathbf{k}', \mathbf{r}, t) \right] \mathbf{v}_{\mathbf{k}}$$

$$= \sum_{\mathbf{k}} \delta n(\mathbf{k}, \mathbf{r}, t) \left(\mathbf{v}_{\mathbf{k}} - \sum_{\mathbf{k}'} f_{\mathbf{k}, \mathbf{k}'} \frac{\partial n_{\mathbf{k}'}^0}{\partial \epsilon_{\mathbf{k}'}} \mathbf{v}_{\mathbf{k}'} \right), \tag{1.126}$$

and where we have used the result $\sum_{\mathbf{k}} I(\delta n(\mathbf{k}, \mathbf{r}, t))_{\text{coll}} = 0$, because the continuity equation expresses the quasiparticle number conservation and collisions can change neither the number of quasiparticles nor the current.

The current expression (1.126) shows that $\mathbf{J}(\mathbf{r}, t) \neq \sum_{\mathbf{k}} \delta n(\mathbf{k}, \mathbf{r}, t) \mathbf{v}_{\mathbf{k}}$, i.e. that the current is not determined by quasiparticle velocity, but there exist non-local dynamic contributions, due to the interaction. On the other hand, if the system is translationally invariant, the current cannot have any contribution from the interaction, but only from the kinetic energy, because it is a constant of motion which commutes with the interaction. This means that one must have

$$\mathbf{J}(\mathbf{r}, t) = \sum_{\mathbf{k}} \delta n(\mathbf{k}, \mathbf{r}, t) \frac{\mathbf{k}}{m}, \tag{1.127}$$

where m is the bare quasiparticle mass. Comparison of equations (1.126) and (1.127) implies

$$\frac{\mathbf{k}}{m} = \mathbf{v_k} - \sum_{\mathbf{k'}} f_{\mathbf{k},\mathbf{k'}} \frac{\partial n^0_{\mathbf{k'}}}{\partial \epsilon_{\mathbf{k'}}} \mathbf{v_{k'}} \,. \tag{1.128}$$

Equation (1.128) is a condition which is imposed on $f_{\mathbf{k},\mathbf{k'}}$ by translational invariance. For an isotropic system both the current and the velocity are parallel to $\mathbf{k}$; therefore, equation (1.128) involves only the spin-symmetric component with $l = 1$ in the expansion (1.121). Using the relationship

$$\frac{\partial n^0_{\mathbf{k}}}{\partial \epsilon_{\mathbf{k}}} = -\delta(\epsilon_k - \epsilon_F) \,, \tag{1.129}$$

which stems from the fact that the equilibrium quasiparticle distribution function is a step function, and from the definition of effective mass $v_{k_F} = k_F/m^*$, and (1.122) and (1.123), we can change equation (1.128) into the relation

$$\frac{m^*}{m} = 1 + \frac{F^s_1}{3} \,. \tag{1.130}$$

Since the effective mass can be evaluated by specific heat experiments, by using relation (1.117), which still holds for the gas of quasiparticles with $\epsilon_F = k_F^2/2m^*$, equation (1.130) enable for the determination of the Landau parameter F^s_1.

In order to establish a connection between F^s_0 and a measurable quantity, let us assume that the hydrodynamic regime holds, and let us look for Euler-like equations for the density variations. To this end, let us multiply the Landau equation by k_j/m, where k_j is one of the momentum components, and let us perform a summation on $\mathbf{k}$; we obtain

$$\frac{\partial}{\partial t} J_j(\mathbf{r},t) + \nabla_{r_i} \sum_{\mathbf{k}} \delta n(\mathbf{k},\mathbf{r},t) v_i \frac{k_j}{m} - \nabla_{r_i} \sum_{\mathbf{k}\mathbf{k'}} \frac{\partial n^0_{\mathbf{k}}}{\partial \epsilon_{\mathbf{k}}} f_{\mathbf{k},\mathbf{k'}} \delta n(\mathbf{k'},\mathbf{r},t) v_i \frac{k_j}{m} = 0 \,, \tag{1.131}$$

where we have used the result $\sum_{\mathbf{k}} k_j I(\delta n(\mathbf{k},\mathbf{r},t))_{\text{coll}} = 0$, which results from the current being conserved during collisions. However, the fact that the collision term does not change the quasiparticle density and their current, does not mean that it is not relevant in the hydrodynamic regimes where $\omega\tau \ll 1$. In the hydrodynamic regime the collisions are important and tend to re-establish the equilibrium distribution n^0. They tend to keep the normal displacement of the Fermi surface $u_{\mathbf{k}}$ at point $\mathbf{k}$ which, for isotropic systems, is defined by

$$\delta n(\mathbf{k},\mathbf{r},t) = \delta(\epsilon_p - \epsilon_F) v_F u_{\mathbf{k}}(\mathbf{r},t) \,, \tag{1.132}$$

at small values, setting to zero all its components associated with deformations with $l > 1$. In this limit $u \simeq a + b\cos\theta$ and it corresponds to an oscillation of the density superimposed on a uniform translation of the fluid. This is what is expected for the propagation of acoustic waves. We are in a regime of local equilibrium.

If we consider isotropic systems for which $\delta n(\mathbf{k}, \mathbf{r}, t)$ is spherical, only terms with $i = j$ survive in (1.131), and using the relationship (1.129) as well as equations (1.122) and (1.123), we easily obtain the following equation

$$\frac{\partial}{\partial t} \mathbf{J}(\mathbf{r}, t) + \frac{2}{3} \frac{\epsilon_F}{m} (1 + F_0^s) \nabla_\mathbf{r} \rho(\mathbf{r}, t) = 0 , \qquad (1.133)$$

which holds only in the hydrodynamic regime. In fact, in the conservation equation (1.131), the $l = 2$ term would survive. However we put it to zero because we have assumed that we are in the hydrodynamic regime. Equation (1.133) resembles the classical one, and together with the continuity equation (1.125) leads to the sound equation

$$\frac{\partial^2}{\partial t^2} \rho(\mathbf{r}, t) - v_1^2 \nabla^2 \rho(\mathbf{r}, t) = 0 , \qquad (1.134)$$

with v_1 the sound velocity in the quantum liquid, given by

$$v_1^2 = \frac{k_F^2}{3 m m^*} (1 + F_0^s) . \qquad (1.135)$$

Equation (1.134) describes the propagation of ordinary sound in quantum liquid and the corresponding propagation velocity (1.135) is connected to the system compressibility by (1.80).

In the case of ^{3}He, the measurements of specific heat and ordinary sound velocity at vapor pressure $(P = 0)$, provide the following values of the Landau parameters: $F_0^s = 10$ and $F_1^s = 6$. From these values it is immediately clear that ^{3}He is very different from a non-interacting Fermi gas. For example, the effective mass turns out to be three times as large as the bare mass.

The Landau parameters F_0^a and F_1^a are connected to the magnetic properties of quasiparticles. For the study of such properties, it is necessary to study the effect of the deviations $\delta n^a(\mathbf{k}, \mathbf{r}) = \delta n_\uparrow(\mathbf{k}, \mathbf{r}) - \delta n_\downarrow(\mathbf{k}, \mathbf{r})$ of the local spin-antisymmetric distribution function $n^a(\mathbf{k}, \mathbf{r}) = n_\uparrow(\mathbf{k}, \mathbf{r}) - n_\downarrow(\mathbf{k}, \mathbf{r})$, with respect to the equilibrium spin-antisymmetric distribution function $n_{\mathbf{k}\uparrow}^0 - n_{\mathbf{k}\downarrow}^0$, which is assumed to have the same form as the distribution of a non-interacting and spin-polarized Fermion gas. In this case, the integral of the distribution $n^a(\mathbf{k}, \mathbf{r}, t)$ in momentum space gives the spatial magnetization of the quasiparticles, $m(\mathbf{r}, t)$. The equations for $\delta n^a(\mathbf{k}, \mathbf{r})$ have the same form as those for $\delta n^s(\mathbf{k}, \mathbf{r}) = \delta n_\uparrow(\mathbf{k}, \mathbf{r}) + \delta n_\downarrow(\mathbf{k}, \mathbf{r})$ that we have studied above, but are characterized by the Landau parameters F_0^a and F_1^a.

The system magnetic susceptibility per particle can be expressed through F_0^a as follows

$$\frac{\chi_\sigma}{N} = -\mu_0 \frac{3m^*}{k_F^2} \frac{1}{1 + F_0^a} , \qquad (1.136)$$

which should be compared to the corresponding value for the non-interacting Fermi gas $\chi_\sigma^{FG}/N = -\mu_0(3m/k_F^2)$. The effect of interaction comes in through m^* and F_0^a. In the case of ^{3}He, F_0^a has a *very* negative value $\simeq -0.7$. Recalling that $m^* = 3m$,

we find that the magnetic susceptibility is approximately 20 times larger than in the Fermi gas. The system is quasi-ferromagnetic, in the sense that it is very easily magnetized. As for the F_1^a parameter, its value can be derived from specific heat measurements in the nonlinear temperature regime. In fact, the magnetic excited states have low energy and affect the specific heat. From such analysis we find $F_1^a = -0.55$.

The Landau theory is easily generalized to the two-dimensional case. In this case the Landau equations keep the same form as equations (1.119), and equations (1.121) and (1.123) should be replaced by

$$f_{\mathbf{k},\mathbf{k}';2D}^{s,a} = \sum_{l=0}^{\infty} f_l^{s,a} \cos l(\theta - \theta') \tag{1.137}$$

and

$$\nu^{2D}(0) = \sum_{\mathbf{k}} \delta(\epsilon_{\mathbf{k}} - \epsilon_F) = \frac{Vm^*}{\pi}. \tag{1.138}$$

It is not simple to connect the Landau parameters to measurable quantities in two dimensions, and in general the parameters themselves are derived from the physical interaction. As happened in the $3D$ case, translational invariance imposes a condition on the quasiparticle current in $2D$ which results in a relationship between the effective mass and the Landau parameter F_1^s:

$$\frac{m^*}{m} = 1 + \frac{F_1^s}{2}. \tag{1.139}$$

It is also possible to derive the sound equations, which keep the form (1.134) unchanged, but where the ordinary sound velocity is given by

$$v_{1,2D}^2 = \frac{k_F^2}{2mm^*}(1 + F_0^s). \tag{1.140}$$

Finally, it is possible to link F_0^a to the system magnetic susceptibility per particle as follows

$$\frac{\chi_{\sigma,2D}}{N} = -\mu_0 \frac{2m^*}{k_F^2} \frac{1}{1 + F_0^a}. \tag{1.141}$$

As last remark, we would like to recall that there also exist Bose quantum liquids (e.g. ^{4}He), and that recently in various laboratories Bose–Einstein condensates of alkali atoms have been realized. The elementary excitations of Bose systems are completely different from those of Fermi systems, and have phonon nature. The different nature of elementary excitations has the consequence that the specific heat of these systems, contrary to (1.117), is proportional to T^3 as $T \to 0$. In the following chapters, we will treat the phonon nature of the elementary excitations of Bose systems in detail.

References to Chapter 1

M.H. Anderson, J.R. Ensher, M.R. Matthews, C.E. Wieman and E.A. Cornell, Science **269**, 198 (1995).

K.B. Davis, M.O. Mewes, M.R. Andrews, N.J. van Druten, D.S. Durfee, D.M. Kurn and W. Ketterle, Phys. Rev. Lett. **75** 3969 (1995).

C.C. Bradley, C.A. Sackett, J.J. Tollet and R.G. Hulet, Phys. Rev. Lett. **75**, 1687 (1995).

F. Dalfovo, S. Giorgini, L.P. Pitaevskii and S. Stringari, Rev. Mod. Phys. **71**, 463 (1999).

A. Bohr and B. Mottelson, Nuclear Structure (Benjamin, New York, 1975).

K. Huang, Statistical Mechanics, Second Edition (John Wiley and Sons, New York 1987).

L.D. Landau, Sov. Phys. JEPT **3**, 920 (1956); **5**, 101 (1957).

D. Pines and P. Nozières, The Theory of Quantum Liquids (Benjamin, New York 1966).

The Hartree–Fock Theory

2.1 Introduction

When the interaction term of (1.1) is included in the theory, the many-Fermion (Boson) wave function is a combination of Slater determinants (symmetric products) that must be determined by means of variational or other more sophisticated techniques. However, even in the presence of the interaction, the ground state of the system can be forced to be a single Slater determinant (symmetric product). This is the idea at the basis of the Hartree–Fock (HF) theory which tries to describe some physical properties of the system with a wavefunction which, as in the independent-particle model (IPM), is the product of single-particle functions. The single Slater determinant (symmetric product) is chosen among all the possible ones in order to minimize the energy of the system, calculated as mean value of the Hamiltonian (1.1) (including the interaction) on the product of single-particle functions. Clearly, the only correlations included in the method are the statistical ones, deriving, for example, from Pauli exclusion principle. Dynamic correlations, which are due to interactions and are responsible for the deviation of the wave function from a product of single-particle functions and of the two-body density from the predictions of the IPM of equations (1.46)–(1.50), are not included in the theory.

One important consequence of this fact is that the HF theory is applicable only to those systems in which the interaction is well behaved and, for example, it does not diverge too fast as the interparticle distance tends to zero. This is clearly seen by calculating, for example, the average value of a two-body potential in the Fermi gas model:

$$\langle SD| \sum_{i<j}^{N} v(\mathbf{r}_{ij})|SD\rangle = \frac{1}{8}\rho N \sum_{\sigma_1 \sigma_2} \int g_{\sigma_1 \sigma_2}(\mathbf{r})v(\mathbf{r})d\mathbf{r}, \qquad (2.1)$$

where ρ is the constant density of the gas (i.e. the diagonal part of the one-body density), while $\sum_{\sigma_1 \sigma_2} g_{\sigma_1 \sigma_2}$ is given by equation (1.87), in the $3D$ case. It is observed that whether the integral in the interaction term will diverge or not will depend on

the shape of the potential $v(\mathbf{r})$ or on the dimensionality of the system under study. This is, for example, the case of the Lennard–Jones potential, which describes the interaction between two atoms and contains terms of the form $1/\mathbf{r}^{12}$, or of the nuclear interaction with a hard core, or of the Coulomb potential for one-dimensional systems.

Therefore, we see that the Hartree–Fock method can be used only with potentials having a soft behavior, which do not cause the divergence of the integrals appearing in the average value of the Hamiltonian on the product functions of equations (1.10) and (1.12).

One evolution of this method is the theory of Brueckner–Hartree–Fock, which introduces an effective potential g^{eff}, defined by

$$v|0\rangle = g^{\text{eff}}|HF\rangle\,, \tag{2.2}$$

where $|0\rangle$ is the true ground state on which the true potential (which may be divergent) operates, while g^{eff} is non-divergent and operates on a non-correlated (mean field) wavefunction. This theory will be considered in Chapter 3.

2.2   The Hartree–Fock Method for Fermions

Let us calculate the energy of the system as the mean value of the Hamiltonian with two-body interaction of (1.1) on a generic Slater determinant, using the formulae of Chapter 1:

$$
\begin{aligned}
E &= \langle SD|H|SD\rangle \\
&= \sum_{i\sigma} \int d\mathbf{r}\varphi_i^*(\mathbf{r},\sigma)\left(\frac{-\nabla^2}{2m} + v_{\text{ext}}(\mathbf{r})\right)\varphi_i(\mathbf{r},\sigma) \\
&\quad + \frac{1}{2}\sum_{ij\sigma\sigma'}\int d\mathbf{r}d\mathbf{r}'\varphi_i^*(\mathbf{r},\sigma)\varphi_j^*(\mathbf{r}',\sigma')v(\mathbf{r}-\mathbf{r}')[\varphi_i(\mathbf{r},\sigma)\varphi_j(\mathbf{r}',\sigma') \\
&\quad - \varphi_i(\mathbf{r}',\sigma')\varphi_j(\mathbf{r},\sigma)]\,,
\end{aligned}
\tag{2.3}
$$

where φ_i are the single-particle wavefunctions which appear in the Slater determinant, that we will determine by using the Hartree–Fock theory.

Let us minimize the energy (2.3) with respect to arbitrary variations of the φ_i functions. Since the φ_i must be normalized, the quantity to be minimized is

$$E - \sum_{i\sigma}\varepsilon_i\int |\varphi_i|^2 d\mathbf{r} \tag{2.4}$$

where the ε_i are N Lagrange multipliers. If we require that equation (2.4) be stationary with respect to variations of φ_i^*:

$$\delta\left(E - \sum_{i,\sigma}\varepsilon_i\int|\varphi_i(\mathbf{r},\sigma)|^2 d\mathbf{r}\right) = 0\,, \tag{2.5}$$

we obtain the Hartree–Fock equations:

$$\left(-\frac{\nabla^2}{2m} + v_{\text{ext}}(\mathbf{r})\right)\varphi_i(\mathbf{r},\sigma) + \sum_{j\sigma'}\int d\mathbf{r}'\varphi_j^*(\mathbf{r}',\sigma')v(\mathbf{r}-\mathbf{r}')$$

$$\times\,[\varphi_i(\mathbf{r},\sigma)\varphi_j(\mathbf{r}',\sigma') - \varphi_i(\mathbf{r}',\sigma')\varphi_j(\mathbf{r},\sigma)] = \varepsilon_i\varphi_i(\mathbf{r},\sigma)\,. \tag{2.6}$$

These equations can be put in a compact way using the following relationships for the one-body diagonal and non-diagonal densities respectively:

$$\rho(\mathbf{r}') = \sum_{j\sigma'}|\varphi_j(\mathbf{r}',\sigma')|^2$$

and

$$[\rho^{(1)}(\mathbf{r},\sigma,\mathbf{r}',\sigma')]^* = \sum_j\varphi_j(\mathbf{r},\sigma)\varphi_j^*(\mathbf{r}',\sigma')\,.$$

In this way we obtain

$$\left(-\frac{\nabla^2}{2m} + v_{\text{ext}}(\mathbf{r})\right)\varphi_i(\mathbf{r},\sigma) + U(\mathbf{r})\varphi_i(\mathbf{r},\sigma)$$

$$-\sum_{\sigma\|\sigma'}\int d\mathbf{r}'[\rho^{(1)}(\mathbf{r},\sigma,\mathbf{r}',\sigma')]^*v(\mathbf{r}-\mathbf{r}')\varphi_i(\mathbf{r}',\sigma') = \varepsilon_i\varphi_i(\mathbf{r},\sigma)\,, \tag{2.7}$$

where

$$U(\mathbf{r}) = \int d\mathbf{r}'\rho(\mathbf{r}')v(\mathbf{r}-\mathbf{r}')\,, \tag{2.8}$$

and $\sigma\|\sigma'$ means that the spins must be parallel, since otherwise the exchange term vanishes.

Note that the Hartree–Fock potential:

$$v^{HF}\varphi_i(\mathbf{r},\sigma) = v_{\text{ext}}(\mathbf{r})\varphi_i(\mathbf{r},\sigma) + U(\mathbf{r})\varphi_i(\mathbf{r},\sigma)$$

$$-\sum_{\sigma\|\sigma'}\int d\mathbf{r}'[\rho^{(1)}(\mathbf{r},\sigma,\mathbf{r}',\sigma')]^*v(\mathbf{r}-\mathbf{r}')\varphi_i(\mathbf{r}',\sigma') \tag{2.9}$$

is a self-consistent field which depends on the φ_i functions which are occupied by the N particles, and that the exchange term [i.e. the last term in (2.9)] is non-local. In the Hartree theory only the local (direct) term $U(\mathbf{r})$ is considered.

The HF equations form a system of N coupled integral-differential equations. The ε_i have the physical meaning of single-particle energies.

The HF equations are solved by means of a *self-consistent iterative method*, i.e. starting from N known single-particle functions $\varphi_i^{(0)}$, which are used to determine $v_{(0)}^{HF}$. Equations (2.7) are then solved and N new wavefunctions are determined, by means of which a new potential $v_{(1)}^{HF}$ is built up. Equations (2.7) are subsequently solved again, and so on, until solutions are obtained which coincide with those used to set up the potential of the previous iterations (self-consistency). The Slater determinant obtained with the solutions of the last iteration is the Hartree–Fock ground state.

Properties of the solutions

The solutions of the Hartree–Fock equations for the wavefunctions φ_i and the single-particle energies ε_i, have the following properties:

- When self-consistency is attained, equations (2.7) provide a complete set of solutions φ_i; only the N states corresponding to the lowest values of the ε_i are used to set up the Slater determinant that gives the Hartree–Fock ground state. However, the remaining states provide a natural basis to describe the $1p - 1h$, $2p - 2h, \ldots$, excited states.
- Wavefunctions φ_i corresponding to different energies are mutually orthogonal.
- The particles are non-self-interacting. The potential acting on the particle described by the state φ_i, has no contribution from such state, but only from the states corresponding to all other particles. This is due to the mutual cancellation of the direct and exchange terms in the HF potential (2.9) when $j = i$. This result follows from the anti-antisymmetrization of the wavefunction. In the Hartree theory, in which the exchange term is neglected, one has the unphysical interaction of a particle with itself.
- The mean value of the system Hamiltonian in the HF state is different from the sum of the single-particle energies ε_i corresponding to the occupied states in the HF ground state:

$$\langle HF|H|HF \rangle \neq \sum_i \varepsilon_i \,. \tag{2.10}$$

In fact, using equations (2.3) and (2.6), we obtain:

$$\langle HF|H|HF \rangle = \frac{1}{2}\left(\sum_i \varepsilon_i + \sum_i t_i + \sum_i v_i \right), \tag{2.11}$$

where

$$t_i = \sum_\sigma \int \varphi_i^*(\mathbf{r}, \sigma) \left(\frac{-\nabla^2}{2m} \right) \varphi_i(\mathbf{r}, \sigma) d\mathbf{r} \,,$$

$$v_i = \sum_\sigma \int \varphi_i^*(\mathbf{r}, \sigma) v_{\text{ext}}(\mathbf{r}) \varphi_i(\mathbf{r}, \sigma) d\mathbf{r} \,. \tag{2.12}$$

Residual interaction

Apart from a constant term, the Hartree–Fock equations define the HF Hamiltonian $H^{HF} = \sum_i H_i^{HF}$:

$$H_i^{HF} \phi_i = (\varepsilon_i + \text{const}) \phi_i \,. \tag{2.13}$$

It is easily verified that the HF ground state is an eigenstate of H^{HF} and its eigenvalue is the Hartree–Fock energy: $E^{HF} = \sum_i (\varepsilon_i + \text{const})$. However it is always possible to choose the value of the constant such as the HF energy coincides with the mean value of the two-body Hamiltonian H in the HF state:

$$E^{HF} = \langle HF|H|HF \rangle = \langle HF|H^{HF}|HF \rangle \,. \tag{2.14}$$

This means that if we write

$$H = H^{HF} + V_{\text{res}} \,, \tag{2.15}$$

then V_{res} is a residual two-body interaction whose mean value in the HF state is zero:

$$\langle HF|V_{\text{res}}|HF \rangle = 0 \,. \tag{2.16}$$

Moreover, it is possible to show that the matrix elements of the residual interaction between the HF ground state and the one-particle–one-hole excited states vanish as well:

$$\langle HF|V_{\text{res}}|i^{-1}, m \rangle = 0 \,. \tag{2.17}$$

On the other hand, the matrix elements of the residual interaction between the HF ground state and the two-particles–two-holes excited states do not vanish:

$$\langle HF|V_{\text{res}}|i^{-1}j^{-1}, mn \rangle \neq 0 \,. \tag{2.18}$$

Equation (2.17), can be rewritten as

$$\langle HF|H|i^{-1}, m \rangle = 0 \,, \tag{2.19}$$

and is a particular case of the more general condition

$$\langle HF|[H, F]|HF \rangle = 0 \,, \tag{2.20}$$

where F is any one-body operator. This condition means that $|HF\rangle$ is the Slater determinant which minimizes the system energy. In fact, if equation (2.20) did not hold, then by using the transformation $e^{\alpha[H,F]}$ on the HF state it would be possible to lower the HF energy, which is impossible by definition of the HF state.

2.2.1 *Examples of physical systems treated by the Hartree–Fock method*

Metal clusters

The Hartree–Fock method was employed initially in the field atomic and molecular physics, and provided very good results for atoms with a small number of electrons and simple molecules like diatomic ones. In recent years the method has also been used for calculations on metal clusters and quantum dots. In the following we will shortly describe the two latter systems, describing their main characteristics and showing the results of HF calculations.

Metal clusters, that we will consider here, are clusters of alkali metals which are obtained experimentally by evaporating the metal inside a container where a noble gas is also introduced, which acts as a catalyzer (Knight et al. 1985; de Heer et al. 1987). If a micro-hole (of the order of a few μm) is made in the container, the gas (which initially has given values of pressure and temperature) undergoes a supersonic expansion which produces a lowering of temperature and the formation of metallic aggregates called clusters.

The resulting beam consists of different aggregates containing different numbers of atoms; it is of interest to measure the relative abundance of clusters of a given type as a function of the number N of constituting atoms. This kind of experiments (see Fig. 2.1) provides a spectrum of abundance, showing a series of peaks corresponding to some values of N, which are a sort of magic numbers analogous to those observed, for example, in the ionization energies of the atoms and nuclear separation.

One of the most well-known results obtained by this technique is the discovery of fullerene (Kroto et al. 1985; Kratschmer et al. 1990), i.e. an allotropic state of carbon consisting of 60 atoms placed on the vertices of the icosahedral structure with 12 pentagonal and 20 hexagonal faces shown in Fig. 2.2. This structure is the one used to make soccer balls, and this is the reason for the name "soccer-like carbon cluster" commonly used in the literature to indicate fullerene.

The simplest model for these systems is the so called jellium model (Ekardt 1984; Yannouleas et al. 1989; Bertsch et al. 1991; Van Giai and Lipparini 1992; Guet and Johnson 1992; Lipparini et al. 1994; Broglia et al. 2002), and is obtained by considering the aggregate as a set of electrons (the valence electrons of the cluster atoms) which feel the electrostatic field produced by a homogeneous distribution of positive ions inside a tridimensional sphere of radius R (metal clusters) or on the surface of a sphere (fullerene). The electrons interact mutually by the repulsive
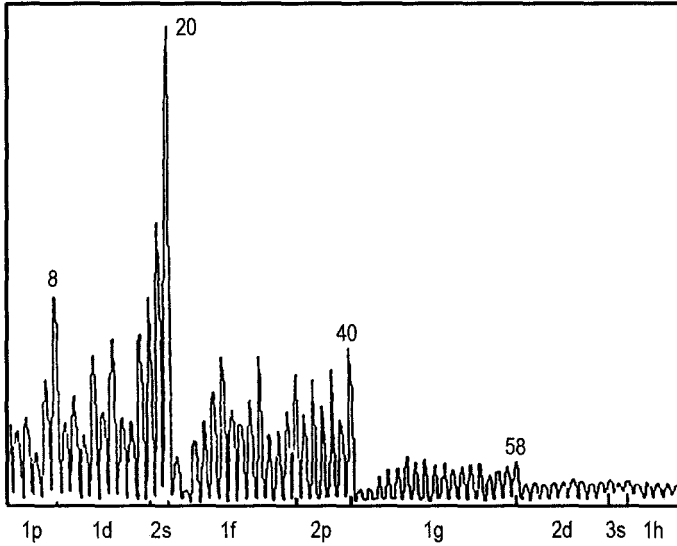
Fig. 2.1   Abundance spectrum for Na clusters.
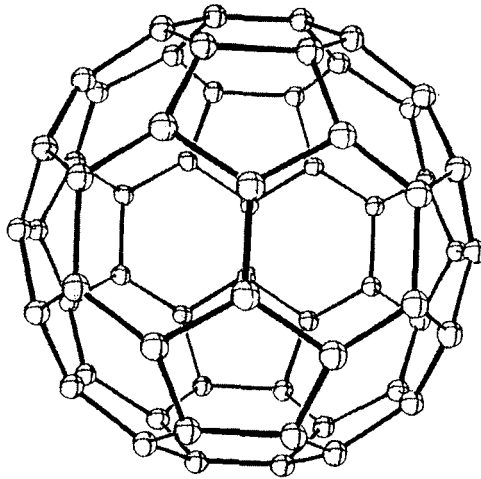
Fig. 2.2   Geometrical structure of fullerene C_{60}.

Coulomb force. This model is expected to work rather well especially for alkali metal aggregates, where the single valence electron is nearly free. In this case (which is the only one that we consider in the following) the number of valence electrons coincides with the number N of atoms in the aggregate and with the number of ions as well. The ions are considered as rigid, in the sense that they do not interact

with possible external fields.

Therefore, in the case of metal clusters the ion density can be schematized as follows

$$\rho_I(\mathbf{r}) = \rho_b \vartheta(R - \mathbf{r}) \,, \tag{2.21}$$

where ρ_b is the bulk density, i.e. the constant density of ions (which coincides with the electron density) in the homogeneous system, and ϑ is the step function. Using atomic units [where $m = e^2 = \hbar = 1$, the energy is in Hartree units H ($1H = 27.2$ eV), and length is in units of the Bohr radius a_0 ($1 \ a_0 = 0.529$ Å)], the Hamiltonian of the N electrons is given by

$$H = \sum_{i=1}^{N} \left(\frac{\mathbf{p}_i^2}{2} - \int \frac{\rho_I(\mathbf{r}')}{|\mathbf{r}_i - \mathbf{r}'|} d\mathbf{r}' \right) + \sum_{i<j}^{N} \frac{1}{|\mathbf{r}_i - \mathbf{r}_j|} \,, \tag{2.22}$$

where the confinement potential of the ions

$$V_+(\mathbf{r}) = - \int \frac{\rho_I(\mathbf{r}')}{|\mathbf{r} - \mathbf{r}'|} d\mathbf{r}' \,, \tag{2.23}$$

for the distribution (2.21) is given by

$$V_+(\mathbf{r}) = 2\pi\rho_b \begin{cases} \dfrac{1}{3}r^2 - R^2 & \text{if } r \leq R \\[2mm] -\dfrac{2R^3}{3r} & \text{if } r > R \end{cases} \,, \tag{2.24}$$

and the radius of the sphere where the ions are uniformly distributed is fixed by the relation

$$\frac{4}{3}\pi\rho_b R^3 = N_I \,, \tag{2.25}$$

with N_I being the number of ions in the cluster.

The HF equations for the Hamiltonian (2.22) become

$$\left[-\frac{\nabla^2}{2} + \int \frac{\rho(\mathbf{r}') - \rho_I(\mathbf{r}')}{|\mathbf{r} - \mathbf{r}'|} d\mathbf{r}' \right] \varphi_i(\mathbf{r}, \sigma)$$

$$- \sum_{\sigma \| \sigma'} \int d\mathbf{r}' (\rho^{(1)}(\mathbf{r}, \sigma, \mathbf{r}', \sigma'))^* \frac{1}{|\mathbf{r} - \mathbf{r}'|} \varphi_i(\mathbf{r}', \sigma') = \varepsilon_i \varphi_i(\mathbf{r}, \sigma) \,, \tag{2.26}$$

where

$$\rho(\mathbf{r}) = \sum_{i,\sigma} |\varphi_i(\mathbf{r}, \sigma)|^2 \,,$$

and

$$[\rho^{(1)}(\mathbf{r}, \sigma, \mathbf{r}', \sigma')]^* = \sum_{j} \varphi_j(\mathbf{r}, \sigma) \varphi_j^*(\mathbf{r}', \sigma') \,.$$

Note that for the homogeneous system, to which the cluster tends when $N \to \infty$, one has $\rho_e = \rho_I$, and in the HF equation only the kinetic energy and exchange terms survive. It is then clear that the bonding is due to the exchange term, which is a quantum effect. The same holds for clusters (i.e. the non-homogeneous system) because the exchange term is stronger than the sum of the ionic potential with the direct term deriving from electron–electron interaction.

In Fig. 2.3, we compare the single-particle spectra of sodium clusters formed by
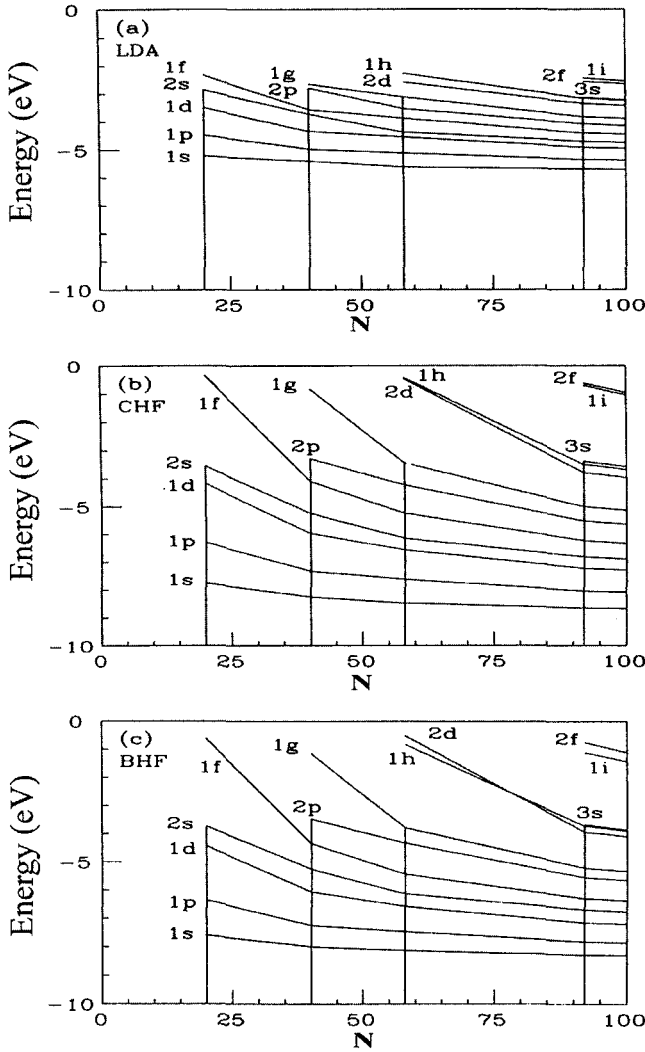
Fig. 2.3 Single-particle energies of Na clusters with 20,40,58, and 92 atoms in the spherical jellium model. Part (a) is within LDA, (b) within Coulomb HF, and (c) within BHF. The height of the vertical lines indicate the filled levels in each cluster. The (n, l) of the levels are indicated.

20, 40, 58, 92 atoms, as obtained by the Coulomb Hartree–Fock method (CHF), to those derived by more refined theories (Brueckner–Hartree–Fock (BHF), see Chapter 3) and by the density functional theory (LDA) (see Chapter 4), which take into account the dynamic interactions in an approximate way. In all kinds of calculations the confinement potential of (2.24) with $R = r_s N^{1/3}$ and the Wigner–Seitz radius $r_s = 4$ (in atomic units) is used (r_s is by definition the radius in atomic units of the sphere which encloses one electron). It can be noted that the LDA spectrum is strongly compressed with respect to the other two, and that the gap between the highest occupied level and the lowest unoccupied one is much larger in HF and BHF than is in LDA. The strong bonding of lowest-energy levels in HF and BHF derives from the fact that the Coulomb exchange term in the HF scheme depends strongly on the state. Inclusion of the correlation term in BHF causes a stronger compression of the spectrum than it does in HF, where the dynamic correlation terms are completely neglected. The difficulty that the LDA theory encounters in predicting that $N = 40$ is a magic number for sodium clusters (in agreement with the experimental abundance spectra), is absent in the HF scheme, where the $2s$–$1f$ and $2p$–$1g$ gaps are much larger than in LDA. On the other hand, as will be discussed in the following, the LDA theory is not expected to be a good theory for the single-particle spectrum, but only for the total energies and for the density of the ground state. In HF and BHF the highest-energy occupied states have energy close to the ionization potentials determined experimentally, in agreement with the Koopmans theorem, which proves their coincidence in the $N \to \infty$ case. For example, in Na$_{20}$ (sodium cluster with 20 atoms) the experimental value is 3.75 eV, which should be compared with the HF and BHF predictions of 3.54 and 3.72 eV, respectively. In Na$_{40}$ the corresponding values are 3.60 eV, 3.28 eV, and 3.47 eV, respectively. The LDA predictions are 4.03 eV in Na$_{20}$ and 3.75 eV in Na$_{40}$.

TABLE 2.1

N	HF	BHF	LDA	MC
20	-1.237	-1.846	-2.019	-1.860
40	-1.200	-1.840	-2.048	—
58	-1.241	-1.926	-2.093	—
92	-1.237	-1.931	-2.119	—
∞	-1.236	-2.035	-2.154	-2.154

In Table 2.1, we report the total energies per particle (in eV) for some sodium clusters and for the homogeneous system ($N = \infty$), as predicted by the HF calculation, together with the LDA and BHF results (Lipparini et al. 1994). In the same table are also reported the Monte Carlo (see Chapter 6) results for the homogeneous system (Ceperley 1978; Ceperley and Alder 1980), and for Na$_{20}$ (Ballone et al. 1992). The Monte Carlo results should be considered as those of best possible calculation. From the table we can see the importance of the dynamic correlations
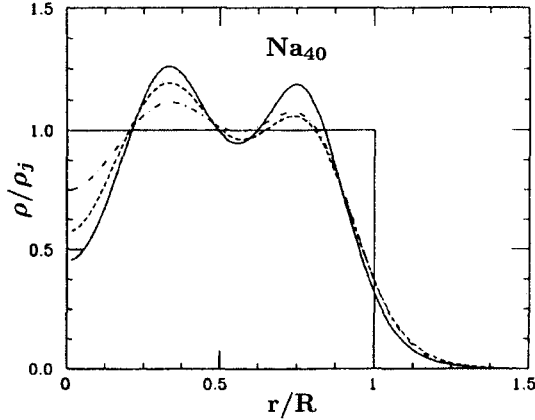
Fig. 2.4 Electronic density profiles in rm Na$_{40}$ in the three approaches. The dotted-dashed, dashed and full lines refer to the *LDA*, *HF* and *BHF* results, respectively. The square curve shows the jellium density ρ_j.

in determining the total binding energy. It can also be noted that the *HF* and *BHF* results have an oscillatory behavior, and that *BHF* tends to the bulk value more slowly than the *LDA* theory.

In Fig. 2.4, we report the electronic densities of Na$_{40}$, computed by the three different methods. The three densities are similar, but show some marked difference in the central part, reflecting the smaller amplitude of the s state wavefunction at the centre in *HF* and *BHF* with respect to *LDA*. It can be shown that the inclusion in the *HF* density of the effects due to long range correlations (*RPA*, see Chapter 9) increases the density profile at the centre, in agreement with the *LDA* approach.

As was discussed at the beginning of this subsection, the *HF* and *LDA* calculations, in the jellium approximation of equations (2.21) and (2.23) for the electron–ion interaction potential, became of common use during the 1990s. In spite of its simplicity, the jellium model provides a good description of the optical properties of some metal clusters, in particular those of sodium and potassium (see Chapter 8). However, for other clusters such as the lithium ones, this approach cannot reproduce experimental data. This fact urged some authors (Blundell and Guet 1993; Serra et al. 1993; Yabana and Bertsch 1995; Lipparini et al. 1994; Alasia et al. 1995) to modify the electron–ion potential of the jellium model so as to take into account the effects of ionic structure. This was accomplished by means of the use of pseudo-potentials, which during the atomic calculations allow an atom and its core to be replaced by a pseudo-atom with only the valence electrons. In this way, equation (2.23) is replaced by the expression $V_+(\mathbf{r}) = \int \rho_I(\mathbf{r'})v_{ps}(|\mathbf{r}-\mathbf{r'}|)d\mathbf{r'}$, where the ionic density is still given by (2.21), i.e. the atoms are still uniformly distributed on a sphere, but instead of describing the electron-ion interaction by $-|\mathbf{r}-\mathbf{r'}|^{-1}$ one uses the pseudo-potential $v_{ps}(|\mathbf{r}-\mathbf{r'}|)$. In the literature this model is commonly named

pseudo-jellium. In order to show the differences between the jellium and the pseudo-jellium results, we report in Table 2.2 the *LDA* values of the static polarizability of some metal clusters, normalized to the classical polarizability $\alpha_{cl} = R^3 = r_s^3 N_I$, in the different approximations. The *LDA* polarizability is obtained by adding to the Kohn-Sham equations (see Chapter 4) a static electric dipole constraint (see also Chapter 8).

<div align="center">

TABLE 2.2

α/α_{cl}	$PPJM$	$PHJM$	JM	Expt.
Na_{20}	1.92	1.90	1.37	1.76 ± 0.10
Na_{40}	1.75	1.73	1.33	1.71 ± 0.10
K_{20}	1.92	1.91	1.28	1.73 ± 0.20
Li_{20}	2.14	2.07	1.47	
Li_{139}^{+}	1.48	1.45	1.20	

</div>

The values $r_s = 3.25$, 3.93 and 4.86 a.u. have been used for Li, Na and K, respectively. The experimental values were taken from Knight et al. (1985). *PPJM* indicates the approximation with pseudo-potential of Bachelet et al. (1982), *PHJM* indicates the approximation with the pseudo-Hamiltonian of Bachelet et al. (1989). As can be seen from the table, the pseudo-potential and pseudo-Hamiltonian models, when compared to jellium model (*JM*), much reduce the discrepancy between experimental and *LDA* results.

Quantum dots

Recently, nanotechnologies (1 nanometre $= 10^{-9}$ metres) based on semiconductor heterostructures (for example, GaAs/Ga$_x$Al$_{1-x}$As) allowed the realization of quantum wires and dots: these are specific objects to study the physics of low-dimensionality electrons. Quantum wires and dots are realized by lateral confinement of two-dimensional electron gas (2DEG) at the boundary of the heterostructure. The procedure to construct these systems can be explained schematically as follows. The heterostructure is the union of two materials having different electronic properties. In general, the bottom of the conduction band E_C, and the top of the valence band E_V, lie at different energies in the two materials. Therefore, there is a discontinuity in both E_C and E_V at the contact surface. Electric equilibrium between the two materials is reached when the Fermi levels E_F of the two materials coincide. This equilibrium can be reached by a charge (electron) transfer, which produces a potential gap in the contact area which in turn levels the E_F's, and at the same time bends the conduction and valence bands of the semiconductor. In some cases, between the curvature and the discontinuity it is possible that in the conduction band a quantum hole is produced, in which the electric charges are
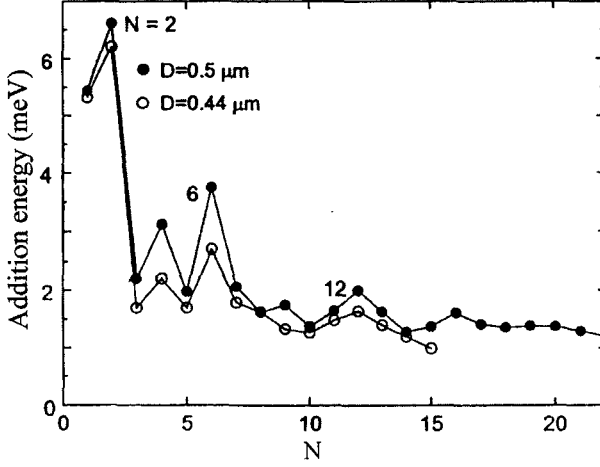
Fig. 2.5 Addition energy (Tarucha et al. 1996) as a function of the number of electrons for two dots of different size.

trapped at an energy lower than E_F. The trapped electrons are obliged to move in a very limited region and, in practice, in the contact plane between the two semi-conductors. In this way, we have a two dimensional electron gas. Using lithographic techniques, it is then possible to make structures (wires or dots) having size of the order of, or less than, a few hundred nanometres. For a recent review on quantum dots, see Reimann and Manninen (2002). At present, these techniques allow the construction of quantum dots, or artificial atoms, with the number N of electrons ranging from zero to a few hundred.

This allowed a detailed study of the correlated ground state of the quantum dot; the many-particle ground state strongly depends on the number N of electrons and obeys the Hund rules, well known in atomic physics. These characteristics are particularly evident in the experiments (see Fig. 2.5) on addition energy (Tarucha et al. 1996) necessary to put an additional electron on the quantum dot, $\Delta_N = \mu(N+1) - \mu(N)$ where $\mu(N) = E(N) - E(N-1)$ is the chemical potential of the system.

The theoretical predictions of the $E(N)$ energy are based on the study of the following Hamiltonian:

$$H = H_0 + H_{\text{int}} = \sum_{i=1}^{N} \left(\frac{p_i^2}{2m} + v_{\text{ext}}(\mathbf{r}_i) \right) + \frac{e^2}{\epsilon} \sum_{i<j}^{N} \frac{1}{|\mathbf{r}_i - \mathbf{r}_j|}, \qquad (2.27)$$

which describes the motion of N electrons confined into the $z = 0$ plane $[\mathbf{r} \equiv (r, \vartheta)]$. In equation (2.27), $m = m^* m_e$ is the effective mass of the electron inside the semiconductor, ϵ is the dielectric constant of the semiconductor, and $v_{\text{ext}}(\mathbf{r})$ is the confinement potential which in the following will be of parabolic shape:

$$v_{\text{ext}}(\mathbf{r}) = m\omega_0^2 r^2 / 2 \,.$$

Moreover, in the following we will employ effective atomic units or dot units (d.u.), defined by $\hbar = e^2/\varepsilon = m = 1$. In this system of units the length unit is Bohr radius a_0 times ε/m^*, which we will indicate by a_0^*, and the energy unit H^* is the Hartree times m^*/ε^2. For GaAs quantum dots we consider in this section, we have $\varepsilon = 12.4$, $m^* = 0.067$, $a_0^* = 97.94$ Å and $H^* \simeq 11.86$ meV.

First of all, let us check that the independent-particle model does not provide results for Δ_N which agree with experimental data. We solve the eigenvalue problem

$$H_0 \varphi_i(\mathbf{r}, \sigma) = \varepsilon_i \varphi_i(\mathbf{r}, \sigma). \qquad (2.28)$$

Since $[H, L_z] = [H_0, L_z] = 0$, we can choose common eigenfunctions for H_0 and for the z component of the angular momentum $L_z = \sum_{i=1}^{N} l_{z_i}$, where l_{z_i} is the single-particle angular momentum. Remembering that in polar coordinates $l_z = -i\frac{\partial}{\partial \vartheta}$, we find that the eigenfunctions of l_z are $e^{-il\vartheta}$ with eigenvalues $l = 0, \pm 1, \pm 2, \ldots$ and that the eigenfunctions of H_0 may be written as

$$\varphi_{n,l,m_s}(\mathbf{r}, \sigma) = R_{nl}(\mathbf{r}) e^{-il\vartheta} \chi_{m_s}(\sigma), \qquad (2.29)$$

where R_{nl} is the radial part which depends on the n and l quantum numbers.

Subsequent solution of the Schrödinger equation for R_{nl} with a confinement potential given by the two-dimensional harmonic oscillator, provides the single-particle energies:

$$\varepsilon_{nl} = (2n + 1 + |l|)\omega_0 = (N + 1)\omega_0, \qquad (2.30)$$

with $N = 0, 1, 2 \ldots$. The filling pattern of the orbitals is schematized in Table 2.3:

TABLE 2.3

$N = 2n + |l|$	n, l	Degeneracy
0	(0,0)	2
1	(0, ±1)	4
2	(1,0), (0, ±2)	6
3	(1, ±1), (0, ±3)	8
.	⋯	.

From Table 2.3, we see that the independent-particle model predicts the existence of the magic numbers: 2, 6, 12, 20, etc. (note that these are different from those of the tridimensional case, and that dimensionality plays an important role). Using $E(N) = \sum_{i=1}^{N} \varepsilon_i$, which holds in the independent-particle model, it is easily found that in such model the addition energy has peaks of height ω_0 at the magic numbers, while it vanishes for the other values of N. The agreement with experimental data of Fig. 2.5 is quite poor and all the features observed in the figure are due to interaction.

The HF equations "for the Hamiltonian (2.27), (2.28)" are written as

$$\left(\frac{-\nabla^2}{2} + \frac{\omega_0^2 r^2}{2} + \int \frac{\rho(\mathbf{r}')}{|\mathbf{r} - \mathbf{r}'|} d\mathbf{r}' \right) \varphi_i$$

$$- \sum_{\sigma \| \sigma'} \int d\mathbf{r}' (\rho^{(1)}(\mathbf{r}, \sigma, \mathbf{r}', \sigma'))^* \frac{1}{|\mathbf{r} - \mathbf{r}'|} \varphi_i(\mathbf{r}', \sigma') = \varepsilon_i \varphi_i . \qquad (2.31)$$

In what follows we discuss the results obtained on the basis of their solutions.

TABLE 2.4

N	HF	$LSDA$	MC
2	1.1420	1.0468	1.02167(7)
3	2.4048	2.2631	2.2339(3)
4	3.9033	3.6864	3.7135(5)
6	8.0359	7.6349	7.5996(8)
8	13.1887	12.7276	12.6903(7)
10	19.4243	18.7636	18.7244(5)
13	30.4648	29.5363	29.4942(7)

In Table 2.4, we report the HF energies (in H^* units and with $\omega_0 = 2.8$) for the GaAs dots with $N = 2, 3, 4, 6, 8, 10, 13$, and compare them to the $LSDA$ and Monte Carlo (MC) results (Pederiva et al. 2000).

In Fig. 2.6, we plot the correlation energy computed as difference between the MC total energy and the HF energy, as a function of the number of electrons N in the dot. The dashed line indicates the $LSDA$ results, and gives an idea about how good the local density approximation (see Chapter 4) is.

From the table we see that HF overestimates by some percent the MC energy.

In Fig. 2.7, we compare the electronic densities for $N = 20$ in HF, BHF, LDA and Diffusion Monte Carlo (DMC). The agreement between the LDA and MC curves is very good, and covers the whole r range including the boundary where the density gradients are large. It is also seen that the BHF theory definitely improves the HF results when compared to MC.

Finally, in Fig. 2.8, we plot the addition energies of the various methods. Structures and peaks are observed at the electron numbers 2, 4, 6, 9 and 12, in good agreement with the experimental results of Fig. 2.5. The spin polarizations P $= N \uparrow - N \downarrow$ are also reported:

$$P = \langle 0| \sum_i \sigma_i^z |0\rangle , \qquad (2.32)$$

which turn out to be the same for all curves in agreement with Hund's rule, according to which the total spin takes on the maximum value consistent with the fact that the electrons are all in the same shell and with Pauli's principle. For HF this is a consequence of the fact that the exchange term is attractive and different from zero only for parallel spins.
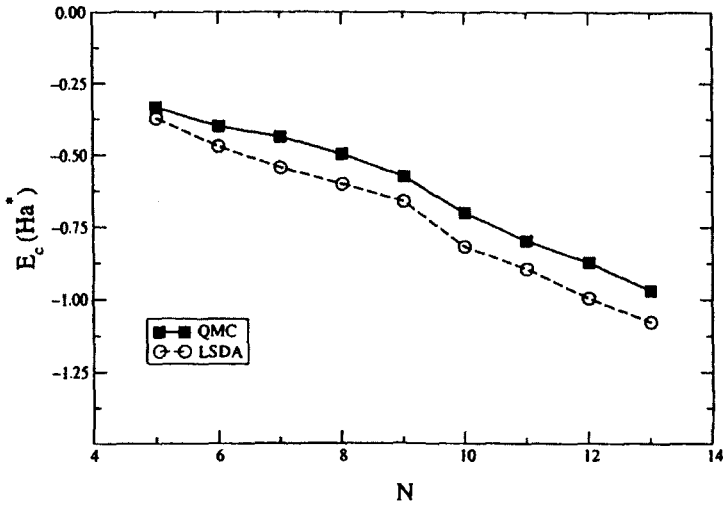
Fig. 2.6   Correlation energies E_c for a series of parabolic dots, computed by Diffusion Monte Carlo (full squares) and *LSDA* (open circles).
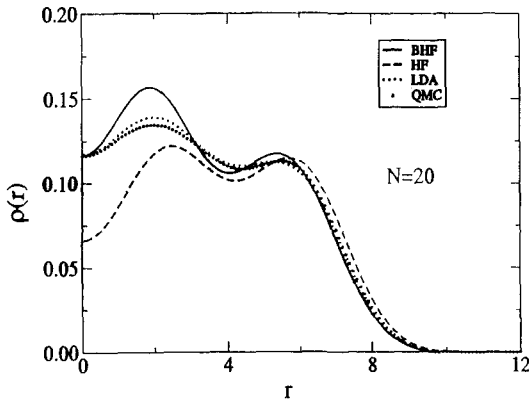
Fig. 2.7   Electronic density profiles for a dot with 20 electrons in different theories.

2.2.2   *Examples of infinite systems treated by the Hartree–Fock method*

Electron gas

The interacting-electron gas model can be used with good results to describe in three dimensions the valence electrons of an alkali metal. The electrons are considered as quasi-free electrons which move in the electrostatic field produced by the uniform distribution of the positive charge metallic ions, and which interact mutually through the Coulomb force.
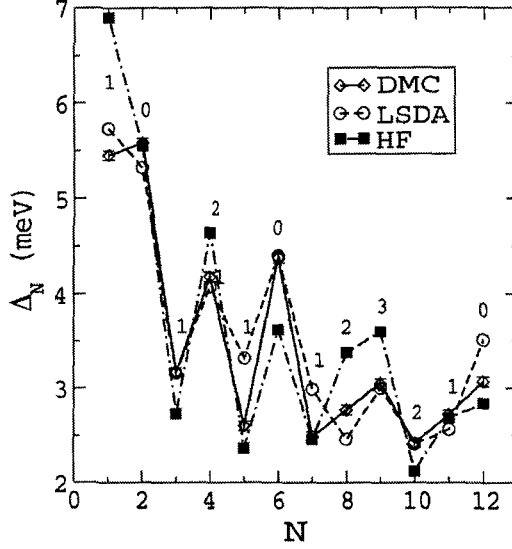
Fig. 2.8 Addition energies Δ_N as a function of the number of electrons in the dot. In the plot are reported the spin polarizations $P = N_\uparrow - N_\downarrow$, which are the same for all curves.

In two dimensions, an analogous model is used to describe the electrons which are confined on the boundary surface of a semiconductor heterostructure (quantum well).

In the case of an infinite system the HF equations become particularly simple since it is possible to exploit the translational invariance of the system, which requires $\rho_I = \rho_e = const$. The constant-density solutions of the HF equations exist and are plane waves

$$\varphi_i(\mathbf{r}, \sigma) = \frac{1}{\sqrt{L^D}} e^{i\mathbf{k}\cdot\mathbf{r}} \chi_{m_s}(\sigma)\,,$$

where D is the system dimensionality.

The electron gas is described by Hamiltonian (2.22), and the HF equations (2.26) for the homogeneous system become

$$-\frac{\nabla^2}{2}\varphi_i(\mathbf{r}, \sigma) - \frac{1}{(2\pi)^D} \int d\mathbf{r}' \int d\mathbf{k}' n_{\mathbf{k}'} \frac{e^{i\mathbf{k}'\cdot(\mathbf{r}-\mathbf{r}')}}{|\mathbf{r}-\mathbf{r}'|} \varphi_i(\mathbf{r}', \sigma) = \varepsilon_i \varphi_i(\mathbf{r}, \sigma)\,, \quad (2.33)$$

where for the one-body non-diagonal density we used the result of (1.81).

By inserting the plane wave solutions in (2.33), we get the following result for the single-particle energies:

$$\varepsilon_{\mathbf{k}} = \frac{k^2}{2} - \frac{1}{(2\pi)^D} \int d\mathbf{k}' n_{\mathbf{k}'} v(|\mathbf{k} - \mathbf{k}'|) , \qquad (2.34)$$

where $v(|\mathbf{k} - \mathbf{k}'|) = 4\pi/|\mathbf{k} - \mathbf{k}'|^2$ in $3D$, and $v(|\mathbf{k} - \mathbf{k}'|) = 2\pi/|\mathbf{k} - \mathbf{k}'|$ in $2D$.

The second term in (2.34) is the self-energy term $\Sigma_x(k)$ due to the exchange interaction, which introduces a k-dependence of ε which in turn modifies the quadratic law of the kinetic term. For example, in $3D$ we obtain

$$\Sigma_x(k) = -\frac{k_F}{\pi} \left(1 + \frac{1 - y^2}{2y} \ln \left| \frac{1 + y}{1 - y} \right| \right) , \qquad (2.35)$$

with $y = k/k_F$.

The self-energy (2.35) produces an effective mass defined by $(\varepsilon_k^0 = k^2/2)$:

$$\frac{1}{m^*} = \frac{1}{k} \frac{\partial \varepsilon_k}{\partial k} = 1 + \frac{\partial \Sigma_x(k)}{\partial \varepsilon_k^0} , \qquad (2.36)$$

which in the present case turns out to be given by

$$\frac{1}{m^*} = \frac{1}{2\pi k_F} \frac{1}{y^2} \left(\frac{1 + y^2}{2y} \ln \left| \frac{1 + y}{1 - y} \right| - 2 \right) . \qquad (2.37)$$

The effective mass in (2.37) diverges at the Fermi energy, where $y \to 1$. The cause of this logarithmic divergence is the long range nature of the Coulomb interaction, together with the HF approximation. It is a non-physical divergence, and is removed in theories which treat the Coulomb interaction at higher order than HF, like, for example, the RPA that will be discussed later on. In this regard, it should be noted that for homogeneous systems (and only for them) the HF theory coincides with the first-order perturbation theory (in the interaction). As for the Coulomb energy, the second-order perturbation correction for the ground state energy diverges, and the lowest-order non-trivial and consistent approximation for the electron gas energy is given by the RPA theory; the latter sums a series of diagrams which are individually divergent but their sum is finite.

The electron gas HF energy per particle is obtained by adding to the kinetic energy per particle of the Fermi gas the exchange energy given by

$$\frac{E_x}{N} = \frac{1}{2\rho} \int \frac{d\mathbf{k}}{(2\pi)^D} n_{\mathbf{k}} \Sigma_x(k) . \qquad (2.38)$$

From equation (2.38), we see that the self-energy $\Sigma_x(k)$ can be obtained from E_x by taking the functional derivative of E_x with respect to $n_{\mathbf{k}}$.

The electron gas exchange energy per particle in different dimensions is given by

$$\frac{E_x}{N} = -\frac{2}{\pi} \frac{D}{D^2 - 1} \frac{1}{\alpha r_s} , \qquad (2.39)$$

where the Wigner-Seitz radius r_s is connected to the density by

$$r_s = \begin{cases} (3/4\pi\rho)^{1/3} & \text{for } D = 3 \\ (1/\pi\rho)^{1/2} & \text{for } D = 2 \\ 1/2\rho & \text{for } D = 1 \end{cases}, \qquad (2.40)$$

and

$$\alpha = \begin{cases} (4/9\pi)^{1/3} & \text{for } D = 3 \\ 1/\sqrt{2} & \text{for } D = 2 \end{cases}. \qquad (2.41)$$

Note that in the $1D$ case the exchange integral is not defined, and one should introduce the width a and change the potential $1/\sqrt{(x-x')^2}$ with

$$1/\sqrt{(x-x')^2 + (y-y')^2} \simeq 1/\sqrt{(x-x')^2 + a^2}.$$

These cases are called quasi-$1D$ ($Q1D$) cases, and have applications in the quantum wires. For the potential $\sqrt{(x-x')^2 + a^2}$, one obtains

$$\frac{E_x^{Q1D}}{N} = -\frac{k_F}{2\pi} \int_{-\infty}^{+\infty} \frac{j_0^2(k_F x)}{\sqrt{x^2 + a^2}} dx, \qquad (2.42)$$

where $j_0(y) = \sin(y)/y$. A more sophisticated approximation for the $Q1D$ electron gas is obtained by the substitution

$$1/\sqrt{(x-x')^2 + (y-y')^2} \rightarrow \int_{-\infty}^{+\infty} 1/\sqrt{(x-x')^2 + (y-y')^2} |\varphi(y)|^2 |\varphi(y')|^2 dy dy'$$

of the $2D$ potential with the direct matrix element in the y-direction, between single-particle states which are the lowest-energy states of some confinement potential.

The electron gas exchange energy per particle can also be put in an analytic form for the case of a partially polarized system with polarization ξ. Using the formalism of Section 1.8.2, we obtain

$$\frac{E_x}{N}(r_s, \xi) = -\frac{2\sqrt{2}}{3\pi r_s}[(1+\xi)^{3/2} + (1-\xi)^{3/2}], \qquad (\text{in } 2D), \qquad (2.43)$$

and

$$\frac{E_x}{N}(r_s, \xi) = -\frac{3}{8\pi r_s}\left(\frac{9\pi}{4}\right)^{1/3}[(1+\xi)^{4/3} + (1-\xi)^{4/3}], \qquad (\text{in } 3D). \qquad (2.44)$$

In the $3D$ case, the HF energy per particle for the non-polarized system can be written as (in Hartree units):

$$\frac{E_{3D}^{HF}}{N} = \frac{1.105}{r_s^2} - \frac{0.458}{r_s}, \qquad (2.45)$$

where the two contributes are the kinetic and exchange ones, respectively. One may wonder about the limits of validity of such expression. To this end, let us consider the system Hamiltonian and write it in terms of the variable $\xi = \frac{r}{r_s}$:

$$H = \sum_{i=1}^{N} \left(-\frac{1}{2} \frac{\partial^2}{\partial \mathbf{r}_i^2} \right) + \sum_{i<j}^{N} \frac{1}{|\mathbf{r}_i - \mathbf{r}_j|} = \frac{1}{r_s^2} \left[\sum_{i=1}^{N} \left(\frac{-\partial^2}{2\partial \xi_i^2} \right) + r_s \sum_{i<j}^{N} \frac{1}{|\xi_i - \xi_j|} \right]. \quad (2.46)$$

For large density ($r_s \to 0$), and from equation (2.46), we see that the kinetic term dominates the potential one. Moreover, the exchange term gives the first-order correction in the potential, and from equation (2.45), it is intuitive that in this limit the ground state energy is a power series of the variable r_s. Although it is in general very unreliable to extrapolate from only two terms, this is just what happens in this case: for small r_s the energy actually is a series in r_s. This result was obtained by Gell-Mann and Brueckner (1957), and is known as the result of the *RPA* theory:

$$\frac{E_{3D}^{RPA}}{N} = \frac{1.105}{r_s^2} - \frac{0.458}{r_s} - 0.047 + 0.0311 \ln(r_s) + \cdots \quad (2.47)$$

If we define the correlation energy as the difference between the ground state energy as provided by a given theory, and the *HF* energy: $E_c/N = E/N - E_{HF}/N$, we have that the *RPA* correlation energy is given by

$$E_c^{RPA}(3D) = -0.047 + 0.0311 \ln(r_s) + O(r_s).$$

For small density ($r_s \to \infty$), the kinetic term is negligible with respect to the potential one, and the system tends to find a configuration such as to minimize the repulsive Coulomb interaction. Wigner first showed that the most effective way to minimize this energy is to localize the electrons on the sites of a lattice. This phenomenon, which is called Wigner crystallization, shows that the lowest-energy solution may loose the initial (translational) symmetry of the Hamiltonian (see Section 4.11). For a cubic lattice Wigner found that in the $r_s \to \infty$ limit the potential energy of the lattice is given by $-0.9/r_s$. This is the total Coulomb energy, i.e. including exchange and correlation. If we subtract from this the exchange energy $E_x = -0.46/r_s$ we find a correlation energy given by $E_c^{WIG}(3D) = -0.44/r_s$.

Metals have values of r_s in the range 2–6. It is then clear that the two limiting cases cannot be applied to physical systems. Therefore, Wigner produced a *formula for the correlation energy* that extrapolates between the high-density and low-density limits:

$$\frac{E_c(3D)}{N} = -\frac{0.44}{r_s + 7.8}, \quad (2.48)$$

which was largely employed in past years. Nowadays, interpolations obtained from Monte Carlo results (see Section 4.5) are normally used.

For the two-dimensional electron gas the energies which correspond to equations (2.45) and (2.47) are (see for example Isihara 1989):

$$\frac{E_{2D}^{HF}}{N} = \frac{0.5}{r_s^2} - \frac{0.6}{r_s}, \tag{2.49}$$

$$\frac{E_{2D}^{RPA}}{N} = \frac{0.5}{r_s^2} - \frac{0.6}{r_s} - 0.192 - 0.086 r_s \ln(r_s) + \cdots . \tag{2.50}$$

From these we see that the kinetic energy of the system in two dimensions is about $1/2$ of the $3D$ case at the same r_s, while the exchange energy in $2D$ is slightly larger than in $3D$, and the correlation energy in the RPA is much larger. The RPA correlations are stronger in $2D$ than in $3D$.

2.3   The Hartree–Fock Method for Bosons

In the case of a system of N Bosons with Hamiltonian

$$H = \sum_{i=1}^{N} \left(\frac{p^2}{2m} + v_{\text{ext}} \right)_i + \sum_{i<j}^{N} v(\mathbf{r}_i, \mathbf{r}_j) ,$$

the Hartree–Fock equations are obtained starting from the energy, obtained as the mean value of H on the following symmetrized product of single-particle wavefunctions:

$$\phi(\mathbf{r}_1 \mathbf{r}_2, \ldots \mathbf{r}_N) = \varphi(\mathbf{r}_1) \varphi(\mathbf{r}_2) \cdots \varphi(\mathbf{r}_N) , \tag{2.51}$$

where the φ are all equal. Using the formulae of Chapter 1, we find

$$\langle \phi | H | \phi \rangle = N \int \varphi^*(\mathbf{r}) \left(-\frac{\nabla^2}{2m} \right) \varphi(\mathbf{r}) d\mathbf{r} + N \int |\varphi(\mathbf{r})|^2 v_{\text{ext}} d\mathbf{r}$$

$$+ \frac{N(N-1)}{2} \int \int d\mathbf{r} d\mathbf{r}' \varphi^*(\mathbf{r}) \varphi^*(\mathbf{r}') v(\mathbf{r} - \mathbf{r}') \varphi(\mathbf{r}) \varphi(\mathbf{r}') . \tag{2.52}$$

Note that the structure is very similar to the one for the Fermion case, but it is much simpler since the single-particle wavefunctions are all equal in the ground state; in the last term the exchange part, produced by the antisymmetrization of the Fermion wavefunction, is obviously missing.

If we apply the variational principle with the constraint that the single-particle wavefunction is normalized:

$$\delta(E - \mu N \int |\varphi(\mathbf{r})|^2 d\mathbf{r}) = 0 , \tag{2.53}$$

where μ is the only Lagrange multiplier that appears in the Boson case, and its physical meaning is that of a chemical potential, we find the Hartree–Fock equation:

$$\left\{ -\frac{\nabla^2}{2m} + v_{\text{ext}} + \frac{(N-1)}{N} \int dr' \rho(\mathbf{r}')v(\mathbf{r}-\mathbf{r}') \right\} \varphi(\mathbf{r}) = \mu\varphi(\mathbf{r}) . \qquad (2.54)$$

This equation looks like a nonlinear Schrödinger equation, where the nonlinearity is derived from the mean field term proportional to the density $\rho(\mathbf{r}) = N|\varphi(\mathbf{r})|^2$. The solution of (2.54) is obtained by iteration (with the self-consistent method). The Hartree–Fock energy is given by

$$E^H = \frac{1}{2m} \int (\nabla\sqrt{\rho(\mathbf{r})})^2 dr$$

$$+ \int v_{\text{ext}}\rho(\mathbf{r})dr + \frac{(N-1)}{2N} \int dr dr' \rho(\mathbf{r})\rho(\mathbf{r}')v(\mathbf{r}-\mathbf{r}') , \qquad (2.55)$$

where the density is the self-consistent one. The first term of (2.55) correspond to the quantum kinetic energy due to the uncertainty principle. It is usually named "quantum pressure" and vanishes for homogeneous systems.

By direct integration of (2.54), one finds

$$\mu = \int dr \varphi^*(\mathbf{r}) \left\{ -\frac{\nabla^2}{2m} + v_{\text{ext}} + \frac{N-1}{N} \int dr' \rho(\mathbf{r}')v(\mathbf{r}-\mathbf{r}') \right\} \varphi(\mathbf{r}) , \qquad (2.56)$$

that is

$$\mu = \frac{1}{N}(E_{\text{kin}} + 2E_{\text{int}} + E_{\text{ext}}) , \qquad (2.57)$$

where E_{kin} is the kinetic energy, E_{int} is the interaction energy, and E_{ext} is the energy of the external field.

2.4   The Gross–Pitaevskii Equations

The solutions of the Hartree–Fock equations for Bosons, in general, are a worse starting point for more refined theories than in the Fermion case, since they contain no correlation of any kind (not even the statistical ones due to Pauli principle which are present in the Fermion solutions). There exists, however, a case in which they provide an extremely good solution to the problem, i.e. the case of the dilute and cold atomic gas which has been recently realized with the Bose–Einstein condensation (BEC) of alkali atoms in magnetic traps. For such systems, only low-energy collisions between pairs of atoms are important. These collisions are characterized by only one parameter, the s-wave scattering length, irrespective of the details of the two-body potential. This allows the two-body interaction in the Hamiltonian to be replaced by an effective interaction given by

$$V(\mathbf{r} - \mathbf{r}') = g\delta(\mathbf{r} - \mathbf{r}') , \qquad (2.58)$$

where the coupling constant g is related to the scattering length a by

$$g = \frac{4\pi\hbar^2 a}{m}.$$ (2.59)

This replacement works well in the limit where the (diluted-gas) condition holds:

$$\rho|a|^3 \ll 1.$$

Using the potential (2.58) in the Hartree–Fock equations (2.54), and taking

$$(N-1)/N = 1,$$

we obtain the Gross–Pitaevskii equations (Gross 1961; Pitaevskii 1961) (see also Section 8.6) for the ground state:

$$\left\{ -\frac{\nabla^2}{2m} + v_{\text{ext}} + g\rho(\mathbf{r}) \right\} \varphi(\mathbf{r}) = \mu\varphi(\mathbf{r}),$$ (2.60)

which are known to provide the good theory for dilute systems (see Dalfovo et al. 1999). For example, the corrections to the mean field energy due to dynamic correlations behave as $(\rho|a|^3)^{1/2}$ and are typically of the order of 1% (see Chapter 9).

The numerical solutions of the Gross-Pitaevskii equations, obtained using equation (2.60), in the case of a harmonic-oscillator external potential with parameter ω_{ho}, and for different values of the parameter $N|a|/a_{ho}$ ($a_{ho} = (\hbar/m\omega_{ho})^{1/2}$), are plotted in Fig. 2.9 for attractive interaction among the atoms ($a < 0$) and in Fig. 2.10 for repulsive interaction ($a > 0$). The effects of interaction are manifested in the departure from Gaussian shape predicted by the model without interaction. Comparison of these solutions with the low-temperature experimental profiles, as well as with Monte Carlo calculations, gives excellent agreement.

If the forces are attractive ($a < 0$), the system density tends to increase at the trap centre in order to lower the interaction energy (see Fig. 2.9). This tendency is balanced by the kinetic term which can stabilize the system. In any case, if the central density increases too much the kinetic term cannot avoid gas collapse. For a given type of atoms, and of external potential (i.e. the trap), one expects collapse when the number of particles in the condensate overcomes a given critical value N_{cr} of the order of $a_{ho}/|a|$. Clearly, in the homogeneous system where quantum pressure due to the kinetic term is absent, the condensate is always unstable. N_{cr} can be calculated by the Gross–Pitaevskii equations and turns out to be given by $N_{cr} = 0.575 a_{ho}/|a|$, in good agreement with experimental data.

2.5 Hartree–Fock in Second Quantization Language

Given a complete set of single-particle states φ_i, in second quantization formalism the Slater determinant built with the $\varphi_1 \cdots \varphi_N$ states is written as

$$|SD\rangle = c_1^+ \cdots c_N^+ |\,\rangle,$$ (2.61)
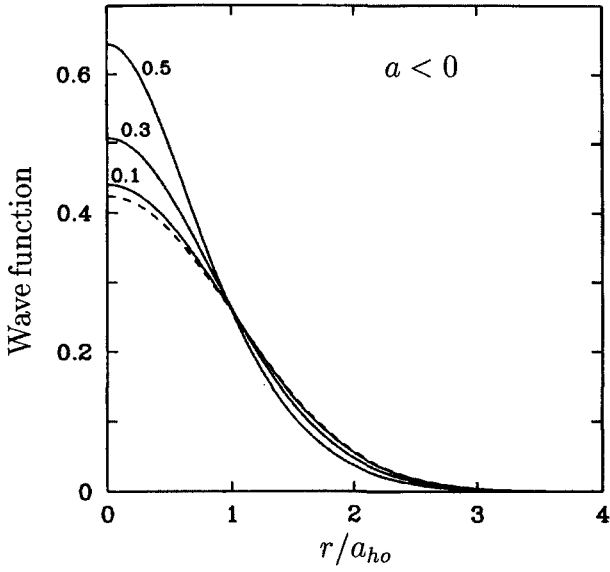
Fig. 2.9   Wavefunction of the condensate, at $T = 0$, obtained by numerical solution of the Gross–Pitaevskii equations (2.60) in a spherical harmonic-oscillator trap with negative scattering length. The three curves correspond to $N|a|/a_{ho} = 0.1, 0.3$ and 0.5. The dashed line is the ideal-gas prediction. The curves are normalized to 1.
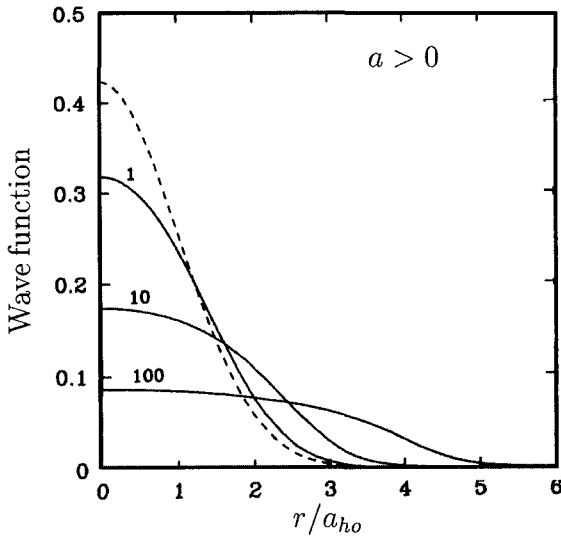
Fig. 2.10   The same as Fig. 2.9, but for repulsive interaction $(a > 0)$ and $N|a|/a_{ho} = 1$, 10 and 100.

where $|\ \rangle$ is the particle vacuum state and c_δ^+ are the creation operators in the state φ_δ. The requirement that $|SD\rangle$ is antisymmetric produces the following anticommutation relations for the c and c^+ operators:

$$\{c_\delta, c_\gamma^+\} = \delta_{\lambda,\gamma}, \qquad \{c_\delta, c_\gamma\} = 0, \qquad \{c_\delta^+, c_\gamma^+\} = 0, \qquad (2.62)$$

where c_δ, the hermitian conjugate of c_δ^+, is the annihilation operator of the particle in state δ. The operator $n_\delta = c_\delta^+ c_\delta$ has the property $n_\delta^2 = n_\delta$, and gives the occupation number of state δ, which can be either 0 or 1.

In the case of Boson systems, the function $|\Phi\rangle$, which is the product of single-particle functions φ_i, is written as

$$|\Phi\rangle = a_1^+ \cdots a_N^+ |\ \rangle, \qquad (2.63)$$

where $|\ \rangle$ is again the particle vacuum state, and a_δ^+ and a_δ are the creation and annihilation operators of a Boson in state φ_δ, analogous to c_δ^+ and c_δ^-. The requirement that $|\Phi\rangle$ is symmetric leads to commutation relations for the a and a^+ operators, instead of the anticommutation relations of the Fermion case:

$$[a_\delta, a_\gamma^+] = \delta_{\lambda,\gamma}, \qquad [a_\delta, a_\gamma] = 0, \qquad [a_\delta^+, a_\gamma^+] = 0. \qquad (2.64)$$

In second-quantization language the basic Hamiltonian for a many-Fermion system [see Eq. (1.1)] is written as

$$H = \sum_{\delta\gamma} h_{\delta\gamma} c_\delta^+ c_\gamma + \sum_{\delta\gamma\alpha\beta} \frac{1}{2} V_{\delta\gamma\alpha\beta} c_\gamma^+ c_\beta^+ c_\alpha c_\delta, \qquad (2.65)$$

where

$$h_{\delta\gamma} = \sum_\sigma \int d\mathbf{r} \varphi_\delta^*(\mathbf{r}, \sigma) \left(\frac{-\nabla^2}{2m} + v_{\text{ext}}(\mathbf{r}) \right) \varphi_\gamma(\mathbf{r}, \sigma) \qquad (2.66)$$

and

$$V_{\delta\gamma\alpha\beta} = \sum_{\sigma\sigma'} \int d\mathbf{r} d\mathbf{r}' \varphi_\gamma^*(\mathbf{r}, \sigma) \varphi_\beta^*(\mathbf{r}', \sigma') v(\mathbf{r} - \mathbf{r}') \varphi_\delta(\mathbf{r}, \sigma) \varphi_\alpha(\mathbf{r}', \sigma'). \qquad (2.67)$$

The HF ground state is determined by the following equation

$$\langle HF | [H, c_\delta^+ c_\gamma] | HF \rangle = 0, \qquad (2.68)$$

where δ and γ represent both hole and particle states. This equation is completely equivalent to the HF equations (2.6), and may be derived (see, for example, Rowe 1970) starting from the variational condition $\delta\langle SD | H | SD \rangle = 0$, by using the Thouless theorem (Thouless 1972). This theorem states that any Slater determinant $|SD'\rangle$ which is not orthogonal to $|SD\rangle$ can be written as

$$|SD'\rangle = e^{\sum_{mi} b_{mi} c_m^+ c_i} |SD\rangle, \qquad (2.69)$$

where i and m are hole and particle states for $|SD\rangle$ but not for $|SD'\rangle$. Therefore, an arbitrary and infinitesimal variation $\delta|SD\rangle$ can be written as

$$\delta|SD\rangle = \sum_{mi} \delta b_{mi} c_m^+ c_i |SD\rangle .$$

For a homogeneous system, the natural basis set is provided by plane waves, so that the set of quantum numbers that defines the state δ is given by $(\mathbf{p}, \lambda)$, where λ is the spin component ($\uparrow$ or $\downarrow$), and the Hamiltonian takes on the form

$$H = \sum_{\mathbf{p},\lambda} \epsilon_p c_{\mathbf{p},\lambda}^+ c_{\mathbf{p},\lambda} + \sum_{\mathbf{p},\mathbf{q},\lambda} v_{\text{ext}}(\mathbf{q}) c_{\mathbf{p}+\mathbf{q},\lambda}^+ c_{\mathbf{p},\lambda}$$
$$+ \frac{1}{2} \sum_{\mathbf{p}_1,\mathbf{p}_2,\mathbf{q},\lambda,\lambda'} V(\mathbf{q}) c_{\mathbf{p}_1+\mathbf{q},\lambda}^+ c_{\mathbf{p}_2-\mathbf{q},\lambda'}^+ c_{\mathbf{p}_2,\lambda'} c_{\mathbf{p}_1,\lambda} , \qquad (2.70)$$

where $V(q)$ is the Fourier transform of the interaction and $\epsilon_p = p^2/2m$.

Equations (2.65)–(2.70) are easily generalized to the Boson case.

For the electron gas (jellium model) the Hamiltonian becomes

$$H = \sum_{\mathbf{p},\lambda} \epsilon_p c_{\mathbf{p},\lambda}^+ c_{\mathbf{p},\lambda} + \frac{1}{2} \sum_{\mathbf{p}_1,\mathbf{p}_2,\mathbf{q}\neq 0,\lambda,\lambda'} V(\mathbf{q}) c_{\mathbf{p}_1+\mathbf{q},\lambda}^+ c_{\mathbf{p}_2-\mathbf{q},\lambda'}^+ c_{\mathbf{p}_2,\lambda'} c_{\mathbf{p}_1,\lambda} , \quad (2.71)$$

where the $\mathbf{q} = 0$ is missing in the electron–electron interaction because this part of the potential is canceled by the positive charge background field. The HF energy for the electron gas is obtained by taking the mean value of Hamiltonian (2.71) in the ground state of the Fermi gas, in which all the plane-wave states with momentum smaller or equal to the Fermi momentum are occupied. The occupation number operator, defined by

$$c_{\mathbf{p},\lambda}^+ c_{\mathbf{p},\lambda} |HF\rangle = n_{\mathbf{p},\lambda} |HF\rangle , \qquad (2.72)$$

takes the form of (1.73). When the potential energy term in (2.71) acts on the ground state, it destroys a pair of particles $(\mathbf{p}_1, \lambda)$ $(\mathbf{p}_2, \lambda')$ inside the Fermi sphere. One obtains a non-vanishing result only if these particles are simultaneously created by the operators $c_{\mathbf{p}_1+\mathbf{q},\lambda}^+ c_{\mathbf{p}_2-\mathbf{q},\lambda'}^+$. This happens if $\mathbf{q} = 0$ (but this case must be excluded because in our case $\mathbf{q}$ is always different from zero (jellium model) or if $\mathbf{p}_2 - \mathbf{q} = \mathbf{p}_1$ and $\lambda' = \lambda$. Therefore, the HF energy is

$$E^{HF} = \sum_{\mathbf{p},\lambda} \epsilon_p n_{\mathbf{p},\lambda} + \frac{1}{2} \sum_{\mathbf{p}_1,\mathbf{q}\neq 0,\lambda} V(\mathbf{q}) \langle HF| c_{\mathbf{p}_1+\mathbf{q},\lambda}^+ c_{\mathbf{p}_1,\lambda}^+ c_{\mathbf{p}_1+\mathbf{q},\lambda} c_{\mathbf{p}_1,\lambda} |HF\rangle . \quad (2.73)$$

Using the anticommutation relations (2.62), one obtains the following expression in terms of the distribution function $n_{\mathbf{p},\lambda}$:

$$E^{HF} = \sum_{\mathbf{p},\lambda} \epsilon_p n_{\mathbf{p},\lambda} - \frac{1}{2} \sum_{\mathbf{p},\mathbf{q},\lambda} V(\mathbf{q}) n_{\mathbf{p}+\mathbf{q},\lambda} n_{\mathbf{p},\lambda} . \qquad (2.74)$$

The first term in (2.74) is the kinetic energy of the non-interacting Fermi gas; the second term is the exchange energy which in $3D$, for example, may be rewritten as

$$E_x = - \sum_{p_1 \leq k_F, p_2 \leq k_F} \frac{2\pi e^2}{|p_1 - p_2|^2} \,, \tag{2.75}$$

and
once integration is performed it reproduces the result of (2.39).

2.6 Hartree–Fock at Finite Temperature

At finite temperature the equilibrium state of a system of particles is a statistical mixture defined by the density matrix

$$D = \sum_n p_n |n\rangle\langle n| \,, \tag{2.76}$$

where p_n represents the occupation probability of state $|n\rangle$ at the considered temperature.

Using the density matrix, it is possible to write the expectation value of a generic observable O as

$$\langle O \rangle = \sum_n p_n \langle n|O|n \rangle = \sum_{ijn} \langle n||j\rangle\langle j|O|i\rangle\langle i||n\rangle p_n$$

$$= \sum_{ij} \langle j|O|i\rangle\langle i|D|j\rangle = Tr(DO) \,. \tag{2.77}$$

The observable that we will consider in the following is the thermodynamic grand potential

$$G = E - TS - \mu\langle N \rangle \,, \tag{2.78}$$

where μ is the chemical potential, $\langle N \rangle$ the average number of particles in the system,

$$E = \langle H \rangle = Tr(D\,H) = \sum_n p_n E_n \tag{2.79}$$

is the system mean energy, and

$$S = -K\,Tr(D \ln D) = -K \sum_n p_n \ln p_n \tag{2.80}$$

its entropy (K is Boltzmann constant). The value of μ determines the average number of particles at temperature T.

Using the above equations we can write

$$G = Tr(D[H - \mu N - \beta^{-1} \ln D]) \,, \tag{2.81}$$

where $\beta = 1/KT$. For given values of β and μ, D is determined by the functional equation

$$\frac{\delta G}{\delta D} = 0. \tag{2.82}$$

This equation has the formal solution:

$$D = Z^{-1}e^{-\beta(H-\mu N)}, \tag{2.83}$$

with

$$Z = Tr(e^{-\beta(H-\mu N)}). \tag{2.84}$$

Due to the structure of H, the operator D obtained in this way is very complex, and it is practically impossible to carry out calculation starting from this expression.

In the HF approximation, the following form is imposed *a priori* on D, in the case of Fermions (see e.g. Des Cloiseaux 1967):

$$D_{HF} = \prod_\nu [f_\nu(c_\nu^\dagger c_\nu) + (1 - f_\nu)(c_\nu c_\nu^\dagger)], \tag{2.85}$$

where c_ν and $c_\nu^\dagger$ are the annihilation and creation operators of the single particle-state $|\nu\rangle$, and f_ν its occupation probability. Using expression (2.85), the entropy is written as

$$S = -K \sum_\nu [f_\nu \ln f_\nu + (1 - f_\nu) \ln(1 - f_\nu)], \tag{2.86}$$

which is the usual expression for the entropy of free Fermions. Now the problem is that of determining the basis $|\nu\rangle$, the energies ϵ_ν (which are the parameters of the theory) and the occupation numbers f_ν, by minimizing the HF grand potential defined as

$$G_{HF} = E_{HF} - TS_{HF} - \mu\langle N\rangle, \tag{2.87}$$

with $\langle N\rangle = \sum_\nu f_\nu$, and where E_{HF} is the HF energy given by

$$E = \frac{1}{2m} \int \tau(\mathbf{r})d\mathbf{r} + \int \rho(\mathbf{r})v_{\text{ext}}(\mathbf{r})d\mathbf{r}$$
$$+ \frac{1}{2} \int [\rho(\mathbf{r})\rho(\mathbf{r}') - |\rho^{(1)}(\mathbf{r}, \mathbf{r}')|^2]v(\mathbf{r} - \mathbf{r}')d\mathbf{r}d\mathbf{r}', \tag{2.88}$$

where the densities are defined in terms of the occupation numbers f_ν and of the single-particle wavefunctions ϕ_ν as follows:

$$\rho(\mathbf{r}) = \sum_\nu f_\nu |\phi_\nu(\mathbf{r})|^2\,,$$

$$\tau(\mathbf{r}) = \sum_\nu f_\nu |\nabla\phi_\nu(\mathbf{r})|^2\,, \tag{2.89}$$

$$\rho^{(1)}(\mathbf{r},\mathbf{r}') = \sum_\nu f_\nu \phi_\nu^*(\mathbf{r})\phi_\nu(\mathbf{r}')\,.$$

By minimizing $\hat{G} = G - \sum_i \lambda_i \langle \phi_\nu | \phi_\nu \rangle$ with respect to the wavefunctions, we obtain the HF equations at finite temperature ($\hbar = 1$):

$$\left(-\frac{\nabla^2}{2m} + v_{\text{ext}} + \int \rho(\mathbf{r}')v(\mathbf{r}-\mathbf{r}')d\mathbf{r}'\right)\phi_\nu(\mathbf{r},\sigma)$$

$$-\sum_{\sigma\|\sigma'}\int d\mathbf{r}'(\rho^{(1)}(\mathbf{r},\sigma,\mathbf{r}',\sigma'))^*\phi_\nu(\mathbf{r}',\sigma')v(\mathbf{r}-\mathbf{r}')$$

$$= \frac{\lambda_\nu}{f_\nu}\phi_\nu(\mathbf{r},\sigma) \equiv \varepsilon_\nu \phi_\nu(\mathbf{r},\sigma)\,. \tag{2.90}$$

By minimizing $\hat{G}$ with respect to the f_ν and using the HF equations we obtain

$$\varepsilon_\nu + KT\ln\frac{f_\nu}{1-f_\nu} - \mu = 0\,, \tag{2.91}$$

and thus

$$f_\nu = \frac{1}{1+\exp[(\varepsilon_\nu - \mu)/KT]}\,. \tag{2.92}$$

The chemical potential is subsequently determined by the condition

$$\langle N \rangle = \sum_\nu \frac{1}{1+\exp[(\varepsilon_\nu - \mu)/KT]}\,. \tag{2.93}$$

In the case of Bosons, in the HF approximation, the following form is imposed *a priori* on D:

$$D_{HF} = \prod_\nu [f_\nu(a_\nu^\dagger a_\nu) - (1+f_\nu)(a_\nu a_\nu^\dagger)]\,, \tag{2.94}$$

which yields the expression

$$S = -K\sum_\nu [f_\nu \ln f_\nu - (1+f_\nu)\ln(1+f_\nu)]\,, \tag{2.95}$$

for the entropy. In the thermodynamic limit ($f_\nu/N = 0$ for all $\nu \neq 0$), one gets for the HF energy of the Bosons (Huse and Siggia 1982):

$$E = N_0 \langle 0|H_0|0\rangle + \sum_{\nu \neq 0} f_\nu \langle \nu|H_0|\nu\rangle + \frac{1}{2}N_0^2 \langle 00|V|00\rangle$$

$$+ 2N_0 \sum_{\nu \neq 0} f_\nu \langle 0\nu|V|0\nu\rangle + \sum_{\nu \neq 0}\sum_{\mu \neq 0} f_\nu f_\mu \langle \nu\mu|V|\nu\mu\rangle \,, \tag{2.96}$$

where $f_0 = N_0$ is the occupation number of the lowest single-particle state φ_0 and

$$\langle \nu|H_0|\mu\rangle = \int d\mathbf{r}\, \varphi_\nu^*(\mathbf{r}) \left(\frac{-\nabla^2}{2m} + v_{\mathrm{ext}}(\mathbf{r}) \right) \varphi_\mu(\mathbf{r}) \,,$$

$$\langle \nu\mu|V|\alpha\lambda\rangle = \int d\mathbf{r}d\mathbf{r}'\, \varphi_\nu^*(\mathbf{r})\varphi_\mu^*(\mathbf{r}')v(\mathbf{r}-\mathbf{r}')\varphi_\alpha(\mathbf{r})\varphi_\lambda(\mathbf{r}') \,, \tag{2.97}$$

and in the following we will approximate the interparticle potential $v(\mathbf{r} - \mathbf{r}')$ as a δ-function with weight $g = 4\pi a/m$ where a is the s-wave scattering length. By minimizing $\hat{G} = G - \sum_i \lambda_i \langle \phi_\nu|\phi_\nu\rangle$ with respect to φ_0 and φ_ν with $\nu \neq 0$, we obtain the HF equations for trapped Bosons at finite temperature (Goldman et al. 1981; Huse and Siggia 1982):

$$\left(-\frac{\nabla^2}{2m} + v_{\mathrm{ext}} + 2\rho_T(\mathbf{r})g + \rho_0(\mathbf{r})g \right) \phi_0(\mathbf{r}) = \frac{\lambda_0}{N_0}\phi_0(\mathbf{r}) \equiv \varepsilon_0\phi_0(\mathbf{r}) \,,$$

$$\left(-\frac{\nabla^2}{2m} + v_{\mathrm{ext}} + 2[\rho_T(\mathbf{r}) + \rho_0(\mathbf{r})]g \right) \phi_\nu(\mathbf{r}) = \frac{\lambda_\nu}{f_\nu}\phi_\nu(\mathbf{r}) \equiv \varepsilon_\nu\phi_\nu(\mathbf{r}) \quad \nu \neq 0 \,, \tag{2.98}$$

where $\rho_T = \sum_{\nu \neq 0} |\phi_\nu(\mathbf{r})|^2$ is the density of uncondensed particles (the thermal component) and $\rho_0 = N_0|\phi_0(\mathbf{r})|^2$ is the condensate density. Note that in the form (2.98), the HF equations do not guarantee that $\langle \nu|0\rangle = 0$ for $\nu \neq 0$. For macroscopic systems this has negligible consequences for all but possibly a very few $\nu \neq 0$ single-particle states and, from a practical point of view, one can safely ignore the problem. Formally, however, one can guarantee the condition $\langle \nu|0\rangle = 0$ following the prescriptions of Huse and Siggia (1982).

By minimizing $\hat{G}$ with respect to the f_ν and using the HF equations we finally obtain

$$\varepsilon_\nu + KT \ln \frac{f_\nu}{1 + f_\nu} - \mu = 0 \,, \tag{2.99}$$

and thus

$$f_\nu = \frac{1}{\exp[(\varepsilon_\nu - \mu)/KT] - 1} \,. \tag{2.100}$$

The chemical potential is subsequently determined by the condition

$$\langle N \rangle = \sum_{\nu} \frac{1}{\exp[(\varepsilon_{\nu} - \mu)/KT] - 1} \,, \tag{2.101}$$

with $N_0 = (\exp[(\varepsilon_0 - \mu)/KT] - 1)^{-1}$.

The *HF* equations and the normalization conditions (2.93), (2.101) are to be solved in a self-consistent way by using iterative methods. The fluctuation of the particle number can be expressed in terms of the thermal occupation numbers. For example, in the case of Fermions one gets

$$(\Delta N)^2 = \langle N^2 \rangle - \langle N \rangle^2 = \sum_{\nu} f_{\nu}(1 - f_{\nu}) \,. \tag{2.102}$$

The quantity $\Delta N/N$ should be small. Otherwise, the use of the grand-canonical ensemble may be inadequate to describe a finite system (see for example Gross 1997).

As we have already discussed at the end of Chapter 1, in the homogeneous case the normal spectrum of a system of Bosons has a phononlike behavior. For such a system the *HF* description at finite temperature is then expected to be incorrect. However for confined systems, like the one recently built in magnetic traps, the *HF* description at finite temperature for Bosons works quite well, apart from the description of a very few low-energy states. This point is discussed in detail in the paper by Giorgini, Pitaevskii and Stringari (1997) and will be the object of further discussion in Chapter 8.

2.7 Hartree–Fock–Bogoliubov and *BCS*

Normal metals have a single-particle excitation spectrum which is analogous to that of a non-interacting electron gas, i.e. a continuum starting from zero. The degeneracy associated to this spectrum produces a linear temperature-dependence for the specific heat near absolute zero, and to large electric and thermal conductivities for metals. In the superconducting phase, which is observed below a critical temperature T_c, the single-particle excitation spectrum is completely different from that of normal metals. In order to create a single-particle excitation from the ground state in superconductors, one needs a minimum energy of 2Δ, known as the energy gap. This mere fact is at the origin of all superconductivity-related phenomena, like, for example, the different (nonlinear) T-dependence of the specific heat of superconductors when $T \leq T_c$. This difference between the excitation spectra is reflected in a difference between the wavefunctions of the two phases. In fact, it can be shown that while in the normal phase the probability that two single-particle states $(\mathbf{k}, \lambda)$ and $(\mathbf{k}', \lambda')$ are simultaneously occupied, is a smooth function of $\mathbf{k}$ and $\mathbf{k}'$, in the superconducting phase such probability increases by a finite amount for given pairs of states. This singular behavior of the pair correlation function actualizes London's

idea that superconductivity is due to electron condensation in momentum space. When one considers the residual interaction, which is usually neglected in describing normal states, these pair correlations which lead to superconductivity emerge clearly. The Hartree–Fock–Bogoliubov (HFB) theory is the one that introduces such correlations in the wavefunctions. The HFB theory generalizes the HF theory since it minimizes the system energy not in the space of Slater determinants, but in the space of the following states

$$|\Psi\rangle = \prod_{\nu \rangle 0}(u_\nu + v_\nu c_\nu^+ c_{\bar\nu}^+)|\rangle\,, \tag{2.103}$$

where $\bar\nu$ defines the time-reversed state, $u_\nu = u_{\bar\nu}$ and $v_\nu = -v_{\bar\nu}$; u_ν and v_ν are real and $\nu > 0$ indicates that the pair ν and $\bar\nu$ appears only once in (2.103). If u_ν and v_ν satisfy the condition

$$u_\nu^2 + v_\nu^2 = 1 \quad \forall\, \nu\,, \tag{2.104}$$

then the state $|\Psi\rangle$ is normalized to 1. Moreover, the state $|\Psi\rangle$ has the property

$$\alpha_\mu|\Psi\rangle = 0 \quad \forall\, \mu\,, \tag{2.105}$$

with

$$\alpha_\mu = u_\mu c_\mu - v_\mu c_\mu^+\,. \tag{2.106}$$

Therefore, this represents the annihilation operator of a quasiparticle which occupies state φ_μ. The operators α and α^+ obey anticommutation relations identical to those in (2.62). The usual Slater determinants are obtained from $|\Psi\rangle$ by taking $u_\nu = 0$ and $v_\nu = 1$ if ν lies below the Fermi level, and $u_\nu = 1$ and $v_\nu = 0$ if ν is above the Fermi level. In general $|\Psi\rangle$ contains pair correlations. Moreover, it can be shown that the state $|\Psi\rangle$ does not have a definite number of particles, i.e. it violates the particle-number conservation symmetry. Clearly, in order that the theory be realistic, the particle-number fluctuations should be small. In order to apply the variational principle the system Hamiltonian is written in terms of the quasiparticle operators (2.106) and their hermitian conjugates, by utilizing the inverse transformations, and the following quantity is minimized

$$\langle\Psi|H - \mu N|\Psi\rangle\,, \tag{2.107}$$

where $|\Psi\rangle$ is given by (2.103) and

$$N = \sum_{\nu > 0}(c_\nu^+ c_\nu + c_{\bar\nu}^+ c_{\bar\nu}) \tag{2.108}$$

is the particle-number operator, while the parameter μ is fixed at the end of the calculation to reproduce the correct mean value of N. The minimization procedure provides the set of HFB wavefunctions φ_ν and the weights u_ν and v_ν.

The *BCS* theory is a simplified approach to the *HFB* theory, in which the pairs, correlated by (2.103), are made up by the plane wave states $(\mathbf{k}, \uparrow)$ and $(-\mathbf{k}, \downarrow)$, having energy close to the Fermi energy, and the effective Hamiltonian is the pairing Hamiltonian

$$H = \sum_{\mathbf{k},\lambda} \frac{k^2}{2m} c^+_{\mathbf{k},\lambda} c_{\mathbf{k},\lambda} + \sum_{k,l} V_{kl} c^+_{\mathbf{k}\uparrow} c^+_{-\mathbf{k}\downarrow} c_{-l\downarrow} c_{l\uparrow} , \qquad (2.109)$$

with $V_{kl} = \langle k, -k|V|l, -l\rangle$. In order that the phenomenon of superconductivity takes place, it is necessary that the matrix element V_{kl} is mainly negative near the Fermi surface. This attraction is due to the presence of the crystal lattice and to the electron–phonon interaction which screens the repulsive electron–electron interaction, until the sign of the effective interaction is changed.

At mean-field level, the Hamiltonian (2.109) is written

$$H = \sum_{\mathbf{k},\lambda} \frac{k^2}{2m} c^+_{\mathbf{k},\lambda} c_{\mathbf{k},\lambda} + \sum_{k,l} V_{kl} X^+_{\mathbf{k}} c_{-l\downarrow} c_{l\uparrow} + \sum_{k,l} V_{kl} X_l c^+_{\mathbf{k}\uparrow} c^+_{-\mathbf{k}\downarrow} , \qquad (2.110)$$

where

$$X^+_{\mathbf{k}} = -\langle c^+_{-\mathbf{k}\downarrow} c^+_{\mathbf{k}\uparrow}\rangle = -Tr(D c^+_{-\mathbf{k}\downarrow} c^+_{\mathbf{k}\uparrow}) , \qquad (2.111)$$

and the density matrix is given by (2.83). The grand-canonical Hamiltonian $K = H - \mu N$ can be written in the form

$$K = \sum_{\mathbf{k}} (\, c^+_{\mathbf{k}\uparrow} \quad c_{-\mathbf{k}\downarrow} \,) \begin{pmatrix} \epsilon_k & \Delta_{\mathbf{k}} \\ \Delta^+_{\mathbf{k}} & -\epsilon_k \end{pmatrix} \begin{pmatrix} c_{\mathbf{k}\uparrow} \\ c^+_{-\mathbf{k}\downarrow} \end{pmatrix} , \qquad (2.112)$$

where $\epsilon_k = k^2/2m - \mu$,

$$\Delta_{\mathbf{k}} = \sum_l V_{kl} X_l , \qquad (2.113)$$

and energies are measured starting from the Fermi energy. The Hamiltonian (2.112) is a Hamiltonian for the quasiparticles meant as the ensemble of particles created outside the Fermi sphere and the holes created inside the Fermi sphere. This Hamiltonian can be put into diagonal form by applying a Bogoliubov unitary transformation

$$c_{\mathbf{k}\uparrow} = u_{\mathbf{k}} \alpha_{\mathbf{k}-} + v_{\mathbf{k}} \alpha^+_{\mathbf{k}+}, \quad c^+_{-\mathbf{k}\downarrow} = u_{\mathbf{k}} \alpha^+_{\mathbf{k}+} - v_{\mathbf{k}} \alpha_{\mathbf{k}-} , \qquad (2.114)$$

where the quasiparticle operator $\alpha_{\mathbf{k}-}$ lowers the system momentum by $\mathbf{k}$, and lowers the spin by unity [it annihilates a particle with quantum numbers $(\mathbf{k} \uparrow)$ and creates one with quantum numbers $(-\mathbf{k} \downarrow)$], while $\alpha_{\mathbf{k}+}$ increases the system momentum by $\mathbf{k}$ and increases the spin by unity. If we impose that the transformation diagonalizes

the Hamiltonian, i.e. it should result in

$$K = \sum_{\mathbf{k}\lambda} E_{\mathbf{k}\lambda} \alpha_{\mathbf{k}\lambda}^{+} \alpha_{\mathbf{k}\lambda} \,, \tag{2.115}$$

we then obtain

$$E_{\mathbf{k}\mp} = \pm\omega_{\mathbf{k}} = \pm\sqrt{\epsilon_k^2 + \Delta_{\mathbf{k}}^2} \,, \tag{2.116}$$

and

$$u_{\mathbf{k}}^2 = \frac{1}{2}\left(1 + \frac{\epsilon_k}{\sqrt{\epsilon_k^2 + \Delta_{\mathbf{k}}^2}}\right), \qquad v_{\mathbf{k}}^2 = \frac{1}{2}\left(1 - \frac{\epsilon_k}{\sqrt{\epsilon_k^2 + \Delta_{\mathbf{k}}^2}}\right). \tag{2.117}$$

From the transformations (2.114), we obtain for the system density

$$\rho = \frac{N}{V} = \frac{1}{V}\left\langle \sum_{\mathbf{k}} c_{\mathbf{k}}^{+} c_{\mathbf{k}} \right\rangle = \frac{1}{V} \sum_{\mathbf{k}} \left(\frac{u_{\mathbf{k}}^2}{e^{\beta\omega_{\mathbf{k}}}+1} + \frac{v_{\mathbf{k}}^2}{e^{-\beta\omega_{\mathbf{k}}}+1} \right)$$

$$= \frac{1}{V} \sum_{\mathbf{k}} \frac{1}{2}\left(1 - \frac{\epsilon_{\mathbf{k}}}{\omega_{\mathbf{k}}} \tanh\left(\frac{\beta\omega_{\mathbf{k}}}{2}\right) \right), \tag{2.118}$$

and using equation (2.113) as well, the self-consistent equation for the gap

$$\Delta_l = -\frac{1}{2} \sum_{\mathbf{k}} V_{kl} \frac{\Delta_{\mathbf{k}}}{\omega_{\mathbf{k}}} \tanh\left(\frac{\beta\omega_{\mathbf{k}}}{2}\right). \tag{2.119}$$

An explicit solution for equation (2.119) is obtained by approximating V_{kl} with the following potential

$$V_{kl} = \begin{cases} -g/V & \text{if } \left|\mu - \dfrac{k^2}{2m}\right| \le \Delta\epsilon \quad \text{and} \quad \left|\mu - \dfrac{l^2}{2m}\right| \le \Delta\epsilon \\ 0 & \text{otherwise} \end{cases}, \tag{2.120}$$

where g is a constant, so that V_{kl} is attractive in a layer of thickness $2\Delta\epsilon$ centered on the Fermi surface. In this case, since the right-hand side of (2.119) does not depend on l, the gap itself must be a constant depending solely on temperature:

$$\Delta_l = \begin{cases} \Delta(T) & \text{if } \left|\mu - \dfrac{l^2}{2m}\right| \le \Delta\epsilon \\ 0 & \text{otherwise} \end{cases}. \tag{2.121}$$

By changing the summation into integration and approximating $k^2 dk = k_F^2 dk$, where k_F is the Fermi momentum, we obtain

$$1 = gN(0) \int_0^{\Delta\epsilon} d\epsilon_{\mathbf{k}} \frac{\tanh(\beta\omega_{\mathbf{k}}/2)}{\omega_{\mathbf{k}}} \,, \tag{2.122}$$

where $N(0) = mk_F/(2\pi^2)$ is the quasiparticle density of the states at the Fermi surface per unit volume. At the critical temperature the gap is zero and we can write

$$1 = gN(0) \int_0^{\Delta\epsilon} d\epsilon_{\mathbf{k}} \frac{\tanh(\beta_c\epsilon_{\mathbf{k}}/2)}{\epsilon_{\mathbf{k}}} = gN(0)\ln(2\gamma\beta_c\Delta\epsilon/\pi) \,, \qquad (2.123)$$

with $\beta_c = (KT_c)^{-1}$ and $\ln\gamma = 0.5772$. Therefore, from equation (2.123), the following result is obtained

$$KT_c = 2\frac{\gamma}{\pi}\Delta\epsilon e^{-1/N(0)g} \qquad (2.124)$$

for the critical temperature of the BCS transition. From this equation we see that the critical temperature is an analytic function of the interaction intensity, so that a perturbative treatment starting from the normal phase cannot produce this result until an infinite number of graphs of a given class is summed.

Equation (2.122) can also be used to find the gap at zero temperature, where the hyperbolic tangent is equal to 1. We obtain

$$\Delta(T = 0) = 2\Delta\epsilon e^{-1/N(0)g} \,, \qquad (2.125)$$

and therefore the important result

$$\frac{\Delta(T = 0)}{KT_c} = 1.764 \,, \qquad (2.126)$$

which is valid in the limit of weak coupling $N(0)g \le 1/4$. This ratio is in reasonable agreement with the experimental results on superconductors with weak coupling, while it is too small in the case of lead and mercury where damping effects, that we have neglected, are important.

For a detailed discussion on the HFB and BCS theory one should see the books by Schrieffer (1964) and Fetter and Walecka (1971). For applications of the BCS theory to nuclear physics see the book of Rowe (1970).

References to Chapter 2

W.D. Knight, K. Clemenger, W.A. de Heer and W.A. Saunders, Phys. Rev. B **31**, 445 (1985); W.A. de Heer, W.D. Knight, M.Y. Chou and M.L. Cohen, Solid State Physics, **40**, 93 (1987).

H.W. Kroto, J.R. Heath, S.C. O'Brien, R.F. Curl and R.E. Smalley, Nature **318**, 162 (1985).

W. Kratschmer, L.D. Lamb, K. Fostiropoulos and D.R. Huffman, Nature **347**, 354 (1990).

W. Ekardt, Phys. Rev. Lett. **52**, 1925 (1984); Phys. Rev. B **32**, 1961 (1985).

C. Yannouleas, R.A. Broglia, M. Brack and P.F. Bortignon, Phys. Rev. Lett. **63**, 255 (1989).

G.F. Bertsch, A. Bulgac, D. Tomanek and Y. Wang, Phys. Rev. Lett. **67**, 2690 (1991).

N. Van Giai and E. Lipparini, Z. Phys. D **27**, 193 (1993).

C. Guet and W.R. Johnson, Phys. Rev. B **45**, 11283 (1992).

E. Lipparini, Ll. Serra and K. Takayanagi, Phys. Rev. B **49**, 16733 (1994).

R.A. Broglia, G. Colo, G. Onida and H.E. Roman, Solid State Physics of Finite Systems: Metal Clusters, Fullerenes, Atomic Wire (CUSL, Milan, 2002).

D. Ceperley, Phys. Rev. B **18**, 3126 (1978); D.M. Ceperley and B.J. Alder, Phys. Rev. Lett. **45**, 566 (1980).

P. Ballone, C.J. Umrigar and P. Delaly, Phys. Rev. B **45**, 6293 (1992).

S.E. Blundell and C. Guet, Z. Phys. D **28**, 81 (1993).

Ll. Serra, G.B. Bachelet, Nguyen Van Giai and E. Lipparini, Phys. Rev. B **48**, 14708 (1993).

K. Yabana and G.F. Bertsch, Z. Phys. D **32**, 329 (1995).

F. Alasia et al., Phys. Rev. B **52**, 8488 (1995).

W.D. Knight, K. Clemenger, W.A. de Heer and W.A. Saunders, Phys. Rev. B **31**, 445 (1985).

G.B. Bachelet, D.R. Hamann and M. Schluter, Phys. Rev. B **26**, 4199 (1982).

G.B. Bachelet, D.M. Ceperley and M.G.B. Chiocchetti, Phys. Rev. Lett. **62**, 2088 (1989).

S. Tarucha, D.G. Austing, T. Honda, R.J. van der Hage and L.P. Kouwenhoven, Phys. Rev. Lett. **77**, 3613, 1996.

S.M. Reimann and M. Manninen, Rev. Mod. Phys. **74**, 1283 (2002).

F. Pederiva, C.J. Umrigar and E. Lipparini, Phys. Rev. B **62**, 8120 (2000).

M. Gell-Mann and K.A. Brueckner, Phys. Rev. **106**, 364 (1957).

E.P. Wigner, Phys. Rev. **46**, 1002 (1934).

A. Isihara, Solid State Physics **42**, 271 (1989).

E.P. Gross, Nuovo Cimento **20**, 454 (1961).

L.P. Pitaevskii, Sov. Phys. JEPT **13**, 451 (1961).

F. Dalfovo, S. Giorgini, L.P. Pitaevskii and S. Stringari, Rev. Mod. Phys. **71**, 463 (1999).

D.J. Rowe, Nuclear Collective Motion (Methuen, London, 1970).

D.J. Thouless, The Quantum Mechanics of Many Body Systems (Academic Press 1972).

J. Des Cloiseaux, in Many-Body Physics, Les Houches 1967 (Gordon and Breach Science Publishers, New York).

V.V. Goldman, I.F. Silvera and A.J. Legget, Phys. Rev. B **24**, 2870 (1981).

D.A. Huse and E.D. Siggia, J. Low Temp. Phys. **46**, 137 (1982).

S. Giorgini, L.P. Pitaevskii and S. Stringari, J. Low Temp. Phys. **109**, 309 (1997).

D.H.E. Gross, Phys. Rep. **279**, 119 (1997).

J.R. Schrieffer, Theory of Superconductivity (Benjamin, Reading, Massachusetts, 1964).

A.L. Fetter and J.D. Walecka, Quantum Theory of Many Body Systems (McGraw Hill Book Company, 1971).

This page is intentionally left blank

The Brueckner–Hartree–Fock (BHF) Theory

3.1 Introduction

In several many-body problems, the strongly repulsive nature of the short-range interactions does not allow direct use of either mean field theories or ordinary perturbation theory. As a consequence, during the 50's and 60's the g matrix theory was developed by Brueckner. In this theory, the effective interaction of two particles in the presence of all the others is defined in a self-consistent way. This theory is particularly simple in the homogeneous system, where the single-particle states are plane waves, and we are only faced with the problem of determining g. The problem is much more complex in finite systems because the states need to be determined self-consistently together with g (double self-consistency problem).

A possible way of simplifying the problem in finite systems is to use the results of the homogeneous problem, by using the local density approximation (LDA). In LDA, one first determines the g matrix in the homogeneous system, and then uses it as an effective interaction in HF self-consistent calculations in finite systems.

Calculations of this kind have been carried out in nuclear physics, on ^{3}He and on the electron gas. In the first two systems the g matrix theory does not work as well as in the electron gas case. This is due to the fact that the g matrix takes into account only two-body interactions, and three-body and four-body interactions are important for nucleons and ^{3}He, while they are negligible in the electron case.

3.2 The Lippman–Schwinger Equation

Let us consider the elastic scattering of two particles having the same mass m. Let us separate the system Hamiltonian into a one-body term H_0, plus the two-body interaction V: $H = H_0 + V$. Let us assume that the scattering takes place at energy E (i.e. the sum of the energies of the two particles in the initial state). Let ϕ be the wavefunction of H_0 with energy E, i.e. $H_0\phi = E\phi$ where $E = \epsilon_1 + \epsilon_2$. Let ψ be the wavefunction corresponding to the same energy E, which describes the interacting system: $H\psi = E\psi$.

From the two equations:

$$(H_0 - E)\phi = 0 \,, \tag{3.1}$$

and

$$(H_0 - E)\psi = -V\psi \,, \tag{3.2}$$

by subtraction one gets

$$\psi = \phi - \frac{V}{H_0 - E}\psi \,, \tag{3.3}$$

which is an exact relationship between the correlated wavefunction ψ and the non-correlated one ϕ, in the form of an integral equation. Then we introduce the operator g such that

$$g\phi = V\psi \,. \tag{3.4}$$

From equations (3.3) and (3.4) we immediately obtain

$$g\phi = V\phi - \frac{Vg}{H_0 - E}\phi \,,$$

which, in operator form, can be rewritten as

$$g = V - \frac{V}{H_0 - E}g \,, \tag{3.5}$$

and is the Lippman–Schwinger equation. Note that, formally, we can write

$$g = \frac{V}{1 + \frac{V}{H_0 - E}} \,,$$

and from this equation it follows that g is finite even if V is divergent at short distance.

Taking equation (3.5) between the initial state, where the particles have momenta $\mathbf{k}_1, \mathbf{k}_2$, and the final one characterized by momenta $\mathbf{k}'_1, \mathbf{k}'_2$, we obtain the following integral equation:

$$\langle \mathbf{k}_1, \mathbf{k}_2 | g | \mathbf{k}'_1, \mathbf{k}'_2 \rangle = \langle \mathbf{k}_1, \mathbf{k}_2 | V | \mathbf{k}'_1, \mathbf{k}'_2 \rangle$$

$$+ \sum_{\mathbf{t}_1, \mathbf{t}_2} \langle \mathbf{k}_1, \mathbf{k}_2 | V | \mathbf{t}_1, \mathbf{t}_2 \rangle \frac{1}{E - \epsilon_{t_1} - \epsilon_{t_2}} \langle \mathbf{t}_1, \mathbf{t}_2 | g | \mathbf{k}'_1, \mathbf{k}'_2 \rangle \,, \tag{3.6}$$

where we have introduced a complete set of 2-particle intermediate states $|\mathbf{t}_1, \mathbf{t}_2\rangle$ which are eigenstates of H_0 (plane waves) with eigenvalue $\epsilon_{t_1} + \epsilon_{t_2} = \frac{t_1^2}{2m} + \frac{t_2^2}{2m}$, and the initial energy E is given by $E = \frac{k_1^2}{2m} + \frac{k_2^2}{2m}$.

The solution of (3.6) represents the summation of the ladder diagrams of Fig. 3.1, where the dashed line represents the interaction V. The first order diagram [i.e. the first term in Eq. (3.6)] represents the Born approximation to the elastic scattering
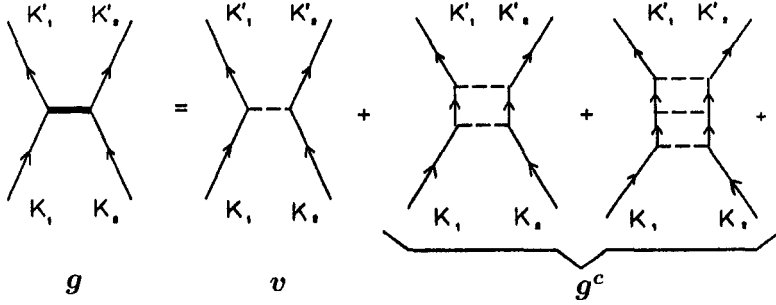
Fig. 3.1   Graphical representation of Eq. (3.6). The dashed lines represent the bare interaction.

of two particles. All other diagrams are obtained by iteration. As in the RPA (see Chapter 8), the individual diagrams may diverge, but the sum converges.

Taking into account that in the scattering the sum of momenta is conserved, the integral equation (3.6) can be rewritten so as to stress the dependence of g on three momenta, i.e. the initial momenta $\mathbf{k}_1$ and $\mathbf{k}_2$, and the transfer momentum $\mathbf{q} = \mathbf{k}'_1 - \mathbf{k}_1 = \mathbf{k}_2 - \mathbf{k}'_2$. In this way we obtain

$$g(\mathbf{k}_1, \mathbf{k}_2, \mathbf{q}) = V(\mathbf{q}) + \int \frac{d\mathbf{k}}{(2\pi)^D} \frac{V(|\mathbf{q} - \mathbf{k}|)g(\mathbf{k}_1, \mathbf{k}_2, \mathbf{k})}{\frac{k_1^2}{2m} + \frac{k_2^2}{2m} - \frac{(\mathbf{k}_1 + \mathbf{k})^2}{2m} - \frac{(\mathbf{k}_2 - \mathbf{k})^2}{2m}} \cdot \qquad (3.7)$$

This integral equation needs to be solved numerically for each $\mathbf{q}$, once $\mathbf{k}_1$ and $\mathbf{k}_2$ are fixed.

3.3   The Bethe–Goldstone Equation

The theory reported in the previous Section solves the problem of elastic scattering of two particles in vacuum. The Brueckner–Hartree–Fock theory, that is usually employed for Fermions, replaces the vacuum with a medium of particles of the same type. Due to the presence of the medium, the interaction between the two particles is modified. The way this modification is accounted for, requires that interactions other than two-body ones are negligible, and approximates the many-body medium by a non-interacting Fermi gas characterized by momenta which are all smaller than the Fermi momentum.

The role of the Fermi sea is that of limiting the summation on the intermediate states in (3.6) and (3.7), so as not to include occupied states below the Fermi surface. This idea is implemented in the Bethe–Goldstone equation for the effective interaction $g(\mathbf{k}_1, \mathbf{k}_2, \mathbf{q})$ between any two particles of momenta $\mathbf{k}_1$ and $\mathbf{k}_2$:

$$g(\mathbf{k}_1, \mathbf{k}_2, \mathbf{q}) = V(\mathbf{q}) + \int \frac{d\mathbf{k}}{(2\pi)^D} V(|\mathbf{q} - \mathbf{k}|)$$

$$\times \frac{(1 - n_{\mathbf{k}_1 + \mathbf{k}})(1 - n_{\mathbf{k}_2 - \mathbf{k}})}{\frac{k_1^2}{2m} + \frac{k_2^2}{2m} - \frac{(\mathbf{k}_1 + \mathbf{k})^2}{2m} - \frac{(\mathbf{k}_2 - \mathbf{k})^2}{2m}} g(\mathbf{k}_1, \mathbf{k}_2, \mathbf{k}), \qquad (3.8)$$

where $n_{\mathbf{k}}$ is the usual Fermi distribution function at zero temperature [see Eq. (1.73)]. The $n_{\mathbf{k}}$ introduce a dependence on the medium density in the effective interaction through the Fermi momentum.

In the Boson case there is no limitation on the intermediate states because, as known, the Pauli principle plays no role in this case. Therefore, equation (3.7) still holds. Moreover, for Bosons, in the ground state it is possible to take $\mathbf{k}_1 = \mathbf{k}_2 = 0$. Therefore, we obtain the integral equation

$$g(\mathbf{q}) = V(\mathbf{q}) - m \int \frac{d\mathbf{k}}{(2\pi)^D} V(|\mathbf{q} - \mathbf{k}|) \frac{g(\mathbf{k})}{k^2} . \tag{3.9}$$

The Bethe–Goldstone integral equation (3.8) for Fermions can be solved by standard techniques (e.g. see Suwa 2002) and yields the matrix $g(\mathbf{k}_1, \mathbf{k}_2, \mathbf{q})$. From this quantity it is possible to calculate the interaction energy in the ground state, or directly the correlation energy, by taking the expectation value of the second term on the right-hand side of (3.8) in a Slater determinant of plane waves.

For example, in the case where the interaction depends solely on the interparticle distance (V=V(r)), the correlation energy is given by (Nagano, Singwi and Ohnishi 1984):

$$E_c = 4E_d + 2E_x , \tag{3.10}$$

where E_d and E_x are the direct and exchange contributions respectively (the factors 4 and 2 result from summation on spin variables), and are given by

$$E_d = \frac{1}{2} \sum_{\mathbf{k}_1, \mathbf{k}_2, \mathbf{q}} V(\mathbf{q}) H(\mathbf{k}_1, \mathbf{k}_2, \mathbf{q}) g(\mathbf{k}_1, \mathbf{k}_2, \mathbf{q}) \tag{3.11}$$

and

$$E_x = -\frac{1}{2} \sum_{\mathbf{k}_1, \mathbf{k}_2, \mathbf{q}} V(\mathbf{k}_1 - \mathbf{k}_2 + \mathbf{q}) H(\mathbf{k}_1, \mathbf{k}_2, \mathbf{q}) g(\mathbf{k}_1, \mathbf{k}_2, \mathbf{q}) , \tag{3.12}$$

where

$$H(\mathbf{k}_1, \mathbf{k}_2, \mathbf{q}) = \frac{n_{\mathbf{k}_1}(1 - n_{\mathbf{k}_1+\mathbf{q}}) n_{\mathbf{k}_2}(1 - n_{\mathbf{k}_2-\mathbf{q}})}{\frac{k_1^2}{2m} + \frac{k_2^2}{2m} - \frac{(\mathbf{k}_1+\mathbf{q})^2}{2m} - \frac{(\mathbf{k}_2-\mathbf{q})^2}{2m}} . \tag{3.13}$$

3.4   The One-Dimensional Fermion System

As an example of the application of the *BHF* theory, in the following we will consider the case of a one-dimensional system of Fermions interacting through a potential whose Fourier transform is a constant given by $V(\mathbf{q}) = 2C$ (Nagano and Singwi 1983). In coordinate space the interaction is given by $V(x) = 2C\delta(x)$ where x is the distance between Fermions on the x axis.

Though this system is very simple and of little relevance as regards interesting physical systems such as quasi-one-dimensional conductors and quantum wires, it is very instructive to study because the exact solution for the ground state energy is known, and can be solved analytically for many models including the BHF one.

In this case the Bethe–Goldstone equation becomes

$$g(k_1, k_2) = 2C + 2C \int \frac{dk}{(2\pi)} \frac{(1 - n_{k_1+k})(1 - n_{k_2-k})}{\frac{k_1^2}{2m} + \frac{k_2^2}{2m} - \frac{(k_1+k)^2}{2m} - \frac{(k_2-k)^2}{2m}} g(k_1, k_2), \quad (3.14)$$

whose solution is

$$g(k_1, k_2) = \frac{2C}{1 - 2CA(k_1, k_2)}, \quad (3.15)$$

where

$$A(k_1, k_2) = \int \frac{dk}{(2\pi)} \frac{(1 - n_{k_1+k})(1 - n_{k_2-k})}{\frac{k_1^2}{2m} + \frac{k_2^2}{2m} - \frac{(k_1+k)^2}{2m} - \frac{(k_2-k)^2}{2m}}. \quad (3.16)$$

The integral in Eq. (3.16) is analytic and turns out to be equal to

$$A(k_1, k_2) = \begin{cases} \dfrac{m}{\pi} \dfrac{1}{k_1 - k_2} \ln \left| \dfrac{k_2 + k_F}{k_1 + k_F} \right| & \text{if } 0 \le k_1 + k_2 \le 2k_F \\[2mm] \dfrac{m}{\pi} \dfrac{1}{k_2 - k_1} \ln \left| \dfrac{k_2 - k_F}{k_1 - k_F} \right| & \text{if } -2k_F \le k_1 + k_2 < 0 \end{cases}, \quad (3.17)$$

where the Fermi momentum is connected to the linear density by $N/L = \rho = 2k_F/\pi$ (see Section 1.8).

The ground state energy per unit length E/L is the kinetic energy plus the interaction energy. Using $E_{kin}/L = 2\epsilon_0^F k_F/(3\pi)$ [see Eq. (1.76)], where ϵ_0^F is the Fermi energy, and the expectation value of (3.15) for the interaction energy, we find

$$\frac{E}{L} = \frac{2}{3} \frac{k_0^F \epsilon_0^F}{\pi} + \int_{-k_F}^{k_F} \frac{dk_1}{2\pi} \int_{-k_F}^{k_F} \frac{dk_2}{2\pi} g(k_1, k_2). \quad (3.18)$$

A simple calculation yields the energy per unitary length expressed in dimensionless units $\epsilon = E/(L\epsilon_0^F k_F)$:

$$\epsilon = \frac{2}{3\pi} + \frac{C_p}{2\pi^2} \int_{-1}^{1} dx \left(\int_{-x}^{1} dy \frac{1}{1 + C_p h(x, y)} + \int_{-1}^{-x} dy \frac{1}{1 + C_p h(-x, -y)} \right), \quad (3.19)$$

where

$$h(x, y) = -\frac{1}{\pi} \frac{1}{x - y} \ln \left(\frac{y + 1}{x + 1} \right),$$

and we have introduced the dimensionless parameter

$$C_p = \frac{C k_F}{\epsilon_F} = \frac{4mC}{\pi \rho}.$$

For $C_p \ll 1$ $(\rho \to \infty)$, equation (3.19) reduces to

$$\epsilon = \frac{2}{3\pi} + 8\frac{C_p}{\pi^2},\tag{3.20}$$

which is the result one obtains in HF.

For $C_p = \infty$ $(\rho \to 0)$, we have

$$\epsilon = \frac{2}{3\pi} + \frac{1}{2\pi} \times 5.120 = 1.03.\tag{3.21}$$

The exact result is $\epsilon = 8/(3\pi)$. Therefore, even in the extreme case of an infinite coupling constant, the BHF result does not differ from the exact one by more than 20%. For values of $C_p \leq 6$, the BHF calculation yields values which depart from the exact ones by less than 3%.

In Fig. 3.2 we show the plot of the energy ϵ as a function of the parameter C_p for the different available many-body theories and for the exact calculation. We note that the RPA and HF theories work well only for small C_p values, i.e. for small r_s.

The $STLS$ approximation, that will be described later, though better than the previous ones, is not quantitatively good for $C_p > 2$. The BHF approximation works really well with the interaction used.
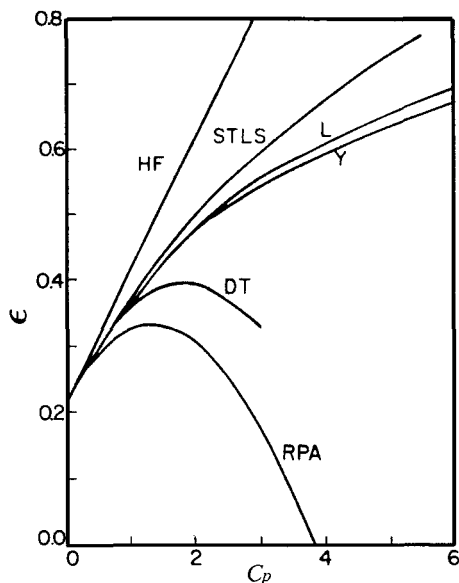

Fig. 3.2   Energy density ϵ as a function of the dimensionless parameter C_P in different theories: HF, $STLS$, $L \equiv BHF$, RPA and Y, which indicates the exact result based on the Yang integral equation (Yang 1967). DT is the dynamic theory developed by Nagano and Singwi (1983).

3.5   Numerical Results of *BHF* Calculation in Different Systems

Numerical solutions of the Bethe–Goldstone equation were obtained for nuclear matter, ^{3}He, and the two and three dimensional electron gas.

In the case of nuclear matter the first step is to take a "realistic" nucleon-nucleon interaction, for example of the type of the softcore Reid potential (Reid 1968). This is a phenomenological interaction which fits the properties of deuterium and the scattering data in the non-relativistic energy range. Subsequently, one solves numerically the integral equation for the g matrix using this interaction.

The next step is to approximate the g matrix, which in general is non-local in co-ordinate space, by a sum of local functions which depend on the Fermi momentum k_F. More precisely, the effective interaction is subdivided into a central part $V_c(r)$, a spin-orbit part $V_{LS}(r)\mathbf{L}\cdot\mathbf{S}$ and a tensor part $V_T(r)S_{12}$. Then, in each spin-isospin channel (S,T) (S and T are the spin and the isospin of the pair of nucleons, respectively) one looks for a parametrization of each part in the form

$$V(r) = \sum_i C_i(k_F)e^{-\frac{r^2}{\lambda_i^2}} , \qquad (3.22)$$

where the coefficients $C_i(k_F)$ and the ranges λ_i are fitted to obtain, for each value of the density:

- a good approximation for the diagonal matrix elements of the g matrix.
- general agreement with the non-diagonal matrix elements of the g matrix.

This program has been carried out, e.g. by Sprung and Banerjee (1971) who looked for different k_F-dependencies of the g matrix.

The energy per nucleon, E/A, obtained by the g matrix as computed directly from the Reid potential either without any parametrization or with some of its parametrizations ($G_0 - G_3$), is plotted in Fig. 3.3 as a function of k_F.

The saturation point (i.e. the minimum of the curves) is found to correspond to a density value $k_F = 1.43$ fm^{-1} which is too high with respect to the experimental one, 1.37 fm^{-1}, and to an energy value which is too small ($E/A = -11$ MeV to be compared to the experimental value of -17.04 MeV). This is due to the fact that the g matrix takes into account only the two-body contributions to the ladder diagrams. The three-body and four-body contributions to E/A are important, and when added to the previous ones make the calculated energy values agree well with the experimental value. Since it is very difficult to calculate accurately the three-body and four-body contributions to the effective interaction, what one does is simply to renormalize in an empirical way the effective interaction by slightly changing some of the Gaussian ranges in (3.22). In this way, by introducing two further parameters, it is possible to have saturation at $k_F = 1.35$ fm^{-1} and $E/A = -16.5$ MeV. Such renormalized interaction is then used for HF calculations in finite
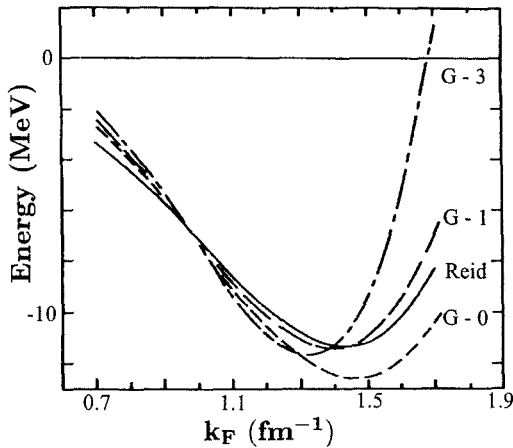
Fig. 3.3   Energy per nucleon as a function of k_F obtained in BHF using the Reid potential and some of its parametrizations $G_0 - G_3$.

nuclei using the local density approximation, in which k_F is replaced by its relation with density.

The HF calculations in finite nuclei, using the g matrix parametrizations and the local density approximation, were developed by Negele (1970) and by Campi and Sprung (1972). These calculations yield very satisfying results. In particular, the binding energies and the densities of closed-shell nuclei are very well reproduced. More recent g matrix calculations, as well as further references, may be found in Song et al. (1998).

In the case of ^{3}He and of the electron gas, the problem of the g matrix is simpler because the bare interaction is much simpler than in nuclear matter. Nonetheless, for ^{3}He the numerical solution yield unsatisfying results for the binding energy. This is due to the fact that ^{3}He is a very correlated system, in which many body interactions play a fundamental role. For example, they produce an effective mass that is more than three times greater than the bare mass of ^{3}He atoms. The effective interaction as computed using the Bethe–Goldstone equation and a two-body potential, is completely unable to reproduce such value. Therefore, in the following we will concern ourselves with the electron gas, for which the situation is much more satisfying.

In the case of the Coulomb potential, once the equation (3.8) for g is solved, one computes the correlation energy directly from equations (3.10)–(3.13). This was done by Nagano, Singwi and Ohnishi (1984), Takayanagi and Lipparini (1996) and Suwa, Takayanagi and Lipparini (2003) in $2D$, and by Lowy and Brown (1975), Bedell and Brown (1978) and Lipparini, Serra and Takayanagi (1994) in $3D$.

TABLE 3.1

r_s	ϵ_c^{MC}	ϵ_c^{L}	ϵ_c^{RPA}
1	−2.99	−2.60	−5.40
5	−1.34	−1.23	−3.10
10	−0.83	−0.76	−2.24
20	−0.48	−0.44	−1.61

The results for the $2D$ electron gas are reported in Table 3.1, together with the Monte Carlo results of Tanatar–Ceperley (Tanatar and Ceperley 1989), as well as the RPA results, for the sake of comparison. Energies are in eV. From the table we see that there is very good agreement between Monte Carlo and the ladder theory for large values of r_s. At small values of r_s long-range correlations, which are taken into account by the RPA theory, are important. As we discussed previously, and as can be seen from the table, RPA is the good theory only for $r_s \to 0$. A similar level of agreement between the ladder approximation and Monte Carlo calculations is also obtained in three dimensions.

In order to stress further the role of dynamic correlations, in Fig. 3.4 we plot the pair correlation function $g_{\uparrow\downarrow}(r)$ for antiparallel spins in $3D$, computed in the ladder approximation and compared to the RPA (see Chapter 9), for different density values. In this case statistical exchange correlations are absent, and the HF calculation yields a constant $g_{\uparrow\downarrow}(r)$ value with r equal to 1.
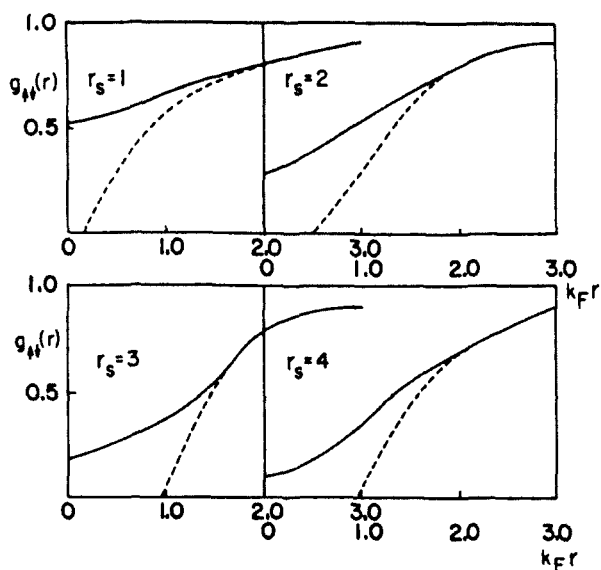

Fig. 3.4 Pair correlation function g(r) for antiparallel spins. This function represents the correlations in the absence of exchange. The full line is the result of the ladder approximation. The dashed line is the RPA result.

From this figure we can see that at short distance the correlation function is very different from the classical value, and that the RPA correlations become unphysical (i.e. negative) at short distance, faster and faster as the r_s value is increased.

3.6 The g Matrix for the $2D$ Electron Gas

In this Section we report in detail the solution of the Bethe–Goldstone equation for the g matrix, for the case of the $2D$ electron gas, and derive some approximations for g which allow to use it in a simple and practical way for both static and dynamic calculations. These approximations were used also in nuclear physics and for the $3D$ electron gas.

For the $2D$ and $3D$ electron gas, where the HF theory is well defined, it is better to solve the Bethe–Goldstone integral equation for the quantity

$$g^c = g - V\,, \tag{3.23}$$

rather than for the g matrix, where V is the Coulomb potential [i.e. the first term in Eq. (3.8)], and g^c is the correlation due to multiple-scattering processes [i.e. the second term in Eq. (3.8)]. g^c obeys the integral equation

$$g^c = V \frac{Q}{E - H_0} V + V \frac{Q}{E - H_0} g^c\,, \tag{3.24}$$

where, for simplicity, we have indicated by Q the Pauli operator that limits the intermediate states to the excited states with momentum greater than the Fermi momentum, and changes the Lippman–Schwinger equation (3.6) into the Bethe–Goldstone (3.8).

The solution of the integral equation (3.24), evaluated on a plane wave Slater determinant, gives directly the correlation energy of the electron gas.

3.6.1 *Decomposition in partial waves*

As we saw previously, the solution of the Bethe–Goldstone equation depends on three momenta: those of the initial states k_1 and k_2 and the transfer momentum q. These three momenta may be replaced by $p_1 = \frac{k_1 - k_2}{2}$, $p_2 = \frac{k_1' - k_2'}{2}$, $P = k_1 + k_2$, i.e. the relative momenta of the initial and final states and the total momentum. This means that it is possible to put the matrix elements between two-particle states of Fig. 3.1 into the following form

$$\langle k_1 k_2 | g^c | k_1' k_2' \rangle = (2\pi)^2 \delta(k_1 + k_2 - k_1' - k_2') \langle p_1 | g_P^c | p_2 \rangle\,, \tag{3.25}$$

where $p_1 = (p_1, \alpha_1)$ and $p_2 = (p_2, \alpha_2)$.

The angles α_1 and α_2 are measured starting from the fixed direction of P. Note that g_P^c can be interpreted as an effective interaction operating onto the relative wavefunction with fixed P. In what follows we describe the techniques suitable

for solving equation (3.24) and for obtaining the matrix elements $\langle \mathbf{p}_1 | g_P^c | \mathbf{p}_2 \rangle$ in (relative) momentum space, for a fixed value of $\mathbf{P}$.

The Coulomb interaction in (relative) co-ordinate space is given by

$$\langle \mathbf{r}_1 | V | \mathbf{r}_2 \rangle = \delta(\mathbf{r}_1 - \mathbf{r}_2) \frac{1}{|\mathbf{r}_1 - \mathbf{r}_2|} \exp(-\mu|\mathbf{r}_1 - \mathbf{r}_2|), \qquad (3.26)$$

where $\mathbf{r}_1$ and $\mathbf{r}_2$ are the relative coordinates of the initial and final states, respectively, and we have introduced the damping factor $\exp(-\mu|\mathbf{r}_1 - \mathbf{r}_2|)$ using the cutoff parameter $\mu(> 0)$, that will be discussed later. Using the following expansion for the plane wave, which is valid in $2D$,

$$e^{i\mathbf{p}\cdot\mathbf{r}} = \sum_{n=-\infty}^{\infty} i^n J_n(pr)e^{in(\alpha-\phi)}, \qquad (3.27)$$

where $\mathbf{p} = (p, \alpha)$ and $\mathbf{r} = (r, \phi)$, and J_n is the Bessel function, we may put the matrix element in momentum space in the form:

$$\langle \mathbf{p}_1 | V | \mathbf{p}_2 \rangle = \int d\mathbf{r}_1 d\mathbf{r}_2 e^{-i\mathbf{p}_1 \cdot \mathbf{r}_1} \langle \mathbf{r}_1 | V | \mathbf{r}_2 \rangle e^{i\mathbf{p}_2 \cdot \mathbf{r}_2}$$

$$= \sum_{n_1,n_2=-\infty}^{\infty} (-i)^{n_1} \frac{e^{in_1\alpha_1}}{\sqrt{2\pi}} \langle p_1 n_1 | V | p_2 n_2 \rangle i^{n_2} \frac{e^{-in_2\alpha_2}}{\sqrt{2\pi}}, \qquad (3.28)$$

where the partial wave components are calculated by

$$\langle p_1 n_1 | V | p_2 n_2 \rangle = \delta_{n_1 n_2} (2\pi)^2 \int r dr \, J_{n_1}(p_1 r) J_{n_1}(p_2 r) \frac{e^{-\mu r}}{r}$$

$$= \delta_{n_1 n_2} \frac{4\pi}{\sqrt{p_1 p_2}} Q_{|n_1|-\frac{1}{2}} \left(\frac{p_1^2 + p_2^2 + \mu^2}{2 p_1 p_2} \right), \qquad (3.29)$$

and Q_n is the Legendre function of the second kind. Note that the above expression becomes very large for $p_1 \sim p_2$. In fact, it would diverge for $p_1 = p_2$ in the absence of the cutoff μ.

Let us now consider the Pauli operator

$$\langle \mathbf{p}_1 | Q_P | \mathbf{p}_2 \rangle = (2\pi)^2 \delta(\mathbf{p}_1 - \mathbf{p}_2) \theta \left(\left| \frac{\mathbf{P}}{2} + \mathbf{p}_1 \right| - k_F \right) \theta \left(\left| \frac{\mathbf{P}}{2} - \mathbf{p}_1 \right| - k_F \right), \qquad (3.30)$$

which depends explicitly on the center of mass momentum $\mathbf{P}$ and on the Fermi momentum k_F, and makes the g matrix dependent on these quantities as well. The

partial wave decomposition of the Pauli operator is given by

$$\langle \mathbf{p}_1 | Q_P | \mathbf{p}_2 \rangle = (2\pi)^2 \frac{\delta(p_1 - p_2)}{p_1}$$

$$\times \sum_{n_1, n_2} (-i)^{n_1} \frac{e^{in_1\alpha_1}}{\sqrt{2\pi}} \langle n_1 | Q_P(p_1) | n_2 \rangle i^{n_2} \frac{e^{-in_2\alpha_2}}{\sqrt{2\pi}} , \qquad (3.31)$$

where

$$\langle n_1 | Q_P(p) | n_2 \rangle = \begin{cases} \delta_{n_1, n_2} & \cdots \ k_F \le \left| \dfrac{P}{2} - p \right| \\ \dfrac{1 + (-1)^N}{2} \dfrac{2\gamma}{\pi} \dfrac{\sin N\gamma}{N\gamma} & \cdots \ \left| \dfrac{P}{2} - p \right| \le k_F \le \sqrt{\dfrac{P^2}{4} + p^2} \\ 0 & \cdots \ \text{otherwise} . \end{cases} \qquad (3.32)$$

In the above expression we have defined

$$\gamma = \sin^{-1}\left(\frac{\frac{P^2}{4} + p^2 - k_F^2}{Pp} \right), \quad N = n_1 - n_2 , \qquad (3.33)$$

and we have assumed that

$$\frac{\sin N\gamma}{N\gamma} = 1 \quad \text{for} \quad N = 0 . \qquad (3.34)$$

Note that the Pauli operator $\langle \mathbf{p}_1 | Q_P | \mathbf{p}_2 \rangle$ depends separately on the angles α_1 and α_2, and thus is not invariant under rotations. Therefore, the above expression for the exact Pauli operator mixes the components with different angular momentum n, and makes the numerical calculation rather complex.

The problem of the coupling of different partial waves may be avoided by defining a Pauli operator which is averaged over angles, $\bar{Q}_P$ by averaging over angle α_1 in the previous expression (Bethe and Goldstone 1957; Lowy and Brown 1975). In this way, equation (3.32) is replaced by

$$\langle n_1 | \bar{Q}_P(p) | n_2 \rangle = \delta_{n_1, n_2} \begin{cases} 1 & \cdots \ k_F \le \left| \dfrac{P}{2} - p \right| \\ 2\gamma/\pi & \cdots \ \left| \dfrac{P}{2} - p \right| \le k_F \le \sqrt{\dfrac{P^2}{4} + p^2} \\ 0 & \cdots \ \text{otherwise} \end{cases} \qquad (3.35)$$

which is diagonal with respect to the angular momentum n. The numerical calculations that we report here (Suwa et al. 2003) were carried out both with exact Pauli operator of (3.32), and with the angle-averaged Pauli operator of (3.35). As we will discuss in what follows, the difference between the two calculations is small.

The matrix g_P^c can then be expanded in the same way as equation (3.28) for V as follows:

$$\langle \mathbf{p}_1 | g_P^c | \mathbf{p}_2 \rangle = \sum_{n_1,n_2=-\infty}^{\infty} (-i)^{n_1} \frac{e^{in_1\alpha_1}}{\sqrt{2\pi}} \langle p_1 n_1 | g_P^c | p_2 n_2 \rangle i^{n_2} \frac{e^{-in_2\alpha_2}}{\sqrt{2\pi}} . \qquad (3.36)$$

Using the above partial wave expansions, equation (3.24) reduces to the following one-dimensional integral equation:

$$\langle p_1 n_1 | g_P^c | p_2 n_2 \rangle = \sum_{n,n'} \int_0^\infty \frac{p\,dp}{(2\pi)^2} \langle p_1 n_1 | V | pn \rangle \frac{\langle n | Q_P(p) | n' \rangle}{p_1^2 - p^2 + i\eta} \langle pn' | V | p_2 n_2 \rangle$$

$$+ \sum_{n,n'} \int_0^\infty \frac{p\,dp}{(2\pi)^2} \langle p_1 n_1 | V | pn \rangle \frac{\langle n | Q_P(p) | n' \rangle}{p_1^2 - p^2 + i\eta} \langle pn' | g_P^c | p_2 n_2 \rangle , \qquad (3.37)$$

where we put $E = p_1^2$ for the (vector) initial state with relative momentum p_1 (note that the reduced mass is one half). In other words, we choose the initial energy E in such a way that the vector initial state is on its energy shell. As a consequence, if the two particles in the initial states are below the Fermi energy then the energy denominator of (3.37) cannot vanish, and the matrix elements of the g matrix are real and symmetric. Since we wish to determine an effective interaction to describe the ground state and the low-energy excited states, we may assume that the above condition is fulfilled in cases we are interested in. In any case, in order to study the overall structure of g, it is worth calculating it also in the cases where one or both particles in the ground states are outside the Fermi surface. In these cases, the initial energy is large enough to allow real scattering processes to take place, and the g matrix becomes complex. In these cases too, we retain only the real part of the g matrix, and g is still real and symmetric in momentum space. It is easy to show that

$$\langle p_1 n_1 | g_P^c | p_2 n_2 \rangle = \langle p_1 - n_1 | g_P^c | p_2 - n_2 \rangle .$$

The coupled integral equation (3.37) may be solved, for example, by the method of matrix inversion to yield $\langle p_1 n_1 | g_P^c | p_2 n_2 \rangle$, and thus the matrix element $\langle \mathbf{p}_1 | g_P^c | \mathbf{p}_2 \rangle$ of equation (3.36). In any case, it is clear that the dependence of the g^c matrix on $\mathbf{P}$ in momentum space, leads to a g^c matrix in co-ordinate space which depends on $\mathbf{R}_1 - \mathbf{R}_2$, i.e. difference of the co-ordinates of the centre of mass of the two particles between the initial and final states. Obviously, an effective interaction of this kind is not convenient for practical uses. In order to get an effective interaction which depends solely on the relative co-ordinates of the two particles, in (3.36) the centre-of-mass momentum P is replaced by the square root of its mean square value $\bar{P} = \sqrt{\langle \mathbf{P}^2 \rangle}$ for all two-particle states below the Fermi level. At the same time equation (3.36) is averaged over the directions of $\mathbf{P}$ in order to make the resulting expression invariant under rotations. After these manipulations it is possible to

define the matrix element of g^c as a function of $\mathbf{p}_1$ and $\mathbf{p}_2$:

$$\langle \mathbf{p}_1 | \, g^c \, | \mathbf{p}_2 \rangle = \frac{1}{2\pi} \sum_{n=-\infty}^{\infty} e^{in(\alpha_1 - \alpha_2)} \langle p_1 n | \, g_{\bar{P}}^c \, | p_2 n \rangle$$

$$= \frac{1}{2\pi} \sum_{n=0}^{\infty} \epsilon_n \langle p_1 n | g^c | p_2 n \rangle \cos n(\alpha_1 - \alpha_2) \,, \qquad (3.38)$$

where we have defined

$$\epsilon_n = \begin{cases} 1 & \text{for } n = 1 \\ 2 & \text{for } n \neq 1 \end{cases}, \qquad (3.39)$$

and have used the fact that the matrix elements

$$\langle p_1 n | g^c | p_2 n \rangle = \langle p_1 - n | g^c | p_2 - n \rangle$$

are real. The above expression for $\langle \mathbf{p}_1 | g^c | \mathbf{p}_2 \rangle$ is real and depends only on the combination $\alpha_1 - \alpha_2$, thus showing explicitly that it is invariant under the simultaneous rotation of $\mathbf{p}_1$ and $\mathbf{p}_2$. This means that in co-ordinate space the g^c matrix depends only on the initial and final relative co-ordinates and is invariant under rotations. By taking the Fourier transform of (3.38), one arrives at the effective interaction

$$\langle r_1 | g^c | r_2 \rangle = \frac{1}{2\pi} \sum_{n=0}^{\infty} \epsilon_n \, \langle r_1 n | g^c | r_2 n \rangle \cos n(\phi_1 - \phi_2) \,, \qquad (3.40)$$

where $\mathbf{r}_i = (r_i, \phi_i)$, and

$$\langle r_1 n | g^c | r_2 n \rangle = \frac{1}{(2\pi)^2} \int p_1 dp_1 p_2 dp_2 J_n(p_1 r_1) J_n(p_2 r_2) \langle p_1 n | g^c | p_2 n \rangle \,. \qquad (3.41)$$

The interaction (3.40) has finite range and is not diagonal in the initial and final relative co-ordinates (nonlocal interaction), and rendering this rather useless for practical applications. Therefore, in the following, we show how to turn it into a simple and useful interaction.

3.6.2   *The separable approximation*

In order to put the matrix g^c ($\langle \mathbf{r}_1 | g^c | \mathbf{r}_2 \rangle$) into the form of an effective interaction that can be used for practical purposes, we need two successive steps. The first one corresponds to the so-called separable approximation, which will be explained and justified in what follows; the second step is the g^c expansion that will be described in the next Section.

In the separable approximation it is assumed that the matrix elements of g^c of equation (3.38) in momentum space, may be approximated by the product of a local

factor $v(q)$ and a nonlocal one $c(p)$ as follows:

$$\langle \mathbf{p}_1 | g^c | \mathbf{p}_2 \rangle = c\left(\frac{1}{2}|\mathbf{p}_1 + \mathbf{p}_2|\right) v(|\mathbf{p}_1 - \mathbf{p}_2|) = c(p)v(q)\,, \qquad (3.42)$$

where we have introduced $p = |\mathbf{p}| = |\mathbf{p}_1 + \mathbf{p}_2|/2$ and $q = |\mathbf{q}| = |\mathbf{p}_1 - \mathbf{p}_2|$. This expression assumes that the p- and q-dependencies of g^c are separable. The form of g^c in (3.42) is a different way of representing the g matrix which, contrary to the one described in Section 3.5 in the case of nuclear matter, takes into account the nonlocal parts of g^c.

Taking the Fourier transform of the above separable form, we obtain the g^c matrix in coordinate space:

$$\langle \mathbf{r}_1 | g^c | \mathbf{r}_2 \rangle = \tilde{c}(|\mathbf{r}_1 - \mathbf{r}_2|)\tilde{v}\left(\frac{1}{2}|\mathbf{r}_1 + \mathbf{r}_2|\right) = \tilde{c}(s)\tilde{v}(r)\,, \qquad (3.43)$$

where $s = |\mathbf{s}| = |\mathbf{r}_1 - \mathbf{r}_2|$ and $r = |\mathbf{r}| = |\mathbf{r}_1 + \mathbf{r}_2|/2$.

This is still an intricate nonlocal interaction depending on the s and r coordinates separately. We note that in the case where $\tilde{c}(|\mathbf{r}_1 - \mathbf{r}_2|) \propto \delta(\mathbf{r}_1 - \mathbf{r}_2)$, the above interaction becomes the usual two-body interaction which is diagonal in the relative coordinates of the two interacting particles.

In the separable approximation, the local part $v(q)$ and the nonlocal part $c(p)$ of equation (3.42), are computed as follows. First of all, we eliminate the ambiguity in the normalization of $v(q)$ and $c(p)$ as defined in (3.42), by putting $c(0) = 1$. Next, if we let $\mathbf{p}_1 = \mathbf{q}/2$ and $\mathbf{p}_2 = -\mathbf{q}/2$ in (3.38) and (3.42), we have

$$\left\langle \frac{\mathbf{q}}{2} \middle| g^c \middle| -\frac{\mathbf{q}}{2} \right\rangle = \frac{1}{2\pi} \sum_{n=0}^{\infty} \epsilon_n (-1)^n \left\langle \frac{q}{2}n_1 \middle| g^c \middle| \frac{q}{2}n_2 \right\rangle$$

$$= c(0)v(q) = v(q)\,. \qquad (3.44)$$

In the same way we have

$$\langle \mathbf{p} | g^c | \mathbf{p} \rangle = \frac{1}{2\pi} \sum_{n=0}^{\infty} \epsilon_n \langle pn_1 | g^c | pn_2 \rangle = c(p)v(0)\,. \qquad (3.45)$$

From these equations we derive the following expressions for $v(q)$ and $c(p)$:

$$v(q) = \frac{1}{2\pi} \sum_{n=0}^{\infty} \epsilon_n (-1)^n \left\langle \frac{q}{2}n \middle| g^c \middle| \frac{q}{2}n \right\rangle\,, \qquad (3.46)$$

$$c(p) = \frac{1}{v(0)} \frac{1}{2\pi} \sum_{n=0}^{\infty} \epsilon_n \langle pn | g^c | pn \rangle\,. \qquad (3.47)$$

It is clear that $v(q)$ is evaluated using the exchange process for forward scattering and thus it has the phase factor $(-1)^n$, which is absent in $c(p)$, since $c(p)$ is computed by the direct process.
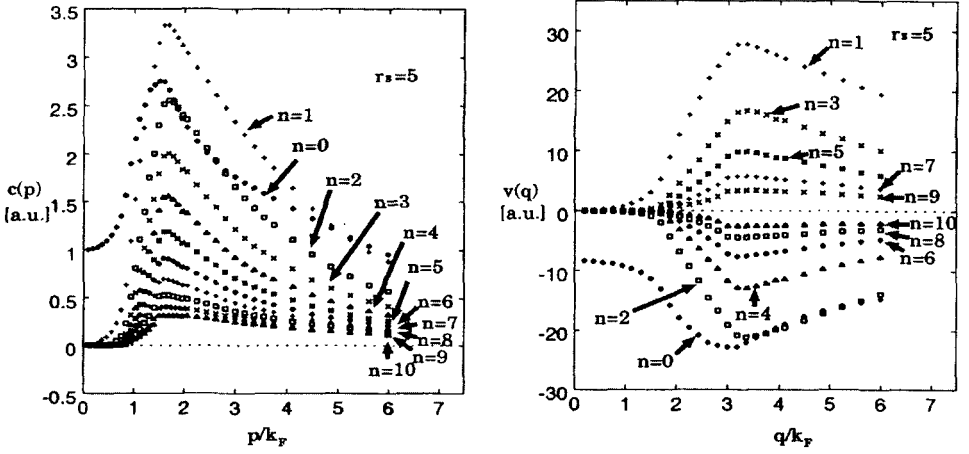
Fig. 3.5   Partial waves of c(p) and v(q) based on Eqs. (3.47) and (3.46) at $r_s = 5$ in atomic units, where $p = |\mathbf{p}_1 + \mathbf{p}_2|/2$ and $q = |\mathbf{p}_1 - \mathbf{p}_2|$.

In Fig. 3.5, for $r_s = 5$ we display how each partial wave contributes to the sum in (3.46) and (3.47), for values of q and p up to several times the Fermi momentum to show the overall structure of the interaction. It can be seen that all the partial wave contributions have a rapid increase at about $p \sim k_F$ for $c(p)$, and $q/2 \sim k_F$ for $v(q)$. This behavior can be explained in the following way. Assume we have two particles below the Fermi energy; then the condition $p \sim k_F$ requires that the relative initial and final momenta of the two particles fulfill $p_2 \sim p_1 \sim k_F$, which in turn means that both particles are near the Fermi surface. Then these particles may be easily excited from the Fermi sea with large amplitude because only a small transfer momentum is required, and this leads to a rapid increase in each partial wave component $\langle pn|\, g^c\, |pn \rangle$ for $p \sim k_F$. It is evident that this argument explains the increase of each partial wave component of $v(q)$ for $q/2 \sim k_F$.

The resulting interactions, $c(p)$ and $v(q)$, are shown in Fig. 3.6. It is seen that all partial waves contribute coherently in $c(p)$, so that convergence is slow and exhibits a very pronounced peak for $p \sim k_F$. For $v(q)$, equation (3.46) is the sum of an alternate series and converges quickly; the resulting peak at $q/2 \sim k_F$ is not very high. Note, further, that if one looks at the region where $q, p \ll k_F$ and from which the effective interaction will be derived later, one sees that only a few partial waves are needed in order to obtain a converging result.

The separable approximation can be justified only *a posteriori* by comparing the matrix elements using the two expressions for the g^c matrix, i.e. the original one (3.38) and the separable form (3.42). Here we will report some comparisons. In Fig. 3.7 we compare $\langle \mathbf{p}_1|g^c|\mathbf{p}_2 \rangle$ of Eq. (3.38) and $c(\frac{1}{2}|\mathbf{p}_1 + \mathbf{p}_2|)v(|\mathbf{p}_1 - \mathbf{p}_2|)$ for the cases where the two vectors $\mathbf{p}_1$ and $\mathbf{p}_2$ obey $p_1 = p_2 = p$, and for the angles $\alpha = \alpha_1 - \alpha_2$ equal to $\pi/4$, $\pi/2$ and $3\pi/4$. Note that for $\alpha = 0, \pi$ the matrix elements
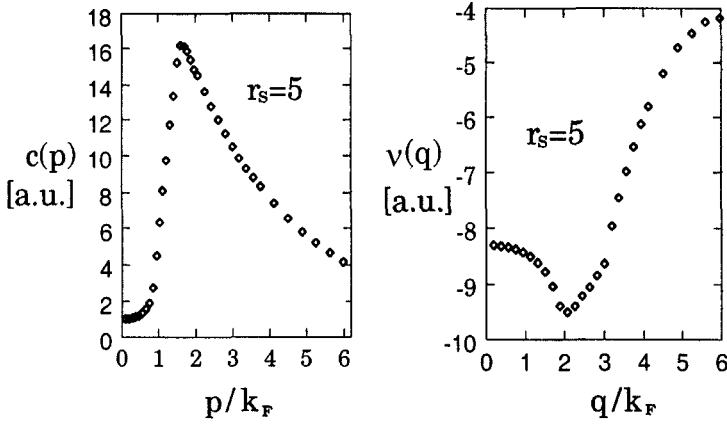
Fig. 3.6   Local $v(q)$ and nonlocal $c(p)$ components, in atomic units, of the correction to the g matrix, g^c, written in the separable form of Eq. (3.42), as functions of the momenta $q = |\mathbf{p}_1 - \mathbf{p}_2|$ and $p = |\mathbf{p}_1 + \mathbf{p}_2|/2$.

Fig. 3.7   Comparison between the matrix elements $\langle \mathbf{p}_1 | g^c | \mathbf{p}_2 \rangle$ and the separable potential $c(p)v(q) = c(\frac{1}{2}|\mathbf{p}_1 + \mathbf{p}_2|)v(|\mathbf{p}_1 - \mathbf{p}_2|)$, as a function of $p_1 = p_2 = p$ for $\alpha = \alpha_1 - \alpha_2$ equal to $\pi/4, \pi/2$ and $3\pi/4$ to $r_s = 5$.
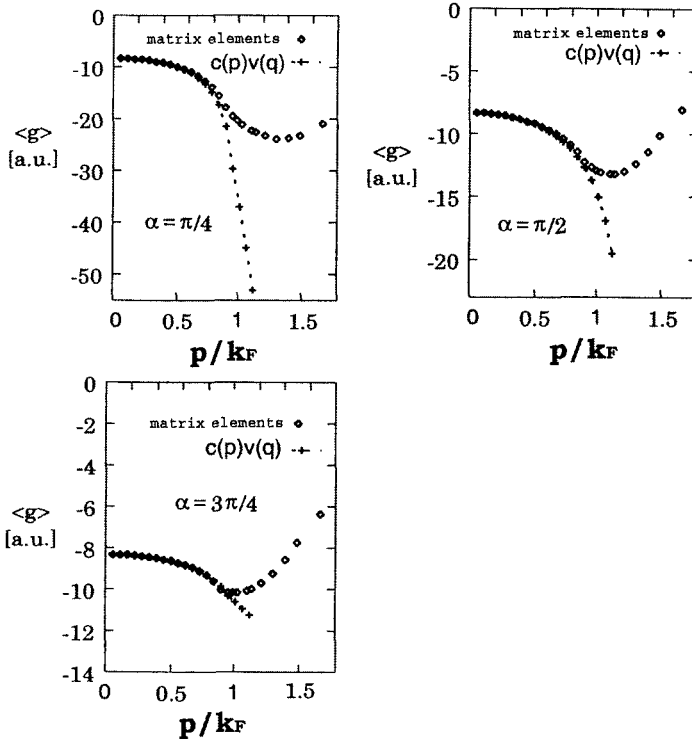
of g^c are used to compute $c(p)$ and $v(q)$, and so can be deduced exactly from the separable form. From the figure it is seen that the separable approximation works extremely well for $p \leq k_F$, where the two particles are below the Fermi surface in the initial state and no real scattering can take place. For $p \geq k_F$ there is no way of putting both particles within the Fermi circle. In this case the initial energy is high enough to allow real scattering processes and to produce a phase shift in the asymptotic form of the relative wavefunction. This change in the physical situation produces a slope change in the matrix element $\langle \mathbf{p}_1 | \, g^c \, | \mathbf{p}_2 \rangle$ of Eq. (3.38) to $p \sim k_F$ (threshold effect), which cannot be reproduced by the separable approximation, as seen in the figure. Moreover, in the cases where $p_1 \neq p_2$, one finds that the separable approximation works well for all cases where $p_1, p_2 \leq k_F$. This means that the matrix element $\langle \mathbf{p}_1 | \, g^c \, | \mathbf{p}_2 \rangle$ is very well approximated by the separable potential $c(p)v(q)$ in the range $p \leq k_F$ and $q \leq 2k_F$, i.e. for all particles below the Fermi surface.

Finally, we note that the matrix element g^c is negative as can be seen from Figs. 3.5 and 3.6. This fact can be understood as follows: the multiple scattering processes account for the effects of short range interactions which cause distortion of the uncorrelated many-body function, which are such as to minimize the repulsive potential of other electrons, and so to lower the total system energy. The g matrix turns these effects into an effective interaction for the uncorrelated states, and so is necessarily an attractive interaction.

3.6.3 *The g matrix expansion*

From the separable potential $c(p)v(q)$ in momentum space it is in principle possible to compute the potential $\tilde{c}(s)\tilde{v}(r)$ of equation (3.43) in coordinate space. However, this potential would be a complex nonlocal interaction with a finite range for both r and s, and would be of little use for practical applications. Therefore, a final approximation is made (i.e. the g matrix expansion) which stems from the inspection of the matrix elements of the separable potential $\tilde{c}(s)\tilde{v}(r)$, in order to get a simpler expression of the interaction. The matrix elements of g^c between any two states $|\psi\rangle$ and $| \varphi \rangle$, in the separable approximation can be written as

$$\langle \psi | g^c | \varphi \rangle = \int d\mathbf{r}_1 d\mathbf{r}_2 \psi^*(\mathbf{r}_1) \langle \mathbf{r}_1 | g^c | \mathbf{r}_2 \rangle \varphi(\mathbf{r}_2)$$

$$= \int d\mathbf{r}_1 d\mathbf{r}_2 \psi^* \left(\mathbf{r} + \frac{\mathbf{s}}{2} \right) \tilde{c}(s) \tilde{v}(r) \varphi \left(\mathbf{r} - \frac{\mathbf{s}}{2} \right)$$

$$= \int d\mathbf{r} \psi^*(\mathbf{r}) g^c(\mathbf{r}, \nabla) \varphi(\mathbf{r}) . \tag{3.48}$$

In the previous expression we have defined

$$g^c(\mathbf{r}, \nabla) = \int d\mathbf{s} \exp \left(\frac{\mathbf{s}}{2} \cdot \overleftarrow{\nabla} \right) \tilde{c}(s) \tilde{v}(r) \exp \left(-\frac{\mathbf{s}}{2} \cdot \overrightarrow{\nabla} \right) , \tag{3.49}$$

where $\nabla = i\mathbf{p} = \partial/\partial\mathbf{r}$ operates on the relative co-ordinate of the two interacting particles and $\overleftarrow{\nabla}$ operates on the left, whereas $\overrightarrow{\nabla}$ operates on the right.

In the above expression for $g^c(\mathbf{r}, \nabla)$ we can assume that the maximum value of ∇ is of the order of k_F for particles in the ground state and in the low-energy excited states. Therefore, we can evaluate equation (3.49) by expanding the exponential and retaining the first two terms (g matrix expansion), provided that $k_F r_c \leq 1$, where r_c is the range of $\tilde{c}(s)$. From Fig. 3.5, this range is estimated to be of the order of $r_c \sim 1/k_F$ due to the behavior of $c(p)$ in the small momentum region, where the separable approximation holds. Therefore, the above condition for expanding equation (3.49) is only marginally fulfilled. We will discuss this point again in the next Section, where we will compare the correlation energies as computed with and without the expansion. We will find that the correlation energy is under-estimated by the g matrix expansion, and this is the price to be paid in order to obtain a simple expression for the effective interaction.

By expanding the exponential functions of (3.49) and retaining only terms up to second order in ∇, we have

$$g^c(\mathbf{r}, \nabla) = \int d\mathbf{s} \left(1 + \frac{\mathbf{s}^2}{16}\overleftarrow{\nabla}^2 + \frac{\mathbf{s}}{2} \cdot \overleftarrow{\nabla}\right) \tilde{c}(s)\tilde{v}(r) \left(1 + \frac{\mathbf{s}^2}{16}\overrightarrow{\nabla}^2 - \frac{\mathbf{s}}{2} \cdot \overrightarrow{\nabla}\right)$$

$$= c_1\tilde{v}(r) + \frac{c_3}{16}\{\overleftarrow{\nabla}^2\tilde{v}(r) + \tilde{v}(r)\overrightarrow{\nabla}^2 - 2\overleftarrow{\nabla}\tilde{v}(r) \cdot \overrightarrow{\nabla}\}, \qquad (3.50)$$

where we have defined the momenta $c(s)$ as

$$c_i = 2\pi \int_0^\infty ds\, s^i \tilde{c}(s), \quad i = 1, 3, \ldots. \qquad (3.51)$$

Here $\tilde{v}(r)$ is further expanded around the zero-range interaction as follows. The Fourier transform of $\tilde{v}(r)$ can be developed in power series of q^2 as

$$v(q) = \int d\mathbf{r}\, e^{-i\mathbf{q}\cdot\mathbf{r}}\tilde{v}(r) = 2\pi \int r\, dr\, \tilde{v}(r) J_0(qr)$$

$$= v_1 - \frac{v_3}{4}q^2 + \frac{v_5}{64}q^4 + \cdots, \qquad (3.52)$$

where the momenta v_i of $\tilde{v}(r)$ are defined as

$$v_i = 2\pi \int_0^\infty dr\, r^i \tilde{v}(r), \quad i = 1, 3, \ldots. \qquad (3.53)$$

We then Fourier-transform (3.52) and retain terms up to second order in ∇, which yields

$$\tilde{v}(r) = \int \frac{d\mathbf{q}}{(2\pi)^2} e^{i\mathbf{q}\cdot\mathbf{r}} v(q) \cong v_1\delta(\mathbf{r}) + \frac{v_3}{4}\{\nabla^2\delta(\mathbf{r})\}$$

$$= v_1\delta(\mathbf{r}) + \frac{v_3}{4}\{\overleftarrow{\nabla}^2\delta(\mathbf{r}) + \delta(\mathbf{r})\overrightarrow{\nabla}^2 + 2\overleftarrow{\nabla}\delta(\mathbf{r}) \cdot \overrightarrow{\nabla}\}. \qquad (3.54)$$

It can be shown that the maximum value of q in (3.52), which is relevant for particles below the Fermi surface, is about $2k_F$. It can be further noted from Fig. 3.5 that the range of $\tilde{v}(r)$ is of the order of $r_v \sim 1/2k_F$, which shows that the maximum value of the exponent $\mathbf{q} \cdot \mathbf{r}$ in (3.54) is about $2k_F r_v \sim 1$. This justifies the above expansion at the same level of accuracy as the expansion of equation (3.49).

By substituting (3.54) into (3.50), we arrive at the following final expression for the effective interaction:

$$g^c(\mathbf{r}, \nabla) = u\delta(\mathbf{r}) + v\{\overleftarrow{\nabla}^2\delta(\mathbf{r}) + \delta(\mathbf{r})\overrightarrow{\nabla}^2\} + 2w\overleftarrow{\nabla}\delta(\mathbf{r}) \cdot \overrightarrow{\nabla} , \qquad (3.55)$$

where the coefficients u, v and w are defined as

$$u = v_1 , \qquad (3.56)$$

$$v = \frac{1}{16}v_1 c_3 + \frac{1}{4}v_3 , \qquad (3.57)$$

$$w = -\frac{1}{16}v_1 c_3 + \frac{1}{4}v_3 . \qquad (3.58)$$

The effective interaction of (3.55) is a zero-range interaction depending on the momentum, of the same type as the Skyrme ones largely used in nuclear physics (Vautherin and Brink 1972, see Chapter 4). The c_i and v_i momenta can be computed numerically from the potential in momentum space as

$$c_1 = c(0) = 1 ,$$

$$c_3 = -2 \left. \frac{d^2}{dp^2}c(p) \right|_{p=0} ,$$

$$v_1 = v(0) ,$$

$$v_3 = -2 \left. \frac{d^2}{dq^2}v(q) \right|_{q=0} .$$

These expressions, together with (3.46) and (3.47), show that in order to obtain the effective interaction of (3.55), it is enough to know the diagonal matrix elements $\langle pn|g^c|pn\rangle$ of the g^c matrix in the low-energy limit ($p \sim 0$). A closer inspection of (3.38) shows that only the $\langle pn|g^c|pn\rangle$ matrix elements with $n = 0, 1$ contribute to the above coefficients. This is a direct consequence of the fact that the first two terms of the right hand side of (3.55) represent the s wave interaction ($n = 0$), and the third term the p wave one ($n = 1$). In other words, the g matrix expansion only simulates the s and p wave matrix elements of the separable potential, and neglects all other components with higher angular momentum. However, it should be noted that the s and p components are enough to describe the low-energy phenomena.
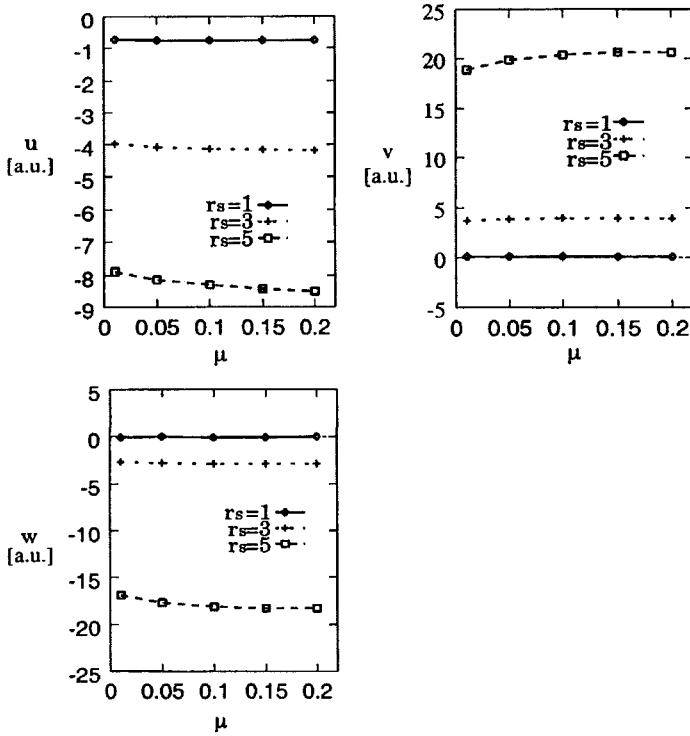
Fig. 3.8 Dependence of the u, v and w coefficients on the cutoff parameter μ (in units of k_F) for $r_s = 1, 3, 5$.

3.6.4 *Numerical results and discussion*

First of all, we discuss the role of the Pauli operator in numerical calculations. If we take the angle-averaged operator of (3.35), it is enough to retain only terms with $n = 0, 1$ in the integral equation (3.37) in order to calculate the effective interaction of (3.55). On the other hand, if we use the exact expression (3.32) for the Pauli operator, all partial wave components are coupled and we will need to consider many partial waves to obtain a convergent result for $n = 0, 1$. The largest n value required to have a convergent result in the case of the $2D$ electron gas is typically about 10, depending on the value of r_s.

Let us next discuss the cutoff parameter μ in the definition of the Coulomb interaction in (3.26). The value of μ should be so small that all numerical results are stable against variations of μ itself. In order to show that this is indeed possible, in Fig. 3.8 we report the numerical results of u, v and w for r_s ($= 1, 3$ and 5), as a function of the cutoff parameter μ. From this figure it is seen that u, v and w approach their convergent values smoothly as μ decreases and, thus, that the use of a damping factor is legitimate. The numerical values of u, v and w in atomic units are reported in Table 3.2 for several values of r_s.

TABLE 3.2

r_s	u	v	w
1	−0.800	0.124	−0.059
3	−4.363	5.411	−3.745
5	−8.828	28.602	−23.831
10	−21.253	258.71	−269.89
20	−47.890	2262.7	−2795.6

In the g matrix theory the correlation energy per electron is expressed as follows in terms of the effective interaction of (3.55):

$$\varepsilon_c^{DME} = \frac{1}{\rho}\langle 0|g^c|0\rangle = \rho\left(\frac{u}{4} - \frac{v}{8}k_F^2 + \frac{3w}{8}k_F^2\right), \tag{3.59}$$

where $|0\rangle$ indicates the ground state of the non-interacting system.

The correlation energies of (3.59) computed either with the exact Pauli operator or with the angle-averaged one, turn out to be practically the same, and the difference between the two results increases slightly with increasing r_s. This shows that the mixing of states with different angular momenta becomes relevant only in the low-density region.

If we use the separable potential of (3.42) without any expansion, we get the following expression instead of (3.59) (see appendix):

$$\varepsilon_c = \frac{1}{2\rho}\int^{k_F}\frac{d\mathbf{k}_1}{(2\pi)^2}\frac{d\mathbf{k}_2}{(2\pi)^2}\{4c(|\mathbf{k}_1 - \mathbf{k}_2|/2)v(0) - 2c(0)v(|\mathbf{k}_1 - \mathbf{k}_2|)\}. \tag{3.60}$$

The correlation energies of equations (3.60) ($\langle c(p)v(q)\rangle$) and (3.59) (ϵ_c^{DME}) are reported in Table 3.3 in eV/electron, together with the Monte Carlo results.

TABLE 3.3

r_s	ϵ_c^{MC}	$\langle c(p)v(q)\rangle$	ϵ_c^{DME}
1	−2.99	−2.60	−2.34
3	−1.83	−1.65	−1.49
5	−1.34	−1.23	−1.11
10	−0.83	−0.76	−0.69
20	−0.48	−0.44	−0.40

It can be noted that the QMC correlation energies can be well reproduced by the separable potential, especially in the high r_s range. In the region of small r_s, where the long range RPA correlations are important, there is an expected discrepancy between the g matrix and Monte Carlo results. It is also possible to show that the correlation energy of (3.59) underestimates that of (3.60) by about 10%, and this is the price to be paid when passing from the separable potential to the Skyrme-like interaction.

As is clear from the derivation of the effective interaction of (3.55), this error originates from (i) neglecting the contributions of partial waves with $n \geq 2$, and (ii) inaccurate treatment of the s wave and p wave contributions.

The effective interaction of (3.55) can be readily employed to study the dynamic and static properties of finite systems such as electron systems confined in an external field (quantum dots). For these systems the effective Hamiltonian to be used in BHF like calculations is given by (in effective atomic units):

$$H^{eff} = \sum_{i=1}^{N} \left(-\frac{\vec{\nabla}^2}{2} + v_{\text{ext}} \right)_i + \sum_{i<j} \left(\frac{1}{|\mathbf{r}_i - \mathbf{r}_j|} + g^c(\mathbf{r}_{ij}) \right), \qquad (3.61)$$

where $g^c(\mathbf{r}_{ij})$ is given by Eq. (3.55) and the dependence on the density of the u, v and w coefficients is to be treated in local density approximation.

The BHF energy functional for an external potential produced by a jellium of positive charge, is given by the following expression

$$E^{BHF} = \frac{1}{2} \int \tau d\mathbf{r} + \frac{1}{4} \int u(\rho)\rho^2 d\mathbf{r} - \int t_1(\rho)(\rho\tau - j^2)d\mathbf{r} - \int t_2(\rho)(\nabla\rho)^2 d\mathbf{r}$$

$$+ \frac{1}{2} \int \frac{(\rho - \rho_+)_{\mathbf{r}_1}(\rho - \rho_+)_{\mathbf{r}_2}}{|\mathbf{r}_1 - \mathbf{r}_2|} d\mathbf{r}_1 d\mathbf{r}_2 - \frac{1}{2} \int \frac{|\rho^{(1)}(\mathbf{r}, \mathbf{r}')|^2}{|\mathbf{r} - \mathbf{r}'|} d\mathbf{r} d\mathbf{r}', \quad (3.62)$$

where

$$t_1 = \frac{1}{4}(v - 3w), \quad t_2 = \frac{3}{16}\left(v + w + 2/3\rho\frac{\partial v}{\partial \rho} \right),$$

and

$$\tau(\mathbf{r}) = \sum_i |\nabla\varphi_i(\mathbf{r})|^2, \quad \mathbf{j}(\mathbf{r}) = -\frac{1}{2i}\sum_i (\varphi_i(\mathbf{r})\nabla\varphi_i^*(\mathbf{r}) - h.c.),$$

$$\rho^{(1)}(\mathbf{r}, \mathbf{r}') = \sum_i \varphi_i^*(\mathbf{r})\varphi_i(\mathbf{r}'), \quad \rho(\mathbf{r}) = \sum_i |\varphi_i(\mathbf{r})|^2,$$

are the kinetic energy, current, one-body non-diagonal and diagonal densities, respectively. The $\varphi_i(\mathbf{r})$ are the single-particle wavefunctions, and the last terms in equation (3.62) are the electron–electron (both direct and exchange), electron–ion, and ion–ion Coulomb contributions. Besides the pure HF functional, the energy functional (3.62) has the correlation term

$$E_c(\rho, \tau) = \int \left(\frac{1}{4}u\rho^2 - t_2(\nabla\rho)^2 - t_1(\rho\tau - j^2) \right) d\mathbf{r}. \qquad (3.63)$$

This term is very easily handled both in static and dynamic calculations. Clearly, the term in $(\nabla\rho)^2$ vanishes for homogeneous systems, for which ρ is a constant. On the other hand, the current term is zero for time-reversal invariant systems.

The single-particle wavefunctions which appear in (3.62) are to be determined in a self-consistent way by solving the BHF equations:

$$\left\{ -\frac{1}{2}\vec{\nabla}[1 - 2t_1(\rho)\rho(\mathbf{r})] \cdot \vec{\nabla} + V_c(\rho,\tau) + \int \frac{\rho(\mathbf{r}') - \rho_+(\mathbf{r}')}{|\mathbf{r} - \mathbf{r}'|} d\mathbf{r}' \right\} \varphi_i(\mathbf{r})$$

$$+ \sum_{j\|i}^{N} \int \frac{\varphi_j^*(\mathbf{r}')\varphi_i(\mathbf{r}')}{|\mathbf{r} - \mathbf{r}'|} d\mathbf{r}' \varphi_j(\mathbf{r}) = \varepsilon_i \varphi_i(\mathbf{r}), \qquad (3.64)$$

where $j\|i$ means that the spins must be parallel, and

$$V_c(\rho,\tau) = \frac{1}{2}u\rho + \frac{1}{4}u'\rho^2 + \frac{1}{4}(3w - v)\tau + \frac{1}{4}(3w' - v')\rho\tau$$

$$+ \frac{1}{16}(5v' + 3w' + 2v''\rho)\left(\frac{d\rho}{dr}\right)^2 + \frac{3}{8}(v + w + 2/3v'\rho)\nabla^2\rho, \qquad (3.65)$$

is the correlation potential, and the $'$ and $''$ mean first and second derivatives of the u v and w functions, with respect to the density.

Equations (3.64) constitute a set of coupled integral-differential equations; they have been solved for quantum dots (T. Suwa et al. 2003) and the resulting density in the case of a dot with 20 electrons was shown in Fig. 2.7.

Calculations analogous to the $2D$ ones reported in this Section were carried out in the $3D$ case by Lipparini et al. (1994) in metal clusters, and the results concerning the single-particle energies, the ionization energies, the total energies and the densities of some sodium clusters were shown in Section 2.2.1.

In general, it may be concluded that the BHF theory is a very good microscopic theory, in the sense that it improves the HF theory by including the ladder correlations, which are important ones especially at physical densities.

3.6.5   *Appendix*

Starting from equation (3.42) it is possible to calculate the ground state energy E^{BHF} of the electron gas. To this end, it is convenient to use the second quantization formalism, in which the two-body interaction is written as (see Section 2.5):

$$\frac{1}{2} \sum_{\mathbf{k}_1,\mathbf{k}_2,\mathbf{q},\sigma,\sigma'} V(\mathbf{q})c^+_{\mathbf{k}_1+\mathbf{q},\sigma}c^+_{\mathbf{k}_2-\mathbf{q},\sigma'}c_{\mathbf{k}_2,\sigma'}c_{\mathbf{k}_1,\sigma},$$

where the operators c^+_λ and c_λ are creation and annihilation operators which obey the anticommutation relations

$$\{c_\lambda, c^+_{\lambda'}\} = \delta_{\lambda,\lambda'}, \qquad \{c_\lambda, c_{\lambda'}\} = 0, \qquad \{c^+_\lambda, c^+_{\lambda'}\} = 0.$$

Using the transformations $\mathbf{p}_1 = 1/2(\mathbf{k}_1 - \mathbf{k}_2)$ and $\mathbf{p}_2 = 1/2(\mathbf{k}'_1 - \mathbf{k}'_2)$ where $\mathbf{k}'_1 = \mathbf{k}_1 + \mathbf{q}$ and $\mathbf{k}'_2 = \mathbf{k}_2 - \mathbf{q}$, we find $\mathbf{p}_2 - \mathbf{p}_1 = \mathbf{q}$ and $1/2(\mathbf{p}_1 + \mathbf{p}_2) = 1/2(\mathbf{k}_1 - \mathbf{k}_2 + \mathbf{q})$,

and finally

$$g^c = \frac{1}{2} \sum_{\mathbf{k}_1,\mathbf{k}_2,\mathbf{q},\sigma,\sigma'} c(|\mathbf{k}_1 - \mathbf{k}_2 + \mathbf{q}|/2)v(|\mathbf{q}|)c^+_{\mathbf{k}_1+\mathbf{q},\sigma}c^+_{\mathbf{k}_2-\mathbf{q},\sigma'}c_{\mathbf{k}_2,\sigma'}c_{\mathbf{k}_1,\sigma} \ . \quad (3.66)$$

From this expression, one finds for the BHF energy

$$E^{BHF} = E^{HF} + \frac{1}{2} \sum_{\mathbf{k}_1,\mathbf{k}_2,\sigma,\sigma'} v(0)c(|\mathbf{k}_1 - \mathbf{k}_2|/2)\langle HF|c^+_{\mathbf{k}_1,\sigma}c^+_{\mathbf{k}_2,\sigma'}c_{\mathbf{k}_2,\sigma'}c_{\mathbf{k}_1,\sigma}|HF\rangle$$

$$+ \frac{1}{2} \sum_{\mathbf{k}_1,\mathbf{q},\sigma} c(0)v(|\mathbf{q}|)\langle HF|c^+_{\mathbf{k}_1+\mathbf{q},\sigma}c^+_{\mathbf{k}_1,\sigma}c_{\mathbf{k}_1+\mathbf{q},\sigma}c_{\mathbf{k}_1,\sigma}|HF\rangle \ , \quad (3.67)$$

where E^{HF} is the HF energy

$$E^{HF} = \sum_{\mathbf{k},\sigma} \epsilon^{HF}_{\mathbf{k},\sigma} n_{\mathbf{k},\sigma} \ , \quad (3.68)$$

written in terms of the distribution functions $n_{\mathbf{k},\sigma}$ ($= 1$, $k \le k_F$, $= 0$ $k > k_F$) and of the single-particle HF energies, and the other terms give the correlation energy.

From equation (3.67), and using the commutation relations for operators c and c^+, and $c^+_{\mathbf{k},\sigma}c_{\mathbf{k},\sigma}|HF\rangle = n_{\mathbf{k},\sigma}|HF\rangle$, we obtain the following expression for E^{BHF}:

$$E^{BHF} = E^{HF} + \frac{1}{2} \sum_{\mathbf{k}_1,\mathbf{k}_2,\sigma,\sigma'} v(0)c(|\mathbf{k}_1 - \mathbf{k}_2|/2)n_{\mathbf{k}_1,\sigma}n_{\mathbf{k}_2,\sigma'}$$

$$- \frac{1}{2} \sum_{\mathbf{k}_1,\mathbf{k}_2,\sigma,\sigma'} c(0)v(|\mathbf{k}_1 - \mathbf{k}_2|)n_{\mathbf{k}_1,\sigma}n_{\mathbf{k}_2,\sigma'}\delta_{\sigma,\sigma'} \ . \quad (3.69)$$

Next, the single-particle energies and the self-energy in BHF are obtained by differentiation with respect to $n_{\mathbf{k},t}$:

$$\epsilon^{BHF}_{\mathbf{k},t} = \epsilon^{HF}_{\mathbf{k},t} + \sum_{\mathbf{k}_2,\sigma'} [v(0)c(|\mathbf{k} - \mathbf{k}_2|/2)n_{\mathbf{k}_2,\sigma'} - c(0)v(|\mathbf{k} - \mathbf{k}_2|)n_{\mathbf{k}_2,\sigma'}\delta_{t,\sigma'}]$$

$$+ \frac{1}{2} \sum_{\mathbf{k}_1,\mathbf{k}_2,\sigma,\sigma'} \left[\frac{\partial}{\partial \rho}(v(0)c(|\mathbf{k}_1 - \mathbf{k}_2|/2) - c(0)v(|\mathbf{k}_1 - \mathbf{k}_2|)\delta_{\sigma,\sigma'}) \right]$$

$$\times n_{\mathbf{k}_1,\sigma}n_{\mathbf{k}_2,\sigma'} \ . \quad (3.70)$$

In the derivation of Eq. (3.70) we took into account the dependence of the correlation energy on density, and used

$$\frac{\partial}{\partial n_{\mathbf{k},t}} = \frac{\partial}{\partial \rho}\frac{\partial \rho}{\partial n_{\mathbf{k},t}}$$

with $\partial \rho/\partial n_{\mathbf{k},t} = 1$.

The effective mass in BHF is therefore given by

$$\frac{1}{m^*} = \frac{1}{k}\frac{\partial \epsilon_k^{BHF}}{\partial k} = 1 + \frac{m}{k}\frac{\partial}{\partial k}\Sigma_x(k) + \frac{m}{k}\frac{\partial}{\partial k}\Sigma_c^{BHF}(k)\,, \qquad (3.71)$$

where $\Sigma_x(k)$ is the exchange self energy and $\Sigma_c^{BHF}(k)$ is the BHF correlation contribution. Although in the literature there exist no accurate numerical calculation of $\Sigma_c^{BHF}(k)$, an approximate estimate of such quantity shows that the correlation contribution to the effective mass has opposite sign with respect to the exchange one, and tends to cancel it.

References to Chapter 3

K.A. Brueckner and C.A. Levinson, Phys. Rev. **97**, 1344 (1955); K.A. Brueckner, J.L. Gammel and H. Weitzner, Phys. Rev. **110**, 431 (1958).

T. Suwa, Doctoral thesis, Sophia University, Tokyo, 2002.

S. Nagano, K. Singwi and S. Ohnishi, Phys. Rev. B **29**, 1209 (1984).

S. Nagano and K. Singwi, Phys. Rev. B **27**, 6732 (1983).

C.N. Yang, Phys. Rev. Lett. **19**, 1312 (1967).

R.V. Reid, Annals of Phys. **50**, 411 (1968).

D.W.L. Sprung and P.K. Banerjee, Nucl. Phys. A **168**, 273 (1971).

J. Negele, Phys. Rev. C **1**, 1260 (1970).

X. Campi and D.W.L. Sprung, Nucl. Phys. A **194**, 401 (1972).

H.Q. Song, M. Baldo, G. Giansiracusa and U. Lombardo, Phys. Rev. Lett. **81**, 1584 (1998).

T. Suwa, K. Takayanagi and E. Lipparini, Phys. Rev. B 2003, in publication.

E. Lipparini, Ll. Serra and K. Takayanagi, Phys. Rev. B **49**, 16733 (1994); K. Takayanagi and E. Lipparini, Phys. Rev. B **54**, 8122 (1996).

D.N. Lowy and G.E. Brown, Phys. Rev. B **12**, 2138 (1975); K. Bedell and G.E. Brown, Phys. Rev. B **17**, 4512 (1978).

B. Tanatar and D.M. Ceperley, Phys. Rev. B **39**, 5005 (1989).

T. Suwa, K. Takayanagi, E. Lipparini and F. Pederiva, to be published.

D. Vautherin and D. Brink, Phys. Rev. C **5**, 626 (1972).

This page is intentionally left blank

Chapter 4

The Density Functional Theory (DFT)

4.1 Introduction

Hohenberg and Kohn, in a famous paper of 1964, were the first who proved in a rigorous way that the properties of the ground state of an N-particle system can be expressed as functionals of its density $\rho(\mathbf{r})$, i.e. they are determined by the knowledge of the density. The total energy E can be expressed in terms of such a functional and $E(\rho)$ obeys a variational principle. The Thomas–Fermi model for the atom is a special case of this formalism, and the same is true for the Gross–Pitaevskii theory for the ground state of a dilute Boson gas.

The density functional theory has been applied most of all to systems of electrons like atoms, molecules, homogeneous solids, surfaces and interfaces, quantum wells and quantum dots, etc. As we will discuss in the following, this theory has been used for the description of liquid helium and atomic nuclei as well.

The self-consistent single-particle equations that were derived from the variational principle by Kohn and Sham (1965) describe the properties of the ground state (energy and density) in a way that, formally, takes into account all many-body effects. Their solution, in the local density approximation, is as simple as the solution of the Hartree equations (without exchange terms) and leads to results better than the Hartree–Fock ones, though the latter are much more complicated, and in some cases even almost impossible, to obtain. The reason for this is that the Kohn and Sham solutions treat accurately both exchange and correlation effects, while the HF ones treat exchange exactly but completely neglect correlations.

4.2 The Density Functional Formalism

In what follows we report Levy's (1979) proof of the theorems on which is based the formalism of the density functional theory. Let us consider N interacting particles that move in an external field $v_{\text{ext}}(\mathbf{r})$ whose Hamiltonian will be written as

$$H = T + V + \sum_{i=1}^{N} v_{\text{ext}}(\mathbf{r}_i) \,, \tag{4.1}$$

where T is the kinetic energy and V the interparticle interaction.

Let us consider all possible densities $\rho(\mathbf{r})$, i.e. those that can be obtained from any N-particle wavefunction $\Psi(\mathbf{r_1}, \mathbf{r_2}, \dots, \mathbf{r_N})$ through

$$\rho(\mathbf{r}) = \langle \Psi | \sum_{i=1}^{N} \delta(\mathbf{r} - \mathbf{r}_i) | \Psi \rangle \,, \tag{4.2}$$

and let us define the functional

$$F(\rho) = \min_{\Psi \to \rho} \langle \Psi | T + V | \Psi \rangle \,, \tag{4.3}$$

where the minimum is with respect to all $|\Psi\rangle$ which produce the density ρ. $F(\rho)$ is universal in the sense that it does not refer to any specific system or to the external potential. Indicating by E_{GS}, Ψ_{GS} and ρ_{GS} the energy, wavefunction and density of the ground state, respectively, the two basic theorems of the density functional theory are

$$E(\rho) = \int dr v_{\text{ext}}(\mathbf{r}) \rho(\mathbf{r}) + F(\rho) \geq E_{GS} \,, \tag{4.4}$$

for any density (4.2), and

$$\int dr v_{\text{ext}}(\mathbf{r}) \rho_{GS}(\mathbf{r}) + F(\rho_{GS}) = E_{GS} \,. \tag{4.5}$$

In order to prove the variational principle (4.4) let us indicate by Ψ_{min}^{ρ} a wavefunction that minimizes (4.3), so that

$$F(\rho) = \langle \Psi_{\text{min}}^{\rho} | T + V | \Psi_{\text{min}}^{\rho} \rangle \,. \tag{4.6}$$

By writing

$$V_{\text{ext}} = \sum_{i=1}^{N} v_{\text{ext}}(\mathbf{r}_i) \,,$$

we have

$$\int dr v_{\text{ext}}(\mathbf{r}) \rho(\mathbf{r}) + F(\rho) = \langle \Psi_{\text{min}}^{\rho} | T + V_{\text{ext}} + V | \Psi_{\text{min}}^{\rho} \rangle \geq E_{GS} \,, \tag{4.7}$$

as follows from the minimum properties of the ground state. This proves the inequality (4.4). Using again the minimum property, we then find

$$E_{GS} = \langle \Psi_{GS} | T + V_{\text{ext}} + V | \Psi_{GS} \rangle \leq \langle \Psi_{\text{min}}^{\rho_{GS}} | T + V_{\text{ext}} + V | \Psi_{\text{min}}^{\rho_{GS}} \rangle \,. \tag{4.8}$$

By subtracting V_{ext}, we obtain

$$\langle \Psi_{GS} | T + V | \Psi_{GS} \rangle \leq \langle \Psi_{\min}^{\rho_{GS}} | T + V | \Psi_{\min}^{\rho_{GS}} \rangle. \tag{4.9}$$

On the other hand, the definition of $\Psi_{\min}^{\rho_{GS}}$ leads to an opposite inequality between the two sides of (4.9). This is possible only if

$$\langle \Psi_{GS} | T + V | \Psi_{GS} \rangle = \langle \Psi_{\min}^{\rho_{GS}} | T + V | \Psi_{\min}^{\rho_{GS}} \rangle. \tag{4.10}$$

Therefore we have

$$
\begin{aligned}
E_{GS} &= \int d\mathbf{r} v_{\text{ext}}(\mathbf{r}) \rho_{GS}(\mathbf{r}) + \langle \Psi_{GS} | T + V | \Psi_{GS} \rangle \\
&= \int d\mathbf{r} v_{\text{ext}}(\mathbf{r}) \rho_{GS}(\mathbf{r}) + \langle \Psi_{\min}^{\rho_{GS}} | T + V | \Psi_{\min}^{\rho_{GS}} \rangle \\
&= \int d\mathbf{r} v_{\text{ext}}(\mathbf{r}) \rho_{GS}(\mathbf{r}) + F(\rho_{GS}),
\end{aligned} \tag{4.11}
$$

which completes the proof of the basic theorems. From equation (4.10) follows the important result that if the ground state is not degenerate, then $\Psi_{\min}^{\rho_{GS}} = \Psi_{GS}$. If, on the contrary, it is degenerate, then $\Psi_{\min}^{\rho_{GS}}$ equals one of the ground state wavefunctions, and the others can be obtained as well. Therefore, the ground state density determines the wavefunction (or the wavefunctions) through which it is possible to compute all the properties of the ground state. Thus, these properties are functions of the density. This theorem is the formal justification for dealing with the density instead of the wavefunctions.

These theorems provide a general framework for calculating the ground state properties. One needs to find an approximation for $F(\rho)$ and to minimize $E(\rho)$ in equation (4.4) for the potential of interest V_{ext}. This leads to the corresponding approximation for E_{GS} and ρ_{GS}. Then, if we have an approximation for the functional $X(\rho)$ describing a given property X of the ground state, the same procedure leads to approximations for X itself.

4.3 Examples of Application of the Density Functional Theory

4.3.1 *The Thomas–Fermi theory for the atom*

In this approximation, the atom electrons are treated as independent particles, so that the system energy is given by the average value of the Hamiltonian (expressed in atomic units)

$$H = \sum_{i=1}^{N} \left(-\frac{\vec{\nabla}_i^2}{2} + v_{\text{ext}}(\mathbf{r}_i) \right) + \sum_{i<j} \frac{1}{|\mathbf{r}_i - \mathbf{r}_j|}, \tag{4.12}$$

(where $v_{\text{ext}}(\mathbf{r}_i) = -Z/r_i$ is the Coulomb potential of the nucleus) taken on a Slater determinant:

$$
E = \int \frac{\tau}{2} d\mathbf{r} + \int v_{\text{ext}} \rho(\mathbf{r}) d\mathbf{r} + \frac{1}{2} \int d\mathbf{r} d\mathbf{r}' \frac{\rho(\mathbf{r})\rho(\mathbf{r}')}{|\mathbf{r} - \mathbf{r}'|}
$$
$$
- \frac{1}{2} \sum_{\sigma,\sigma'} \int d\mathbf{r} d\mathbf{r}' \frac{|\rho^{(1)}(\mathbf{r}, \sigma, \mathbf{r}', \sigma')|^2}{|\mathbf{r} - \mathbf{r}'|} . \tag{4.13}
$$

Further approximations consist in neglecting the exchange term [i.e. the last one in Eq. (4.13)] and employing the local density approximation for the kinetic energy density τ:

$$
\tau = \tau(\rho) = \frac{3}{5}(3\pi^2)^{2/3} \rho(\mathbf{r})^{5/3} , \tag{4.14}
$$

which means that we assume that τ is given by the kinetic energy of a non-interacting electron gas with density ρ [see Eqs. (1.74) and (1.76)]. This is a good approximation if $\rho(\mathbf{r})$ varies slowly enough in space, so that an electron located at $\mathbf{r}$ practically feels a homogeneous medium of density $\rho(\mathbf{r})$. Therefore, the Thomas–Fermi density functional is

$$
E(\rho) = \frac{3}{10}(3\pi^2)^{2/3} \int \rho(\mathbf{r})^{5/3} d\mathbf{r} + \int v_{\text{ext}} \rho(\mathbf{r}) d\mathbf{r} + \frac{1}{2} \int d\mathbf{r} d\mathbf{r}' \frac{\rho(\mathbf{r})\rho(\mathbf{r}')}{|\mathbf{r} - \mathbf{r}'|} . \tag{4.15}
$$

The equation that controls the system behavior is obtained by minimizing the energy functional under the constraint that the number of electrons $N = \int \rho d\mathbf{r}$ is constant:

$$
\delta(E - \mu \int \rho d\mathbf{r}) = 0 . \tag{4.16}
$$

In this way the Thomas–Fermi equations are obtained

$$
\frac{5}{3}\alpha\rho^{2/3} + v_{\text{ext}} + \int d\mathbf{r}' \frac{\rho(\mathbf{r}')}{|\mathbf{r} - \mathbf{r}'|} - \mu = 0 , \tag{4.17}
$$

where $\alpha = \frac{3}{10}(3\pi^2)^{2/3}$. Once solved, these equations yield ρ as a function of μ; the chemical potential is subsequently found by using the relationship that fixes the number of particles $N = \int \rho d\mathbf{r}$.

The Thomas–Fermi method describes only roughly the density and electrostatic potential of the atomic electrons. The main shortcoming of the model is that the density diverges at the nucleus and does not decay exponentially at infinity, but rather as r^{-6}. When applied to molecules it does not produce binding, and cannot predict the shell structure of atoms.

4.3.2 The Gross–Pitaevskii theory for the ground state of a dilute gas of Bosons

In Section 2.3, we saw that the mean field theories for Bosons in an external field lead to the following density functional

$$E(\rho) = \frac{1}{2m} \int (\vec{\nabla}\sqrt{\rho})^2 d\mathbf{r} + \int v_{\text{ext}}\rho d\mathbf{r} + \frac{N-1}{2N} \int d\mathbf{r} d\mathbf{r}' \rho(\mathbf{r})\rho(\mathbf{r}')v(|\mathbf{r}-\mathbf{r}'|), \quad (4.18)$$

and that in the case of dilute systems, where the condition $\rho|a|^3 \ll 1$ is fulfilled, it is possible to replace the two-body interaction by an effective interaction given by $V(\mathbf{r}-\mathbf{r}') = g\delta(\mathbf{r}-\mathbf{r}')$, where the coupling constant g is connected to the scattering length a by $g = 4\pi\hbar^2 a/m$. Thus we obtain the Gross–Pitaevskii functional:

$$E(\rho) = \frac{1}{2m} \int (\vec{\nabla}\sqrt{\rho})^2 d\mathbf{r} + \int v_{\text{ext}}\rho d\mathbf{r} + \frac{g}{2} \int \rho^2 d\mathbf{r}, \quad (4.19)$$

for the Bose–Einstein condensate, which is known to be the good theory, in the sense that the corrections to the mean field energy, due to dynamic correlations, behave as $(\rho|a|^3)^{1/2}$ (see Chapter 9) and are typically of the order of 1%.

The above functional is probably the best realization of the density functional theory.

In the case of atoms subject to repulsive interaction and confined in a parabolic external field, in the limit $Na/a_{ho} \gg 1$ $(a_{ho} = (\hbar/m\omega_{ho})^{1/2})$, which turns out to be accomplishable in the experiments, the functional (4.19) leads to particularly simple solutions. In fact, in this limit the atoms of the condensate are pushed outwards and the central density is very flat (see Fig. 2.10), and the kinetic term (which is proportional to the gradient of the density) is negligible. In this approximation, which is known as Thomas–Fermi approximation, minimization of the functional with the constraint of constant number of electrons yields the equations

$$v_{\text{ext}} + g\rho - \mu = 0, \quad (4.20)$$

whose solution is

$$\rho = \begin{cases} g^{-1}[\mu - v_{\text{ext}}] & \mu > v_{\text{ext}} \\ 0 & \text{otherwise} \end{cases}. \quad (4.21)$$

The constraint on the particle number gives the value of μ:

$$\mu = \frac{\hbar\omega_{ho}}{2} \left(\frac{15Na}{a_{ho}} \right)^{2/5}. \quad (4.22)$$

Moreover, since $\mu = \partial E/\partial N$, the energy per particle is given by

$$\frac{E}{N} = \frac{5}{7}\mu. \quad (4.23)$$

In this case, the Thomas–Fermi solutions turn out to be a very good approximation for the density and for the energy per particle of the condensate, when the number of atoms is of the order of 10^5–10^6.

The Thomas–Fermi approximation is employed also in the case of anisotropic traps where the external potential is described by

$$v_{\text{ext}}(\mathbf{r}) = \frac{1}{2} m(\omega_\perp^2 (x^2 + y^2) + \omega_z^2 z^2).$$ (4.24)

This choice of the confinement potential reproduces very well most of the experimental conditions.

The Thomas–Fermi solution yields values of the average values of one-body operators which are quite different from those obtained from the independent-particle model, i.e. by neglecting the interaction. For example, for the potential (4.24), a simple calculation leads to the following results for the mean square radii and anisotropy of the velocity distributions:

$$\frac{\langle p_z^2 \rangle}{\langle p_x^2 \rangle} = \frac{\langle x^2 \rangle}{\langle z^2 \rangle} = \frac{\omega_z^2}{\omega_\perp^2}$$ (4.25)

in the case of the Thomas–Fermi approximation, and

$$\frac{\langle p_z^2 \rangle}{\langle p_x^2 \rangle} = \frac{\langle x^2 \rangle}{\langle z^2 \rangle} = \frac{\omega_z}{\omega_\perp}$$ (4.26)

in the case of the independent-particle model.

A detailed treatment of the results of the Gross–Pitaevskii theory when applied to the Bose–Einstein condensation phenomena, can be found in the review paper by Dalfovo et al. (1999). The time-dependent Gross–Pitaevskii theory will be treated in Chapter 8.

4.4   The Kohn–Sham Equations

In 1965 Kohn and Sham proposed a method to obtain an exact, single-particle like, description of a many body system. The method is based on the following separation of the energy functional:

$$E(\rho) = T_0(\rho) + \int d\mathbf{r} \rho(\mathbf{r}) \left[v_{\text{ext}}(\mathbf{r}) + \frac{1}{2} U(\mathbf{r}) \right] + E_{xc}(\rho),$$ (4.27)

where $T_0(\rho)$ is the kinetic energy of the non-interacting system with density ρ, $U(\mathbf{r}) = \int d\mathbf{r}' \rho(\mathbf{r}') v(|\mathbf{r} - \mathbf{r}'|)$ is the Hartree potential (which in the case of electrons is the classical Coulomb potential) and $E_{xc}(\rho)$ can be thought of as the definition of the exchange-correlation energy. Though $T_0(\rho)$ is different from the real kinetic energy, it has comparable magnitude and is treated exactly in this method. The exact treatment of $T_0(\rho)$ eliminates some of the shortcomings of the Thomas–Fermi approach to the Fermion system, like for example the lack of shell effects or the

absence of bonding in molecules and solids. All terms of (4.27), except E_{xc}, can be treated exactly. Therefore, the unavoidable approximations of the method concern only the exchange-correlation energy.

Application of the variational principle to (4.27), with the constraint of particle number conservation, leads to

$$\frac{\partial T_0(\rho)}{\partial \rho} + v_{\text{ext}}(\mathbf{r}) + U(\mathbf{r}) + \frac{\partial E_{xc}(\rho)}{\partial \rho} = \mu, \tag{4.28}$$

where μ is the Lagrange multiplier related to the conservation of N. By comparing this equation with the corresponding one for a system of particles moving in an effective potential $V_{\text{eff}}(\mathbf{r})$, but without any two-body interaction, i.e.

$$\frac{\partial T_0(\rho)}{\partial \rho} + V_{\text{eff}}(\mathbf{r}) = \mu, \tag{4.29}$$

we see that the two problems are identical provided that

$$V_{\text{eff}}(\mathbf{r}) = v_{\text{ext}}(\mathbf{r}) + U(\mathbf{r}) + \frac{\partial E_{xc}(\rho)}{\partial \rho}. \tag{4.30}$$

Therefore, the solution of equation (4.29) can be found simply by solving the single-particle equation for the non-interacting particles:

$$\left(-\frac{\vec{\nabla}^2}{2m} + V_{\text{eff}}(\mathbf{r}) \right) \varphi_i(\mathbf{r}) = \epsilon_i \varphi_i(\mathbf{r}), \tag{4.31}$$

which yields

$$\rho(\mathbf{r}) = \sum_{i=1}^{N} |\varphi_i(\mathbf{r})|^2. \tag{4.32}$$

The constraint (4.30) is fulfilled by a self-consistent procedure. Finally, one obtains the density and energy of the ground state, and all quantities related to these two. In particular, to compute the energy one uses

$$\sum_i \epsilon_i = \sum_i \langle \varphi_i | -\frac{\vec{\nabla}^2}{2m} + V_{\text{eff}}(\mathbf{r}) | \varphi_i \rangle = T_0(\rho) + \int d\mathbf{r} \rho(\mathbf{r}) V_{\text{eff}}(\mathbf{r}) \tag{4.33}$$

and

$$E = \sum_i \epsilon_i - \frac{1}{2} \int d\mathbf{r} \rho(\mathbf{r}) U(\mathbf{r}) + E_{xc}(\rho) - \int d\mathbf{r} \rho(\mathbf{r}) \frac{\partial E_{xc}(\rho)}{\partial \rho}. \tag{4.34}$$

From the numerical point of view, the solution of the Kohn–Sham equations (4.30) and (4.31) is much simpler than that of the HF equations, since, contrary to the HF potential, the effective potential is local.

Note that, contrary to the HF theory, in the density functional theory the single-particle wavefunctions and energies have no physical meaning, but are rather just

mathematical tools through which the physical quantities, ρ and the energy, are calculated. In particular, the occupied single-particle energies do not represent the physical energies required to excite the particles to the continuum.

The physical excitation energies $\hat{\epsilon}_i$ are the solutions of the Dyson equation:

$$-\frac{\vec{\nabla}^2}{2m}\hat{\varphi}_i(\mathbf{r}) + \int d\mathbf{r}'\Sigma(\mathbf{r},\mathbf{r}';\hat{\epsilon}_i)\hat{\varphi}_i(\mathbf{r}') = \hat{\epsilon}_i\hat{\varphi}_i(\mathbf{r}),\qquad(4.35)$$

where $\Sigma(\mathbf{r},\mathbf{r}';\hat{\epsilon})$ is the non-local self-energy operator. This operator is clearly different from the local operator $V_{\text{eff}}(\mathbf{r})$ of the Kohn–Sham equations, and contrary to the real eigenvalues ϵ_i, the $\hat{\epsilon}_i$ of equation (4.35) are in general complex, which reflects the finite lifetime of the ionized states. There are examples showing that the real parts of ϵ_i and $\hat{\epsilon}_i$ differ as well.

However, there exists a very important special case, i.e. that in which N is made to tend to infinity. In this case, it is possible to show that the highest-energy occupied KS eigenvalue ϵ_N equals the true chemical potential $\mu = \hat{\epsilon}_N$. For the density functional theory, this is the analogue of the Koopmans theorem (Koopmans 1933).

4.5   The Local Density Approximation for the Exchange-Correlation Energy

For a system with slowly varying density, the local density approximation can be made:

$$E_{xc}(\rho) = \int \epsilon_{xc}(\rho(\mathbf{r}))\rho(\mathbf{r})d\mathbf{r},\qquad(4.36)$$

where $\epsilon_{xc}(\rho(\mathbf{r}))$ is the exchange-correlation energy per particle of the uniform system having density ρ. We have

$$\epsilon_{xc}(\rho(\mathbf{r})) = \epsilon_x(\rho(\mathbf{r})) + \epsilon_c(\rho(\mathbf{r})).\qquad(4.37)$$

For electron systems, the exchange energy per particle as a function of density is given by (2.39). For example, in $2D$ we have $\epsilon_x = -4/3\sqrt{2\rho/\pi}$. The best correlation energy per particle is surely the one given by the Monte Carlo calculations of Ceperley and coworkers. The calculated numerical values at different r_s, are fitted by Padè approximants which, in the two-dimensional case taken as an example, are of the type

$$\epsilon_c(r_s,\xi) = a_0\frac{1+a_1x}{1+a_1x+a_2x^2+a_3x^3},\qquad(4.38)$$

with $x = (r_s)^{1/2}$ and $r_s = (\pi\rho)^{-1/2}$. This Padè form behaves as $\sim a + br_s$ for $r_s \to 0$, which is the correct high-density expansion, and has the asymptotic form

$$\epsilon_c \sim \frac{a}{r_s} + \frac{b}{r_s^{3/2}} + \frac{c}{r_s^2} \qquad (4.39)$$

for $r_s \to \infty$. The best fit a_i coefficients for the correlation energies for the normal ($\xi = 0$) and polarized ($\xi = 1$) fluids are reported in Table 4.1 in Rydberg units (1 atomic unit = 2 Rydberg).

TABLE 4.1

	$\xi = 0$	$\xi = 1$
a_0	−0.3568	−0.0515
a_1	1.1300	340.5813
a_2	0.9052	75.2293
a_3	0.4165	37.0170

Most of the calculations with the Kohn–Sham equations were carried out under the local density approximation, which produces surprisingly good results even in the cases where the density does not change slowly. The quality of the *LDA* can be appreciated from the results of Table 2.1 and Fig. 2.7, where the results of this approach for the energies and densities, are compared to those of Monte Carlo, *HF* and *BHF*, for metal clusters and quantum dots. The *LDA* also produces very good results for the binding energy of atoms and diatomic molecules, and for the cohesion energies of metals (for an exhaustive discussion see Lundqvist and March 1983).

4.6 The Local Spin Density Approximation (*LSDA*)

The formalism of density functional shows that, in principle, it is possible to determine the total energy by using a functional which depends only on density, and not on spin density. However, the task of determining a good approximation for the exchange-correlation energy, is much simpler if the functional is expressed in terms of the spin densities. For electron systems, this is the simplest way of fulfilling the demand that high-spin states tend to be energetically favored (Hund's rule). Contrary to *LDA*, the *LSDA* approach obeys Hund's rule and gives results in good agreement with Monte Carlo. This is shown in Table 2.4 and Figs. 2.6–2.8 and 4.1, where the energies and densities of this approach are compared to those of Monte Carlo for metal clusters and quantum dots.

The *LSDA* approximation can be expressed as

$$E_{xc}^{LSDA} = \int \epsilon_{xc}(\rho(\mathbf{r}), \xi(\mathbf{r}))\rho(\mathbf{r})d\mathbf{r}, \qquad (4.40)$$

where $\epsilon_{xc}(\rho(\mathbf{r}), \xi(\mathbf{r}))$ is the exchange-correlation energy per particle of a homogeneous, spin-polarized system with spin-up and spin-down densities $\rho_+(\mathbf{r})$ and $\rho_-(\mathbf{r})$,
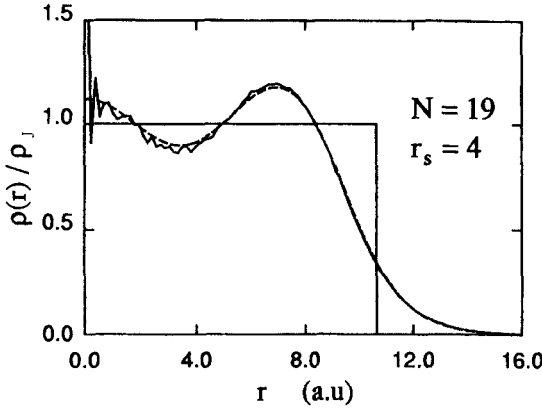
Fig. 4.1   Electronic density profiles of the sodium cluster with 19 electrons in *LSDA* (dashed line), and in variational Monte Carlo (full line) (Ballone et al. 1992). The square curve shows the jellium density ρ_j.

respectively, and $\xi = (\rho_+ - \rho_-)/\rho$ is the spin polarization. The parametrization most widely used in the literature for the exchange-correlation energy is that of Tanatar and Ceperley (1988) of equation (4.38) in $2D$, and that of Ceperley and Alder (1980) in $3D$ for the non-polarized ($\xi = 0$) and ferromagnetic ($\xi = 1$) cases. For intermediate polarizations one uses (von Barth and Hedin 1972):

$$\epsilon_{xc}(\rho, \xi) = \epsilon_{xc}(\rho, 0) + f(\xi)[\epsilon_{xc}(\rho, 1) - \epsilon_{xc}(\rho, 0)]. \tag{4.41}$$

The function $f(\xi)$ is the same that, used in (4.41) for the exchange energy alone, reproduces the exact calculation of equations (2.43) and (2.44), i.e. we have

$$f(\xi) = \frac{(1 + \xi)^{3/2} + (1 - \xi)^{3/2} - 2}{2^{3/2} - 2} \qquad \text{(in } 2D\text{)} \tag{4.42}$$

and

$$f(\xi) = \frac{(1 + \xi)^{4/3} + (1 - \xi)^{4/3} - 2}{2^{4/3} - 2} \qquad \text{(in } 3D\text{)}. \tag{4.43}$$

Like in the case of unpolarized systems, from equation (4.27), with $E_{xc} = E_{xc}^{LSDA}$, we can derive a set of self-consistent equations, by treating the single-particle kinetic-energy functional T_0 exactly. The following set of coupled equations for spin-up and spin-down particles is obtained:

$$\left\{ -\frac{\vec{\nabla}^2}{2m} + v_{\text{ext}}(\mathbf{r}) + \int d\mathbf{r}' \rho(\mathbf{r}') v(|\mathbf{r} - \mathbf{r}'|) + v_{xc}(\mathbf{r}) + \sigma W_{xc}(\mathbf{r}) \right\} \varphi_{i,\sigma}(\mathbf{r})$$

$$= \epsilon_{i,\sigma} \varphi_{i,\sigma}(\mathbf{r}), \tag{4.44}$$

where $\sigma = \pm 1$, and

$$v_{xc}(\mathbf{r}) = \frac{\partial E_{xc}(\rho, m)}{\partial \rho(\mathbf{r})} = \frac{\partial \rho \epsilon_{xc}(\rho, \xi)}{\partial \rho(\mathbf{r})}, \qquad W_{xc}(\mathbf{r}) = \frac{\partial E_{xc}(\rho, m)}{\partial m(\mathbf{r})} = \frac{\partial \epsilon_{xc}(\rho, \xi)}{\partial \xi(\mathbf{r})}, \quad (4.45)$$

and

$$\rho(\mathbf{r}) = \sum_{\sigma} \rho_{\sigma}(\mathbf{r}), \qquad m(\mathbf{r}) = \rho_+ - \rho_-, \qquad \rho_{\sigma}(\mathbf{r}) = \sum_{i=1} |\varphi_{i,\sigma}(\mathbf{r})|^2 . \quad (4.46)$$

The $LSDA$ theory was applied very successfully to atoms, molecules and metal clusters with non-zero spin and thus non-zero magnetization. An exhaustive description of the results obtained in these cases can be found in Lundqvist and March (1983), and Jones and Gunnarsson (1989).

The theory was also employed to calculate the magnetic susceptibility χ_{σ} of paramagnetic metals. To do this one has to solve equations (4.44) in the presence of a weak magnetic field B which introduces a further term $\mu_0 B \sigma$ in (4.44), where $\mu_0 = e\hbar/2mc$ is Bohr's magneton, and then calculate the total magnetization m [see also Eq. (1.110)]:

$$m = \frac{\chi_{\sigma} B}{L^D} . \quad (4.47)$$

A method which is equivalent to the solution of the $LSDA$ equations in a magnetic field, is that of calculating the linear response function for the spin density operator $\hat{\rho} = \sum_i e^{i\mathbf{q} \cdot \mathbf{r}_i} \sigma_i^z$, by using the time-dependent form of the $LSDA$ theory (see Section 8.9.1), and then computing the static response in the limit of zero transfer momentum q. In this way we find ($\chi_{\sigma} = \mu_0 \chi^{m,m}$ of Section 8.91) in atomic units:

$$\chi_{\sigma} = \frac{\mu_0 \chi_0}{1 - \frac{F_0^a}{L^D} \chi_0} , \quad (4.48)$$

where $F_0^a = \frac{\partial^2 E_{xc}(\rho, m)}{\partial m^2}|_{m=0}$ and χ_0 is the static response of the free electron gas in the $q \to 0$ limit:

$$\frac{\chi_0}{L^D} = \begin{cases} -mk_F/\pi^2 & \text{for D=3} \\ -m/\pi & \text{for D=2} \\ -2m/(\pi k_F) & \text{for D=1} \end{cases} . \quad (4.49)$$

From equations (4.48) and (4.49), by using the expressions for the exchange energies of the partially polarized electron gas of Chapter 2, we find for the spin-susceptibility of the electron gas:

$$\frac{\chi_{\sigma}}{\mu_0 \chi_0} = \begin{cases} 1 - (2/3\pi^2)^{2/3} r_s + 3(4/9\pi)^{2/3} r_s^2 (\partial^2 \epsilon_c/\partial \xi^2)_{\xi=0} & \text{for } D = 3 \\ 1 - (\sqrt{2}/\pi) r_s + r_s^2 (\partial^2 \epsilon_c/\partial \xi^2)_{\xi=0} & \text{for } D = 2 \\ 1 + (8r_s^2/\pi^2)(\partial^2 \epsilon_{xc}/\partial \xi^2)_{\xi=0} & \text{for } D = 1 \end{cases} \quad (4.50)$$

In Table 4.2 we compare the results of (4.50) with the correlation energy obtained from Monte Carlo calculations, and the ξ dependence of (4.41) with the results of

the variational calculation of Vosko et al. (1975) as well as with the experimental results for alkali metals which, in nature, are the closest realization of the three-dimensional interacting electron gas.

TABLE 4.2

metal	variational	response	Exp.
Na	1.62	1.59	1.65
K	1.79	1.78	1.70
Rb	1.78	1.87	1.72
Cs	2.20	1.99	$1.76 - 2.24$

As can be seen from this table, there is a rather good agreement between theory and experiment.

4.7   Inclusion of Current Terms in *DFT* (*CDFT*)

The *LSDA* formalism was extended by Vignale and Rasolt (1987, 1988) who included, in the exchange-correlation energy, terms depending on the strength of the magnetic field applied to the system. This theory, which is known as the "current density functional theory" (*CDFT*), provides a method for describing a system of interacting electrons in a gauge field.

The most important case of application of the *CDFT* theory concerns quantum dots in a magnetic field. In this case one has N electrons moving in the $z = 0$ plane where they are confined by a circularly symmetric potential $v_{ext}(r)$ with $r = \sqrt{x^2 + y^2}$. A constant magnetic field B is applied normal to the plane, which in the symmetric gauge is described by the vector potential $\mathbf{A} = \frac{B}{2}(-y, x, 0)$. By introducing the cyclotron frequency $\omega_c = eB/mc$, we can write the *CDFT* grand potential as (see also Section 2.6) $G = E - TS - \mu N$ by adding to the total energy (we use effective atomic units with Boltzmann's constant $K = 1$):

$$E = \frac{1}{2} \int d\mathbf{r}\, \tau(\mathbf{r}) + \frac{\omega_c}{2} \int d\mathbf{r}\, r\, j_p(\mathbf{r}) + \frac{1}{8}\omega_c^2 \int d\mathbf{r}\, r^2\, \rho(\mathbf{r})$$

$$+ g^* \mu_0 B \sum_i f_i\, s_{z_i} + \int d\mathbf{r}\, v_{ext}(\mathbf{r})\rho(\mathbf{r})$$

$$+ \frac{1}{2} \int \int d\mathbf{r}\, d\mathbf{r}'\, \frac{\rho(\mathbf{r})\rho(\mathbf{r}')}{|\mathbf{r} - \mathbf{r}'|} + \int d\mathbf{r}\, \mathcal{E}_{xc}(\rho(\mathbf{r}), \xi(\mathbf{r}), \mathcal{V}(\mathbf{r})), \qquad (4.51)$$

the temperature times the total entropy S given by

$$S = -\sum_i [f_i \ln f_i + (1 - f_i) \ln(1 - f_i)], \qquad (4.52)$$

and the electron chemical potential μ times the number of electrons $N = \sum_i f_i$. The introduction of temperature in the *CDFT* formalism is necessary in the case

of non-vanishing magnetic field, even when one describes the system at zero temperature. This is due to the fact that at zero temperature, for some values of B (see Chapter 5) the energy levels near to the Fermi surface are very close in energy and it is impossible to achieve good convergence of the Kohn–Sham equations other than by first obtaining convergence at finite temperature, and by subsequent gradual lowering of the temperature itself, until convergence of the zero-temperature solution is attained.

The second and third terms of (4.51) originate from the modified kinetic energy term of the Hamiltonian of the electrons with charge $-e$ in the magnetic field $(\mathbf{p}^2/2 \to (\mathbf{p}+e/c\mathbf{A})^2/2)$. The fourth term represents the Zeeman interaction energy between the magnetic moment of the electrons (whose effective gyromagnetic factor is g^*) and the external magnetic field. In equations (4.51), (4.52) s_{z_i} is the z components of the spin ($\pm 1/2$), and f_i is the occupation number of the i-th single-particle level. The density $\rho(\mathbf{r})$, the kinetic energy density $\tau(\mathbf{r})$ and the paramagnetic current density $\mathbf{j}_p(\mathbf{r})$ are all defined in terms of the single-particle occupation numbers f_i and wavefunctions ϕ_i as follows:

$$\rho(\mathbf{r}) = \sum_i f_i \mid \phi_i(\mathbf{r}) \mid^2 \tag{4.53}$$

$$\tau(\mathbf{r}) = \sum_i f_i \mid \nabla\phi_i(\mathbf{r}) \mid^2 \tag{4.54}$$

$$\mathbf{j}_p(\mathbf{r}) = j_p(r)\hat{e}_\theta = -\frac{1}{r}\sum_i f_i l_i \mid \phi_i(\mathbf{r}) \mid^2 \hat{e}_\theta , \tag{4.55}$$

where $\hat{e}_\theta$ is the azimuthal unit vector.

The exchange-correlation energy in (4.51) is written in the local density approximation (LDA):

$$E_{xc} = \int d\mathbf{r}\rho(r)\epsilon_{xc}[\rho(r), \xi(r), \mathcal{V}(r)] , \tag{4.56}$$

and is a functional of the density ρ, of the local spin polarization ξ and of the local vorticity $\mathcal{V}(r)$:

$$\mathcal{V}(r) = \mathcal{V}(r)\,\hat{e}_z = -\frac{c}{er}\frac{\partial}{\partial r}(r\,\frac{j_p}{\rho})\hat{e}_z . \tag{4.57}$$

Following Ferconi and Vignale's (1994) indications, we take

$$\epsilon_{xc}[\rho, \xi, \mathcal{V}] = \frac{1}{1+\nu^4}\epsilon_{xc}^{LWM}[\rho, \nu] + \frac{\nu^4}{1+\nu^4}\epsilon_{xc}^{TC}[\rho, \xi] , \tag{4.58}$$

where $\nu = 2\pi\mathcal{L}^2\rho$ is the local filling factor (see Chapter 5), and $\mathcal{L}$ is the magnetic length $\mathcal{L}^2 = \hbar c/eB = \hbar/m\omega_c$. This expression is a Padè interpolation between Levesque, Weis and MacDonald's (1984) results for the exchange-correlation energy

at high magnetic field, $\epsilon_{xc}^{LWM}[\rho, \nu]$, and those of Tanatar and Ceperley at zero magnetic field, $\epsilon_{xc}^{TC}[\rho, \xi]$ [see Eqs. (4.41),(4.42)].

In the LDA, the vorticity $\mathcal{V}$ is taken to be proportional to the applied magnetic field $\mathcal{V} = -e\mathbf{B}/mc$, which allows the filling factor to be related to the vorticity as follows:

$$\nu = 2\pi\rho\frac{\hbar}{m}\frac{1}{\mathcal{V}}. \tag{4.59}$$

This completely defines the $CDFT$ functional.

In order to obtain the single-particle wavefunctions $\phi_i(\mathbf{r})$ and the occupation numbers f_i, one needs to minimize G under the constraint that the single-particle wavefunctions are orthonormal. By minimizing with respect to the single-particle wavefunctions one gets the Kohn–Sham (KS) equations:

$$\left[-\frac{1}{2}\left(\frac{d^2}{dr^2} + \frac{1}{r}\frac{d}{dr} - \frac{l^2}{r^2} \right) - \frac{\omega_c}{2}l + \frac{1}{8}\omega_c^2 r^2 + v_{\text{ext}}(r) \right.$$

$$\left. + \int d\mathbf{r}'\, \frac{\rho(\mathbf{r}')}{|\mathbf{r} - \mathbf{r}'|} - \frac{e}{c}l\frac{A_{xc}(r)}{r} + V_{xc\sigma}(r) + \frac{1}{2}g^*\mu_0 B\sigma \right] u_{nl\sigma} = \epsilon_{nl\sigma}u_{nl\sigma}\,, \quad (4.60)$$

where we used the circular symmetry of the wavefunctions

$$\phi_i(\mathbf{r}) = e^{-\imath l\theta}u_{nl\sigma}(r)\,, \tag{4.61}$$

with $\sigma = \pm 1$, $n = 0, 1, 2, \ldots$, and $l = 0, \pm 1, \pm 2, \pm 3, \ldots$. These wavefunctions are eigenstates of l_z [see also Eq. (2.29)] with eigenvalue $-l$. At $B \neq 0$, the single-particle level i is non-degenerate, and in the above expression we used the notation $i \equiv \{n, l, \sigma\}$.

In equation (4.60) one has

$$V_{xc\sigma}(r) = \left. \frac{\delta E_{xc}(\rho, \xi, \mathcal{V})}{\delta\rho_\sigma} \right|_{\rho_{-\sigma}, \mathcal{V}} - \frac{e}{c}\mathbf{A}_{xc}(r) \cdot \frac{\mathbf{j}_p}{\rho}\,, \tag{4.62}$$

where $\mathbf{A}_{xc}$ is the exchange-correlation vector potential:

$$\frac{e}{c}\mathbf{A}_{xc}(r) = \frac{e}{c}A_{xc}\hat{e}_\theta = \frac{c}{e\rho}\frac{d}{dr}\left(\rho\left.\frac{\delta\mathcal{E}_{xc}}{\delta\mathcal{V}}\right|_{n,\xi} \right)\hat{e}_\theta\,. \tag{4.63}$$

By minimizing G with respect to f_i, and using the KS equations, one obtains the occupation numbers:

$$f_i = \frac{1}{1 + e^{(\epsilon_i - \mu)/T}}\,. \tag{4.64}$$

Next, the chemical potential is determined by normalization:

$$N = \sum_i f_i = \sum_i (1 + e^{(\epsilon_i - \mu)/T})^{-1}\,.$$

As can be seen by comparing the present Section with Section 2.6, the finite-temperature treatment is formally the same for HF and for the density functional theories.

The KS differential equations (4.60) and the normalization condition were solved in a self-consistent way by several authors (Ferconi and Vignale 1994; Lipparini et al. 1997; Pi et al. 1998; Steffens et al. 1998). The numerical results will be reported in the next Chapter, which treats quantum dots under magnetic field in the different theories.

4.8 Ensemble Density Functional Theory

The density functional theory has been generalized to treat the case of degenerate Kohn–Sham ground states, producing the Ensemble DFT ($EDFT$) (Dreizler and Gross 1995). In fact, there are cases in which the true density of the system cannot be represented by a single Slater determinant of single-particle wavefunctions. For example, in the case where the KS orbitals are degenerate at the Fermi energy (which coincides with the highest single-particle energy of the occupied orbitals), so that there exists ambiguity as to how the degenerate orbitals should be occupied. As mentioned in the previous Section, this case is realized for KS orbitals of quantum dots in the presence of a strong magnetic field. A way of tackling the problem is that of carrying out finite-temperature calculations, and then lowering the temperature gradually; an alternative method is to use the $EDFT$, that we describe in the following.

$EDFT$ is the theory that describes the true density of the system as an ensemble of Slater determinants of KS orbitals. While it is possible to show that the representation is rigorous, it is not possible to show how the degenerate KS orbitals at the Fermi energy should be occupied, i.e. there exists no practical calculation procedure for the $EDFT$ theory. Only recently has a practical generalization of $EDFT$ been proposed and applied to the fractional quantum Hall effect. In what follows we briefly describe such method (Heinonen et al. 1995).

In $EDFT$, any physical density $\rho(\mathbf{r})$ can be represented by

$$\rho(\mathbf{r}) = \sum_{mn} f_{mn} |\phi_{mn}(\mathbf{r})|^2 ,$$

where the f_{mn} are occupation numbers which obey $0 \leq f_{mn} \leq 1$, and the orbitals follow the generalized KS equation

$$H^{KS} \phi_{mn}(\mathbf{r}) = \epsilon_{mn} \phi_{mn}(\mathbf{r}) , \tag{4.65}$$

where H^{KS} is the effective KS Hamiltonian which depends on the various densities. The problem lies in the determination of the KS orbitals and of their occupation numbers in the presence of degeneracy. In the scheme proposed by Heinonen et al., we start from a given set of input orbitals and occupation numbers, and iterate the

system N_{eq} times using the KS scheme. N_{eq} is large enough to ensure that the density is close to the final density after N_{eq} iterations (in practice, 20–40 iterations). If it were possible to represent the system density by a single Slater determinant of KS orbitals, the calculation would be finished. However, in the system there are many degenerate or quasi-degenerate orbitals at the Fermi energy. After each iteration step, the KS scheme chooses to occupy the N_{eq} orbitals with the lowest eigenvalues, which corresponds to building up with these orbitals a Slater determinant different from all the others. However, there are small density fluctuations between successive iteration steps, which cause a different occupation of these degenerate (or quasi-degenerate) orbitals after each step. This corresponds to building up different Slater determinants after each step, and the occupation numbers f_{mn} of these orbitals are either 0 or 1 after each step, nearly at random. This means that the calculation will never converge. In any case, the averaged occupations, i.e. the occupation numbers as averaged over many iteration steps, are well defined and tend towards a well-defined value. As a consequence, one uses these average occupation numbers to build up an ensemble by storing average occupations $\langle f_{mn} \rangle$ after the first N_{eq} iteration steps:

$$\langle f_{mn} \rangle = \frac{1}{(N_{it} - N_{eq})} \sum_{i=N_{eq}+1}^{N_{it}} f_{mn,i}, \qquad (4.66)$$

where $f_{mn,i}$ is the occupation number (either 0 or 1) of orbital ϕ_{mn} after the i-th step; this is used to build up the density.

Basically, this algorithm takes a different degenerate (or quasi degenerate) Slater determinant after each iteration step, and all of these determinants are equally weighted in the ensemble.

Clearly, this scheme reduces to the KS one for systems whose density can be represented by a single Slater determinant of KS orbitals. Moreover, it can be verified numerically that the finite-temperature version of the method reproduces the finite-temperature $CDFT$ distributions down to extremely low temperatures (see Section 5.6).

4.9 DFT for Strongly Correlated Systems: Nuclei and Helium

In the case of strongly correlated systems like nuclei and liquid ^{3}He, dynamic correlations are responsible for nonlocal effects which result in effective masses m^* which are very different from the bare mass m, and depend on the system density. For example, for liquid ^{3}He one finds that m^* is strongly density-dependent and equal to about three times the bare mass at saturation density (zero-pressure value).

Nonlocal effects of this kind are predicted in the Brueckner–Hartree–Fock theory, which is the only applicable "mean field" theory because the nucleon-nucleon and

atom-atom interactions cannot be treated in HF and one needs to find effective interactions (see Chapter 3).

As can be seen from equation (3.63), if we expand the effective interaction as was done in Section 3.6, the energy not only depends on the density ρ, but also on the kinetic energy density τ and on terms in $\nabla\rho$. Moreover, expression (3.63) generates, in the BHF equations (3.64), an effective mass

$$m^* = \frac{m}{1 + 2am\rho}, \tag{4.67}$$

with $a = -t_1$. These considerations suggested, for nuclei with the same number of neutrons (N) and protons (Z) and closed shells (Vautherin and Brink 1972) and for liquid helium (Stringari 1984; Dalfovo 1989), the use of density functionals of the type

$$E[\rho, \tau] = \int \left\{ \frac{\tau}{2m^*} + \frac{1}{2}b\rho^2 + d(\nabla\rho)^2 + \frac{1}{2}c\rho^{2+\gamma} \right\} d\mathbf{r}, \tag{4.68}$$

where the last term is added to keep into account more-than-two-body correlations which are neglected in the BHF theory, but are important for nuclei and helium. In the case of ^{4}He, more refined functionals have been introduced, which take into account finite-range effects for both local and non-local parts. For a discussion of the results that can be attained by these functionals we refer the reader to the paper by Dalfovo et al. (1995).

In the case of nucleons, the effective mass is parametrized exactly as in (4.67), while for ^{3}He one uses

$$m^* = \frac{m}{(1 - \frac{\rho}{\rho_c})^2}, \tag{4.69}$$

where ρ_c is a parameter. In the case of liquid ^{4}He, in the functional (4.68) it is necessary to take $m^* = m$ and $\tau = (\nabla\rho)^2/4\rho$, which is the correct expression for the kinetic energy density for Boson systems (see also Section 2.3).

In the case of nuclei the functional (4.68) is next generalized to take into account the spin-orbit interaction, Coulomb interaction between protons, and the isospin degrees of freedom when $N \neq Z$ (see Section 4.10).

The parameters that appear in the effective mass, as well as b, d, c and γ, are fitted to reproduce the values of some known experimental quantities and are reported in Table 4.3 for the various systems ($SIII$ is the effective interaction of the nuclei).

TABLE 4.3

Sist.	a	ρ_c	b	c	d	γ
SIII	44.38	–	−846.56	1750	62.97	1
³He	–	0.0406	−683.0	1.405057×10^6	2222	2.1
⁴He	–	–	−888.81	1.04554×10^7	2383	2.8

The parameter values in the table are in MeV fm^5 for a and d, in MeV fm^3 for b and in MeV fm^6 for c in the case of the *SIII* for the nuclei; for ³He and ⁴He, ρ_c is in Å^{-3}, b in °K Å^3, c in °K Å$^{3(1+\gamma)}$ and d in °K Å^5.

From equation (4.68), for homogeneous Fermi systems we obtain the following form for the energy per particle

$$\frac{E}{N} = \frac{3}{5} \frac{(3\pi^2)^{2/3}}{2m^*(\rho)} \rho^{2/3} + \frac{1}{2}b\rho + \frac{1}{2}c\rho^{1+\gamma}, \qquad (4.70)$$

where $\rho = vk_F^3/6\pi^2$ with $v = 2$ in the case of ³He and $v = 4$ in the case of nucleons, while for ⁴He the first term vanishes identically and the density is a constant. From the above expression we derive the pressure

$$\frac{P}{\rho} = \rho \frac{\partial E/N}{\partial \rho}, \qquad (4.71)$$

and the compressibility

$$\frac{1}{K\rho} = \frac{\partial P}{\partial \rho} = \frac{\partial}{\partial \rho} \rho^2 \frac{\partial E/N}{\partial \rho}. \qquad (4.72)$$

The saturation density ρ_0 is determined by putting $P = 0$ in (4.71). By inserting $\rho = \rho_0$ in equations (4.70) and (4.72), we obtain the binding energy and the compressibility at $P = 0$, which are to be compared with the experimental data in order to extract the values of some of the parameters in Table 4.3. The other values are obtained by fitting, in the case of helium the surface tensions, and in the case of nucleons some properties of magic nuclei. The obtained numerical values for the saturation densities, binding energy per particle, compressibilities, and effective masses of the homogeneous systems, and the surface tensions σ of the semi-infinite systems, are reported in Table 4.4. For the homogeneous and semi-infinite nuclear matter, the values reported in the table refer to systems with $N = Z$.

TABLE 4.4

Sist.	ρ_0	E/N	$(K\rho_0)^{-1}$	m^*/m	σ
SIII	0.145	−15.85	355.4/9	0.763	1.07
³He	1.6347×10^{-2}	−2.49	12.1	2.8	0.113
⁴He	2.1836×10^{-2}	−7.15	27.2	1	0.274

The values of the parameters in the table are in fm^{-3} for ρ_0, in MeV for E/N and $(K\rho_0)^{-1}$, and in Mev fm^{-2} for σ in the case of the $SIII$ parametrization for nuclei; on ^{3}He and ^{4}He, ρ_0 is in $Å^{-3}$, E/N and $(K\rho_0)^{-1}$ in $°K$, and σ in $°K\ Å^{-2}$.

The equations of state for the ^{3}He and ^{4}He systems, predicted from Eq. (4.71), are reported in Figs. 4.2 and 4.3 respectively, together with the experimental data of Wheatley (1975) and Watson et al. (1969).

As can be seen from these figures, there is good agreement between theory and experiment over the whole pressure range. The same is true for compressibility.

The surface tension may be calculated starting from the functional (4.68), using the Wilets method; the latter, in the case of Fermion systems, uses the extended Thomas–Fermi approximation for the kinetic energy density:

$$\tau = \frac{3}{5}(3\pi^2)^{2/3}\rho^{5/3} + \beta\frac{(\nabla\rho)^2}{\rho} + \delta\nabla^2\rho\,, \tag{4.73}$$

where $\beta = 1/18$ and $\delta = 1/3$. In the homogeneous limit, τ reduces to the Thomas–Fermi term (4.14). Expression (4.73) is deduced by a semiclassical expansion of the energy of a Fermion system (Ring and Schuck 1980). The surface tension of the semi-infinite system in the $z \leq 0$ half space with a free surface is written as

$$\sigma = \int_{-\infty}^{+\infty} [\epsilon(\rho, \rho') - \mu\rho]dz\,, \tag{4.74}$$

where z is the co-ordinate perpendicular to the system, ρ' is the density derivative with respect to z (in the other directions, the density is a constant and equals the bulk one), and

$$\epsilon(\rho, \rho') = h(\rho) + \frac{1}{2m^*(\rho)}\beta\frac{(\rho')^2}{\rho} + d_1(\rho')^2\,, \tag{4.75}$$

with

$$h(\rho) = \frac{1}{2m^*(\rho)}\frac{3}{5}(3\pi^2)^{2/3}\rho^{5/3} + \frac{1}{2}b\rho^2 + \frac{1}{2}c\rho^{2+\gamma} \tag{4.76}$$

and

$$d_1 = d - \frac{\delta}{2}\left(\frac{\partial}{\partial\rho}\frac{1}{m^*(\rho)}\right)\,. \tag{4.77}$$

The equilibrium density, which is used to calculate the surface tension through equation (4.74), is found using Euler equation

$$\frac{\partial}{\partial\rho(z)}\int_{-\infty}^{+\infty} [\epsilon(\rho, \rho') - \mu\rho]dz = 0\,. \tag{4.78}$$

Clearly, the Wilet method can be used in the case of ^{4}He as well using, where one replaces in place of equation (4.73), the expression $\tau = (\rho')^2/4\rho$, i.e. the right one for the kinetic energy density of Bosons. The surface tension of metal surfaces has
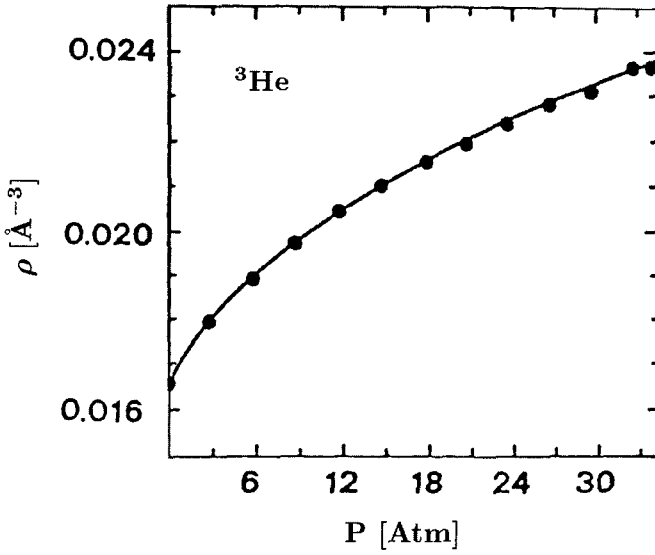
Fig. 4.2   Equation of state for liquid ^{3}He. The full line is from Eq. (4.71) and the experimental points are taken from Wheatley (1975).
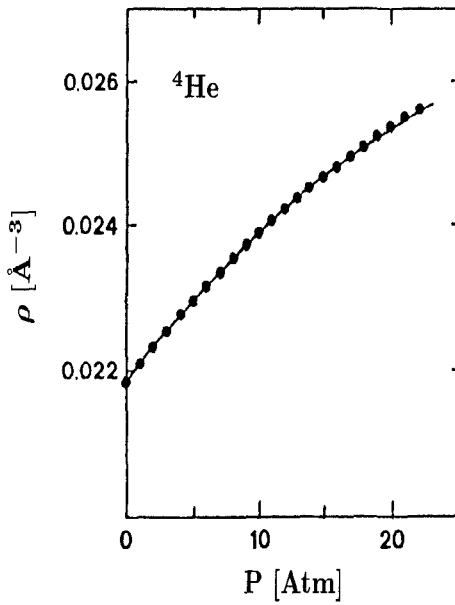

Fig. 4.3   Equation of state of ^{4}He. The full line is deduced from Eq. (4.71) and the experimental points are taken from Watson et al. (1969).

been studied by Lang and Kohn (1970) within the jellium model and by techniques similar to the previous ones, using the density functional theory.

The Kohn–Sham equations which derive from the functional in (4.68) are written as

$$\left\{ -\vec{\nabla} \frac{1}{2m^*} \cdot \vec{\nabla} + U(\rho, \tau) \right\} \varphi_i(\mathbf{r}) = \varepsilon_i \varphi_i(\mathbf{r}) , \qquad (4.79)$$

where the self-consistent field U is given by

$$U(\rho, \tau) = \frac{1}{2} \tau \frac{\partial}{\partial \rho} \frac{1}{m^*(\rho)} + b\rho - 2d\nabla^2\rho + \frac{1}{2}c(2 + \gamma)\rho^{1+\gamma} . \qquad (4.80)$$

Assuming spherical symmetry, the single-particle states which enter the definition of the various densities of equations (4.79) and (4.80) can be factorized in the form $\varphi_i(\mathbf{r}) = R_{n,l}(r)Y_{l,m}(\theta, \varphi)\chi_{m_s}(\sigma)$ and equation (4.79) turns into a non-linear system of differential equations for the radial part of the wavefunctions, to be solved by iterative self-consistent methods. The calculation is carried out for nuclei and helium clusters, in which the $2(2l + 1)$ degenerate states of the (n, l) level are completely occupied (closed-shell nuclei and clusters) and for which the spherical symmetry of the density and of the average potential is guaranteed. In the case of ^{4}He, the Kohn–Sham equations become a differential equation for the density:

$$-\frac{1}{4m}\nabla^2\rho + \frac{1}{8m}\frac{(\nabla\rho)^2}{\rho} + b\rho^2 - 2d\rho\nabla^2\rho + \frac{1}{2}c(2 + \gamma)\rho^{1+\gamma} = \mu\rho. \qquad (4.81)$$

Equation (4.81) is solved numerically by requiring that the density vanishes at large r values, and that its first derivative is zero at the centre $(r = 0)$. The chemical potential μ is determined by the normalization condition of the density.

Tables 4.5 and 4.6 report the results, relative to different N values, for the binding energy per particle, the chemical potential, the surface thickness t, the

TABLE 4.5

N	$E/N[^\circ K]$	$\mu(N)[^\circ K]$	$r_0(N)$ [Å]	$t(N)$ [Å]	$\rho_0(N)[10^{-2}$ Å$^{-3}]$
8	−0.40	−1.06	4.19	6.7	0.76
20	−1.27	−2.52	3.11	8.8	1.61
40	−2.18	−3.57	2.74	9.0	2.06
70	−2.93	−4.24	2.57	9.2	2.22
112	−3.51	−4.70	2.47	9.3	2.28
168	−3.96	−5.04	2.41	9.3	2.30
240	−4.31	−5.26	2.36	9.3	2.30
330	−4.60	−5.46	2.33	9.3	2.30
728	−5.19	−5.87	2.28	8.8	2.28
∞	−7.15	−7.15	2.22	7.0	2.19

TABLE 4.6

N	$E/N[°K]$	$\mu^-(N)[°K]$	$\mu^+(N)[°K]$	$r_0(N)[\text{Å}]$	$t(N)[\text{Å}]$	$\rho_0(N)[10^{-2}\text{Å}^{-3}]$
20	+0.08	−0.48	−0.15	3.99	8.6	0.85
40	−0.19	−1.04	−0.68	3.13	8.8	1.42
70	−0.50	−1.34	−0.94	2.90	8.8	1.61
112	−0.75	−1.53	−1.13	2.78	9.5	1.69
168	−0.95	−1.60	−1.28	2.69	9.6	1.73
240	−1.11	−1.65	−1.47	2.64	9.5	1.75
330	−1.25	−1.67	−1.63	2.61	9.4	1.75
∞	−2.49	-2.49	−2.49	2.44	8.3	1.65

TABLE 4.7

N	^{4}He $E/N[°K]$	$r_0(N)[\text{Å}]$	^{3}He $E/N[°K]$	$r_0(N)[\text{Å}]$
8	−0.60	—	—	—
20	−1.57	2.77	0.21	—
40	−2.39	2.54	−0.044	3.29
70	−3.03	2.48 − 2.50	−0.28	3.01
112	−3.50	2.43	−0.46	2.89
168	—	—	−0.62	2.78
240	−4.19	2.37	−0.74	2.71
728	−4.94	2.32	—	—

density at the centre ρ_0, and the unit radius defined as

$$r_0(N) = \sqrt{\frac{5}{3}\langle r^2(N)\rangle}N^{-1/3}, \qquad (4.82)$$

where $\langle r^2\rangle$ is the mean square radius for ^{4}He and ^{3}He clusters, respectively. In the case of ^{3}He, μ^- and μ^+ are single particle energies of the highest occupied level and of the lowest non-occupied level, respectively, and coincide with the chemical potential in the limit $N \to \infty$. The surface thickness t is defined as the distance between the points at which the density decreases from 90% to 10% of the central density.

For comparison, in Table 4.7 we report the results of calculations carried out using the variational Monte Carlo method, for the binding energy and the unit radius, and in Figs. 4.4 and 4.5 the densities of two clusters, as obtained with both methods.

Let us first discuss the ^{4}He results. From Table 4.5 and Fig. 4.4 we see that:

- The ^{4}He clusters are bound for all values of N.
- For large N values the surface thickness, the central density and the unit radius, tend to the values which correspond to the semi-infinite matter (i.e. the values in the three last columns of the row labelled ∞). The convergence of the binding
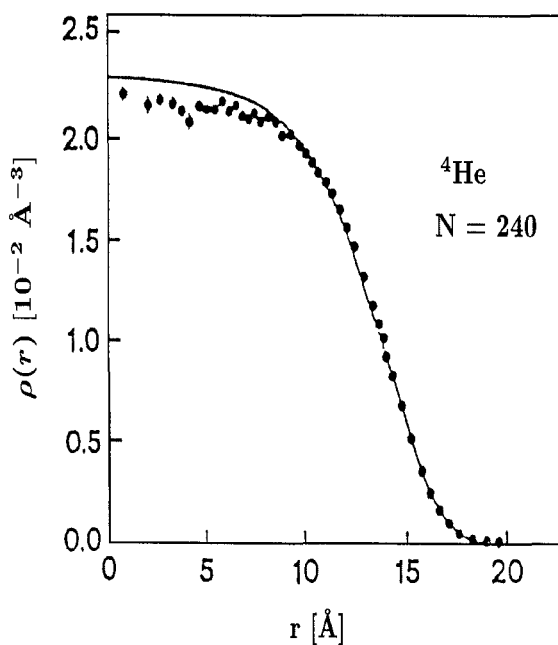
Fig. 4.4   Density profile for a cluster with 240 ^{4}He atoms. The dots refer to the *MC* calculation of Pandharipande et al. (1986).
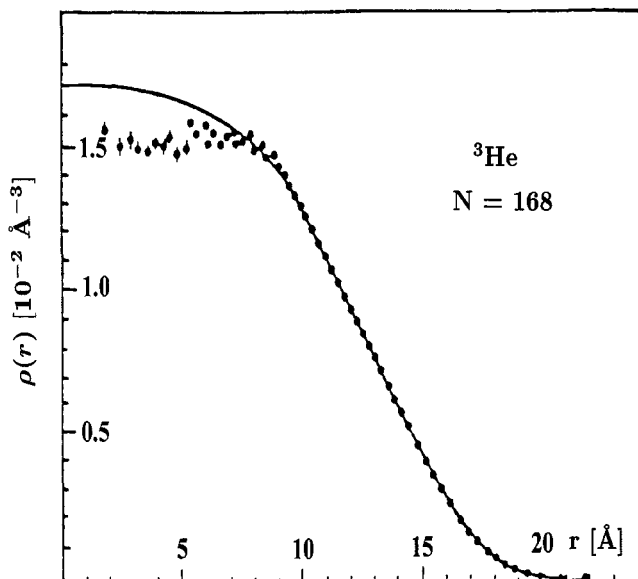

Fig. 4.5   Density profile for a cluster with 168 ^{3}He atoms. The dots refer to the *MC* calculation of Pandharipande et al. (1986).

energy towards the bulk value is quite slow, and can be represented by a mass formula typical of drop models for quantum liquids

$$E(N) = a_v N + a_s N^{2/3} + \left(a_c - \frac{2}{9} a_s^2 \rho_0 K \right) N^{\frac{1}{3}} + a_0 \,, \qquad (4.83)$$

with $a_v = -7.15 \; ^\circ K$, $a_s = 16.95 \; ^\circ K$, $a_c = 10.45 \; ^\circ K$, and $a_0 = 29 \; ^\circ K$.

• The results of density functional method are in good agreement with those of Monte Carlo calculations (Pandharipande et al. 1986).

As from ^{3}He clusters, from the results of Table 4.6 and Fig. 4.5, it emerges that:

• The ^{3}He clusters are bound only for N values larger than $N_{min} \simeq 30$. This result is consistent with the value $N_{min} \simeq 40$ obtained by Monte Carlo calculations of Table 4.7. Clusters with $N < N_{min}$ can exist as metastable states clusters, as long as the chemical potential (which is proportional to the derivative of the energy per particle with respect to N) is negative. The lower limit for metastability is $N \simeq 16$.

• The ^{3}He clusters have a shell structure. The average field has a form that is similar to the potential of a spherical harmonic oscillator (only for very large clusters the surface thickness is small with respect to the radius, and the potential is approximately a square well). The single-particle levels, i.e. the solutions of equations (4.79) and (4.80), turn out to be grouped following the order of the degenerate levels of the harmonic oscillator, and the most bound clusters correspond to the occupation of the respective major shells, i.e. $N = 40, 70, 112, 168, 240, \ldots$ (see also the table in Section 1.3). The gap per particle $(\mu^- - \mu^+)$ for the closed-shell clusters is of the order of 0.2–0.4 $^\circ K$, and decreases as $N^{-1/3}$ for large N values. The gap value depends strongly on the value of the effective mass. The lower the mass, the greater the kinetic contribution to (4.79).

• Contrary to the case of metal clusters (see Section 2.2.1) and of atomic nuclei, the shell structure of ^{3}He clusters does not entail density oscillations due to the filling of single-particle levels. These oscillations are energetically unfavored due to the relatively high value of the surface tension and to the low system compressibility.

• The convergence of the binding energy towards the homogeneous system value can be expressed by the mass formula (4.83) with $a_v = -2.49 \; ^\circ K$, $a_s = 8.42 \; ^\circ K$, $a_c = 5.39 \; ^\circ K$, and $a_0 = -19.8 \; ^\circ K$.

• In the case of ^{3}He as well, the method of density functional yields results in good agreement with the Monte Carlo calculations (Pandharipande et al. 1986).

In Table 4.8 we report the binding energy and the charge radius of some closed-shell nuclei for the $SIII$ parametrization (Beiner et al. 1975), together with the experimental values. The charge radius is defined as

$$r_c(N) = \sqrt{\langle r_c^2(N) \rangle}, \qquad \langle r_c^2(N) \rangle = \frac{1}{N} \int \rho_c(\mathbf{r}) r^2 d\mathbf{r} \,, \qquad (4.84)$$

where $\rho_c(\mathbf{r})$ is the charge density of the nucleus.

TABLE 4.8

Nucleus	E^{exp} [MeV]	E^{SIII} [MeV]	r_c^{exp} [fm]	r_c^{SIII} [fm]
^{16}O	127.6	128.2	2.73	2.69
^{40}Ca	342.1	341.9	3.49	3.48
^{48}Ca	416.0	418.2	3.48	3.53
^{90}Zr	783.9	785.2	4.27	4.32
^{140}Ce	1172.7	1172.4	4.88	–
^{208}Pb	1636.5	1636.6	5.50	5.57

The table shows that the experimental results for the binding energies and the charge radii are very well reproduced by the $SIII$ parametrization, for both light and heavy nuclei. In general, the nuclei have a strong shell structure which is strongly affected by the spin-orbit and isospin terms in the mean field, which for simplicity were omitted in (4.80). These terms are discussed in detail in the papers by Vautherin and Brink (1972) and Beiner et al. (1975), and in the following Section. As in the case of ^{3}He, the value of the effective mass strongly affects the single-particle spectrum, and there exist parametrizations other than the one discussed here, i.e. $SIII$, which reproduce the binding energies and the charge radii as precisely as $SIII$ itself, but which yield rather different single-particle spectra. However, we would like to recall that in theories based on the density functional, the single-particle spectrum is not expected to have physical meaning. The nuclear densities exhibit oscillations due to the filling of single-particle levels; this effect is shown in Fig. 4.6.

Finally, the $SIII$ parametrization produces a mass formula (4.83) with $a_v = -15.849$ MeV, $a_s = 18.8$ MeV, $a_c = 10$ MeV, and $a_0 = -5$ MeV.

4.10 *DFT* for Mixed Systems

The density functional theory has also been used to study the properties of two-component systems. Examples of two-component systems where the DFT has been employed successfully are protons and neutrons in nuclei that we mentioned previously, electron-hole drops in semiconductors, and the ^{3}He–^{4}He mixtures. The DFT for many-component systems can be found in the book edited by Lundqvist and March (1983) and in Baym and Pethick (1978), here we limit ourselves to illustrating the problem taking as a specific examples the ^{3}He–^{4}He mixtures (Dalfovo and Stringari 1985) and nuclei.

Let us start with the ^{3}He–^{4}He mixtures. Let us indicate with

$$\rho = \rho_4 + \rho_3, \quad x = \frac{\rho_3}{\rho}, \tag{4.85}$$

the total system density and the concentration of ^{3}He atoms, respectively. The density functional is set up of requiring that for $x = 0$ and $x = 1$ it coincides with the respective functionals of pure ^{4}He and ^{3}He [Eq. (4.68), with the parameters of
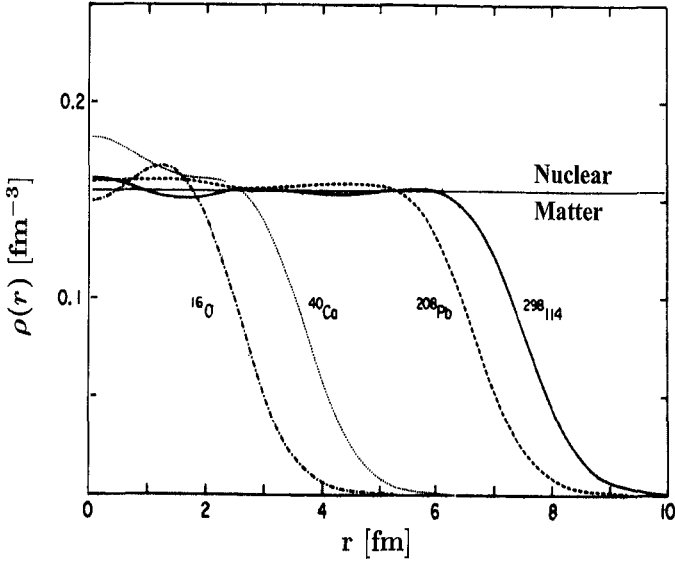
Fig. 4.6   Nuclear density profiles computed by the density functional derived from the *SIII* effective interaction.

Table 4.3]. The addition of a small number of mixed terms accounts for the effective interaction typical of the mixture. The functional is written as

$$E = \int dr \left[\frac{\tau_4}{2m_4} + \frac{1}{2} b_4 \rho_4^2 + d_4 (\nabla \rho_4)^2 + \frac{1}{2} c_4 \rho_4^2 \rho^{\gamma_4} + \frac{\tau_3}{2m_3^*} + \frac{1}{2} b_3 \rho_3^2 + d_3 (\nabla \rho_3)^2 \right.$$

$$\left. + \frac{1}{2} c_3' \rho_3^2 \rho^{\gamma_3} + \frac{1}{2} c_3'' \rho_3^{2+\gamma_3} + b_{34} \rho_3 \rho_4 + c_{34} \rho_3 \rho_4 \rho^{\gamma_{34}} + d_{34} (\nabla \rho_3)(\nabla \rho_4) \right] , \quad (4.86)$$

where

$$m_3^* = \frac{m_3}{(1 - \frac{\rho_3}{\rho_{3c}} - \frac{\rho_4}{\rho_{4c}})^2} . \qquad (4.87)$$

The parameter ρ_{4c} accounts for mass renormalization of ^{3}He atoms due to the excitations induced in the surrounding ^{4}He, and may be determined by the value of the effective mass of a ^{3}He atom in solution, in the $x \to 0$ limit. The parametrization (4.87) turns out to be consistent with the experimental data relative to dilute solutions and yields the correct value of the effective mass of pure ^{3}He. For homogeneous solutions the energy per particle takes the form

$$\frac{E}{N} = \rho^{-1} \left[\frac{1}{2} b_4 \rho_4^2 + \frac{1}{2} c_4 \rho_4^2 \rho^{\gamma_4} + \frac{3}{5} \frac{(3\pi^2)^{2/3}}{2m_3^*} \rho_3^{5/3} + \frac{1}{2} b_3 \rho_3^2 \right.$$

$$\left. + \frac{1}{2} c_3' \rho_3^2 \rho^{\gamma_3} + \frac{1}{2} c_3'' \rho_3^{2+\gamma_3} + b_{34} \rho_3 \rho_4 + c_{34} \rho_3 \rho_4 \rho^{\gamma_{34}} \right] . \qquad (4.88)$$

From this we see that for $\rho = \rho_4$ one obtains again the expression of E/N for pure ^{4}He, while for $\rho = \rho_3$ one obtains again the expression of E/N for pure ^{3}He, provided that $c_3 = c_3' + c_3''$. Five interaction parameters are left to be determined in the functional (4.86). The parameters b_{34}, c_{34} and c_3'' are fitted to reproduce the experimental values at $P = 0$ of the maximum solubility of ^{3}He in ^{4}He at zero temperature, of the chemical potential of ^{3}He in the $x \to 0$ limit, and of the ratio of the specific volumes of ^{3}He and ^{4}He in the same limit. For γ_{34} we take a value intermediate between $\gamma_3 = 2.1$ and $\gamma_4 = 2.8$. Finally, for the parameter d_{34} we take $d_{34} = d_3 + d_4$. As concerns the choice of these values, we note that the precise value of the parameters γ_{34} and d_{34} has little influence on the results derived from the functional (4.86). The values of the above parameters are reported in Table 4.9.

TABLE 4.9

ρ_{4c} [Å^{-3}]	b_{34}[°K Å^3]	c_{34}[°K Å$^{3(1+\gamma_{34})}$]	c_3''[°K Å$^{3(1+\gamma_3)}$]	γ_{34}
0.062	-777.29	4.564748×10^6	-5.0683×10^4	2.5

The physical quantities that distinguish the behavior of homogeneous solutions at equilibrium, are all deduced from equation (4.88). For example, for pressure we have

$$\frac{P}{\rho} = \rho \left(\frac{\partial E/N}{\partial \rho} \right)_x , \qquad (4.89)$$

from which we extract the equilibrium density $\rho(P, x)$. The volume increase induced by ^{3}He is described by the volume excess parameter defined by

$$\alpha_0(P) = -\lim_{x \to 0} \frac{1}{\rho} \left(\frac{\partial \rho}{\partial x} \right)_P . \qquad (4.90)$$

The enthalpy per particle is given by

$$\frac{H}{N} = \frac{E}{N} + \frac{P}{N} , \qquad (4.91)$$

from which we obtain the chemical potentials of ^{3}He and ^{4}He:

$$\mu_3(x, P) = \frac{H}{N} + (1 - x) \left(\frac{\partial}{\partial x} \frac{H}{N} \right)_P , \qquad (4.92)$$

$$\mu_4(x, P) = \frac{H}{N} + x \left(\frac{\partial}{\partial (1-x)} \frac{H}{N} \right)_P , \qquad (4.93)$$

and the osmotic pressure

$$\Pi(x, P) = \rho(0, P)[\mu_4(0, P) - \mu_4(x, P)] , \qquad (4.94)$$

that is the pressure difference between the two liquids when a container containing the ^{3}He–^{4}He mixture is connected to a pure ^{4}He reservoir through a capillary.

In Figs. 4.7–4.9 we compare the results for the excess volume, the chemical potentials and the osmotic pressure as obtained starting from functional (4.88) with the corresponding experimental results (Ebner and Edwards 1970; Watson et al. 1969; Seligmann et al. 1969; Ghozlan and Varoquaux 1979). As can be seen, the agreement is quite good.

In the case of nuclei with $N \neq Z$, the functional (4.68) is generalized as follows:

$$
E = \int d\mathbf{r} \left[\frac{\tau}{2} + a(\rho\tau - j^2) + \frac{1}{2}b\rho^2 + d(\nabla\rho)^2 + \frac{1}{2}c\rho^{2+\gamma} \right.
$$

$$
\left. + a_1(\rho_1\tau_1 - j_1^2) + \frac{1}{2}b_1\rho_1^2 + d_1(\nabla\rho_1)^2 + \frac{1}{2}c_1\rho^\gamma\rho_1^2 \right] + E_{so} + E_C, \quad (4.95)
$$

where

$$
\rho = \rho_n + \rho_p = \sum_{i\sigma,q} \varphi_i^*(\mathbf{r},\sigma,q)\varphi_i(\mathbf{r},\sigma,q),
$$

$$
\rho_1 = \rho_n - \rho_p = \sum_{i\sigma,q} q\varphi_i^*(\mathbf{r},\sigma,q)\varphi_i(\mathbf{r},\sigma,q), \quad (4.96)
$$

with ρ_n and ρ_p the neutron and proton densities, respectively ($q = \pm 1$, where $+1$ indicates the neutron and -1 the proton), and the same for the kinetic energy densities τ and τ_1, and for the current densities j and j_1. E_{so} and E_C are the contributions of the spin-orbit and Coulomb interactions to the energy, respectively. The parameters a_1, b_1, c_1, d_1 for the *SIII* parametrization are reported in Table 4.10.

TABLE 4.10

a_1 [MeVfm^5]	b_1 [MeVfm^3]	c_1 [MeVfm^6]	d_1 [MeVfm^5]
-30.6	536.2	-3500.0	-17.0

From the functional (4.95) one obtains the following set of coupled equations for the single-particle wavefunctions of neutrons and protons:

$$
\left[-\frac{\vec{\nabla}}{2m^*} \cdot +a\mathbf{j} \cdot i\nabla\vec{\nabla} - a_1\nabla\rho_1 \cdot \nabla + qa_1\mathbf{j_1} \cdot i\nabla + U(\mathbf{r}) + qW(\mathbf{r}) + V_{so} + V_C \right] \varphi_{i,q}(\mathbf{r})
$$

$$
= \varepsilon_{i,q}\varphi_{i,q}(\mathbf{r}), \quad (4.97)
$$

with the self-consistent U and W fields given by

$$
U = b\rho + \frac{1}{2}c(2+\gamma)\rho^{1+\gamma} + \frac{1}{2}c_1\gamma\rho^{\gamma-1}\rho_1^2 + a\tau - 2d\nabla^2\rho, \quad (4.98)
$$

and

$$
W = b_1\rho_1 + c_1\rho^\gamma\rho_1 + a_1\tau_1 - 2d_1\nabla^2\rho_1, \quad (4.99)
$$
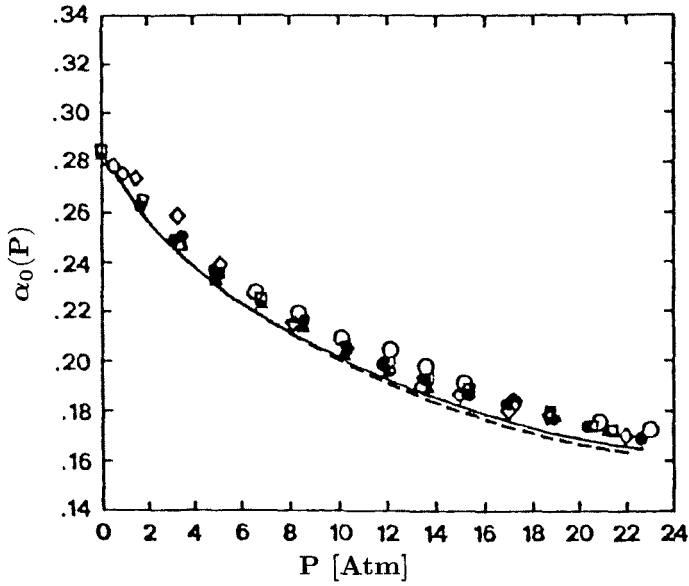
Fig. 4.7 Volume excess parameter as a function of pressure. The full line is the prediction of the theories obtained from the functional (4.88). The experimental data are from Watson et al. (1969).
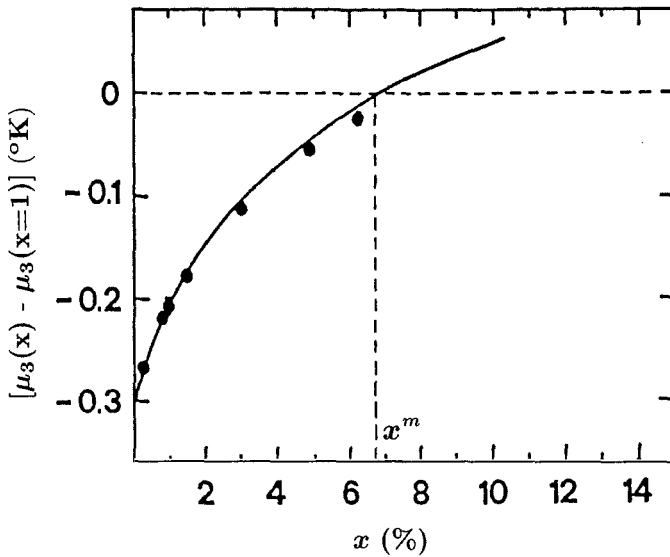

Fig. 4.8 Chemical potential of the ^{3}He atoms as a function of concentration. The full line is the prediction of the theories obtained from the functional (4.88). The experimental data are from Seligmann et al. (1969). The concentration x_m indicates the maximum solubility.
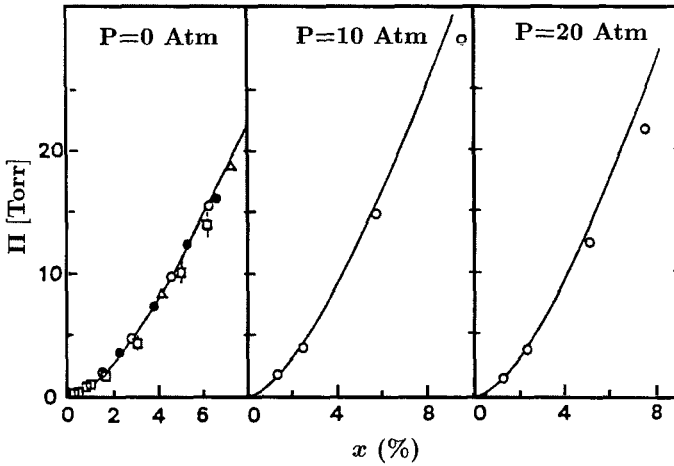
Fig. 4.9 Osmotic pressure as a function of x for three different pressures. The full line is the prediction of the theories obtained from the functional (4.88). The experimental data are from Ghozlan and Varoquaux (1979) and Ebner and Edwards (1970).

the effective mass from equation (4.67) and where V_{so} and V_C are the spin-orbit and Coulomb potentials, respectively. Equations (4.97)–(4.99) are solved by iteration and their solutions have been widely used to study the properties of finite nuclei.

It is interesting to notice the analogy existing between the $LSDA$ equations (4.44) for the systems of spin-polarized electrons, and the equations (4.97) for nuclei with $N \neq Z$ (isospin polarized). In particular, the exchange-correlation potential W_{xc}, which is a functional of the system magnetization m, is the analogue of the symmetry potential W of equation (4.99), which is a functional of the isovector density ρ_1. As we will see later, these potentials play a fundamental role in the propagation of spin and isospin waves in electron and nucleon systems, respectively.

4.11 Symmetries and Mean Field Theories

The Hamiltonian H of the N-body system has the symmetry S if H and S commute:

$$[H, S] = 0 . \qquad (4.100)$$

From equation (4.100) it follows that if $|n\rangle$ is a non-degenerate eigenstate of H, it has the symmetry S. Spontaneous symmetry breaking can occur in the exact case only if there is degeneracy. For example, if the ground state of H is degenerate and S is a symmetry of the problem, by linearly combining the degenerate states it is possible to set up an eigenstate of H which is not an eigenstate of S.

In mean field theories, such as the HF and the Kohn–Sham theories, it is by no means granted that the single-particle Hamiltonian H^{SP}, which determines the single-particle states through the solution of the HF or Kohn–Sham equations, has

the same symmetries as H. Indeed, it may be that

$$[H^{sp}, S] \neq 0. \tag{4.101}$$

In general, this means that also the mean field ground state does not have the symmetry S, and so there may occur a symmetry breaking. Examples of symmetry breaking in mean field theories are the breakdown of translational invariance in the electron gas (Wigner crystallization), the breakdown of rotational invariance in deformed nuclei, and the violation of particle-number conservation in HF-Bogoliubov calculations (superconductivity).

Recently, some symmetry breaking effects have been pointed out in HF and $LSDA$ calculations on quantum dots. In particular, in the absence of an external magnetic field, some quantum dots have zero total spin, but exhibit a locally non-vanishing magnetization, a so-called spin density wave (SDW) (Koskinen et al. 1997; Yannouleas and Landman 1999; Puente and Serra 1999). This can be observed in Fig. 4.10, where the polarization $\xi(x,y)$ is plotted for the case of the $S_z = 0$ ground state of a 34-electron dot. As seen in the figure, though $\int \xi d\mathbf{r} = 0$, ξ exhibits an pronounced radial oscillation, which just recalls the phenomenon of spin density waves in the bulk. Another symmetry breaking effect evidenced by $CDFT$ calculations on quantum dots is the breakdown of time-reversal (Steffens et al. 1998). In some cases this breakdown gives rise to spontaneously induced orbital currents

$S = 0$
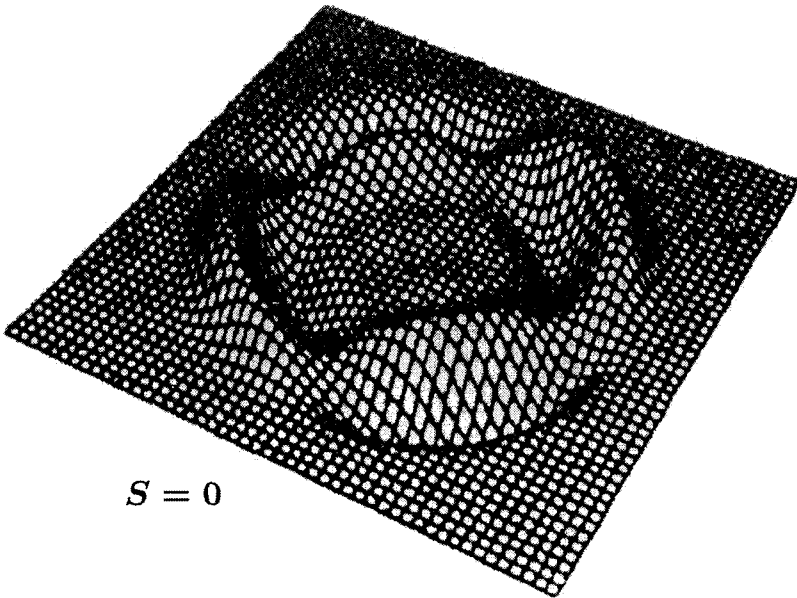
Fig. 4.10 Polarization $\xi(x,y)$ of the ground state with $S = 0$ of the 34-electron dot, computed in $LSDA$ without requiring circular symmetry.

and to non-zero magnetization also for ground states which have zero total angular momentum. Moreover, at low densities breakdown of the circular symmetry has been found in quantum dots, which is analogous to the ones observed in nuclear physics for deformed nuclei. This symmetry breaking has been confirmed by calculations based on the exact diagonalization of the Hamiltonian, which exhibits rotational-band-like spectra.

Finally we note that symmetry breaking of (4.101) affects the dynamic properties of mean field theories. If we want to study the system excitations by employing the eigenstates of H^{sp}, it is possible to obtain non-zero excitation energies for operators S which are symmetries of the system. This leads to spurious states in the excitation spectrum of the system itself. As we will see in the following, the use of the RPA theory for excited states can eliminate such spurious states.

References to Chapter 4

P. Hohenberg and W. Kohn, Phys. Rev. B **136**, 864 (1964).

W. Kohn and L.J. Sham, Phys. Rev. A **140**, 1133 (1965).

M. Levy, Proc. Natl. Acad. Sci. (USA) **76**, 6062 (1979).

F. Dalfovo, S. Giorgini, L.P. Pitaevskii and S. Stringari, Rev. Mod. Phys. **71**, 463 (1999).

T.C. Koopmans, Physica **1**, 104 (1933).

P. Ballone, C.J. Umrigar and P. Delaly, Phys. Rev. B **45**, 6293 (1992).

D. Ceperley, Phys. Rev. B **18**, 3126 (1978); D.M. Ceperley and B.J. Alder, Phys. Rev. Lett. **45**, 566 (1980); B. Tanatar and D.M. Ceperley, Phys. Rev. B **39**, 5005 (1989).

S. Lundqvist and N.H. March, Theory of the Inhomogeneous Electron Gas, (Plenum, New York, 1983).

V. von Barth and L. Hedin, J. Phys. C **5**, 1629 (1972).

R.O. Jones and O. Gunnarsson, Rev. Mod. Phys. **61**, 689 (1989).

S.H. Vosko, J.P. Perdew and A.H. MacDonald, Phys. Rev. Lett. **35**, 1725 (1975).

G. Vignale and M. Rasolt, Phys. Rev. Lett **59**, 2360 (1987); Phys. Rev. B **37**, 10 685 (1988).

M. Ferconi and G. Vignale, Phys. Rev. B **50**, 14722 (1994).

D. Levesque, J.J. Weiss and A.H. MacDonald, Phys. Rev. B **30**, 1056 (1984).

E. Lipparini, N. Barberan, M. Barranco, M. Pi and Ll. Serra, Phys. Rev. B **56**, 12375 (1997); M. Pi, M. Barranco, A. Emperador, E. Lipparini and Ll. Serra, Phys. Rev. B **57**, 14783 (1998).

O. Steffens, U. Rössler and M. Suhrke, Europhys. Lett. **42**, 529 (1998); O. Steffens, M. Suhrke and U. Rössler, Europhys. Lett. **44**, 222 (1998).

R.M. Dreizler and E.K.U. Gross, Density Functional Theory (Springer-Verlag, Berlin, 1990).

O. Heinonen, M.I. Lubin and M.D. Johnson, Phys. Rev. Lett. **75**, 4110 (1995).

D. Vautherin and D.M. Brink, Phys. Rev. C **5**, 626 (1972).

S. Stringari, Phys. Lett. A **106**, 267 (1984).

F. Dalfovo, Tesi di Dottorato dell'Università di Trento, 1989.

F. Dalfovo et al., Phys. Rev. B **52**, 1193 (1995).

J.C. Wheatley, Rev. Mod. Phys. **47**, 467 (1975).

A.E. Watson, J.D. Reppy and R. Richardson, Phys. Rev. **188**, 384 (1969).

P. Ring and P. Schuck, The Nuclear Many-Body Problem (Springer Verlag, N.Y. 1980).

N.D. Lang and W. Kohn, Phys. Rev. B **1**, 4555 (1970).

V.R. Pandharipande, S.C. Pieper and R.B. Wiringa, Phys. Rev. B **34**, 4571 (1986).

M. Beiner, H. Flocard, Nguyen Van Giai and Ph. Quentin, Nucl. Phys. A **238**, 29 (1975).

G. Baym and C.J. Pethick, in The Physics of Liquid and Solid Helium, Part ii, ed. K.H. Bennemann and J.B. Ketterson (Wiley, 1978), pp. 1–175.

F. Dalfovo and S. Stringari, Phys. Lett. A **112**, 171 (1985).

C. Ebner and D.O. Edwards, Phys. Rep. **2**, 77 (1970).

P. Seligmann, D.O. Edwards, R.E. Sarwinsky and J.T. Tough, Phys. Rev. **181**, 415 (1969).

A. Ghozlan and E. Varoquaux, Ann. Phys. Fr. 4, 239 (1979).

M. Koskinen, M. Manninen and S.M. Remann, Phys. Rev. Lett. **79**, 1389 (1999).

C. Yannouleas and U. Landman, Phys. Rev. Lett. **82**, 5325 (1999).

A. Puente and Ll. Serra, Phys. Rev. Lett. **83**, 3266 (1999).

Chapter 5

Quantum Dots in a Magnetic Field

5.1 Introduction

In this Chapter we will apply the theories discussed in the previous Chapters to the case of quantum dots in an external magnetic field. This field, which is applied perpendicularly to the dot itself, can completely spin-polarize the electrons of the system. Its presence strongly affects the motion of the electrons in the dot and gives rise to substantial fluctuations in the static and dynamic properties of the dot. These fluctuations have been related to the integer and fractional quantum Hall effect that is exhibited by the resistivity of a two-dimensional surface in the presence of a perpendicular magnetic field. The detailed microscopic study of such correspondence is one of the main purposes of this Chapter.

5.2 The Independent-Particle Model

Let us consider the electrons belonging to a two-dimensional quantum dot, confined by a harmonic potential in the plane $z = 0$; the electrons are subject to a magnetic field in the z direction: $\mathbf{B} = B\hat{k}$ described by a vector potential $\mathbf{A} = \frac{B}{2}(-y, x, 0)$. Suppose the electrons can be described by the Pauli Hamiltonian:

$$H = \sum_i \left\{ \frac{1}{2m} \left[\mathbf{p} + \frac{e}{c}\mathbf{A}(\mathbf{r}) \right]^2 + \frac{1}{2}m\omega_0^2 r^2 + \frac{e\hbar}{2m_e c}\, \boldsymbol{\sigma} \cdot (\boldsymbol{\nabla} \times \mathbf{A}) \right\}_i$$

$$+ \frac{e^2}{\varepsilon} \sum_{i<j}^{N} \frac{1}{|\mathbf{r}_i - \mathbf{r_j}|}, \tag{5.1}$$

where $m = m^* m_e$ is the effective mass of the electrons, $-e$ their charge, ε the dielectric constant of the semiconductor, and $\boldsymbol{\sigma}$ Pauli's vector matrix. Note that $\mathbf{A} = (\mathbf{B} \times \mathbf{r})/2$, so that $\boldsymbol{\nabla} \cdot \mathbf{A} = 0$. In equation (5.1) there is a one-body part, that in the following we will indicate as H_0, and a two-body part given by the Coulomb interaction. For the moment, let us focus our attention on H_0, and let us study its

eigenvalues and eigenfunctions. If we define

$$\Omega^2 \equiv \omega_0^2 + \frac{1}{4}\omega_c^2 \,, \tag{5.2}$$

where $\omega_c = eB/mc$ is the cyclotron frequency, and recalling the definition of angular momentum relative to the z axis $l_z = -i\hbar\partial/\partial\theta$, the one-body part of (5.1) can be rewritten as

$$H_0 = \sum_i \left\{ \frac{\mathbf{p}^2}{2m} + \frac{1}{2}\omega_c \, l_z + \frac{1}{2}m^* \Omega^2 \, r^2 + \frac{e\hbar}{2m_ec}B\,\sigma_z \right\}_i \,. \tag{5.3}$$

Since

$$[H_0, L_z] = 0, \quad [H_0, S_z] = 0 \,, \tag{5.4}$$

where $L_z = \sum_i l_z^i$ and $S_z = \frac{1}{2}\sum_i \sigma_z^i$ are the z components of the angular momentum and of the total spin, it is possible to write the single-particle wavefunctions as $\phi(\mathbf{r}, \sigma) = e^{-il\theta}u(r)\chi_\sigma$. These functions correspond to a quantum-number of the angular momentum along z equal to $-l$, and to a z spin component equal to $\pm 1/2$; by introducing the effective gyromagnetic factor g^* (for the bare electron $g^* = g = 2$), Bohr's magneton $\mu_0 = \hbar e/2m_ec$, and $\sigma \equiv \pm 1$, $u(r)$ is the solution of the radial Schrödinger equation:

$$\left[-\frac{\hbar^2}{2m}\left(\frac{d^2}{dr^2} + \frac{1}{r}\frac{d}{dr} - \frac{l^2}{r^2} \right) + \frac{m}{2}\Omega^2 r^2 - \frac{\hbar\omega_c}{2}l + \frac{g^*}{2}\mu_0 B\,\sigma \right] u_{nl\sigma} = \epsilon_{nl\sigma}u_{nl\sigma} \,. \tag{5.5}$$

The physically acceptable solutions of this equation were determined by Fock (1928) and Darwin (1930). One finds

$$\epsilon_{nl\sigma} = \hbar\Omega(2n + |l| + 1) - \frac{1}{2}\hbar\omega_c l + \frac{1}{2}g^*\mu_0 B\sigma \,, \tag{5.6}$$

with $n = 0, 1, 2, \ldots$ and $l = 0, \pm 1, \pm 2, \ldots$. The normalized wavefunctions are written in terms of generalized Laguerre polynomials:

$$\phi(\mathbf{r})_{n,l,\sigma} = \frac{e^{-il\theta}}{\sqrt{2\pi}}\frac{1}{a}\sqrt{\frac{n!}{2^{|l|}(n+|l|)!}}\left(\frac{r}{a}\right)^{|l|}e^{-(\frac{r}{2a})^2}L_n^{|l|}\left(\frac{r^2}{2a^2}\right)\chi_\sigma \,, \tag{5.7}$$

where $a \equiv \sqrt{\hbar/2m\Omega}$. In the following, we study the two relevant limiting cases $\omega_0 >> \omega_c$ e $\omega_c >> \omega_0$.

5.2.1 *The $\omega_0 >> \omega_c$ case*

If we set ω_c equal to zero, equation (5.6) becomes

$$\epsilon_{nl} = \hbar\omega_0(N + 1) \,, \tag{5.8}$$

where we have defined $N \equiv 2n + |l|$ with $N = 0, 1, 2, \ldots$. These are the levels of a two-dimensional harmonic oscillator. Each level is $2(N + 1)$-fold degenerate

(by taking due account of the spin). As has already been discussed in Section 2.2.1, dots with a number of electrons $N_e = 2, 6, 12, 20, 30, 42, 56, \ldots$, are closed-shell dots. These values are part of the sequence $(p+1)(p+2)$ with $p = 0, 1, 2, \ldots$, which equals the number of fully occupied shells. The shell structure is such that for a given N, n varies from zero to the integer value of $N/2$, and there are values of $|l|$ up to N, with the same parity as N. For example, when $N = 6$ we have $n = 0, 1, 2, 3$, $l = 0, \pm2, \pm4, \pm6$, while with $N = 5$ we have $n = 0, 1, 2$, $l = \pm1, \pm3, \pm5$. This means that not all transitions of a given multipolarity L can take place between adjacent shells. Dipole transitions with $L = 1$, which involve jumps with odd ΔN can always occur, but for quadrupole transitions $(L = 2)$ to take place jumps with even ΔN are required.

Equation (5.8) shows that for a fixed n, the single-particle levels are distributed according to straight lines as a function of $|l|$. If one used a different confinement potential, like for example the one produced by a uniform distribution of positive charges on a disk of fixed radius, there would be some distortion, but the levels are still distributed in a very regular way.

Furthermore, retaining terms linear in B we find

$$\epsilon_{nl} = \hbar\omega_0(N+1) - \frac{\hbar\omega_c}{2}l + \frac{1}{2}g^*\mu_0\,B\,\sigma\,. \tag{5.9}$$

The l and σ degeneracies are lifted by the B-linear terms, which push upwards the levels with $l < 0$ and $\sigma < 0$ (provided $g^* < 0$ like in GaAs), and push downwards the levels with $l > 0$ and $\sigma > 0$, thus introducing a pattern of intersections in the single-particle spectrum as a function of B, which can result in a shell structure for the dots which is quite different from the $B = 0$ one (see Fig. 5.1).

5.2.2 The $\omega_c \gg \omega_0$ case

If we put ω_0 equal to zero, equation (5.6) becomes

$$\epsilon_{nl\sigma} = \hbar\omega_c\left(M + \frac{1}{2}\right) + \frac{1}{2}g^*\mu_0\,B\,\sigma\,, \tag{5.10}$$

where we have introduced the label of the Landau levels $M \equiv n + \frac{1}{2}(|l| - l)$. We can see that the electronic states with the same spin are distributed in infinitely l-degenerate levels, characterized by the values of $M = 0, 1, 2, \ldots$. If $g^* < 0$ like in GaAs then the levels $(M, \uparrow)$ are lower in energy than the levels $(M, \downarrow)$. For each of the two spin values, we see that the first Landau level consists of states with $n = 0$ and non-negative l-values, $l = 0, 1, 2, \ldots$. The second Landau level $M = 1$ is built up by states with $n = 1$, and non-negative l-values plus the state $n = 0, l = -1$. The third Landau level $M = 2$ is built up by $n = 2$, non-negative l-values plus the states $n = 1, l = -1$ and $n = 0, l = -2$, and so on.
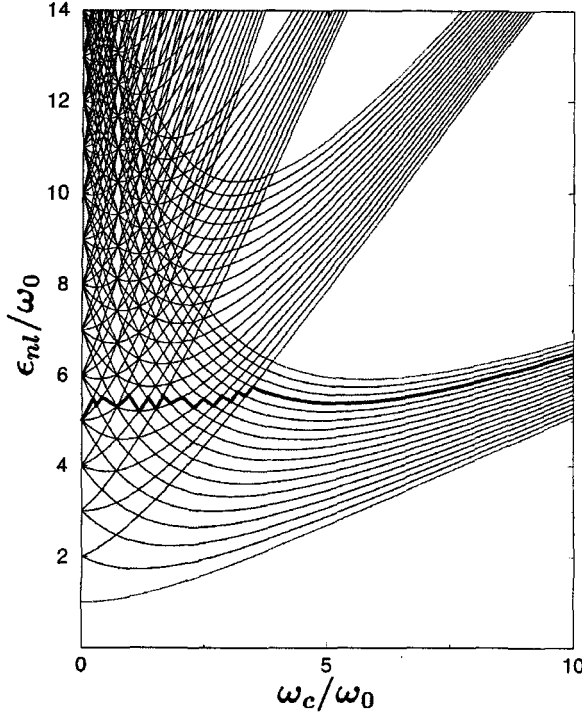
Fig. 5.1   Single-particle energy levels of Eq. (5.6) in ω_0 units, as a function ω_c/ω_0. The Zeeman term has been neglected for simplicity.

At the lowest order in ω_0/ω_c one gets

$$\epsilon_{nl\sigma} = \hbar\omega_c\left(M + \frac{1}{2}\right) + \hbar\frac{\omega_o^2}{\omega_c}(2n + |l| + 1) + \frac{1}{2}g^*\mu_0 B\,\sigma\,. \qquad (5.11)$$

The l degeneracy is broken by a positive linear term. Once B, g^* and the electron number N are fixed, the filling of the Landau levels occurs according to the energy balance of the three terms of (5.11).

In Fig. 5.1 we show the single-particle energy levels of (5.6) in ω_0 units, as a function of ω_c/ω_0, and by neglecting the Zeeman term. The evolution of the harmonic oscillator spectrum towards the Landau spectrum as ω_c increases is clearly observed, together with the level degeneracy. The full line shows the Fermi energy of a 30-electron dot in this approximation.

It is important to stress again that the harmonic-oscillator level structure and the Landau one are very different as regards the respective contents of single-particle angular momentum.

We mentioned above that in the case of the harmonic oscillator, transitions with $\Delta N = 1$ are impossible for any multipolarity of the excitation operator. On the other hand, since the Landau levels have practically no limitation as to the l

value of their single-particle components, any multipole transition between Landau levels with $\Delta M = 1$ is possible. The implications of this fact are both simple and important for the interpretation of the experimental spectra:

If the electron–electron interaction is neglected, at low B the energies of the dipole $(L = 1)$, quadrupole $(L = 2)$ and octupole $(L = 3) \dots$ modes are $\hbar w_0 (\Delta N = 1)$, $2\hbar w_0 (\Delta N = 2)$ and $3\hbar w_0 (\Delta N = 3) \dots$, respectively. At high B, all of the above modes are at energy $\hbar \omega_c (\Delta M = 1)$. The residual interaction and finite-dimension effects (N is finite) change quantitatively this scenario which, however, is still valid from a qualitative point of view (Schuller et al. 1998; Barranco et al. 1999).

5.2.3 *The MDD (maximum density droplet) state*

Let us assume that the value of B is so high, that the gap between Landau levels is such that only the first Landau level $(M = 0, \uparrow)$ may be occupied, both in the ground state and for a large number of N-electron excited states.

Putting $M = 0$, and thus $n = \frac{1}{2}(l - |l|)$ in (5.11), we obtain

$$\epsilon_l = \frac{1}{2}\hbar\omega_c + \hbar\frac{\omega_o^2}{\omega_c}(l + 1) + \frac{1}{2}g^*\mu_0 B \,. \tag{5.12}$$

From equation (5.12) we derive the energy of the eigenstates of H_0:

$$E = \sum_l^{occ} \epsilon_l = \text{const.} + \gamma L \,, \tag{5.13}$$

where $\gamma = \hbar\frac{\omega_o^2}{\omega_c}$ and L is the eigenvalue (with opposite sign) of the total angular momentum operator

$$L = -\langle\Psi| \sum_{i=1}^{N} l_{iz} |\Psi\rangle = \sum_l^{occ} l \,. \tag{5.14}$$

Since the energy is linear in angular momentum, it follows that the ground state is the one with the lowest value of L. Let this value be L_0; this will result from the summation of lowest possible values of the single-particle angular momenta:

$$L_0 = \sum_{l=0}^{N-1} l = \frac{N(N-1)}{2} \,. \tag{5.15}$$

All states with $L > L_0$ are excited states. Apart from the $L_0 + 1$ state (dipole excited state), all other excited states that can be built up starting from the single-particle states belonging to the first Landau level, are degenerate. In the case of 3 electrons, some of these states are reported, as an example, in Table 5.1.

TABLE 5.1

l_1	l_2	l_3	L
0	1	2	$3 = L_0$
0	1	3	4
0	1	4	5
0	2	3	5

As seen from the table, only the $L = 3$ and $L = 4$ states are not degenerate.

The Coulomb interaction modifies this scheme. However, if B is so large that it is possible to disregard the Coulomb mixing with other Landau levels, and consider only the first Landau level for the description of the system at such B value, the $|L_0\rangle$ and $|L_0 + 1\rangle$ states, which are non-degenerate eigenstates of H_0 and L_z, are eigenstates of the true Hamiltonian H (i.e. including the Coulomb interaction) as well, since H commutes with L_z. Therefore, it appears that values of B and N exist, for which the above conditions are realized, and so the true ground state of the system is the Slater determinant:

$$
\Psi_0 = \frac{1}{\sqrt{N!}} \begin{vmatrix} \phi_0(\mathbf{r}_1) & \cdots & \phi_{N-1}(\mathbf{r}_1) \\ \vdots & \ddots & \vdots \\ \phi_0(\mathbf{r}_N) & \cdots & \phi_{N-1}(\mathbf{r}_N) \end{vmatrix} , \tag{5.16}
$$

where, for $\omega_c \gg \omega_0$:

$$
\phi_l = \frac{1}{\sqrt{2\pi \mathcal{L}^2}} \frac{1}{\sqrt{l!}} \left(\frac{r e^{-i\vartheta}}{\sqrt{2}\mathcal{L}} \right)^l e^{-\frac{r^2}{4\mathcal{L}^2}} , \tag{5.17}
$$

and $\mathcal{L} = \sqrt{\frac{\hbar c}{eB}}$ is the magnetic length. In the literature. The state in (5.16) is called the MDD state (Maximum Density Droplet State). It is a completely spin-polarized state ($\langle \Psi_0 | S_z | \Psi_0 \rangle = \frac{N}{2}$) and its one-body diagonal density is given by

$$
\rho = \sum_{l=0}^{N-1} |\phi_l|^2 = \sum_{l=0}^{N-1} \frac{1}{2\pi \mathcal{L}^2} \frac{1}{l!} \left(\frac{r}{\sqrt{2}\mathcal{L}} \right)^{2l} e^{-\frac{r^2}{2\mathcal{L}^2}} , \tag{5.18}
$$

while the one-body non-diagonal density is given by

$$
\rho^{(1)}(\mathbf{r_1}, \mathbf{r_2}) = \sum_{l=0}^{N-1} \phi_l^*(\mathbf{r_1})\phi_l(\mathbf{r_2}) = \sum_{l=0}^{N-1} \frac{1}{2\pi \mathcal{L}^2} \frac{1}{l!} \left(\frac{r_1 r_2}{2\mathcal{L}^2} \right)^l e^{-\frac{r_1^2 + r_2^2}{4\mathcal{L}^2}} e^{il(\vartheta_1 - \vartheta_2)} . \tag{5.19}
$$

For large N values the one-body diagonal density is characterized by the constant value

$$
\rho = \frac{1}{2\pi \mathcal{L}^2} = \frac{eB}{2\pi\hbar c} \tag{5.20}
$$

within the circle of radius $R = \mathcal{L}\sqrt{2N}$, and by a boundary thickness of the order of the magnetic length.

The diagonal two-body density of the MDD state for $N \to \infty$ is given by

$$\rho^{(2)}(|\mathbf{r_1} - \mathbf{r_2}|) = \rho^2 - |\rho^{(1)}(\mathbf{r_1}, \mathbf{r_2})|^2 = \left(\frac{1}{2\pi\mathcal{L}^2}\right)^2 \left(1 - e^{-\frac{|\mathbf{r_1} - \mathbf{r_2}|^2}{2\mathcal{L}^2}}\right), \quad (5.21)$$

and it allows the evaluation of the average value of two-body operators in the ground state of the system. For example, the Coulomb exchange energy per particle

$$\frac{E_x}{N} = \frac{1}{2}\frac{1}{2\pi\mathcal{L}^2}\int d^2r \frac{e^2}{r}[g(r) - 1] = -\frac{1}{2}\frac{e^2}{\mathcal{L}}\sqrt{\frac{\pi}{2}}, \quad (5.22)$$

where $g(|\mathbf{r_1} - \mathbf{r_2}|) = 1 - e^{-\frac{|\mathbf{r_1} - \mathbf{r_2}|^2}{2\mathcal{L}^2}}$ is the pair correlation function for the MDD state.

In the limit of infinite N, expression (5.20) allows us to define the filling factor of Landau levels. In fact, once the density is fixed, it is necessary that the magnetic field has the value (that we indicate B_0) in order that the system is in the MDD state, where all the single-particle states of the first Landau level are occupied. Therefore, as an indicator of the filling of Landau levels we introduce the filling factor ν defined as

$$\nu = \rho \frac{2\pi\hbar c}{eB}, \quad (5.23)$$

whose value is 1 when all the electrons are in the first Landau level $(B = B_0)$. By progressively decreasing the magnetic field, some electrons will be placed in the second Landau level until, when $\nu = 2$, in the independent-particle model the second level is completely filled, and at $\nu = 3$ the third level will be filled, and so on. The corresponding, closed-shell states are very stable and are called incompressible, integer filling states.

5.3 Fractional Regime

If the external magnetic field is higher than B_0 the filling factor is smaller than one: in this case we enter the so-called fractional regime, for which the ground state is no longer the MDD state, but is rather a strongly correlated state whose wavefunction, in some cases, was guessed by Laughlin (1983).

In order to understand the form of the ground state for the fractional regime suggested by Laughlin, it is convenient to write the Slater determinant (5.16) describing the MDD state in the following way (Vandermonde way):

$$\Psi(q_1, q_2 \cdots q_N) = \text{const} \begin{vmatrix} q_1^0 & \cdots & q_1^{N-1} \\ \vdots & \ddots & \vdots \\ q_N^0 & \cdots & q_N^{N-1} \end{vmatrix} e^{-\sum_{i=1}^N \frac{|q_i|^2}{4}}$$

$$= \text{const} \prod_{i<j=1}^{N} (q_i - q_j) e^{-\sum_{i=1}^{N} \frac{|q_i|^2}{4}} , \tag{5.24}$$

where $q_i = (x_i - iy_i)/\mathcal{L}$ (lengths are in units of the magnetic length $\mathcal{L}$); the normalization constant is given by

$$\text{const} = (N!)^{-1/2} (2\pi\mathcal{L}^2)^{-N/2} 2^{-N(N-1)/4} \prod_{j=0}^{N-1} (j!)^{-1/2} .$$

Laughlin suggested the following generalization of the wavefunction (5.24), valid for $B \geq B_0$, and where m is an odd integer in order that Fermi statistics holds:

$$\Psi_m(q_1, q_2 \cdots q_N) = \prod_{i<j=1}^{N} (q_i - q_j)^m e^{-\sum_{i=1}^{N} \frac{|q_i|^2}{4}} . \tag{5.25}$$

This ansatz for the wavefunction implies that all the electrons are in the first Landau level, and that all spins are oriented along the magnetic field.

The Laughlin states have the following properties:

- They are eigenstates of the angular momentum with eigenvalue $m\frac{N(N-1)}{2}$.
- They are closely connected with the one-component classical plasma. In fact, writing

$$|\Psi_m|^2 = e^{-\beta\Phi} , \tag{5.26}$$

with $\beta = 1/m$ playing the role of $\beta = 1/KT$, we find

$$\Phi = -\sum_{i<j=1}^{N} 2m^2 ln|q_i - q_j| + \frac{1}{2}m \sum_{i=1}^{N} |q_i|^2 . \tag{5.27}$$

We see that Φ is the potential energy of the two-dimensional plasma of N particles with charge $\sqrt{2}m$. For $\mathcal{L} = 1$, the first term is the repulsive interaction while the second is the interaction with a background of positive charges, uniformly distributed in the system with density $1/(\sqrt{2\pi})$. For some density values this plasma is expected to have a uniform charge distribution. Actually, Monte Carlo simulations (Caillol et al. 1982) showed that such a system is a fluid if $\Gamma = \sqrt{\pi\rho}e^2\beta = \sqrt{2m}$ is smaller than 140; for higher values it forms a hexagonal crystal. It is expected that the Laughlin state also has a constant density and may be connected with a quantum-liquid-like state. $|\Psi_m|^2$ corresponds to a system whose constant density is given by:

$$\rho = \frac{1}{2\pi} \frac{1}{m} , \tag{5.28}$$

which in turn corresponds to a fractional filling factor: $\nu = 1/m$.

- In the Laughlin states the energy per particle is lower than in any other state that has been proposed, for example HF and Charge Density Wave, and is very close to the fixed phase Monte Carlo calculations.

5.4 Hall Effect

The Hall effect manifests itself in two-dimensional electron systems under a uniform magnetic field perpendicular to the electron mobility plane (for example the xy plane). By applying an electric field in the x direction (in this way inducing a current density j_x), because of the Lorentz force a difference of potential V_y is created between the two surface boundaries parallel to the x axis. It is then possible to define the Hall transverse resistivity

$$\rho_{yx} \equiv \frac{E_y}{j_x}. \tag{5.29}$$

From classical calculations, this quantity is proportional to the magnetic field and inversely proportional to the electron density:

$$\rho_{yx} = \frac{F_y}{e} \frac{1}{e\rho v_x} = \frac{ev_x B}{ce} \frac{1}{e\rho v_x} = \frac{B}{\rho ec}. \tag{5.30}$$

In experiments (von Klitzing, Dorda, and Pepper 1980; Ebert et al. 1982), such linear dependence of the resistivity on B is observed at low B values. However, at low temperature, by increasing the value of B, one observes plateaux in the B-dependence of the resistivity, when the magnetic field value is the inverse of an integer times the electron density:

$$B = \frac{2\pi\hbar c}{e} \rho \frac{1}{\nu}, \qquad \nu = 1, 2, 3, \ldots. \tag{5.31}$$

Moreover, the longitudinal resistivity $\rho_{xx} = E_x/j_x$ exhibits a minimum for these values of the magnetic field.

These facts can be explained by the theory developed in the previous Sections, by considering the quantum motion of the electrons. When the Landau levels are filled, the many-electron wavefunction produces very stable incompressible states and robust against changes in B, and the Hall resistivity stays constant, thereby causing the plateau. Moreover, the longitudinal resistivity becomes small because there exists a large energy gap for exciting the electrons, due to the closed shells. These closed shells, i.e. the above incompressible states, are formed when the magnetic field value is the inverse of an integer number times the density.

Plateaux of the Hall resistivity and minima of the longitudinal resistivity have also been observed (Tsui, Stormer and Gossard 1982; Willet et al. 1987) at low temperature and high field, when B is the inverse of a fractional number times the

density:

$$B = \frac{2\pi\hbar c}{e}\rho\frac{1}{1/m}, \qquad m = 1, 2, \ldots \tag{5.32}$$

This fractional quantum Hall effect is observed when the first Landau level is partially filled, and is due to the electron correlations induced by the mutual interaction, contrary to the case of the integer quantum Hall which is explained within the independent-particle model, and is described by the Laughlin correlated states.

5.5   Elliptical Quantum Dots

In this Section we will consider the properties of quantum dots in the case of anisotropic confinement. There exist many experimental (Dahl et al. 1991; Sasaki et al. 1998; Austing et al. 1999) and theoretical (Peeters 1990; Madhav and Chakraborty 1994) studies of the electronic properties of quantum dots of this kind, as a function of anisotropy and applied external magnetic field. In the case of zero field, there are some theoretical works (Reimann et al. 1998; Puente and Serra 1999) in the *LSDA* approximation for quantum dots with complex shapes. In what follows we will study the independent-particle model for elliptical dots under external magnetic field, for which it is possible to deduce analytical results. At the end of this Section we will briefly discuss some *LSDA* results for anisotropic systems.

If we define

$$\Omega_x^2 \equiv \omega_x^2 + \frac{1}{4}\omega_c^2, \qquad \Omega_y^2 \equiv \omega_y^2 + \frac{1}{4}\omega_c^2, \tag{5.33}$$

the one-body Hamiltonian for elliptical quantum dots under magnetic field turns out to be given by:

$$H_{xy} = \sum_i h_{xy}^i = \sum_i \left\{ \frac{p_x^2 + p_y^2}{2m} + \frac{1}{2}\omega_c(xp_y - yp_x) \right.$$

$$\left. + \frac{1}{2}m(\Omega_x^2 x^2 + \Omega_y^2 y^2) + \frac{1}{2}g^*\mu_0 B\,\sigma_z \right\}_i. \tag{5.34}$$

The Schrödinger equation

$$h_{xy}\Psi_{n_x n_y}(x,y) = \epsilon_{n_x n_y}\Psi_{n_x n_y}(x,y), \tag{5.35}$$

may be re-written in the form (Dippel et al. 1994):

$$h_3\Phi_{n_x n_y}(x,y) = \epsilon_{n_x n_y}\Phi_{n_x n_y}(x,y), \tag{5.36}$$

where

$$h_3 = U^{-1}h_{xy}U, \qquad \Psi_{n_x n_y} = (U\Phi_{n_x n_y})(x,y), \tag{5.37}$$

and the unitary operator U is given by

$$U = e^{i\alpha xy} e^{i\beta p_x p_y} , \qquad (5.38)$$

with

$$\alpha = -\frac{m}{2}\left(\frac{\omega_x^2 - \omega_y^2}{\omega_c}\right) + \text{sgn}[\omega_x^2 - \omega_y^2]\frac{m}{2\omega_c}\sqrt{(\omega_x^2 + \omega_y^2 + \omega_c^2)^2 - 4\omega_x^2\omega_y^2}$$

$$\beta = \frac{1}{m}\text{sgn}[\omega_x^2 - \omega_y^2]\frac{\omega_c}{\sqrt{(\omega_x^2 + \omega_y^2 + \omega_c^2)^2 - 4\omega_x^2\omega_y^2}} , \qquad (5.39)$$

where $\text{sgn}[\omega_x^2 - \omega_y^2]$ is +1 if $\omega_x^2 \geq \omega_y^2$, and -1 if $\omega_x^2 \leq \omega_y^2$. Therefore, the transformed Hamiltonian can be written in terms of squared co-ordinate and momentum operators alone:

$$h_3 = \frac{p_x^2}{2M_1} + \frac{p_y^2}{2M_2} + \frac{1}{2}M_1\Omega_1^2 x^2 + \frac{1}{2}M_2\Omega_2^2 y^2 + \frac{1}{2}g^*\mu_0 B\sigma_z \qquad (5.40)$$

with

$$M_{1,2} = -\frac{2m\sqrt{(\omega_x^2 + \omega_y^2 + \omega_c^2)^2 - 4\omega_x^2\omega_y^2}}{\text{sgn}[\omega_x^2 - \omega_y^2](\omega_x^2 - \omega_y^2 \pm \omega_c^2) + \sqrt{(\omega_x^2 + \omega_y^2 + \omega_c^2)^2 - 4\omega_x^2\omega_y^2}} ,$$

$$\Omega_{1,2} = \frac{1}{\sqrt{2}}\left[\omega_x^2 + \omega_y^2 + \omega_c^2 \pm \text{sgn}[\omega_x^2 - \omega_y^2]\sqrt{(\omega_x^2 + \omega_y^2 + \omega_c^2)^2 - 4\omega_x^2\omega_y^2}\right]^{1/2} . \qquad (5.41)$$

These results can be easily obtained using the Baker–Hausdorff formula

$$e^{i\lambda G}Ae^{-i\lambda G} = A + i\lambda[G, A] + \frac{i^2\lambda^2}{2!}[G, [G, A]]]$$

$$+ \cdots + \frac{i^n\lambda^n}{n!}[G, [G, \cdots [G, A]\cdots]] + \cdots , \qquad (5.42)$$

and by requiring that in the transformed Hamiltonian non-quadratic terms vanish.

The eigenvalues of h_3, which are eigenvalues of h_{xy} as well, are given by (where we have dropped the spin part for simplicity)

$$\epsilon_{n_x n_y} = \left(n_x + \frac{1}{2}\right)\Omega_1 + \left(n_y + \frac{1}{2}\right)\Omega_2, \quad n_x, n_y = 0, 1, 2, \ldots \qquad (5.43)$$

The eigenfunctions of h_3 are products $\Phi_{n_x n_y} = \varphi_{n_x}(x)\varphi_{n_y}(y)$ of one-dimensional harmonic oscillator eigenfunctions φ_i, with frequencies Ω_i and masses M_i. The eigenfunctions of h_{xy} are very complex and may be obtained by transformations (5.38) and (5.39). The same transformation allows an easy evaluation of interesting

quantities such as the mean square radii:

$$\langle x^2 \rangle = \frac{1}{N} \sum_{n_x, n_y, \sigma} \langle n_x n_y | x^2 | n_x n_y \rangle_\Psi \,,$$

$$\langle y^2 \rangle = \frac{1}{N} \sum_{n_x, n_y, \sigma} \langle n_x n_y | y^2 | n_x n_y \rangle_\Psi \,,$$

without explicit knowledge of the wavefunction. In fact, we have

$$\langle n_x n_y | x^2 | n_x n_y \rangle_\Psi = \langle n_x n_y | U^{-1} x^2 U | n_x n_y \rangle_\Phi \,,$$
$$\langle n_x n_y | y^2 | n_x n_y \rangle_\Psi = \langle n_x n_y | U^{-1} y^2 U | n_x n_y \rangle_\Phi \,,$$

$$(5.44)$$

and using equation (5.42):

$$U^{-1} x^2 U = x^2 - 2\beta x p_y + \beta^2 p_y^2, \qquad U^{-1} y^2 U = y^2 - 2\beta y p_x + \beta^2 p_x^2 \,, \quad (5.45)$$

with $\langle n_x n_y | x p_y | n_x n_y \rangle_\Phi = \langle n_x n_y | y p_x | n_x n_y \rangle_\Phi = 0$ and the virial theorem

$$\langle n_x n_y | \frac{p_x^2}{M_1} | n_x n_y \rangle_\Phi = \langle n_x n_y | M_1 \Omega_1^2 x^2 | n_x n_y \rangle_\Phi = \left(n_x + \frac{1}{2} \right) \Omega_1 \,,$$

$$(5.46)$$

$$\langle n_x n_y | \frac{p_y^2}{M_2} | n_x n_y \rangle_\Phi = \langle n_x n_y | M_2 \Omega_2^2 y^2 | n_x n_y \rangle_\Phi = \left(n_y + \frac{1}{2} \right) \Omega_2 \,,$$

we obtain

$$\langle x^2 \rangle = \frac{1}{N} \sum_{n_x, n_y, \sigma} \left(\frac{1}{M_1 \Omega_1} \left(n_x + \frac{1}{2} \right) + \beta^2 M_2 \left(n_y + \frac{1}{2} \right) \Omega_2 \right) \,,$$

$$\langle y^2 \rangle = \frac{1}{N} \sum_{n_x, n_y, \sigma} \left(\frac{1}{M_2 \Omega_2} \left(n_y + \frac{1}{2} \right) + \beta^2 M_1 \left(n_x + \frac{1}{2} \right) \Omega_1 \right) \,.$$

$$(5.47)$$

The energies (5.43) have the following limiting behavior: at zero magnetic field the system behaves like a pair of harmonic oscillators in the x, y directions. For high magnetic field ($\omega_c \gg \omega_x, \omega_y$; $\omega_y > \omega_x$), we obtain

$$\Omega_1 \to 0 \quad \text{and} \quad \epsilon_{n_x, n_y} = (n_y + 1/2)\omega_c \,,$$

i.e. Landau levels are formed as in the case of isotropic parabolic confinement. When $\omega_x = \omega_y$ and the confinement is isotropic parabolic, $n_x = n + |l|/2 - l/2$ and $n_y = n + |l|/2 + l/2$, where n and l are the principal and azimuthal quantum numbers, respectively. Also in the case $\omega_x \simeq \omega_y$, the energy levels are very similar to the isotropic ones, apart from the fact that the $2n + |l| + 1$ fold degeneracy at $B = 0$ is broken by deformation.

In Fig. 5.2(a) we show (Madhav and Chakraborty 1994) the magnetic-field dependence of the energy levels (5.43) for a dot with $\omega_x = 1.0$ meV and $\omega_y = 1.1$ meV.

For this choice, the deviation from circular symmetry is very small and the energy levels are very similar to those of the circular dot, apart from the origin
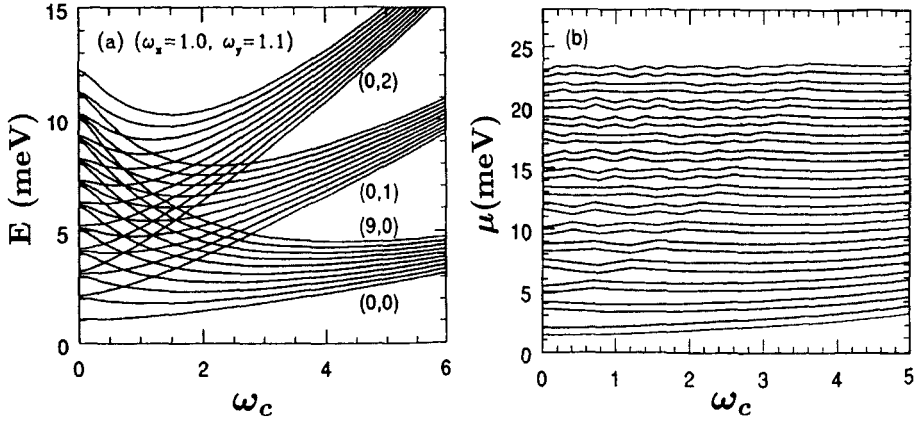
Fig. 5.2 (a) Energy levels of a anisotropic dot as a function of ω_c (meV) for $\omega_x = 1.0$ meV and $\omega_y = 1.1$ meV. The lines are drawn in increasing order of (n_x, n_y), as indicated. (b) Chemical potential in the CI approximation for the energy levels of (a).

where a shift of the degenerate level due to deformation shows up. In Fig. 5.2(b) we show the chemical potential calculated in the constant-interaction model (CI), where the total energy is written as

$$E(N) = \sum_i^N \epsilon_i + \frac{1}{2}N^2 V , \qquad (5.48)$$

where V is the electron–electron interaction energy, and ϵ_i is the energy of the i-th electron. Therefore, in this model the chemical potential is

$$\mu = E(N) - E(N-1) = \epsilon_N + \left(N - \frac{1}{2}\right)V . \qquad (5.49)$$

The result of the calculation reported in the figure (for N values in the range 1 to $\simeq$ 30) also includes the Zeeman energy suitable for GaAs. We have used $V = 0.6$ meV, taken from the work of Ashoori et al. (1993).

The energies and chemical potentials for $\omega_x = 1.0$ meV and $\omega_y = 5$ and 10 meV are plotted in Figs. 5.3 and 5.4. We can clearly see that as ω_y increases, the level crossing takes place at higher energies, and the oscillations of the chemical potentials are quenched at lower energies. For example, when $\omega_y = 5$, the oscillations are quenched for $N = 1 - 12$, and when $\omega_y = 10$, for $N = 1 - 22$. Moreover, the amplitude of the oscillations strongly decreases with increasing anisotropy. On the other hand, the magnetic field value beyond which the chemical potential oscillations disappear, increases by increasing ω_y. As the threshold magnetic field value does, the oscillations also shift towards higher magnetic fields, similar to what is observed experimentally (Ashoori 1993).

LSDA calculations in elliptical quantum dots have been carried out by Austing et al. (1999) and Serra, Puente and Lipparini (2002). These calculations show that
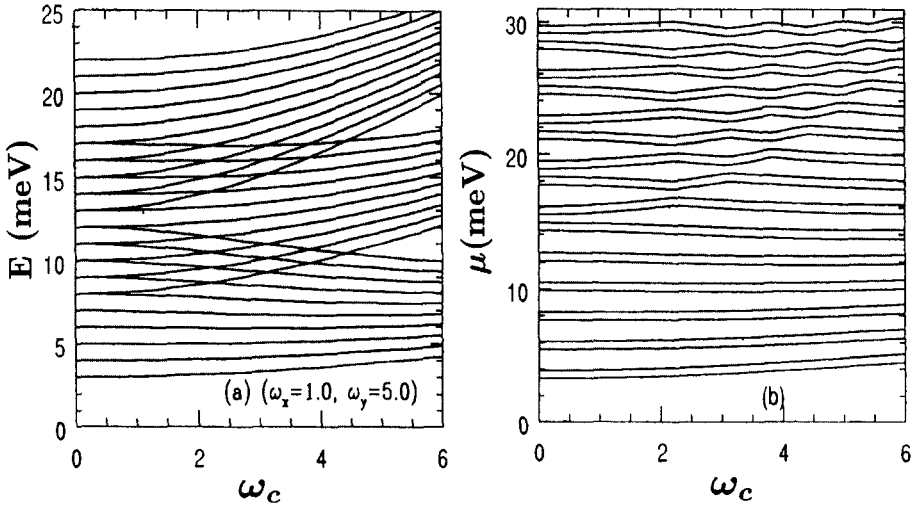
Fig. 5.3   Same as Fig. 5.2, but for $\omega_y = 5.0$ meV.
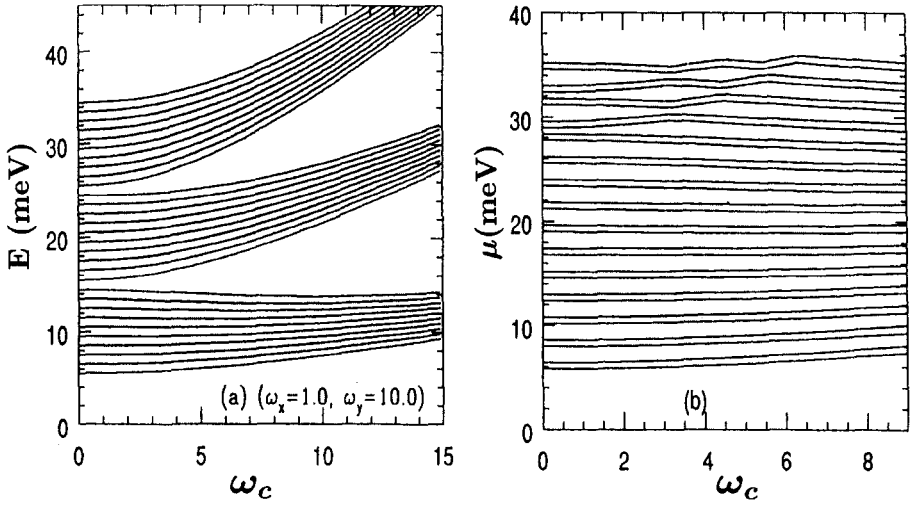
Fig. 5.4   Same as Fig. 5.2, but for $\omega_y = 10.0$ meV.

the deformation has the effect of quenching the shell structure, which is very evident for circular dots in the addition energy spectra of Figs. 2.5 and 2.8, exhibiting very prominent peaks at the magic numbers $2, 6, 12, 20, \ldots$. In elliptical dots the resulting spectra consist of a series of low, similar peaks, without clear shell effects. Moreover, the deformation favors the appearance of spin-density-wave states (SDV) (see Section 4.11).

Finally, we note that the frequencies (5.41) yield the exact excitation energies of the electric dipole modes excited by the centre-of-mass operators $D_x = \sum_{i=1}^{N} x_i$ and $D_y = \sum_{i=1}^{N} y_i$. In fact, due to the translational invariance of the interaction, the two-body interaction gives no contribution to the excitation energy of dipolar modes, which is affected solely by the external potential (see also Section 8.10.1). These excitations are produced by transitions with $\Delta n_x = 0$ and $\Delta n_y = 1$, or with $\Delta n_x = 1$ and $\Delta n_y = 0$, and therefore occur at energies Ω_1 and Ω_2.

5.5.1 Analogies with the Bose–Einstein condensate in a rotating trap

Let us consider a dilute gas of Bosons interacting through repulsive forces, at zero temperature and placed in a harmonic trap with frequencies $\omega_x, \omega_y \ll \omega_z$. If the confinement potential rotates around the z-axis with angular velocity Ω, the Hamiltonian of this N-particle, "quasi-two-dimensional" system, in the rotating reference frame is written as

$$H = \sum_i \left\{ \frac{p_x^2 + p_y^2}{2m} - \Omega l^z + \frac{1}{2} m(\omega_x^2 x^2 + \omega_y^2 y^2) \right\}_i + \frac{2\pi \hbar^2}{m} g \sum_{i<j=1}^{N} \delta(\mathbf{r}_i - \mathbf{r}_j), \quad (5.50)$$

where the position vector in the delta-like interaction are in the x–y plane.

The two-dimensional Hamiltonian (5.50), in the $\Omega = 0$ case, has been studied by several groups (Haugset and Haugerud 1998; Pitaevskii and Rosch 1997; Bhaduri et al. 1999; Petrov, Holzmann and Shlyapnikov 2000), and in the three-dimensional case and $\Omega \neq 0$ by A. Recati, F. Zambelli and S. Stringari (2001).

The dimensionless coupling constant g in the two-dimensional, δ-like interaction may be related to the scattering length a for the s-wave three-dimensional scattering. This is done starting from the three-dimensional δ-like potential (see Section 4.3.2) and calculating the expectation value of the δ function in the z direction, in the ground state wavefunction of the one-dimensional harmonic oscillator. In this way we obtain the effective two-dimensional interaction of (5.50), with coupling constant

$$g = \sqrt{\frac{2}{\pi}} \frac{a}{b_z}, \quad (5.51)$$

where $b_z = \sqrt{\hbar/m\omega_z}$ is the confinement length in z direction. This quasi-two-dimensional description of the trap in three dimensions is only valid for dilute systems, whose scattering length fulfills the condition $a \ll b_z \ll b_x, b_y$, where $b_x = \sqrt{\hbar/m\omega_x}$ and $b_y = \sqrt{\hbar/m\omega_y}$. Therefore, from equation (5.51) it follows that in (5.50) we have $g \ll 1$. From simple estimates it turns out that Hamiltonian (5.50) is experimentally realizable for a gas of Rubidium atoms with $N \simeq 10^4$ with $g \simeq 0.05$.

By comparing the one-body part of the Hamiltonian (5.50) with equation (5.34), we note that the formulae previously derived for the electron gas in an elliptical trap

under external magnetic field, can be generalized to the case of a Boson system in a rotating trap. The analogues of equations (5.39) and (5.41), are ($\omega_x > \omega_y$):

$$\alpha = \frac{m}{4}\left(\frac{\omega_x^2 - \omega_y^2}{\Omega}\right) - \frac{m}{4\Omega}\sqrt{(\omega_x^2 - \omega_y^2)^2 + 8\Omega^2(\omega_x^2 + \omega_y^2)}$$

$$\beta = -\frac{2}{m}\frac{\Omega}{\sqrt{(\omega_x^2 - \omega_y^2)^2 + 8\Omega^2(\omega_x^2 + \omega_y^2)}},$$

(5.52)

and

$$M_{1,2} = \frac{2m\sqrt{(\omega_x^2 - \omega_y^2)^2 + 8\Omega^2(\omega_x^2 + \omega_y^2)}}{(\omega_x^2 - \omega_y^2 \pm 2\Omega^2) + \sqrt{(\omega_x^2 - \omega_y^2)^2 + 8\Omega^2(\omega_x^2 + \omega_y^2)}}$$

$$\Omega_{1,2} = \frac{1}{\sqrt{2}}\left[\omega_x^2 + \omega_y^2 + 2\Omega^2 \pm \sqrt{(\omega_x^2 - \omega_y^2)^2 + 8\Omega^2(\omega_x^2 + \omega_y^2)}\right]^{1/2}.$$

(5.53)

From equations (5.52) and (5.53), it follows directly that the Schrödinger equation for the non-interacting Bose gas has no stationary solutions in the rotating system in the region $\Omega > \omega_y$ and $\Omega < \omega_x$, where $\Omega_{1,2}$ become imaginary. This is the main difference with respect to the electron gas under magnetic field, for which the frequencies (5.41) are always real. In the case of the dilute Boson gas, the δ-like interaction has important effects and may change the situation by generating stationary solutions different from the ones predicted by the non-interacting model (A. Recati, F. Zambelli and S. Stringari 2001). However, it does not affect the oscillation frequencies of the dipolar modes which are given by Ω_1 and Ω_2 of equation (5.53).

It is also very interesting to remark that, in the case $\Omega = \omega_x = \omega_y$, the one-body part of Hamiltonian (5.50), yields a single-particle spectrum:

$$\epsilon_{nl} = \hbar 2\Omega\left(M + \frac{1}{2}\right),$$

(5.54)

where we have introduced the label $M \equiv n + \frac{1}{2}(|l| + l)$. Therefore, we see that the Boson states in the rotating system are distributed among infinitely-l-degenerate levels, which are the analogues of the Landau levels for electrons, characterized by the values of $M = 0, 1, 2, \ldots$. The $M = 0$ level contains states with $n = 0$, and non-positive values of l, i.e. $l = 0, -1, -2, \ldots$. Therefore, in this situation there is a very close analogy with the quantum Hall effect. Such analogy leads to the identification, also in the case of Bosons in a rotating trap, of ground states of Laughlin type. For a discussion of this point, see for example Peredes et al. (2001).

5.6   Spin-Orbit Coupling and Spintronics

A novel technology based on the use of the electron spin, as opposed to the more traditional use of the electron charge, is emerging under the name of spintronics.

Several spin-based electronic devices have already proved their importance, even at a commercial level, such as the spin-valve read heads. A review of the status of this incipient field can be found in Wolf et al. (2001).

The spin-orbit (SO) coupling is an essential mechanism for most spintronics devices, since it links the spin and the charge dynamics, opening the possibility of spin control through electric fields (Datta and Das 1990). Indeed, recent experimental and theoretical investigations have shown that the SO coupling affects the charge transport and, more specifically, the conductance fluctuations of chaotic quantum dots in a parallel magnetic field (Folk et al. 2001; Halperin et al. 2001; Aleiner and Fal'ko 2001). It also affects the dot far-infrared absorption, introducing peculiar correlations between the charge and spin oscillating densities (Valín-Rodríguez, Puente and Serra 2002). Finally, a sufficiently strong SO coupling can lead (Valín-Rodríguez et al. 2002) to spin inversion, with an alternating B-dependence, similar to the observations from capacitance spectroscopy experiments of both vertical (Ashoori 1996) and lateral quantum dots (Voskoboymikov et al. 2001).

In this Section we analyze the combined effects of SO coupling, weak vertical magnetic (B) fields, and spatial deformation in fixing the spin and other ground state properties of model semiconductor dots. We consider the SO coupling terms as reviewed by Voskoboynikov et al. (2001). Assuming a $2D$ system and the effective Hamiltonian formalism, the relevant Dresselhaus contribution for the standard (001) plane of GaAs reads

$$\mathcal{H}_D = \frac{\lambda_D}{\hbar} \sum_{i=1}^{N} [P_x \sigma_x - P_y \sigma_y]_i \,, \tag{5.55}$$

where the σ's are the Pauli matrices and

$$\mathbf{P} = -i\hbar\nabla + \frac{e}{c}\mathbf{A}$$

represents the canonical momentum given in terms of the vector potential $\mathbf{A}$, taken in the symmetric gauge. The Dresselhaus parameter λ_D is determined by the dot vertical width z_0 as (Voskoboynikov et al. 2001) $\lambda_D \approx \gamma(\pi/z_0)^2$, with a material-specific constant γ that for GaAs is $\gamma = 27.5$ eV $\mathring{A}^3$ (Knap et al. 1996). In the following we will not consider a SO coupling of Rashba type, proportional to $\ell \cdot \sigma$ (Voskoboynikov et al. 2001), since its contribution to the results for GaAs turns out to be negligible.

Neglecting the Coulomb interaction the complete Hamiltonian reads $\mathcal{H} = \mathcal{H}_0 + \mathcal{H}_D + \mathcal{H}_Z$, where $\mathcal{H}_0$ consists of the kinetic and confinement energies, i.e.

$$\mathcal{H}_0 = \sum_{i=1}^{N} \left[\frac{\mathbf{P}^2}{2m} + \frac{1}{2}m(\omega_x^2 x^2 + \omega_y^2 y^2) \right]_i .$$

The Zeeman term $\mathcal{H}_Z$ depends on the total vertical spin S_z, the Bohr magneton μ_B and the effective gyromagnetic factor g^*, which for bulk GaAs is -0.44. Namely, $\mathcal{H}_Z = g^* \mu_B B S_z$.

Assuming $\mathcal{H}_0 \gg \mathcal{H}_D \gg \mathcal{H}_Z$ and expanding in powers of λ_D an analytic diagonalization to $O(\lambda_D^3)$ in spin space is possible with a unitary transformation (Aleiner and Fal'ko 2001) $\tilde{\mathcal{H}} = U_1^+ \mathcal{H} U_1$, where

$$U_1 = exp\left[-i\lambda_D \frac{m}{\hbar^2} \sum_{i=1}^{N} (x\sigma_x - y\sigma_y)_i \right], \qquad (5.56)$$

giving the transformed Hamiltonian:

$$\tilde{\mathcal{H}} = \sum_{j=1}^{N} \left[\frac{\mathbf{P}^2}{2m} + \frac{1}{2}m(\omega_x^2 x^2 + \omega_y^2 y^2) + \lambda_D^2 \frac{m}{\hbar^3} \mathcal{L}_z \sigma_z + \frac{1}{2}g^* \mu_B B \sigma_z \right]_j$$

$$- N\lambda_D^2 \frac{m}{\hbar^2} + O(\lambda_D^3), \qquad (5.57)$$

where we have defined the *canonical* angular momentum operator $\mathcal{L}_z = xP_y - yP_x$. Despite the spin diagonalization, the x and y degrees of freedom in (5.57) are still coupled through the vector potential in the kinetic energy and in $\mathcal{L}_z$. With a second transformation of the same type used in Section 5.5, each spin component can be recast in a separable form. Specifically, defining $\hat{\mathcal{H}}_\eta = U_{2\eta}^+ \tilde{\mathcal{H}}_\eta U_{2\eta}$, with $\eta = \uparrow, \downarrow$ and U given by equation (5.38), we obtain

$$\hat{\mathcal{H}}_\eta = \sum_{j=1}^{N_\eta} \left[\frac{p_x^2}{2M_{1\eta}} + \frac{M_{1\eta}}{2}\Omega_{1\eta}^2 x^2 + \frac{p_y^2}{2M_{2\eta}} + \frac{M_{2\eta}}{2}\Omega_{2\eta}^2 y^2 + \frac{1}{2}g^* \mu_B B s_\eta \right]_j$$

$$- N_\eta \lambda_D^2 \frac{m}{\hbar^2} + O(\lambda_D^3), \qquad (5.58)$$

where $s_\eta = \pm 1$ for $\eta = \uparrow, \downarrow$. Assuming, without the loss of generality, $\omega_x \geq \omega_y$ the masses and frequencies of the decoupled oscillators are

$$M_{k\eta} = \frac{2m\sqrt{(\omega_x^2 + \omega_y^2 + \omega_{c\eta}^2)^2 - 4\omega_x^2\omega_y^2}}{\omega_x^2 - \omega_y^2 \pm \omega_{c\eta}^2 + \sqrt{(\omega_x^2 + \omega_y^2 + \omega_{c\eta}^2)^2 - 4\omega_x^2\omega_y^2}},$$

$$\Omega_{k\eta} = \frac{1}{\sqrt{2}}\left[\omega_x^2 + \omega_y^2 + \omega_{c\eta}^2 \pm \sqrt{(\omega_x^2 + \omega_y^2 + \omega_{c\eta}^2)^2 - 4\omega_x^2\omega_y^2} \right]^{1/2} \qquad (5.59)$$

with the upper (lower) sign in $\pm$ corresponding to $k = 1(2)$. We have defined in (5.59) a spin dependent cyclotron frequency which incorporates the SO correction,

$$\omega_{c\uparrow,\downarrow} = \frac{eB}{mc} \pm 2\lambda_D^2 \frac{m}{\hbar^3}. \qquad (5.60)$$

The solution to equation (5.58) is given by products of x and y harmonic oscillator functions which, when transformed back to the laboratory frame, yield the desired solutions to the original Hamiltonian. The eigenvalues for each spin can be labelled
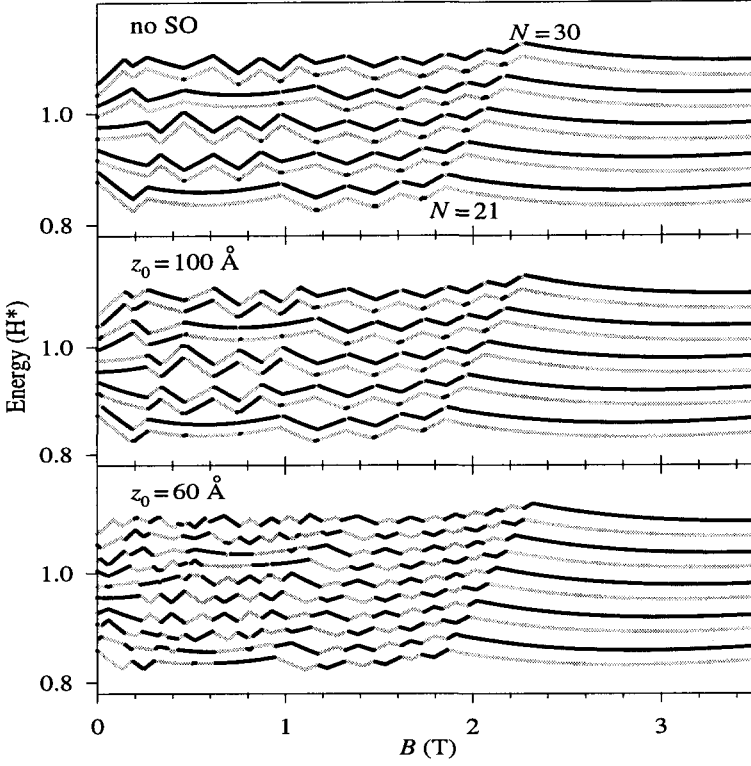
Fig. 5.5 Single-particle energies in effective atomic units in the noninteracting model. Circular symmetry with $\omega_x = \omega_y = 1.1$ meV has been assumed. Each line has been shifted vertically by a small amount representing the charging energy. Light and dark gray color correspond to up and down spin, respectively.

by the number of quanta in the x and y oscillators:

$$\varepsilon_{N_1 N_2 \eta} = \left(N_1 + \frac{1}{2}\right) \hbar\Omega_{1\eta} + \left(N_2 + \frac{1}{2}\right) \hbar\Omega_{2\eta} + s_\eta \frac{1}{2} g^* \mu_B B - \lambda_D^2 \frac{m}{\hbar^2}. \quad (5.61)$$

Figure 5.5 displays the magnetic field evolution of the single-particle energies (5.61) for a circular dot, except for a constant representing the charging energy. These values give the chemical potential of the dot for varying electron number, as measured for instance in capacitance spectroscopy experiments (Ashoori 1996; Ciorga et al. 2000). (Notice that, unlike the results reported in Figs. 5.2–5.4, they do not include the effect of the interaction calculated in the constant interaction model. Consequently the results reported in the top of Fig. 5.5, differ from the ones of Fig. 5.2 by a constant). Actually the parabola coefficient has been taken from a fit to the experiments. The spin is indicated in Fig. 5.5 with the light and dark gray tones. In the absence of SO coupling each line corresponds to a given spin, except for a very small fluctuation due to the Zeeman energy at some cusps and valleys.

In this case the traces arrange themselves in parallel pairs of up and down spin. As shown in the two lower panels of Fig. 5.5, the SO coupling produces sizeable up and down fluctuations of the spin. For $z_0 = 100$ Å, i.e. weak SO coupling, the fluctuations start at low magnetic fields and they extend up to $B \approx 1$ T. An even stronger SO ($z_0 = 60$ Å) produces spin inversions up to the last level crossing, which marks the filling factor $\nu = 2$ line. Besides, in the latter case the traces are no longer paired but, instead, anticorrelated with a π phase shift; specially in the region just before $\nu = 2$. The results of Fig. 5.5 can help to interpret the experiments of Ashoori (1996) and Ciorga et al. (2000), which observed anticorrelated behavior in the traces and spin alternation with increasing B, respectively.

The effects of deformation and Coulomb interaction have been analyzed by Valín-Rodríguez et al. (2002) using the local-spin density approximation within a spinorial formalism, since the spin-orbit term breaks the symmetry of a single spin quantization axis.

As an example, Fig. 5.6 shows $\langle S_z \rangle$ as a function of B and the intensity of the SO coupling, given by z_0, for for $N = 9$ electrons in a circular confining potential with $\omega_x = \omega_y = 6$ meV. In agreement with the above discussion, for $B \leq 2.2$ T the noninteracting model predicts spin inversion when decreasing the dot width. The *LSDA* also yields spin-inverted regions although with some conspicuous differences. The interaction inhibits the spin flip at low magnetic fields and low widths, shifting the inversion region to 1.8 T $\leq B \leq$ 2.6 T and leaving only a small residue for $z_0 \leq 40$ Å and $B \leq 1.2$ T. It is worth mentioning that although in the laboratory
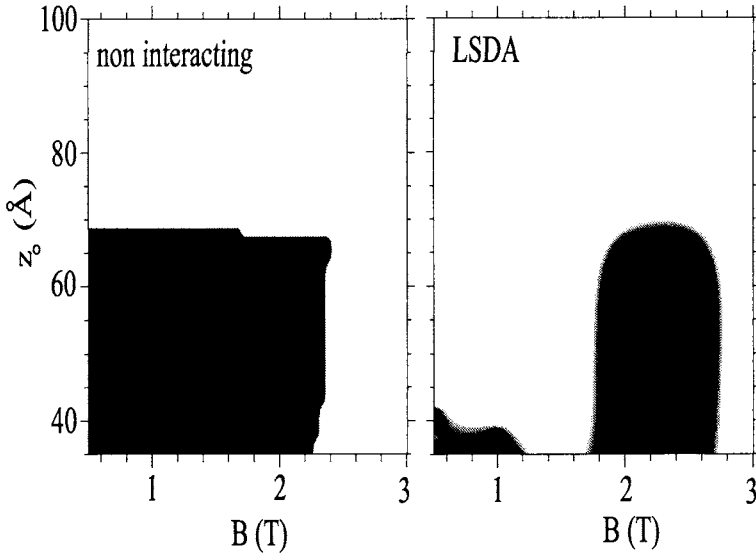
Fig. 5.6   Vertical spin evolution in the B–z_0 plane for the for a circular dot with $N = 9$ electrons, $\hbar\omega_x = \hbar\omega_y = 6$ meV. White (black) color indicates upward (downward) total spin.

frame $\langle S_z \rangle$ is not restricted to discrete values (because of the transformation U_1), in practice its fluctuations increase with the SO strength but they are generally small.

5.7 *DFT* for Quantum Dots in a Magnetic Field

In this Section we present the results for two GaAs quantum dots ($g^* = -0.44$, $\epsilon = 12.4$, $m^* = 0.067$) with $N = 25$ and $N = 210$ electrons, under constant external magnetic field (Lipparini et al. 1997; Pi et al. 1998); the results were obtained using the *CDFT* theory described in Section 4.7. The reason for this choice is that these dots have been studied experimentally (Demel et al. 1990), and are good examples of small and large dots. We will also briefly discuss the results obtained by *HF* and Ensemble *DFT* calculations (see Section 4.8).

The *CDFT* calculations were carried out at low temperature, $T \leq 0.1$ °K. This makes the calculation possible in the case of configurations with non-integer filling factor ν, and produces no appreciable thermal effect. For integer ν, the calculation was carried out at $T = 0$.
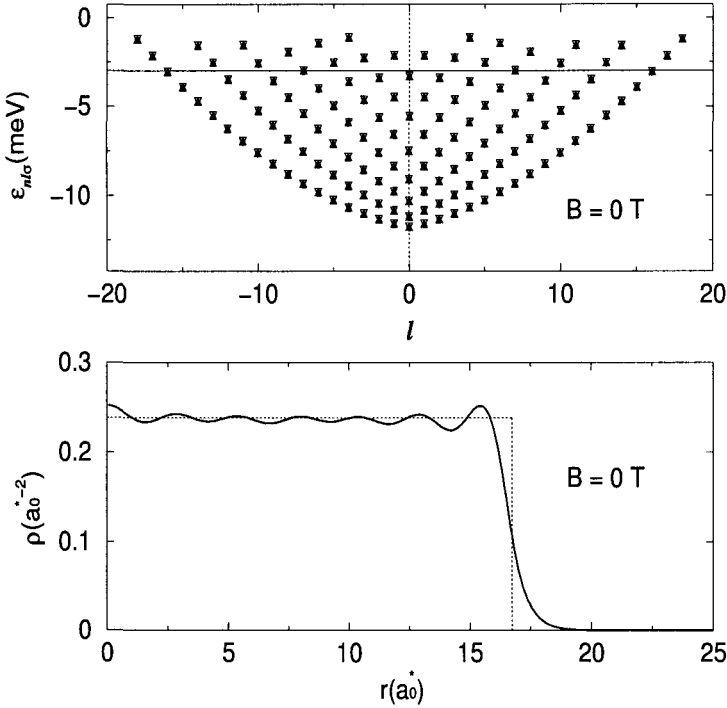
Fig. 5.7 Top: single-particle energies as a function of l for the $N = 210$ dot at $B = 0$. The full triangles represent spin-up states, the open triangle the spin-down states. The horizontal line represents the chemical potential of electrons. Bottom: Electron density ρ as a function of r. The dotted line is the density of the jellium disc.

Two different models of the $N = 25$ dot were employed. In the first one, the external confinement potential was the one produced by a jellium disc with a radius R of 100 nanometres, one which on can find uniformly distributed $N^+ = 28$ positive charges. This potential is analytic:

$$v_{\text{ext}}(r) = \frac{4N^+}{\pi R^2} \times \begin{cases} R\,\mathbf{E}(r/R) & r < R \\ r\{\mathbf{E}(R/r) - [1 - (R/r)^2]\mathbf{K}(R/r)\} & r > R. \end{cases} \quad (5.62)$$

In this equation, $\mathbf{K}$ and $\mathbf{E}$ are the complete elliptic integrals of the first and second kind respectively. In the second model, a harmonic oscillator potential was employed with $\omega_0 = 2.78$ meV. For the $N = 210$ dot only the disc was used, with radius $R = 160$ nm and $N^+ = N$.

The density and the single-particle energies of the $N = 210$ at $B = 0$ are plotted in Fig. 5.7. The single-particle energies, as a function of l, are distributed on parabolic curves, each curve being characterized by a different quantum number n. The figure shows the degeneracy of each single-particle level, corresponding to the possible choices $\pm|l|$, $\sigma = \pm 1$. Figure 5.8 shows the same results for the 25-electron dot and the two different confinement potentials. From the middle
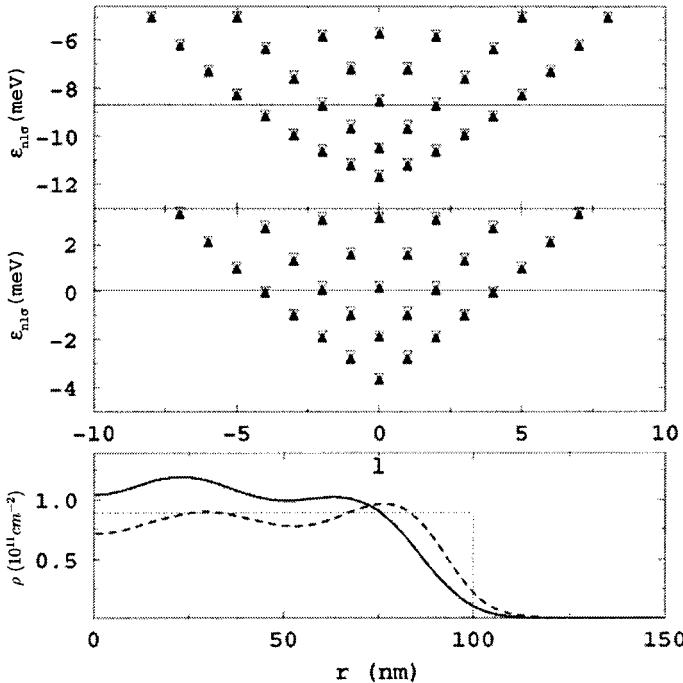
Fig. 5.8   Top: the same as the top of Fig. 5.7, but for the $N = 25$ dot with confinement produced by the jellium disc. Middle: it is same as top, but with parabolic confinement. Bottom: the corresponding electron densities ρ as a function of r. Full line: disc confinement; dashed line: parabolic confinement. The dotted line represents the density of the jellium disc.

panel of Fig. 5.8, we note that the contributions of the Hartree potential and of the exchange-correlation potential, affect very little the linear dependence on l predicted by the independent-particle model [see Eq. (5.8)].

Figure 5.9 shows the single-particle spectra for the $N = 210$ dot, as a function of l and for B values in the range 1.29–10.28 T (Tesla), which correspond to the incompressible states with reported ν value. In order to evaluate ν we used equation (5.23) with $\rho = 210/(\pi R^2)$ and $R = 160$ nm. At $B = 10.28$ T $(\nu = 1)$, the system is completely spin-polarized. Note that, due to the sign of the term linear in l in the KS equations (4.60), most occupied levels have a positive l, i.e. a negative angular momentum, and that the $(M, \uparrow)$ band is lower in energy than the $(M, \downarrow)$ band due to the negative value of g^* used in the calculation. For this reason, in the following we indicate by L_z the value of the total orbital angular momentum with opposite sign, and by S_z the component of the total spin in the z direction.
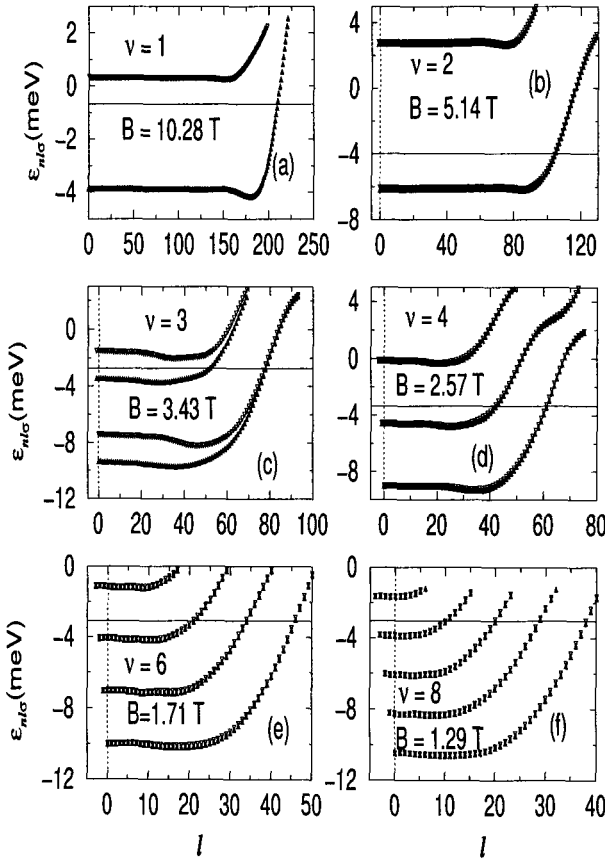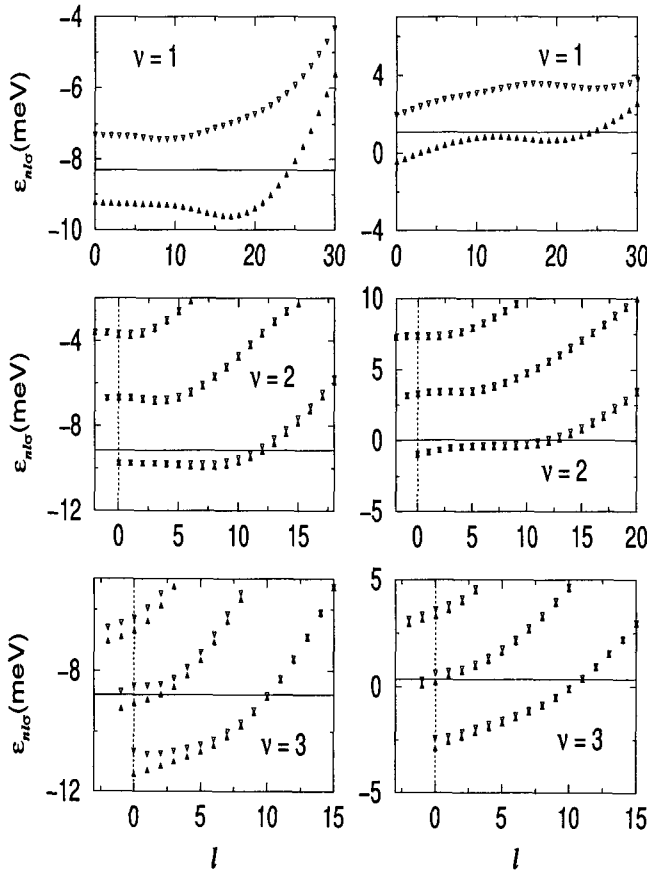

Fig. 5.9 Single-particle energies of the $N = 210$ dot as a function of l for $\nu = 1$–6, 8. The full triangles represent the $(M, \uparrow)$ bands, and the open triangles the $(M, \downarrow)$ bands. The horizontal line is the chemical potential of the electrons.

It is remarkable that, for the 210 electron dot, the magnetic fields corresponding to the different ν values follow the law which holds for the bulk, i.e. $B(\nu) = \frac{1}{\nu}B(1)$, up to ν values as large as $\nu = 11$. A similar behavior is observed also in the $N = 25$ case, up to $\nu = 6$. Confinement potentials like those produced by a disc, favor the existence of incompressible regions in the inner region of the dot, because the electrons in these regions tend to establish a density close to that of the positive background in order to screen the Coulomb potential. This can be seen, for example, in the incompressible states shown in Fig. 5.9.

Figure 5.10 shows some electronic densities and magnetizations $m(r) = \rho_+ - \rho_-$ for the 210-electron dot, together with the L_z and $2S_z$ values predicted by the calculation. From this figure we see that these states are the finite-dimension-analogues of the Landau incompressible states with $\nu = 1 - 4, 6$ and 8; the latter, for an electronic density of 2.61×10^{11} cm^{-2}, would be realized exactly at the same B values. Actually, the densities in Fig. 5.10 have a step-like shape, whose plateau has the value $\rho = \nu B/2\pi c$.
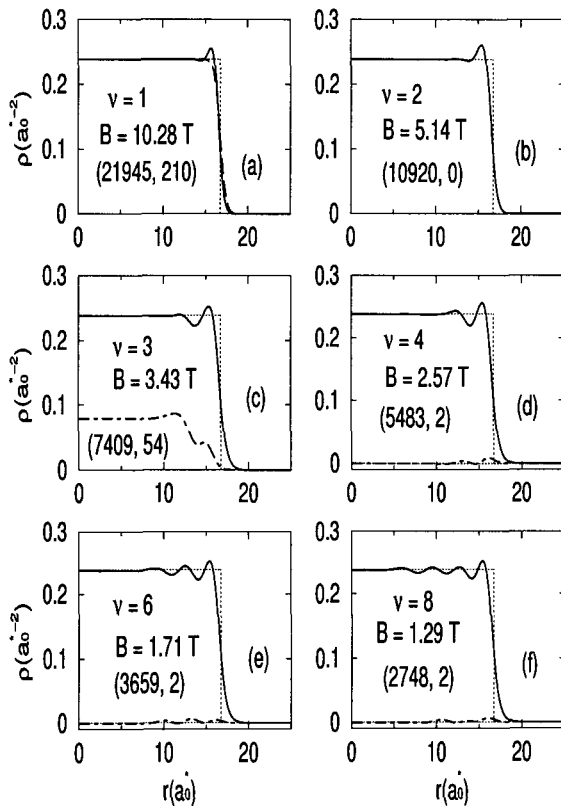
Fig. 5.10   Electron densities $\rho(r)$ (Full curves), and spin magnetizations (dotted-dashed curves) corresponding to some of the configurations of Fig. 5.9. The dashed curve in the top left panel represents the density of the MDD state. The values of $(L_z, 2S_z)$ are also plotted.

Let us discuss now the results relative to the 25-electron dot, obtained by using the two different confinement potentials. In particular, let us compare the results at the same values of ν rather than B. Note that the completely polarized states $\nu = 1$ correspond to $B = 3.56$ T in the case of disc confinement, and to $B = 4.58$ T in the harmonic oscillator case. For $\nu > 1$, the B values obey the law $B(\nu) = \frac{1}{\nu}B(1)$.

Figure 5.11 shows the single-particle energies for $\nu = 1, 2$ and 3, and Fig. 5.12 the electron densities. It is interesting to notice that the two confinement potentials, whose parameters were fixed so as to reproduce the experimental energy of the dipole mode at $B = 0$, yield rather different electronic densities. In general, the ground state configurations corresponding to parabolic confinement are more compact.

We will now describe some results for the 210-electron dot obtained by Pi et al. (1998). In the case of such large dot, it is found that the values of the angular

Fig. 5.11   Single-particle energies of the $N = 25$ dot as a function of l for $\nu = 1, 2, 3$. Full triangles represent the (M,↑) bands, and the open triangles the (M,↓) bands. The horizontal line is the chemical potential of electrons. The panels on the left correspond to disc confinement, those on the right to parabolic confinement.
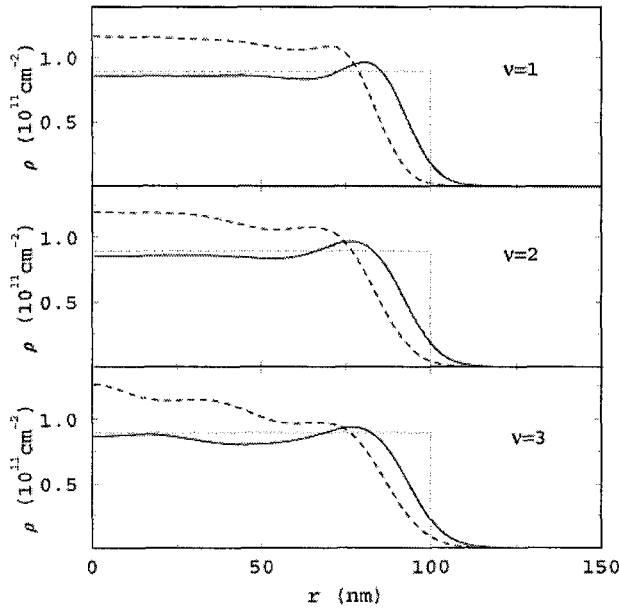
Fig. 5.12   Electron densities $\rho(r)$ for the $N = 25$ dot, for disc confinement (full lines), and for parabolic confinement (dashed lines), corresponding to the configurations of Fig. 5.11.

momentum at different B follow the law

$$L_z = \nu^{-1} \frac{N(N-1)}{2} , \tag{5.63}$$

and the spin is approximately given by

$$2S_z = \begin{cases} 0 & \nu \quad \text{even} \\ N/\nu & \nu \quad \text{odd} \end{cases} \tag{5.64}$$

and these expressions are valid in the limit of large N values for incompressible Landau states. The validity of these equations is explicit from Fig. 5.13, where we plotted the orbital and spin angular momenta as a function of B. The small plateaux found along the $L_z(B)$ curve at integer ν values, which appear in the $2S_z(B)$ curve as well, demonstrate the robustness of these states against changes in B, and their resistance toward L_z and S_z changes. In fact, because of the term $\omega_c^2 r^2$ in (4.51), when B increases starting from a given value $B(\nu)$, the electronic density is compressed, thereby increasing the electrostatic energy of the dot. This energy is abruptly compensated by a sudden increase of the angular momentum through the population of single-particle levels with higher l values. This effect is fast due to the low density of single-particle states around the Fermi surface when ν is integer, and is quite similar to the effect described for smaller dots (Ferconi and Vignale 1994). On the other hand, the high density of single-particle states at the
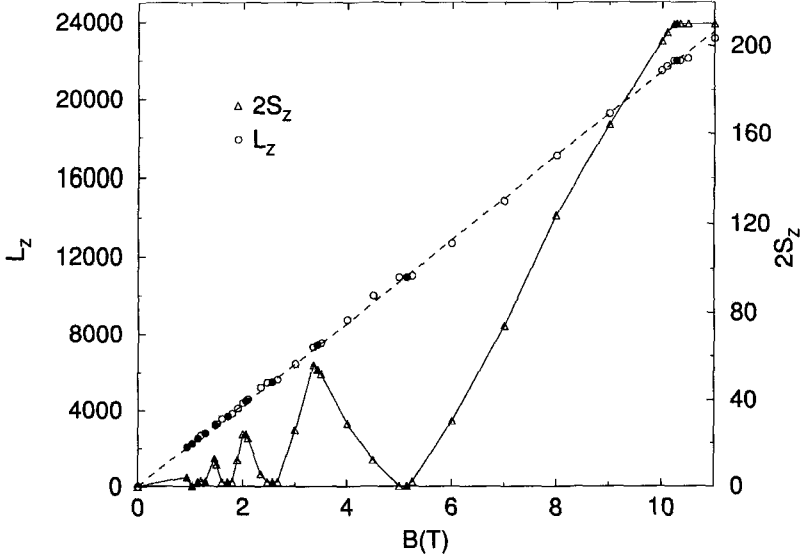
Fig. 5.13 L_z (circles and left-hand scale) and $2S_z$ (triangles and right-hand scale), as a function of B for the $N = 210$ dot. The values corresponding to integer filling factors from 1 to 11 are the full symbols, and the line connecting the $2S_z$ points is a guide to the eye. The dashed line is from Eq. (5.63).

Fermi energy, when the state is compressible (i.e. $\nu > 1$ is not an integer), makes L_z increase gradually with B.

In the $\nu = 1$ panel of Fig. 5.10 the density (5.18) of the MDD state is plotted. Recall that for $N \to \infty$ this state is the incompressible state with $\nu = 1$ of the quantum Hall effect, and that for sufficiently high magnetic fields this state has an exact expression, i.e. a Slater determinant of single-particle orbitals with angular momenta $0, 1, \ldots, N - 1$, belonging to the first Landau level.

The natural question, to which people have tried to give an answer in many papers (see for example Ferconi and Vignale 1997), is whether the MDD state can be the ground state of a quantum dot. The stability region of such completely spin-polarized state in the N-B plane, is bound to the left by the line B_f which, for a given number of electrons, represents the magnetic field for which $2S_z = N$. To the right it is bound by the line B_r where the reconstruction of the quantum dot boundary begins, which means the process by which electrons begin to be transferred to single-particle states with $l > N - 1$. This region is very narrow because after complete polarization of the system, the magnetic field is very effective in reconstructing the dot boundary. For the $N = 25$ dot, one finds $B_f = 4.46 \leq B \leq B_r = 4.70$ T for harmonic confinement, and $B_f = 3.42 \leq B \leq B_r = 3.70$ T for the disc. For parabolic confinement the stability region of the MDD state narrows as N increases, and vanishes beyond a critical N value. For example, in the case of the 210-electron dot, it has been impossible to find the B value corresponding to the MDD state for

parabolic confinement. These results appear to have been confirmed by the recent experimental work of Oosterkamp et al. (1999).

For the jellium disc confinement, and for $N = 210$, it seems that the MDD state exists, as indicated by Figs. 5.9 and 5.10. As can be seen from the top left panel of Fig. 5.10, the two densities [i.e. the one yielded by the $CDFT$ calculation and the one from Eq. (5.18)] are very similar, with only one difference arising at the boundary. The protuberance in the $CDFT$ density at the boundary is due to both the confinement potential which changes abruptly at the boundary, and to the exchange-correlation energy which also varies very fast there.

It is also very interesting to consider the energy splitting $\Delta E_{\downarrow\uparrow}$ between the Landau bands $(M, \uparrow)$ and $(M, \downarrow)$, reported for example in Fig. 5.9. This difference is very small for even values of ν, which correspond to ground states with $S_z \simeq 0$ (paramagnetic states), because the Zeeman term in (4.51) and (4.60) is also very small (for example, $\simeq 0.26$ meV at $B = 10.28$ T), and $\Delta E_{\downarrow\uparrow} \simeq |g^* \mu_0 B|$. On the contrary, the energy splitting is large for odd ν values, even when the applied magnetic field is small; compare, for example, the cases $\nu = 3$ and $\nu = 6$ in the same figure. These ground states have rather high values of S_z (they are ferromagnetic states) and the large splitting is due to the exchange-correlation potential, which depends on the magnetization: $\Delta E_{\downarrow\uparrow} \simeq 2|W_{xc}|$. W_{xc} is zero for paramagnetic states, and large for ferromagnetic ones, giving rise to an energy splitting much larger than that due to the Zeeman term. The HF, $LSDFT$, and $CFDT$ calculations yield this large splitting, while the Hartree approximation does not. The exchange and correlation effects are the origin of the simple structure of the MDD state, since they prevent the two $(0, \uparrow)$ and $(0, \downarrow)$ Landau bands from being close in energy at $\nu = 1$, and so from contributing to setting up the ground state. As we already stressed in Chapter 4, these spin splittings are similar to the isospin ones that occur in nuclei for which the number of neutrons differs from the number of protons. The exchange-correlation potential that produces them is the analogue of the symmetry potential in the nuclei.

The B-dependence of the total energy E of the 210-electron dot is shown in Fig. 5.14. Local minima of E are clearly observed at ν values corresponding to the paramagnetic states of the dot. On the other hand, local maxima occur at ν values corresponding to ferromagnetic states. The energy exhibits an inflection point at the ferromagnetic state $\nu = 1$ with $2S_z = 210$. Therefore, in this dot, which has quite a large N value, one observes several transitions from paramagnetic to ferromagnetic states. In dots with small number of electrons this does not occur, and normally one observes just one transition between these two states. In the bottom panel of the same figure, we report the L_z-dependence of E, exhibiting local minima in correspondence with the paramagnetic states. The existence of many paramagnetic states plays a fundamental role in keeping the dot energy around its value at $B = 0$. $|E|$ decreases as S_z increases, and vice-versa. Only beyond the $\nu = 2$ state does E increase monotonously with S_z, and finally reaches its full-polarization value at about $\nu = 1$.
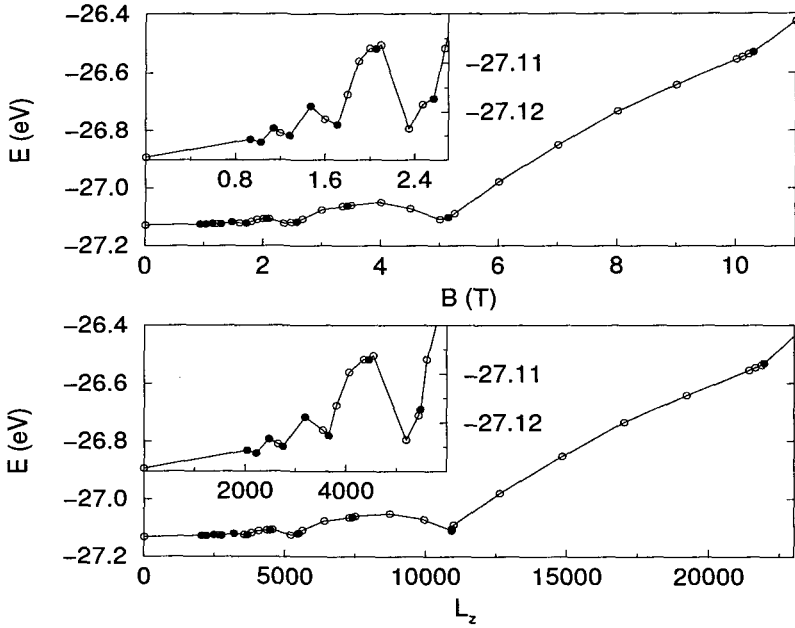
Fig. 5.14 Top: total energy of the $N = 210$ dot as a function of B. The values corresponding to the integer filling factors in the range 1–11 are indicated by full symbols. The line connecting the points is a guide to the eye. The inset shows the low-B region with the relative scale to the right. Bottom: the same as top, but as a function of L_z.

The chemical potential μ and the ionisation potential $IP = E_{N-1} - E_N$ are shown in Fig. 5.15. They exhibit a saw-tooth behavior as a function of B, with an abrupt decrease in the vicinity of integer ν values. The corresponding L_z values are a sort of magic numbers, corresponding to which the dot is especially stable. Note that the large size of this dot is the cause of the great similarity between the μ and IP values, as well as of the large oscillations of the ionisation potential.

Another interesting quantity, that we shall use later on, is the electric field $\mathcal{E}(r)$ produced by the electrons of the dot. This field is plotted in Fig. 5.16 for the B values corresponding to $\nu = 2/3, 1, 4$. $\mathcal{E}(r)$ has a strong peak at the dot boundary, with features reflecting the complex structure of the dot density in that region.

So far we have considered mainly incompressible states with ν values integer and ≥ 1. These are particularly simple configurations whose ground states can be described by a single Slater determinant, and that in the density functional theory are normally labelled as pure v-representable states (Dreizler and Gross 1990). Examples of non-v-representable densities are those corresponding to degenerate ground states. Many ground states of quantum dots, corresponding to non-integer ν values, which are compressible, are found to be non-v-representable. An example of such configurations is shown in Fig. 5.17, where we plot the single-particle energies of the $N = 210$ dot, for $B = 4, 7$ and 9 T. These results were obtained at a temperature of 0.1 °K.
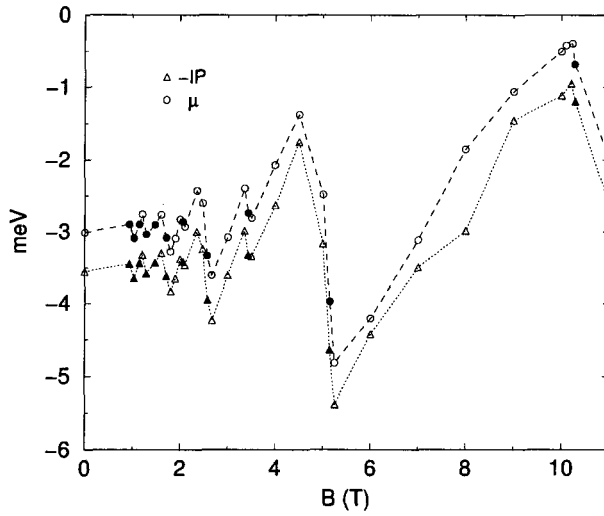
Fig. 5.15 Chemical potential of the electrons (circles) and *-IP* (ionisation potential, triangles) of the $N = 210$ dot, as a function of B. The points corresponding to integer filling factors in the range 1–11, are indicated by full symbols.
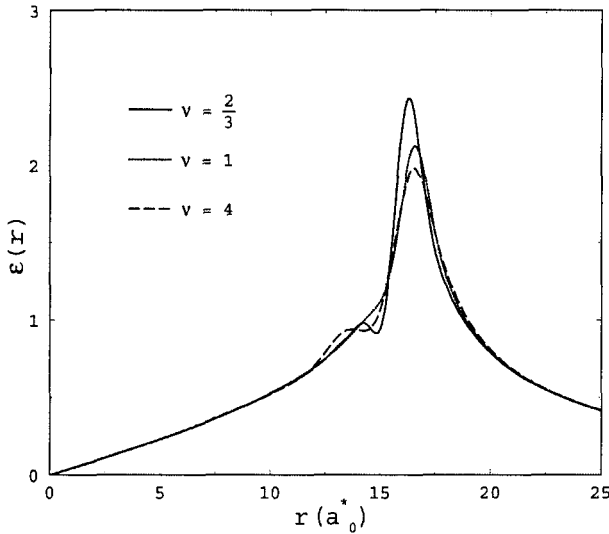
Fig. 5.16 Electric field $\mathcal{E}(r)$ produced by the electrons of the $N = 210$ dot, as a function of r for the reported filling factors.

Contrary to the incompressible configurations described above, it can be shown that these ground states are highly degenerate, with many electronic levels whose energies are very close to the chemical potential. The panels on the left side of Fig. 5.18 show the thermal occupation numbers f_i [see Eq. (4.64)] for the same values of B, and those on the left side of Fig. 5.19 show the corresponding densities
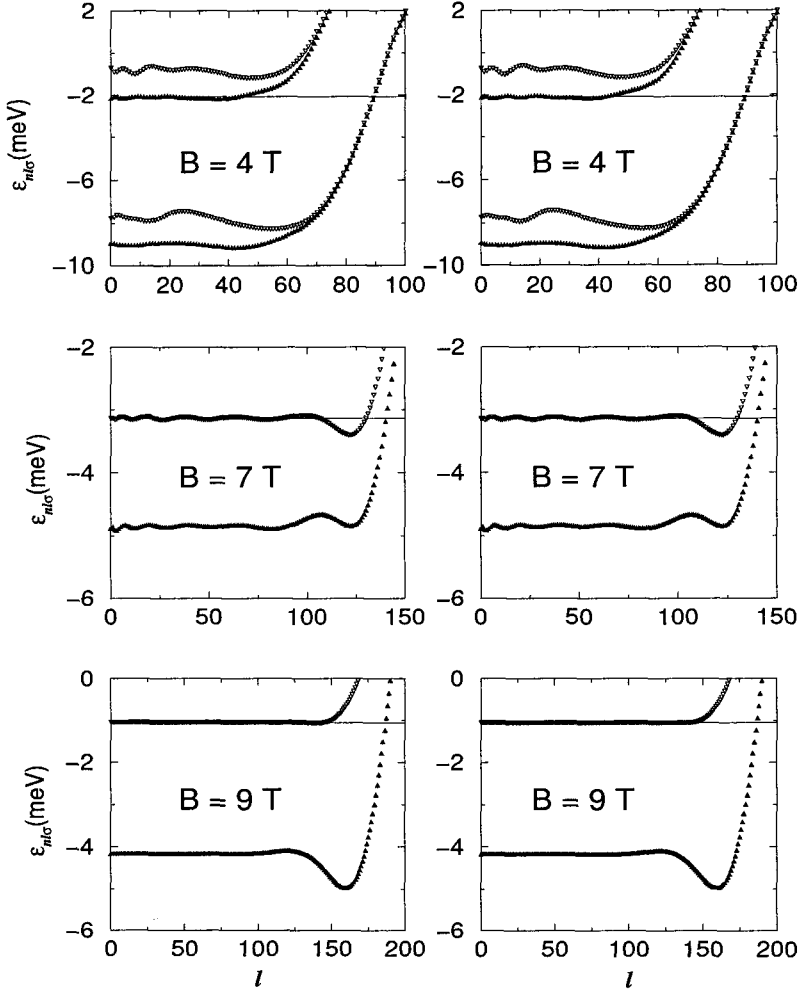
Fig. 5.17 Single-particle energies of the $N = 210$ dot as a function of l for $B = 4, 7$ and 9 T, respectively. The horizontal line is the chemical potential of the electrons. The labelling is the same as in Fig. 5.9. Panels on the left: *DFT* results at $T = 0.1$ °K. Panels on the right: *EDFT* results.

and magnetisations. The corresponding EDTF values are shown in the panels on the right sides of the two figures in question. The L_z and $2S_z$ values predicted by the two theories are reported in Table 5.2. We recall that the *EDFT* theory is a generalisation of the density functional theory, which is used to treat cases of degenerate Kohn–Sham ground states (see Section 4.8).

As can be seen from the table, the particle number fluctuations, given by $\Delta N/N$, are small and thus allow the use of the grand canonical ensemble to describe the dot (see Section 4.7).
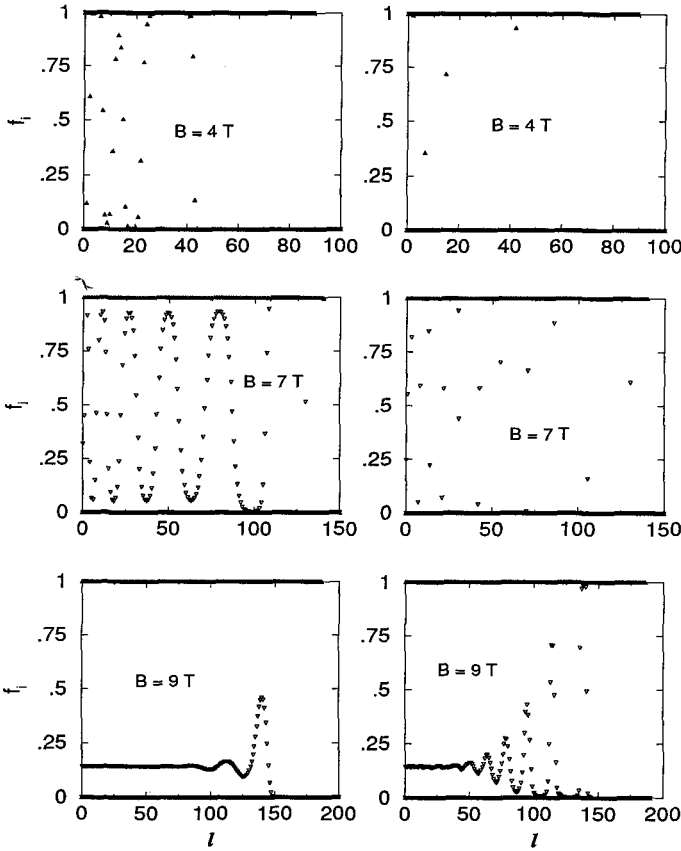
Fig. 5.18 Single-particle occupation numbers of the $N = 210$ dot as a function of l for $B = 4, 7$ and 9 T, respectively. Panels on the left: DFT results at $T = 0.1$ °K. Panels on the right: $EDFT$ results.

TABLE 5.2

	E (eV)		L_z		$2S_z$		$\Delta N/N$ (%)	
B (T)	CDFT	EDFT	CDFT	EDFT	CDFT	EDFT	CDFT	EDFT
4	-27.05	-27.05	8729	8730	30	30	0.8	0.3
7	-26.85	-26.85	14812	14811	72	72	1.6	0.8
9	-26.64	-26.64	19217	19218	164	164	2.1	1.8

From inspection of Figs. 5.17–5.19 and of Table 5.2, it may be concluded that the finite-temperature version of the $CDFT$ theory allows us to solve the technical problem that arises when the single-particle density of states is large, and it is not possible to solve the Kohn–Sham equations at zero temperature with occupation numbers 0 or 1. Moreover, it allows us to obtain the electron densities and other characteristics of highly correlated states that cannot be described even
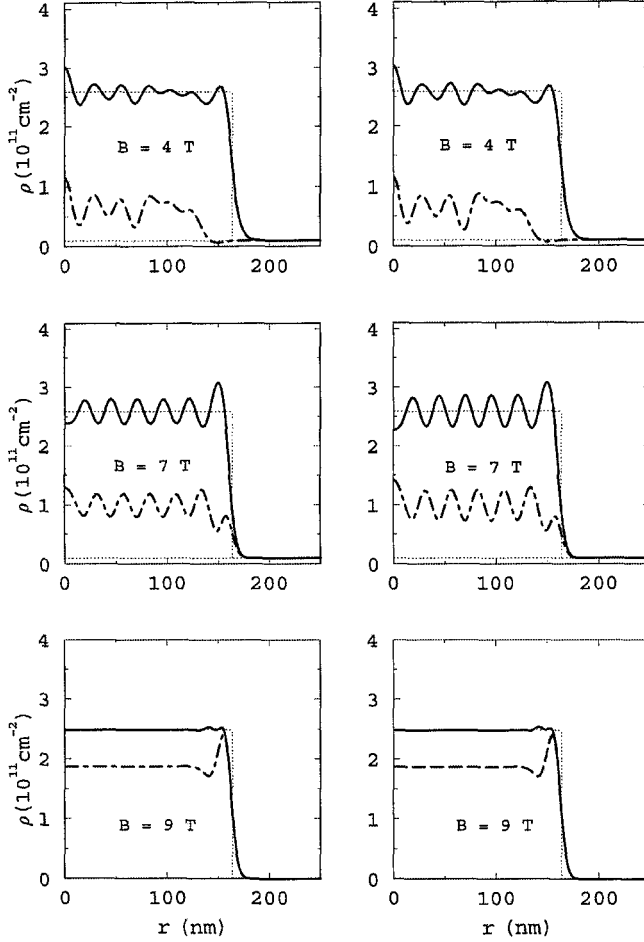
Fig. 5.19 Electronic densities ρ (r) (full curves), and spin magnetisations (dashed curves) of the $N = 210$ dot as a function of r for $B = 4, 7$ and 9 T, respectively. Panels on the left: DFT results at $T = 0.1$ °K. Panels on the right: $EDFT$ results.

approximately in terms of integer occupation numbers. Of course, it is necessary that the correlations are included in the density functional.

The finite-temperature $CDFT$ and $EDFT$ theories were also applied to the study of configurations corresponding to fractional and values of ν which is small than or equal to 1 (Heinonen et al. 1995; Lubin et al. 1997; Pi et al. 1998). The results that were found, for example for the density, are very similar to what one obtains starting from the Laughlin wavefunctions.

Finally, we note that the $CDFT$ single-particle energies for the integer filling factors of Fig. 5.9, are very similar to the results obtained in the HF approximation (Gudmundsson and Palacios 1995). On the contrary, the energies obtained in the range $1 < \nu < 2$ are qualitatively different. In this region, and for dots with few
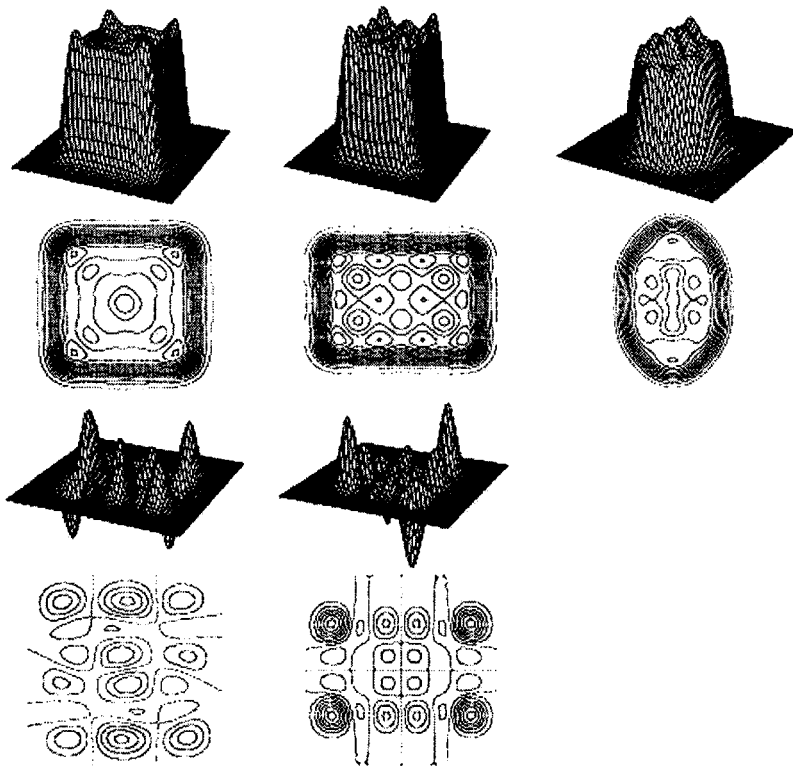
Fig. 5.20   Density ρ(x,y) (top figures) and magnetisations $m(x, y)$ of the $N = 20$ dot confined by a square jellium, a rectangular jellium, and an anisotropic parabola, respectively. The magnetisation of the deformed parabola is identically zero everywhere.

electrons, the HF approximation results in a crossing of the $(0, \uparrow)$ and $(0, \downarrow)$ bands, which is not reproduced by the $CDFT$ calculations for similar N values. It is likely that cancellations that occur between the exchange term (which is generally over-estimated by HF) and the correlation one, prevent such level crossing in density functional calculations.

Very recently, $LSDA$ calculations have been carried out for dots where the electrons are confined by anisotropic potentials (Reimann et al. 1998; Puente and Serra 1999). As an example of these results, we report (Puente and Serra 1999) in Fig. 5.20 the densities and magnetisations of a 20-electron dot, in a square jellium, in a rectangular jellium, and in a deformed parabola. For the square jellium one obtains a very rapidly varying density exhibiting maxima at the corners and four additional maxima arranged according to square symmetry. A similar structure appears for rectangular geometry. In the case of the deformed parabola, the density has an ellipsoidal shape, with an axis ratio close to ω_x/ω_y. In the inner part of the dot we notice three areas of local maxima, aligned along the major axis. It is interesting to note that, while for the parabola the magnetisation is identically zero,

for the square and the rectangle there is a magnetisation wave in the ground state. The amplitude of this wave is about 15% and 25% of the density maximum height in the two cases.

5.8 The Aharanov-Bohm Effect and Quantum Rings

Recently, the availability of nanoscopic semiconductor ring structures (Garcia et al. 1997; Lorke and Luyken 1998; Lorke et al. 2000; Warburton et al. 2000; Keyser et al. 2002) has stimulated a strong interest in the properties of quantum rings, in particular those related to the fractional Aharonov–Bohm oscillations of the energy and of the persistent current in the ring. These oscillations have been observed in mesoscopic (Mailly, Chapelier and Benoit 1993) and nanoscopic (Fuhrer et al. 2001; Keyser et al. 2002) rings in a GaAlAs/GaAs heterostructures and studied within many theoretical approaches (see, for example, Viefers et al. 2000 and references therein).

The Aharanov–Bohm effect is a direct consequence of the properties of eigenfunctions of isolated one-dimensional quantum rings, which cause the periodicity of all physical quantities. The reason for this behavior is due to the observation (Hund 1938; Byers and Yang 1961; Bloch 1970; Buttiker, Imry and Landauer 1983; Cheung et al. 1988) that in the case of an ideal one-dimensional ring without impurities, which encloses a magnetic flux Φ, the vector potential can be eliminated from the Schröedinger equation for the free motion of the electrons:

$$\frac{1}{2m}\left(-i\hbar\frac{d}{dx} + \frac{e}{c}A(x)\right)\psi_\ell(x) = \epsilon_\ell\psi_\ell(x)\,, \tag{5.65}$$

by introducing a gauge transformation. The result is that the field enters now the calculation via the flux-modified boundary condition:

$$\psi_\ell(L) = \exp\left[\frac{i2\pi\Phi}{\Phi_0}\right]\psi_\ell(0)\,, \tag{5.66}$$

where L is the ring circumference, $\Phi_0 = hc/e$ and we have used as spatial variable $x = L\theta/2\pi$, so that x varies between 0 and L. The situation is then analogous to the one-dimensional Bloch problem, as seen by identifying $2\pi\Phi/\Phi_0$ and kL. The energy levels of the ring, given by

$$\epsilon_\ell = \frac{\hbar^2}{2m}\left[\frac{2\pi}{L}\left(\ell - \frac{\Phi}{\Phi_0}\right)\right]^2, \quad \ell = 0, \pm 1, \pm 2, \ldots, \tag{5.67}$$

form microbands as a function of Φ with period Φ_0, analogous to the Bloch electron bands in the extended k-zone picture (see Fig. 5.21). The current carried by level ϵ_ℓ at zero temperature is

$$I_\ell = -\frac{ev_\ell}{L}, \quad v_\ell = \frac{1}{\hbar}\frac{\partial\epsilon_\ell}{\partial k_\ell}\,, \tag{5.68}$$
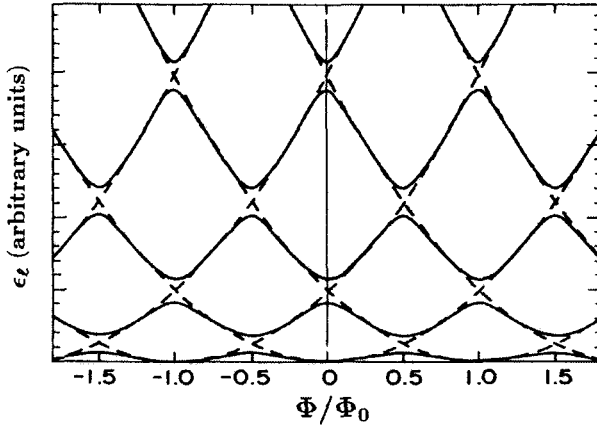
Fig. 5.21 Schematic diagram of the energy levels (5.67) as a function of the flux Φ/Φ_0 in a one-dimensional ring with (solid curve) and without impurities (dashed curve).

or, using the above analogy

$$I_\ell = -c\frac{\partial \epsilon_\ell}{\partial \Phi}. \tag{5.69}$$

Figure 5.21 shows schematically the energies of the eigenstates as a function of flux. In the absence of impurities in the ring, the curves form intersecting parabolas. In the presence of disorder, there are gaps at the points of intersection, in the same way as band gaps form in the band structure problem. Whereas the eigenenergies of the one-dimensional ring are symmetric in the flux, the current carried by an eigenstate, which is given by

$$I_\ell = \frac{2\pi e\hbar}{mL^2}\left[\ell - \frac{\Phi}{\Phi_0}\right], \quad \ell = 0, \pm 1, \pm 2, \ldots, \tag{5.70}$$

is antisymmetric in the flux. Moreover, since at an integer or half-integer flux quantum, the energy is maximum or minimum, at these values of Φ the current is zero.

  Up to now we have considered a single electron moving in the ideal one-dimensional ring. For many electron, it is possible to observe new effects in the current due to the crossings of the energy levels. For example, one can place two electrons in the state $\ell = 0$. If $N = 3$, the third electron, for $\Phi/\Phi_0 \simeq 0$, can be placed in either the $\ell = 1$ state or the $\ell = -1$ state, depending on whether Φ/Φ_0 is infinitesimally negative or positive. These rearrangements, when permitted by Fermi statistics, lead to discontinuous jumps in the current, with a change of sign. Repeating the analysis for cases $N = 4\ell$, $4\ell + 1$, $4\ell + 2$, $4\ell + 3$ leads to the results given in the article by Loss and Golbart (1991). For odd numbers of electrons they find that there is an approximate half-quantum flux periodicity, which however improves as the number of electrons increases. For even number of electrons there is one quantum flux periodicity as in the case of spinless electrons.

The electron–electron interaction can change the previous picture and yield a decrease of period and amplitude of the oscillations of the ground state energy and persistent current. This so-called "fractional Aharonov–Bohm effect" is due to electron correlations and has been studied by means of exact diagonalization (Niemela et al. 1996) of the many-electron Hamiltonian (5.1) with the parabolic potential $m\omega_0^2 r^2/2$ substituted by a shifted parabolic potential

$$v_{\text{ext}}(r) = \frac{1}{2}m\omega_0^2(r - R_0)^2 \,, \tag{5.71}$$

which better models the lateral confinement potential in the case of a ring. Calculations with the $LSDA$ theory and diffusion Monte Carlo have been also performed (Emperador, Pederiva and Lipparini 2003), and in the following we present some results obtained by these authors. Taking $R_0 = 20$ nm, $\omega_0 = 330$ meV, an effective mass $m = 0.063\,m_e$ and a dielectric constant $\epsilon = 12.4$, the electron density turns out to extend over a region with a width that is 15% of R_0. The ring is therefore nearly equivalent to a quantum wire with periodic boundary conditions at both ends, and can be regarded as quasi one-dimensional. The flux across the ring is $\Phi = \pi R_0^2 B$, where B is the applied magnetic field.

In Fig. 5.22 we plot the $LSDA$ ground state energy as a function of B in the case of $N = 10$ electrons in the ring. With $R_0 = 20$ nm, a magnetic field intensity
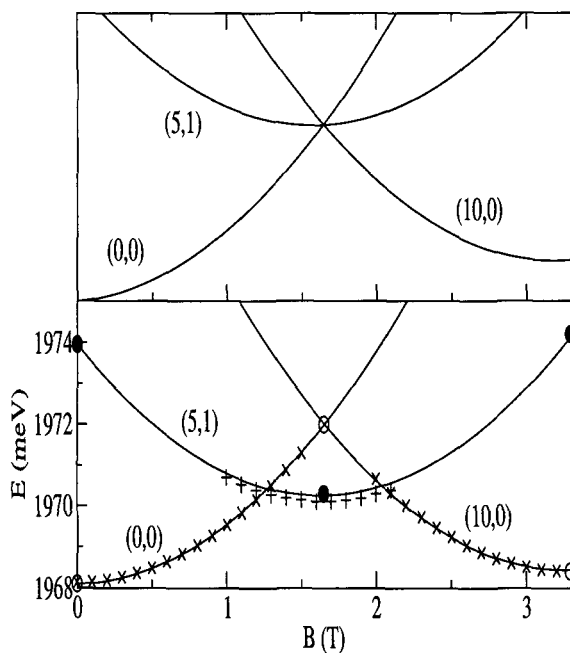
Fig. 5.22 Ground state energy as a function of B for a $N = 10$ quasi one-dimensional ring. Upper panel: non-interacting electrons. Lower panel: $LSDA$ (crosses and plus symbols) and DFM (empty and full circles) results. The (L,S) of each configuration is indicated.

of 3.29 T corresponds to one flux quantum crossing the ring. The upper panel of the figure shows the ground state energy for the ring containing non-interacting electrons in different (L,S) configurations. The lower panel gives the energy for the same configurations as calculated in $LSDA$ and in diffusion Monte Carlo. The full curves correspond to the quantity

$$E(\Phi) = E(0) + \frac{\hbar^2}{2mR_0^2} \sum_\alpha \left(\ell_\alpha - \frac{\Phi}{\Phi_0} \right)^2 + a\frac{\Phi}{\Phi_0}, \qquad (5.72)$$

where the sum runs over the occupied single particle levels for each configuration and $E(0)$ is the diffusion Monte Carlo interaction energy of each configuration at $B = 0$. The last term is a small energy associated to the compression of the single particle wave functions by the magnetic field, and the constant a tends to zero for a strictly one-dimensional ring. The validity of equation (5.72) implies that the electron–electron interaction is essentially independent on the magnetic field.

In the case of non-interacting electrons, the three electronic configurations shown in the upper panel of the figure are degenerate at $\Phi = \Phi_0/2$, corresponding to $B = 1.645$ T. The interaction decreases the energy of the $(L, S) = (5, 1)$ configuration in agreement with Hund's rule, and yields an alternation of spin singlet ($S = 0$) and spin triplet ($S = 1$) ground states as a function of B which leads to a period of $\Phi_0/2$ of the Aharonov–Bohm oscillations to be compared with the period of one flux for the non-interacting case.

Increasing the radius of the ring, the density of electrons in the ring lowers and the single particle energies become almost degenerate. The interaction mixes the quasidegenerate single particle levels and destroys circular symmetry in the intrinsic frame of reference of the system (Koskinen et al. 2001; Bormann and Harting 2001; Puente and Serra 2001; Pederiva et al. 2002) by means of a localization of the electrons in this frame. In the case of total localization, the Wigner molecule rotates as a rigid body and all the electrons have the same angular momentum $\ell = L/N$. The total energy becomes

$$E(\Phi) = E(0) + \frac{\hbar^2}{2mNR_0^2} \left(L - \frac{\Phi}{\Phi_0}N \right)^2 + a\frac{\Phi}{\Phi_0}, \qquad (5.73)$$

where $E(0)$ is now a constant independent on L, S and the magnetic field. Hence, in this case the period of the Aharonov–Bohm oscillations is Φ_0/N. This result is confirmed by the exact diagonalization calculation by Niemela et al. (1996) of low density quasi-one-dimensional quantum rings containing up to four electrons, in which they just find a period Φ_0/N of the Aharonov–Bohm oscillations.

References to Chapter 5

V. Fock, Z. Physik **47**, 446 (1928).

C.G. Darwin, Proc. Cambridge Philos. Soc. **27**, 86 (1933).

C. Schüller, K. Keller, G. Biese, E. Ulrichs, L. Rolf, C. Steinebach, D. Heitmann and K. Eberl, Phys. Rev. Lett. **80**, 2673 (1998).

M. Barranco, L. Colletti, E. Lipparini, M. Pi and Ll. Serra, Phys. Rev. B **61**, 8289 (2000).

R.B. Laughlin, Phys. Rev. Lett. **50**, 1395 (1983).

J.M. Caillol, D. Levesque, J.J. Weis and J.P. Hansen, Stat. Phys. **28**, 25 (1982).

K. von Klitzing, G. Dorda and M. Pepper, Phys. Rev. Lett. **45**, 494 (1980).

G. Ebert, K. von Klitzing, C. Probst and K. Ploog, Solid State Commun. **44**, 95 (1982).

D.C. Tsui, H. Stormer and A.C. Gossard, Phys. Rev. Lett. **48**, 1559 (1982).

R. Willet, J.P. Eisenstein, H. Stormer, D.C. Tsui, A.C. Gossard and J.H. English, Phys. Rev. Lett. **59**, 1776 (1987).

S. Sasaki, D.G. Austing and S. Tarucha, Physica B **256**, 157 (1998).

D.G. Austing et al., Phys. Rev. B **60**, 11514 (1999).

F.M. Peeters, Phys. Rev. B **42**, 1486 (1990).

A.V. Madhav and T. Chakraborty, Phys. Rev. B **49**, 8163 (1994).

S.M. Reimann et al., Phys. Rev. B **58**, 8111 (1998).

A. Puente and Ll. Serra, Phys. Rev. Lett. **83**, 3266 (1999).

O. Dippel, P. Schmelcher and L.S. Cederbaum, Phys. Rev. A **49**, 4415 (1994).

R.C. Ashoori et al., Phys. Rev. Lett. **71**, 613 (1993).

Ll. Serra, A. Puente and E. Lipparini, Physica E **14**, 391 (2002).

T. Haugset and H. Haugereud, Phys. Rev. A **57**, 3809 (1998).

L.P. Pitaevskii and A. Rosch, Phys. Rev. A **55**, R853 (1997).

R.K. Bhaduri, S.M. Reimann, A. Ghose Choudhuri and M.K. Srivastava, cond. matt/9908210 (1999).

D.S. Petrov, M. Holzmann and G.V. Shlyapnikov, Phys. Rev. Lett. **84**, 2551 (2000).

A. Recati, F. Zambelli and S. Stringari, Phys. Rev. Lett. **86**, 377 (2001).

B. Peredes, P. Fedichev, J.I. Chirac and P. Zoller, Phys. Rev. Lett. **87**, 402 (2001).

S.A. Wolf, D.D. Awschalom, R.A. Buhrman, J.M. Daughton, S. von Molnár, M.L. Roukes, A.Y. Chtchelkanova and D.M. Treger, Science **294**, 1488 (2001).

S. Datta and B. Das, Appl. Phys. Lett. **56**, 665 (1990).

J.A. Folk, S.R. Patel, K.M. Birnbaum, C.M. Marcus, C.I. Duruöz and J.S. Harris, Phys. Rev. Lett. **86**, 2102 (2001).

B.I. Halperin, A. Stern, Y. Oreg, J.N.H.J. Cremers, J.A. Folk and C.M. Marcus, Phys. Rev. Lett. **86**, 2106 (2001).

I.L. Aleiner and V.I. Fal'ko, Phys. Rev. Lett. **87**, 256801 (2001).

M. Valín-Rodríguez, A. Puente and Ll. Serra, Phys. Rev. B **66**, 045317 (2002).

M. Valín-Rodríguez, A. Puente, Ll. Serra and E. Lipparini, Phys. Rev. B **66**, 165302 (2002).

R.C. Ashoori, Nature **379**, 413 (1996); see also references therein.

M. Ciorga, A.S. Sachrajda, P. Hawrylak, C. Gould, P. Zawadzki, S. Jullian, Y. Feng and Z. Wasilewski, Phys. Rev. B **61**, R16315 (2000).

O. Voskoboynikov, C.P. Lee and O. Tretyak, Phys. Rev. B **63**, 165306 (2001).

W. Knap, C. Skierbiszewski, A. Zduniak, E. Litwin-Staszewska, D. Bertho, F. Kobbi, J.L. Robert, G.E. Pikus, F.G. Pikus, S.V. Iordanskii, V. Mosser, K. Zekentes and Yu. B. Lyanda-Geller, Phys. Rev. B **53**, 3912 (1996).

E. Lipparini, N. Barberan, M. Barranco, M. Pi and Ll. Serra, Phys. Rev. B **56**, 12375 (1997).

M. Pi, M. Barranco, A. Emperador, E. Lipparini and Ll. Serra, Phys. Rev. B **57**, 14783 (1998).

T. Demel, D. Heitmann, P. Grambow and K. Ploog, Phys. Rev. Lett. **64**, 788 (1990).

M. Ferconi and G. Vignale, Phys. Rev. B **50**, 14 722 (1994); Phys. Rev. B **56**, 12 108 (1997).

T.H. Oosterkamp, J.W. Janssen, L.P. Kouwenhoven, D.G. Austing, T. Honda and S. Tarucha, Phys. Rev. Lett. **82**, 2931 (1999).

R.M. Dreizler and E.K.U. Gross, Density Functional Theory (Springer-Verlag, Berlin, 1990).

O. Heinonen, M.I. Lubin and M.D. Johnson, Phys. Rev. Lett. **75**, 4110 (1995).

M.I. Lubin, O. Heinonen and M.D. Johnson, Phys. Rev. B **56**, 10373 (1997).

V. Gudmundsson and J.J. Palacios, Phys. Rev. B **52**, 11266 (1995).

J.M. Garcia et al., Appl. Phys. Lett. **71**, 2014 (1997).

A. Lorke and R.J. Luyken, Physica B **256**, 424 (1998).

A. Lorke et al., Phys. Rev. Lett. **84**, 2223 (2000).

R.J. Warburton et al., Nature **405**, 926 (2000).

U.F. Keiser et al., e-print cond-mat/0206262.

D. Mailly, C. Chapellier and A. Benoit, Phys. Rev. Lett. **70**, 2020 (1993).

A. Fuhrer et al., Nature **413**, 822 (2001).

S. Viefers et al., Phys. Rev. B **62**, 16777 (2000).

F. Hund, Ann. Phys. (Leipzig) **32**, 102 (1938).

N. Byers and C.N. Yang, Phys. Rev. Lett. **7**, 46 (1961).

F. Bloch, Phys. Rev. B **2**, 109 (1970).

M. Buttiker, Y. Imry and R. Landauer, Phys. Lett. A **96**, 365 (1983).

H.F. Cheung et al., Phys. Rev. B **37**, 6050 (1988).

D. Loss and P. Goldbart, Phys. Rev. B **43**, 13762 (1991).

K. Niemela et al., Europhys. Lett. **36**, 533 (1996).

A. Emperador, F. Pederiva and E. Lipparini preprint (2003).

M. Koskinen et al., Phys. Rev. B **63**, 205323 (2001).

P. Bormann and J. Harting, Phys. Rev. Lett. **86**, 3120 (2001).

A. Puente and Ll. Serra, Phys. Rev. B **63**, 125334 (2001).

F. Pederiva, A. Emperador and E. Lipparini, Phys. Rev. B **66**, 165314 (2002).

Chapter 6

Monte Carlo Methods

6.1 Introduction

The term *Monte Carlo* was used for the first time in the forties by a group of sci-
entists who were working in Los Alamos at the Manhattan Project, to indicate a
class of mathematical methods for the numerical solution of integration problems
by probabilistic methods. Although the ideas underlying Monte Carlo methods were
already known in the eighteenth century (Comte de Buffon 1777), the development
of these algorithms is recent, in part due to the facility of their implementation on
the computer. In many cases, Monte Carlo methods are the only efficient approach
to the evaluation of many-dimensional integrals of physical interest. The time re-
quired to evaluate an integral with standard integration methods (like, for example,
the Simpson rule) depends exponentially on the dimensionality of the space under
consideration. As we will see, the stochastic integration methods have the property
that they require a computational effort which depends only algebraically on the
dimensionality.

6.2 Standard Quadrature Formulae

Suppose we want to compute the integral of a function defined in a space of dimen-
sion D, on a hyper-cube of side L:

$$I(D) = \int_0^L dx_1 \cdots \int_0^L dx_D \ F(x) \,. \tag{6.1}$$

For $D = 1$, the numerical value of the integral can be approximated by subdivid-
ing the area subtended by the curve $y = F(x)$, into rectangles with fixed base h
(Simpson rule). The smaller h, the smaller the error in the approximation of the
subtended area. By adding all the rectangle areas, we obtain an approximate es-
timate which, in the limit where the base tends to zero, equals the value of the
integral. By generalizing this procedure to a function defined in a space with D
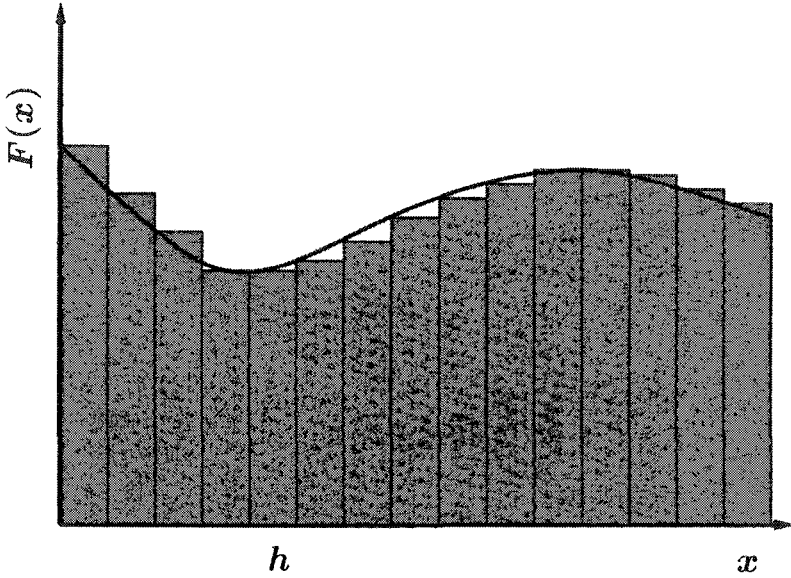
Fig. 6.1   Integration by the first Simpson rule in one dimension: the integral is approximated by the sum of the areas of rectangles with base h and height determined by the values of the function, evaluated on a grid of points.

dimensions, we have

$$I(D) \approx h^D \sum F(x) \,, \tag{6.2}$$

where the summation extends over all the points of a lattice defined in the integration hyper-cube.

If the lattice base h is made to tend to zero, we will obtain the exact value of the integral, like in the one-dimensional case discussed previously. An upper limit of the error made in the i-th interval, for a one-dimensional curve, may be obtained by the derivative of the function:

$$\Delta = h^2 \frac{d}{d\,x_i} F(x_i) \,.$$

By generalizing to D dimensions:

$$\Delta = h^{D+1} \nabla F(x) \approx h^{D+1} \,,$$

where, for the approximation on the right-hand side, we assumed that the gradient of the function is finite in the considered integration interval. Therefore, the total error may be estimated by adding the contributions of the N intervals:

$$\Delta_{\text{TOT}} \approx N h^{D+1} \,.$$

If L is the side of the hyper-cube, the number of lattice points can be expressed as

$$N = \left(\frac{L}{h}\right)^D .$$

Then, the total error becomes

$$\Delta_{\text{TOT}} \approx \left(\frac{L}{h}\right)^D h^{D+1} = L^D h = V h , \tag{6.3}$$

where $V = L^D$ is the volume of the hyper-cube. It is possible to write the previous equation in terms of N, thus obtaining

$$\Delta_{\text{Tot}} = \frac{LV}{N^{\frac{1}{D}}} .$$

This allows us to estimate the number of points required to obtain a precision of the order of ε for the numerical evaluation of the integral:

$$\varepsilon = N^{-\frac{1}{D}} \implies N = \varepsilon^{-D} .$$

In a typical case, for example, the calculation of statistical averages in a system with 20 particles ($D = 60$), the requirement of an error of the order of $\varepsilon = 0.1$ entails the use of $N = 10^{60}$ points. Even with a Tflop computer (i.e. capable of performing 10^{12} operations per second), the time required for the calculation will not be less than 10^{48} seconds, which largely exceeds the age of the universe. Therefore, in general the standard integration methods are unsuitable for many body problems.

6.3 Random Variable Distributions and Central Limit Theorem

In order to introduce the Monte Carlo methods, it is useful to briefly recall some elementary notions of statistics. The main object of our treatment are the so-called *random variables*, or *stochastic variables*. These variables may be defined by the following properties:

(1) The ensemble of the values that they may take: $\{x\}$.
(2) The probability law $P(x)$ for each value of the variable (also called the *probability density*). This function must have the following properties:

$$P(x) \geq 0 \quad \forall\, x ,$$

$$\int P(x)dx = 1 . \tag{6.4}$$

N variables are said to be *independent* if

$$P(x_1, x_2, \ldots, x_N) = P(x_1)P(x_2)\cdots P(x_N).\tag{6.5}$$

The Monte Carlo methods are based on one of the fundamental theorems of statistics, the so-called *central limit theorem*. Let us consider a function f with real values. Let S_N be the stochastic variable defined by

$$S_N = \frac{1}{N}\sum_{i=1}^{N} f(x_i),\tag{6.6}$$

where x is a stochastic variable. Whichever $P[x]$, in the limit $N \longrightarrow \infty$, the probability distribution of S_N is given by

$$P[S_N] \overset{N\to\infty}{=} \frac{1}{\sqrt{2\pi\sigma_N}}\exp\left[-\frac{(S_N - \langle f \rangle)^2}{2\sigma_N}\right],\tag{6.7}$$

where

$$\langle f \rangle = \int f(x)P(x)dx,$$

$$\sigma_N^2 = \frac{1}{N}\sigma_S^2,\tag{6.8}$$

and

$$\sigma_S^2 = \int f^2(x)P(x)dx - \langle f \rangle^2.$$

Therefore, the central limit theorem tells us that the distribution of a sum of values obtained as a function of *any* stochastic variable, is always a Gaussian, which possesses mean value and variance that can be calculated.

6.4   Calculation of Integrals by the Monte Carlo Method

Suppose we want to calculate the integral of a function $F(x)$ defined in an n-dimensional space, and let us consider a probability density P from which we can extract values for the variable x (the latter, in general, will be an n-dimensional vector). The integral can be written in the following form:

$$\int F(x)dx = \int \frac{F(x)}{P(x)}P(x)dx \equiv \int f(x)P(x)dx.\tag{6.9}$$

From the central limit theorem, it follows that the stochastic variable

$$S_N = \frac{1}{N} \sum_{i=1}^{N} f(x_i),$$
(6.10)

has a Gaussian distribution around the mean value $\langle f \rangle$ (which is precisely the integral to be computed), with a statistical error

$$\sigma_N \propto \frac{1}{\sqrt{N}}.$$
(6.11)

Therefore, the Monte Carlo (MC) integration method consists in generating a sequence of points distributed according to a probability density P, and in estimating the integral of a given function by means of (6.10). Such estimate is affected by a statistical error which, as can be seen from (6.11), decreases as the reciprocal of the square root of the number of generated points. Therefore, it is possible to compare the efficiency of the MC method with that of standard integration procedures. In the MC method, the number of points required to reach a pre-fixed precision, ε, depends on σ_S^2 (i.e. the *variance* of S), and increases as ε^{-2} *irrespective of the dimensionality of the integral under consideration*. Hence, the MC method becomes computationally advantageous, as soon as the dimension of the space in which the integrand is defined exceeds a few.

6.5 Markov Chains

The main problem one faces in the application of MC methods, is the successful generation of sequences of points distributed according to a probability density, which is established *a priori* by the problem under study. As an example, let us assume we need to calculate expectation values of physical observables for a quantum system of N interacting particles. We also assume we know the wavefunction of the system in the ground state, $\Psi(\mathbf{r_1} \ldots \mathbf{r_N})$. The calculation of the expectation value of an observable O, requires the evaluation of integrals of the kind:

$$\langle \Psi | \hat{O} | \Psi \rangle = \int |\Psi(\mathbf{r}_1 \cdots \mathbf{r}_N)|^2 O(\mathbf{r}_1 \cdots \mathbf{r}_N) \, d\mathbf{r}_1 \cdots d\mathbf{r_N}.$$
(6.12)

In this case, the MC method has a direct intuitive meaning: by generating points distributed according to $|\Psi|^2$ (which represents the probability of finding the particles in a given configuration), and by calculating the respective values of operator $\hat{O}$, it is possible to obtain the required expectation value.

It is known that in a classical system the trajectories of the particles are the solutions of equation of motion of the system. This fact allows us to define an algorithm which generates successive configurations for the positions and velocities of the particles, obeying Boltzmann statistics. Intuitively, it would be convenient to exploit some analogous feature, to generate configurations of a quantum system.

Indeed, it is possible to define a sort of stochastic dynamics which relates, one to the other, sequentially generated configurations, in such a way that their final distribution conforms with a given probability density. Such pseudo-dynamics, which does not have any physical meaning, can be formalized by the theory of Markov chains. A *Markov chain* is defined as a sequence of stochastic variables $\{x_i\}$, such that

$$x_1 \quad \text{has probability} \quad P_1(x),$$
$$P_k(x) = w(x_k|x_{k-1})P_{k-1}(x_{k-1}). \tag{6.13}$$

The function $w(x_k|x_{k-1})$ is called *transition probability* or *transition matrix*. In general, it depends on the value of index k.

A Markov chain is *stationary* when the transition probability w does not depend on index k. From this definition, it follows immediately that a stationary chain is completely defined once the distribution probability for the first variable in the chain $P_1(x)$ and the transition probability w are established. In fact, we will have

$$P_2(x_2) = \sum_{\{x_1\}} w(x_2|x_1)P_1(x_1),$$
$$P_3(x_3) = \sum_{\{x_2\}} w(x_3|x_2)P_2(x_2) = \sum_{\{x_2\}}\sum_{\{x_1\}} w(x_3|x_2)w(x_2|x_1)P_1(x_1),$$
$$\vdots \tag{6.14}$$
$$P_k(x_k) = \sum_{\{x_1 \cdots x_{k-1}\}} w(x_k|x_{k-1})\cdots w(x_2|x_1)P_1(x_1) = \sum_{\{x_1\}} w^{k-1}(x_k|x_1)P_1(x_1),$$

and hence

$$P_k = w^{k-1}P_1. \tag{6.15}$$

Let us now assume that w exists, and that it can be easily sampled. Given an initial configuration x_1 (that we can imagine as being sampled by a uniform probability density), a relevant question is whether the configurations which are generated successively do converge towards some limiting distribution P_∞. In general, it is difficult to prove the existence of this limit. However, in the cases of physical interest, all necessary conditions are fulfilled. Therefore, in what follows we will rely on some assumptions:

• The limit:

$$P_\infty = \lim_{k\to\infty} w^k P_1 \tag{6.16}$$

exists and corresponds to a good probability distribution.

- The transition probability w has the ergodicity property: given two points x and y in configuration space, it must be that

$$\exists\, N < \infty \quad \text{such that} \quad w^N(x|y) > 0\,. \tag{6.17}$$

This means that it is always possible to reach a given point in space, starting from any other point, in a finite number of steps.

If the limit P_∞ exists, it is an eigenvector of the matrix w. In fact,

$$wP_\infty = \lim_{k\to\infty} w^{k+1}P_1 = P_\infty\,. \tag{6.18}$$

Therefore, the transition matrices have the property that all of their eigenvalues are located on the circle of unit radius in the complex plane, and this implies the uniqueness of P_∞. To prove this, we first note that since the probability distributions are normalized, there can exist no eigenvalue $\lambda > 1$. Let us suppose we have a basis of eigenfunctions φ_n of w, and let us expand the distribution P_1 on this basis. We will have

$$w^k P_1 = \sum_n c_n w^k \varphi_n \Rightarrow w^k P_1 = \sum_n c_n \lambda^k \varphi_n\,, \tag{6.19}$$

and if $\lambda < 1$, then

$$\lim_{k\to\infty} w^k P_1 = 0\,. \tag{6.20}$$

There is a further condition that, in general, we wish that it is satisfied in a real physical system. If the system is at equilibrium, the stochastic pseudo-dynamics should not generate configurations that are distributed in an inhomogeneous way. For example, if we compute some properties of a gas or a liquid in a container, we do not want the configurations to fill only a part of the available volume. This requirement is reflected in a constraint imposed upon w and P, which is known as the condition of *detailed balance*:

$$P_\infty(x)w(y|x) = P_\infty(y)w(x|y)\,. \tag{6.21}$$

This means that the probability of moving the configuration from the neighborhood of point x to the neighborhood of point y, should be proportional only to the values of the probability function P, and should not depend on the particular event under consideration. In other words,

$$\frac{w(x|y)}{w(y|x)} = \frac{P_\infty(x)}{P_\infty(y)}\,. \tag{6.22}$$

This condition may be used to sample the transition matrix w (which in general is unknown) which yields, as a limit, the $P_\infty(x) \equiv P$ that we want to sample. Let us

factorize the matrix w into the two following factors:

(1) A "proposal" for the next position, T.
(2) A probability of accepting the next position, A.

Therefore, we will have

$$w(x, y) = T(x, y)A(x, y).$$ (6.23)

The matrix T can be suitably chosen and, in general, it will be a distribution that we know how to sample. From the previous relations, we find that the matrix A should have the following property:

$$\frac{A(y|x)}{A(x|y)} = \frac{P(y)T(x|y)}{P(x)T(y|x)} \Rightarrow A(y|x) = F\left(\frac{P(y)}{P(x)}\frac{T(x|y)}{T(y|x)}\right),$$ (6.24)

where the function F should be such that

$$\frac{F(x)}{F(1/x)} = x.$$ (6.25)

The following are examples of functions which satisfy the above relations:

(1) $F(x) = \min(1, x)$,
(2) $F(x) = x/(1 + x)$.

In order to sample an arbitrary probability distribution P, it is enough to define a transition probability T that we know how to sample and then, starting from an arbitrary point x_1 in configuration space, to generate the subsequent configuration distributed according to

$$\sum_{\{x_1\}} T(x_2|x_1)P(x_1).$$

In order to ensure detailed balance, the new configuration will be either retained or rejected with a probability A defined by (6.24). Such ensemble of points in configuration space, which constitute a Markov chain, is often called a *random walk*, and the moving point is called the *walker*.

6.6   The Metropolis Algorithm $[M(RT)^2]$

This algorithm constitutes the simplest practical implementation of the scheme described in the previous sections. The acronym by which it is indicated derives from the names of its developers (N. Metropolis, A.W. Rosenbluth, M.N. Rosenbluth, A.H. Teller and E. Teller 1953); however, it is often referred to as the Metropolis algorithm. In this algorithm the transition proposal T is assumed to be uniform in
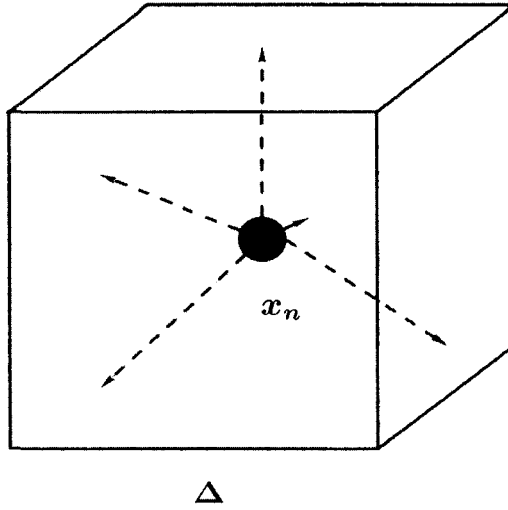
Fig. 6.2 In the $M(RT)^2$ algorithm the positions of the particles are chosen at random inside a cube of side Δ.

a D-dimensional hyper-cube of side Δ. Therefore, given a point $\mathbf{x}_i$, the next point in the Markov chain is generated in the following way:

$$\mathbf{x}_{n+1} = \mathbf{x}_n + \Delta \xi', \tag{6.26}$$

where the components of the vector ξ are extracted at random in the interval

$$-\frac{1}{2} \leq \xi' \leq \frac{1}{2}.$$

The transition proposal is symmetrical and the acceptance probability A depends only on $P(x_n)$ and $P(x_{n+1})$. A possible choice is the following

$$A(x,y) = \min\left(1, \frac{P(y)}{P(x)}\right). \tag{6.27}$$

In order to decide whether a proposed move is accepted or not, one extracts a random number ξ in the interval $(0,1)$ and compares it to A. The next move is then determined according to the following criterion:

$$\begin{cases} x_{n+1} = \text{new position} & \text{if } \xi < \dfrac{P(y)}{P(x)} \\[2ex] x_{n+1} = x_n & \text{if } \xi > \dfrac{P(y)}{P(x)} \end{cases}. \tag{6.28}$$

After a number of steps, this algorithm generates a distribution of points x_i according to the probability distribution P. Therefore, after the generation of N

points the estimate of an integral of the form

$$\int dx P(x) F(x),$$

will be given by

$$\frac{1}{N} \sum_{i=1}^{N} F(x_i).$$

6.7   Variational Monte Carlo for Liquid ^{4}He

As an example of application to a real physical system, we will compute the energy per particle of the helium isotope with mass 4, at the temperature of 0 K and zero pressure. These atoms have spin $S = 0$, and therefore, at temperatures close to absolute zero behave like quantum particles which obey the Bose–Einstein statistics. The interaction between He atoms is known with great accuracy. A good approximation for the inter-atomic potential is given by a potential of the Lennard–Jones type:

$$V(r_{12}) = 4\epsilon \left[\left(\frac{\sigma}{r_{12}} \right)^{12} - \left(\frac{\sigma}{r_{12}} \right)^{6} \right]. \tag{6.29}$$

To simulate the liquid phase, the system is modelled as an ensemble of N atoms confined inside a box, which is periodically replicated in space. The Hamiltonian of such system is

$$H = -\frac{\hbar^2}{2m} \sum_{i=1}^{N} \nabla^2 + \sum_{i<j} V(r_{ij}). \tag{6.30}$$

Since we do not know the wavefunction of the ground state, we look for an approximate solution of the Schrödinger equation:

$$H\Psi_0 = E_0 \Psi_0, \tag{6.31}$$

where E_0 is the energy of the ground state.

Let us consider the following *trial function* (McMillan 1965):

$$\Psi_T = \prod_{i<j} e^{-\frac{1}{2}\left(\frac{b}{r_{ij}}\right)^m} = \prod_{i<j} f(r_{ij}). \tag{6.32}$$

This Ψ has the right symmetry properties for a system of Bosons (i.e. it is symmetric under the exchange of two particles), and has the property of canceling out when $r_i = r_j$. Accordingly, the probability of finding two atoms very close to each other is very small, as expected in the presence of an inter-atomic potential which is strongly repulsive at the origin.
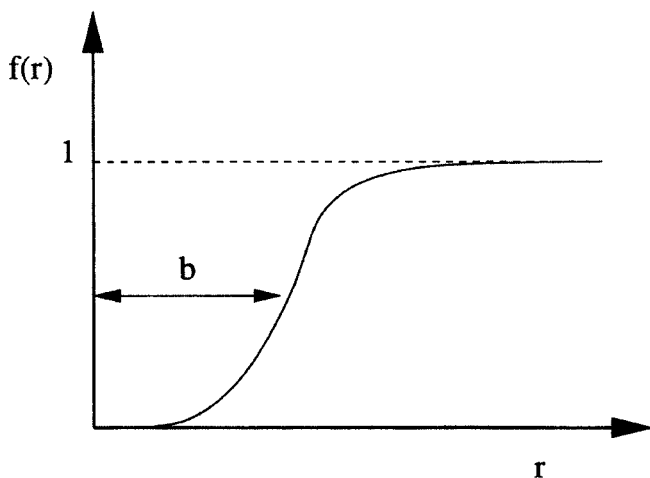
Fig. 6.3 The function $u(r_{ij})$ used in the VMC calculation of the energy of liquid ^{4}He. This function cancels out in correspondence with the repulsive part of the inter-atomic potential, and is ~ 1 for large distances. The parameter b describes the amplitude of the correlation well of the particle.

Let us now consider the variational principle (Riesz theorem):

$$E_T = \frac{\langle \Psi_T | H | \Psi_T \rangle}{\langle \Psi_T | \Psi_T \rangle} \geq \frac{\langle \Psi_0 | H | \Psi_0 \rangle}{\langle \Psi_0 | \Psi_0 \rangle} = E_0 \,. \tag{6.33}$$

In general, if we chose a trial function which depends on a set of parameters $\{\alpha\}$, the best representation of the ground state is given by the condition:

$$\frac{\partial E_T}{\partial \{\alpha\}} = 0 \,. \tag{6.34}$$

This derivative is not known analytically. It is necessary to compute the integrals in (6.33) numerically, and to minimize the function $E_T(\alpha)$ so obtained. The integral that provides the value E_T is calculated by means of the $M(RT)^2$ algorithm by considering

$$P = \prod_{i<j} e^{-(\frac{b}{r_{ij}})^m} \,. \tag{6.35}$$

The latter expression is not normalized, but this is not a problem since in the algorithm it appears only in the ratio $P(y)/P(x)$.

As a first step, one generates a random distribution of points in the simulation box (i.e. the distribution P_1 of the previous sections). Subsequently, new atomic positions are generated according to (6.26), and the value of the wavefunction is computed in the new point of configuration space. The move is either accepted or rejected according to (6.27). Hence, the Monte Carlo estimate for the energy per

particle becomes

$$E_T \cong \frac{1}{N} \sum_{i=1}^{N} \frac{H\psi_T(r_i)}{\psi_T(r_i)} \, . \tag{6.36}$$

By taking for the inter-atomic potential the parameter values $\epsilon = 10.4$ °K (we are using energy units such that $\hbar = 1$ and $K_B = 1$) and $\sigma = 2.556$ Å, we obtain the estimate $E_{VMC} = -5.72$ °K for the energy per particle (McMillan 1965). This should be compared with the experimental value -7.14 °K. With a simple model like this, it is also possible to obtain information on other properties of ^{4}He. In particular, it is possible to estimate the fraction of Bose–Einstein condensate, which turns out to be about 8%, in good agreement with experimental data.

6.8   Monte Carlo Methods and Quantum Mechanics

The most successful application of Monte Carlo methods in physics, is the possibility of solving exactly the quantum many body problem, at least in some cases. These algorithms are often generically referred to as *Quantum Monte Carlo (QMC)* methods. However, it is possible to identify at least three great families of *QMC* algorithms:

(1) Variational Monte Carlo. We expounded this method with an example in the previous section. In general, *VMC* consists in finding an approximate solution of the Schrödinger equation, depending on some parameters, and in utilizing the variational principle for the determination of the best value of the parameters themselves.*

(2) Projection Methods. These are methods that solve exactly the Schrödinger equation for the ground state of a system of interacting Bosons at temperature $T = 0$. They may be used to yield approximate, but extremely optimized, solutions for Fermion systems. The two main algorithms are the *Diffusion Monte Carlo (DMC)* and the *Green's Function Monte Carlo (GFMC)*.

(3) Path Integral Monte Carlo. It consists in evaluating averages on the density matrix of a system (and thus, at finite temperature), using a path-integral-like expansion. It is exact for Boson systems, and can be used in approximate form for Fermions (Ceperley 1995).

In the following, we will consider only projection methods, and will describe one of their possible derivations and their main characteristics.

---

*For a general discussion see for example Ceperley and Kalos (1986).

6.9 Propagation of a State in Imaginary Time

In quantum mechanics, the propagation of a state from time t_0 to time t is given by the following expression:

$$\psi(R, t) = e^{-iH(t-t_0)/\hbar}\psi(R, t_0)\,, \tag{6.37}$$

where $R = \{\mathbf{r}_1 \ldots \mathbf{r}_N\}$ are the co-ordinates of the N particles. Let us reparametrize time by means of an *imaginary time* $\tau = it$. Formally, we can rewrite the same propagator in the following way:

$$\psi(R, \tau) = e^{-H(\tau-\tau_0)/\hbar}\psi(R, \tau_0)\,. \tag{6.38}$$

Let us set $\hbar = 1$, so that the imaginary time has the dimension of a reciprocal energy. Moreover, let us put $\tau_0 = 0$. Next we expand the state ψ on a basis of eigenstates of H:

$$\psi(R, 0) = \sum_n c_n \phi_n(R)\,. \tag{6.39}$$

By applying the propagator (6.38), we obtain

$$\psi(R, \tau) = e^{-H\tau}\psi(R, 0) = \sum_n c_n e^{-E_n\tau}\phi_n(R)\,, \tag{6.40}$$

where the E_n are the eigenvalues corresponding to the ϕ_n. From (6.40), we note that the components $c_n e^{-\tau E_n}$ of the propagated state along the eigenstates of H decay exponentially with different characteristic times which is proportional to the excitation energy.

However, it is possible to normalize the wavefunction in such a way as to keep the component along one of the eigenstates constant. In particular, by considering the following function:

$$\psi'(R, \tau) = e^{E_0\tau}\psi(R, \tau)\,, \tag{6.41}$$

the expansion (6.40) becomes

$$\psi'(R, \tau) = \sum_n c_n e^{-\tau(E_n-E_0)}\phi_n(R)\,. \tag{6.42}$$

In the $\tau \to \infty$ limit, we obtain

$$\lim_{\tau \to \infty} \psi'(R, \tau) = c_0\phi_0(R)\,, \tag{6.43}$$

i.e. the normalized state, propagated in imaginary time, tends to the ground state, at most, multiplied by a constant. In general, *the propagation in imaginary time of an arbitrary wavefunction of a system, projects from this function the eigenstate of H which has the lowest energy, among those along which the initial state has a non-vanishing component.* For a many body system, if one does not impose any constraint, H has both symmetric and antisymmetric eigenstates with respect to

particle exchange. It can be shown that the lowest-energy solution, and hence the state projected by imaginary time propagation, is always symmetric. The projection algorithm can then be straightforwardly applied only to Boson systems and therefore, for simplicity we will assume for the moment that the system under consideration consists only of Bosons.

6.10   Schrödinger Equation in Imaginary Time

Equation (6.38) represents the formal solution of a many-body Schrödinger equation in imaginary time:

$$-\frac{\partial}{\partial \tau}\psi(R,\tau) = H\psi(R,\tau)\,, \tag{6.44}$$

that is

$$-\frac{\partial}{\partial \tau}\psi(R,\tau) = -\frac{\hbar^2}{2m}\sum_{i=1}^{N}\nabla_i^2\psi(R,\tau) + V(R)\psi(R,\tau)\,, \tag{6.45}$$

where $R = \{\mathbf{r}_1, \mathbf{r}_2, \dots \mathbf{r}_N\}$. Equation (6.45) is equivalent to a diffusion equation with an absorption term. To better understand its meaning, it is interesting to examine it in two important limiting cases.

(a) Zero-mass limit

If the mass is very small, the kinetic term becomes dominant, and the equation reduces to

$$-\frac{\partial}{\partial \tau}\psi(R,\tau) = -\frac{\hbar^2}{2m}\sum_{i=1}^{N}\nabla_i^2\psi(R,\tau)\,. \tag{6.46}$$

It is possible to express the exact solution of (6.46) in integral form:

$$\psi(R,\tau) = \int G(R - R',\tau)\psi(R',0)dR'\,, \tag{6.47}$$

where the Green's function is given by

$$G(R - R',\tau) = \frac{1}{(4\pi D\tau)^{\frac{dN}{2}}}\exp\left\{-\frac{(R - R')^2}{4D\tau}\right\}\,, \tag{6.48}$$

where d is the dimensionality of the system, N is the number of particles and $D = \hbar^2/2m$. The latter quantity plays the role of a diffusion constant.

The function $\psi(R,\tau)$ describes the probability that a particle is at point R at time τ, while the Green's function describes the probability of passing from R to R' in a time interval τ. Finally, $\psi(R',0)$ is the probability of being at R' at time $\tau = 0$. Therefore, to generate system configurations distributed according to the

solution of (6.46), it is sufficient to start from an arbitrary particle distribution $\psi(R',0)$, and then to generate displacements according to the Green's function G, i.e. to generate a vector in $d \times N$ dimensions in which each component is a random number extracted from the Gaussian distribution G, and then sum it to the initial positions of the particles. Therefore, the pseudo-dynamics for the walker is given by the equation:

$$r_i' = r_i + \xi_i. \tag{6.49}$$

The positions $\{r_i'\}$ will be distributed according to $\psi(R, \tau)$.

(b) Infinite-mass limit

If the mass becomes very large, the dominant term is that of the potential energy and we obtain the following equation:

$$-\frac{\partial}{\partial \tau}\psi(R, \tau) = V(R)\psi(R, \tau). \tag{6.50}$$

For a normalized state $e^{\tau E_0}\psi(R, \tau)$ the equation is modified in the following way:

$$-\frac{\partial}{\partial \tau}\psi(R, \tau) = [V(R) - E_0]\psi(R, \tau), \tag{6.51}$$

and its solution is:

$$\psi(R, \tau) = P_B = e^{-[V(R) - E_0]\tau}. \tag{6.52}$$

Equation (6.52) is interpreted as the probability that a walker, which is at R, survives in this same position after a time τ. Therefore, the walker population tends to increase where $V(R) < E_0$, and to vanish where $V(R) > E_0$. From the point of view of the algorithm, this means that we should compute the value of equation (6.52) at point R, and generate at the same point a number of walkers equal to $[P_B + \xi]$, where ξ is a random number uniformly distributed between 0 and 1. If the resulting number is 0, the walker is destroyed. This process is called *branching*.

In general, the situation is intermediate between these two limits, and the algorithm will have to implement both the diffusive dynamics and the branching process. To this purpose, we note that the propagator can be decomposed by using the Trotter formula:

$$e^{-\tau H} = e^{-\tau(T+V)} \approx e^{-\tau T}e^{-\tau V} + o(\tau). \tag{6.53}$$

In the $\tau \to 0$ limit, the decomposition becomes exact. This disagrees with the fact that, in order to arrive at a correct projection of the ground state, propagation should take place for long imaginary times, at least of the order of a few of the decay time $\tau_0 = 1/(E_1 - E_0)$ of the component along the first excited state. However, it is

possible to split the propagation in time τ, into M propagation steps $\Delta\tau = \tau/M$. If M is large, the approximation (6.53) is quite accurate.

The previous considerations yield a first possible structure of the projection algorithm:

- Generation of a walker population distributed according to $\psi(R, 0)$.
- Diffusion of the walkers following (6.49) for a short time $\Delta\tau$.
- Calculation of the survival and/or multiplication probability of a walker according to (6.52).
- Back to step 1, and repeat until propagation for a sufficiently long time τ is achieved.

The required ground state eigenvalue, is the value of E_0 that makes the population stationary.

6.11 Importance Sampling

If the potential V has divergences (as, for example, in a system of electrons interacting through the Coulomb potential), the expression for the branching probability may diverge, and this causes large fluctuations in the walker population. In these cases it is convenient to employ an approximate wavefunction (obtained, for example, by a VMC calculation) to drive the walkers in such a way that they avoid classically forbidden regions of configuration space. For example, in the presence of a repulsive potential, the wavefunction should cancel or have a minimum on the hyperplanes defined by $r_i = r_j$. Let us consider, then, a trial function $\psi_T(R)$, known as *importance function*. We sample the walkers from a density $f(R, \tau) = \psi_T(R)\phi(R, \tau)$ which evolves in imaginary time, and which in the $\tau \to \infty$ limit is proportional to $\psi_T(R)\phi_0(R)$. We are interested in finding the equation which governs the distribution $f(R, \tau)$, i.e. the analogue of the Schrödinger equation in imaginary time introduced in the previous sections. Let us define the *pseudo-force* acting on particle i:

$$F_i(R) = 2\nabla_i \ln \psi_T(R) = 2\frac{\nabla_i \psi_T(R)}{\psi_T(R)} \, .$$

It may be noted that

$$\nabla(f(R, \tau)F(R)) = 2\nabla\psi_T(R)\nabla\phi(R, \tau) + 2\phi(R, \tau)\nabla^2\psi_T(R) \, ,$$
$$\nabla^2 f(R, \tau) = \psi_T(R)\nabla^2\phi(R, \tau) + 2\nabla\psi_T(R)\nabla\phi(R, \tau) + \phi(R, \tau)\nabla^2\psi_T(R) \, .$$
(6.54)

By combining these expressions, it is possible to obtain an expression for the Laplacian of the function $\phi(R, \tau)$:

$$\psi_T(R)\nabla^2\phi(R, \tau) = \nabla^2 f(R, \tau) - \nabla[f(R, \tau)F(R)] + f(R, \tau)\frac{\nabla^2\psi_T(R)}{\psi_T(R)} \, . \quad (6.55)$$

In order to obtain the desired distribution in the $\tau \to \infty$ limit, the function $\phi(R, \tau)$ must satisfy the imaginary-time dependent Schrödinger equation:

$$\frac{\partial}{\partial \tau} \phi(R, \tau) = D \sum_{i=1}^{N} \nabla_i^2 \phi(R, \tau) - V(R)\phi(R, \tau).$$ (6.56)

By multiplying both sides of Eq. (6.56) by $\psi_T(R)$, and inserting (6.55), we obtain the following equation for the probability density $f(R, \tau)$:

$$\frac{\partial}{\partial \tau} f(R, \tau) = D \sum_{i=1}^{N} \nabla_i^2 f(R, \tau) - D \sum_{i=1}^{N} \nabla_i \cdot [f(R, \tau)F_i(R)]$$

$$- E_L(R)f(R, \tau),$$ (6.57)

where

$$E_L(R) = -D \sum_{i=1}^{N} \frac{\nabla_i^2 \psi_T(R)}{\psi_T(R)} + V(R) = \frac{H\psi_T(R)}{\psi_T(R)},$$

is the *local energy* operator.

Equation (6.57) is a Fokker–Planck equation with a source term. To understand the walker dynamics associated with this equation, let us carry out the same kind of analysis as for the Schrödinger equation in imaginary time, i.e. let us consider the two limits of zero mass and infinite mass. The former case corresponds to neglecting the term depending on the local energy. In this way we obtain a simplified equation:

$$\frac{\partial}{\partial \tau} f(R, \tau) = D \sum_{i=1}^{N} (\nabla_i^2 f(R, \tau) - \nabla_i \cdot [f(R, \tau)F_i(R)]),$$ (6.58)

which, for $\tau \to \infty$, has the solution

$$f(R, \tau) = \psi_T^2(R).$$

In fact, if we put the limit of $f(R, \tau)$ in the following form:

$$\lim_{\tau \to \infty} f(R, \tau) = e^{-\mathcal{V}(\mathcal{R})},$$

and

$$\mathcal{F}(\mathcal{R}) = -\nabla \mathcal{V}(\mathcal{R}),$$

then by substituting in (6.58), we have:

$$\mathcal{F}(\mathcal{R}) = 2\nabla \ln \psi_T^2(R),$$

$$\mathcal{V}(\mathcal{R}) = \ln \psi_T^2(R),$$

$$e^{-\mathcal{V}(\mathcal{R})} = \psi_T^2(R).$$

This means that, if we neglect the branching process, the Fokker–Planck equation in imaginary time for $f(R, \tau)$ corresponds to a suitable dynamics for the sampling of the variational probability density $\psi_T^2(R)$. The Green's function for equation (6.58) is a Gaussian similar to (6.48) and its centre, contrary to what happens for the free diffusion equation, is shifted along the gradient of the wavefunction ψ_T with respect to the origin R. Thus, the Monte Carlo dynamics has a new term, called the *drift* term, which describes the effect of the pseudo-force on the evolution of the walker population. Therefore, starting with a walker at position R in the $d \times N$-dimensional space, the new position R' is generated moving each particle according to the following expression:

$$r_i' = r_i + D \frac{2\nabla_i \psi_T(R)}{\psi_T(R)} \Delta\tau + \xi_i \,,$$

where ξ is a vector in which each component is a random number with Gaussian distribution as in (6.49).

In the $m \to \infty$ limit, we have for the normalized function:

$$\frac{\partial}{\partial \tau} f(R, \tau) = [E_0 - E_L(R)] f(R, \tau) \,. \tag{6.59}$$

Now the branching probability becomes

$$P_B = e^{-\Delta\tau(E_L(R) - E_0)} \,.$$

Therefore, the introduction of the importance function modifies two steps of the algorithm:

(1) Addition of the drift term in the walker dynamics.
(2) Use of the local energy in place of the potential energy in the branching term.

This procedure drastically reduces the walker population fluctuations, even in the presence of diverging potentials. In fact, a proper choice of the analytic form of $\psi_T(R)$ guarantees that $E_L(R)$ is always finite (*cusp condition*), a condition that is exactly fulfilled if $\psi_T(R)$ is an exact eigenstate of the Schrödinger equation. Another advantage of this algorithm is that it is possible to define in a natural way an energy estimator, other than the normalization constant. In the limit of propagation for an infinite imaginary time, the mean value of the local energy $E_L(R)$ computed on the distribution $f(R, \tau)$ is exactly the ground state energy. In fact,

$$E_0 = \frac{\langle \psi_T(R) | H\phi_0(R) \rangle}{\langle \psi_T(R) | \phi_0(R) \rangle} \,, \tag{6.60}$$

but since the operator H is hermitian, we have

$$E_0 = \frac{\langle \phi_0(R) | H\psi_T(R) \rangle}{\langle \phi_0(R) | \psi_T(R) \rangle} = \lim_{\tau \to \infty} \frac{\int f(R, \tau) \frac{H\psi_T(R)}{\psi_T(R)} \, dR}{\int f(R, \tau) dR} \,. \tag{6.61}$$
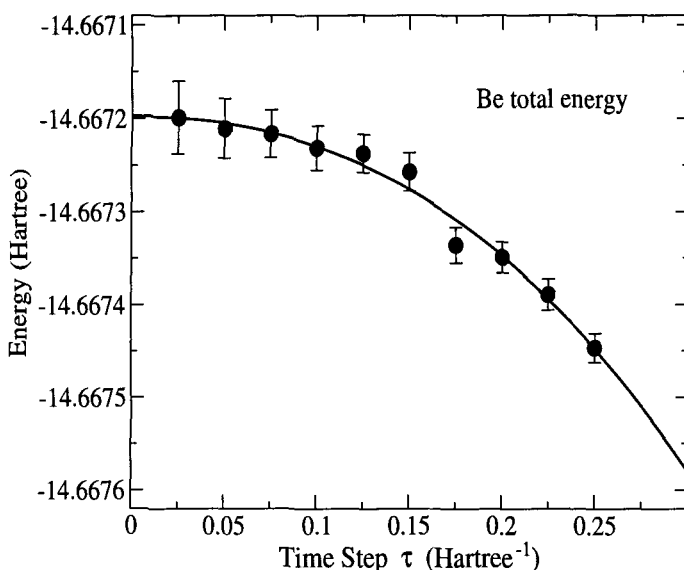
Fig. 6.4   Dependence of the total energy on the time-step τ in the calculation of the total energy of Be atom in various variants of the *DMC* algorithm (courtesy C.J. Umrigar).

Therefore, the energy eigenvalue may be obtained as the mean value of the local energy on the distribution $f(R, \tau)$. For any other estimator, one does not get mean values on the ground state, but rather matrix elements between the ground state and the trial variational state. However, let us suppose that for an operator $\hat{O}$ there exists a value $\epsilon << 1$ such that $|\psi_T\rangle - |\phi_0\rangle \sim \epsilon|\psi_{\text{res}}\rangle$, where $|\psi_{\text{res}}\rangle$ is a suitable combination of excited states of the system. It is easily verified that the estimator

$$2\langle\phi_0|\hat{O}\psi_T\rangle - \langle\psi_T|\hat{O}\psi_T\rangle \qquad (6.62)$$

differs from the matrix element on the ground state by an order of ϵ^2. Such corrected estimator is named *mixed estimator*. More complicated methods for finding pure estimators, are present in the literature.

A final consideration concerns the validity of approximation (6.53). In general, the terms $o(\tau)$ which are neglected in the implementation of the algorithm have a non-negligible effect on the energy value (*time-step error*). For this reason it is, in general, necessary to carry out a τ-extrapolation of the results. By suitable modifications of the algorithm, the effects of the time-step error can be reduced. In Fig. 6.4, we see how different implementations of the *DMC* lead to very different τ-dependencies of the results.[†]

[†] An exhaustive discussion about the dependence of the time-step error on the details of the algo-rithm, may be found in the paper by Umrigar, Nightingale and Runge (1993).

6.12   Fermion Systems and the Sign Problem

Let us suppose we want to use a DMC-like algorithm to study a many-body Fermion (e.g. electron) system. We might consider starting from an antisymmetric variational trial function ψ_T, and then applying the algorithm as described above. From the expression (6.61), which gives the mean value of the energy, we deduce that the result is, in principle, correct if we take as energy reference E_0^A (i.e. the energy of the antisymmetric ground state), because the components on the symmetric states vanish by orthogonality. Therefore, the term in (6.42) which includes $e^{-\tau(E_0 - E_0^A)}$ and would be diverging, gives actually no contribution. However, if we compute the variance of the ground state energy E_0^A:

$$\sigma^2 = \left| \langle H \rangle^2 - \langle H^2 \rangle \right|, \tag{6.63}$$

then the symmetric components survive in the following expression:

$$\langle H^2 \rangle = \frac{\int \phi_0(R) \psi_T(R) \left(\frac{H \psi_T(R)}{\psi_T(R)} \right)^2 dR}{\int \phi_0(R) \psi_T(R) dR}, \tag{6.64}$$

and the term

$$\sum_n c_n \exp\{-(E_n - E_0^A)\tau\} \phi_{0n} \tag{6.65}$$

diverges exponentially. Thus, it is possible to obtain exact mean eigenvalues, but affected by infinitely large error.

This problem is known as the *sign problem* and, up until now, it constitutes the most severe limit to the application of the DMC method to Fermion systems.

In any case, there are a certain number of approximations that make the use of DMC possible and, in some cases, yield almost exact results. The most widespread of these is the *fixed-node approximation*. Essentially, it consists in imposing artificial boundary conditions on the problem, by requiring that the DMC projected wavefunction has the same zeroes as the antisymmetric trial function. In this way, the problem is reduced to a standard calculation for the positive (or negative) part of the wavefunction. The antisymmetry and continuity of the wavefunction imply that it must become zero on a $(3N - 1)$-dimensional hyper-surface in the $3N$-dimension space of the system under study. Such hyper-surface (the *nodal structure*) in general is not known, but it may be optimized by means of variational methods. Though the resulting error may be estimated, it cannot be determined *a priori*.

The following is an example of trial function for a system of electrons:

$$\psi_T = \sum_{i<j} U(r_{ij}) \sum_i D_i^\uparrow D_i^\downarrow, \tag{6.66}$$

where $D_i^\uparrow$ and $D_i^\downarrow$ are Slater determinants, made up of suitable single-particle wavefunctions, and which represent the antisymmetric part. The $U(r_{ij})$ is the correlation
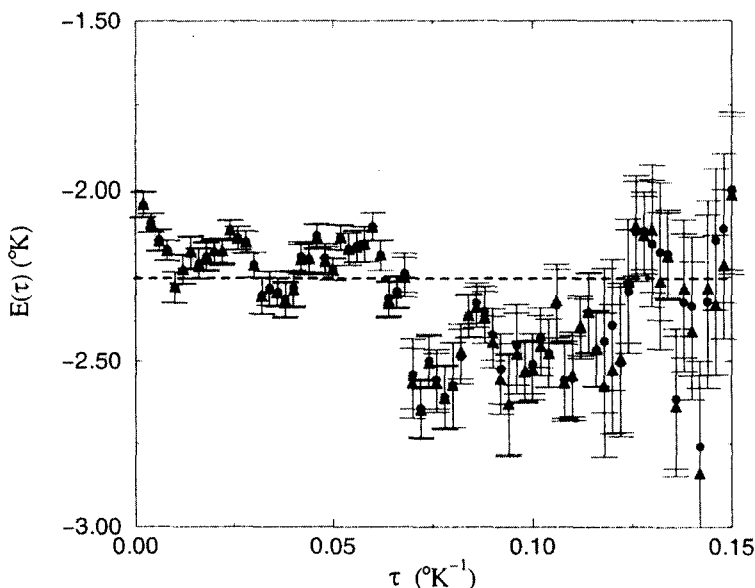
Fig. 6.5 Evolution of the mean value of energy in a DMC calculation with free nodes for 14 ^{3}He particles. Note that the error bars rapidly increase with imaginary time.

function, and may include up to more than ten parameters. Let us assume that we made a good choice for ψ_T, i.e.

$$\sigma^2(H) \approx 0. \tag{6.67}$$

The calculation goes on by modifying with DMC the trial function only in the regions with constant sign, removing the walkers that pass from one region to the other. The results that one obtains are, in general, good for electron systems (they have been presented several times in this book), while in other cases (like ^{3}He) the method is not as satisfactory.

Recently, remarkable progress has been made in the development of an algorithm which is able to exactly project the ground state of Fermion systems (Kalos and Pederiva 1999). At present, this is still an active research field.

References to Chapter 6

G.E.P. and M.E. Muller, A Note on the Generation of Random Normal Deviates, Ann. Math. Stati. **29**, 610 (1958).

D.M. Ceperley and M.H. Kalos, Monte Carlo Methods in Statistical Physics, ed. by K. Binder (Springer-Verlag, Berlin 1986), p. 145.

D.M. Ceperley, Rev. Mod. Phys. **67**, 279 (1995).

G. Comte de Buffon, Essai d'arithmétique morale, Supplément à l' Histoire Naturelle, Vol. 4 (1777).

M.H. Kalos and F. Pederiva, Quantum Monte Carlo Methods in Physics and Chemistry, ed by C.J. Umrigar and M.P. Nightingale (Kluwer Acadcmic Publishing, 1999), p. 263.

W.L. McMillan, Phys. Rev. A **138**, 442 (1965).

N. Metropolis, A.W. Rosenbluth, M.N. Rosenbluth, A.H. Teller and E. Teller, J. Chem. Phys. **21**, 1087 (1953).

C.J. Umrigar, M.P. Nightingale and K.J. Runge, J. Chem. Phys. **99**, 2865 (1993).

As general references to the Monte Carlo simulation in classical and quantum systems, the following texts may be useful:

M.P. Allen and D.J. Tildesley, Computer Simulation of Liquids (Clarendon, Oxford 1987).

M.H. Kalos and P.A. Withlock, Monte Carlo Methods: Basic, Vol. 1 (J. Wiley and Sons, New York, 1986).

PART 2

The Linear Response Function Theory

7.1 Introduction

The second part of this book is devoted to the study of the excited states of inter-acting many particle systems, which can be described by a Hamiltonian like that in (1.1). Moreover, the particles interact with an external oscillating field (responsible for the excitation of the system) through an interaction Hamiltonian H_{int}.

As we did in the first part of the book, which is devoted to the study of the ground state of a many body system, we will consider both homogeneous and finite systems of Fermions and Bosons. In any case, the interesting quantities that can be tested experimentally are the matrix elements

$$|\langle n|F|0\rangle|^2 \tag{7.1}$$

of an observable F between the ground and excited states of H (which in turn are the solutions of the equation $H|n\rangle = E_n|n\rangle$), and the corresponding excitation energies

$$E_n - E_0 . \tag{7.2}$$

In Chapter 1 we showed that these quantities can be easily computed for a one-body operator $F = \sum_{i=1}^{N} f(x_i)$, in the case of the independent-particle model (IPM) where two-body interaction is neglected in H. The relevant excited states are the one-particle–one-hole states $|i^{-1}m\rangle$, and the matrix elements of the operator F are given by (1.19) for Fermions, and (1.21) for Bosons. The corresponding excitation energies are given by the difference $\epsilon_{mi} = \epsilon_m - \epsilon_i$ between the single-particle energies of the hole and of the particle. It might be asked whether the IPM predictions are in agreement with experimental data, or fail completely. To try to give an answer to this question, let us compute, for a homogeneous system of Fermions and Bosons, the dynamic form factor:

$$S(\mathbf{q}, \omega) = \sum_n |\langle n|\rho_{\mathbf{q}}|o\rangle|^2 \delta(\omega - \omega_{no}), \qquad \omega_{no} = E_n - E_0 , \tag{7.3}$$

for the density operator:

$$\rho_{\mathbf{q}} = \sum_{i=1}^{N} e^{i\mathbf{q}\cdot\mathbf{r}_i} = \int d\mathbf{r} \, e^{i\mathbf{q}\cdot\mathbf{r}} \rho(\mathbf{r}), \tag{7.4}$$

with $\rho(\mathbf{r}) = \sum_{i=1}^{N} \delta(\mathbf{r} - \mathbf{r}_i)$. This quantity, which was previously introduced in Section 1.8.1, can be directly measured by inelastic scattering experiments, and in the IPM is given by

$$S(\mathbf{q}, \omega) = \sum_{mi} |\langle mi^{-1}|\rho_{\mathbf{q}}|0\rangle|^2 \delta(\omega - \epsilon_{mi}), \tag{7.5}$$

where the sum runs on all the one-particle–one-hole states. In the case of non-interacting homogeneous systems, the single-particle wavefunctions are plane waves.

In the $3D$ Fermion case, the calculation of $S(\mathbf{q}, \omega)$ was carried out in Section 1.8.1 for small q (i.e. q much smaller than the Fermi momentum), and we obtained the following analytical result

$$S(\mathbf{q}, \omega) = \begin{cases} V\dfrac{m^2\omega}{2\pi^2 q} & \text{for } 0 \leq \omega \leq \dfrac{qk_F}{m} \\[3mm] 0 & \text{for } \omega > \dfrac{qk_F}{m} \end{cases}, \tag{7.6}$$

which shows that for any value of q, the dynamic form factor $S(\mathbf{q}, \omega)$ tends to zero when $\omega \to 0$, as a consequence of the Pauli principle which limits the number of low-energy excitations for Fermions. The excitation spectrum is a continuum in the range

$$0 \leq \epsilon_{mi} \leq qk_F/m.$$

In the case of a three-dimensional homogeneous system of Bosons at zero temperature, whose IPM ground state is the product function

$$|0\rangle = \varphi_{i_o}(x_1)\varphi_{i_o}(x_2)\cdots\varphi_{i_o}(x_n), \tag{7.7}$$

where the $\varphi_{i_o}(x)$ are all equal to each other, and is given by the plane waves $\varphi_{i_o} = e^{i\mathbf{p}\cdot\mathbf{r}}/\sqrt{V}$ characterized by the momentum $\mathbf{p}$ (which can be put equal to zero), the calculation of the matrix element (1.21) for the density operator leads immediately to the result

$$\langle mi_o^{-1}|\rho_{\mathbf{q}}|0\rangle = \sqrt{N}, \tag{7.8}$$

and to the existence of only one possible excited state at energy $\epsilon_{mi_o} = q^2/2m$. Therefore, for a system of non-interacting Bosons we have the following expression for the dynamic form factor:

$$S(\mathbf{q}, \omega) = N \cdot \delta\left(\omega - \frac{q^2}{2m}\right). \tag{7.9}$$

In summary, the independent-particle model makes the following predictions for the dynamic form factor: for Fermions, the existence of a continuum of single-particle states with energy ω between 0 and qk_F/m, among which the strength is distributed, and which — for all (small) q-values — goes to zero when ω goes to zero; for Bosons it is the existence of only one single-particle state at energy $q^2/2m$ which picks up all of the available strength.

In nature, the closest realization of an interacting Fermi gas in three dimensions, is an alkali metal: for example, in sodium each atom has a valence electron which is nearly free because it is very far apart from the core electrons placed into closed shells. The ensemble of such valence electrons constitutes a gas of nearly-free electrons, which move in the field of the uniformly distributed ions, and under the effect of their mutual Coulomb interaction. The excitation of this valence-electron gas is realized by striking an electron beam on the alkali metal, and measuring the inelastic cross section of this process at various transferred momenta, as a function of the energy transferred to the system. The inelastic cross section is proportional to the dynamic form factor.

The data of Fig. 7.1 show that $S(\mathbf{q},\omega)$ behaves quite differently from the prediction of the independent-particle model in the limit of small q. The cross section at
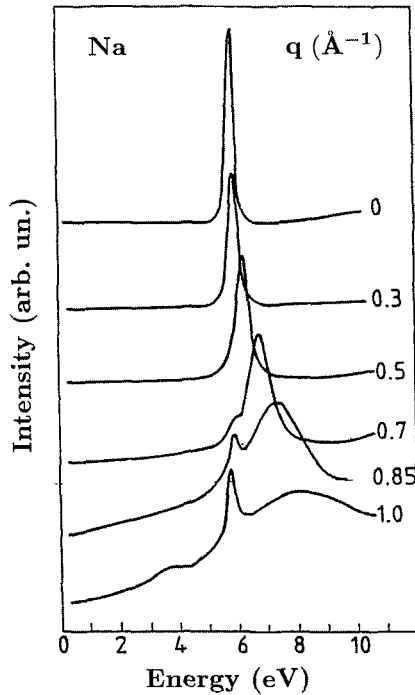
Fig. 7.1 Experimental excitation spectrum of Sodium (Von Felde et al. 1989) as a function of energy, for different values of the transferred momentum.
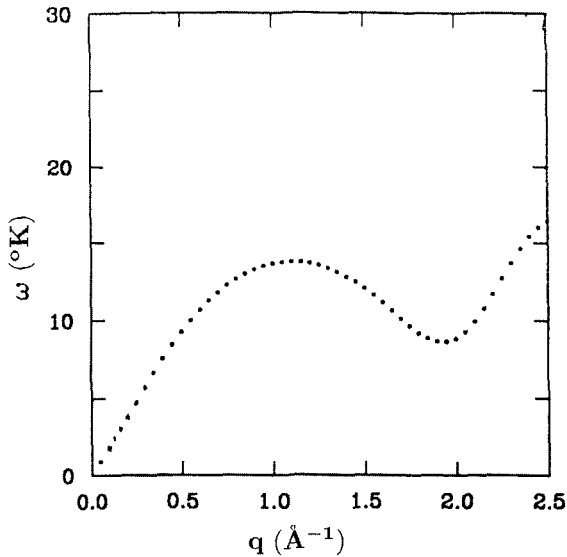
Fig. 7.2 Experimental data (Donnelly et al. 1981) on the dispersion of elementary excitations in superfluid ^{4}He.

fixed q, as a function of the energy absorbed by the system, is characterized by the presence of a peak at a well defined energy, which does not go to zero when q tends to zero, and which collects practically all of the excitation strength of the process. It is only at high values of q that this state decays into low-energy single-particle states. This excited state, at small values of the transferred momentum, has nothing in common with the single-particle states of the IPM, and is a collective excitation of the system called plasmon.

As regards Bosons, if we consider superfluid ^{4}He as an example of homogeneous system of Bosons, the experimental data of Fig. 7.2 show that at low q, these excitations have phonon nature with a q-linear dispersion law which has nothing in common with the IPM predictions.

Therefore, the comparison with experimental data evidences the shortcomings of the independent-particle model for the description of the excited states of a Fermion or Boson quantum liquid, and poses us the problem of setting up a general theory for the description of these states. Such theory should take into account the interaction among particles.

By "quantum liquids", we mean both the "real" quantum liquids that are found in nature, i.e. ^{4}He (Bose) and ^{3}He (Fermi) which have the property of being liquid in such a low temperature range that quantum effects connected to degeneracy and interaction cannot be neglected, and the conduction electrons in metals, semi-metals and semiconductors, as well as nuclear matter and the very recently realized Bose condensates of alkali atoms.

7.2   General Formalism

An N-particle system described by Hamiltonian H can be excited by making it interact with a beam of external particles, and subsequently studied by measuring its response to the external field that describes this interaction. If the interaction is sufficiently weak, the system response is linear and completely determined by the system's intrinsic properties (i.e. those in the absence of the external field).

   The theory of the linear response function allows the study of the excited homogeneous and non-homogeneous states, of interacting systems, both at zero and at finite temperature. We will begin with the zero-temperature response, and discuss the finite-temperature effects in another Section.

   The interaction Hamiltonian of a system with an external field that oscillates in time with frequency ω, may be written as

$$H_{\text{int}} = \lambda(G^\dagger e^{-i\omega t} + G e^{i\omega t})e^{\eta t} . \tag{7.10}$$

   The quantity λ gives the field intensity. G is an operator which depends on the space, spin, isospin, ..., variables of the N particles of the system, and contains the physical information pertaining to the type of excitations to which the system is subjected. The factor $e^{\eta t}$, with η positive and small, guarantees that as $t \to -\infty$ the system is described by the unperturbed Hamiltonian H and is in the ground state $|0\rangle$.

   The interaction (7.10) produces time dependence in the N particles wavefunction $|\psi(t)\rangle$ which is the solution of the equation:

$$(H + H_{\text{int}})|\psi(t)\rangle = i\frac{\partial}{\partial t}|\psi(t)\rangle , \tag{7.11}$$

and, consequently, the mean value of an operator F on such a state, can be written as

$$\langle\psi(t)|F|\psi(t)\rangle - \langle 0|F|0\rangle = F_+ e^{-i\omega t}e^{\eta t} + F_- e^{i\omega t}e^{\eta t} . \tag{7.12}$$

Equation (7.11) is to be solved with the boundary condition that for $t \to -\infty$ the system is in the ground state $|0\rangle$.

   The linear response function of the system to the external field (7.10) is defined as

$$\chi(F, G, \omega) = \lim_{\lambda \to 0}\frac{F_+}{\lambda} . \tag{7.13}$$

Note that this definition generalizes to the quantum case the classical definition of linear response. For example, consider the electrostatic polarizability α of a classical system. This is the linear response of the system to an external electric field E. If P is the induced dipole moment, we will have

$$\alpha = \lim_{E \to 0}\frac{P}{E} . \tag{7.14}$$

The linear response function to an electric field that oscillates in time, is also known as dynamic polarizability.

Using the usual procedures of perturbation theory, let us look for solutions of (7.11) of the form

$$|\psi(t)\rangle = \sum_n a_n(t) e^{-iE_n t} |n\rangle, \qquad (7.15)$$

where the boundary condition corresponds to

$$a_n(-\infty) = \begin{cases} 1 & \text{if } n = 0 \\ 0 & \text{if } n \neq 0 \end{cases}. \qquad (7.16)$$

By retaining only the first order terms in λ, we find $(n \neq 0)$:

$$a_n(t) = \lambda \left[\frac{\langle n|G^\dagger|0\rangle}{\omega - \omega_{no} + i\eta} e^{(-i\omega + i\omega_{no} + \eta)t} - \frac{\langle n|G|0\rangle}{\omega + \omega_{no} - i\eta} e^{(i\omega + i\omega_{no} + \eta)t} \right]. \qquad (7.17)$$

Then, at first order in λ we have

$$\langle \psi(t)|F|\psi(t)\rangle - \langle 0|F|0\rangle$$

$$= \sum_n [\langle 0|F|n\rangle a_n(t) e^{-i\omega_{no}t} + \langle n|F|0\rangle a_n^\dagger(t) e^{i\omega_{no}t}]. \qquad (7.18)$$

By substituting (7.17) into (7.18), separating the coefficients of $e^{-i\omega t}$ from those of $e^{i\omega t}$, and bearing in mind that $\langle 0|G|n\rangle^* = \langle n|G^\dagger|0\rangle$, we obtain from the definition (7.13) the following expression for the linear response

$$\chi(F, G, \omega) = \sum_n \left[\frac{\langle 0|F|n\rangle\langle n|G^\dagger|0\rangle}{\omega - \omega_{no} + i\eta} - \frac{\langle 0|G^\dagger|n\rangle\langle n|F|0\rangle}{\omega + \omega_{no} + i\eta} \right]. \qquad (7.19)$$

From equation (7.19) we see that the knowledge of χ means the knowledge of both the excitation energies (i.e. the poles of χ) and the matrix elements of the operators (i.e. the residues in the poles of χ): therefore, if we succeed in calculating the linear response, we automatically achieve what we are looking for, viz. the matrix elements between ground and excited states, and the excitation energies.

If F is Hermitian and equal to G, or if $F = G$ but not Hermitian (e.g. $F = G = \rho_{\mathbf{q}}$) and the unperturbed system is time-reversal invariant (so that $|\langle n|F|0\rangle|^2 = |\langle n|F^\dagger|0\rangle|^2$), then equation (7.19) takes on the simplified form:

$$\chi(F, \omega) = 2 \sum_n \omega_{no} \frac{|\langle n|F|0\rangle|^2}{(\omega + i\eta)^2 - \omega_{no}^2}. \qquad (7.20)$$

Note that in the case of the density operator, the relation $|\langle n|\rho_{\mathbf{q}}|0\rangle|^2 = |\langle n|\rho_{\mathbf{q}}^\dagger|0\rangle|^2$ and consequently equation (7.20) still holds even if the time-reversal symmetry is broken as long as the system retains parity invariance. This case, i.e. the density response, will be discussed in detail in Section 7.5. Note also that in the case of the nuclei, equation (7.20) cannot be derived from equation (7.19) starting from

operators of the form $F = G = \sum_i f(\mathbf{r}_i)\tau^+$, where τ^+ is the isospin operator which, by operating on the proton state produces the neutron state. In fact, for nuclei with an excess of neutron the operators F and $F^\dagger = \sum_i f(\mathbf{r}_i)\tau^-$, (where τ^- changes the neutron state into that of the proton) excite different states and the two excitation strengths

$$|\langle n|\sum_i f(\mathbf{r}_i)\tau^+|0\rangle|^2$$

and

$$|\langle n|\sum_i f(\mathbf{r}_i)\tau^-|0\rangle|^2\,,$$

are different.

Using the Dirac relation

$$\lim_{\eta\to 0} \frac{1}{x - a + i\eta} = \mathrm{P}\left(\frac{1}{x-a}\right) - i\pi\delta(x-a)\,, \tag{7.21}$$

we have that the real and imaginary parts of χ are related to the dynamic form factor

$$S(F,\omega) = \sum_n |\langle n|F|0\rangle|^2\delta(\omega - \omega_{no})\,, \tag{7.22}$$

which generalizes the definition (7.3) to any excitation operator F, by

$$\mathrm{Re}\ \chi(F,\omega) = \int_0^\infty d\omega' S(F,\omega')\mathrm{P}\left(\frac{2\omega'}{\omega^2 - \omega'^2}\right)\,, \tag{7.23}$$

and

$$S(F,\omega) - S(F,-\omega) = -\frac{1}{\pi}\mathrm{Im}[\chi(F,\omega)]\,. \tag{7.24}$$

Note that at zero temperature, $S(F,-\omega)$ is identically zero for $\omega > 0$ because the excitation energies ω_{no} are always positive since the system is initially in the ground state. Therefore, for positive ω-values, $S(F,\omega)$ and the imaginary part of χ coincide. As we will see, at finite temperature this is no longer the case.

If $F = G$ but not Hermitian such as in the case of the following operators

$$F = G = \sum_i^N x_i\sigma_i^+ \qquad \sigma^+ = \frac{1}{2}(\sigma_x + i\sigma_y)$$

or

$$F = G = \sum_i^N r_i e^{i\theta}\,,$$

and if the system is not time-reversal invariant (i.e. it is either spin-polarized or angular momentum-polarized), or if we have a nucleus with an excess of neutrons

and we are considering charge-exchange processes described by operators like those discussed previously, then in these cases χ takes the form

$$\chi = \sum_n \left[\frac{|\langle n|F^\dagger|0\rangle|^2}{\omega - \omega_{no} + i\eta} - \frac{|\langle n|F|0\rangle|^2}{\omega + \omega_{no} + i\eta} \right]. \tag{7.25}$$

In this case the operators F and $F^\dagger$ excite different states of the system and $S(F,\omega) \neq S(F^\dagger,\omega)$, and the following relation holds

$$-\frac{1}{\pi}\text{Im }\chi(\omega) = S(F^\dagger,\omega) - S(F,-\omega), \tag{7.26}$$

This relation allows us to extract both $S(F^\dagger)$ and $S(F)$, once the imaginary part of the linear response is known along the whole (positive and negative) ω axis.

7.3   Linear Response Function and Sum Rules

The linear response function (7.20) can be related to the moments m_k of the dynamic form factor (7.22), defined by

$$m_k = \int_0^\infty d\omega\,\omega^k S(F,\omega) = \sum_n \omega_{no}^k |\langle 0|F|n\rangle|^2, \tag{7.27}$$

by expanding $\chi(F,\omega)$ as a function of ω. In the two cases of $\omega \to \infty$ and $\omega \to 0$ we obtain

$$\lim_{\omega\to\infty} \chi(F,\omega) = \frac{2}{\omega^2}\left(m_1 + \frac{1}{\omega^2}m_3 + \cdots \right) \tag{7.28}$$

and

$$\lim_{\omega\to 0} \chi(F,\omega) = -2(m_{-1} + \omega^2 m_{-3} + \cdots), \tag{7.29}$$

respectively.

By using the completeness relation $\sum_n |n\rangle\langle n| = 1$ and the equation $H|n\rangle = E_n|n\rangle$, it is possible to write the moments (7.27) with $k \geq 0$ as the mean values on the ground state of commutators [ ] and anticommutators { } of the excitation operator F and of the Hamiltonian H. For time-reversal-invariant systems, the following sum rules are derived:

$$
\begin{aligned}
m_0 &= \frac{1}{2}\langle 0|\{F, F^\dagger\}|0\rangle - \langle 0|F|0\rangle^2, \\[6pt]
m_1 &= \frac{1}{2}\langle 0|[F, [H, F^\dagger]]|0\rangle, \\[6pt]
m_2 &= \frac{1}{2}\langle 0|\{[F, H], [H, F^\dagger]\}|0\rangle, \\[6pt]
m_3 &= \frac{1}{2}\langle 0|[[F, H], [H, [H, F^\dagger]]]|0\rangle.
\end{aligned}
\tag{7.30}
$$

Note that in the odd sum rules only commutators appear, while in the even ones anticommutators appear as well, and that in the expansion (7.28) only odd moments with $k > 0$ appear. The moments with $k < 0$ may also be expressed through commutators and anticommutators. For example, we can write

$$m_{-1} = \frac{1}{2}\langle 0|[[X^\dagger, H], X]|0\rangle\,,$$

$$m_{-2} = \frac{1}{2}\langle 0|\{X^\dagger, X\}|0\rangle\,,$$

(7.31)

where the operator X is the solution of the following equation

$$[H, X] = F\,.$$

(7.32)

In the expansion (7.29) only moments with negative odd k enter. Among these, the most important is certainly m_{-1}, which is connected to the static polarizability $\chi(F, 0)$ of the system by the relation

$$m_{-1} = \sum_n \frac{|\langle 0|F|n\rangle|^2}{\omega_{no}} = -\frac{\chi(F, 0)}{2}\,.$$

(7.33)

As an example of the calculation of a sum rule, let us compute m_1 for the electric dipole operator

$$F = D = e\sum_{i=1}^{N} z_i\,,$$

in the case where the system is a neutral atom with N electrons and Hamiltonian given by

$$H = \sum_{i=1}^{N}\left(\frac{p^2}{2m} - \frac{Ne^2}{r}\right)_i + \sum_{i<j}\frac{e^2}{|\mathbf{r}_i - \mathbf{r}_j|}\,.$$

The dynamic form factor for the operator D is directly observable. For example, in photo-absorption experiments where the cross section $\sigma(\omega)$ is related to $S(D, \omega)$ by the relationship

$$\sigma(\omega) = 4\pi^2\omega S(D, \omega)\,.$$

(7.34)

The evaluation of the double commutator of equation (7.30) is very simple, because the dipole operator commutes with both the one-body nuclear potential and the two-body Coulomb interaction, because both are local terms, and the only contribution comes from the kinetic energy. The result is

$$m_1(D) = \frac{N\hbar^2 e^2}{2m}\,,$$

(7.35)

independent of the model and known as the Thomas–Reich–Kuhn sum rule. Using equation (7.34) we have

$$\int \sigma(\omega)d\omega = 4\pi^2 m_1(D) = 2\pi^2 \frac{N\hbar^2 e^2}{m}, \tag{7.36}$$

which means that the area underlying the photo-absorption cross section plotted as a function of the photon energy, is proportional to the atomic charge.

The sum rules (7.30) may be generalized to any operator F and G, starting from the following mixed expression:

$$m_k^{\pm} = \frac{1}{2} \sum_n \omega_{no}^k (\langle 0|F|n\rangle\langle n|G^{\dagger}|0\rangle \pm \langle 0|G^{\dagger}|n\rangle\langle n|F|0\rangle)$$

$$= \frac{1}{2}(\langle 0|F(H - E_0)^k G^{\dagger}|0\rangle \pm \langle 0|G^{\dagger}(H - E_0)^k F|0\rangle). \tag{7.37}$$

For $k = 0, 1, 2$ we obtain

$$m_0^+ = \frac{1}{2}\langle 0|\{F, G^{\dagger}\}|0\rangle,$$

$$m_1^+ = \frac{1}{2}\langle 0|[F, [H, G^{\dagger}]]|0\rangle, \tag{7.38}$$

$$m_2^+ = \frac{1}{2}\langle 0|\{[F, H], [H, G^{\dagger}]\}|0\rangle,$$

and

$$m_0^- = \frac{1}{2}\langle 0|[F, G^{\dagger}]|0\rangle,$$

$$m_1^- = \frac{1}{2}\langle 0|\{F, [H, G^{\dagger}]\}|0\rangle, \tag{7.39}$$

$$m_2^- = \frac{1}{2}\langle 0|[[F, H], [H, G^{\dagger}]]|0\rangle.$$

Clearly, when $G = G^{\dagger} = F$, we will have m_0^+, m_1^+, m_2^+ coincide with the sum rules of equation (7.30), while m_0^-, m_1^-, m_2^- vanish. This holds also in the $F = G = \rho_{\mathbf{q}}$ case, provided the unperturbed system is parity or time-reversal invariant.

The sum rules m_0^-, m_1^+, m_2^-, ... enter into the $\omega \to \infty$ expansion of the linear response $\chi(F, G, \omega)$ of (7.19):

$$\lim_{\omega \to \infty} \chi(F, G, \omega) = \frac{2}{\omega}\left(m_0^- + \frac{1}{\omega}m_1^+ + \frac{1}{\omega^2}m_2^- \cdots\right). \tag{7.40}$$

As an example of application of the mixed sum rules (7.37), let us consider a quantum dot under the effect of a static magnetic field perpendicular to the electron motion (which is confined on the x, y plane), with Hamiltonian H given

by equation (5.1), and let us compute the sum rules m_0^-, m_1^+, m_2^- and m_3^+ for the operators

$$F = F^- = \sum_{j=1}^{N} r_j e^{-i\theta_j}$$

and

$$G^\dagger = F^+ = \sum_{j=1}^{N} r_j e^{+i\theta_j} \, .$$

These are dipole operators with angular momentum -1 and $+1$, respectively, and if the dot in its ground state is angular-momentum-polarized and has $\langle 0|L_z|0\rangle = -L_0$, with $L_0 = \sum_i^{occ} l_i$, then they excite states with $\Delta L_z = \mp 1$, respectively. For a high external magnetic field, these two excitations — at IPM level — are one-particle–one-hole excitations among single-particle states belonging to one Landau level in the first case (edge excitations), and among states belonging to two different Landau levels (bulk-like) in the second case.

The calculation of the commutators is very simple because the two-body inter-action commutes both with $F^\pm$ and with the results of the commutation between H and $F^\pm$, which is given by

$$[H, F^\pm] = \pm \frac{\omega_c}{2} F^\pm - iP^\pm \, , \qquad P^\pm = \sum_{j=1}^{N} (p_x \pm ip_y)_j \, .$$

We can thus find (in effective atomic units) the following

$$
\begin{aligned}
m_0^- &= 0 \, , \\
m_1^+ &= N \, , \\
m_2^- &= \omega_c N \, , \\
m_3^+ &= (\omega_0^2 + \omega_c^2) N \, .
\end{aligned}
\tag{7.41}
$$

The results for the above moments, may be used to compute the excited state frequencies of the operators $F^\pm$, if one makes the further hypothesis that such moments are saturated by only two modes with frequencies $\omega_\pm$, which are excited respectively by the operators $F^\pm$:

$$S^\pm(\omega) = \sigma^\pm \delta(\omega - \omega_\pm) \, , \tag{7.42}$$

where $\sigma^\pm = |\langle \omega_\pm | F^\pm | 0 \rangle|^2$ are the corresponding strengths. The hypothesis (7.42), in conjunction with the result $m_0^- = 0$, implies $\sigma^+ = \sigma^-$. In this case, then, one immediately finds

$$\omega_+ - \omega_- = \frac{m_2^-}{m_1^+} = \omega_c \, , \tag{7.43}$$

and

$$\frac{\omega_+^3 + \omega_-^3}{\omega_+ + \omega_-} = \frac{m_3^+}{m_1^+} = \omega_0^2 + \omega_c^2, \tag{7.44}$$

from which it follows that

$$\omega_\pm = \sqrt{\omega_0^2 + \frac{1}{4}\omega_c^2} \pm \frac{\omega_c}{2}, \tag{7.45}$$

which is an exact result for the Hamiltonian (5.1) of the quantum dot (generalized Kohn theorem, see also Section 8.10.1).

Review papers on sum rules, where many applications of this method are discussed, are those of Leonardi and Rosa-Clot (1971); Bohigas, Lane and Martorell (1979); Lipparini and Stringari (1989) and Orlandini and Traini (1990).

7.4   Finite Temperature

The formalism of the linear response function at finite temperature is very similar to that of the zero-temperature developed above. However, there are some differences worthy of being stressed.

At zero temperature the excitation operator F induces a transition between the ground state $|0\rangle$ and one of the excited states $|n\rangle$ with $n \neq 0$. If the system is at equilibrium at a finite temperature T, then the ground state is a statistical mixture defined by the density matrix (2.76):

$$D = \sum_k p_k |k\rangle\langle k|,$$

where p_k is the probability of finding the system in the state $|k\rangle$, given by

$$p_k = \frac{e^{-\beta E_k}}{Z}, \tag{7.46}$$

with $Z = \sum_k e^{-\beta E_k}$ equals to the partition function. The dynamic form factor associated with the excitation operator F is generalized from equation (7.22) to

$$S_T(F,\omega) = \sum_{k \neq n} p_k |\langle n|F|k\rangle|^2 \delta(\omega - \omega_{nk}), \tag{7.47}$$

where $\omega_{nk} = E_n - E_k$.

During the interaction of the system with a test particle at finite temperature, it is possible to transfer energy both from the particle to the system, and from the system to the test particle because negative excitation energies ω_{nk} are admissible. At thermal equilibrium, the two probabilities (which are proportional to $S(F,\omega)$ and $S(F,-\omega)$, respectively) are not independent. The relationship existing between

$S(F, \omega)$ and $S(F, -\omega)$ is known as the principle of detailed balance. To derive it, it is sufficient to interchange the indexes n and k in (7.47), obtaining

$$S_T(F, \omega) = Z^{-1} \sum_{k \neq n} e^{-\beta E_n} |\langle k|F|n \rangle|^2 \delta(\omega + \omega_{nk})$$

$$= Z^{-1} \sum_{k \neq n} e^{-\beta(E_n - E_k)} e^{-\beta E_k} |\langle n|F^\dagger|k \rangle|^2 \delta(\omega + \omega_{nk})$$

$$= e^{\beta \omega} S_T(F^\dagger, -\omega). \tag{7.48}$$

Assuming time-reversal invariance so that $S_T(F^\dagger, -\omega) = S_T(F, -\omega)$, we finally find

$$S_T(F, \omega) = e^{\beta \omega} S_T(F, -\omega). \tag{7.49}$$

At zero temperature the imaginary part of the response function and the dynamic form factor coincide for positive ω, and only processes by which energy is transferred to the system are allowed. At finite temperature these two functions are quite different for small $\beta \omega$ values. This can be easily seen starting from the Kubo result for the linear response function at finite temperature:

$$\chi(F, \omega) = Z^{-1} \sum_{kn} e^{-\beta E_k} |\langle n|F|k \rangle|^2 \frac{2\omega_{nk}}{(\omega + i\eta)^2 - \omega_{nk}^2}, \tag{7.50}$$

which holds for time-reversal invariant systems. Using relation (7.21), the imaginary part of χ can be written as

$$\text{Im } \chi(\omega) = -\pi[S_T(F, \omega) - S_T(F, -\omega)], \tag{7.51}$$

and using the detailed balance condition (7.49) we obtain the relation

$$\text{Im } \chi(\omega) = -\pi[1 - e^{-\beta \omega}] S_T(F, \omega) \tag{7.52}$$

known as the fluctuation-dissipation theorem. Relation (7.52) shows that the imaginary part of the linear response function and $S_T(F, \omega)$ can be different at finite temperature. In general, $S_T(F, \omega)$ is much more temperature dependent than $\text{Im } \chi(\omega)$ which, for this reason, is a more fundamental quantity from the point of view of many body theory. It is also known as the dissipative component of the response function of the system. In fact, by means of second order perturbation theory, it is possible to connect $\text{Im } \chi(\omega)$ to the energy transferred per unit time by the external field to the system (see Section 7.5).

The moments of the dynamic form factor (7.47) are given by the following generalization of (7.27):

$$m_p = \int_{-\infty}^{+\infty} S_T(F, \omega) \omega^p d\omega = \sum_{k \neq n} p_k |\langle n|F|k \rangle|^2 \omega_{nk}^p. \tag{7.53}$$

Note that these moments, contrary to the $T = 0$ case, get contribution from negative ω as well. It can be shown that the moments defined as in Eq. (7.53) obey the usual sum rules, i.e. that the m_p with $p > 0$ are the mean values on the statistical mixture D. For example, in the case of the energy-weighted sum rule m_1 for the Hermitian operator F, we have

$$
\begin{aligned}
m_1 &= \frac{1}{2}\text{Tr}\{D[F,[H,F]]\} \\
&= \frac{1}{2}\text{Tr}\{D(2FHF - HF^2 - F^2H)\} \\
&= \frac{1}{2}\sum_{k \neq n} |\langle n|F|k\rangle|^2 (2E_n - E_k - E_k)p_k \\
&= \sum_{k \neq n} |\langle n|F|k\rangle|^2 (E_n - E_k)p_k \, .
\end{aligned}
\tag{7.54}
$$

In what follows, for the sake of simplicity, we will indicate the mean value of an operator A on the statistical mixture D by $\langle A \rangle$, which will stand for[*]

$$
\text{Tr}(DA) = \sum_n p_n \langle n|A|n\rangle \, .
$$

7.5 The Density Response

The density response is a quantity that allows one to study the dynamic behavior of an interacting many body system, both at zero and finite temperature. It can be measured by inelastic scattering reactions and can be used to provide important information both on the collective states that are excited at small transferred momentum, and on the momentum distribution which characterizes the system at high-transferred momentum.

As we have already discussed in Section 7.2, the density response corresponds to the case $F = G = \rho_\mathbf{q}$ in (7.19). If the unperturbed system is parity-invariant or time-reversal-invariant, it is possible to write the density response $\chi(\mathbf{q},\omega)$ as

$$
\chi(\mathbf{q},\omega) = 2\sum_{kn} p_k \omega_{nk} \frac{|\langle n|\rho_\mathbf{q}|k\rangle|^2}{(\omega + i\eta)^2 - \omega_{nk}^2} \, .
\tag{7.55}
$$

It can be written as a function of the dynamic form factor (7.47) as

$$
\chi(\mathbf{q},\omega) = \int_{-\infty}^{+\infty} d\omega' \left[\frac{S(\mathbf{q},\omega)}{\omega - \omega' + i\eta} - \frac{S(-\mathbf{q},\omega)}{\omega + \omega' + i\eta} \right],
\tag{7.56}
$$

[*]See Eq. (2.77).

and the real and imaginary parts of χ can be expressed as

$$\text{Re } \chi(\mathbf{q},\omega) = \int_{-\infty}^{+\infty} d\omega' \left[S(\mathbf{q},\omega) P \frac{1}{\omega - \omega'} - S(-\mathbf{q},\omega) P \frac{1}{\omega + \omega'} \right] \qquad (7.57)$$

and

$$S(\mathbf{q},\omega) - S(-\mathbf{q},-\omega) = -\frac{1}{\pi} \text{Im}[\chi(\mathbf{q},\omega)]. \qquad (7.58)$$

If the system interacts weakly with a test particle, and $v(\mathbf{q})$ is the Fourier transform of the interaction, the probability per unit time that the particle transfers momentum $\mathbf{q}$ and energy ω to the system, $P(\mathbf{q},\omega)$, is related to the dynamic form factor $S(\mathbf{q},\omega)$ by the relation

$$P(\mathbf{q},\omega) = 2\pi |v(\mathbf{q})|^2 S(\mathbf{q},\omega). \qquad (7.59)$$

As was discussed in Section 7.4, at finite temperature the test particle can either transfer momentum $\mathbf{q}$ and energy ω to the system, or extract them from the system. The energy transferred per unit time between the external field and the system is given by

$$\frac{dE}{dt} = 2\pi |v(\mathbf{q})|^2 \omega(S(\mathbf{q},\omega) - S(-\mathbf{q},-\omega)) = -2|v(\mathbf{q})|^2 \omega \text{Im}[\chi(\mathbf{q},\omega)]. \qquad (7.60)$$

Equations (7.53) and (7.58), together with the identity $S(\mathbf{q},\omega) = S(-\mathbf{q},\omega)$ which holds for parity- or time-reversal-invariant systems, allow us to write the following relation among the odd moments of $S(\mathbf{q},\omega)$ and the imaginary part of χ:

$$m_{2p+1} = -\frac{1}{\pi} \int_0^\infty \omega^{2p+1} \text{Im } [\chi(\mathbf{q},\omega)] d\omega, \qquad (7.61)$$

independent of temperature. For example, the sum rule m_1 also known as the f-sum rule in the case of local potentials, for which

$$[H, \rho_\mathbf{q}] = \mathbf{q} \cdot \mathbf{j}_\mathbf{q} \qquad (7.62)$$

where

$$\mathbf{j}_\mathbf{q} = \frac{1}{2m} \sum_{i=1}^N (\mathbf{p}_i e^{i\mathbf{q}\cdot\mathbf{r}_i} + e^{i\mathbf{q}\cdot\mathbf{r}_i} \mathbf{p}_i), \qquad (7.63)$$

takes the value

$$m_1 = \frac{N\mathbf{q}^2}{2m}. \qquad (7.64)$$

The result (7.64) holds for any q and at all temperatures, and does not depend on the model used to derive it. For example, the independent particle model which,

for small q and zero temperature, yields the result (7.6) for $S(\mathbf{q}, \omega)$, reproduces the f-sum rule:

$$m_1 = \int_0^{\frac{qk_F}{m}} \frac{m^2 V}{2\pi^2 q} \cdot \omega^2 d\omega = \frac{q^2 V}{2m} \cdot \frac{k_F^3}{3\pi^2} = \frac{q^2}{2m} \cdot V\rho = \frac{Nq^2}{2m} . \qquad (7.65)$$

Another important odd sum rule is the m_3 given by

$$m_3 = \frac{1}{2} \langle [[\rho_\mathbf{q}, H], [H, [H, \rho_{-\mathbf{q}}]]] \rangle . \qquad (7.66)$$

For local potentials, for which (7.62) holds, we see that the m_3 is determined by the double commutator of the Hamiltonian with the component of the current (7.63) parallel to $\mathbf{q}$.

Among the odd negative moments let us consider m_{-1}, which is related to the static polarizability $\chi(\mathbf{q}, 0)$ by the relation

$$m_{-1} = -\frac{1}{2}\chi(\mathbf{q}, 0) . \qquad (7.67)$$

In the $\mathbf{q} \to \mathbf{0}$ limit and for homogeneous systems, it is easy to show (Pines and Nozières 1966) that the static polarizability of neutral systems is related to the isothermal compressibility K of the system by the relation (compressibility sum rule)

$$\lim_{q\to 0} \chi(\mathbf{q}, 0) = -2 \lim_{q\to 0} \int_{-\infty}^{+\infty} S(\mathbf{q}, \omega) \frac{1}{\omega} d\omega = -N\rho K , \qquad (7.68)$$

where ρ is the density of the homogeneous system and the compressibility K is defined by

$$\frac{1}{K\rho} = \frac{\partial P}{\partial \rho} , \qquad (7.69)$$

and the pressure P can be obtained from the energy of the system

$$P = \rho^2 \frac{\partial(E/N)}{\partial \rho} . \qquad (7.70)$$

The isothermal compressibility can also be expressed through the isothermal sound velocity v as $(K\rho)^{-1} = mv^2$.

The even moments are more difficult to evaluate and, as we will see, their relation with $\text{Im}(\chi)$ depends explicitly on temperature. Let us consider, for example, the moment m_0 given by

$$m_0 = \int_{-\infty}^{+\infty} S(\mathbf{q}, \omega) d\omega = NS(\mathbf{q}) , \qquad (7.71)$$

where $S(\mathbf{q})$ is the static form factor:

$$S(\mathbf{q}) = \frac{1}{N} \sum_{k \neq n} p_k |\langle n|\rho_\mathbf{q}|k\rangle|^2$$

$$= \frac{1}{N} \left(\sum_{k,n} p_k |\langle n|\rho_\mathbf{q}|k\rangle|^2 - \sum_k p_k |\langle k|\rho_\mathbf{q}|k\rangle|^2 \right)$$

$$= \frac{1}{N} \left(\sum_{k,n} p_k \langle k|\rho_{-\mathbf{q}}|n\rangle\langle n|\rho_\mathbf{q}|k\rangle - \sum_k p_k |\langle k|\rho_\mathbf{q}|k\rangle|^2 \right)$$

$$= \frac{1}{N} (\langle \rho_{-\mathbf{q}}\rho_\mathbf{q}\rangle - |\langle \rho_\mathbf{q}\rangle|^2) , \tag{7.72}$$

which, as obvious from (7.72), is determined by the density fluctuations.

In the limit of zero temperature, $S(\mathbf{q})$ can be expressed through the ground state two-body density matrix as

$$S(\mathbf{q}) = 1 + \frac{1}{N} \int d\mathbf{r}_1 d\mathbf{r}_2 [\rho^{(2)}(\mathbf{r}_1, \mathbf{r}_2) - \rho^{(1)}(\mathbf{r}_1)\rho^{(1)}(\mathbf{r}_2)] e^{i\mathbf{q}\cdot(\mathbf{r}_1 - \mathbf{r}_2)} . \tag{7.73}$$

If the system is homogeneous, $\rho^{(2)}(\mathbf{r}_1, \mathbf{r}_2)$ can only depend on $r = |\mathbf{r}_1 - \mathbf{r}_2|$ due to translational invariance, and we have

$$\rho^{(2)}(\mathbf{r}_1, \mathbf{r}_2) = \rho^2 g(r) , \tag{7.74}$$

where

$$g(r) = \frac{1}{4} \sum_{\sigma,\sigma'} g_{\sigma,\sigma'}(r)$$

is the spin-averaged probability of finding two particles at relative distance r, while ρ is the one-body diagonal density which is a constant of the system. Therefore, we obtain

$$S(\mathbf{q}) = 1 + \rho \int d\mathbf{r}(g(r) - 1)e^{i\mathbf{q}\cdot\mathbf{r}} . \tag{7.75}$$

This formula allows us to derive $g(r)$ from $S(\mathbf{q})$ by taking the Fourier transform. Note that for large $\mathbf{q}$, $S(\mathbf{q}) \to 1$. In this limit, only incoherent processes are important, in which the particle is scattered by the individual constituents of the system, and only the $i = j$ term in the sum $\rho_{-\mathbf{q}}\rho_\mathbf{q} = \sum_{i,j} e^{i\mathbf{q}\cdot(\mathbf{r}_i - \mathbf{r}_j)}$ contributes to the static structure factor. In the same limit, the dynamic form factor can be written as

$$S(\mathbf{q}, \omega) = \int n(\mathbf{p})\delta \left(\omega - \left(\frac{q^2}{2m} - \frac{\mathbf{q}\cdot\mathbf{p}}{m} \right) \right) d\mathbf{p} , \tag{7.76}$$

and is entirely determined by the momentum distribution $n(\mathbf{p})$ of the system (P. Hohenberg and P. Platzman 1966). The situation is completely different at small $\mathbf{q}$, where coherent processes dominate.

By using the relation (7.52), together with the antisymmetry property of $\text{Im}(\chi)$ under the exchange of ω into $-\omega$ [see Eq. (7.51)], it is possible to put $S(\mathbf{q})$ in the following form

$$NS(\mathbf{q}) = \int_{-\infty}^{+\infty} S(\mathbf{q},\omega)d\omega = -\frac{1}{2\pi} \int_{-\infty}^{+\infty} \text{Im } \chi(\mathbf{q},\omega) \coth\frac{\beta\omega}{2} d\omega. \qquad (7.77)$$

When $\mathbf{q}$ is small, the integral in (7.77) is dominated by the region where $\omega \ll KT$ and it is possible to replace the cotangent by the reciprocal of its argument. Then, if we use the result of equation (7.68), we find

$$\lim_{q\to 0} S(\mathbf{q}) = \frac{\rho K}{\beta}, \qquad (7.78)$$

This shows that at low transferred momentum the density fluctuations have thermal origin. In any case, at very low temperature thermal fluctuations are quenched and the validity of (7.78) is limited to very low momenta.

7.6   The Current Response to an Electromagnetic Field

The current response to an electromagnetic field is the quantity that allows for the study of the conductivity and diamagnetic properties of an interacting charged many-body system.

Of particular interest is the transverse current response function defined by

$$\chi_\perp(\mathbf{q},\omega) = 2\sum_n \omega_{n0} \frac{|\langle n|j_{\mathbf{q},\perp}|0\rangle|^2}{(\omega + i\eta)^2 - \omega_{n0}^2}, \qquad (7.79)$$

where $j_{\mathbf{q}}$ is the current operator:

$$\mathbf{j_q} = \frac{1}{2m}\sum_{i=1}^{N}(\mathbf{p}_i e^{i\mathbf{q}\cdot\mathbf{r}_i} + e^{i\mathbf{q}\cdot\mathbf{r}_i}\mathbf{p}_i),$$

and $j_{\mathbf{q},\perp}$ is an arbitrary component of $\mathbf{j_q}$ perpendicular to $\mathbf{q}$. $\chi_\perp(\mathbf{q},\omega)$ is related (see, for example, Pines and Nozières 1966) to the transverse conductivity by

$$\sigma_\perp(\mathbf{q},\omega) = \frac{ie^2}{\omega}\left(\chi_\perp(\mathbf{q},\omega) + \frac{N}{m}\right), \qquad (7.80)$$

and its static part $\chi_\perp(\mathbf{q},0)$ is connected to the magnetic permeability μ_M by

$$\mu_M = \lim_{q\to 0} \frac{1}{1 + \frac{4\pi e^2}{c^2 q^2}(\chi_\perp(\mathbf{q},0) + \frac{N}{m})}. \qquad (7.81)$$

The corresponding diamagnetic susceptibility χ_D is then given by

$$\chi_D = \frac{\mu_M - 1}{4\pi} \, . \tag{7.82}$$

The longitudinal current response function, defined as

$$\chi_{\parallel}(\mathbf{q}, \omega) = \frac{2}{q^2} \sum_n \omega_{n0} \frac{|\langle n|\mathbf{q} \cdot \mathbf{j_q}|0\rangle|^2}{(\omega + i\eta)^2 - \omega_{n0}^2} \, , \tag{7.83}$$

can be related to the density response $\chi(\mathbf{q}, \omega)$ of the previous Section using the identity

$$\chi_{\parallel}(\mathbf{q}, \omega) + \frac{N}{m} = \frac{\omega^2}{q^2} \chi(\mathbf{q}, \omega) \, , \tag{7.84}$$

which immediately follows from equation (7.62) and (7.64). The result (7.84) expresses the gauge invariance of the theory. The relevant excited states in (7.83) involve single-pair, collective states (plasmons) and multi-pair excitations. On the other hand, plasmons do not contribute to the transverse current response function (7.79), since transverse excitations do not involve density changes which are at the origin of plasmons (see Section 8.4).

From equation (7.84) it follows that

$$\chi_{\parallel}(\mathbf{q}, 0) = -\frac{N}{m} \, . \tag{7.85}$$

This result is directly equivalent to the f-sum rule. In the opposite limit, $\mathbf{q} \equiv 0$ and $\omega \neq 0$, the longitudinal and transverse current responses coincide, and the relevant matrix elements entering their expressions are also the ones determining absorption of light on the system [see Eq. (7.34)] since the dipole operator $\mathbf{D} = \sum_i z_i$ is connected to the momentum operator by $[H, \mathbf{D}] = -(i/m)\mathbf{P}$, where $\mathbf{P} = \sum_i \mathbf{p}_i$. For translationally invariant systems for which the identity $[H, \mathbf{P}] = 0$ holds, one obtains

$$\chi_{\parallel}(0, \omega) = \chi_{\perp}(0, \omega) = 0 \, , \tag{7.86}$$

as follows immediately from equations (7.79), (7.83) and the result

$$\omega_{n0}\langle n|\mathbf{P}|0\rangle = \langle n|[H, \mathbf{P}]|0\rangle = 0 \, . \tag{7.87}$$

In the $q \equiv 0$ limit the conductivity is given by

$$\sigma(0, \omega) = \frac{iNe^2}{m\omega} \, , \tag{7.88}$$

and hence

$$\mathrm{Re}\,[\sigma(0, \omega)] = 0 \, . \tag{7.89}$$

The DC conductivity which is obtained from the real part of the conductivity by taking the $\mathbf{q} \to \mathbf{0}$ limit and subsequently the $\omega \to 0$ limit, is zero for translationally invariant systems. The homogeneous electron gas does not absorb any light. The possibility of nearly free-particle systems to absorb light and to conduct is due therefore to its imperfections or deviations from homogeneity.

In the general case (non-translationally invariant systems) one has

$$\text{Re}\,[\sigma(0,\omega)] = -e^2 \text{Im}\,\left[\frac{\chi(P_\alpha/m,\omega)}{\omega}\right] = \pi e^2 \frac{S(P_\alpha/m,\omega)}{\omega}\,, \qquad (7.90)$$

where $S(P_\alpha/m,\omega)$ is the strength of the operator P_α/m:

$$S(P_\alpha/m,\omega) = \sum_n |\langle n|P_\alpha/m|0\rangle|^2 \delta(\omega - \omega_{no})\,, \qquad (7.91)$$

and P_α/m is an arbitrary component of $\mathbf{P}/m$. It is straightforward to demonstrate that the conductivity (7.90) fulfills the sum rule:

$$\int \text{Re}\,[\sigma(0,\omega)]d\omega = \int \pi e^2 \frac{S(P_\alpha/m,\omega)}{\omega}d\omega = \frac{\pi e^2 N}{2m}\,. \qquad (7.92)$$

Using the formalism introduced in the previous two Sections, it is then easy to generalize result (7.90) to the case of finite temperature. The result is

$$\text{Re}\,[\sigma(0,\omega)] = \pi e^2 \frac{1}{\omega}[1 - e^{-\beta\omega}]S_T(P_\alpha/m,\omega)\,, \qquad (7.93)$$

where

$$S_T(P_\alpha/m,\omega) = \sum_{kn} p_k |\langle n|P_\alpha/m|k\rangle|^2 \delta(\omega - \omega_{nk})\,, \qquad (7.94)$$

and

$$p_k = e^{-\beta E_k}/Z, \qquad Z = \sum_k e^{-\beta E_k}\,.$$

For non-translationally invariant systems the Hamiltonian can be written as $H = H_0 + V$, where H_0 is the homogeneous electron gas part, while V is the potential which causes other forces besides electron–electron interactions. For example, V could be the sum of the interactions with the crystalline potential, with impurities of density operator $\rho_i(\mathbf{q})$, or with phonons. In this case one has

$$\left[H,\frac{P_\alpha}{m}\right] = \left[V,\frac{P_\alpha}{m}\right] = \frac{i}{m}\nabla_\alpha V = -\frac{i}{m}F_\alpha\,, \qquad (7.95)$$

where F_α is the force due to the potential V. By using the result

$$\langle n|[H,\frac{P_\alpha}{m}]|0\rangle = \omega_{n0}\langle n|\frac{P_\alpha}{m}|0\rangle = -\frac{i}{m}\langle n|F_\alpha|0\rangle\,, \qquad (7.96)$$

equation (7.90) yields the following expression for conductivity

$$\text{Re}\,[\sigma(0,\omega)] = \frac{\pi e^2}{m^2 \omega^3} S(F_\alpha, \omega)\,, \tag{7.97}$$

where

$$S(F_\alpha, \omega) = -\frac{1}{\pi}\text{Im}\,[\chi(F_\alpha, \omega)] = \sum_n |\langle n|F_\alpha|0\rangle|^2 \delta(\omega - \omega_{no})\,. \tag{7.98}$$

Equations (7.97) and (7.98) are easily generalized to the case of finite temperature and serve as another possible starting point for the evaluation of the conductivity. Applications of these formulae for several different kinds of potentials V can be found in the book by Mahan (1981).

We now discuss the diamagnetic properties of a many-body system. These are obtained from the transverse current response (7.79) by taking at first $\omega = 0$ and then the $\mathbf{q} \to 0$ limit.

In a homogeneous system, the main contribution to the static transverse current response, in the $\mathbf{q} \to 0$ limit comes from single-pair excitations (the longitudinal plasmon mode does not contribute for reasons of symmetry, while multi-pair excitations are negligible in the long wavelength limit). The static response is given by

$$\chi_\perp(\mathbf{q}, 0) = -\frac{2}{m^2} \sum_p \frac{n_\mathbf{p}(1 - n_{\mathbf{p+q}})(\mathbf{p} \cdot n_\perp)^2}{\omega_{\mathbf{pq}}}\,, \tag{7.99}$$

where $n_\mathbf{p}$ is the Fermi distribution (1.73), $\omega_{\mathbf{pq}}$ is the excitation energy (1.93) and $n_\perp$ is a unit vector perpendicular to $\mathbf{q}$. It is easy to show, by a suitable interchange of indices that Pauli exclusion principle plays no role in the summation over p in (7.99). We then obtain

$$\chi_\perp(\mathbf{q}, 0) = -\frac{2}{m} \sum_{p \leq p_F} \frac{(\mathbf{p} \cdot n_\perp)^2}{\mathbf{p} \cdot \mathbf{q} + q^2/2}\,. \tag{7.100}$$

Replacing the sum with an integral and carrying out the angular integrations, one gets

$$\chi_\perp(\mathbf{q}, 0) = -\frac{N}{2m} + \frac{1}{2\pi^2 mq} \int_0^{p_F} dp\, p\, (p^2 - q^2/4) \ln\left(\frac{p - q/2}{p + q/2}\right)\,. \tag{7.101}$$

Expanding the logarithm in powers of $q/2p$ one finally obtains

$$\lim_{q \to 0} \chi_\perp(\mathbf{q}, 0) = -\frac{N}{m} + \frac{N}{m}\frac{q^2}{4p_F^2}\,, \tag{7.102}$$

where the term of order q^2 is responsible for the weak diamagnetism first calculated by Landau. The magnetic permeability is then given by

$$\mu_M = \frac{1}{1 + N\pi e^2/mc^2 p_F^2},$$ (7.103)

and the corresponding diamagnetic susceptibility is given by

$$\chi_D = \frac{\mu_M - 1}{4\pi} \simeq -\frac{Ne^2}{4mc^2 p_F^2} = -\frac{1}{3}\chi_P,$$ (7.104)

where χ_P is the paramagnetic spin susceptibility for the non-interacting electron gas ($\chi_P = -\mu_0\chi_\sigma$ of Chapter 1).

In a finite size many particle system, the static transverse current response can be calculated exactly at order q^2 for the many-body Hamiltonian (1.1). In order to reach the goal, it is convenient to write $j_{\mathbf{q},\perp}$ as

$$j_{\mathbf{q},\perp} = \frac{i}{2}\left([H, O] - \frac{q}{m}Q\right),$$ (7.105)

where

$$O = \sum_{i=1}^{N}(x_i e^{iqy_i} + e^{iqy_i} x_i),$$

and

$$Q = \sum_{i=1}^{N}(x_i p_i^y e^{iqy_i} + e^{iqy_i} x_i p_i^y).$$

Using the result of (7.105) one can write

$$\chi_\perp(\mathbf{q}, 0) = -2\sum_n \frac{|\langle n|j_{\mathbf{q},\perp}|0\rangle|^2}{\omega_{n0}}$$

$$= -\frac{1}{2}\sum_n \omega_{n0}|\langle n|O|0\rangle|^2$$

$$+ \frac{q}{2m}\langle 0|Q^\dagger O + O^\dagger Q|0\rangle - \frac{q^2}{2m^2}\sum_n \frac{|\langle n|Q|0\rangle|^2}{\omega_{n0}}.$$ (7.106)

This expression, truncated at order q^2, gives

$$\chi_\perp(\mathbf{q}, 0) = -\frac{N}{m} + \frac{Nq^2}{4m}\langle x^2 + y^2\rangle - \frac{q^2}{2m^2}\sum_n \frac{|\langle n|L_z|0\rangle|^2}{\omega_{n0}},$$ (7.107)

where

$$N\langle x^2 + y^2\rangle = \langle 0|\sum_i (x_i^2 + y_i^2)|0\rangle$$

and L_z is the z-component of the angular momentum. Using the results

$$\Theta = 2 \sum_n \frac{|\langle n|L_z|0\rangle|^2}{\omega_{n0}}$$

and

$$\Theta_{rig} = mN\langle x^2 + y^2 \rangle,$$

where Θ is the moment of inertia of the system (see Section 10.1.4) and Θ_{rig} the rigid value of Θ one gets for the magnetic permeability:

$$\mu_M = \frac{1}{1 + \frac{\pi e^2}{m^2 c^2}(\Theta_{rig} - \Theta)}, \tag{7.108}$$

and for the diamagnetic susceptibility:

$$\chi_D = \frac{\mu_M - 1}{4\pi} \simeq -\frac{e^2}{4m^2 c^2}\Theta_{rig}\left(1 - \frac{\Theta}{\Theta_{rig}}\right). \tag{7.109}$$

In the case of spherical systems $\Theta = 0$, since the eigenstates of the Hamiltonian are also the eigenstates of the angular momentum, hence χ_D takes the usual value

$$\chi_D = -\frac{e^2}{4mc^2}N\langle x^2 + y^2 \rangle.$$

However for deformed systems, Θ is different from zero and may give a large contribution to the diamagnetic susceptibility.

7.7 The Density Response for Non-Interacting Homogeneous Systems

The density response in the case of homogeneous non-interacting systems (both Bosons and Fermions) can be computed analytically. Though the contribution of the interaction is essential for the correct calculation of the density response, and especially so at low $\mathbf{q}$, it is important to know the free response because it is an essential ingredient in theories which take interaction into account. At zero temperature, the free response function [hereafter indicated as $\chi_0(\mathbf{q}, \omega)$] is given by the following expression

$$\chi_0(\mathbf{q}, \omega) = \sum_{mi} 2\epsilon_{mi} \frac{|\langle mi^{-1}|\rho_{\mathbf{q}}|0\rangle|^2}{(\omega + i\eta)^2 - \epsilon_{mi}^2}. \tag{7.110}$$

where the summation runs over all one-particle–one-hole states.

In the case of Bosons, and using the result (7.8), the calculation of the matrix element of the density operator in (7.110) leads immediately to the following result

$$\chi_0^B(\mathbf{q}, \omega) = \frac{\frac{q^2}{m} \cdot N}{(\omega + i\eta)^2 - (\frac{q^2}{2m})^2},$$ (7.111)

from which it is seen that $\chi_0^B(\mathbf{q}, \omega)$ has only one pole at energy $q^2/2m$. From equation (7.111), we can very easily obtain the result (7.9), which holds for positive ω. Then, by taking the limit $\omega \to \infty$, we have

$$\lim_{\omega \to \infty} \chi_0^B(\mathbf{q}, \omega) = \frac{Nq^2}{m\omega^2} \left(1 + \frac{1}{\omega^2} \left(\frac{q^2}{2m} \right)^2 + \cdots \right)$$ (7.112)

and so the correct value for the m_1 sum rule is $m_1 = Nq^2/2m$, and for m_3 the prediction is $m_3 = m_1(q^2/2m)^2$. The latter reflects the fact that in the ideal Boson gas there is only one excited state at energy $q^2/2m$.

Moreover, from equation (7.111) it follows that for $\mathbf{q} \to 0$ the static response diverges as $1/q^2$, a result that is due to the infinite compressibility of an ideal Boson gas.

The Fermion case is somewhat more complex, because in the Fermi gas there is a continuum of one-particle–one-hole excited states, with excitation energies given by

$$\omega_{mi} = \epsilon_m - \epsilon_i = \frac{(\mathbf{p} + \mathbf{q})^2}{2m} - \frac{\mathbf{p}^2}{2m}.$$ (7.113)

Using the results of Section 1.8.1, it is possible to write the free response function of Fermions as:

$$\chi_0^F(\mathbf{q}, \omega) = 2 \sum_{\substack{p < k_F \\ |\mathbf{p}+\mathbf{q}| > k_F}} \frac{\frac{2\mathbf{p}\cdot\mathbf{q}}{m} + \frac{q^2}{m}}{\omega^2 - (\frac{\mathbf{p}\cdot\mathbf{q}}{m} + \frac{q^2}{2m})^2},$$ (7.114)

where the factor 2 takes into account the sum over the spin index. Therefore, the calculation of the response function is reduced to an integration over the region of momentum space such that $p < k_F$ and $|\mathbf{p} + \mathbf{q}| > k_F$, out of which one-particle–one-hole pairs with total momentum $\mathbf{q}$ may be excited. This region depends on the dimensionality of the system. It is a portion of a sphere in $3D$, of the Fermi circle in $2D$, and of the Fermi segment in $1D$. The free response function of Fermions is known as the Lindhard function.

Introducing the distributions (1.73), equation (7.114) can be rewritten as

$$\chi_0^F(\mathbf{q}, \omega) = 2L^D \int \frac{d\mathbf{p}}{(2\pi)^D} n_{\mathbf{p}} (1 - n_{\mathbf{p}+\mathbf{q}}) \frac{\frac{2\mathbf{p}\cdot\mathbf{q}}{m} + \frac{q^2}{m}}{\omega^2 - (\frac{\mathbf{p}\cdot\mathbf{q}}{m} + \frac{q^2}{2m})^2}.$$ (7.115)

By means of the change of variable $\mathbf{p'} = -\mathbf{p} - \mathbf{q}$, it is easy to show that the second integral in (7.115):

$$I_2 = \int \frac{d\mathbf{p}}{(2\pi)^D} n_\mathbf{p} n_{\mathbf{p}+\mathbf{q}} \frac{\frac{2\mathbf{p}\cdot\mathbf{q}}{m} + \frac{q^2}{m}}{\omega^2 - (\frac{\mathbf{p}\cdot\mathbf{q}}{m} + \frac{q^2}{2m})^2}$$

vanishes because $I_2 = -I_2$. Therefore, we are left with the calculation of

$$\chi_0^F(\mathbf{q}, \omega) = 2L^D \int \frac{d\mathbf{p}}{(2\pi)^D} n_\mathbf{p} \frac{\frac{2\mathbf{p}\cdot\mathbf{q}}{m} + \frac{q^2}{m}}{\omega^2 - (\frac{\mathbf{p}\cdot\mathbf{q}}{m} + \frac{q^2}{2m})^2}$$

$$= 2L^D \int \frac{d\mathbf{p}}{(2\pi)^D} n_\mathbf{p} \left(\frac{1}{\omega - (\frac{\mathbf{p}\cdot\mathbf{q}}{m} + \frac{q^2}{2m})} - \frac{1}{\omega + (\frac{\mathbf{p}\cdot\mathbf{q}}{m} + \frac{q^2}{2m})} \right). \quad (7.116)$$

In the one-dimensional case, taken as an example, we have

$$\chi_0^{1D}(\mathbf{q}, \omega) = \frac{L}{\pi} \cdot \int_{-k_F}^{k_F} dp \left[\frac{1}{\omega - (\frac{pq}{m} + \frac{q^2}{2m})} - \frac{1}{\omega + (\frac{pq}{m} + \frac{q^2}{2m})} \right]$$

so that

$$\chi_0^{1D}(\mathbf{q}, \omega) = \frac{L}{\pi} \cdot \left[-\frac{m}{q} \ln \left(\omega - \frac{pq}{m} - \frac{q^2}{2m} \right) - \frac{m}{q} \ln \left(\omega + \frac{pq}{m} + \frac{q^2}{2m} \right) \right]_{-k_F}^{k_F}$$

$$= -\frac{m}{q} \frac{L}{\pi} \left[\ln \left(\frac{\omega - \frac{k_F q}{m} - \frac{q^2}{2m}}{\omega + \frac{k_F q}{m} - \frac{q^2}{2m}} \right) + \ln \left(\frac{\omega + \frac{k_F q}{m} + \frac{q^2}{2m}}{\omega - \frac{k_F q}{m} + \frac{q^2}{2m}} \right) \right]$$

$$= -\frac{m}{q} \frac{L}{\pi} \ln \left[\frac{\omega^2 - (\frac{k_F q}{m} + \frac{q^2}{2m})^2}{\omega^2 - (\frac{k_F q}{m} - \frac{q^2}{2m})^2} \right]. \quad (7.117)$$

Note that for $\mathbf{q}$ fixed and smaller than $2k_F$, we find that $\chi_0^{1D}(\mathbf{q}, \omega)$ has a finite negative value for $\omega = 0$. This free respond function has a continuum of poles which correspond to the continuum of single-particle excited states (see also Section 1.8.1) in the range

$$\frac{k_F q}{m} - \frac{q^2}{2m} \leq \omega \leq \frac{k_F q}{m} + \frac{q^2}{2m},$$

and it tends to zero starting from positive ω when ω tends to infinity. If q is small, the region of the poles gets narrower and the one-dimensional Fermi gas resembles a Boson gas, because in the $q \to 0$ limit the continuum of excited states tends to only one single-particle excited state at energy $\omega = k_F q/m$ (see Fig. 7.3).
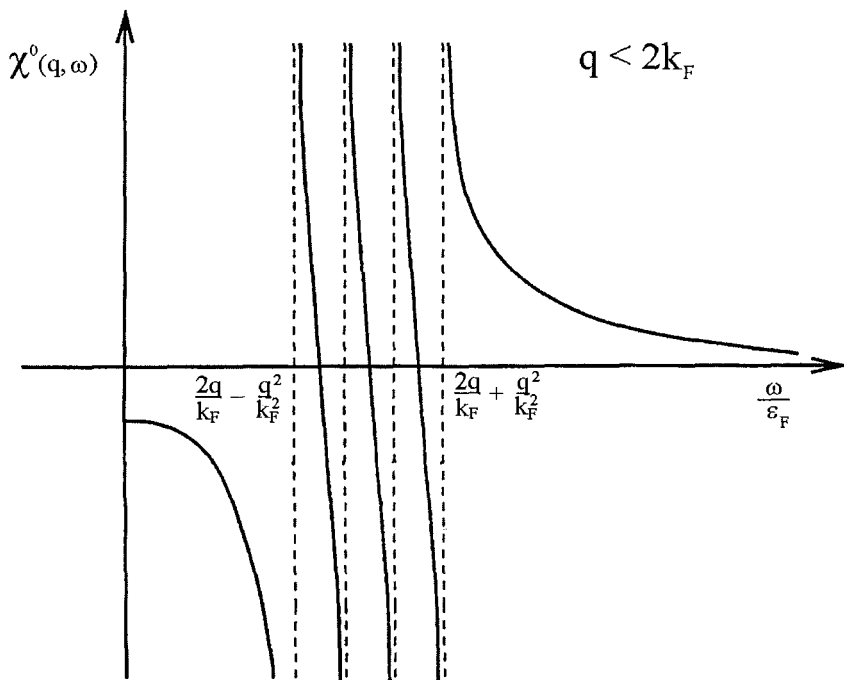
Fig. 7.3   Free response function of the one-dimensional Fermi gas, at fixed q.

From equation (7.117), the following result is obtained for the static polarizability of the one-dimensional Fermi gas:

$$\frac{\chi_0^{1D}(\mathbf{q},0)}{L} = -\frac{2m}{q\pi}\ln\left(\frac{\frac{k_F q}{m} + \frac{q^2}{2m}}{\frac{k_F q}{m} - \frac{q^2}{2m}}\right)$$

$$= -\frac{2m}{q\pi}\ln\left(\frac{1 + \frac{q}{2k_F}}{1 - \frac{q}{2k_F}}\right)$$

$$= -\frac{2m}{q\pi}\left[\ln\left(1 + \frac{q}{2k_F}\right) - \ln\left(1 - \frac{q}{2k_F}\right)\right], \qquad (7.118)$$

and thus

$$\lim_{q\to 0}\frac{\chi_0^{1D}(\mathbf{q},0)}{N} = -\frac{2m}{q\pi\rho}\left[\frac{q}{2k_F} + \frac{q}{2k_F}\right] = -\rho\frac{4m}{\pi^2\rho^3}, \qquad (7.119)$$

from which we derive the value $K = 4m/\pi^2\rho^3$ for the system compressibility. This value coincides with the one that can be obtained starting from the expression for the energy of the free one-dimensional gas given in (1.76), using relation (1.79).

For homogeneous systems in two and three dimensions, the free response functions in terms of the following dimensionless quantities:

$$\hat{q} = \frac{q}{k_F}, \qquad \hat{\omega} = \frac{m\omega}{k_F^2}, \qquad \hat{\chi}_0(\hat{q},\hat{\omega}) = \frac{1}{\nu_0}\chi_0(q,\omega), \qquad (7.120)$$

where ν_0 are the densities of states at the Fermi surface, which in turn are given by

$$\nu_0 = \begin{cases} L^3 \dfrac{mk_F}{\pi^2} & \text{for } D = 3 \\[2mm] L^2 \dfrac{m}{\pi} & \text{for } D = 2 \\[2mm] L \dfrac{2m}{\pi k_F} & \text{for } D = 1 \end{cases}, \qquad (7.121)$$

turn out to have the form ($\omega = \omega_1 + i\omega_2$)

$$\hat{\chi}_{3D}^0(\hat{q},\hat{\omega})$$

$$= \frac{1}{4\hat{q}}\left[\left(\frac{1-a^2+c^2}{2} - iac\right)\ln\frac{(1+a)^2+c^2}{(1-a)^2+c^2}\right.$$

$$- \left(\frac{1-b^2+c^2}{2} - ibc\right)\ln\frac{(1+b)^2+c^2}{(1-b)^2+c^2}$$

$$+ (-2ac - i(1+c^2-a^2))\left(\tan^{-1}\frac{1+a}{c} + \tan^{-1}\frac{1-a}{c}\right)$$

$$\left. + (2bc + i(1+c^2-b^2))\left(\tan^{-1}\frac{1+b}{c} + \tan^{-1}\frac{1-b}{c}\right) - 4b\right] \quad \text{(in } 3D) \quad (7.122)$$

where

$$a = \hat{\omega}_1/\hat{q} - \hat{q}/2, \, b = \hat{\omega}_1/\hat{q} + \hat{q}/2, \, c = \hat{\omega}_2/\hat{q},$$

and

$$\hat{\chi}_{2D}^0(\hat{q},\hat{\omega}) = -1 - \frac{\sqrt{(a+ic)^2 - 1} - \sqrt{(b+ic)^2 - 1}}{\hat{q}} \qquad \text{(in } 2D) \quad (7.123)$$

where the square root is defined by the choice of the cut in the upper semi-plane. Finally, the one-dimensional response (7.117) in terms of dimensionless quantities, is written as

$$\hat{\chi}_{1D}^0(\hat{q},\hat{\omega}) = \frac{1}{2\hat{q}}\ln\left[\frac{\hat{\omega}^2 - (\hat{q} - \hat{q}^2/2)^2}{\hat{\omega}^2 - (\hat{q} + \hat{q}^2/2)^2}\right].$$

The behavior of the free response functions in $2D$ and $3D$, as a function of ω_1, is analogous to the one-dimensional case. The only difference is in the range of the continuum of poles, which for $q \leq 2k_F$ is limited between 0 and $k_F q/m + q^2/2m$. The linear response function in the $3D$ case is schematically shown in Fig. 7.4. The
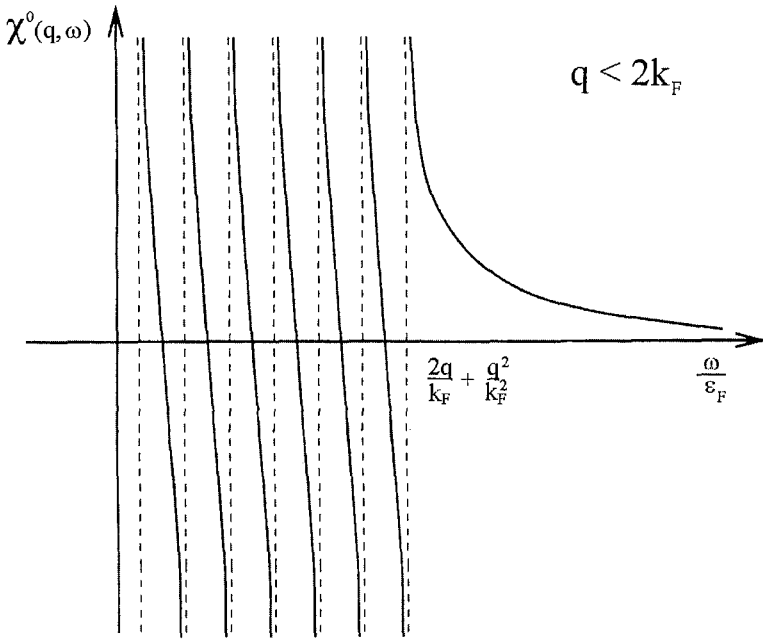
Fig. 7.4   Free response function for the three-dimensional Fermi gas, at fixed q.

one suitable for the $2D$ case is absolutely similar. The generalization of the Lindhard response function to finite temperature, is discussed by Khanna and Glyde (1976). Finally, note that in the case of nuclear matter, in the computation of the above quantities one should take into account the isospin degeneracy, which has the effect that many of such quantities should be multiplied by two.

References to Chapter 7

A. Von Felde, A. Sprosser-Prou and J. Fink, Phys. Rev. B **40**, 10181 (1989).

R.J. Donnelly, J.A. Donnelly and R.N. Hills, J. Low Temp. Phys. **44**, 471 (1981).

R. Kubo, Can. J. Phys. **34**, 1274 (1956); J. Phys. Soc. Japan, **12**, 570 (1957).

D. Pines and P. Nozières, The Theory of Quantum Liquids (Benjamin, New York 1966).

R. Leonardi and M. Rosa-Clot, Riv. Nuovo Cimento **1**, 1 (1971).

O. Bohigas, A.M. Lane and J. Martorell, Phys. Rep. **51**, 267 (1979).

E. Lipparini and S. Stringari, Phys. Rep. **175**, 103 (1989).

G. Orlandini and M. Traini, Rep. Prog. Phys. **54**, 257 (1991).

P. Hohenberg and P. Platzman, Phys. Rev. **152**, 198 (1966).

G.D. Mahan, "Many Particle Physics" (Plenum Press, New York and London 1981).

F.C. Khanna and H.R. Glyde, Can. J. Phys. **54**, 648 (1976).

This page is intentionally left blank

Chapter 8

The Linear Response Function in Different Models

8.1   The Linear Response Function in Landau Theory

In this Section we will discuss the linear response of a homogeneous Fermi liquid to an external field which oscillates at a given frequency and wavelength (Pines and Nozières 1966). In the limit where the wavevector q and energy ω related to the excitation fulfill the conditions $qv_f, \omega \ll \epsilon_F$, which guarantee that only $1p - 1h$ excitations contribute to the dynamic response, the system response is correctly described by the Landau theory of normal Fermi liquids. This theory allowed Landau to predict the existence of the "zero sound" in liquid ^{3}He, before its experimental observation. The propagation of zero sound, unlike that of normal (first) sound which takes place in hydrodynamic regime (see Section 1.9), is related to a collisionless (elastic) regime, and is produced by the mean self-consistent field.

In the presence of an external perturbation, which interacts with the system through an interaction potential H_{int} of the form of equation (7.10) with

$$G^{s,a} = \rho_{\mathbf{q}}^{s,a} = \sum_{j=1}^{N_\uparrow} e^{-i\mathbf{q}\cdot\mathbf{r}_j} \pm \sum_{j=1}^{N_\downarrow} e^{-i\mathbf{q}\cdot\mathbf{r}_j}, \tag{8.1}$$

it is necessary to add to the Landau equations (1.119) an external-field term describing the flow of particles in phase space; this flow is induced by the force $\mathcal{F}$ corresponding to H_{int}, that is

$$\mathcal{F}^{s,a} = -i\lambda\mathbf{q}(\rho_{\mathbf{q}}^{s,a})^* e^{-i\omega t} + c.c. \tag{8.2}$$

The external-field term, corresponding to the force $\mathcal{F}$, has the form (see Section 1.9):

$$\mathcal{F}^{s,a} \cdot \mathbf{v_k} \frac{\partial n_{\mathbf{k}}^0}{\partial \epsilon_{\mathbf{k}}}. \tag{8.3}$$

In the above equations, the suffixes s, a indicate the symmetric and antisymmetric parts, respectively, of the densities and of the external forces [in Eq. (8.1), the $+$ sign corresponds to G^s, and the $-$ sign corresponds to G^a], and the term (8.3) should

be added in its symmetric (antisymmetric) part to the Landau equation for the symmetric (antisymmetric) distribution function. Moreover, for simplicity, in the following we will assume that the system has zero initial spin, so that the density and spin-density response functions are uncoupled. The effects due to coupling of the two responses will be discussed in one of the forthcoming Sections. Therefore, in the absence of the collision term (elastic regime), the Landau equations under external field become

$$\frac{\partial}{\partial t}\delta n_{\mathbf{k}}^{s,a}(\mathbf{r},t) + \mathbf{v}_{\mathbf{k}} \cdot \nabla_{\mathbf{r}}\delta n_{\mathbf{k}}^{s,a}(\mathbf{r},t)$$

$$-\nabla_{\mathbf{k}}n_{\mathbf{k}}^0 \cdot \sum_{\mathbf{k}'} f_{\mathbf{k},\mathbf{k}'}^{s,a} \nabla_{\mathbf{r}}\delta n_{\mathbf{k}'}^{s,a}(\mathbf{r},t) + \mathcal{F}^{s,a} \cdot \mathbf{v}_{\mathbf{k}}\frac{\partial n_{\mathbf{k}}^0}{\partial \epsilon_{\mathbf{k}}} = 0. \qquad (8.4)$$

The external field in (8.4) induces oscillations of the distribution function, which may be written as

$$\delta n_{\mathbf{k}}^{s,a}(\mathbf{r},t) = \delta n_{\mathbf{k}}^{s,a}(\mathbf{q},\omega)e^{i\mathbf{q}\cdot\mathbf{r}}e^{-i\omega t} + c.c. \qquad (8.5)$$

Next, the linear response function is obtained by evaluating the density fluctuations:

$$\langle \rho_{\mathbf{q}}^{s,a} \rangle = \frac{1}{V}\int \rho^{s,a}(\mathbf{r},t)e^{-i\mathbf{q}\cdot\mathbf{r}}d\mathbf{r}$$

$$= \frac{1}{(2\pi)^3}\int d\mathbf{k}\delta n^{s,a}(\mathbf{r},t)e^{-i\mathbf{q}\cdot\mathbf{r}}d\mathbf{r}$$

$$= \sum_{\mathbf{k}}\delta n_{\mathbf{k}}^{s,a}(\mathbf{q},\omega)e^{-i\omega t}. \qquad (8.6)$$

Using equations (7.13) and (8.6), we finally obtain the response functions:

$$\chi^s(q,\omega) = \chi(\rho_{\mathbf{q}}^s,\rho_{\mathbf{q}}^s,\omega) = \frac{1}{\lambda}\sum_{\mathbf{k}}\delta n_{\mathbf{k}}^s(\mathbf{q},\omega),$$

$$\chi^a(q,\omega) = \chi(\rho_{\mathbf{q}}^a,\rho_{\mathbf{q}}^a,\omega) = \frac{1}{\lambda}\sum_{\mathbf{k}}\delta n_{\mathbf{k}}^a(\mathbf{q},\omega). \qquad (8.7)$$

It is convenient to put the quantity $\delta n_{\mathbf{k}}^{s,a}(\mathbf{q},\omega)$ in the form

$$\delta n_{\mathbf{k}}^{s,a}(\mathbf{q},\omega) = \delta(\epsilon_k - \epsilon_F)v_F u_{\mathbf{k}}(\mathbf{q},\omega),$$

where $u_{\mathbf{k}}$ is the normal displacement of the Fermi surface at point $\mathbf{k}$, [see also Eq. (1.132)], $v_F = k_F/m^*$ is the Fermi velocity, and ϵ_F is the Fermi energy. The equation for $u_{\mathbf{k}}$ is attained by substituting (8.5) into (8.4):

$$(\mathbf{q}\cdot\mathbf{v}_{\mathbf{k}} - \omega)u_{\mathbf{k}}^{s,a} + \mathbf{q}\cdot\mathbf{v}_{\mathbf{k}}\sum_{\mathbf{k}'} f_{\mathbf{k},\mathbf{k}'}^{s,a}\delta(\epsilon_{k'} - \epsilon_F)u_{\mathbf{k}'}^{s,a} + \lambda\frac{\mathbf{q}\cdot\mathbf{v}_{\mathbf{k}}}{v_F} = 0, \qquad (8.8)$$

where we have used (1.129). By taking, without the loss of generality, $\mathbf{q}$ parallel to the z-axis of momentum space, where the directions of $\mathbf{k}$ and $\mathbf{k}'$ are identified by

the (θ, ϕ) and (θ', ϕ') angles, respectively, equation (8.8) may be rewritten as

$$qv_F(\cos\theta - s)u^{s,a}(\theta, \phi)$$

$$+ qv_F \cos\theta \nu(0) \int \frac{d\Omega'_{\mathbf{k}'}}{4\pi} f^{s,a}(k\hat{k}')u^{s,a}(\theta', \phi') + \lambda q \cos\theta = 0\,, \qquad (8.9)$$

where $\nu(0)$ is the density of states at the Fermi surface (1.123) and $s = \omega/qv_F$. (Note that in the case of nuclear matter $\nu(0) = 2Vm^*k_F/\pi^2$ due to isospin degeneracy.) In what follows, we will look for solutions of (8.9) in the form

$$u^{s,a}(\theta, \phi) = \sum_{l,m} u^{s,a}_{l,m} Y_{l,m}(\cos\theta)\,.$$

If we use expansion (1.121) for the interaction, we see that equations (8.9) are equations in which m is conserved, i.e. the nature of the solutions is determined by m, and not by l, which is mixed. The solutions with $m = 0$ are solutions in which the density is changed ($\int d\Omega u(\theta, \phi) \neq 0$), and give rise to propagation of longitudinal waves. Those with $m \neq 0$ do not cause a density change and are responsible for transverse waves ($m = 1$), quadrupolar waves ($m = 2$), etc. In what follows we will consider the longitudinal case ($m = 0$), which is the only one that involves density fluctuations and, thus, represents the high-frequency counterpart of ordinary sound. For the longitudinal mode, the following expansion holds

$$u^{s,a}(\theta, \phi) = \sum_l u^{s,a}_l P_l(\cos\theta)\,, \qquad (8.10)$$

where

$$u^{s,a}_l \equiv u^{s,a}_{l,0}\sqrt{\frac{2l+1}{4\pi}}\,.$$

Then we obtain

$$(\cos\theta - s)\sum_l u^{s,a}_l P_l(\cos\theta) + \cos\theta \sum_{l'} \frac{u^{s,a}_{l'}}{2l'+1} P_{l'}(\cos\theta)F^{s,a}_{l'} + \lambda\frac{\cos\theta}{v_F} = 0\,, \qquad (8.11)$$

where we have used (1.122), $P_l(\cos k\hat{k}') = P_l(\cos\theta)P_l(\cos\theta')$ and

$$\int_{-1}^{1} P_l(\cos\theta)P_{l'}(\cos\theta)d\cos\theta = \frac{2}{2l+1}\delta_{l,l'}\,.$$

Furthermore, from equation (8.11) we have

$$\frac{u^{s,a}_l}{2l+1} + \sum_{l'}\Omega_{l,l'}F^{s,a}_{l'}\frac{u^{s,a}_{l'}}{2l'+1} = -\frac{\lambda}{v_F}\Omega_{l,0}\,, \qquad (8.12)$$

with

$$\Omega_{l,l'} = \Omega_{l',l} = \frac{1}{2}\int_{-1}^{1} dx P_l(x)\frac{x}{x-s}P_{l'}(x)\,, \qquad (8.13)$$

from which we obtain

$$\Omega_{0,0} = 1 + \frac{s}{2}\ln\frac{s-1}{s+1} = 1 + \frac{s}{2}\ln\left|\frac{s-1}{s+1}\right| + i\frac{\pi}{2}s\Theta(1-s),$$

$$\Omega_{l,1} = s\Omega_{l,0} + \frac{1}{3}\delta_{l,1},$$

$$\Omega_{2,0} = \frac{1}{2} + \frac{3s^2-1}{2}\Omega_{0,0},$$
(8.14)

$$\Omega_{2,2} = \frac{1}{5} + \frac{3s^2-1}{2}\Omega_{2,0}.$$

In what follows we will use the following limits:

$$\Omega_{0,0}|_{s\to\infty} = -\frac{1}{3s^2} - \frac{1}{5s^4} - \frac{1}{7s^6} + \cdots,$$
(8.15)

$$\Omega_{0,0}|_{s\to1+} = 1 + \frac{1}{2}\ln\frac{s-1}{2} + \cdots.$$

From equation (8.7), we then obtain the response function

$$\chi^{s,a}(q,\omega) = \frac{1}{\lambda}v_F\nu(0)\frac{1}{4\pi}\int u^{s,a}(\theta,\phi)d\Omega = \frac{1}{\lambda}v_F\nu(0)u_0^{s,a}.$$
(8.16)

In order to derive $u_0^{s,a}$ from equations (8.11) and (8.12), taking into account the three first Landau parameters (F_0, F_1, F_2), it is convenient to proceed in the following way. From equation (8.11), taking $\frac{1}{2}\int_{-1}^{1}d\cos\theta$, we obtain the relation

$$su_0^{s,a} = \frac{1}{3}\left(1 + \frac{1}{3}F_1^{s,a}\right)u_1^{s,a},$$
(8.17)

which represents quasiparticle number conservation. Then, taking

$$\frac{1}{2}\int_{-1}^{1}\cos\theta\,d\cos\theta$$

we obtain the relation

$$su_1^{s,a} - (1 + F_0^{s,a})u_0^{s,a} - \frac{2}{5}\left(1 + \frac{1}{5}F_2^{s,a}\right)u_2^{s,a} = \frac{\lambda}{v_F},$$
(8.18)

which expresses quasiparticle current conservation. Eliminating $u_1^{s,a}$ from the two above equations, we find

$$\left[s^2 - \frac{1}{3}\left(1 + \frac{1}{3}F_1^{s,a}\right)(1 + F_0^{s,a})\right]u_0^{s,a} - \frac{2}{15}\left(1 + \frac{1}{3}F_1^{s,a}\right)\left(1 + \frac{1}{5}F_2^{s,a}\right)u_2^{s,a}$$

$$= \frac{1}{3}\left(1 + \frac{1}{3}F_1^{s,a}\right)\frac{\lambda}{v_F}.$$
(8.19)

From equation (8.12), taking $l = 0$ we have the relation

$$u_0^{s,a} + \Omega_{0,0}F_0^{s,a}u_0^{s,a} + \Omega_{0,1}F_1^{s,a}\frac{u_1^{s,a}}{3} + \Omega_{0,2}F_2^{s,a}\frac{u_2^{s,a}}{5} = -\frac{\lambda}{v_F}\Omega_{0,0}, \qquad (8.20)$$

and taking $l = 2$ we have

$$\frac{u_2^{s,a}}{5} + \Omega_{2,0}F_0^{s,a}u_0^{s,a} + \Omega_{2,1}F_1^{s,a}\frac{u_1^{s,a}}{3} + \Omega_{2,2}F_2^{s,a}\frac{u_2^{s,a}}{5} = -\frac{\lambda}{v_F}\Omega_{2,0}. \qquad (8.21)$$

By dividing these two relations side by side, and using the identities $\Omega_{0,1} = s\Omega_{0,0}$ and $\Omega_{2,1} = s\Omega_{2,0}$, we finally obtain the relation

$$\frac{u_2^{s,a}}{5} = \frac{\Omega_{2,0}u_0^{s,a}}{\Omega_{0,0} + F_2^{s,a}(\Omega_{2,2}\Omega_{0,0} - \Omega_{2,0}^2)}. \qquad (8.22)$$

From equations (8.19) and (8.22) we arrive at the desired equation for $u_0^{s,a}$ and, thus, to the dynamic polarizabilities, we have

$$\chi^{s,a}(q,\omega) = \frac{\frac{1}{3}\nu(0)(1 + \frac{F_1^{s,a}}{3})}{s^2 - \frac{1}{3}(1 + \frac{F_1^{s,a}}{3})(1 + F_0^{s,a}) - \frac{2}{3}\frac{(1 + \frac{1}{3}F_1^{s,a})(1 + \frac{1}{5}F_2^{s,a})\Omega_{2,0}}{\Omega_{0,0} + F_2^{s,a}(\Omega_{2,2}\Omega_{0,0} - \Omega_{2,0}^2)}}. \qquad (8.23)$$

From equation (8.23), taking the $\omega \to 0$ and $\omega \to \infty$ limits [see Eqs. (7.28) and (7.29)], and taking account of equations (8.14) and (8.15), it is possible to derive the following analytic expressions for the sum rules:

$$m_{-1}^{s,a} = \frac{N}{2}\frac{3}{1 + F_0^{s,a}}\frac{m^*}{k_F^2}, \qquad (8.24)$$

$$m_1^{s,a} = \frac{N}{2}\frac{q^2}{m^*}\left(1 + \frac{F_1^{s,a}}{3}\right), \qquad (8.25)$$

$$m_3^{s,a} = \frac{N}{2}\frac{q^4k_F^2}{m^{*3}}\left(1 + \frac{F_1^{s,a}}{3}\right)^2\left(\frac{3}{5} + \frac{1}{3}F_0^{s,a} + \frac{4}{75}F_2^{s,a}\right). \qquad (8.26)$$

The m_{-3} sum rule diverges due to the linear ω dependence of the strength (Im (χ)) for small ω. In equations (8.24)–(8.26), the effective mass is related to the F_1^s Landau parameter through the equation (1.130):

$$m^*/m = 1 + F_1^s/3. \qquad (8.27)$$

The m_{-1}^s sum rule is known as the hydrodynamic sum rule, because it is directly related to ordinary sound velocity $v_1^2 = k_F^2(1 + F_0^s)/3mm^*$ [see Eq. (1.135)]. The m_1^s sum rule is the f-sum rule; as a consequence of equation (8.27) it does not depend on the interaction, in agreement with the direct calculation of m_1^s from equation (7.30) [see also Eq. (7.64)]. The m_3^s sum rule has been less discussed in the literature. As remarked by Lipparini and Stringari (1989), and as we will see later on, it is related to the elastic properties of the Fermi systems.

In the case of the m_k^a sum rules for the spin-density operator $\rho_{\mathbf{q}}^a$, the following remarks apply. The m_{-1}^a sum rule can be expressed in terms of the system magnetic susceptibility [see Eq. (1.136)], through the relation

$$m_{-1}^a = -\frac{1}{2\mu_0}\chi_\sigma \, . \tag{8.28}$$

Unlike the symmetric case, the m_1^a sum rule gets contribution from the interaction. In fact, in the case of the spin channel, there is no cancellation between the combination $1 + F_1^a/3$ and the one that characterizes the effective mass, $m^*/m = 1 + F_1^s/3$.

The spin channel has deep analogies with the isospin channel of nuclear matter, with N neutrons and Z protons and $A = N + Z$ nucleons. In this case, which is the most interesting for nuclear matter because it leads to the excitation of strongly collective isovector modes (giant resonances), we have

$$G^a = \rho_{\mathbf{q}}^a = \sum_{j=1}^{N} e^{-i\mathbf{q}\cdot\mathbf{r}_j} - \sum_{j=1}^{Z} e^{-i\mathbf{q}\cdot\mathbf{r}_j} \, , \tag{8.29}$$

and there is total analogy between spin and isospin operators. As remarked before, in the case of nuclear matter one should bear in mind that the density of states at the Fermi energy is twice the amount with respect to other cases due to isospin degeneracy. In the isovectorial case, the m_{-1}^a sum rule can be expressed in terms of the b_{sym} coefficient of the volume-symmetry-energy that appears in the semi-empirical mass formula of nuclei (Weizsacker 1935; Bethe and Bacher 1936):

$$E = b_{\mathrm{vol}}N - b_{\mathrm{surf}}N^{2/3} - \frac{1}{2}b_{\mathrm{sym}}\frac{(N-Z)^2}{A} - \frac{3}{5}\frac{Z^2 e^2}{R_c} \, , \tag{8.30}$$

through the relation

$$m_{-1}^a = \frac{A}{2b_{\mathrm{sym}}} \, , \tag{8.31}$$

where the parameters b_{sym} and F_0^a are connected by

$$b_{\mathrm{sym}} = \frac{2}{3}\epsilon_F(1 + F_0^a) \, . \tag{8.32}$$

Using the values $b_{\mathrm{sym}} = 50$ MeV and $\epsilon_F \simeq 37$ Mev, corresponding to a nuclear mass density $\rho = 0.17$ nucleons fm^{-3}, we have $F_0^a \simeq 1$ for nuclear matter from equation (8.32). Let us recall that for ^{3}He it is $F_0^a = -0.7$ and $F_0^s = 9.15$. The Landau parameter F_0^s of nuclear matter is connected to the compressibility χ_{nm} of nuclear matter, by the relation $\chi_{nm}/9 = 2\epsilon_F(1 + F_0^s)/3$. The value of χ_{nm} is not very well determined experimentally. Using the value $\chi_{nm} \simeq 200$ MeV, we find $F_0^s \simeq -0.1$. The Landau parameters for nuclear matter can be deduced by the effective, Skyrme-like forces, like for example the *SIII* described in Chapter 4. In Table 8.1 we report the values of the parameters $F_0^s, F_0^a, F_1^s, F_1^a$ for some of these forces (Garcia-Recio et al. 1992) (k_F in fm^{-1}):

TABLE 8.1

	$SIII(k_F = 1.29)$	$SkM(k_F = 1.33)$	$SGII(k_F = 1.33)$
F_0^s	0.299	-0.235	-0.235
F_0^a	0.865	0.975	0.733
F_1^s	-0.708	-0.630	-0.652
F_1^a	0.489	0.574	0.524

In what follows, as an example of the application of equation (8.23), we will discuss the dynamic polarizability in the simplified case where only the $F_0^{s,a}$ Landau parameter is assumed to be non-zero. Using relations (8.14) and putting $F_1 = F_2 = 0$ in (8.23), we find the result

$$\chi^{s,a}(q,\omega) = \frac{-\nu(0)\Omega_{0,0}}{1 + F_0^{s,a}\Omega_{0,0}} \, . \tag{8.33}$$

The poles of equation (8.33) are given by the solutions of

$$\frac{1}{F_0^{s,a}} = \frac{s}{2}\ln\frac{s+1}{s-1} - 1 \, , \tag{8.34}$$

where we used the result (8.14) for $\Omega_{0,0}$. The dynamic form factor (strength function) is given by

$$S^{s,a}(q,\omega) = -\frac{1}{\pi}\text{Im }\chi^{s,a}(q,\omega) \, . $$

First of all, we notice that if $F_0 = 0$, we find the result

$$S^{s,a}(q,\omega) = \frac{\nu(0)}{\pi}\text{Im }\Omega_{0,0} = \frac{Vm^2}{2\pi^2}\frac{\omega}{q}\Theta\left(1 - \frac{\omega}{qv_F}\right) \, , \tag{8.35}$$

using equation (8.14), which is the same as that of (1.98) for the single-particle strength of the Fermi gas. However, if $F_0 > 0$, the interaction produces a discrete peak at $\omega > qv_F$. In fact, in this case (i.e. $F_0^{s,a} > 0$, corresponding to a repulsive interaction among the quasiparticles) equation (8.34) has a real solution for $s = \omega/qv_F$, such that $s > 1$. This solution (collective) corresponds to an excitation mode of the system with no attenuation, whose phase velocity $v = \omega/q$ is greater than v_F. However, if $-1 < F_0^{s,a} < 0$, the solution of (8.34) has imaginary components and the corresponding mode is damped (Landau damping). Finally, if the attraction among quasiparticles is so strong that $F_0^{s,a} < -1$ then the solution is unstable.

In the ^{3}He case, the first case ($F_0^{s,a} > 0$) is realized for the density channel (symmetric spin), and the second one for the spin-density channel (antisymmetric spin). For the isovectorial modes of nuclear matter we are again in the first case.

We now discuss the undamped solution for ^{3}He, i.e. zero sound. In this case, $F_0^s = 9.15$ is large enough that we are justified in looking for solutions of (8.34) in

the limit of large s. Therefore, using the expansion of equation (8.15), we obtain

$$s^2 = \frac{F_0^s}{3}\left(1 + \frac{9}{5F_0^s} + \cdots\right) \qquad (8.36)$$

and a wave phase velocity

$$v_0^2 = \frac{\omega^2}{q^2} = v_F^2 \frac{F_0^s}{3}\left(1 + \frac{9}{5F_0^s} + \cdots\right). \qquad (8.37)$$

If we compare this with the ordinary sound wave, as obtained from the hydrodynamic equations (1.135), taken the same limit ($F_1^s = 0$), and which are given by

$$v_1^2 = v_F^2 (F_0^s/3)(1 + 1/F_0^s + \cdots),$$

we find that the two velocities are different. The difference increases if we take into account the other Landau parameters as well. For example, the ordinary sound velocity v_1 does not depend on F_2, while the velocity v_0 of zero sound does. This mode has elastic nature and its frequency is well described by the energy

$$\omega^2 = \frac{m_3^s}{m_1^s} = \frac{m^*}{m} q^2 v_F^2 \left(\frac{3}{5} + \frac{F_0^s}{3} + \frac{4}{75}F_2^s\right). \qquad (8.38)$$

The difference between the energies of the hydrodynamic (with collisions) and elastic (collisionless) modes, can be detected experimentally by studying the velocity of sound in ^{3}He as a function of temperature, i.e. of the collision time. Two regimes are found, the low-temperature one in which sound propagation takes place at velocity v_0 [see Eq. (8.37)], and the high-temperature one where sound propagation occurs at ordinary sound velocity v_1. In these regimes, there is no sound attenuation. However, there is an intermediate range in which sound attenuation is not zero and varies with temperature.

The sound attenuation can be studied in the Landau theory using the "single time" approximation (Khalatninov and Abrikosov 1958) for the collision integral:

$$I(\delta n^s)_{\text{coll}} = -\frac{1}{\tau}[\delta \tilde{n}_{\mathbf{k}}^s - \delta \tilde{n}_{\mathbf{k}}^s(l = 0, l = 1)], \qquad (8.39)$$

where

$$\delta \tilde{n}_{\mathbf{k}}^s = \delta n_{\mathbf{k}}^s - \frac{\partial n_{\mathbf{k}}^0}{\partial \epsilon_{\mathbf{k}}} \sum_{\mathbf{k}'} f_{\mathbf{k},\mathbf{k}'}^s \delta n_{\mathbf{k}'}^s \qquad (8.40)$$

is the local deformation of the distribution function, while $\delta \tilde{n}_{\mathbf{k}}^s(l = 0, l = 1)$ corresponds to the components of $\delta \tilde{n}_{\mathbf{k}}^s$ which have $l = 0$ and $l = 1$ angular momentum in momentum space, and ensures mass and momentum conservation during collisions. The use of $\delta \tilde{n}_{\mathbf{k}}^s$ in place of $\delta n_{\mathbf{k}}^s$ ensures local energy conservation of quasiparticles. τ is the characteristic time of collision. The collision integral (8.39) changes the

Landau equation under external field (8.11) into the following one:

$$(\cos\theta - \xi)u^s(\theta) + \cos\theta\left(\frac{\lambda}{v_F} + F_0^s u_0 + \frac{1}{3}F_1^s u_1 \cos\theta + \frac{1}{5}F_2^s u_2(3\cos^2\theta - 1)\right)$$

$$= \frac{1}{\sigma}(u_0 + u_1\cos\theta), \qquad (8.41)$$

where $\xi = s + i/(\tau q v_F)$ and $\sigma = i\tau q v_F$, and we have retained Landau parameters up to F_2. From (8.41) it is possible to derive the system linear response in the presence of the collision term. The equation for the poles of the response function describes sound dispersion in a Fermi liquid in the presence of the collision term. We are going to describe the visco-elastic model (Bedell and Pethick 1982) for sound attenuation. This model is based on a truncated solution of (8.41). This equation yields the following linear system of equations

$$\begin{vmatrix} -s & \dfrac{G_1}{\sqrt{3}} & 0 & 0 & \cdots \\[2ex] \dfrac{G_0}{\sqrt{3}} & -s & \dfrac{2G_2}{\sqrt{15}} & 0 & \cdots \\[2ex] 0 & \dfrac{2G_1}{\sqrt{15}} & -\xi\left(1 - \dfrac{F_2}{5\sigma\xi}\right) & \dfrac{3G_3}{\sqrt{35}} & \cdots \\[2ex] 0 & 0 & \dfrac{3G_2}{\sqrt{35}} & -\xi\left(1 - \dfrac{F_3}{7\sigma\xi}\right) & \cdots \\[2ex] 0 & 0 & 0 & \dfrac{4G_3}{\sqrt{63}} & \cdots \\[2ex] \cdots & \cdots & \cdots & \cdots & \cdots \end{vmatrix} \cdot \begin{vmatrix} u_0 \\ u_1 \\ u_2 \\ u_3 \\ \cdots \\ \cdots \end{vmatrix} = -\frac{\lambda}{v_F}\begin{vmatrix} 0 \\ 1 \\ 0 \\ 0 \\ 0 \\ \cdots \end{vmatrix}, \qquad (8.42)$$

where $G_l = 1 + F_l/(2l+1)$. The structure of these equations shows that, for $l > 2$, we have $u_{l+1} \simeq u_l/s$, so that the contributions from high multipolarities are less and less important, provided that $s > 1$. This suggests that the set of equations be truncated at a given order in l. The visco-elastic model consists in truncating the system of equations at order $l \le 2$, which means considering only the three first lines and columns of the matrix equation (8.42). By requiring that the determinant of the coefficients of the homogeneous system be zero, we find

$$-\xi\left(1 - \frac{F_2}{5\sigma\xi}\right)(s^2 - s_1^2) + \frac{4}{15}sG_1G_2 = 0 \qquad (8.43)$$

where $s_1^2 = (v_1/v_F)^2$. Assuming ω is real, equation (8.43) yields two equations for the real q_R and imaginary q_I parts of $q(\omega)$, from which we get the sound velocity $v = \omega/q_R$ and the sound attenuation coefficient $\gamma = q_I$. Assuming further that the imaginary part of s is much smaller than the real part, we find

$$v^2 = v_1^2 + \frac{4}{15}v_F^2 G_1 G_2 \frac{(\omega\tau)^2}{G_2 + (\omega\tau)^2}, \qquad (8.44)$$

and

$$\gamma = \frac{2}{15} \frac{v_F^2}{v^3} G_1 G_2 \frac{\omega^2 \tau}{G_2 + (\omega\tau)^2} \,. \tag{8.45}$$

Equations (8.44) and (8.45) describe the transition from the collisionless regime ($\omega\tau \gg 1$) to the hydrodynamic one ($\omega\tau \ll 1$). In the first case the sound velocity is given by

$$v_0^2 = v_1^2 + 4v_F^2 G_1 G_2/15 \,,$$

and the attenuation coefficient becomes

$$\gamma_0 = 2v_F^2 G_1 G_2/(15v_0^3\tau) \,.$$

In the second case the sound velocity is the ordinary one and the attenuation coefficient behaves like $\omega^2\tau$. The above results, in the case of ^{3}He, reproduce rather well the experimental data (Abel, Anderson and Wheatley 1966). They were also applied to the study of nuclear resonances at finite temperature (Denisov 1989; Baran et al. 1995). Finally, we note that the visco-elastic model yields an expression for the dynamic polarizability which is identical to the one obtained previously, provided all the Landau parameters other than F_0 and F_1 are neglected, and an $1/s^2$-expansion is performed.

The Landau theory has been generalized to charged Fermi systems by Silin (Silin 1957). Silin was the first who realized that the problems due to the long-range Coulomb interactions (which are singular in the $\mathbf{q} \to 0$ limit), might be overcome by partitioning the total interaction among charged quasiparticles into a regular part $f_{\mathbf{k},\mathbf{k}'}$ (which is the equivalent of the total interaction among neutral quasiparticles), and a singular part given by the Fourier transform of the Coulomb interaction. The latter, is to be treated in terms of a mean polarization field acting on the quasiparticles. Such mean polarization field $\mathcal{E}(\mathbf{r},t)$ is connected to the density fluctuations by the equation:

$$\text{div } \mathcal{E}(\mathbf{r},t) = 4\pi e \delta n_{\mathbf{k}}^s(\mathbf{r},t) \,, \tag{8.46}$$

and appears in the Landau equations (8.4) for $\delta n_{\mathbf{k}}^s(\mathbf{r},t)$, through an additional external-force term of the form (8.3), i.e. $-e\mathcal{E} \cdot \mathbf{v}_{\mathbf{k}} \partial n^0/\partial \epsilon_{\mathbf{k}}$, while it does not change the Landau equation for the spin density fluctuations. $\mathcal{E}(\mathbf{r},t)$ can be interpreted as an additional applied field, which screens the interaction between two quasiparticles due to the presence of all the other quasiparticles. Using the result

$$\mathcal{E}(q,\omega) = -i\mathbf{q}\frac{4\pi e}{q^2} \sum_{\mathbf{k}} \delta n_{\mathbf{k}}^s(q,\omega) \,, \tag{8.47}$$

one obtains, in charged systems, the following equation for $u_{\mathbf{k}}^s$

$$(\mathbf{q} \cdot \mathbf{v}_{\mathbf{k}} - \omega)u_{\mathbf{k}}^s + \mathbf{q} \cdot \mathbf{v}_{\mathbf{k}} \sum_{\mathbf{k}'} \left(f_{\mathbf{k},\mathbf{k}'}^s + \frac{4\pi e^2}{q^2} \right) \delta(\epsilon_{\mathbf{k}'} - \epsilon_F)u_{\mathbf{k}'}^s + \lambda\frac{\mathbf{q} \cdot \mathbf{v}_{\mathbf{k}}}{v_F} = 0 \,. \tag{8.48}$$

The solution of such equation goes on like in the case of neutral systems. The final formulae for the dynamic polarizability $\chi^s(q,\omega)$, and for the sum rules, are obtained from equations (8.23)–(8.26) by simply replacing the Landau parameter F_0^s with $F_0^s + \nu(0)4\pi e^2/q^2$.

TABLE 8.2

r_s	F_0^s	F_0^a
1	-0.17	-0.13
2	-0.36	-0.23
3	-0.55	-0.32
4	-0.74	-0.38
5	-0.95	-0.44
10	-2.03	-0.65

Much effort has been devoted to deriving the Landau parameters for the $3D$ electron gas, starting from the microscopic interaction (see for example Pines and Nozières 1966; Hedin and Lundqvist 1969). What emerges clearly from these calculations is that for the $3D$ electron gas the ratio m^*/m is practically equal to 1, so that the value of the Landau parameter F_1^s might be zero. The same can be assumed to hold for the corresponding parameter in the spin channel: $F_1^a \simeq 0$. The only parameters which are definitely non-zero are F_0^s and F_0^a. The most reliable values for these parameters can be deduced from the Monte Carlo values of the compressibility and magnetic susceptibility (Vosko, Wilk and Nusair 1980; Iwamoto and Pines 1984), and are reported in Table 8.2 for different values of the density. The excited state of the $3D$ electron gas which correspond to the zero sound in ^{3}He, is called plasmon, and has been observed in numerous experiments. One of the most complete among these experments is the one published by vom Felde, Sprosser-Prou and Fink (1989). We will describe it in Section 8.4.

To conclude, let us discuss the linear response in the two-dimensional Landau theory. In $2D$ the equation corresponding to Eq. (8.9) is

$$(\cos\theta - s)u^{s,a}(\theta) + \cos\theta\,\nu(0)\int \frac{d\theta'}{2\pi} f_{2D}^{s,a}(\theta,\theta')u^{s,a}(\theta') = -\frac{\lambda}{v_F}\cos\theta, \quad (8.49)$$

where the $2D$ level density $\nu(0)$ at the Fermi surface is given by (1.138). Employing the expansion (1.137) for the $2D$ interaction, and the analogue for the displacements u:

$$u^{s,a}(\theta) = \sum_l u_l^{s,a}\cos l\theta, \quad (8.50)$$

we find

$$(\cos\theta - s)\sum_l u_l^{s,a}\cos l\theta + \cos\theta\left(u_0^{s,a}F_0^{s,a} + \sum_{l>0}u_l^{s,a}\frac{F_l^{s,a}}{2l}\cos l\theta\right) = -\frac{\lambda}{v_F}\cos\theta.$$

$$(8.51)$$

From this equation, dividing by $(\cos\theta - s)$ and then multiplying by $\cos m\theta$, and then performing the integration $\int_0^{2\pi} \frac{d\theta}{2\pi}$, we obtain

$$u_0^{s,a} + F_0^{s,a} u_0^{s,a} \Lambda_{0,0} + \sum_{l>0} \Lambda_{0,l} \frac{F_l^{s,a}}{2l} u_l^{s,a} = -\frac{\lambda}{v_F} \Lambda_{0,0},$$

$$\frac{u_m^{s,a}}{2} + F_0^{s,a} u_0^{s,a} \Lambda_{m,0} + \sum_{l>0} \Lambda_{m,l} \frac{F_l^{s,a}}{2l} u_l^{s,a} = -\frac{\lambda}{v_F} \Lambda_{m,0}, \quad m \neq 0,$$

(8.52)

with

$$\Lambda_{m,l} = \int_0^{2\pi} \frac{d\theta}{2\pi} \cos m\theta \frac{\cos\theta}{\cos\theta - s} \cos l\theta.$$

The Λ functions have the following properties:

$$\Lambda_{0,0} = \begin{cases} 1 + i \dfrac{s}{\sqrt{1-s^2}} & \text{if } s \leq 1 \\[3mm] 1 - \dfrac{s}{\sqrt{s^2-1}} & \text{if } s > 1 \end{cases},$$

(8.53)

and

$$\Lambda_{1,0} = s\Lambda_{0,0}, \quad \Lambda_{2,0} = 1 + (2s^2 - 1)\Lambda_{0,0},$$

$$\Omega_{2,1} = s\Lambda_{2,0}; \quad \Lambda_{2,2} = \frac{1}{2} + (2s^2 - 1)\Lambda_{2,0}.$$

(8.54)

From equation (8.52), performing the integration $\int_0^{2\pi} \frac{d\theta}{2\pi}$ we have

$$su_0^{s,a} = \frac{u_1^{s,a}}{2}\left(1 + \frac{F_1^{s,a}}{2}\right),$$

(8.55)

and performing the integration $\int_0^{2\pi} \cos\theta \frac{d\theta}{2\pi}$:

$$s\frac{u_1^{s,a}}{2} - \frac{u_0^{s,a}}{2}(1 + F_0^{s,a}) - \frac{u_2^{s,a}}{4}\left(1 + \frac{F_2^{s,a}}{4}\right) = \frac{\lambda}{2v_F}.$$

(8.56)

From the two previous equations we find

$$\left[s^2 - \frac{1}{2}(1 + F_0^{s,a})\left(1 + \frac{F_1^{s,a}}{2}\right)\right] u_0^{s,a} - \frac{u_2^{s,a}}{4}\left(1 + \frac{F_1^{s,a}}{2}\right)\left(1 + \frac{F_2^{s,a}}{4}\right)$$

$$= \left(1 + \frac{F_1^{s,a}}{2}\right)\frac{\lambda}{2v_F}.$$

(8.57)

Moreover, from (8.52) we consider those with $m = 0$ and $m = 2$, divide them side by side to obtain

$$u_2^{s,a} = \frac{2u_0^{s,a}\Lambda_{2,0}}{\Lambda_{0,0} + \frac{F_2^{s,a}}{2}(\Lambda_{2,2}\Lambda_{0,0} - \Lambda_{2,0}^2)}.$$

(8.58)

By substituting this equation into (8.57), we arrive at the following expression:

$$u_0^{s,a} = \frac{\frac{1}{2}(1 + \frac{F_1^{s,a}}{2})\frac{\lambda}{v_F}}{s^2 - \frac{1}{2}(1 + F_0^{s,a})(1 + \frac{F_1^{s,a}}{2}) - \frac{1}{2}\frac{(1+\frac{F_1^{s,a}}{2})(1+\frac{F_2^{s,a}}{4})\Lambda_{2,0}}{\Lambda_{0,0}+\frac{F_2^{s,a}}{2}(\Lambda_{2,2}\Lambda_{0,0}-\Lambda_{2,0}^2)}} \tag{8.59}$$

and for the linear response $\chi^{s,a}(q,\omega) = v_F\nu(0)u_0^{s,a}/\lambda$, we find the expression

$$\chi_{2D}^{s,a}(q,\omega) = \frac{\frac{1}{2}\nu(0)(1 + \frac{F_1^{s,a}}{2})}{s^2 - \frac{1}{2}(1 + \frac{F_1^{s,a}}{2})(1 + F_0^{s,a}) - \frac{1}{2}\frac{(1+\frac{F_1^{s,a}}{2})(1+\frac{F_2^{s,a}}{4})\Lambda_{2,0}}{\Lambda_{0,0}+\frac{F_2^{s,a}}{2}(\Lambda_{2,2}\Lambda_{0,0}-\Lambda_{2,0}^2)}}. \tag{8.60}$$

From the latter, it is possible to derive the following expressions for the sum rules:

$$m_{-1,2D}^{s,a} = \frac{N}{2}\frac{1}{1+F_0^{s,a}}\frac{2m^*}{k_F^2}, \tag{8.61}$$

$$m_{1,2D}^{s,a} = \frac{N}{2}\frac{q^2}{m^*}\left(1 + \frac{F_1^{s,a}}{2}\right), \tag{8.62}$$

$$m_{3,2D}^{s,a} = \frac{N}{2}\frac{q^4 k_F^2}{m^{*3}}\left(1 + \frac{F_1^{s,a}}{2}\right)^2\left(\frac{3}{4} + \frac{1}{2}F_0^{s,a} + \frac{1}{16}F_2^{s,a}\right). \tag{8.63}$$

The frequency of ordinary sound in $2D$ is well represented by the energy

$$\omega^2 = \frac{m_1^s}{m_{-1}^s} = q^2\epsilon_F(1 + F_0^{s,a}) \tag{8.64}$$

while that of the elastic mode (zero sound in $2D$) is well represented by the energy

$$\omega^2 = \frac{m_3^s}{m_1^s} = \frac{m^*}{m}q^2 v_F^2\left(\frac{3}{4} + \frac{1}{2}F_0^{s,a} + \frac{1}{16}F_2^{s,a}\right). \tag{8.65}$$

Like in the three-dimensional case, the $2D$ Landau theory can be generalized to charged Fermi systems by introducing a mean polarization field $\mathcal{E}(\mathbf{r},t)$, related to the density fluctuations by

$$\mathcal{E}(q,\omega) = -i\mathbf{q}\frac{2\pi e}{q}\sum_{\mathbf{k}}\delta n_{\mathbf{k}}^s(q,\omega), \tag{8.66}$$

which is the Fourier transform of the Coulomb interaction in $2D$, and by adding to the $2D$ Landau equation the following term

$$-e\mathcal{E}\cdot\mathbf{v_k}\frac{\partial n_{\mathbf{k}}^0}{\partial\epsilon_{\mathbf{k}}}. \tag{8.67}$$

From this point on, the calculation of the linear response function proceeds as in the case of neutral systems. The final formulae for the dynamic polarizability $\chi^s(q,\omega)$ and for the sum rules are obtained from equations (8.60)–(8.63), simply by replacing the Landau parameter F_0^s with $F_0^s + \nu(0)2\pi e^2/q$. For the $2D$ electron

gas, a variational Monte Carlo calculation for the Landau parameters is available (Kwon, Ceperley and Martin 1994). The results of such calculation for some density values are reported in Table 8.3.

TABLE 8.3

	$r_s = 1$	$r_s = 2$	$r_s = 3$	$r_s = 5$
F_0^s	−0.60	−0.99	−1.63	−3.70
F_0^a	−0.34	−0.41	−0.49	−0.5
F_1^s	−0.14	−0.10	−0.03	0.12
F_1^a	−0.19	−0.24	−0.26	−0.27
F_2^s	−0.07	−0.16	−0.27	−0.50
F_2^a	0.01	0.07	0.14	0.32

The $2D$ electron gas can be realized at the interfaces of heterostructures of $GaAs/Al_xGa_{1-x}As$ (Ando, Fowler and Stern 1982) and of other structures. The response function of such systems has been studied by means of inelastic scattering of polarized light (Pinczuk et al. 1989; Luo et al. 1993; Eriksson et al. 1999). These experiments, which evidence the existence of "zero sound" — like collective states, will be discussed later.

8.2   Time Dependent Hartree (TDH) for Homogeneous Systems: The RPA

The time-dependent Hartree–Fock (HF) equations, are the time-dependent version of the static HF equations (2.7) and are written as ($\hbar = 1$):

$$i\frac{\partial}{\partial t}\varphi_i(\mathbf{r}, \sigma, t) = H^{HF}\varphi_i(\mathbf{r}, \sigma, t), \qquad (8.68)$$

where the single-particle wavefunctions $\varphi_i(\mathbf{r}, \sigma, t)$, and the one-body densities: $\rho(\mathbf{r}, t)$ (diagonal) and $\rho^{(1)}(\mathbf{r}, \sigma; \mathbf{r}', \sigma', t)$ (non-diagonal), upon which H^{HF} depends, are functions of time. Equations (8.68) can be obtained by requiring that the action integral

$$I = \int_{t_1}^{t_2} \langle \psi_{SD}(t)|H - i\frac{\partial}{\partial t}|\psi_{SD}(t)\rangle dt, \qquad (8.69)$$

computed for a generic Slater determinant, be stationary against an arbitrary variation of ψ_{SD} in the space of Slater determinants:

$$\frac{\delta I}{\delta \psi_{SD}} = 0. \qquad (8.70)$$

The time-dependent Hartree equations (TDH), are obtained by replacing the HF Hamiltonian by the Hartree Hamiltonian (which depends only on the diagonal,

one-body density) in (8.68):

$$H^H = \frac{-\nabla^2}{2m} + v_{\text{ext}}(\mathbf{r}) + \int \rho(\mathbf{r}', t) v(\mathbf{r} - \mathbf{r}') d\mathbf{r}' . \tag{8.71}$$

The time-dependent Hartree equations in the presence of a time-oscillating external field of the form (7.10) are written as

$$i\frac{\partial}{\partial t}\varphi_i(\mathbf{r}, t) = \left[\frac{-\nabla^2}{2m} + v_{\text{ext}}(\mathbf{r}) + \int \rho(\mathbf{r}', t) v(\mathbf{r} - \mathbf{r}') d\mathbf{r}' \right.$$

$$\left. + \lambda(g^\dagger e^{-i\omega t} + h.c.) \right] \varphi_i(\mathbf{r}, t) , \tag{8.72}$$

and for a homogeneous system have the same form for both Fermions and Bosons.

In the following, we will discuss the solutions of these equations for a homogeneous system in the case where

$$G = \sum_{i=1}^{N} g(r_i) = \sum_{i=1}^{N} e^{-i\mathbf{q}\cdot\mathbf{r}_i} ,$$

and subsequently we will compute the Hartree response function $\chi(F, G, \omega)$ for the operator

$$F = \sum_{i=1}^{N} f(r_i) = \sum_{i=1}^{N} e^{i\mathbf{q}\cdot\mathbf{r}_i}$$

i.e. the density response. For a homogeneous system, the static external field $v_{\text{ext}}(\mathbf{r})$ in (8.72) will be equated to zero in the cases of ^{3}He, nuclear matter and Bosons, and equal to the potential generated by a jellium of positive charge (ρ_+) in the case of electrons. In the latter case, equations (8.72) have the form

$$i\frac{\partial}{\partial t}\varphi_i(\mathbf{r}, t) = \left[\frac{-\nabla^2}{2m} + e^2 \int \frac{\rho(\mathbf{r}', t) - \rho_+}{|\mathbf{r} - \mathbf{r}'|} d\mathbf{r}' \right.$$

$$\left. + \lambda \cdot \left(e^{i(\mathbf{q}\cdot\mathbf{r} - \omega t)} + e^{-i(\mathbf{q}\cdot\mathbf{r} - \omega t)} \right) \right] \varphi_i(\mathbf{r}, t) . \tag{8.73}$$

In the homogeneous case, due to translational invariance, equation (8.72) for $\rho(\mathbf{r}, t)$ will yield solutions of the form

$$\rho(\mathbf{r}, t) = \rho_0 + \delta\rho(\mathbf{r}, t) , \tag{8.74}$$

where ρ_0 is the (constant) density of the (unperturbed) ground state, and

$$\delta\rho(\mathbf{r}, t) = \delta\rho\left(e^{i(\mathbf{q}\cdot\mathbf{r} - \omega t)} + e^{-i(\mathbf{q}\cdot\mathbf{r} - \omega t)} \right) , \tag{8.75}$$

where $\delta\rho$ is a constant to be determined. Therefore, the fluctuation of the operator

$$F = \sum_{i=1}^{N} e^{i\mathbf{q}\cdot\mathbf{r}_i}$$

is given by

$$\delta F(G,\omega) = \langle\psi(t)|F|\psi(t)\rangle - \langle 0|F|0\rangle$$

$$= \int d\mathbf{r} e^{i\mathbf{q}\cdot\mathbf{r}}(\rho(\mathbf{r},t) - \rho_0)_G = L^D\delta\rho e^{i\omega t}, \qquad (8.76)$$

where L^D is the volume of the system in dimension D. Moreover, the dynamic polarizability [see Eq. (7.13)] is given by

$$\chi(q,\omega) = \frac{L^D\delta\rho}{\lambda}. \qquad (8.77)$$

In order to determine $\delta\rho$, we will insert $\rho(\mathbf{r},t)$ of equations (8.74) and (8.75) into (8.72), and linearize the equations. This means writing the self-consistent Hartree mean field, i.e. $U(\mathbf{r},\rho(\mathbf{r},t)) = \int \rho(\mathbf{r}',t)v(\mathbf{r}-\mathbf{r}')d\mathbf{r}'$, as

$$U(\mathbf{r},\rho(\mathbf{r},t)) = U(\mathbf{r},\rho_0) + \left.\frac{\partial U}{\partial\rho(\mathbf{r},t)}\right|_{\rho=\rho_0}\delta\rho(\mathbf{r},t). \qquad (8.78)$$

Therefore, from equations (8.72) and (8.78) we obtain

$$i\frac{\partial}{\partial t}\varphi_i(\mathbf{r},\sigma,t) = \left[\frac{-\nabla^2}{2m} + v_{\text{ext}}(\mathbf{r}) + U(\mathbf{r},\rho_0)\right.$$

$$\left. + (\delta\rho v(q) + \lambda)\cdot(e^{i(\mathbf{q}\cdot\mathbf{r}-\omega t)} + e^{-i(\mathbf{q}\cdot\mathbf{r}-\omega t)})\right]\varphi_i(\mathbf{r},\sigma,t), \qquad (8.79)$$

where $v(q)$ is the Fourier transform of the interaction potential.

For example, if the interacting potential is the Coulomb potential then $v(q)$ is given by

$$v(q) = \begin{cases} (1D) & 2e^2 K_0(|qa|) \\ (2D) & 2\pi e^2/q \\ (3D) & 4\pi e^2/q^2 \end{cases}, \qquad (8.80)$$

where for the "one-dimensional" case we took a Coulomb interaction of the form $1/\sqrt{(x-x')^2 + a^2}$, and K_0 is a modified Bessel function of the second kind (see e.g. Gradshteyn and Ryzhik 1980) for which, in the limit $|qa| \to 0$, we have

$$K_0(|qa|) \sim |\ln qa|. \qquad (8.81)$$

Equation (8.79) can be rewritten as

$$i\frac{\partial}{\partial t}\varphi_i(\mathbf{r},\sigma,t) = \left[\frac{-\nabla^2}{2m} + v_{\text{ext}}(\mathbf{r}) + U(\mathbf{r},\rho_0)\right.$$

$$\left. + \lambda' \cdot \left(e^{i(\mathbf{q}\cdot\mathbf{r}-\omega t)} + e^{-i(\mathbf{q}\cdot\mathbf{r}-\omega t)}\right)\right]\varphi_i(\mathbf{r},\sigma,t)\,, \tag{8.82}$$

with

$$\lambda'(q) = \lambda + \delta\rho v(q)\,. \tag{8.83}$$

In the homogeneous systems we are considering, the static Hartree potential $U(\mathbf{r},\rho_0)$ is a constant which, in the case of the electron gas, cancels exactly the one originating from v_{ext} (for the other systems, $v_{\text{ext}} = 0$) and, apart from this inessential constant, equation (8.82) coincides with that of a non-interacting system coupled to an external time-oscillating field, with a coupling constant λ' given by equation (8.83). For such system, the density response function is the (single-particle) free response $\chi_0((\mathbf{q},\omega)$ that we studied in Section 7.7. Therefore, in the time-dependent Hartree theory, the particles of the N-body interacting system respond like non-interacting particles to the combined effect of the external field (λ) plus the polarization field induced by the density fluctuations in the self-consistent Hartree mean-field. From equation (8.77) and from the analogous relation for the free response function:

$$\chi^0(q,\omega) = \frac{L^D\delta\rho}{\lambda'(q)}\,, \tag{8.84}$$

we then obtain

$$\lambda\chi(q,\omega) = \lambda'(q)\chi^0(q,\omega) = L^D\delta\rho\,, \tag{8.85}$$

which are known as the *RPA* equations. The solution of these equations is given by

$$\chi^{RPA}(q,\omega) = \frac{\chi^0(q,\omega)}{1 - \frac{v(q)}{L^D}\chi^0(q,\omega)}\,, \tag{8.86}$$

and is called the *RPA* response function.

The energies of the *RPA* excited states of the system are given by the poles of equation (8.86), and are obtained from the solutions of

$$1 - \frac{v(q)}{L^D}\chi^0(q,\omega) = 0\,. \tag{8.87}$$

The graphical solution of this equation is obtained by plotting the free response $\chi^0(q,\omega)$ for fixed q, as a function of ω, and finding the intersections of $\chi^0(q,\omega)/L^D$ with the straight line $1/v(q)$, parallel to the ω axis.

The *RPA* matrix elements of the density operator $\rho_{\mathbf{q}} = F = \sum_{i=1}^{N} e^{i\mathbf{q}\cdot\mathbf{r}_i}$, between the ground state and the *RPA* excited states with energies ω, given by the

solutions of (8.87) for the poles of $\chi^{RPA}(q, \omega)$, are found by calculating the residues of $\chi^{RPA}(q, \omega)$ in such poles. To perform such calculation, let us put equation (8.86) in the following form:

$$\frac{1}{\chi^{RPA}(q, \omega)} = \frac{1}{\chi^0(q, \omega)} - \frac{v(q)}{L^D}, \tag{8.88}$$

and let us expand it around the generic pole of energy $\bar{\omega}$, keeping in mind that in the pole $(\chi^{RPA}(q, \bar{\omega}))^{-1} = 0$, so that $(\chi^0)^{-1} = v(q)/L^D$. As a result, we obtain

$$\frac{1}{\chi^{RPA}(q, \omega)} \sim \frac{\partial}{\partial \omega}\left(\frac{1}{\chi^0}\right)\bigg|_{\omega = \bar{\omega}} (\omega - \bar{\omega}) = -\left(\frac{v(q)}{L^D}\right)^2 \frac{\partial \chi^0}{\partial \omega}\bigg|_{\omega = \bar{\omega}} (\omega - \bar{\omega}), \tag{8.89}$$

that is

$$\chi^{RPA}(q, \omega) \sim -\left(\frac{L^D}{v(q)}\right)^2 \frac{1}{\chi_0'(\omega = \bar{\omega})} \frac{1}{\omega - \bar{\omega}}, \tag{8.90}$$

where $\chi_0' = \frac{\partial \chi^0}{\partial \omega}$. Therefore, the desired matrix element is given by

$$|\langle 0|\rho_{\mathbf{q}}|\bar{\omega}\rangle|^2 = -\left(\frac{L^D}{v(q)}\right)^2 \frac{1}{\chi_0'(\omega = \bar{\omega})}. \tag{8.91}$$

Equations (8.86), (8.87) and (8.91) hold for both Fermion and Boson systems. As discussed in Section 7.7, what is quite different in the two cases is the form of the free response $\chi^0(q, \omega)$. As will appear later, such difference leads to a great diversity in the RPA solutions in the two cases.

Another important difference between Fermion and Boson systems, concerns the range of validity of the RPA equations (8.86) at finite temperature. In these equations, the thermal effects show themselves only through the free response function, which includes the occupation numbers of the single-particle states. Whereas for Fermions the use of the Fermi–Dirac thermal occupation numbers is appropriate and the ensuing RPA equations at finite temperature make sense (see e.g. Braghin and Vautherin 1994; Hernandez et al. 1995), in the Boson case the use of the thermal Bose–Einstein occupation numbers leads to equations which, when solved, produce wrong results.

This behavior is due to the different nature of low-energy elementary excitations for the two systems, i.e. p–h excitations for Fermions and phonons for Bosons. While the starting point for the time-dependent theory that leads to the RPA equations, i.e. the Hartree–Fock ground state, in the case of finite temperature is a good one for Fermions, this is not the case for Bosons and leads to wrong results. It is only at zero temperature that the RPA equations for Bosons do provide a good solution for the excited states of the system. This fact will be discussed in Section 8.5. Subsequently, in Section 8.6 we will briefly discuss a finite-temperature approach for Bosons, known as the Popov approximation, which produces correct results for these systems.

8.3   *TDH* for the Density Matrix and the Landau Equations

From the time-dependent Hartree equations

$$i\hbar\frac{\partial}{\partial t}\varphi_i(\mathbf{r},t) = \left[\frac{-\hbar^2\nabla^2}{2m} + \int \rho(\mathbf{r}',t)v(\mathbf{r}-\mathbf{r}')d\mathbf{r}'\right]\varphi_i(\mathbf{r},t)\,, \qquad (8.92)$$

where for simplicity we have omitted the irrelevant external-field term, by multiplying on the left hand ride by $\varphi_i^*(\mathbf{r}',t)$ and performing a summation on occupied states, and recalling the definition of the non-diagonal, one-body density matrix, i.e.:

$$\rho^{(1)}(\mathbf{r},\mathbf{r}',t) = \sum_i \varphi_i^*(\mathbf{r},t)\varphi_i(\mathbf{r}',t)\,,$$

it is easy to obtain the equation

$$i\hbar\frac{\partial}{\partial t}\rho^{(1)}(\mathbf{r},\mathbf{r}',t)$$

$$= \left[\frac{-\hbar^2}{2m}(\nabla_\mathbf{r}^2 - \nabla_{\mathbf{r}'}^2) + (U(\mathbf{r},\rho(\mathbf{r},t)) - U(\mathbf{r}',\rho(\mathbf{r}',t)))\right]\rho^{(1)}(\mathbf{r},\mathbf{r}',t) \quad (8.93)$$

where

$$U(\mathbf{r},\rho(\mathbf{r},t)) = \int \rho(\mathbf{r}',t)v(\mathbf{r}-\mathbf{r}')d\mathbf{r}'$$

is the Hartree self-consistent mean field. Then, introducing the relative and centre-of-mass variables: $\mathbf{s} = \mathbf{r} - \mathbf{r}'$, $\mathbf{R} = (\mathbf{r}+\mathbf{r}')/2$, equation (8.93) can be rewritten as

$$\left\{i\hbar\frac{\partial}{\partial t} + \frac{\hbar^2}{2m}\nabla_\mathbf{s}\cdot\nabla_\mathbf{R} - \left[U\left(\mathbf{R}-\frac{\mathbf{s}}{2},t\right) - U\left(\mathbf{R}+\frac{\mathbf{s}}{2},t\right)\right]\right\}\rho^{(1)}(\mathbf{R},\mathbf{s},t) = 0\,. \quad (8.94)$$

Let us now introduce the distribution function

$$f(\mathbf{R},\mathbf{p},t) = \frac{1}{(2\pi)^D}\int ds e^{\frac{i}{\hbar}\mathbf{p}\cdot\mathbf{s}}\rho^{(1)}(\mathbf{R},\mathbf{s},t)\,, \qquad (8.95)$$

which gives the probability of finding a particle at position $\mathbf{R}$ with momentum $\mathbf{p}$ at time t. Apart from a constant, the distribution function f coincides with the Landau distribution function $n(\mathbf{R},\mathbf{p},t)$ as defined in Section 1.9. This can easily be seen by computing f starting from the density expression $\rho^{(1)}(\mathbf{R},\mathbf{s})$ built up by means of a static, plane-wave Slater determinant. In this case, apart from a constant, f coincides with the ground state distribution (1.73). By transforming equation (8.94), the following equation for f is obtained

$$\frac{\partial}{\partial t}f(\mathbf{R},\mathbf{p},t) + \frac{\mathbf{p}}{m}\cdot\nabla_\mathbf{R}f(\mathbf{R},\mathbf{p},t)$$

$$- \frac{1}{i\hbar}\int ds e^{\frac{i}{\hbar}\mathbf{p}\cdot\mathbf{s}}\left[U\left(\mathbf{R}-\frac{\mathbf{s}}{2},t\right) - U\left(\mathbf{R}+\frac{\mathbf{s}}{2},t\right)\right]\rho^{(1)}(\mathbf{R},\mathbf{s},t) = 0\,. \quad (8.96)$$

By expanding, for small **s**, the difference

$$U\left(\mathbf{R} - \frac{\mathbf{s}}{2}, t\right) - U\left(\mathbf{R} + \frac{\mathbf{s}}{2}, t\right)$$

appearing in the last term of equation (8.96), and using the relation

$$-\frac{1}{i\hbar} \int ds e^{\frac{i}{\hbar}\mathbf{p}\cdot\mathbf{s}} \mathbf{s} \cdot (\nabla_\mathbf{R} U(\mathbf{R}, t)) \rho^{(1)}(\mathbf{R}, \mathbf{s}, t) = \nabla_\mathbf{R} U(\mathbf{R}, t) \cdot \nabla_\mathbf{p} f(\mathbf{R}, \mathbf{p}, t),$$

we obtain

$$\frac{\partial}{\partial t} f(\mathbf{R}, \mathbf{p}, t) + \frac{\mathbf{p}}{m} \cdot \nabla_\mathbf{R} f(\mathbf{R}, \mathbf{p}, t) - \nabla_\mathbf{R} U(\mathbf{R}, t) \cdot \nabla_\mathbf{p} f(\mathbf{R}, \mathbf{p}, t) + O(\hbar^2) = 0. \quad (8.97)$$

Equation (8.97) is the semiclassical limit ($\hbar \to 0$) of the time-dependent Hartree equation, and holds in the long-wavelength limit, where the momentum transferred to the system is small, and the expansion of the Hartree potential used for its derivation is correct. By writing $f(\mathbf{R}, \mathbf{p}, t) = f_\mathbf{p}^0 + \delta f(\mathbf{R}, \mathbf{p}, t)$, and using the relations

$$
\begin{aligned}
\nabla_\mathbf{R} U(\mathbf{R}, t)) &= \left.\frac{\partial U}{\partial \rho(\mathbf{R}, t)}\right|_{\rho(\mathbf{R},t)=\rho_0} \nabla_\mathbf{R} \delta\rho(\mathbf{R}, t), \\
\sum_\mathbf{p} \delta f(\mathbf{R}, \mathbf{p}, t) &= \delta\rho(\mathbf{R}, t),
\end{aligned}
\quad (8.98)
$$

we can immediately identify such equation with the Landau–Vlasov equation (1.119) in the absence of collisions, and with the only non-zero Landau parameter F_0 given by

$$F_0 = \nu(0) \left.\frac{\partial U}{\partial \rho}\right|_{\rho=\rho_0}, \quad (8.99)$$

where $\nu(0)$ is the density of states at the Fermi surface [see Eqs. (1.123) and (1.138)]. The Landau–Vlasov equations have been extensively used to study the collective modes of nuclei (see e.g. Brink, Dellafiore and Di Toro 1986).

The connection between the time-dependent Hartree theory and the Landau theory can also be evidenced in a direct fashion starting from the *RPA* response of equation (8.86). In fact, in the $q \to 0$, $\omega \to 0$ limit the free responses $\chi^0(q, \omega)$ of Section 7.7 have the limits

$$\chi_0^{3D}(q, \omega) = -\nu^{3D}(0)\Omega_{0,0}(s), \qquad \chi_0^{2D}(q, \omega) = -\nu^{2D}(0)\Lambda_{0,0}(s), \quad (8.100)$$

where $\Omega_{0,0}(s)$ and $\Lambda_{0,0}(s)$, with $s = \omega/qv_F$, are the functions which appear in the Landau theory, and are defined in (8.14) and (8.53), respectively. The Fourier transform of the interaction potential, in the same limit, tends to

$$v(0) = L^D \left.\frac{\partial U}{\partial \rho}\right|_{\rho=\rho_0}.$$

Hence, it is immediate to verify that in the $q \to 0$, $\omega \to 0$ limit, equation (8.86) tends to the results of equations (8.23) and (8.60), with $F_1 = F_2 = 0$ and with F_0 given by (8.99).

The identification of the RPA and Landau theories is feasible only in the $\hbar \to 0$ limit, i.e. long wavelength. The RPA theory incorporates quantum effects, which are absent in the Landau theory; as we will see, such terms may be important. Moreover, the RPA theory can be generalized to non-homogeneous systems like nuclei, metal clusters, quantum dots and free surfaces.

8.4 The RPA for the Electron Gas in Different Dimensions: The Plasmon

As an example of Fermion system, let us consider the electron gas in different dimensions, and let us study the RPA solutions. The energies of the RPA states are given by the solutions of equation (8.87) where $v(q)$ is given, in the different cases, in (8.80), and the free response functions were studied in Section 7.7. The graphical solution of such equation in $2D$ and $3D$ is outlined in Fig. 8.1, where we plot $\chi^0(q, \omega)$, for q fixed and much smaller than $2k_F$, as a function of ω, as well as the straight line for constant $1/v(q)$. Given the form of $v(q)$ for the electron gas, such straight line lies in the upper semi-plane, and the smaller q is, the nearer it is to the ω axis.
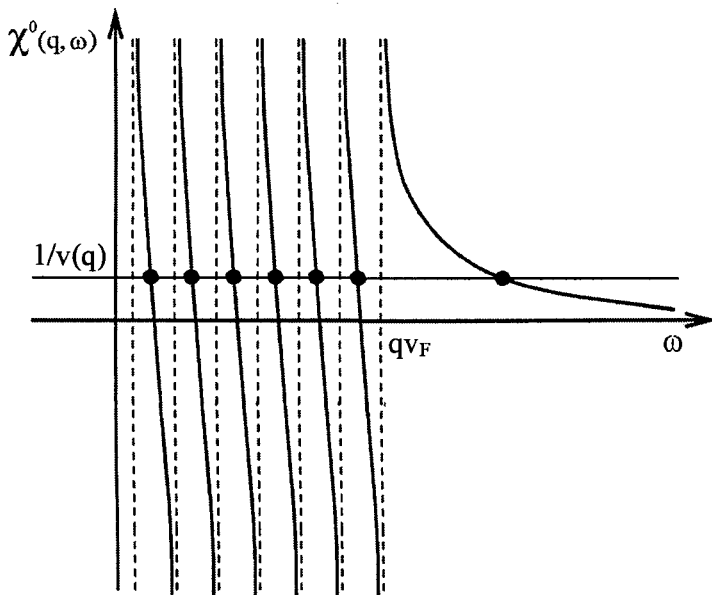
Fig. 8.1   Graphical solution of equation (8.87), for the $2D$ and $3D$ electron gas.

From this figure, we notice that the RPA energies, in the region of the poles of $\chi^0(q, \omega)$, are practically identical to the single-particle energies ϵ_{mi}, but besides these solutions, a new one emerges. This solution is, in general, known as the RPA "collective solution" (zero sound ^{3}He, plasmon for the electron gas, giant resonances for nuclei), in order to differentiate it from single-particle-like solutions. The smaller q is, the farther away the energy of such solution is from the single-particle continuum. Therefore, in order to study this new (with respect to the single-particle excitations) type of excitation, let us consider the limit of small q. In this limit we have $\omega \gg \epsilon_{mi}$, so that for $\chi^0(q, \omega)$ we can use the expansion

$$\chi^0(q, \omega) = \frac{2}{\omega^2} \left(m_1^{sp} + \frac{1}{\omega^2} m_3^{sp} + \cdots \right), \qquad (8.101)$$

where

$$m_1^{sp} = \frac{1}{2} \langle SD | [[\rho_{\mathbf{q}}^\dagger, [T, \rho_{\mathbf{q}}]]] | SD \rangle = \frac{Nq^2}{2m} \qquad (8.102)$$

and

$$m_3^{sp} = \frac{1}{2} \langle SD | [[\rho_{\mathbf{q}}^\dagger, T], [T, [T, \rho_{\mathbf{q}}]]] | SD \rangle = \frac{NT_0^D}{m^2} q^4 \qquad (8.103)$$

are the sum rules for the density operator of the non-interacting system (T is the kinetic energy operator, and $|SD\rangle$ is the ground state of the Fermi gas), and where T_0^D is the kinetic energy per particle of the Fermi gas:

$$T_0^D = \frac{D}{D+2} \frac{k_F^2}{2m}. \qquad (8.104)$$

Inserting these results into equation (8.87) we find for the energy of the RPA collective state the following

$$\omega_{RPA}^2 = \omega_p^2 + \frac{2T_0^D}{m} q^2, \qquad (8.105)$$

which is valid at order q^2, and where ω_p is the plasma frequency given by

$$\omega_p = \begin{cases} (1D) & \sqrt{\dfrac{2\lambda e^2}{m} q^2 |\ln qa|} \\[2ex] (2D) & \sqrt{\dfrac{2\pi e^2 q\sigma}{m}} \\[2ex] (3D) & \sqrt{\dfrac{4\pi e^2 \rho_0}{m}} \end{cases}, \qquad (8.106)$$

and $\lambda = N/L$ is the linear density, $\sigma = N/L^2$ the surface density, and $\rho_0 = N/L^3$ the bulk density.

Now let us compute the strength of the collective solution (8.105), using equation (8.91) in the limit of small q, in which the expansion of equations (8.101)–(8.103) for $\chi^0(q, \omega)$ holds. Using

$$\chi^0(q, \omega) \simeq \frac{Nq^2}{m\omega^2} \left(1 + \frac{2T_0^D}{m\omega^2} q^2 \right) ,$$

a simple calculation leads to the following result:

$$|\langle 0 | \rho_{\mathbf{q}} | \omega_{RPA} \rangle|^2 = \left(\frac{L^D}{v(q)} \right)^2 \frac{m\omega_{RPA}^3}{2Nq^2 (1 + \frac{4T_0^D q^2}{m\omega_{RPA}^2})} , \qquad (8.107)$$

from which we immediately have

$$\omega_{RPA} |\langle 0 | \rho_{\mathbf{q}} | \omega_{RPA} \rangle|^2 = \frac{Nq^2}{2m} , \qquad (8.108)$$

which is valid at order q^2, which means that the collective state completely exhausts the f-sum rule in the limit of small q. Therefore, in this limit, the whole strength is in this one state, and the dynamic form factor $S(\mathbf{q}, \omega)$, in the RPA approximation and for small q, can be written as

$$S^{RPA}(\mathbf{q}, \omega) \sim \frac{Nq^2}{2m\omega_p} \delta(\omega - \omega_p) . \qquad (8.109)$$

If we compare this result with the one of the independent-particle model, which in $3D$ case (that we took as an example, see Section 1.8.1) yielded for $q \ll k_F$:

$$S_{3D}(\mathbf{q}, \omega) = V \frac{m^2 \omega}{2\pi^2 q} \qquad \text{for } \omega < q v_F ,$$

$$S_{3D}(\mathbf{q}, \omega) = 0 \qquad \text{for } \omega > q v_F ,$$

we immediately see that the interaction has crucial effects, which lead to the prediction of a new kind of excited state, the plasmon, which was observed experimentally in the $3D$ case, by inelastic electron scattering on alkali metals (see Fig. 7.1) at an energy value that is in very good agreement with the RPA prediction (for $q \simeq 0$). For example, in the case of Sodium which has an experimental density corresponding to $r_s = 3.93$, one finds $(\omega_p = 4\pi e^2 \rho_0 / m)^{1/2} = 5.93$ eV, which is a value very close to the peak energy of Fig. 7.1 for $q \simeq 0$. Moreover, the q-dispersion of the RPA energy is positive, in agreement with the experimental data of Fig. 7.1 for Sodium.

The RPA strength taken by the collective state can be computed, not only in the small q limit, but for any q. The fraction $F(q)$ of f-sum rule exhausted by the collective state as a function of q is plotted in Fig. 8.2, as calculated in the $TDLDA$ theory (see Section 8.9.1), which takes into account the effect of exchange and correlations in some approximate way. From such figure we see that starting from a given q value (critical q), as q increases the strength taken by the collective
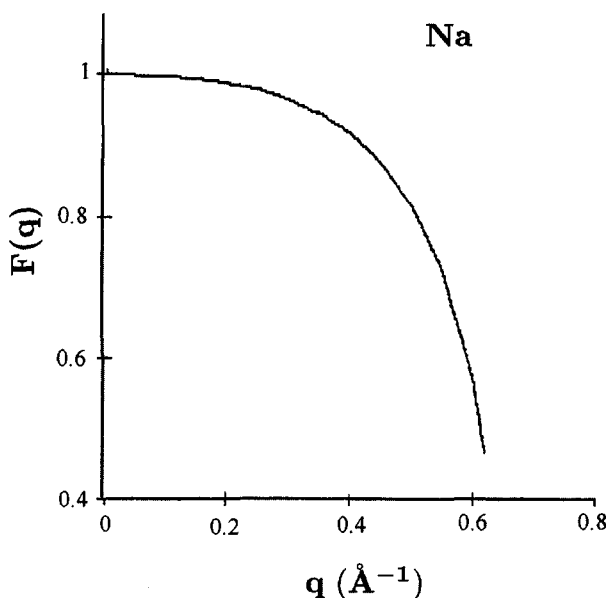
Fig. 8.2   Fraction $F(q)$ of m_1 f-sum rule for the density operator, concentrated in the volume plasmon for Sodium ($r_s = 3.93$).

state quickly drops to zero. The critical q is the q value at which the collective solution joins the continuum of one-particle–one-hole excited states, and the so-called Landau fragmentation of the strength takes place, or Landau damping of the collective state into single-particle states takes place. The Landau damping can be observed in the experimental curve of Fig. 7.1 as a broadening of the collective state with increasing q, which corresponds to the fragmentation of the strength into many states, rather than just into a collective one.

However, the agreement between the RPA theory and finite-q experiment is only qualitative. From a quantitative standpoint, there are important discrepancies, which are highlighted in Fig. 8.3. In this figure we plot the dispersion coefficient α of the experimental bulk plasmon dispersion, defined by the equation

$$E(q) = E(0) + \frac{\alpha}{m} q^2 , \qquad (8.110)$$

and normalized to the RPA dispersion coefficient: $\alpha_{RPA} = 3\epsilon_F/5\omega_p$, as a function of the Wigner-Seitz radius r_s. The experimental values were obtained by inelastic scattering experiments on Na, K, Rb and Cs (vom Felde et al. 1989), to which correspond the r_s values of 3.93, 4.86, 5.20 and 5.62, respectively. From this figure we notice that the experiment predicts a strong variation of α/α_{RPA} with r_s, which disagrees with the RPA theory. Even negative dispersion coefficients are observed for the r_s value corresponding to cesium. The divergences between the RPA results for the dispersion of the bulk plasmon and the experimental results, will form the object of further discussion in forthcoming Sections.
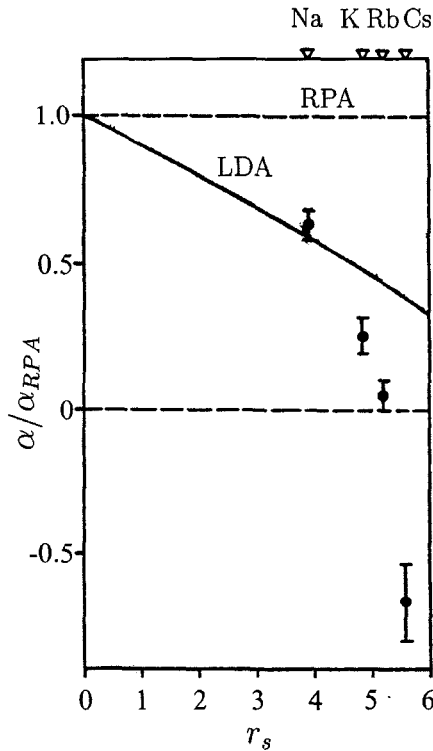
Fig. 8.3 Dispersion coefficient of the bulk plasmon, normalized to the *RPA* coefficient, as a function of r_s. The experimental data are from vom Felde et al. 1989. The constant dashed line at value 1 is the *RPA* prediction, the full line is the *TDLDA* prediction.

Unlike the $3D$ case, the plasmon frequency in $2D$ and $1D$ vanishes in the limit of small q. This important feature of the low-dimensionality plasmon was observed in $2D$ by Allen et al. (1986) in inversion layers, by Grimes and Adams (1976) for electrons on liquid helium, and in $1D$ by Goni et al. (1991) in quantum wires of GaAs. In Fig. 8.4 we report the experimental dispersion of the plasmon in the GaAs quantum wire, together with the *RPA* prediction of Quiang Li and Das Sarma (1989), (1991) and the *TDLDA* ones (see Section 8.9). As seen from the figure, there seems to be good agreement between theory and experiment.

As regards the dimensionality effects on the collective nature of the plasmon, we notice what follows. In $2D$ the behaviour of the *RPA* strength as a function of transferred momentum q is quite analogous to the $3D$ one, shown in Fig. 8.2. However, the situation is very different in one dimension. The fraction $F(q)$ of f-sum rule m_1 of the density operator, that is taken by the quasi-one-dimensional plasmon, and which specifies the relative importance of the plasmon and single-particle excitations, is plotted as a function of q in Fig. 8.5 for GaAs quantum wires of varying width and density.
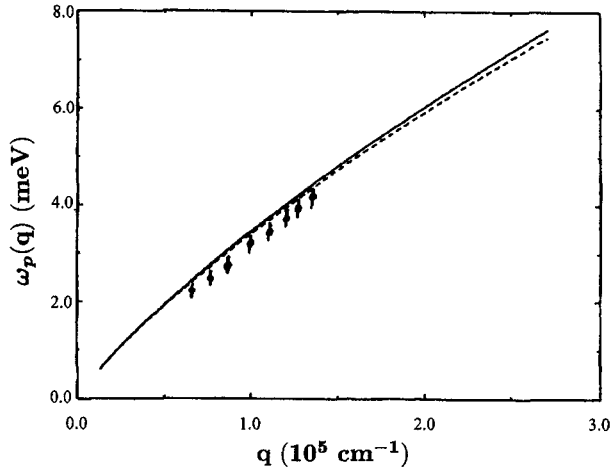
Fig. 8.4   Experimental results for the one-dimensional plasmon (Goñi et al. 1991), compared with the *RPA* (full line) and *TDLDA* (dashed line) theories.
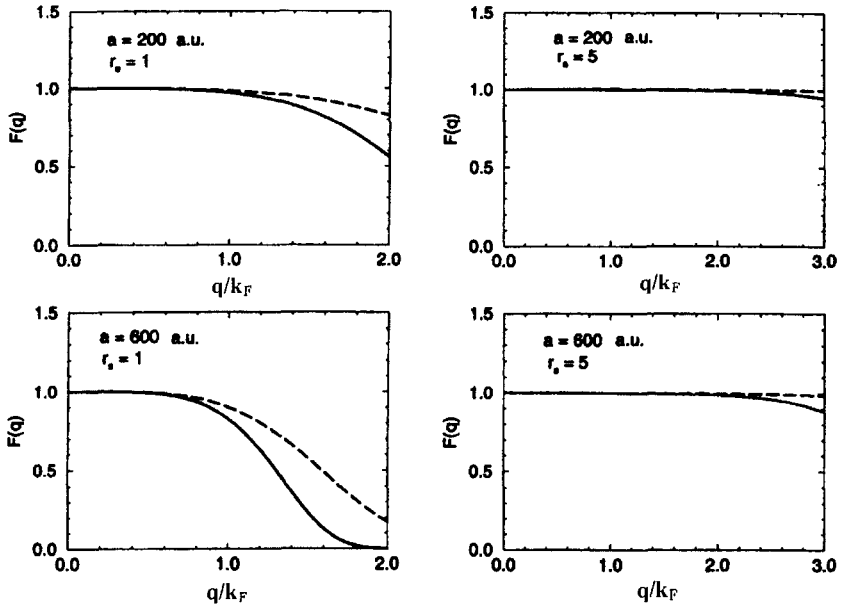
Fig. 8.5   The fraction $F(q)$ of f-sum rule m_1 for the density operator taken by the quasi-one-dimensional plasmon, for quantum wires of various widths and densities. The dashed lines are the *RPA* results, the full ones are the *TDLDA* ones (Agosti et al. 1998).

From the figures, it can be seen that the plasmon collective state in $1D$ dominates the excitation process in a very wide range of q values, much wider than in $3D$ and $2D$. Moreover, unlike the $3D$ and $2D$ cases, in $1D$ the continuum of single-particle states has a gap [see Eq. (1.95) and Fig. 7.3]. This has the consequence that there exist (undamped) collective states for the $1D$ system even for attractive interaction for which $v(q)$ is negative, and that for a wide range of q-values the excitation spectrum in $1D$, unlike the $2D$ and $3D$ ones, is always dominated by collective states. As we will see in the next section, this is analogous to what happens for Boson systems. As a result, the $1D$ system is more resemblance of a Tomonaga-Luttinger liquid (Tomonaga 1950; Luttinger 1963), where it is assumed that the excitations have Boson nature, rather than to a Fermi liquid in which the excitations are of the Fermion type.

8.5 RPA for Bosons

For systems of Bosons, the energies of the RPA states are still given by the solutions of equation (8.87), where $v(q)$ is now the Fourier transform of the interaction among Boson atoms, and the free response function was studied in Section 7.7 and is given in (7.111):

$$\chi_0^B(\mathbf{q}, \omega) = \frac{\frac{Nq^2}{m}}{\omega^2 - (\frac{q^2}{2m})^2}.$$

Using the result of (8.87), we obtain for the energy of the RPA solution:

$$\omega = \sqrt{\frac{\rho q^2 v(q)}{m} + \left(\frac{q^2}{2m}\right)^2}. \tag{8.111}$$

In the limit of small transferred momentum q, equation (8.111) leads to the phonon-like dispersion relation:

$$\omega \simeq cq, \qquad c = \sqrt{\frac{\rho v(0)}{m}}, \tag{8.112}$$

whlich is linear in q. Therefore, at small q the interaction changes the q-dependence of the RPA excitations with respect to the q^2 term of the independent-particle model. The elementary excitations of the Bose systems are different from the single-particle excitations, and are of phonon type. This fact has a very important consequence on the thermodynamics of Boson systems. In fact, thermodynamic properties based on phonon-like elementary excitations are completely different from those based on single-particle-like elementary excitations. For example in a system of Boson atoms, the specific heat is no longer linear with the temperature as in (1.117) (which holds for Fermions), but rather grows like T^3 (see for example Huang 1987).
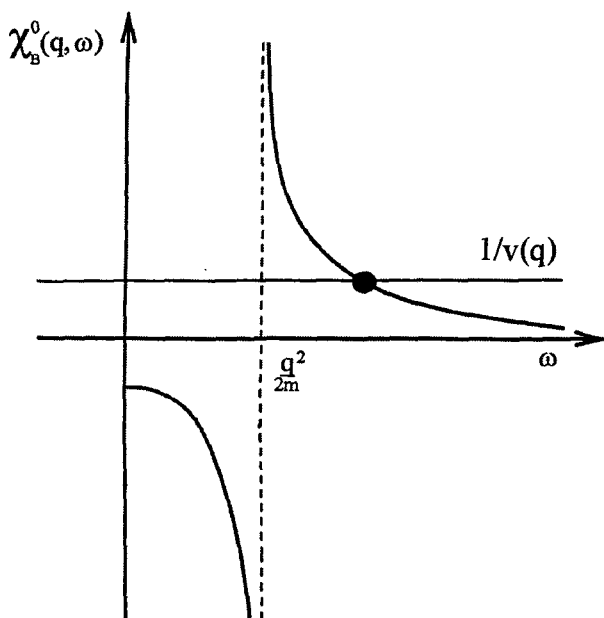
Fig. 8.6   Graphical solution of equation (8.87), for Bosons.

The graphical solution of the RPA equations for Bosons is outlined in Fig. 8.6, where we plot $\chi^0(q,\omega)$ as a function of ω, as well as the straight line of constant value $1/v(q)$.

From this figure we see that the single-particle state at $q^2/2m$ disappears completely, and what is left is only the collective phonon state with dispersion law given by (8.111). Such dispersion law is plotted in Fig. 8.7 for superfluid ^{4}He, together with the experimental data of Donnelly et al. (1981). The function $v(q)$ is fixed, through equation

$$\chi(q) = \frac{\chi^0(q)}{1 - \frac{v(q)}{L^D}\chi^0(q)}, \qquad (8.113)$$

by the static response function, which is experimentally known in superfluid ^{4}He and is plotted in Fig. 8.8.

As can be observed from Fig. 8.7, the RPA prediction explains quite well all the features of the experimental excitation spectrum, i.e. the low-q phonon linear regime, the single-particle quadratic regime at high q when the interaction term in equation (8.111) becomes negligible, and lastly the roton minimum at intermediate q. However, from a quantitative point of view, it over-estimates the experimental result. Such discrepancy between theory and experiment will be further discussed later on, together with the discrepancy found in the case of bulk plasmon dispersion.
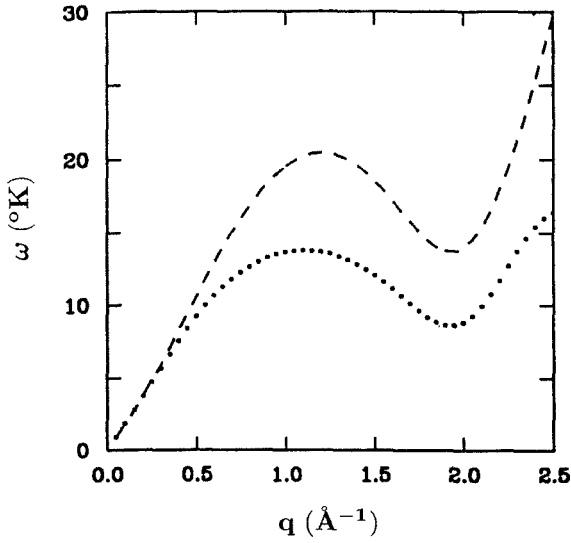
Fig. 8.7 Dispersion of the elementary excitations in superfluid ^{4}He. The dashed line is the *RPA* result (8.111). The dots are the experimental data by Donnelly et al. (1981).
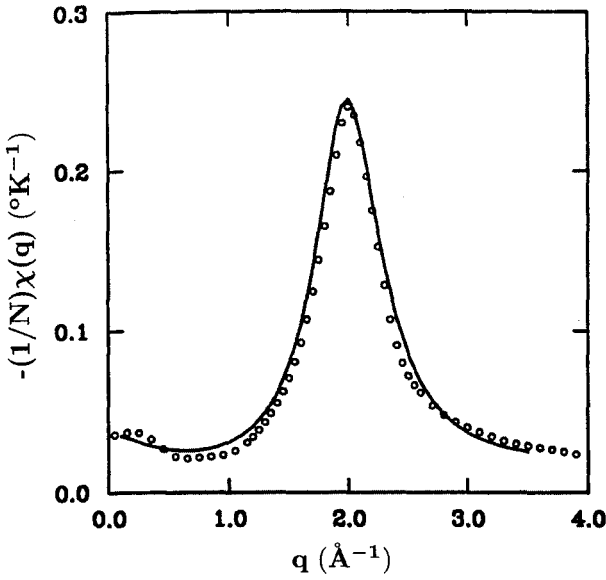
Fig. 8.8 Static response function of superfluid ^{4}He. The full line is the density functional result of Dalfovo et al. (1995). The dots are the experimental results by Woods and Cowley (1973).

Recalling that in the $q \to 0$ limit the static polarizability $\chi(q)$ tends to $-N\rho K$, where K is the isothermal compressibility of the system, and that for Bosons the compressibility of the non-interacting system is infinite, thus starting from equation (8.113), it is possible to connect the interaction $v(q)$ (for $q \to 0$) to the compressibility:

$$v(0) = \frac{1}{K\rho^2} \, . \tag{8.114}$$

Therefore, the coefficient c of the phonon dispersion relation (8.112) is determined by the system compressibility:

$$c = \sqrt{\frac{1}{mK\rho}} \, , \tag{8.115}$$

and gives the propagation velocity of sound in the system. In the case of a cold and dilute Boson gas, for which it is possible to replace the two-body interaction by an effective interaction given by $v(r) = g\delta(r)$, where the constant g is determined by the scattering length a through $g = 4\pi a/m$, we have $v(q) = g$, and in this case the *RPA* frequency dispersion is given by

$$\omega = \sqrt{\frac{\rho q^2 g}{m} + \left(\frac{q^2}{2m}\right)^2} \, . \tag{8.116}$$

Note that for attractive interactions $(a < 0)$, the frequency ω becomes imaginary at small q, evidencing a system instability (see Section 2.4).

From an unrestricted point of view, the following general considerations apply to quantum liquids with elementary-excitation dispersion law having a form as in Fig. 8.7:

(i) At thermal equilibrium, most of the elementary excitations of the system have energies close to the minima of the curve $\omega(q)$, i.e. near $\omega = 0$ and $\omega(q_0)$, where q_0 is the momentum value where the roton minimum lies. Therefore, such minima have a paramount importance for the properties of the quantum liquid. In particular, in the neighborhood of the roton minimum it is possible to expand $\omega(q)$ as a function of $q - q_0$, thus obtaining, at second order, $\omega(q) = \Delta + (q - q_0)^2/2m^*$. Starting from this result it is possible to compute the contribution of rotons (i.e. the elementary excitations with this energy) to the thermodynamic functions of the system; the roton contribution may by greater than that of the phonon at sufficiently high temperatures.

(ii) These systems have the property of superfluidity, i.e. of flowing through narrow capillaries or fissures with no viscosity.

For a detailed description of these phenomena, see for example the books of Lifchitz and Pitaevskii (1981) and Pines and Nozières (1990).

8.6 The Time-Dependent Gross–Pitaevskii Theory

The Hamiltonian of N interacting Bosons can be written in second-quantization formalism as

$$\hat{H} = \int dr \hat{\Phi}^\dagger(\mathbf{r}) \left(\frac{-\nabla^2}{2m} + v_{\text{ext}}(\mathbf{r}) \right) \hat{\Phi}(\mathbf{r})$$

$$+ \frac{1}{2} \int dr dr' \hat{\Phi}^\dagger(\mathbf{r}) \hat{\Phi}^\dagger(\mathbf{r}') v(\mathbf{r} - \mathbf{r}') \hat{\Phi}(\mathbf{r}) \hat{\Phi}(\mathbf{r}'), \qquad (8.117)$$

where $\hat{\Phi}(\mathbf{r})$ and $\hat{\Phi}^\dagger(\mathbf{r})$ are the Boson field operators which annihilate and create a particle, respectively, at $\mathbf{r}$. Note that using in (8.117) the expansion $\hat{\Phi}(\mathbf{r}) = \sum_\alpha \varphi_\alpha(\mathbf{r}) a_\alpha$, where the $\varphi_\alpha(\mathbf{r})$ are single-particle wavefunctions and a_α are the corresponding annihilation operators, we obtain for Bosons, the equivalent of equations (2.65)–(2.67), which were derived in Section 2.5 in the case of N interacting Fermions.

For a homogeneous gas in a volume V, we have

$$\hat{\Phi}(\mathbf{r}) = \frac{1}{\sqrt{V}} \sum_{\mathbf{p}} e^{i\mathbf{p}\cdot\mathbf{r}} a_{\mathbf{p}}, \qquad N = \int dr \hat{\Phi}^\dagger(\mathbf{r}) \hat{\Phi}(\mathbf{r}) = \sum_{\mathbf{p}} a_{\mathbf{p}}^\dagger a_{\mathbf{p}}. \qquad (8.118)$$

The Bose–Einstein condensation (BEC) occurs when the number n_0 of atoms that occupy a particular single-particle state becomes very large: $n_0 \equiv N_0 \gg 1$, and the ratio N_0/N stays finite in the thermodynamic limit $N \to \infty$. BEC occurs in a single-particle state $\varphi_0 = 1/\sqrt{V}$ with momentum $\mathbf{p} = 0$, and the operators relative to such state, a_0 and $a_0^\dagger$, can be treated as numbers: $a_0 = a_0^\dagger = \sqrt{N_0}$. Therefore, the field operator $\hat{\Phi}(\mathbf{r})$ can be decomposed in the form

$$\hat{\Phi}(\mathbf{r}) = \sqrt{\frac{N_0}{V}} + \hat{\Phi}'(\mathbf{r}). \qquad (8.119)$$

Treating the operator $\hat{\Phi}'(\mathbf{r})$ as a perturbation, Bogoliubov (1947) set up a first-order theory for the elementary excitations of Bose gases which, as we will see, yields the same *RPA* results of Section 8.5.

The generalization of the Bogoliubov theory for non-uniform systems and time-dependent configurations is given by

$$\hat{\Phi}(\mathbf{r}, t) = \Psi(\mathbf{r}, t) + \hat{\Phi}'(\mathbf{r}, t), \qquad (8.120)$$

where we used the Heisenberg representation for the field operators. $\Psi(\mathbf{r}, t)$ is a complex function defined as the expectation value of the field operator:

$$\Psi(\mathbf{r}, t) = \langle \hat{\Phi}(\mathbf{r}, t) \rangle.$$

Its modulus identifies the density of the condensate: $\rho_0 = |\Psi(\mathbf{r}, t)|^2$. The function $\Psi(\mathbf{r}, t)$ is a classical field which has the meaning of an order parameter, and is often named "wavefunction of the condensate" (for further considerations, see Dalfovo

et al. 1999). The decomposition (8.120) is especially useful when $\hat{\Phi}'(\mathbf{r}, t)$ is small, i.e. when the number of particles outside the condensate is small. In this case, it is possible to derive an equation for the order parameter by expanding the theory at first order in $\hat{\Phi}'(\mathbf{r}, t)$, like in the case of homogeneous systems. Unlike the latter, we obtain a non-trivial theory at zero order for $\Psi(\mathbf{r}, t)$. To obtain the theory, we start from the Heisenberg equation for the Hamiltonian (8.117) ($\hbar = 1$):

$$i\frac{\partial}{\partial t}\hat{\Phi}^\dagger(\mathbf{r}, t) = [\hat{\Phi}^\dagger, \hat{H}]$$

$$= \left(-\frac{\nabla^2}{2m} + v_{\text{ext}}(\mathbf{r}) + \int d\mathbf{r}'\hat{\Phi}^\dagger(\mathbf{r}', t)v(\mathbf{r} - \mathbf{r}')\hat{\Phi}(\mathbf{r}', t)\right)\hat{\Phi}(\mathbf{r}, t), \quad (8.121)$$

and we replace the operator $\hat{\Phi}$ by the classical field Ψ. This approximation turns out to be a very good one in the case of a cold and dilute atom gas, for which only low-energy two-body interactions are important, which can be described by the effective interaction of Section 2.4: $v(\mathbf{r} - \mathbf{r}') = g\delta(\mathbf{r} - \mathbf{r}')$ with $g = 4\pi a/m$ and a the scattering length in s wave. The use of such effective interaction in (8.121) is consistent with the replacement of $\hat{\Phi}$ by the classical field Ψ, and leads to the time-dependent Gross–Pitaevskii (GP) equations (Gross 1961, 1963; Pitaevskii 1961):

$$i\frac{\partial}{\partial t}\Psi(\mathbf{r}, t) = \left(\frac{-\nabla^2}{2m} + v_{\text{ext}}(\mathbf{r}) + g|\Psi(\mathbf{r}, t)|^2\right)\Psi(\mathbf{r}, t). \quad (8.122)$$

Equations (8.122) hold in the limit where the scattering length is much smaller than the average inter-atomic distance, and when the number of atoms in the condensate is much greater than 1 (for more details, see e.g. Dalfovo et al. 1999).

   Due to the assumption $\Phi' = 0$, the above equations strictly hold only in the limit of zero temperature, when all particles are in the condensate. Before discussing the dynamic behaviour and the finite-temperature generalization, we will consider their stationary solution at zero temperature which, as will be shown, coincides with the Hartree–Fock theory discussed in Section 2.4. In order to obtain the ground state, we write the wavefunction of the condensate as $\Psi(\mathbf{r}, t) = \Psi(\mathbf{r})\exp(-i\mu t)$, where μ is the chemical potential, and Ψ is real and normalized to the total number of particles, $\int d\mathbf{r}\Psi^2 = N_0 = N$. Then, the Gross–Pitaevskii equation (8.122) becomes

$$\left(\frac{-\nabla^2}{2m} + v_{\text{ext}}(\mathbf{r}) + g\Psi^2(\mathbf{r})\right)\Psi(\mathbf{r}) = \mu\Psi(\mathbf{r}), \quad (8.123)$$

and is completely equivalent to the Hartree–Fock equations (2.60) with $\Psi(\mathbf{r}) = \sqrt{N}\varphi(\mathbf{r})$. The solutions of these equations were discussed in Sections 2.4 and 4.3.2.

   In the dynamic case and in the low-temperature limit, where the properties of excitations do not depend on temperature, the excited states may be found from the frequencies ω of the GP equations. We look for solutions of the type

$$\Psi(\mathbf{r}, t) = e^{-i\mu t}[\Psi(\mathbf{r}) + u(\mathbf{r})e^{-i\omega t} + v^*(\mathbf{r})e^{i\omega t}] \quad (8.124)$$

which correspond to small oscillations of the order parameter around the ground-state value. Retaining terms linear in the complex functions u and v, the GP equations (8.122) become

$$\omega u(\mathbf{r}) = [H_0 - \mu + 2g\Psi^2(\mathbf{r})]u(\mathbf{r}) + g\Psi(\mathbf{r})^2 v(\mathbf{r})$$
$$-\omega v(\mathbf{r}) = [H_0 - \mu + 2g\Psi^2(\mathbf{r})]v(\mathbf{r}) + g\Psi(\mathbf{r})^2 u(\mathbf{r})$$

(8.125)

where $H_0 = -\nabla^2/2m + v_{\text{ext}}(\mathbf{r})$. These coupled equations allow the calculation of the energies ω of the excitations. In a homogeneous gas, the amplitudes u and v are plane waves and $\mu = g\Psi^2(\mathbf{r})$. The resulting dispersion law is (Bogoliubov 1947)

$$\omega^2 = \frac{q^2}{2m}\left(\frac{q^2}{2m} + 2g\rho\right).$$

(8.126)

where $\rho = \Psi^2(\mathbf{r})$ is the gas density, and is the same as the *RPA* result of (8.116). For large momentum q the spectrum coincides with the single-particle one, while for low q values the dispersion is phonon-like.

In the case of harmonic confinement of a finite number of atoms, the GP equations yield either single-particle or phonon-like solutions according to whether the ratio Na/a_{ho} ($a_{ho} = \sqrt{1/m\omega_{ho}}$) is much smaller or much larger than 1, respectively.

The coupled equations (8.125) were solved by several authors in order to compute the excited states of confined gases (Edwards et al. 1996; Ruprecht et al. 1996; Singh and Rokhsar 1996; Dalfovo et al. 1997; Esry 1997; Hutchinson and Zaremba 1997; Hutchinson, Zaremba and Griffin 1997; You, Hoston and Lewenstein 1997). Equations (8.125) also allow the calculation of the density of particles flowing out of the condensate at zero temperature (quantum depletion), by summing the squared modulus of the "hole" amplitude v over all excited states: $\rho_{out} = \sum_j |v_j(\mathbf{r})|^2$ (Fetter 1972; Dalfovo et al. 1997; Hutchinson, Zaremba and Griffin 1997).

For spherical traps the solutions of (8.125) are characterized by quantum numbers n_r, l, and m, where n_r is the number of radial nodes, l is the angular momentum of the excitation, and m its z component. For traps with axial symmetry, m is still a good quantum number. In Fig. 8.9 we show the lowest energy solutions of even parity with $m = 0$ and $m = 2$, for a gas of Rubidium atoms confined into an axial symmetry trap ($\omega_x = \omega_y = \omega_\perp$). The deformation parameter of the trap, $\omega_z/\omega_\perp = \sqrt{8}$, corresponds to the experimental conditions of Jin et al. (1996), and values of N up to 10^4 are considered. The agreement between theory and experiment is very good, and evidences the importance of the interaction. In fact, without interaction the two modes would be degenerate at energy $\omega = 2\omega_\perp$.

The spectrum resulting from the numerical solution of the GP equations (8.125) is shown in Fig. 8.10 for a condensate of 10^4 Rubidium atoms in a spherical trap (Dalfovo et al. 1997). Each state with energy ω and angular momentum l, is represented by a full bar. For fixed angular momentum, the number of radial nodes, n_r increases with energy. Looking at the high-energy and high-multipolarity eigenstates, we note that the splitting between even and odd states is approximately
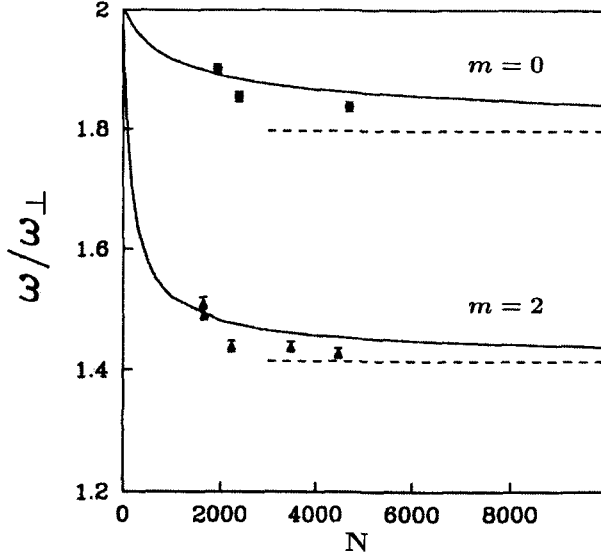
Fig. 8.9 Frequencies (in units of $\omega_\perp$) of collective excitation modes of even parity with $m = 0$ and $m = 2$, for N Rubidium atoms in a symmetric axial trap (see text). The dots are experimental data of Jin et al. (1996). The full lines are the predictions of the Gross–Pitaevskii equations with $a/a_\perp$ equal to $3.37 10^{-3}$ ($a_\perp = \sqrt{1/m\omega_\perp}$). The dashed lines are the asymptotic results for $Na/a_\perp \to \infty$, (Stringari 1996).
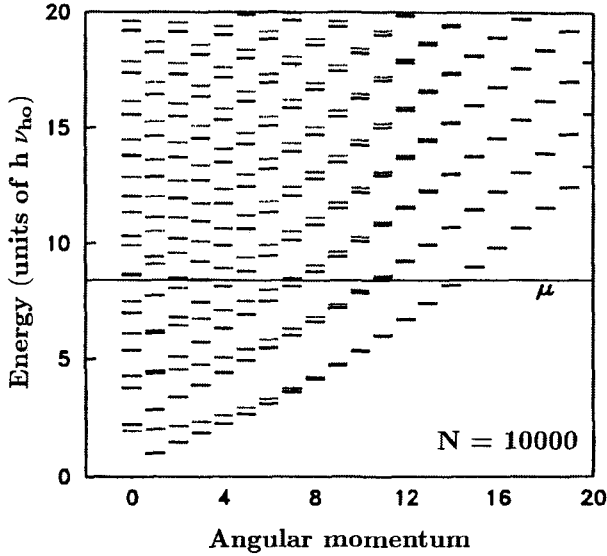
Fig. 8.10 Excitation spectrum of a dilute gas of Rubidium atoms in a spherical trap with $a_{ho} = 0.791\mu m$. Full lines: solutions of the time-dependent GP equations. Dashed lines: single-particle spectrum for the Hamiltonian (8.127). The horizontal line is the chemical potential in units of ω_{ho}.

equal to ω_0, and that the spectrum is similar to that of a $3D$ harmonic oscillator. However, the states with the same value of $2n_r + l$ are not exactly degenerate like in the case of the harmonic oscillator; rather, the states with lower angular momentum are shifted to high energy due to the mean field produced by the condensate in the central region of the trap. The high-energy range of the spectrum is well reproduced by a mean-field description. Such description can be obtained from the GP equations by neglecting the coupling between the positive-energy (u) and negative-energy (v) components of the order parameter (8.124), which is responsible for the collective nature of the solutions. This corresponds to putting $v = 0$ in the first equation (8.125), which reduces to the eigenvalue problem $(H_{sp} - \mu)u = \omega u$, for the single-particle Hamiltonian

$$H_{sp} = \frac{-\nabla^2}{2m} + v_{\text{ext}}(\mathbf{r}) + 2g\rho(\mathbf{r})\,. \tag{8.127}$$

In this case, the eigenfunctions u fulfill the normalization conditions

$$\int d\mathbf{r} u_i^*(\mathbf{r}) u_j(\mathbf{r}) = \delta_{ij}\,.$$

In many body theory, this approximation is identical to the one known as the Tamm-Dancoff approximation (see next Section), and may also be considered as the zero-temperature limit of the HF theory at finite temperature [see the second Eq. (2.98)]. For this reason, in the literature the mean-field spectrum of Fig. 8.10 is sometimes referred to as the HF spectrum. Once we know how to compute the chemical potential and the condensate density through the static GP equations (8.123), it is easy to obtain the mean-field-like spectrum for Hamiltonian (8.127). The mean-field energies are shown in Fig. 8.10 by dashed horizontal bars. We notice that the general structure of the spectrum is very similar to the one yielded by the GP equations, apart from the low-energy, low-multipolarity states. In fact, the latter are the collective states that we discussed previously, which cannot be described by single-particle theories. In principle, one would expect that such low-energy states might influence the Boson system thermodynamics at low temperature, thereby making the finite-temperature mean-field theory incorrect in this range (i.e. around the critical temperature), while the theory should work well at high temperatures where single-particle excitations play the prominent role. In practice, for confined systems the thermodynamics is governed by surface excitations, which are very well reproduced by the mean-field theory even at low energy (Giorgini, Pitaevskii and Stringari 1997). Thus, and unlike what happens in homogeneous systems where phonons dominate the thermodynamic behaviour of the system, and the finite-temperature HF theory is unphysical at low temperature, in confined systems HF at finite temperature may be used to describe the thermodynamics of the system even at very low temperatures.

A theory that describes correctly both the high-temperature and low-temperature regimes, is the so-called Popov approximation (Popov 1965, 1987;

Griffin 1996). This approximation is based on the one hand on the extension to temperature T of the GP equation [see the first of Eq. (2.98)] in which the interaction among atoms of the condensate and outside the condensate is explicitly considered, and on the other hand on Bogoliubov type equations for the system excitations. The equations have the form

$$\left(\frac{-\nabla^2}{2m} + v_{\text{ext}}(\mathbf{r}) + g[\rho_0 + 2\rho_T]\right)\Psi = \mu\Psi\,, \qquad (8.128)$$

and

$$\begin{aligned}
\epsilon_i u_i(\mathbf{r}) &= [H_0 - \mu + 2g\rho(\mathbf{r})]u_i(\mathbf{r}) + g\rho_0(\mathbf{r})v_i(\mathbf{r})\,, \\
-\epsilon_i v_i(\mathbf{r}) &= [H_0 - \mu + 2g\rho(\mathbf{r})]v_i(\mathbf{r}) + g\rho_0(\mathbf{r})u_i(\mathbf{r})\,,
\end{aligned} \qquad (8.129)$$

where $H_0 = -\nabla^2/2m + v_{\text{ext}}(\mathbf{r})$ and $\rho_0 = |\Psi(\mathbf{r})|^2$ is the density of the condensate, while ρ_T is the density of thermal particles, given by

$$\rho_T = \sum_j (|u_j|^2 + |v_j|^2)[\exp(\beta\epsilon_j) - 1]^{-1}, \quad (\beta = 1/KT) \qquad (8.130)$$

with u_j, v_j and ϵ_j solutions of equations (8.129). Now, these quantities depend on temperature. The sum $\rho = \rho_0 + \rho_T$ is the total density. The functions u_j, v_j are normalized according to the condition

$$\int d\mathbf{r}[u_i^*(\mathbf{r})u_j(\mathbf{r}) - v_i^*(\mathbf{r})v_j(\mathbf{r})] = \delta_{ij}\,. \qquad (8.131)$$

In the Popov approximation, the thermal component is treated as a thermal bath that produces a static external field in the condensate equation. One ignores quantum depletion at zero temperature, which is given by $\rho_{\text{out}} = \sum_j |v_j|^2$, and which is very small for the trapped gases. Then, at very low temperature, when ρ_T is negligible with respect to ρ_0, equation (8.128) coincides with the stationary GP equation (8.123), and the equations (8.129) coincide with (8.125). Results obtained by solving the Popov equations are found in Dalfovo et al. (1999) and Giorgini et al. (1997). By comparing the thermodynamic properties of the Boson systems as obtained by the Popov theory with those of the finite-temperature HF theory (see Section 2.6), we note that while for homogeneous gases the phonons (i.e. the low-energy collective states that are taken into account only in the Popov theory) are always relevant in the calculation of thermodynamic properties, in the case of confined gases the HF approximation turns out to be excellent even at relatively low temperatures. As already discussed, this is due to the fact that at such temperatures the main contribution to thermodynamic properties comes from surface excitations, which are well reproduced by the HF theory.

8.7 Time Dependent Hartree–Fock (*TDHF*) and the Matrix *RPAE*

In this Section we look for solutions for the equation:

$$\frac{\delta I}{\delta \phi} = 0 \,,$$

where, in the case of fermions, the action I is given by

$$I = \int_{t_1}^{t_2} \langle \phi_{SD}(t)|H - i\frac{\partial}{\partial t}|\phi_{SD}(t)\rangle dt \,, \tag{8.132}$$

where $H = H_{HF} + V_{\text{res}}$, and $\phi_{SD}(t)$ is a Slater determinant. We recall that (see Chapter 2) the HF Hamiltonian H_{HF} and the residual interaction V_{res} have the following properties:

$$\langle HF|H_{HF}|HF\rangle = E_{HF}, \qquad H_{HF}|i^{-1},m\rangle = \varepsilon_{m,i}|i^{-1},m\rangle \,,$$

where $\varepsilon_{m,i} = \varepsilon_m - \varepsilon_i$, $|HF\rangle$ is the HF ground state and $|i^{-1},m\rangle = a_m^\dagger a_i|HF\rangle$, and

$$\langle HF|V_{\text{res}}|HF\rangle = 0, \qquad \langle HF|V_{\text{res}}|i^{-1},m\rangle = 0 \,,$$

$$V_{m,j,i,n} = \langle i^{-1},m|V_{\text{res}}|j^{-1},n\rangle \neq 0 \,,$$

$$V_{i,j,m,n} = \langle HF|V_{\text{res}}|i^{-1},m,j^{-1},n\rangle \neq 0 \,,$$

$$V_{m,n,i,j} = \langle i^{-1},m,j^{-1},n|V_{\text{res}}|HF\rangle \neq 0 \,.$$

In order to derive the $TDHF$ equations, in the limit of small oscillations around the equilibrium configuration, let us write the generic Slater determinant $\phi_{SD}(t)$ of equation (8.132) by use of the Thouless theorem [see Eq. (2.69)]:

$$|\phi_{SD}(t)\rangle = e^{\sum_{m,i} C_{m,i}(t) a_m^\dagger a_i}|HF\rangle \,. \tag{8.133}$$

Then, the equations for the coefficients $C_{m,i}$ are obtained from equations (8.70), (8.132) and (8.133) by expanding (8.132) up to second order in $C_{m,i}$, and using the above properties. We find

$$\langle \phi_{SD}(t)|H - i\frac{\partial}{\partial t}|\phi_{SD}(t)\rangle$$

$$= E_{HF} + \sum_{m,i}\langle HF|\left(H_{HF} + V_{\text{res}} - i\frac{\partial}{\partial t}\right)C_{m,i}|i^{-1},m\rangle$$

$$+ \sum_{m,i}\langle i^{-1},m|C_{m,i}^*\left(H_{HF} + V_{\text{res}} - i\frac{\partial}{\partial t}\right)|HF\rangle$$

$$+ \sum_{m,i,n,j}\langle i^{-1},m|C_{m,i}^*\left(H_{HF} + V_{\text{res}} - i\frac{\partial}{\partial t}\right)C_{n,j}|j^{-1},n\rangle$$

$$+ \frac{1}{2} \sum_{m,i,n,j} \langle i^{-1}, m, j^{-1}, n | C^*_{m,i} C^*_{n,j} \left(H_{HF} + V_{\text{res}} - i \frac{\partial}{\partial t} \right) | HF \rangle$$

$$+ \frac{1}{2} \sum_{m,i,n,j} \langle HF | \left(H_{HF} + V_{\text{res}} - i \frac{\partial}{\partial t} \right) C_{m,i} C_{n,j} | i^{-1}, m, j^{-1}, n \rangle$$

$$= E_{HF} + \sum_{m,i} |C_{m,i}|^2 \varepsilon_{m,i} + \sum_{m,i,n,j} C^*_{m,i} C_{n,j} V_{m,j,i,n} - i \sum_{m,i} C^*_{m,i} \dot{C}_{m,i}$$

$$+ \frac{1}{2} \sum_{m,i,n,j} C^*_{m,i} C^*_{n,j} V_{m,n,i,j} + \frac{1}{2} \sum_{m,i,n,j} C_{m,i} C_{n,j} V_{i,j,m,n} \, . \tag{8.134}$$

Bt requiring $\delta I = \frac{\delta I}{\delta C^*_{m,i}} \delta C^*_{m,i} = 0$, we find

$$\delta I = \int_{t_1}^{t_2} \left[\sum_{m,i} \left(C_{m,i} \varepsilon_{m,i} + \sum_{n,j} C_{n,j} V_{m,j,i,n} - i \dot{C}_{m.i} \right. \right.$$

$$\left. \left. + \sum_{n,j} C^*_{n,j} V_{m,n,i,j} \right) \delta C^*_{m,i} \right] dt = 0$$

and since the variations $\delta C^*_{m,i}$ are arbitrary, the final equations for the coefficients $C_{m,i}$ are

$$i \dot{C}_{m,i} = C_{m,i} \varepsilon_{m,i} + \sum_{n,j} (C_{n,j} V_{m,j,i,n} + C^*_{n,j} V_{m,n,i,j}) \, . \tag{8.135}$$

Let us now look for solutions to equation (8.135) that oscillate in time with frequency ω, of the form

$$C_{m,i}(t) = Y_{m,i} e^{-i\omega t} + Z^*_{m,i} e^{i\omega t} \, . \tag{8.136}$$

We obtain

$$\varepsilon_{m,i}(Y_{m,i} e^{-i\omega t} + Z^*_{m,i} e^{i\omega t}) + \sum_{n,j} [V_{m,j,i,n}(Y_{n,j} e^{-i\omega t} + Z^*_{n,j} e^{i\omega t})$$

$$+ V_{m,n,i,j}(Y^*_{n,j} e^{i\omega t} + Z_{n,j} e^{-i\omega t})] = \omega Y_{m,i} e^{-i\omega t} - \omega Z^*_{m,i} e^{i\omega t} \, , \tag{8.137}$$

and by equating the coefficients of the exponentials with $\pm \omega$, we find a system of coupled equations for $Y_{m,i}$ and $Z_{m,i}$:

$$\varepsilon_{m,i} Y_{m,i} + \sum_{n,j} [V_{m,j,i,n} Y_{n,j} + V_{m,n,i,j} Z_{n,j}] = \omega Y_{m,i}$$

$$\varepsilon_{m,i} Z_{m,i} + \sum_{n,j} [V_{i,n,m,j} Z_{n,j} + V_{i,j,m,n} Y_{n,j}] = -\omega Z_{m,i} \, . \tag{8.138}$$

[Note that in order to derive these equations, we used $V_{i,j,m,n} = (V_{m,n,i,j})^*$.] Hereafter, equations (8.138) will be denoted as the $RPAE$ equations, in order to distinguish them from the RPA equations in which exchange effects are neglected both in single-particle energies and in the matrix elements. These equations, which are particularly suited to study the excited states of non-homogeneous systems like metal clusters and nuclei, are eigenvalue equations whose solution yields the excitation energies ω of the $RPAE$ states, as well as the matrix elements of an excitation operator F between the ground and the excited states: $\langle 0|F|n\rangle$.

Linear $RPA-TDHF$ equations, of the kind of equations (8.138), can be derived also for Bosons systems like, e.g. the dilute and cold gas of alkali atoms treated in the previous Section by means of the Gross–Pitaevskii theory. In this case, the HF wavefunction of the condensate is written as $|HF\rangle = \phi_i(\mathbf{r_1})\phi_i(\mathbf{r_2})\cdots\phi_i(\mathbf{r_N})$, and the one-particle–one-hole states which appear in the Thouless theorem (8.133) can be obtained starting from the complete set of single-particle wavefunctions which are eigenstates of the Hamiltonian

$$H_{sp} = -\frac{\nabla^2}{2m} + v_{\text{ext}}(\mathbf{r}) + g\rho_0(\mathbf{r})\,,$$

where ρ_0 is the density of the condensate. Following the track of calculation performed above for Fermions, one easily gets the result

$$\varepsilon_{m,i}Y_{m,i} + g\sum_n \left[\int d\mathbf{r}\phi_m^*(\mathbf{r})\phi_n(\mathbf{r})\rho(\mathbf{r})Y_{n,i} + \int d\mathbf{r}\phi_m^*(\mathbf{r})\phi_n(\mathbf{r})\rho(\mathbf{r})Z_{n,i}\right] = \omega Y_{m,i}\,,$$

$$\tag{8.139}$$

$$\varepsilon_{m,i}Z_{m,i} + g\sum_n \left[\int d\mathbf{r}\phi_n^*(\mathbf{r})\phi_m(\mathbf{r})\rho(\mathbf{r})Z_{n,i} + \int d\mathbf{r}\phi_n^*(\mathbf{r})\phi_m(\mathbf{r})\rho(\mathbf{r})Y_{n,i}\right] = -\omega Z_{m,i}\,.$$

The solutions of these equations are identical to those of equations (8.125), as can be easily verified by expanding u and v in the latter equations on the complete set of eigenfunctions of the above Hamiltonian H_{sp}.

In general, the $RPAE$ equations are written in matrix form as

$$\begin{pmatrix} A & B \\ -B^* & -A^* \end{pmatrix} \begin{pmatrix} Y(\omega) \\ Z(\omega) \end{pmatrix} = \omega \begin{pmatrix} Y(\omega) \\ Z(\omega) \end{pmatrix}\,, \tag{8.140}$$

where the matrices A and B are defined in terms of the single-particle wavefunctions as

$$A_{mi,nj} = \varepsilon_{mi}\delta_{mn}\delta_{ij} + \langle mj|V_{\text{res}}|in\rangle_a\,, \qquad B_{mi,nj} = \langle mn|V_{\text{res}}|ij\rangle_a\,, \tag{8.141}$$

and the matrix elements should be antisymmetrized by including exactly the exchange contributions:

$$\langle ab|V_{\text{res}}|cd\rangle_a = \langle ab|V_{\text{res}}|cd\rangle - \langle ab|V_{\text{res}}|dc\rangle\,. \tag{8.142}$$

This is the main difference between the microscopic $HF-RPAE$ calculation and the RPA calculations based on the LDA theory (see Section 8.9), where the exchange contribution is only approximately treated in the energy functional and not in the wavefunction of the ground state.

To solve the $RPAE$ equations, the following procedure is to be followed. First, the static Hartree–Fock problem is solved, from which we get the single-particle energies ε_α, the single-particle wavefunctions φ_α, and the Hartree–Fock ground state $|HF\rangle$. Subsequently, all the one-particle–one-hole states $|i^{-1}, m\rangle$, with their respective excitation energies $\varepsilon_{m,i}$, are set up according to the kind of excitation to be studied. Let us assume, for example, we want to study the photo-absorption cross section of a metal cluster of Sodium atoms, in the limit of long wavelength in which $kR \ll 1$ ($k \simeq 1/\lambda$, with R the metal cluster radius). In this limit, the photo-absorption cross section as a function of the frequency ω of the absorbed photon is given by

$$\sigma(\omega) = 4\pi e^2 \omega S(F, \omega) \,, \qquad (8.143)$$

where

$$F = D = \sum_{i=1}^{N} r_i \cos \vartheta_i$$

is the electric dipole operator, and the sum runs over the valence electrons of the cluster, and

$$S(D, \omega) = \sum_n |\langle 0|D|n\rangle|^2 \delta(\omega - \omega_{n,0}) \qquad (8.144)$$

is the excitation "strength" for the dipole operator.

Then, one selects the one-particle–one-hole states $|i^{-1}, m\rangle$ such that

$$F_{i,m} = D_{i,m} = \langle HF|D|i^{-1}, m\rangle \neq 0$$

(i.e. those which fulfill the selection rule $\Delta l = \pm 1$, valid for the dipole), and cuts the particle–hole space at some energy $\bar\omega$ such that $\varepsilon_{n,i} \leq \bar\omega$. For each particle–hole pair i^{-1}, m in the model space, we compute all the matrix elements of the residual interaction that appear in the $RPAE$ equations (8.138), using the states j^{-1}, n of the model space, and solve the system of coupled equations to obtain the solutions ω and $Y(\omega)_{m,i}, Z_{m,i}(\omega)$. Thus, we have as many solutions as the states i^{-1}, m of the model space, with energies ω different from the energies $\varepsilon_{m,i}$. The $RPAE$ matrix elements $\langle 0|F|\omega\rangle$ are obtained starting from the solutions $Y(\omega)_{m,i}, Z_{m,i}(\omega)$, as

$$\langle 0|F|\omega\rangle = \sum_{m,i} (Y_{m,i}(\omega)F_{m,i}^* + Z_{m,i}(\omega)F_{m,i}) \,, \qquad (8.145)$$

with $F_{i,m} = \langle HF|F|i^{-1}, m\rangle$. The matrix element (8.145) allows us to calculate the excitation strength $S(F, \omega)$ and, in the case taken as the example, where $F = D$, the

$RPAE$ photo-absorption cross section as well. Clearly, the $RPAE$ strength differs from the analogous quantity as computed in HF, given by

$$S_{HF}(F,\omega) = \sum_{m,i} |\langle i^{-1}, m|F|HF\rangle|^2 \delta(\omega - \varepsilon_{m,i})\,. \qquad (8.146)$$

Equation (8.145) can be derived starting from the variance

$$\langle \phi_{SD}(t)|F|\phi_{SD}(t)\rangle - \langle HF|F|HF\rangle\,.$$

Using for $\phi_{SD}(t)$ equation (8.133) expanded to first order in the coefficients $C_{m,i}(t)$ (which in turn are given by $C_{m,i}(t) = Y_{m,i}(\omega)e^{-i\omega t} + Z^*_{m,i}(\omega)e^{i\omega t}$), we obtain

$$\langle \phi_{SD}(t)|F|\phi_{SD}(t)\rangle - \langle HF|F|HF\rangle$$
$$= \sum_{m,i}[(Y_{m,i}F^*_{m,i} + Z_{m,i}F_{m,i})e^{-i\omega t} + (Z^*_{m,i}F^*_{m,i} + Y^*_{m,i}F_{m,i})e^{i\omega t}]\,. \quad (8.147)$$

On the other hand, by writing $|\phi(t)\rangle = |0\rangle + \alpha(t)|\omega\rangle$, where $\alpha(t) = \alpha_0 e^{-i\omega t}$, we obtain

$$\langle \phi(t)|F|\phi(t)\rangle - \langle 0|F|HF\rangle = \alpha_0(\langle 0|F|\omega\rangle e^{-i\omega t} + \langle \omega|F|0\rangle e^{i\omega t}) \qquad (8.148)$$

for the variance so that by comparing equations (8.147) and (8.148), we find (8.145) where the Y and the Z are defined apart from a normalization constant.

The normalization constant for Y and Z can be found in a simple way by introducing the creation and annihilation operators for the RPA excited states starting from (8.145) and the definitions

$$O^\dagger_\omega|0\rangle = |\omega\rangle\,, \qquad . \qquad (8.149)$$

and

$$O_\omega|0\rangle = 0\,, \qquad (8.150)$$

for all ω's. Using the result

$$\langle 0|F|\omega\rangle = \langle 0|FO^\dagger_\omega|0\rangle = \langle 0|[F, O^\dagger_\omega]|0\rangle \approx \langle HF|[F, O^\dagger_\omega]|HF\rangle\,, \qquad (8.151)$$

and comparing it to (8.145), we immediately get for the creation operator

$$O^\dagger_\omega = \sum_{m,i}(Y_{m,i}(\omega)a^\dagger_m a_i - Z_{m,i}(\omega)a^\dagger_i a_m)\,. \qquad (8.152)$$

Moreover, the annihilation operator O_ω is the adjoint operator of $O^\dagger_\omega$. Then, the normalization condition is obtained from

$$1 = \langle \omega \mid \omega \rangle = \langle 0|O_\omega O^\dagger_\omega|0\rangle = \langle 0|[O_\omega, O^\dagger_\omega]|0\rangle \approx \langle HF|[O_\omega, O^\dagger_\omega]|HF\rangle\,. \quad (8.153)$$

Using result (8.152) and the anticommutation relations (2.62) for the operators a and $a^\dagger$ we finally obtain at last:

$$\sum_{m,i}(|Y_{m,i}|^2 - |Z_{m,i}|^2) = 1. \tag{8.154}$$

Different solutions may be orthogonalized in order to fulfill the relation

$$\langle HF|[O_\omega, O_\lambda^\dagger]|HF\rangle = \delta_{\omega,\lambda}.$$

The $RPAE$ equations can also be derived using the method of equations of motion, in which the Schrödinger equation is rewritten using the excited state creation and annihilation operators (8.149) and (8.150) as

$$[H, O_\lambda^\dagger]|0\rangle = (E_\lambda - E_0)O_\lambda^\dagger|0\rangle \equiv \omega_\lambda O_\lambda^\dagger|0\rangle. \tag{8.155}$$

From this equation, it is possible to derive the variational equation for the O and $O^\dagger$ operators

$$\langle 0|[\delta O_\lambda, [H, O_\lambda^\dagger]]|0\rangle = \omega_\lambda \langle 0|[\delta O_\lambda, O_\lambda^\dagger]|0\rangle. \tag{8.156}$$

This equation is exact in the limit when $|0\rangle$ is the true ground state of the system. It is also very useful for we note that in the limit in which the right-hand and left-hand side commutators of the equation are numbers, it turns out to be completely independent on the approximation employed for the ground state, and in the limit in which the commutators are one-body operators their mean values are well reproduced by a mean-field ground state, because for the one-body operators F one expects that $\langle 0|F|0\rangle \approx \langle HF|F|HF\rangle$, even if $|0\rangle \neq |HF\rangle$. These considerations are also the basis for the last steps of equations (8.151) and (8.153).

In the $RPAE$ approximation the excitation operators are taken in the form (8.152), and in the equations of motion (8.156) we replace the mean values of the commutators on the true state by their mean values on the HF state.

By inserting expression (8.152) into the equation of motion (8.156) and allowing δO_λ to span the ensemble of particle-hole creation $(a_m^\dagger a_i)$ and annihilation $(a_i^\dagger a_m)$ operators, one obtains equations (8.138). In such a procedure there is a lack of self-consistence because by including into $O_\lambda^\dagger$ both the creation and the annihilation operators of a particle-hole pair, one automatically excludes the possibility that the $RPAE$ ground state is the HF one which, however, is used to solve the equations of motion. To be consistent, one should use for the ground state in the equations of motion the solution of

$$O_\lambda|RPAE\rangle = 0, \tag{8.157}$$

for all the states λ which defines the $RPAE$ ground state. However, the solution of such system is extremely complex, and in practice to solve the equations of motion one computes the commutators on the $|HF\rangle$ state.

Lastly, we wish to recall the Tamm–Dancoff approximation, that was widely used in past years before the appearance of computers made it possible to solve the $RPAE$ equations. It consists in approximating the ground state $|0\rangle$ by the HF state, and in writing the operators $O_\omega^\dagger$ as creation operators for one-particle–one-hole states:

$$O_\omega^\dagger = \sum_{m,i} Y_{m,i}(\omega) a_m^\dagger a_i \,. \tag{8.158}$$

In this case the equation for the ground state

$$O_\omega |HF\rangle = \sum_{m,i} Y_{m,i}^*(\omega) a_i^\dagger a_m |HF\rangle = 0 \,, \tag{8.159}$$

is satisfied for all particle-hole states. By inserting (8.158) into the equations of motion (8.156), and considering arbitrary variations $\delta Y_{m,i}$, we obtain:

$$\sum_{n,j} \langle HF|[a_i^\dagger a_m, [H, a_n^\dagger a_j]]|HF\rangle Y_{m,j} = \omega_\lambda \langle HF|[a_i^\dagger a_m, a_n^\dagger a_j]|HF\rangle Y_{m,i} \,. \tag{8.160}$$

Using the fact that the HF state obeys the equation (8.159), we arrive at the Tamm–Dancoff equations

$$\sum_{n,j} (\delta_{mn}\delta_{ij}\varepsilon_{m,i} + V_{m,j,i,n}) Y_{n,j} = \omega Y_{m,i} \,. \tag{8.161}$$

Compared to the $RPAE$ solutions, the Tamm–Dancoff approximation completely ignores the dynamic effects due to presence of correlations in the ground state, which are taken into account in $RPAE$ by the term $Z_{m,i}$ in (8.152). This term makes the $RPAE$ state different from the HF one.

In the case of a cold dilute gas of Bosons in a magnetic trap, the Tamm–Dancoff equations lead to solutions which coincide with those of the mean-field, obtained with the single-particle Hamiltonian (8.127). They coincide also with the second HF equation (2.98) at finite temperature only in the zero-temperature limit.

8.8 Examples of Application of the RPA Theory

8.8.1 RPA with separable interactions

The physics described by the matrix $RPAE$ theory can be illustrated in a simple and clear way by a separable interaction of the kind

$$V_{\text{res}} = k \sum_{i<j} Q_i Q_j \,, \tag{8.162}$$

where k is a constant. This interaction emerges in a natural way in the vibrating potential method (Chapter 10), and should be used without including the exchange

terms in the particle-hole matrix elements which, thus, are given by

$$
\begin{aligned}
V_{m,j,i,n} &= \langle mi^{-1}|V_{\text{res}}|nj^{-1}\rangle = kQ_{m,i}Q_{n,j}^* \\
V_{m,n,i,j} &= \langle mi^{-1}nj^{-1}|V_{\text{res}}|HF\rangle = kQ_{m,i}Q_{n,j} \,,
\end{aligned}
\tag{8.163}
$$

where

$$
Q_{m,i} = \langle m|Q|i\rangle = \sum_\sigma \int \varphi_m^*(\mathbf{r},\sigma)q\varphi_i(\mathbf{r},\sigma)d\mathbf{r} \qquad \left(Q = \sum_i q_i\right)
$$

and φ_i are the solutions of the static Hartree–Fock problem.

Equations (8.138) then become

$$
\begin{aligned}
(\varepsilon_{m,i} - \omega)Y_{m,i} + kQ_{m,i}\sum_{n,j}[Q_{n,j}^*Y_{n,j} + Q_{n,j}Z_{n,j}] &= 0\,, \\
(\varepsilon_{m,i} + \omega)Z_{m,i} + kQ_{m,i}^*\sum_{n,j}[Q_{n,j}Z_{n,j}^* + Q_{n,j}^*Y_{n,j}] &= 0\,,
\end{aligned}
\tag{8.164}
$$

with solution

$$
Y_{m,i} = -\frac{NQ_{m,i}}{\varepsilon_{m,i} - \omega}, \qquad Z_{m,i} = -\frac{NQ_{m,i}^*}{\varepsilon_{m,i} + \omega}\,.
\tag{8.165}
$$

The constant N which is given by

$$
N = k\sum_{n,j}[Q_{n,j}^*Y_{n,j} + Q_{n,j}Z_{n,j}]\,,
\tag{8.166}
$$

can be evaluated by the normalization condition (8.154). By eliminating $Y_{m,i}$ and $Z_{m,i}$ from equations (8.165) and (8.166), we obtain the following dispersion relation for the excitation energies ω:

$$
\frac{1}{k} = -2\sum_{m,i}\frac{\varepsilon_{m,i}\,|\,Q_{m,i}\,|^2}{\varepsilon_{m,i}^2 - \omega^2}\,.
\tag{8.167}
$$

Equation (8.167) is completely similar to (8.87), which yields the *RPA* excitation energies for homogeneous systems. It is enough to identify the free response function χ^0 with $-2\sum_{m,i}\varepsilon_{m,i}\,|\,Q_{m,i}\,|\,/(\varepsilon_{m,i}^2 - \omega^2)$ and k with $v(q)/L^D$. The graphical solution of the equation is plotted in Fig. 8.11, and clearly shows that a collective solution emerges apart from the single-particle-like ones. Note that, unlike the homogeneous case, the single-particle spectrum of a finite system like the one considered here, has a gap and is discrete.

The *RPA* matrix elements

$$
\langle \omega|F|HF\rangle = \sum_{m,i}(Y_{m,i}^*F_{m,i} + Z_{m,i}^*F_{m,i}^*)
$$
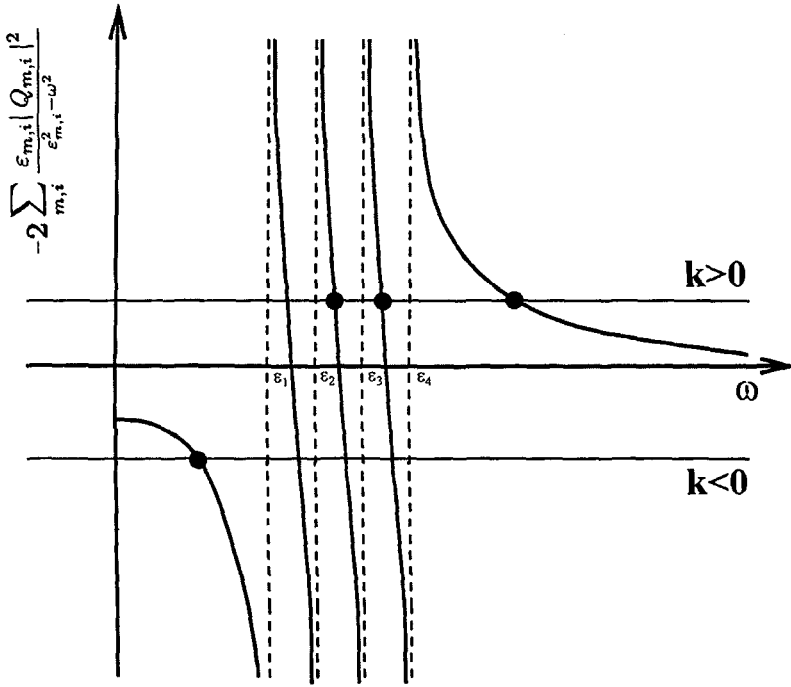
Fig. 8.11   Graphical solution of the dispersion relation (8.167) for the *RPA* theory with separable interactions.

of equation (8.145) are found by computing the normalization constant and using solutions (8.165) for the Y and Z. With a simple calculation we find

$$
N = \left[\sum_{m,i} \left(\frac{4\varepsilon_{m,i}\omega \mid Q_{m,i} \mid^2}{(\varepsilon_{m,i}^2 - \omega^2)^2} \right) \right]^{-1/2}
\tag{8.168}
$$

and

$$
\langle \omega | F | HF \rangle = -N \sum_{m,i} \left(\frac{Q_{m,i}^* F_{m,i}}{\varepsilon_{m,i} - \omega} + \frac{Q_{m,i} F_{m,i}^*}{\varepsilon_{m,i} + \omega} \right) .
\tag{8.169}
$$

An analytic solution for the collective energy can be found in the degeneration limit, in which all the particle-hole energies $\varepsilon_{m,i} = \varepsilon$ are all equal. In this limit, all the *RPA* solutions except one, are trapped at the unperturbed energy ε. The untrapped (collective) solution is obtained from equation (8.167) as

$$
\omega^2 = \varepsilon^2 + 2\varepsilon k \sum_{m,i} \mid Q_{m,i} \mid^2 ,
\tag{8.170}
$$

and assuming that the excitation operator F coincides with Q, we find

$$N^2 = \frac{(\varepsilon^2 - \omega^2)^2}{4\varepsilon\omega\sum_{m,i} |Q_{m,i}|^2} \,, \tag{8.171}$$

and

$$|\langle\omega|Q|HF\rangle|^2 = \frac{\varepsilon}{\omega}\sum_{m,i} |Q_{m,i}|^2 \,. \tag{8.172}$$

The above equations show that the collective state energy is either higher or lower than the unperturbed energy, according to whether the residual interaction is attractive or repulsive, and that the energy-weighted sum rule (f-sum rule)

$$m_1 = \sum_n E_n|\langle 0|Q|n\rangle|^2 = \frac{1}{2}\langle 0|[F,[H,F]]|0\rangle$$

is conserved in the sense that

$$\omega|\langle\omega|F|HF\rangle|^2 = \varepsilon\sum_{m,i} |F_{m,i}|^2 = m_1^{RPA}(\omega)\,. \tag{8.173}$$

Therefore, the same result is obtained when computing m_1^{RPA} either with the RPA matrix element or taking the commutator $\frac{1}{2}\langle HF|[Q,[H,Q]]|HF\rangle$ on the HF state. This is not the case for the $m_0 = \sum_n |\langle 0|Q|n\rangle|^2$ sum rule which, when computed in RPA, is either larger or smaller than the unperturbed one, depending on whether ε/ω is larger or smaller than one. For a general description of the properties of the sum rules mentioned here, see Section 8.10.

8.8.2   *RPAE for metal clusters*

In this Section we will study the response of closed-shell sodium clusters to the electric dipole excitation operator, and use the $RPAE$ theory based on the HF and BHF approximations for the energies of the single-particle wavefunctions. We shall employ both the jellium model for the metal cluster, and a model which uses pseudo-Hamiltonians (Bachelet, Ceperley and Chiocchetti 1989) to describe the ionic potential acting on the valence electrons of the cluster (see Section 2.2.1).

The electric dipole excitations for sodium metal clusters were measured by several authors by means of photo-absorption reaction on a cluster beam (Knight et al. 1985; Pollack et al. 1991; Selby et al. 1991; Borgreen et al. 1993; Ellert et al. 1995; Reiners et al. 1995); the calculations we report here are those by Guet and Johnson (1992) and Lipparini, Serra and Takayanagi (1994). The results are compared with the RPA calculations based on LDA theory of Ekardt (1985) and Yannouleas et al. (1989).

The $RPAE$ calculations based on the HF method with Coulomb interaction, will be henceforth referred to as the Coulomb–HF (CHF) approximation, while those based on the Brueckner–HF method with the effective interaction (3.61),

which is used to determine both the single-particle states and the residual interaction, will be indicated as the BHF approximation.

Thus, the Hamiltonian that describes the motion of the valence electrons of sodium clusters, is given in BHF by (in the following, we use atomic units (a.u.))

$$H = \sum_i \frac{p_i^2}{2} + \sum_{i,j} \left(\frac{1}{|\mathbf{r}_i - \mathbf{r}_j|} + g^c(r_{i,j}, \nabla_{i,j}) \right) + \sum_i \hat{V}_I \,. \tag{8.174}$$

From this, we obtain the CHF Hamiltonian by simply dropping the correlation term g^c.

For the electronic potential

$$V = \sum_{i,j} \left(\frac{1}{|\mathbf{r}_i - \mathbf{r}_j|} + g^c(r_{i,j}, \nabla_{i,j}) \right) , \tag{8.175}$$

of equation (8.174), and for the dipole operator $D = \sum_{i=1}^{N} z_i$, the following property holds

$$[V, D] = 0 \,. \tag{8.176}$$

This condition (8.176) is known as (Bohigas, Lane and Martorell 1979; Lipparini and Stringari 1989) the Galilean invariance of the force, and stems from the translational invariance of the electronic potential (8.175), and from the fact that the dipole operator coincides with the coordinate of the center of mass of the electrons. Then, in the spherical jellium model (JM), where the ionic potential $\hat{V}_I$ is the local operator (2.24) ($\hat{V}_I = V_+$), one finds

$$[H, D] = -\frac{i}{2} P_z \,. \tag{8.177}$$

where $P_z = \sum_i p_i^z$ is the z component of the total momentum of the valence electrons. Thus, using equation (8.177) one obtains for the f-sum rule m_1:

$$m_1^{JM} = \frac{N}{2} \,, \tag{8.178}$$

and for the sum rule cubic in energy:

$$m_3^{JM} = \frac{2\pi}{3} \int_0^\infty \rho(r) \nabla^2 V_+(r) r^2 dr = \frac{2\pi}{r_s^3} \int_0^R \rho(r) r^2 dr \,, \tag{8.179}$$

where $\rho(r)$ is the electron density of the ground state, and in order to obtain the last expression of (8.179) we have used the Poisson equation. The m_3 sum rule depends on the ionic potential V_+ because this external field breaks the translational invariance of the system and thus does not commute with the total momentum operator. In the pseudo-jellium model (PJM), the ionic potential $\hat{V}_I$ of (8.174) is non-local and is given by the expression (Lipparini, Serra and Takayanagi 1994)

$$\hat{V}_I = -\frac{1}{2} \nabla \alpha(r) \cdot \nabla + \mathbf{L}\beta(r) \cdot \mathbf{L} + u(r) \,, \tag{8.180}$$
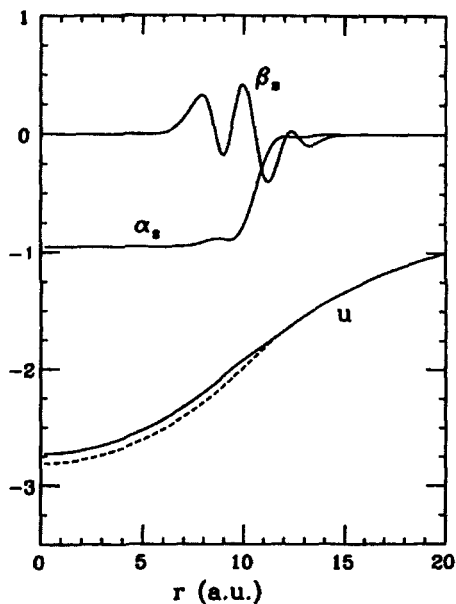
Fig. 8.12   Radial functions α, β and u for the Na_{20} cluster, in atomic units The functions were scaled in the following way: $\alpha_s = 25\alpha$, $\beta_s = 2 \times 10^4\beta$. The local jellium potential of Eq. (2.24) is represented by the dashed line, for comparison.

where **L** is the angular momentum operator and the functions α, β and u are computed from a pseudo-Hamiltonian that takes into account the ionic structure (core electrons) in the interaction between valence electrons and ions. These functions are shown in Fig. 8.12 for the cluster Na_{20}.

The nonlocal character of V_I makes V_I contribute to the commutator $[H, D]$. Taking this contribution into consideration, we get the following result for the f-sum rule

$$m_1^{PJM} = 2\pi \int_0^\infty \left(1 + \alpha(r) + \frac{4}{3}r^2\beta(r) \right) \rho(r)r^2 dr , \qquad (8.181)$$

which differs from the result (8.178) and valid in the jellium model.

The above results for m_1 and m_3 hold in the $RPAE$ approximation, provided one uses the self-consistent mean-field solution for the electron density that appears in expressions (8.179) and (8.181). In fact, it can be shown that the evaluation of the mean value of the commutators

$$m_1 = 1/2\langle 0|[D, [H, D]]|0\rangle ,$$

$$m_3 = 1/2\langle 0|[[D, H], [H, [H, D]]]|0\rangle$$

on the HF state, is equivalent to computing the moments m_1 and m_3 with the $RPAE$ energies and matrix elements (Bohigas, Lane and Martorell 1979; Lipparini
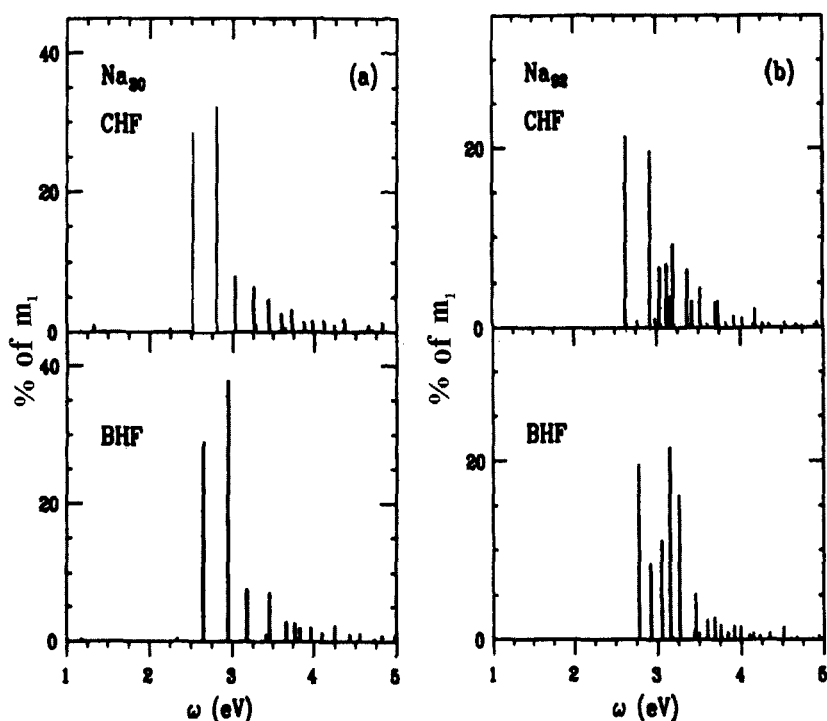
Fig. 8.13 Dipole-energy distribution for the Na_{20} and Na_{92} clusters with the jellium model, in units of the f-sum rule m_1. In all cases the top panel shows the calculation under the $CHF+RPA$ approximation, while the bottom one corresponds to the $BHF + RPA$ approximation.

and Stringari 1989; see also Section 8.10). As regards the inversely energy-weighted sum rule m_{-1}, which is connected to the static polarizability α of the system by the relation

$$m_{-1} = \frac{1}{2}\alpha, \qquad (8.182)$$

it is possible to show in a similar way that the evaluation of the moment

$$m_{-1} = \sum_n E_n^{-1} |\langle n|D|0\rangle|^2$$

using the $RPAE$ energies and matrix elements is equivalent to calculating the polarizability α in a static HF calculation with a dipole constraint. The $RPAE$ calculations that we are going to report in what follows, satisfy these theorems.

In Fig. 8.13 we show the distributions of the dipole strength in the Na_{20} and Na_{92} clusters, computed in CHF and BHF with the spherical jellium model. The strengths are in units of the f-sum rule m_1 of (8.178). As a general feature, the BHF spectrum has an average excitation energy slightly higher than the CHF spectrum, which is reflected in a lower polarizability value. This is shown in Fig. 8.14, where
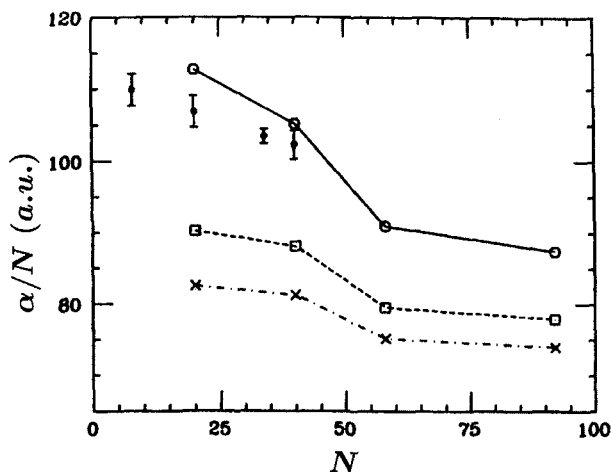
Fig. 8.14   Static dipole polarizability in some closed-shell Sodium clusters. The squares and the crosses correspond to the CHF and BHF approximations, respectively, in the jellium model. The circles are the results of the BHF method with the pseudo-jellium potential.

we plot the electric-dipole polarizability per particle in CHF and BHF (we recall that for the jellium clusters the classical value of α/N is r_s^3). This behaviour can be understood in terms of the role played by electron correlations. Inclusion of these correlations in BHF makes the cluster more rigid than in CHF and, as a consequence, less polarizable by an external electric field and resonant at higher energy.

In Na_{20} the excitation spectrum exhibits two main peaks, in both CHF and BHF. This agrees with the experimental data on the photo-absorption cross sections of Pollack et al. (1991), which exhibit two peaks at 2.4 eV and 2.75 eV. However, the relative intensities of these two peaks are not well reproduced, because in the experiments the second peak is weaker than the first (see Fig. 8.15) and, moreover, the effect of correlations in BHF is to increase the difference between theoretical and measured peak energies, which is already present in CHF, i.e. to increase the blue shift with respect to experiment.

As the size of the cluster increases, the fragmentation of the strength increases as well, and the average excitation energy shifts to higher energies, but in any case staying well below the classical Mie frequency $\omega_{Mie} = \sqrt{4\pi\rho} = \sqrt{3/r_s^3}$ which, for sodium, $(r_s \simeq 4)$ is 3.4 eV. This is shown in the Na_{92} spectrum of Fig. 8.13b.

As for the comparison with the $TDLSDA$ theory (see Section 8.9), the BHF spectra are very close to the $TDLSDA$ ones, and the polarizabilities are practically coincident. The disagreement with experiment cannot be explained within the HF framework, even by taking into account of short-range correlations like in BHF; one should rather include effects due to the ionic structure into the model. To prove this statement, in Fig. 8.15 we show the dipole strengths as computed in the
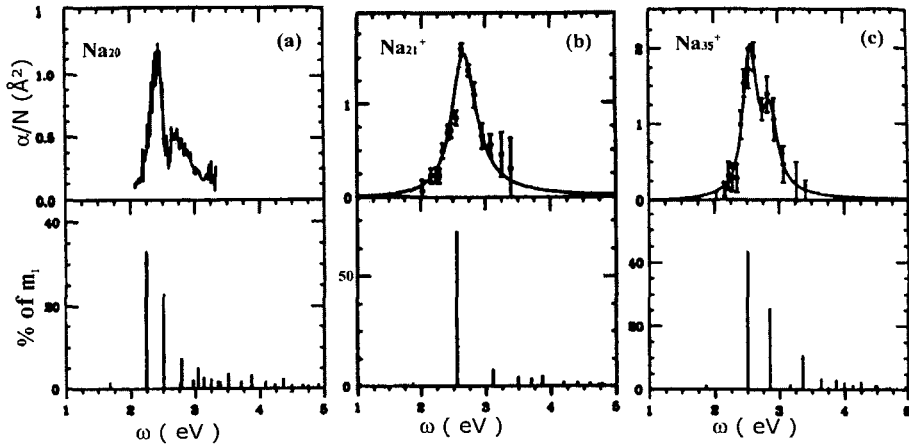
Fig. 8.15   Dipole-strength distributions, in units of the f-sum rule m_1, in the pseudo-jellium model. The results for the Na_{20}, Na_{21}^+ and Na_{35}^+ clusters are reported in (a), (b) and (c), respectively. In all cases the top panel shows the experimental photo-absorption cross section, (Pollack et al. 1991, for (a), Borggreen et al. 1993, for (b) and (c)), while the bottom one shows the theoretical results (Lipparini, Serra and Takayanagi 1994).
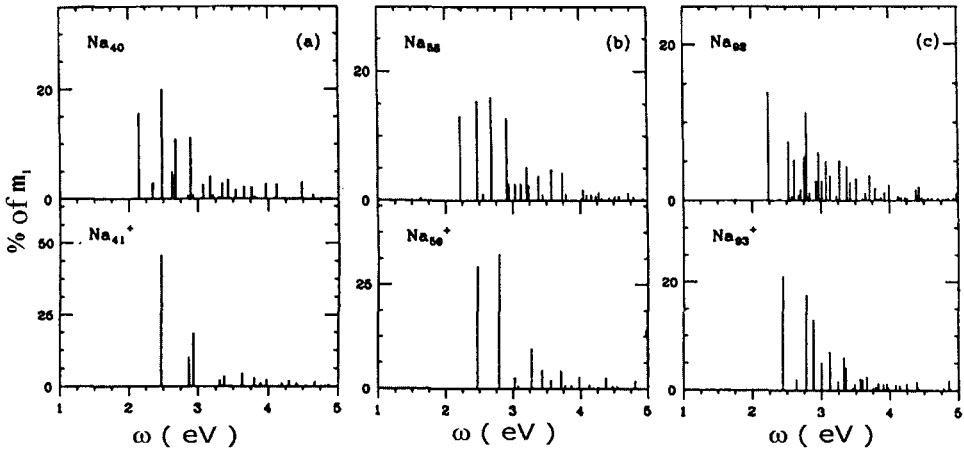
Fig. 8.16   The same as Fig. 8.15, with but for the theoretical results in clusters with 40 (a), 58 (b) and 92 (c) electrons. In all cases the top panel reports the results for neutral clusters, and the bottom one for positively charged ones.

$BHF + PJM$ approximation, for the Na_{20}, Na_{21}^+ and Na_{35}^+ clusters, and compare them with the experimental data. Then, in Fig. 8.16 we report the theoretical calculation in (neutral and positively charged) clusters with 40, 58 and 92 electrons. The strength is given in units of the f-sum rule of (8.181), whose value in the different cases is reported in Table 8.4. In this table, we report the values of $2m_1$ in a.u., which for the jellium equals the number of electrons [see Eq. (8.178)].

As is seen from the table, in sodium clusters m_1^{PJM} is very close to the value of the jellium model, $N/2$ [see Eq. (8.178)]. However, in other cases (like e.g. lithium clusters), m_1^{PJM} is much smaller than m_1^{JM}. This effect, which is due to the non-locality of the pseudo-Hamiltonian, is the important one in order to reproduce the experimental photo-absorption results in lithium clusters (Brechignac et al. 1993), which in the optical region do not saturate the f-sum rule of the jellium model. This was explicitly shown by RPA calculations with pseudo-potentials in lithium clusters (Serra et al. 1993; Blundell and Guet 1993; Alasia et al. 1995).

<div align="center">TABLE 8.4</div>

	Na_{20}	Na_{40}	Na_{58}	Na_{92}	
$2m_1(a.u.)$	19.41	38.76	56.12	88.95	
	Na_{21}^+	Na_{35}^+	Na_{41}^+	Na_{59}^+	Na_{93}^+
$2m_1(a.u.)$	19.38	32.91	38.74	56.09	88.93

From Fig. 8.15 we may conclude that, once the ionic structure effects are included, the spectra predicted by the $BHF + PJM$ theory are in very good agreement with experiment. Especially remarkable is the degree to which it reproduces the fragmentation of the strength (Landau damping) in Na_{20} and Na_{35}^+, and the relative weighs of the peaks. For the Na_{21}^+ cluster the model foresees one dominant state with more than 70% of the strength, in good agreement with the experimental results reported in the figure (Borggreen et al. 1993), as well as with those of Ellert et al. (1995) and Reiners et al. (1995). The spectrum of the Na_{41}^+ cluster also compares very well with the experiments, which evidence a dominant peak at about 2.6 eV, and a tail around 3 eV. The high degree of fragmentation predicted for Na_{40} is also observed in the measurements of Selby et al. (1991).

The dipole polarizability computed in $BHF + PJM$ is shown in Fig. 8.14. From this figure we see that the computed values are very close to the experimental ones of Knight et al. (1985).

8.9   Adiabatic Time Dependent $LSDA$ ($TDLSDA$)

The time-dependent version of the $LSDA$ approximation (see Section 4.6), known as adiabatic $TDLSDA$ (Time Dependent Local Spin Density Approximation) (see for example Gross and Kohn 1990), can be derived through a variational principle on the following action integral

$$I = \int \langle \varphi_{SD}(t)|H^{LSDA} - i\frac{\partial}{\partial t}|\varphi_{SD}(t)\rangle \, dt \qquad (8.183)$$

where $\varphi_{SD}(t)$ is a Slater determinant of single-particle, time-dependent wavefunctions, and

$$\langle\varphi_{SD}(t)|H^{LSDA}|\varphi_{SD}(t)\rangle = E(\rho(\mathbf{r},t),m(\mathbf{r},t))$$

$$= T_0(t) + \int d\mathbf{r}\rho(\mathbf{r},t)\left[v_{\text{ext}}(\mathbf{r}) + \frac{1}{2}U(\mathbf{r},t)\right]$$

$$+ E_{xc}(\rho(\mathbf{r},t),m(\mathbf{r},t)), \qquad (8.184)$$

where

$$U(\mathbf{r},t) = \int d\mathbf{r}'\rho(\mathbf{r}',t)v(|\mathbf{r} - \mathbf{r}'|)$$

is the Hartree potential (for electrons, it is the classical Coulomb potential). If $\varphi_{i,\sigma}$ are the single-particle states that appear in the Slater determinant, for the density appearing in the above equation we have

$$\rho(\mathbf{r},t) = \sum_{\sigma}\rho_{\sigma}(\mathbf{r},t),$$

$$m(\mathbf{r},t) = \rho_{\uparrow}(\mathbf{r},t) - \rho_{\downarrow}(\mathbf{r},t), \qquad (8.185)$$

$$\rho_{\sigma}(\mathbf{r},t) = \sum_{i}|\varphi_{i,\sigma}(\mathbf{r},t)|^2,$$

and

$$T_0(t) = \int d\mathbf{r}\frac{\tau(\mathbf{r},t)}{2m}, \qquad (8.186)$$

where

$$\tau(\mathbf{r},t) = \sum_{i\sigma}|\nabla\varphi_{i,\sigma}(\mathbf{r},t)|^2.$$

By making the stationary condition $\delta I = 0$ to equation (8.183), we obtain the time-dependent Kohn–Sham equations for the $\varphi_i(\mathbf{r},t)$:

$$i\frac{\partial}{\partial t}\varphi_{i,\sigma}(\mathbf{r},t)$$

$$= \left(-\frac{\nabla^2}{2m} + v_{\text{ext}}(\mathbf{r}) + \frac{1}{2}U(\mathbf{r},t) + V_{xc}(\mathbf{r},t) + W_{xc}(\mathbf{r},t)\sigma_z\right)\varphi_{i,\sigma}(\mathbf{r},t), \quad (8.187)$$

where σ_z is the z component of the Pauli spin operator and, in the adiabatic approximation,

$$V_{xc}(\mathbf{r},t) = \frac{\partial E_{xc}(\rho,m)}{\partial\rho(\mathbf{r},t)} \quad \text{and} \quad W_{xc}(\mathbf{r},t) = \frac{\partial E_{xc}(\rho,m)}{\partial m(\mathbf{r},t)} \qquad (8.188)$$

are the exchange-correlation potentials. An exhaustive discussion about the justification of the theory and the validity of $TDLSDA$, is found in Dobson et al. (1998).

Starting from equation (8.187), in the following we will study the $TDLSDA$ response functions of a many-body system to an external, time-oscillating field, by employing a formalism that applies to both homogeneous and non-homogeneous systems, and which also takes account of coupling among different responses which are due to possible spin-polarization in the ground state of the system. We will separate the study of the response into the longitudinal case, in which the system excitations take place without varying the third component of the spin ($\Delta S_z = 0$), and the transverse one, in which the excitations involve a change of spin ($\Delta S_z = \pm 1$).

8.9.1 *The TDLSDA longitudinal response function*

Let us put the system [Eq. (8.187)] in an external, time-oscillating field like that of equation (7.10), where the operator G depends on the spin co-ordinates and is of the form

$$G = G^{s,a} = \sum_{i=1}^{N_\uparrow} g(\mathbf{r}_i) \pm \sum_{i=1}^{N_\downarrow} g(\mathbf{r}_i) \equiv \sum_{i\sigma} g_\sigma(\mathbf{r}_i)|\sigma\rangle\langle\sigma| \,, \qquad (8.189)$$

with $N_\uparrow, N_\downarrow$ the numbers of system particles with spin up and down, respectively. The external potential causes variations in the spin densities of the system (with respect to the static densities), that can be written in the following way

$$\delta\rho_\sigma(\mathbf{r},\omega) = \sum_{\sigma'} \int \alpha_{\sigma,\sigma'}(\mathbf{r},\mathbf{r}',\omega) g_{\sigma'}(\mathbf{r}') \, d\mathbf{r}' \,, \qquad (8.190)$$

where $\alpha_{\sigma,\sigma'}$ is the correlation function that connects the density variation to the external field. Such density variations give rise to changes in the effective $LSDA$ potential of (8.187), which depends on the densities, so that we have $V_{\text{eff}} = V_{\text{eff}}^{gs} + \delta V_{\text{eff}}$. To first perturbation order in δV_{eff}, the effective-potential variation, in turn, causes a density variation which are given by

$$\delta\rho_\sigma(\mathbf{r},\omega) = \sum_{\sigma'} \int \alpha_{\sigma,\sigma'}^0(\mathbf{r},\mathbf{r}',\omega)\delta V_{\text{eff}}^{\sigma'} \, d\mathbf{r}' \,, \qquad (8.191)$$

where the correlation function of the non-interacting particles $\alpha_{\sigma,\sigma'}^0$ (built up through the solutions of the stationary KS equations) is given by the expression

$$\alpha_{\sigma,\sigma'}^0(\mathbf{r},\mathbf{r}',\omega) = \delta_{\sigma,\sigma'} \sum_{mi} \left[\frac{\varphi_{i\sigma}(\mathbf{r})\varphi_{i\sigma}^*(\mathbf{r}')\varphi_{m\sigma}^*(\mathbf{r})\varphi_{m\sigma}(\mathbf{r}')}{\omega + \epsilon_{i\sigma} - \epsilon_{m\sigma}} \right.$$
$$\left. - \frac{\varphi_{i\sigma}^*(\mathbf{r})\varphi_{i\sigma}(\mathbf{r}')\varphi_{m\sigma}(\mathbf{r})\varphi_{m\sigma}^*(\mathbf{r}')}{\omega - \epsilon_{i\sigma} + \epsilon_{m\sigma}} \right] \,, \qquad (8.192)$$

where the indexes i, m refer to hole and particle states, respectively. Noting that at first order in $\delta\rho$ the variation of the effective potential is given by

$$\delta V_{\text{eff}}^{\sigma}(\mathbf{r}) = g_{\sigma}(\mathbf{r}) + \sum_{\sigma'} \int dr' \left(v(|\mathbf{r} - \mathbf{r}'|) + \frac{\partial^2 E_{xc}}{\partial\rho_{\sigma}\partial\rho_{\sigma'}} \right) \delta\rho_{\sigma'}(\mathbf{r}'), \quad (8.193)$$

then from equations (8.190), (8.191) and (8.193) we obtain a Dyson-like integral equation

$$\alpha_{\sigma,\sigma'}(\mathbf{r}, \mathbf{r}', \omega) = \alpha_{\sigma,\sigma'}^{0}(\mathbf{r}, \mathbf{r}', \omega)$$

$$+ \sum_{\sigma_1 \sigma_2} \int \alpha_{\sigma,\sigma_1}^{0}(\mathbf{r}, \mathbf{r_1}, \omega) K_{\sigma_1 \sigma_2}(\mathbf{r_1}, \mathbf{r_2}) \alpha_{\sigma_2 \sigma'}(\mathbf{r_2}, \mathbf{r}', \omega) \, dr_1 \, dr_2 \quad (8.194)$$

which defines the *LSDA* correlation function $\alpha_{\sigma,\sigma'}$ in terms of the free correlation functions $\alpha_{\sigma,\sigma'}^{0}$. The kernel of the integral equation, which is commonly known as particle-hole residual interaction, is given by

$$K_{\sigma_1 \sigma_2}(\mathbf{r_1}, \mathbf{r_2}) = v(|\mathbf{r_1} - \mathbf{r_2}|) + \left. \frac{\partial^2 E_{xc}(\rho, m)}{\partial\rho_{\sigma_1}\partial\rho_{\sigma_2}} \right|_{gs} \delta(\mathbf{r_1} - \mathbf{r_2}), \quad (8.195)$$

where

$$\left. \frac{\partial^2 E_{xc}}{\partial\rho_{\sigma}\partial\rho_{\sigma'}} \right|_{gs} = \left. \frac{\partial^2 E_{xc}}{\partial\rho^2} \right|_{gs} + (\eta_{\sigma} + \eta_{\sigma'}) \left. \frac{\partial^2 E_{xc}}{\partial\rho\partial m} \right|_{gs} + \eta_{\sigma}\eta_{\sigma'} \left. \frac{\partial^2 E_{xc}}{\partial m^2} \right|_{gs}$$

$$\equiv \mathcal{K}(r) + (\eta_{\sigma} + \eta_{\sigma'}) \mathcal{M}(r) + \eta_{\sigma}\eta_{\sigma'} \, \mathcal{I}(r), \quad (8.196)$$

with $\eta_{\uparrow} = 1, \eta_{\downarrow} = -1$. The latter expression is the definition of the functions $\mathcal{K}, \mathcal{M}$, and $\mathcal{I}$.

The dynamic polarizability is given by

$$\chi(F, G, \omega) = \sum_{\sigma'} \int f_{\sigma'}^{*}(\mathbf{r}) \delta\rho_{\sigma'}(\mathbf{r}, \omega) \, dr, \quad (8.197)$$

with $\delta\rho_{\sigma}$ given by (8.190). Then, we obtain

$$\chi(F^s, G^s, \omega) = \int (f_{\uparrow}^{*}(\mathbf{r})\delta\rho_{\uparrow} + f_{\downarrow}^{*}(\mathbf{r})\delta\rho_{\downarrow}) \, dr$$

$$= \int (f_{\uparrow}^{*}(\mathbf{r})\alpha_{\uparrow,\uparrow}g_{\uparrow}(\mathbf{r}') + f_{\uparrow}^{*}(\mathbf{r})\alpha_{\uparrow,\downarrow}g_{\downarrow}(\mathbf{r}')$$

$$+ f_{\downarrow}^{*}(\mathbf{r})\alpha_{\downarrow,\uparrow}g_{\uparrow}(\mathbf{r}') + f_{\downarrow}^{*}(\mathbf{r})\alpha_{\downarrow,\downarrow}g_{\downarrow}(\mathbf{r}'))drdr'. \quad (8.198)$$

Note that if we substitute $\delta\rho_\sigma^0$, as given by

$$\delta\rho_\sigma^0(\mathbf{r},\omega) = \sum_{\sigma'}\int \alpha_{\sigma,\sigma'}^0(\mathbf{r},\mathbf{r}',\omega)g_{\sigma'}(\mathbf{r}')d\mathbf{r}', \qquad (8.199)$$

into (8.197), and use for $\alpha_{\sigma,\sigma'}^0$ the expression (8.192), we obtain the free response function:

$$\chi^0(F,G,\omega) = \sum_{\sigma'mi}\left(\frac{\langle m|f_{\sigma'}^*|i\rangle\langle i|g_{\sigma'}|m\rangle}{\omega - (\epsilon_m - \epsilon_i)} - \frac{\langle m|g_{\sigma'}|i\rangle\langle i|f_{\sigma'}^*|m\rangle}{\omega + (\epsilon_m - \epsilon_i)}\right), \qquad (8.200)$$

where i and m are the single-particle KS states, occupied and non-occupied, respectively, in the ground state of the system. It is also important to notice that, in order to obtain the dynamic polarizability of the system, it is not necessary to go through the solution of the integral equation (8.194) which, from a technical point of view, implies the difficult task of inverting large matrices. In fact, starting from equation (8.194), it is possible to obtain an integral equation for the density variation that enter directly into the definition of χ:

$$\begin{pmatrix}\delta\rho_\uparrow^A \\ \delta\rho_\downarrow^A\end{pmatrix} = \begin{pmatrix}\delta\rho_\uparrow^{(0,A)} \\ \delta\rho_\downarrow^{(0,A)}\end{pmatrix} + \begin{pmatrix}\alpha_{\uparrow\uparrow}^{(0)} & 0 \\ 0 & \alpha_{\downarrow\downarrow}^{(0)}\end{pmatrix} \otimes \begin{pmatrix}K_{\uparrow\uparrow} & K_{\uparrow\downarrow} \\ K_{\downarrow\uparrow} & K_{\downarrow\downarrow}\end{pmatrix} \otimes \begin{pmatrix}\delta\rho_\uparrow^A \\ \delta\rho_\downarrow^A\end{pmatrix}, \qquad (8.201)$$

where the symbols $\otimes$ indicate an implicit spatial integration on the common variable $\mathbf{r}$ of the operands. In this way, the problem of determining the dynamic polarizability is reduced to that of solving the system of $2N_p$ linear equations (8.201), where N_p is the number of points used to solve the Kohn–Sham equations.

The above formalism can be quickly generalized to the finite-temperature case. The only element which changes is the correlation function (8.192), which becomes

$$\alpha_{\sigma,\sigma'}^0(\mathbf{r},\mathbf{r}',\omega) = -\delta_{\sigma,\sigma'}\sum_{\alpha\beta}\varphi_\alpha^*(\mathbf{r})\varphi_\beta(\mathbf{r})\frac{f_\alpha - f_\beta}{\epsilon_\beta - \epsilon_\alpha + \omega}\varphi_\beta^*(\mathbf{r}')\varphi_\alpha(\mathbf{r}'), \qquad (8.202)$$

where the indexes α (β) refer to single-particle levels with spin σ (σ') and thermal occupation numbers f_α (f_β) (see Sections 2.6 and 4.7). The fact that, in the heated system, thermal effects manifest themselves in the RPA or $TDLDA$ equations only through the free correlation function and the density dependence of the residual interaction, which contain the appropriate Fermi–Dirac occupation numbers, has been discussed by many authors (see, for example, Braghin and Vautherin 1994; Hernandez et al. 1996). One can thus realize that the structure of both the RPA and $TDLDA$ equations and its solutions is preserved.

From equation (8.197), taking for F and $G = F$ the symmetric and antisymmetric combinations defined in equation (8.189), it follows that

$$\chi(F^s, F^s, \omega) = \int f^*(\mathbf{r}) f(\mathbf{r}') \alpha_{ss}(r, r', \omega) \, d\mathbf{r} d\mathbf{r}' ,$$

$$\chi(F^a, F^a, \omega) = \int f^*(\mathbf{r}) f(\mathbf{r}') \alpha_{aa}(r, r', \omega) \, d\mathbf{r} d\mathbf{r}' ,$$

$$\chi(F^s, F^a, \omega) = \int f^*(\mathbf{r}) f(\mathbf{r}') \alpha_{sa}(r, r', \omega) \, d\mathbf{r} d\mathbf{r}'$$

$$\chi(F^a, F^s, \omega) = \int f^*(\mathbf{r}) f(\mathbf{r}') \alpha_{as}(r, r', \omega) \, d\mathbf{r} d\mathbf{r}' ,$$

(8.203)

where

$$\alpha_{ss} = \alpha_{\uparrow\uparrow} + \alpha_{\downarrow\downarrow} + \alpha_{\uparrow\downarrow} + \alpha_{\downarrow\uparrow} ,$$

$$\alpha_{aa} = \alpha_{\uparrow\uparrow} + \alpha_{\downarrow\downarrow} - \alpha_{\uparrow\downarrow} - \alpha_{\downarrow\uparrow} ,$$

$$\alpha_{sa} = \alpha_{\uparrow\uparrow} - \alpha_{\downarrow\downarrow} - \alpha_{\uparrow\downarrow} + \alpha_{\downarrow\uparrow} ,$$

$$\alpha_{as} = \alpha_{\uparrow\uparrow} - \alpha_{\downarrow\downarrow} + \alpha_{\uparrow\downarrow} - \alpha_{\downarrow\uparrow} .$$

(8.204)

The simplest physical situation to which it is possible to apply the $TDLSDA$ theory, is the paramagnetic case, in which the magnetization $m_0(r)$ of the ground state is zero, i.e. initially the system is not spin-polarized. In this case we have $\alpha_{\uparrow\uparrow}^{(0)} = \alpha_{\downarrow\downarrow}^{(0)}$, and the function $\mathcal{M}(r)$ of equation (8.196) vanishes identically. It can be easily verified that in such limiting case α_{sa} and α_{as} are zero, and that α_{ss} and α_{aa} obey the Dyson equations

$$\alpha_{ss} = \alpha^{(0)} + \alpha^{(0)} \otimes K_{ss} \otimes \alpha_{ss}$$

$$\alpha_{aa} = \alpha^{(0)} + \alpha^{(0)} \otimes K_{aa} \otimes \alpha_{aa} ,$$

(8.205)

where the kernels are given by $K_{ss} = v(r_{12}) + \mathcal{K}\delta(r_{12})$, $K_{aa} = \mathcal{I}\delta(r_{12})$, and the free correlation function $\alpha^{(0)} = \alpha_{\uparrow\uparrow}^{(0)} + \alpha_{\downarrow\downarrow}^{(0)}$ is the same in the two channels because $\alpha_{\uparrow\uparrow}^{(0)} = \alpha_{\downarrow\downarrow}^{(0)}$. In the paramagnetic limit of longitudinal response, the charge channel (symmetric) and the spin channel (antisymmetric) are uncoupled, and the kernel of the integral equation consists of the Hartree potential term, plus an exchange-correlation term in the former case, and only an exchange-correlation term in the latter. When the system is spin-polarized in the ground state, $\alpha_{\uparrow\uparrow}^{(0)} \neq \alpha_{\downarrow\downarrow}^{(0)}$, $\mathcal{M}(r)$ is not zero, and the two other independent correlation functions α_{sa} and α_{as} produce a (symmetric) density response at F_a, and an (antisymmetric) spin density response at F_s.

Lastly, we note that it can be shown that using the residual interaction given by equation (8.195) in the $RPAE$ equations (8.138), the $RPAE$ solutions for the

energies and matrix elements coincide with the $TDLSDA$ results of the present Section.

In homogeneous systems and when F and $G = F$ are given by the density operator $\rho_q = \sum_i e^{i\mathbf{q}\cdot\mathbf{r}_i}$ and magnetization-density operator $m_q = \sum_i e^{i\mathbf{q}\cdot\mathbf{r}_i}\sigma_i^z$, and in the paramagnetic case, the integral equations (8.205) yield uncoupled algebraic equations for the dynamic polarizabilities in the density and magnetization channels, that are written, respectively, as

$$\chi^{\rho\rho}(q,\omega) = \frac{\chi^0(q,\omega)}{1 - \frac{1}{L^D}(v(q) + \frac{\partial^2 E_{xc}}{\partial\rho^2}|_{gs})\chi^0(q,\omega)}, \qquad (8.206)$$

$$\chi^{mm}(q,\omega) = \frac{\chi^0(q,\omega)}{1 - \frac{1}{L^D}\frac{\partial^2 E_{xc}}{\partial m^2}|_{gs}\chi^0(q,\omega)}. \qquad (8.207)$$

If we compare these equations with the RPA solution (8.86), which was derived in the density channel, we see that the $TDLDA$ theory introduces an explicit dependence on the exchange-correlation energy in the density response, through its second derivative with respect to density. This term changes the dispersion relation of the collective state. For example, in the case of the electron gas, the $TDLDA$ plasmon frequency in the limit of small q becomes

$$\omega^2_{TDLDA}(\mathbf{q}) = \omega_p^2 + \left(\frac{2T_0^D}{m} + \frac{\rho_0}{m}\frac{\partial^2 E_{xc}^D}{\partial\rho^2}\bigg|_{\rho=\rho_0}\right)q^2, \qquad (8.208)$$

where ω_p is given by (8.106). The $TDLDA$ dispersion coefficient, normalized to the RPA dispersion coefficient, is plotted in Fig. 8.3. We see that the agreement with experimental data, though improved with respect to RPA, is still unsatisfactory at high r_s. In the spin-density channel, the $TDLDA$ response is fixed by the second derivative of the exchange-correlation energy with respect to the magnetization, calculated at the magnetization value of the ground state. This quantity is different from zero also for ground states that are not spin-polarized, and is negative. The particle-hole interaction in the magnetic channel is attractive. This has the effect that (see Fig. 8.1) in $2D$ and $3D$ the $TDLDA$ solution, given by the intersection of χ^0/L^D with the (negative) straight line $1/\frac{\partial^2 E_{xc}}{\partial m^2}|_{gs}$, falls into the continuum of single-particle states, so that there is no collective state in the magnetic channel. The situation is different in the $Q1D$ where there exists a gap (see Fig. 7.3) between the continuum of single-particle excited states and the energy zero, so that the $TDLDA$ solution in the $Q1D$ case yields a low-energy collective solution in the magnetic channel.

We finally note that in symmetric nuclear matter (i.e. with the same number of protons and neutrons) it is of special relevance to study the isospin density response in which

$$F^a = G^a = \rho_{1,q} = \sum_i e^{i\mathbf{q}\cdot\mathbf{r}_i}\tau_i^z,$$

where τ_z is the third isospin component. By exploiting the analogy between spin and isospin, and that between equations (4.44) and (4.97), it is possible to write immediately the isospin density response function as

$$\chi^{\rho_1\rho_1}(q,\omega) = \frac{\chi^0(q,\omega)}{1 - \frac{1}{L^D}\frac{\partial W}{\partial \rho_1}|_{gs}\chi^0(q,\omega)}.$$ (8.209)

where W is the symmetry potential of (4.99), and $\rho_1 = \rho_n - \rho_p$ is the isovector density. Therefore, for nuclear matter (and neglecting the small nonlocal a_1 term) we have $\frac{\partial W}{\partial \rho_1}|_{gs} = b_1 + c_1\rho^\gamma$ which, with the parameter values of Tables 4.3, 4.4 and 4.10, leads to the numerical value $\frac{\partial W}{\partial \rho_1}|_{gs} = 28.7$ MeV fm^3. Thus, unlike the magnetic channel, the isospin channel has a repulsive interaction, so that the $TDLDA$ solution yields a collective solution. Such collective solution was experimentally observed in nuclei, and is known as giant resonance (see for example Lipparini and Stringari 1989). The response function of nuclear matter and liquid ^{3}He, was studied in detail starting from density functionals like those described in Section 4.9 [by Garcia-Recio et al. (1992) and Alberico et al. (1991), the one of finite nuclei by Bertsch and Tsai (1975); Liu and Brown (1976) and Liu and N. Van Giai (1983), and that of ^{3}He and ^{4}He clusters by Serra et al. (1991); Barranco et al. (1997) and Casas et al. (1995)].

8.9.2 The TDLSDA transverse response function

Assuming that the spin magnetization is along a fixed direction, that we will take as the z direction, it is possible to derive the transverse spin response in a simple way. The method was developed by Rajagopal (1978), and was applied to quantum dots by Lipparini et al. (1998), (1999). It turns out that the longitudinal and transverse spin responses do not couple. In what follows, we define the spin-flip operators $\sigma_\pm = 1/2(\sigma_x \pm i\sigma_y)$ in such a way that

$$\sigma_+|\uparrow\rangle = \sigma_-|\downarrow\rangle = 0,$$

$$\sigma_+|\downarrow\rangle = |\uparrow\rangle,$$

$$\sigma_-|\uparrow\rangle = |\downarrow\rangle.$$

Let us introduce now a spin magnetization vector $\mathbf{m}$ and assume that the exchange-correlation energy depends only on ρ and $|\mathbf{m}|$, i.e. $E_{xc} = E_{xc}[\rho,|\mathbf{m}|]$. Then, the spin-dependent exchange-correlation potential W_{xc} in equation (8.187)) can be written as

$$\mathbf{W}^{xc}[\rho,|\mathbf{m}|] = W_{xc}[\rho,|\mathbf{m}|]\,\mathbf{m}/|\mathbf{m}|,$$

with

$$W_{xc}[\rho,|\mathbf{m}|] = \partial E_{xc}[\rho,|\mathbf{m}|]/\partial|\mathbf{m}|.$$

At this point, in that equation one performs the change

$$W_{xc}\sigma_z \rightarrow \mathcal{F}_{xc}[\rho, |\mathbf{m}|]\, \mathbf{m} \cdot \boldsymbol{\sigma}\,, \tag{8.210}$$

where $\mathcal{F}_{xc}[\rho, |\mathbf{m}|] \equiv W_{xc}[\rho, |\mathbf{m}|]/|\mathbf{m}|$. Defining the spherical components $\pm$ of the vectors $\mathbf{m}$ and $\boldsymbol{\sigma}$, we have

$$W_{xc}\sigma_z \rightarrow \mathcal{F}_{xc}[\rho, |\mathbf{m}|]\, [m_z \sigma_z + 2(m_+ \sigma_- + m_- \sigma_+)]\,. \tag{8.211}$$

In the static case, the inclusion of the densities m_+ and m_- makes no difference since they vanish identically. The situation is different when the system interacts with a time-dependent field that couples to the electron spin through

$$\mathbf{G} \cdot \boldsymbol{\sigma} = G_z \sigma_z + 2(G_+ \sigma_- + G_- \sigma_+)\,.$$

If the time-dependence is harmonic, the interaction Hamiltonian causing transverse spin excitations may be written as

$$H_{\text{int}} \sim \sum_i [g(\mathbf{r}_i)\, \sigma_-^i\, e^{-\imath \omega t} + g^*(\mathbf{r}_i)\, \sigma_+^i\, e^{\imath \omega t}]\,. \tag{8.212}$$

H_{int} causes non-vanishing variations in the densities m_+ and m_- which, in turn, generate induced potentials through first-order perturbation variations in the mean field of (8.211). This equation shows that the induced interaction is $2\,\mathcal{F}_{xc}\,\delta(\mathbf{r}_1 - \mathbf{r}_2)\,\sigma_-$ for m_+, and $2\,\mathcal{F}_{xc}\,\delta(\mathbf{r}_1 - \mathbf{r}_2)\,\sigma_+$ for m_-, computed for the ground-state values of ρ and m. If we define the transverse correlation function through the equation

$$\delta m^- = \alpha_{-+} \otimes g\,, \tag{8.213}$$

where the symbol $\otimes$ denotes space integration on the space variable common to the operands, and if we require the self-consistency for the density variations like we did in the previous Section, it is easy to reach the following integral equation for α_{-+}:

$$\alpha_{-+} = \alpha_{-+}^{(0)} + 2\,\alpha_{-+}^{(0)} \otimes \mathcal{F}_{xc}\,\delta(r_{12}) \otimes \alpha_{-+}\,, \tag{8.214}$$

in terms of the free correlation function

$$\alpha_{-+}^{(0)}(\mathbf{r}, \mathbf{r}\,'; \omega) = -\sum_{\alpha\beta}(f_\alpha - f_\beta)\frac{\langle\alpha|\sigma_-|\beta\rangle_{\mathbf{r}}\langle\beta|\sigma_+|\alpha\rangle_{\mathbf{r}\,'}}{\epsilon_\beta - \epsilon_\alpha + \omega}\,. \tag{8.215}$$

The dynamic polarizability is further given by

$$\chi_-(\omega) = f^* \otimes \delta m_-\,. \tag{8.216}$$

The expressions for the other transverse channel are

$$\delta m^+ = \alpha_{+-} \otimes g\,, \tag{8.217}$$

$$\alpha_{+-} = \alpha_{+-}^{(0)} + 2\alpha_{+-}^{(0)} \otimes \mathcal{F}_{xc}\,\delta(r_{12}) \otimes \alpha_{+-}\,, \tag{8.218}$$

with

$$\alpha_{+-}^{(0)}(\mathbf{r}, \mathbf{r}'; \omega) = \sum_{\alpha\beta}(f_\alpha - f_\beta)\frac{\langle\alpha|\sigma_+|\beta\rangle_{\mathbf{r}}\langle\beta|\sigma_-|\alpha\rangle_{\mathbf{r}'}}{\epsilon_\alpha - \epsilon_\beta + \omega} . \tag{8.219}$$

And finally

$$\chi_+(\omega) = f^* \otimes \delta m_+ . \tag{8.220}$$

In the homogeneous case when G and F are given by the operators

$$G^- = \sum_i \exp(-i\mathbf{q}\cdot\mathbf{r})_i\sigma_i^- ,$$

$$F^+ = \sum_i \exp(i\mathbf{q}\cdot\mathbf{r})_i\sigma_i^+ ,$$

$$G^+ = \sum_i \exp(-i\mathbf{q}\cdot\mathbf{r})_i\sigma_i^+ ,$$

$$F^- = \sum_i \exp(i\mathbf{q}\cdot\mathbf{r})_i\sigma_i^- ,$$

it is easy to obtain the $TDLSDA$ transverse linear response at zero temperature:

$$\chi_t(q, \omega) = \frac{\chi_t^0(q, \omega)}{1 - \frac{2}{L^D}\mathcal{F}_{xc}\chi_t^0(q, \omega)} . \tag{8.221}$$

with the free transverse linear response given by

$$\chi_t^0(q, \omega) = \sum_{mi}\left(\frac{|\langle m\downarrow|\exp(-i\mathbf{q}\cdot\mathbf{r})\sigma^-|i\uparrow\rangle|^2}{\omega - \epsilon_{mi}} - \frac{|\langle m\uparrow|\exp(i\mathbf{q}\cdot\mathbf{r})\sigma^+|i\downarrow\rangle|^2}{\omega + \epsilon_{mi}}\right). \tag{8.222}$$

In the case of an electron gas in a constant magnetic field that spin-polarizes the system and induces negligible diamagnetic effects, the collective solutions of Eq. (8.221) are not damped, even in the case of attractive p–h interaction, ($\mathcal{F}_{xc} < 0$), and are known as spin-waves. The difference with the longitudinal case, where the collective spin states are always damped for p–h negative interaction, lies in the presence of the magnetic field, which induces magnetization in the system and may generate a gap in the single-particle excitation spectrum for the $2D$ and $3D$ cases like the one shown in Fig. 7.3; for one-dimensional systems such gap is present also for $B = 0$, but not for two-dimensional and three-dimensional systems (see Fig. 7.4).

Spin waves were predicted theoretically by Silin (1958), (1959) and Platzman and Wolf (1967), and observed in alkali metals by Schultz and Dunifer (1967).

In the $TDLSDA$ formalism these spin waves can be obtained as poles of equation (8.221), using for the transverse free-particle wavefunction the expression

$$\chi_t^0(q, \omega) = -\frac{3}{4}\frac{\rho}{\epsilon_F}\left(1 + \frac{\omega}{2qv_F}\ln\frac{\omega - \omega_a - qv_F}{\omega - \omega_a + qv_F}\right), \tag{8.223}$$

which is valid in the $qv_F \ll \epsilon_F$ limit, and where

$$\omega_a = \frac{\omega_L}{\left(1 + \frac{3\rho\mathcal{F}_{xc}}{2\epsilon_F}\right)},$$

with ω_L equal to the Larmor frequency $\omega_L = eB/2mc$. In the high-magnetic field limit: $qv_F/\omega_a < 1$, such free response function is quite different from the $B = 0$ one, and exhibits a gap in the single-particle excitation spectrum. The dispersion of the spin waves, in this case is given by

$$\omega(q) = \omega_L - \frac{1}{3}\frac{q^2 v_F^2}{\omega_a}(1 + F_0^a),   \tag{8.224}$$

with $F_0^a = 3\rho\mathcal{F}_{xc}/2\epsilon_F$. This solution is a collective excitation ($|\text{col}\rangle$) induced by the operator F^-, since it completely exhausts the m_0^- sum rule of Section 7.3, yielding $|\langle\text{col}|F^-|0\rangle|^2 = N_\uparrow - N_\downarrow$; in fact, the strength $|\langle\text{col}|F^+|0\rangle|^2$ is equal to zero owing to the blocking due to the Pauli exclusion principle in the $q \to 0$ limit. To conclude, note that the solution (8.224) obeys the Larmor theorem (see Section 8.10.1).

The above formalism can be applied to the case of liquid ^{3}He (Stringari and Dalfovo 1990), and can be easily generalized to the case of asymmetric nuclear matter ($N \neq Z$), where the transverse collective solution is known as isospin wave (Friman 1980; Lipparini and Stringari 1987). In this latter case the role of the constant magnetic field B is played by the proton Coulomb potential which, in first approximation, produces in the nuclear Hamiltonian a term of the type $-\frac{1}{2}E_C\tau_z$, with E_C equal to the Coulomb energy shift between near nuclei, i.e. the analogue of the Zeeman term present in magnetic-field-polarized systems. Then, for nuclear matter the Larmor frequency turns into the frequency $\omega_C = E_C$.

In the cases of helium and nuclear matter, one can take the interaction parameters F_0^a which appear in the dispersion (8.224) as the Landau parameters, whose values were given in Section 8.1.

8.10   *RPA* and *TDLSDA* Commutators and Symmetry Restoration

In this Section we will discuss a series of results concerning the commutators of a generic, Hermitian, one-body operator, $F = \sum_i f(i)$, with the system Hamiltonian, within the frameworks of the *RPA* and *TDLSDA* theories. In other words, we wish to evaluate the commutator $[H, F]_{RPA} = [H_{RPA}, F]$ where $H_{RPA} = \sum_k \omega_k O_k^\dagger O_k$ and $O_k^\dagger$ (O_k) are the creation (annihilation) operators of the excited *RPA* states k (at frequency ω_k) of equation (8.152). Using the expansion of F in terms of the complete set of *RPA* excitations, and the Boson commutation rules for the operators $O_k^\dagger$ and O_k, we can directly evaluate the commutator $[H_{RPA}, F]$. The *TDLSDA* case can be considered as a particular case of the *RPA* approximation, in which the *RPA* equations (8.138) are solved with the residual particle-hole interaction of

equation (8.195), and with the single-particle wavefunctions and energies obtained as solutions of the Kohn–Sham equations instead of the HF ones. In general, the RPA commutator differs from the true one and, most of all, from the commutator with the static HF (or Kohn–Sham) Hamiltonian, which does not take account of dynamic correlations. The evaluation of the RPA commutator is relevant to the problem of the restoration of symmetries which are broken in the static HF or $LSDA$ theories (see Section 4.11), and for the calculation of the sum rules defined in Section 7.3, taking into account RPA correlations. The results that we are going to show in the following, were proven rigorously in Lipparini and Stringari (1989). For the RPA commutator we obtain the result

$$[H, F]_{RPA} = [H_0^{HF}, F] + \delta H^{HF}(iF), \qquad (8.225)$$

where H_0^{HF} is the static HF Hamiltonian and

$$\delta H^{HF}(iF) = \sum_i \delta H_i^{HF}$$

is the change (linear in F) induced in the HF Hamiltonian by the unitary transformation e^{iF}.

The two terms of (8.225) have different physical meaning: the commutator $[H_0^{HF}, F]$ originates from the static, one-body properties of the Hamiltonian, while the term $\delta H^{HF}(F)$ originates from the renormalization of the self-consistent potential. The latter contribution is essential to take into account the RPA correlations and, in general, to restore the symmetries that are broken by the static theory. In order to expound this point, let us consider the Hamiltonian

$$H = \sum_i \frac{p_i^2}{2m} + g \sum_{i<j} \delta(\mathbf{r}_i - \mathbf{r}_j), \qquad (8.226)$$

which is of relevance for the case of a cold and dilute condensate of Bosons (see Section 2.4). Clearly, this Hamiltonian is invariant under translations, and so it commutes with the total momentum operator $P_z = \sum_i p_i^z$. However, the HF self-consistent Hamiltonian:

$$H^{HF} = \sum_i \left(\frac{p_i^2}{2m} + g\rho(\mathbf{r}_i) \right), \qquad (8.227)$$

where ρ is the Boson density does not commute with P_z when considered from a static point of view but yield the result

$$[H_0^{HF}, iP_z] = -g \sum_i \nabla_z \rho. \qquad (8.228)$$

Nevertheless, if we consider it from the dynamical point of view, it changes due to the variations that take place in its density-dependent terms during the collective

oscillation. The variation

$$\delta H^{HF}(iP_z) = g \sum_i \delta\rho(\mathbf{r}_i), \qquad (8.229)$$

is easily evaluated because the density change, which linear in P_z and induced by the transformation e^{iP_z}, is given by

$$\delta\rho(\mathbf{r}) = \langle HF| \left[\sum_i \delta(\mathbf{r} - \mathbf{r}_i), i \sum_j p_j^z \right] |HF\rangle = \nabla_z \rho(\mathbf{r}). \qquad (8.230)$$

Then we find that the two contributions of equation (8.225) cancel out exactly, and that $[H, P_z]_{RPA} = 0$, thus showing that the RPA theory restores translational symmetry.

As regards the sum rules, the following equalities can be shown:

$$m_1^{RPA} = \frac{1}{2}\langle HF|[F, [H, F^\dagger]_{RPA}]|HF\rangle$$

$$m_3^{RPA} = \frac{1}{2}\langle HF|[[F, H]_{RPA}, [H, [H, F^\dagger]_{RPA}]_{RPA}]|HF\rangle, \qquad (8.231)$$

where $|HF\rangle$ is the HF (or $LSDA$) ground state, and the moments

$$m_k = \sum_n \omega_{no}^k |\langle n|F|0\rangle|^2$$

are computed by using excitation energies and matrix elements given by the solutions of the RPA ($TDLSDA$) equations.

The results (8.231) can be extended to the case of mixed sum rules which involve two different kinds of excitation operators F and G (see Section 7.3):

$$(m_0^-)^{RPA} = \frac{1}{2}\langle HF|[F, G^\dagger]|HF\rangle,$$

$$(m_1^+)^{RPA} = \frac{1}{2}\langle HF|[F, [H, G^\dagger]_{RPA}]|HF\rangle, \qquad (8.232)$$

$$(m_2^-)^{RPA} = \frac{1}{2}\langle HF|[[F, H]_{RPA}, [H, G^\dagger]_{RPA}]|HF\rangle,$$

where, like before, the moments

$$(m_k^\pm)^{RPA} = \sum_n \omega_{no}^k (\langle 0|F|n\rangle\langle n|G^\dagger|0\rangle \pm \langle 0|G^\dagger|n\rangle\langle n|F|0\rangle$$

are computed in the RPA approximation, and the mean values of the RPA commutators, on the HF ground state.

Equations (8.231) and (8.233) show that the calculation of some of the moments of the excitation strength in the RPA ($TDLSDA$) approximation, does not require the explicit solution of the RPA ($TDLSDA$) equations, but only the evaluation of

mean values on the static HF ($LSDA$) state of the RPA commutators that appear in such equations, by using the rule (8.225).

As an example of the application of the above relations, let us compute, starting from the Pauli Hamiltonian (5.1), the m_1^+ sum rule for the operators

$$F = F^+ = \sum_i \exp(i\mathbf{q} \cdot \mathbf{r})_i \sigma_i^+ \,,$$

$$G^\dagger = F^- = \sum_i \exp(-i\mathbf{q} \cdot \mathbf{r})_i \sigma_i^- \,.$$

This sum rule is of relevance in the calculation of the transverse response function of a two-dimensional electron gas confined in a quantum dot, in the presence of an external magnetic field perpendicular to the plane of motion of the electrons. Explicit calculation of

$$m_1^+ = \sum_n \omega_{n0} |\langle n|F^-|0\rangle|^2 + \sum_n \omega_{n0} |\langle n|F^+|0\rangle|^2$$

yields the result:

$$m_1^+ = \frac{Nq^2}{2} - g^* \mu_0 B (N_\uparrow - N_\downarrow) \tag{8.233}$$

where N is the total number of Fermions in the system, and $N_\uparrow$ ($N_\downarrow$) is the number of Fermion with spin up (down), and ($N_\uparrow - N_\downarrow$) is the magnetization of the ground state.

The result of (8.233) for m_1^+ is also reproduced by the $TDLSDA$ theory, if one uses (8.225) to evaluate the $TDLSDA$ commutator in (8.233). Therefore, the transverse spectrum as computed by the $TDLSDA$ theory is such that it satisfies the mixed sum rule m_1^+. On the other hand, the spectra of single-particle models, like those obtained by in the Hartree, HF or Kohn Sham approximations, violate such sum rule. For example, the KS spectrum that one uses to build up the single-particle response function χ^0, leads to the result

$$(m_1^+)^{KS} = \frac{Nq^2}{2} - [g^* \mu_0 B + 2W_{xc}](N_\uparrow - N_\downarrow) \,, \tag{8.234}$$

where W_{xc} is the spin-dependent, exchange-correlation potential that appears in the KS equations (4.44).

In the $TDLSDA$ theory the effect of the induced particle-hole interaction [i.e. the term δH^{HF} of Eq. (8.225)] is crucial in restoring the exact value of m_1^+: in fact, it exactly cancels out the $2W_{xc}$ contribution in (8.234).

8.10.1 The Kohn and Larmor theorems

As was discussed in Section 8.7, using the creation and annihilation operators of the excited states (8.149) and (8.150), one can rewrite the Schrödinger equation as

$$[H, O_\lambda^\dagger]|0\rangle = (E_\lambda - E_0)O_\lambda^\dagger|0\rangle, \tag{8.235}$$

where $|0\rangle$ is the system ground state. This equation (equation of motion) is used, in general, as a starting point to set up approximate theories for the excited states, and the relative excitation energies, of a many body system. However, there are cases where these equations provide exact solutions for such quantities.

Kohn considered the case of a two-dimensional system of N electrons with charge e^-, in a uniform magnetic field perpendicular to the plane where the particles move (i.e. the x–y plane), with Hamiltonian ($\hbar = 1$) given by

$$H = \frac{1}{2m}\sum_{i=1}^{N}\mathbf{P}_i^2 + \sum_{i<j}^{N}V(r_i - r_j) + g\mu_0 B S_z, \tag{8.236}$$

where we chose the vector potential $\mathbf{A}$ in such a way as to give a constant magnetic field along the z axis [e.g. $\mathbf{A} = B(0, x, 0)$], g is the gyromagnetic factor of electrons, and μ_0 is Bohr's magneton. In equation (8.236) S_z is the total spin of the electrons and

$$\mathbf{P} = \sum_{i=1}^{N}(\mathbf{p}_i + \frac{e}{c}\mathbf{A}(\mathbf{r}_i))$$

is their total kinetic momentum ($\mathbf{p}_i = -i\nabla_i$ is the canonical momentum of the i-th electron).

Starting from Eq. (8.236), it is easy to verify that

$$[H, P_+] = \omega_c P_+, \tag{8.237}$$

where $\omega_c = \frac{eB}{mc}$ is the cyclotron frequency, and

$$P_+ = P_x + iP_y, \tag{8.238}$$

because the total momentum $\mathbf{P}$ commutes with the interaction term:

$$\left[\sum_{i<j}^{N}V(r_i - r_j), \mathbf{P}\right] = 0. \tag{8.239}$$

Equation (8.237), together with the equation of motion (8.235), shows that the state $P_+|0\rangle$ is an exact eigenstate of H with energy $E_0 + \omega_c$. This eigenstate is known as the cyclotron resonance of the system, and its frequency cannot be directly affected by any effect caused by inter-particle interaction. This result is known in the literature as the Kohn theorem.

The state $P_+|0\rangle$ is the only state of the system that is excited if we immerse the system in a weak microwave field at frequency ω_c. In fact, describing such field at frequency ω by a vector potential

$$\mathbf{A}' = \left(\frac{E_x}{i\omega}\hat{x} + \frac{E_y}{\omega}\hat{y} \right) e^{-i\omega t},$$

and choosing $E_x = E_y = E$, we find that the interaction Hamiltonian between the system and the homogeneous microwave field is given by

$$H' = \frac{e}{2mc} \sum_{i=1}^{N} (\mathbf{P}_i \cdot \mathbf{A}'_i + \mathbf{A}'_i \cdot \mathbf{P}_i) = \frac{eE}{i\omega mc} P_+ e^{-i\omega t}. \tag{8.240}$$

This operator induces a transition from the ground state $|0\rangle$ to the excited state $P_+|0\rangle$, absorbing the energy ω_c. As a result, a narrow absorption peak emerges at frequency $\omega = \omega_c$.

In the case of a system confined by a potential of parabolic type, such as in quantum dots, it is necessary to add to Hamiltonian (8.236) the confinement potential

$$V_{\text{ext}} = \frac{1}{2}m \sum_{i=1}^{N} \omega_0^2 r_i^2.$$

By using in this case the symmetric gauge $\mathbf{A} = \frac{B}{2}(-y, x, 0)$ and defining $P_\pm = P_x \pm iP_y$, $Q_\pm = Q_x \pm iQ_y$, with

$$Q_x = \sum_{i=1}^{N} x_i \quad \text{and} \quad Q_y = \sum_{i=1}^{N} y_i,$$

and using the commutation relations

$$\left[\frac{P^2}{2m}, Q_\pm \right] = -\frac{i}{m} P_\pm, \quad \left[\frac{P^2}{2m}, P_\pm \right] = \pm\omega_c P_\pm, \quad [V_{conf}, P_\pm] = im\omega_0^2 Q_\pm, \tag{8.241}$$

together with (8.239), it is easy to prove that the following result holds

$$\left[H, Q_\pm - \frac{i\omega_\pm}{m\omega_0^2} P_\pm \right] = \omega_\pm \left(Q_\pm - \frac{i\omega_\pm}{m\omega_0^2} P_\pm \right), \tag{8.242}$$

where $\omega_\pm = \sqrt{\omega_0^2 + 1/4\omega_c^2} \pm \omega_c/2$.

Equation (8.242), together with the equation of motion (8.235), proves that the states $(Q_\pm - i(\omega_\pm/m\omega_0^2)P_\pm)|0\rangle$ are exact eigenstates of H with respective energies $E_0+\omega_\pm$. These eigenstates are the bulk and edge plasmon resonances of the quantum dots under magnetic field, whose frequencies cannot be directly affected by any effect caused by electron interactions. This result is known in the literature as the generalized Kohn theorem. Such plasmon states are the only ones which are

excited in photo-absorption reactions with long-wavelength photons (far-infrared absorption), and have been observed in several experiments (see Section 8.13.2).

The generalized Kohn theorem applies to all systems undergoing harmonic confinement. In the absence of magnetic field, it implies the existence of a collective state at energy ω_0. This state has been observed in cold and dilute Boson gases (see Section 8.6) and in metal clusters (Section 8.8.2).

Starting from (8.236) (with or without confinement potential) it is also easy to verify that the following result is found

$$[H, S_\pm] = \pm \omega_L S_\pm \,, \tag{8.243}$$

where $S_\pm = S_x \pm i S_y$ and $\omega_L = g\mu_0 B$ is the Larmor frequency. Equation (8.243), together with the equation of motion (8.235), proves that for a system with spin polarized ground state ($\langle 0|S_z|0\rangle = (N_\downarrow - N_\uparrow)/2$ for positive g), the state $S_+|0\rangle$ is an exact eigenstate of H with energy $E_0 + \omega_L$. This eigenstate is known as the Larmor state of the system, and its frequency cannot be directly affected by any effect caused by inter-particle interaction. Equation (8.243), together with the result $[H, S_z] = 0$, allows us to write

$$\frac{d\mathbf{S}}{dt} = g\mu_0 \mathbf{S} \wedge \mathbf{B} \,. \tag{8.244}$$

This result is known in the literature as the Larmor theorem, and is the equation for a precessing spin. In the exact theory, precession takes place at the angular frequency $\omega = \omega_L$.

The Kohn and Larmor theorems are not fulfilled by the mean-field theories like the Hartree, HF and Kohn–Sham theories. However, they are satisfied by the RPA and $TDLSDA$ theories. This can be easily shown using the rule (8.225) for the RPA and $TDLSDA$ commutators, and employing such commutators in the equation of motion with the exact ground state replaced by the HF and $LSDA$ ground states. In the forthcoming Sections this point will be expounded in detail for some cases.

8.10.2   *Magneto-conductivity and quantum Hall effect*

By using the results of the previous subsection we now evaluate the transverse conductivity of a two-dimensional electron gas in a magnetic field perpendicular to the plane of motion of the electrons, with Hamiltonian given by (8.236). In the presence of an electric field in the x-direction, giving rise to the interaction Hamiltonian $H' = -\frac{Ej_x}{i\omega}e^{-i\omega t}$, the xx conductivity is given by (see Chapter 7):

$$\sigma_{xx}(0, \omega) = \frac{\langle j_x \rangle}{E} = \frac{i}{\omega} \frac{\sum_n 2\omega_{n0} |\langle n|j_x|0\rangle|^2}{\omega^2 - \omega_{n0}^2} \,, \tag{8.245}$$

so that its real part is given by

$$\text{Re}\left[\sigma_{xx}(0,\omega)\right] = \frac{\pi e^2}{\omega} S\left(\sum_{i=1}^{N} (p_x/m)_i, \omega\right), \tag{8.246}$$

where we have used

$$j_x = -e\sum_{i=1}^{N} p_x/m, \tag{8.247}$$

and the strength S is given by

$$S\left(\sum_{i=1}^{N} (p_x/m)_i, \omega\right) = \sum_n \left| \langle n | \sum_{i=1}^{N} (p_x/m)_i | 0\rangle \right|^2 \delta(\omega - \omega_{n0})$$

$$= \left| \langle 0 | \left[\sum_{i=1}^{N} (p_x/m+)_i, O^\dagger_{\omega_c}\right] | 0\rangle \right|^2 \delta(\omega - \omega_c), \tag{8.248}$$

$$O^\dagger_{\omega_c} = \sqrt{\frac{1}{2Nm\omega_c}} \sum_{i=1}^{N} (-m\omega_c x + i p_x - p_y)_i, \tag{8.249}$$

and we have used results (8.237) and (8.238) and normalized the state $|\omega_c\rangle = O^\dagger_{\omega_c}|0\rangle$ to unity.

From equations (8.248) and (8.249) one gets for the xx conductivity per unit of surface

$$\text{Re}\left[\sigma_{xx}(0,\omega)\right] = \frac{\pi e^2}{2m}\rho\delta(\omega - \omega_c). \tag{8.250}$$

The yx conductivity is then given by

$$\sigma_{yx}(0,\omega) = \frac{\langle j_y\rangle}{E} = \frac{i}{\omega}\sum_n \left(\frac{\langle 0|j_y|n\rangle\langle n|j_x|0\rangle}{\omega - \omega_{n0}} - \frac{\langle 0|j_x|n\rangle\langle n|j_y|0\rangle}{\omega + \omega_{n0}}\right), \tag{8.251}$$

where

$$j_y = -e\sum_{i=1}^{N}(p_y/m + \omega_c x)_i. \tag{8.252}$$

Once more, by using the fact that only the cyclotron state $|\omega_c\rangle = O^\dagger_{\omega_c}|0\rangle$, with $O^\dagger_{\omega_c}$ given by (8.249) can be excited in (8.251), it is easy to show that the real part of the yx conductivity is given by

$$\text{Re}\left[\sigma_{yx}(0,\omega)\right] = -\frac{e^2\rho\omega_c}{m} P\left(\frac{1}{\omega^2 - \omega_c^2}\right). \tag{8.253}$$

The DC yx conductivity, which is obtained by (8.253) taking the $\omega = 0$ limit, coincides with the classical Hall conductivity. We stress, however, that result (8.253) is an exact result of quantum mechanics. It is independent of the Landau-level index ν. Therefore, if ν Landau levels are filled by electrons with density $\rho = \nu\frac{eB}{ch}$, we find

$$\text{Re}\,[\sigma_{yx}] = \frac{ec\rho}{B} = \nu\frac{e^2}{h}\,. \tag{8.254}$$

At the same time, the DC xx conductivity in the direction of the electric field is zero. It is important to notice that even though ν is an integer, the Hall conductivity is actually proportional to the ground state density ρ, which is a continuous variable. That is, the second equality in (8.254) holds only at a particular ρ.

If the magnetic field is so strong that only the first Landau level is filled with a fractional filling factor, as happens for the Laughlin states, then equation (8.254) holds also for $\nu = 1/m$. The integer quantized Hall effect, has been observed in 1980 by von Klitzing et al. and the fractional quantized Hall effect has been measured by Tsui et al. (1982) and Willet et al. (1987).

The calculation of the Hall conductivity is also very instructive in the case of a system confined by a potential of parabolic type for which the exact solutions (8.242) hold. In the presence of an electric field in the x-direction the real part of the xx conductivity is given by (we use now the symmetric gauge):

$$\text{Re}\,[\sigma_{xx}(0,\omega)] = \frac{\pi e^2}{\omega}S\left(\sum_{i=1}^{N}(p_x/m - \omega_c/2y)_i, \omega\right)\,, \tag{8.255}$$

where

$$S\left(\sum_{i=1}^{N}(p_x/m - \omega_c/2y)_i, \omega\right) = \sum_{n}\left|\langle n|\sum_{i=1}^{N}(p_x/m - \omega_c/2y)_i|0\rangle\right|^2 \delta(\omega - \omega_{n0})$$

$$= \left|\langle 0|\left[\sum_{i=1}^{N}(p_x/m - \omega_c/2y)_i, O_+^\dagger\right]|0\rangle\right|^2 \delta(\omega - \omega_+)$$

$$+ \left|\langle 0|\left[\sum_{i=1}^{N}(p_x/m - \omega_c/2y)_i, O_-^\dagger\right]|0\rangle\right|^2 \delta(\omega - \omega_-)\,, \tag{8.256}$$

$$O_\pm^\dagger = \frac{1}{2}\sqrt{\frac{m\bar\omega}{N}}\sum_{i=1}^{N}\left(x \pm iy - \frac{i}{m\bar\omega}(p_x \pm ip_y)\right)_i\,, \tag{8.257}$$

and we have used result (8.242), defined $\bar\omega = \sqrt{\omega_0^2 + \omega_c^2/4}$ so that $\omega_\pm = \bar\omega \pm \omega_c/2$ and normalized the states $|\omega_\pm\rangle = O_\pm^\dagger|0\rangle$ to the unity. Performing the commutators

in (8.256) one gets for the conductivity per unit surface area:

$$\text{Re}\left[\sigma_{xx}(0,\omega)\right] = \frac{\pi e^2}{4m}\frac{\rho}{\bar{\omega}}\left(\omega_+\delta(\omega - \omega_+) + \omega_-\delta(\omega - \omega_-)\right). \qquad (8.258)$$

From this equation, in the limit $\omega_0 \equiv 0$, one recovers immediately equation (8.250), since in this limit $\omega_- = 0$ and $\omega_+ = \omega_c$.

The real part of the yx conductivity can be calculated in an analogous way. One starts from (8.251) and uses as the excited states of this equation the two states $|\omega_\pm\rangle = O_\pm^\dagger|0\rangle$. After a simple calculation one finds

$$\text{Re}\left[\sigma_{yx}\right] = -\frac{e^2\rho}{2m\bar{\omega}}P\left(\frac{\omega_+^2}{\omega^2 - \omega_+^2} - \frac{\omega_-^2}{\omega^2 - \omega_-^2}\right). \qquad (8.259)$$

Once again, we see that from this equation, in the limit $\omega_0 \equiv 0$, one recovers immediately equation (8.253). However for $\omega_0 \neq 0$, differently from the bulk case, the DC conductivity of the dot vanishes since the two excitation branches in the dot contribute to the DC conductivity in an equal and opposite way.

8.11   The Linear Response Based on the Green Functions. *RPAE*

In this Section we will compare the previously discussed *RPA* and *TDLSDA* theories, with the approach to the linear density response function based on the particle-hole (p–h) Green functions. The density response function $\chi(\mathbf{q},\omega)$ is connected to the Green function by the relation (in the following, for simplicity, we ignore spin sums)

$$\chi(\mathbf{q},\omega) = \int\frac{d\mathbf{k}}{(2\pi)^D}G_D^{ph}(\mathbf{k},\mathbf{q},\omega), \qquad (8.260)$$

where D indicates, as usual, the dependence on dimensionality and G_D^{ph} is the p–h Green function for the transition [induced by the external field $(\mathbf{q},\omega)$] from the initial hole (h) state $\mathbf{k}$, to the final particle (p) state $\mathbf{k}+\mathbf{q}$. $G_D^{ph}(\mathbf{k},\mathbf{q},\omega)$ is a solution of the Dyson integral equation:

$$G_D^{ph}(\mathbf{k},\mathbf{q},\omega) = G_{0,D}^{ph}(\mathbf{k},\mathbf{q},\omega)$$

$$+ G_{0,D}^{ph}(\mathbf{k},\mathbf{q},\omega)\int\frac{d\mathbf{p}}{(2\pi)^D}V(\mathbf{k},\mathbf{p},\mathbf{q})G_D^{ph}(\mathbf{p},\mathbf{q},\omega), \quad (8.261)$$

where $G_{0,D}^{ph}(\mathbf{k},\mathbf{q},\omega)$ is the *HF* Green function:

$$G_{0,D}^{ph}(\mathbf{k},\mathbf{q},\omega) = \frac{(1 - n_{\mathbf{k}+\mathbf{q}})n_{\mathbf{k}}}{\omega - \varepsilon_{\mathbf{kq}} + i\eta} - \frac{(1 - n_{\mathbf{k}})n_{\mathbf{k}+\mathbf{q}}}{\omega - \varepsilon_{\mathbf{kq}} - i\eta}, \qquad (8.262)$$

with $n_{\mathbf{k}}$ given by (1.73) and

$$\varepsilon_{\mathbf{kq}} = \frac{(\mathbf{k}+\mathbf{q})^2}{2m} + \Sigma(\mathbf{k}+\mathbf{q}) - \frac{\mathbf{k}^2}{2m} - \Sigma(\mathbf{k})$$

[$\Sigma(\mathbf{k})$ is the Fock self-energy (2.34)], and $V(\mathbf{k}, \mathbf{p}, \mathbf{q})$ is the particle-hole interaction given by the matrix element

$$V(\mathbf{k}, \mathbf{p}, \mathbf{q}) = \langle \mathbf{k}, \mathbf{k}+\mathbf{q} | V | \mathbf{p}+\mathbf{q}, \mathbf{p} \rangle . \qquad (8.263)$$

For example, for the Coulomb interaction the direct and exchange matrix elements are respectively: $4\pi e^2/q^2$ and $4\pi e^2/|\mathbf{k}-\mathbf{p}|^2$ in $3D$, and $2\pi e^2/q$ and $2\pi e^2/|\mathbf{k}-\mathbf{p}|$ in $2D$. The response function obtained from the solution of the Dyson equation with includes exchange effects, is the $RPAE$ response function that we introduced in Section 8.7 starting from the $TDHF$ equations, and that differs from the RPA response because the latter takes into account only the direct matrix elements of the interaction.

The exchange matrix elements make the solution of the integral Dyson equation (8.261) in homogeneous systems a very difficult task. Indeed, much more difficult than in finite systems that we considered in Section 8.8, where spherical symmetry was assumed for the problem. To the best of the Author's knowledge, such equation was solved only in the case of the $2D$ interacting electron gas (Takayanagi and Lipparini 1995; Schulze et al. 2000). For its solution, it is opportune to introduce the "vertex function" $f(\mathbf{k}, \mathbf{q}, \omega)$ defined by

$$G_D^{ph}(\mathbf{k}, \mathbf{q}, \omega) = f(\mathbf{k}, \mathbf{q}, \omega) G_{0,D}^{ph}(\mathbf{k}, \mathbf{q}, \omega) , \qquad (8.264)$$

which satisfies the integral equation

$$f(\mathbf{k}, \mathbf{q}, \omega) = 1 + \int \frac{d\mathbf{p}}{(2\pi)^D} V(\mathbf{k}, \mathbf{p}, \mathbf{q}) f(\mathbf{k}, \mathbf{q}, \omega) G_{0,D}^{ph}(\mathbf{p}, \mathbf{q}, \omega) . \qquad (8.265)$$

Equation (8.265) is still a singular integral equation, like the original Dyson equation, but it has the advantage now the singularities are in the known function $G_{0,D}^{ph}(\mathbf{p}, \mathbf{q}, \omega)$ of equation (8.262). The numerical results show that the exchange contributions to the static and dynamic responses are important, and that such quantities differ much from the RPA predictions, and agree with the Monte Carlo calculations for the static response. The plasmon dispersion and the single-particle transition range for the $2D$ electron gas are reported in Fig. 8.17.

From the curves we observe that in $2D$ the $RPAE$ predicts Landau damping (the plasmon energy touches the border of the single-particle excitations) at q values which are relatively low with respect to the RPA predictions.

The $TDLDA$ approximation can be obtained from equation (8.261), by omitting the exchange contributions in the matrix element (8.263), and the Fock self-energy term in the single-particle energies and identifying the p–h interaction in momentum
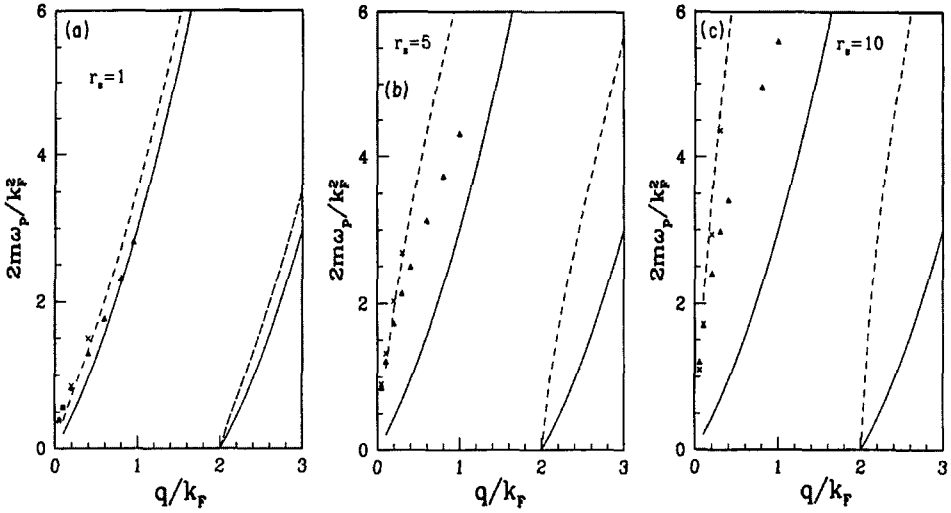
Fig. 8.17   Plasmon dispersion, and single-particle transition range for the 2D electron gas. Crosses and triangles are the plasmon dispersion in $RPAE$ and RPA, respectively. Dashed and full lines give the HF and Hartree single-particle transition ranges, respectively. (a) $r_s = 1$. (b) $r_s = 5$. (c) $r_s = 10$.

space with

$$V(\mathbf{k}, \mathbf{p}, \mathbf{q}) = v(q) + \left. \frac{\partial V_{xc}}{\partial \rho} \right|_{\rho = \rho_0} . \qquad (8.266)$$

Then, $V(\mathbf{k}, \mathbf{p}, \mathbf{q})$ as given by equation (8.266) can be taken out of the integral in (8.261) and, integrating such equation in $d\mathbf{k}$, we obtain an algebraic equation for the response function. By solving the latter yields the $TDLDA$ solution of (8.206). The RPA solution of equation (8.86) is then obtained from (8.261) by taking $V(\mathbf{k}, \mathbf{p}, \mathbf{q}) = v(q)$. Note, further, that in co-ordinate space the p–h interaction (8.266) becomes

$$V_{ph}(|\mathbf{r}_1 - \mathbf{r}_2|) = v(|\mathbf{r}_1 - \mathbf{r}_2|) + \left. \frac{\partial V_{xc}}{\partial \rho} \right|_{\rho = \rho_0} \delta(\mathbf{r}_1 - \mathbf{r}_2), \qquad (8.267)$$

and that the quantity $\left. \frac{\partial V_{xc}}{\partial \rho} \right|_{\rho = \rho_0}$ is connected to the compressibility K of the system by the relation

$$\left. \frac{\partial V_{xc}}{\partial \rho} \right|_{\rho = \rho_0} = \frac{L^D}{\nu(0)_D} \left(\frac{K_0}{K} - 1 \right), \qquad (8.268)$$

where K_0 is the compressibility of the non-interacting system, and $\nu(0)_D$ is the density of states at the Fermi surface. The "vertex function", defined in (8.265), has a very simple expression in the $TDLDA$ theory, given by

$$f^{TDLDA}(\mathbf{q}, \omega) = \frac{1}{1 - (v(q) + \frac{\partial V_{xc}}{\partial \rho}|_{\rho=\rho_0})\chi^0(\mathbf{q}, \omega)}. \qquad (8.269)$$

In the RPA the vertex function is obtained by the above expression setting to zero the derivative of the exchange-correlation potential.

8.12   Screened Response Function and Dielectric Constant

In charged systems, it is convenient to define the screened response function χ^{sc}. This is the response of the system to the sum of the external field plus the Coulomb polarization field. The relation between χ and χ^{sc} in the linear response theory, is easily found from the equation

$$\lambda \chi = [\delta\rho v(q) + \lambda]\chi^{sc} = \delta\rho L^D, \qquad (8.270)$$

which follows from the definitions [see Eq. (8.77)] $\chi = \frac{\delta\rho L^D}{\lambda}$, $\chi^{sc} = \frac{\delta\rho L^D}{\lambda'}$, with $\lambda' = \delta\rho v(q) + \lambda$ equal to the sum of the external field λ plus the Coulomb polarization field $\delta\rho v(q)$. In this way we find

$$\chi(\mathbf{q}, \omega) = \frac{\chi^{sc}(\mathbf{q}, \omega)}{1 - \frac{v(q)}{L^D}\chi^{sc}(\mathbf{q}, \omega)}, \qquad (8.271)$$

which leads to the following results for χ^{sc} in the RPA and in $TDLDA$:

$$\chi^{sc}_{RPA}(\mathbf{q}, \omega) = \chi^0(\mathbf{q}, \omega), \qquad (8.272)$$

$$\chi^{sc}_{TDLDA}(\mathbf{q}, \omega) = \frac{\chi^0(\mathbf{q}, \omega)}{1 - \frac{1}{L^D}\frac{\partial V_{xc}}{\partial \rho}|_{\rho=\rho_0}\chi^0(\mathbf{q}, \omega)}. \qquad (8.273)$$

The screened response has the following property (equivalent to equation (7.68) which is valid for neutral systems)

$$\lim_{q \to 0} \frac{\chi^{sc}(\mathbf{q}, 0)}{L^D} = -\rho^2 K, \qquad (8.274)$$

where K is the system compressibility. Moreover, it is related to the dielectric constant of the system by the relation

$$\epsilon(\mathbf{q}, \omega) = 1 - \frac{v(q)}{L^D}\chi^{sc}(\mathbf{q}, \omega), \qquad (8.275)$$

which follows from the definition

$$\chi^{sc}(\mathbf{q}, \omega) = \epsilon(\mathbf{q}, \omega)\chi(\mathbf{q}, \omega). \qquad (8.276)$$

The dielectric constant $\epsilon(\mathbf{q}, \omega)$ allows us to define a screened static Coulomb potential

$$V_{\text{eff}}(\mathbf{q}) = \frac{v(\mathbf{q})}{e\epsilon(\mathbf{q}, 0)}, \tag{8.277}$$

which gives the Fourier transform of the electrostatic potential $v(\mathbf{r})$ felt by an electron, due to its interaction with a charge e placed at the origin of the plasma. Such external charge polarizes the electrons of the gas in its neighborhood, so that a distant electron responds to both the external charge and the induced polarization charge. In the Thomas–Fermi approximation (Mott and Jones 1936), and in $3D$, we find that

$$V_{\text{eff}}(\mathbf{q}) = \frac{4\pi e}{q^2 + q_{FT}^2}, \tag{8.278}$$

where

$$q_{FT} = \sqrt{\frac{6\pi e^2 \rho_0}{\epsilon_F}}, \tag{8.279}$$

is the Thomas–Fermi momentum. Its reciprocal $\lambda_{FT} = q_{FT}^{-1}$ is known as the "screening length". The ratio of this quantity to the Wigner-Seitz radius is proportional to the square root of the ratio between the mean kinetic and potential energies. For an electron gas at metallic densities (i.e. r_s between 2 and 6), such ratio is approximately 1, so that the screening length and the inter-particle distance are comparable. Thus, it turns out that for the electron gas of physical interest screening is important.

8.13 Examples of Application of the *TDLSDA* Theory

Recently (Eriksson et al. 1999), it has become possible to produce a $GaAs/Al_xGa_{1-x}As$ quantum well containing a high-quality, two-dimensional electron gas, and to vary the density of this gas by changing the density of electron donors in the heterojunction. This experimental realization opened the way for the study of interaction effects in two-dimensional electron systems in the presence of strong magnetic fields, and for the possibility of comparing these studies with the ones carried out on quantum dots where the finite-size effects are important, and different excitation modes (edge modes) are present. In particular, at present the data on inelastic scattering of photons (Raman scattering) are available for both systems (Eriksson et al. 1999; Schuller et al. 1998). These data allow comparison to be made between the excitation spectra of quantum dots and quantum wells, within the framework of the same reaction process. In the next two subsections we will study the excitation spectra of these systems using the *TDLSDA* approximation.

8.13.1   *Quantum wells under very high external magnetic field*

In this subsection we will study the collective states of the two-dimensional electron gas ($2DEG$) under a very high perpendicular magnetic field which, in the ground state of the system, causes full occupation of an integer number of Landau levels. The excited states of the $2DEG$ under very strong magnetic field were studied in the past by several authors. Of particular relevance are the calculations by Kallin and Halperin (1984) and MacDonald (1985), who studied, respectively, the dispersion with transferred momentum q and with the magnetic field B, of the density excitations (CDE) and of the magnetization-density excitations (SDE) in the $2DEG$, within the $RPAE$ and $TDHF$ approximations. The results of the two approaches are fully equivalent. Their agreement with the results of inelastic photon scattering experiments on the dispersion of SDE and CDE modes in the $2DEG$ at filling factor $\nu = 2$, is good only in the limit of high density. At large r_s, large discrepancies between theory and experiment are observed. Instead of only one roton minimum (see Fig. 8.18), and of the instability predicted by $TDHF - RPA$ calculations at $r_s \simeq 3$, the experimental dispersion exhibits two roton minima in the spin channel, and a possible instability only at much larger r_s values (≥ 11) (see Fig. 8.19).

    In the following, we will study the dispersion of longitudinal and transverse density modes in the $2DEG$, by means of the $TDLSDA$ approximation described in the previous Sections (Ghizzi 2000) which, unlike the $TDHF - RPA$ approximation, includes the effects of correlations in the local density approximation. For the longitudinal modes we will limit the calculation to the $\nu = 2$ case, which is of interest and has been studied experimentally. In the transverse channel we will later consider the case $\nu = 1$ as well, in order to evidence the effects of the spin-polarization of the system, which in this channel are of paramount importance. The generalization to other filling factors is direct.
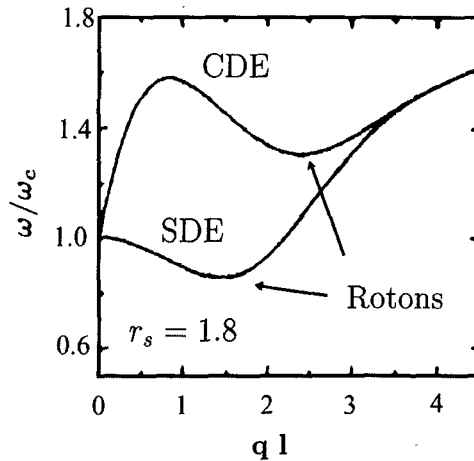
Fig. 8.18   Density excitations (CDE) and magnetization-density excitations (SDE), as a function of the transferred momentum q, in the $TDHF$ approximation. $l = \sqrt{c/eB}$ is the magnetic length.

Density (10^{10} cm^{-2})
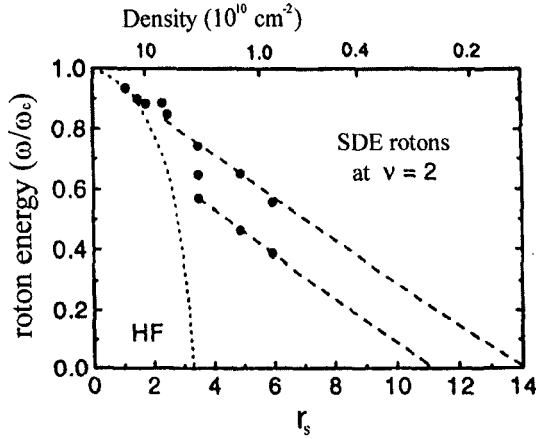
Fig. 8.19 Energies of the rotonic minima in the spin channel SDE, as a function of r_s. Black dots: experimental results. Note that for $r_s \geq 3.3$ more than one rotonic minimum is observed. Dotted line: energy of the rotonic minimum computed in *TDHF*. Dashed line: linear extrapolation of the data.

A. Longitudinal response

In Section 8.9.1 we derived an integral equation for the *TDLSDA* correlation function $\alpha_{\sigma\sigma'}(\mathbf{r}, \mathbf{r}', \omega)$ [see Eqs. (8.194–8.196)], whose main ingredients are the free correlation function, and the residual particle-hole interaction, which were set up starting from the solutions of the KS equations, and from the exchange-correlation potential, respectively. In the case of a homogeneous gas we have that $v_{\text{ext}} + U = 0$ and the exchange-correlation potentials, V_{xc} and W_{xc}, are constant, so that it is only the kinetic energy operator that determines the solutions of the Kohn–Sham equations (apart from the spin-dependent terms which split the single-particle energy levels with different spin). In the case of a very intense magnetic field, directed perpendicularly to the plane of motion of the electrons with charge $-e$, it is convenient to choose the Landau gauge for the vector potential $\mathbf{A}$, for which we have $\mathbf{A} = (0, B_z x, 0)$. Thus, we need to solve the KS equation ($\hbar = 1$):

$$\frac{1}{2m} \left(\mathbf{p} + \frac{e}{c} \mathbf{A} \right)^2 \varphi_i(x, y) = \epsilon_i \varphi_i(x, y), \qquad (8.280)$$

that is

$$\left[-\frac{1}{2m} \left(\frac{\partial^2}{\partial x^2} + \frac{\partial^2}{\partial y^2} \right) - i\omega_c x \frac{\partial}{\partial y} + \frac{1}{2} m\omega_c^2 x^2 \right] \varphi_i(x, y) = \epsilon_i \varphi_i(x, y) \quad (8.281)$$

where $\omega_c = \frac{eB}{mc}$ is the cyclotron frequency. Looking for the general solution in the form

$$\varphi_i(x, y) = \frac{1}{\sqrt{L_y}} e^{-ik_y y} \psi_M(x),$$

where k_y obeys the periodicity condition $k_y = \frac{2\pi}{L_y}n$, for $n = 0, \pm 1, \pm 2, \ldots$, we obtain for $\psi_M(x)$ the following equation

$$\left(-\frac{1}{2m}\frac{\partial^2}{\partial x^2} + \frac{1}{2}m\omega_c^2(x - X)^2\right)\psi_M(x) = \epsilon_M\psi_M(x) \tag{8.282}$$

which is the equation of a harmonic oscillator whose equilibrium position is $X = k_y/m\omega_c$, and whose eigenstates are the Hermite polynomials. Therefore, the eigenfunctions for the Kohn–Sham equation are

$$\varphi_{M,X,\sigma}(x, y) = \frac{e^{-iXy/l^2}}{\sqrt{L_y\pi^{1/2}2^M M!l}}e^{-\frac{(x-X)^2}{2l^2}}H_M\left(\frac{x-X}{l}\right)\chi_\sigma \tag{8.283}$$

where χ_σ is eigenfunction of the spin operator, while $l = (m\omega_c)^{-1/2}$ is the magnetic length and $H_M(\frac{x-X}{l})$ is the Hermite polynomial of degree M defined by

$$H_M(\xi) = (-1)^M e^{\xi^2}\frac{d^M}{d\xi^M}e^{-\xi^2}. \tag{8.284}$$

The eigenvalues of the KS equation, taking account of the spin-dependent (constant) terms as well, are given by ($M = 0, 1, 2, \ldots$):

$$\epsilon_{M,\sigma} = \omega_c\left(M + \frac{1}{2}\right) + \left(W_{xc} + \frac{1}{2}g^*\mu_0 B\right)\sigma. \tag{8.285}$$

We see that the eigenvalues depend only on M, which indicates the different Landau levels, and on the spin $\sigma = \pm 1$, which splits each one of these levels into two sublevels set apart by the constant amount $2W_{xc} + g^*\mu_0 B$. For fixed values of M and σ, the quantum number $X = (2\pi/L_y m\omega_c)n$ for $n = 0, \pm 1, \pm 2 \ldots$ can take on infinite numbers of values; this means that each Landau level is infinitely degenerate. The spin-splitting term is negative, since both W_{xc} and g^* are negative, so that once M is fixed, the states whose spin is parallel to the magnetic field, $\sigma = 1$, have lower energies than those with $\sigma = -1$.

The electron density is given by

$$\rho(x, y) = \sum_\sigma \rho_\sigma = \sum_{MX\sigma}|\varphi_{M,X,\sigma}(x, y)|^2,$$

where the sum covers all the occupied states $MX\sigma$, and it is easy to verify that in the limit $N \to \infty$, it is a constant given by

$$\rho = \frac{eB}{2\pi c}\nu \qquad \nu = 1, 2, 3, \ldots \tag{8.286}$$

where $\nu = \nu_\uparrow + \nu_\downarrow$ is the number of Landau levels occupied by the electrons in the ground state. The density (8.286) is consistent with the initial statement

$$v_{\text{ext}} + U = 0,$$

which allowed us to simplify the KS equations.

The zero-temperature ground state is determined solely by the filling factor $\nu = (2\pi\rho c/eB)$. For example, $\nu = 1$ means that all electrons are in the first Landau level $M = 0$, and have spin up, while $\nu = 2$ means that the electrons occupy the two Landau levels: $M = 0$, $\sigma = \uparrow$ and $M = 0$, $\sigma = \downarrow$. These states are easily obtained experimentally, because the density and the magnetic field are two parameters that can be controlled independently from each other. The *LSDA* theory cannot treat the fractional regime in which $\nu < 1$. However, it can be generalized by the *CDFT* theory (see Section 4.7) to include this regime as well which, however, will not be treated in this Section. Here we will be concerned with $\nu = 2$ and $\nu = 1$ filling.

For $\nu = 2$, the system is not spin-polarized ($S_z = 0$, $W_{xc} = 0$), and in the paramagnetic ground state two Landau levels with $M = 0$ are occupied, and states with spin-up and spin-down are shifted in energy only by the Zeeman term. In this case, as was shown in Section 8.9.1, only the two correlation functions α^{ss} and α^{aa} of equation (8.205) are different from zero, and they describe the density response of the density operator $\rho(q) = \sum_i \exp(i\mathbf{q} \cdot \mathbf{r}_i)$, and the magnetization density response of the spin-density operator $m(q) = \sum_i \exp(i\mathbf{q} \cdot \mathbf{r}_i)\sigma_i^z$, respectively. Since in the integral equations for α^{ss} and α^{aa} the free correlation function is the same, the difference between the *TDLSDA* responses in the two channels is only due to the different kernels (residual interactions). The longitudinal *TDLSDA* response is obtained from the correlation functions as

$$\chi_{AA}(q,\omega) = \int d\mathbf{r}_1 d\mathbf{r}_2 \exp(i\mathbf{q} \cdot (\mathbf{r}_1 - \mathbf{r}_2))\alpha_{AA}(r_1, r_2; \omega), \qquad (8.287)$$

with A equal to ρ or m. As discussed in a paper by Horing (1965), in the case of a two-dimensional electron gas under magnetic field, the correlation functions that appear in the Dyson integral equation are functions only of the module of the spatial distance, as in the case with no magnetic field. Then, the response functions $\chi(q,\omega)$ are obtained from the correlation functions as Fourier transforms, and in this case as well, the integral equations (8.205) yield algebraic equations for the dynamic polarizabilities which in $2D$ are written as

$$\chi_{\rho\rho}(q,\omega) = \frac{\chi^{(0)}(q,\omega)}{1 - \frac{1}{S}(\frac{2\pi}{q} + \mathcal{K})\chi^{(0)}(q,\omega)}, \qquad (8.288)$$

$$\chi_{mm}(q,\omega) = \frac{\chi^{(0)}(q,\omega)}{1 - \frac{1}{S}\mathcal{I}\chi^{(0)}(q,\omega)}. \qquad (8.289)$$

where $\mathcal{K} = \frac{\partial^2 E_{xc}}{\partial \rho^2}$ and $\mathcal{I} = \frac{\partial^2 E_{xc}}{\partial m^2}$. Equations (8.288) and (8.289) are then completely similar to those [i.e. Eqs. (8.206) and (8.207)] for the response functions of the electron gas in the absence of magnetic field. The presence of the field, however, affects the calculation of the free response function substantially. For $\nu = 2$ we have $\chi^{(0)} = \chi_{\uparrow\uparrow}^0 + \chi_{\downarrow\downarrow}^0$ and $\chi_{\uparrow\uparrow}^0 = \chi_{\downarrow\downarrow}^0$. Since single-particle transitions are possible only between states with the same spin, and for which the Landau index M in the final
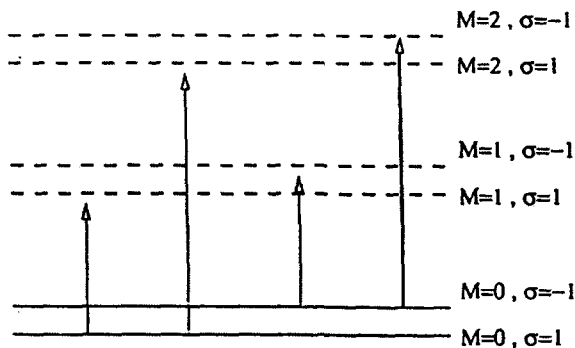
Fig. 8.20   Possible excitations for the three first occupied Landau levels in the case $\nu = 2$. The full line marks the occupied Landau levels in the ground state; the dashed line marks the non-occupied levels.

state differs from the one in the initial state (which is zero, see Fig. 8.20), we have:

$$\chi_{\uparrow\uparrow}^0(q,\omega) = \sum_{M=1}^{\infty} \sum_{X,X'} \frac{2(\epsilon_{M\uparrow} - \epsilon_{0\uparrow})|\langle M\uparrow X|e^{i\mathbf{q}\cdot\mathbf{r}}|0\uparrow X'\rangle|^2}{\omega^2 - (\epsilon_{M\uparrow} - \epsilon_{0\uparrow})^2} . \qquad (8.290)$$

From equation (8.285), we have that $\epsilon_{M\uparrow} - \epsilon_{0\uparrow} = M\omega_c$. Taking $\mathbf{q}$ along the x direction, we find for $\langle M\uparrow X|e^{i\mathbf{q}\cdot\mathbf{r}}|0\uparrow X'\rangle \equiv F_{MX,0X'}$:

$$F_{MX,0X'} = \int \varphi_{MX}^*(x,y)e^{iqx}\varphi_{0X'}(x,y)\,dx\,dy$$

$$= \frac{1}{L_y l\sqrt{\pi 2^M M!}} \int e^{+i\frac{X-X'}{l^2}y}e^{iqx}e^{-\frac{(x-X)^2}{l^2}} H_M\left(\frac{x-X}{l}\right) dx\,dy \quad (8.291)$$

and using

$$\int e^{+i\frac{X-X'}{l^2}y}\,dy = L_y\delta_{X,X'}$$

$$\qquad\qquad\qquad\qquad\qquad\qquad\qquad\qquad\qquad (8.292)$$

$$H_M\left(\frac{x-X}{l}\right) = (-1)^M e^{\frac{(x-X)^2}{l^2}} l^M \frac{d^M}{dx^M} e^{-\frac{(x-X)^2}{l^2}},$$

we obtain

$$F_{MX,0X'} = \frac{\delta_{X,X'}}{l\sqrt{\pi 2^M M!}} \int (-1)^M l^M \frac{d^M}{dx^M}(e^{-\frac{(x-X)^2}{l^2}})e^{iqx}\,dx . \qquad (8.293)$$

The latter integral is easily solved by the well-known property of Fourier transform (that we denote by T):

$$T\left[\frac{d^n}{dx^n}f(x)\right] = (-ik)^n T[f(x)],$$

and bearing in mind that

$$T[e^{-\frac{x^2}{a^2}}] = a^2\sqrt{\pi}e^{-\frac{k^2a^2}{4}} .$$

At last, we obtain

$$F_{MX,0X'} = \delta_{X,X'}\frac{e^{iqX}}{\sqrt{M!}}\left(\frac{iql}{\sqrt{2}}\right)^M e^{-\frac{q^2l^2}{4}} \tag{8.294}$$

so that

$$|F_{MX,0X'}|^2 = \delta_{X,X'}\frac{1}{M!}\left(\frac{q^2l^2}{2}\right)^M e^{-\frac{q^2l^2}{2}} . \tag{8.295}$$

Therefore, we can write the free response function of the system explicitly:

$$\chi^0(q,\omega) = 2N\sum_{M=1}^{\infty}\frac{M\omega_c(\frac{q^2l^2}{2})^M e^{-\frac{q^2l^2}{2}}}{M!(\omega^2 - M^2\omega_c^2)} . \tag{8.296}$$

The excitation energies $\omega(q)$ of the collective density and spin-density modes, as a function of the wavevector q, in the *TDLSDA* approximation may be derived by solving the equations

$$\frac{\chi^{(0)}(q,\omega)}{S} = \left(\frac{2\pi}{q} + \mathcal{K}\right)^{-1} , \qquad \frac{\chi^{(0)}(q,\omega)}{S} = \mathcal{I}^{-1} , \tag{8.297}$$

which yield the poles of $\chi_{\rho\rho}(q,\omega)$ and $\chi_{mm}(q,\omega)$, respectively.

By bounding the model space to the single-particle transitions with energy $1\omega_c$, $2\omega_c$ and $3\omega_c$, in the calculation of the free response function of (8.296), we have

$$\frac{\chi^0}{S} = \frac{2\rho x e^{-x}}{\omega_c}\left(\frac{1}{\lambda - 1} + \frac{x}{\lambda - 4} + \frac{\frac{x^2}{2}}{\lambda - 9}\right) \tag{8.298}$$

where we have set $x = q^2/2l^2$ and $\lambda = \omega^2/\omega_c^2$. Inserting this result into (8.297), we then find:

$$\lambda^3 - \lambda^2\left(14 + A(x)\left(1 + x + \frac{x^2}{2}\right)\right) + \lambda\left(49 + A(x)\left(13 + 10x + \frac{5}{2}x^2\right)\right)$$

$$- 36 - A(x)(36 + 9x + 2x^2) = 0 \tag{8.299}$$

where

$$A(x) = \frac{2\rho x e^{-x}}{\omega_c}\left(\frac{2\pi}{q} + K\right)$$

for the density channel, and

$$A(x) = \frac{2\rho x e^{-x}}{\omega_c}I$$

if we consider the spin-density channel.
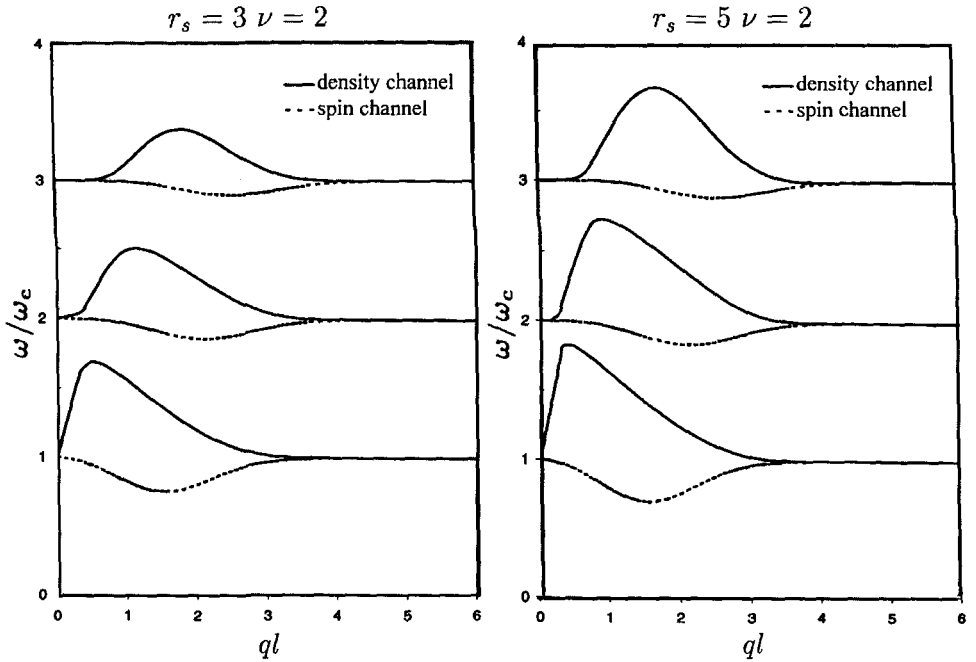
Fig. 8.21   Energies of the collective states in the density and spin-density channels in the case $\nu = 2$, as a function of ql for $r_s = 3, 5$.

In Fig. 8.21 we report the numerical solutions of (8.299) for ω/ω_c, for both density and magnetization channels, as a function of ql and for different values of the density expressed through the Wigner–Seitz radius r_s $(\rho = \pi r_s^2)$.

At small r_s, the $TDLSDA$ dispersion relation is quite similar to the $TDHF - RPA$ results of Kallin and Halperin (1984) and MacDonald (1985). The only relevant difference is found in the $ql \gg 1$ region, where the effect of the residual interaction is negligible and the collective $TDLSDA$ energy tends to $M\omega_c$, while those of the $TDHF - RPA$ always tends to a value larger than $M\omega_c$ due to the self-energy (Fock) shift among the unperturbed single-particle energies. This shift is absent in the $LSDA$ approximation, where the single-particle energies always differ by integer multiples of ω_c. By increasing the value of r_s, the correlation effects in the residual interaction, which are found in $TDLSDA$ only, make the difference between $TDLSDA$ and $TDHF - RPA$ more and more important. While the $TDHF - RPA$ approach predicts an instability in the spin mode at $r_s = 3.3$, the $TDLSDA$ calculation takes care of such instability by means of the correlations. The roton minimum decreases with r_s, but does not show any instability, at least up to $r_s = 10$, which is the maximum value of the considered calculation. The $TDLSDA$ approximation well reproduces the experimental values of Fig. 8.19 for the first roton minimum, while it is unable to reproduce the second roton minimum observed in the spin channel at large ql values.

The strengths relative to the collective states in the density and magnetization channels, whose excitation energies we indicate by ω_ρ and ω_m, respectively, are given by

$$|\langle\omega_\rho(q)|\hat{\rho}(q)|0\rangle|^2 = \frac{1}{\frac{\partial 1/\chi^{(0)}}{\partial\omega}\big|_{\omega=\omega_\rho(q)}}, \qquad (8.300)$$

and

$$|\langle\omega_m(q)|\hat{m}(q)|0\rangle|^2 = \frac{1}{\frac{\partial 1/\chi^{(0)}}{\partial\omega}\big|_{\omega=\omega_m(q)}}. \qquad (8.301)$$

The strength distribution for the three first collective states of density and magnetization excitation is reported in Figs. 8.22 and 8.23, for different values of r_s and ql. From these figures we notice that the low-ql spin state is very collective, unlike the density state, and that the strength breaks up among the possible states with increasing ql.

excitation strengths
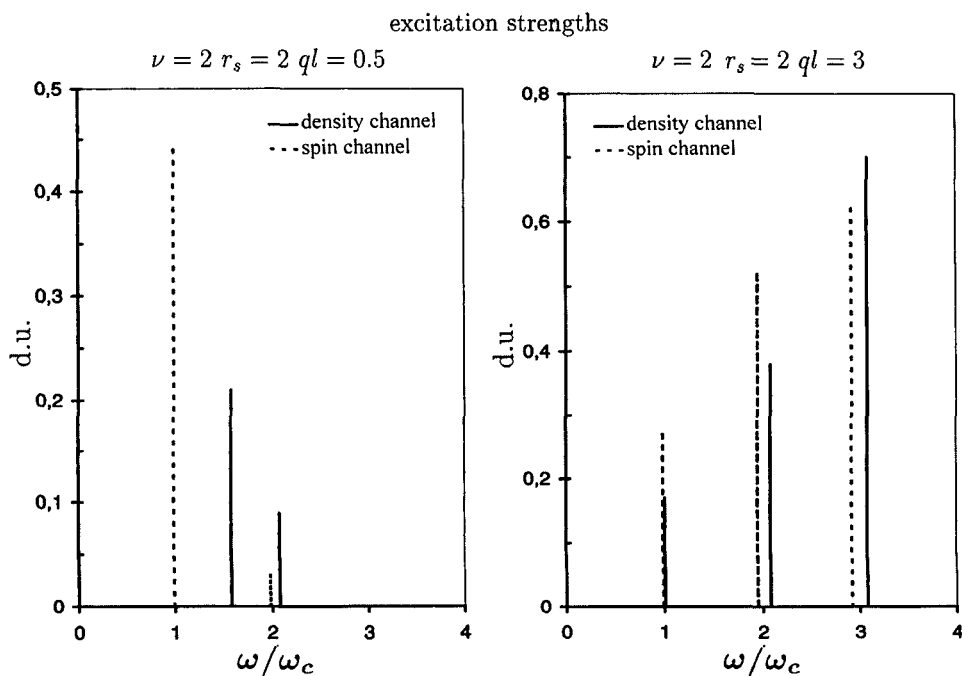
Fig. 8.22 Distribution of strengths in effective atomic units (d.u.) for GaAs samples for the three first collective excitation states in the density and spin-density channels, for various values of ql, in the case of $\nu = 2$, $r_s = 2$.

excitation strengths
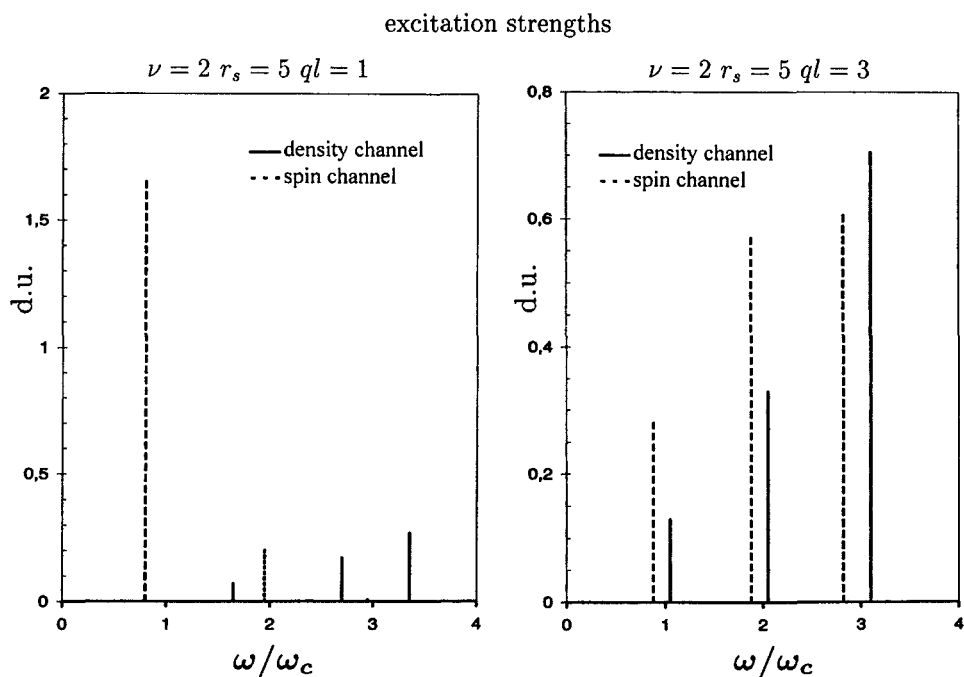
Fig. 8.23   Same as with Fig. 8.22, but for $r_s = 5$.

We further note that the $TDLSDA$ energies and strengths saturate the f-sum rule, given by

$$m_1(\rho\rho, mm) = \frac{Nq^2}{2} .$$ (8.302)

This can be immediately understood by making the limit $\omega \to \infty$ in the expressions of $\chi_{\rho\rho}$ and χ_{mm} [see Eq. (7.28)], and using the result $(x = q^2 l^2/2 = q^2/2\omega_c)$:

$$\sum_{M=1}^{\infty} \frac{M x^M e^{-x}}{M!} = x e^{-x} \sum_{M=1}^{\infty} \frac{x^{M-1}}{(M-1)!} = x .$$ (8.303)

The $TDLSDA$ approximation gives the following results for the sum rule cubic in energy:

$$m_3(\rho\rho) = N \left[\frac{q^6}{8} + \frac{q^2}{2}\omega_c^2 + \frac{3q^4}{4}\omega_c + \frac{\rho q^4}{2}\left(\frac{2\pi}{q} + \mathcal{K}\right) \right]$$ (8.304)

and

$$m_3(mm) = N \left[\frac{q^6}{8} + \frac{q^2}{2}\omega_c^2 + \frac{3q^4}{4}\omega_c + \frac{\rho q^4}{2}\mathcal{I} \right] .$$ (8.305)

The results (8.304), (8.305) were obtained using the result (7.28) of Section 7, and

$$\sum_{M=1}^{\infty} \frac{M^3 x^M e^{-x}}{M!} = x + 3x^2 + x^3 .$$

(8.306)

The results (8.304), (8.305) may also be obtained by directly evaluating the $(TDLDA)$ commutators of the density and magnetization operators with Kohn–Sham Hamiltonian (see Section 8.10). The inversely energy-weighted sum rule $m_{-1} = -\chi(q,0)/2$ can be easily computed using the result:

$$\frac{\chi^{(0)}(q,0)}{S} = \frac{-2\rho}{\omega_c} \exp\left(-\frac{q^2 l^2}{2}\right) \sum_{M=1}^{\infty} \frac{1}{MM!} \left(\frac{q^2 l^2}{2}\right)^M .$$

(8.307)

Finally, we note that the energies which are solutions of (8.297), and the mean energies $E_1 = \sqrt{m_1/m_{-1}}$ and $E_3 = \sqrt{m_3/m_1}$, tend to the limit ω_c when $q \to 0$, in accordance with the Kohn theorem.

B. Transverse response

As in the longitudinal case, the transverse response function for the two-dimensional electron gas under strong magnetic field, is given by the same expression (8.221) derived in Section 8.9.2 in the $B = 0$ case:

$$\chi_t(q,\omega) = \frac{\chi_t^0(q,\omega)}{1 - 2\mathcal{F}_{xc}\chi_t^0(q,\omega)} .$$

(8.308)

In the cases $\nu = 1$ and $\nu = 2$, which we are considering in the following, only the $M = 0$ Landau level is filled in the ground state (spin-up and spin-down levels for $\nu = 2$, and only the spin-up level for $\nu = 1$). The free response function is given by

$$\chi_t^0(q,\omega) = \sum_{M'=0}^{\infty} \sum_{X,X'} \left(\frac{|\langle M' \downarrow X'|F^-|0 \uparrow X\rangle|^2}{\omega - (M'\omega_c + \omega_a)} - \frac{|\langle M' \uparrow X'|F^+|0 \downarrow X\rangle|^2}{\omega + (M'\omega_c - \omega_a)} \right),$$

(8.309)

with $\omega_a = -2\mathcal{F}_{xc}m_0 - g^*\mu_0 B$, where m_0 is the ground state magnetization. In the $\nu = 1$ case, the one-particle–one-hole transitions for the first Landau level are schematized in Fig. 8.24.

Using the results found in the longitudinal case, it is easy to obtain the following expression for the free response function

$$\chi_t^0(q,\omega) = \sum_{M'=0}^{\infty} \frac{1}{M'!} \left(\frac{q^2 l^2}{2}\right)^{M'} e^{-\frac{q^2 l^2}{2}}$$

$$\times \left(\frac{N_\uparrow}{\omega - (M'\omega_c + \omega_a)} - \frac{N_\downarrow}{\omega + (M'\omega_c - \omega_a)} \right),$$

(8.310)
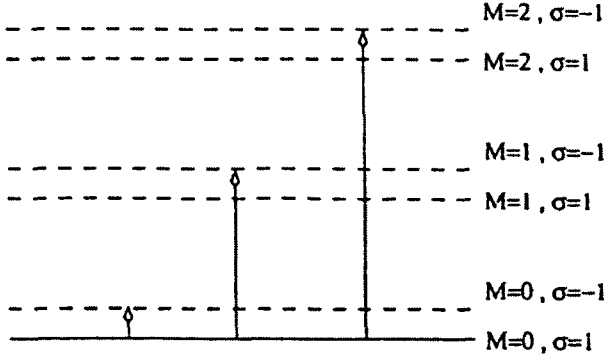
Fig. 8.24   Possible spin-flip excitations for the first Landau levels in the case $\nu = 1$. The full line indicates the Landau levels which are occupied in the ground state, the dashed line indicates unoccupied levels.

where $N_\uparrow = N_\downarrow = N/2$ and hence $m_0 = 0$ for $\nu = 2$ and $N_\uparrow = N$ and $N_\downarrow = 0$ for $\nu = 1$.

Note that when the system is spin-polarized, the $TDLSDA$ transverse response always gives the two sum rules

$$m_0^- = N_\uparrow - N_\downarrow, \quad m_1^+ = \frac{Nq^2}{2} + \omega_L(N_\uparrow - N_\downarrow), \qquad (8.311)$$

where $\omega_L = -g^* \mu_0 B$ is the generalized Larmor frequency. Equations (8.311) follow immediately from the $\omega \to \infty$ limit of the above equations for $\chi_t(q,\omega)$ and $\chi_t^0(q,\omega)$ [see Eq. (7.40)], and from the properties

$$\sum_{M'=0}^{\infty} \frac{1}{M'!} \left(\frac{q^2 l^2}{2} \right)^{M'} e^{-\frac{q^2 l^2}{2}} = 1$$

and

$$\sum_{M'=0}^{\infty} M' \frac{1}{M'!} \left(\frac{q^2 l^2}{2} \right)^{M'} e^{-\frac{q^2 l^2}{2}} = \frac{q^2}{2\omega_c}.$$

The sum rule $m_0^- = \langle 0|[F^+, F^-]|0 \rangle$ is model-independent and determined by the magnetization of the system, while m_1^+ is model-dependent and involves an explicit assumption for the Hamiltonian. Use of the Pauli Hamiltonian in the equation $m_1^+ = \langle 0|[F^+, [H, F^-]]|0 \rangle$, leads exactly to the result (8.311), so that it is possible to conclude that m_1^+ is satisfied by $TDLSDA$. The same does not happen for the free response, that leads to the result $m_1^+(KS) = Nq^2/2 + \omega_a(N_\uparrow - N_\downarrow)$, in which ω_a is present instead of ω_L. Also in the $q \to 0$ limit there is an important difference between the $TDLSDA$ result and the free response one. In fact, from equations

(8.308) and (8.310), it immediately follows that

$$\chi_t^0(q \to 0, \omega) = \frac{m_0}{\omega - \omega_a}, \tag{8.312}$$

$$\chi_t(q \to 0, \omega) = \frac{m_0}{\omega - \omega_L}, \tag{8.313}$$

showing that at the lowest order in q, the $TDLSDA$ pole is given correctly by the Larmor frequency ω_L and not by the renormalized frequency ω_a which gives the poles of $\chi_t^0(q \to 0, \omega)$ in the same limit.

In the case $\nu = 2$, where the system has zero total spin, the lowest excitation energies are of the order of $1\omega_c$, and at $q = 0$, are given by

$$\omega_\pm = \omega_c \pm \omega_L. \tag{8.314}$$

This result differs from the one found in the case where the system is spin-polarized. In fact, at $\nu = 1$, the $\Delta S_z = +1$ channel, excited by the operator $F^+ = \sum_i \exp(+i\mathbf{q} \cdot \mathbf{r})_i \sigma_i^+$, is blocked by the Pauli exclusion principle, and the $\Delta S_z = -1$ channel has the lowest-energy state at $\omega = \omega_L$ and a state "$1\omega_c$" at energy (in the $q \to 0$ limit):

$$\omega_- = \omega_c + \omega_L - 2\mathcal{F}_{xc}. \tag{8.315}$$

The poles of equation (8.308) are solutions of the equation

$$1 - 2\mathcal{F}_{xc}\chi_t^0(q, \omega) = 0, \tag{8.316}$$

which gives the ql-dispersion of the transverse collective states. The only available experimental result concerns the measurement of the Zeeman splitting for $\nu = 2$ at small r_s is that of Eriksson et al. (1999). Such splitting is well reproduced by the calculation.

8.13.2   *Quantum dots under magnetic field*

In this Section we will present and discuss the $TDLSDA$ results for the longitudinal and transverse dipole excitations in quantum dots under external magnetic field (Serra et al. 1999; Lipparini et al. 1999; Steffens and Suhrke 1999). These excitations were observed in photo-absorption experiments in the far infrared region (FIR), where one observes the spectrum excited by the operator $D_s = \sum_{i=1}^N x_i$ (Sikorsky and Merkt 1989; Demel et al. 1990), and more recently in Raman scattering experiments (Strenz et al. 1994; Schuller et al. 1996), where, by the same experiment, it is possible to observe single-particle and collective excitations belonging to both the density and spin-density, and for the latter in both the longitudinal and in the transverse channel. In the dipolar case, these modes are excited by the operators $D_a = \sum_{i=1}^N x_i \sigma_i^z$ and $D_\pm = \sum_{i=1}^N x_i \sigma_i^\pm$, respectively. As mentioned previously, when the dot is spin-polarized (which happens when the dot either has

an odd number of electrons, or is under the action of a magnetic field), the spin response is coupled to the density response, so that the external operator D_s also excites the spin modes, as D_a excites the density ones. When the system is completely spin-polarized, the two modes coincide, while at zero polarization they are uncoupled.

In the following we will assume that the quantum dots under consideration have spherical symmetry. In order to exploit such symmetry, it is suitable to consider the following dipolar external fields, which correspond to the operator G in equation (8.189):

$$D_s^{(\pm 1)} = re^{\pm i\theta}\begin{pmatrix} 1 \\ 1 \end{pmatrix} \quad \text{and} \quad D_a^{(\pm 1)} = re^{\pm i\theta}\begin{pmatrix} 1 \\ -1 \end{pmatrix}, \tag{8.317}$$

with $D_s = (D_s^{(+1)} + D_s^{(-1)})/2$, and likewise for D_a.

In the longitudinal case, the integral equations (8.194) for the correlation functions may be solved as a system of matrix equations in the co-ordinate space, after performing an angular decomposition on $\alpha_{\sigma\sigma'}$ and on the residual interaction.* As can be easily seen by performing the angular integration in (8.190), it is only the modes with $l = \pm L$ that couple to the external fields $G_s^{(\pm L)}$ and $G_a^{(\pm L)}$. Therefore, in the dipolar case the only multipoles which appear into the integral equations for the correlation functions, are those with $L = \pm 1$, and the corresponding response functions $\chi_{AB}^{(\pm 1)}(r, r'; \omega)$, with $A, B = s, a$ are given by:

$$\chi_{AB}(\omega) = \pi^2 \int dr_1\, dr_2\, r_1^2\, r_2^2 [\alpha_{AB}^{(+1)}(r_1, r_2; \omega) + \alpha_{AB}^{(-1)}(r_1, r_2; \omega)]$$

$$\equiv \chi_{AB}^{(+1)}(\omega) + \chi_{AB}^{(-1)}(\omega). \tag{8.319}$$

The imaginary part of $\chi_{AB}(\omega)$ is related to the dynamic structure function by Eq. (7.26), and the following relations hold:

$$\begin{aligned} \text{Re}[\chi_{AB}^{(-1)}(\omega)] &= \text{Re}[\chi_{AB}^{(1)}(-\omega)] \\ \text{Im}[\chi_{AB}^{(-1)}(\omega)] &= -\text{Im}[\chi_{AB}^{(1)}(-\omega)]. \end{aligned} \tag{8.320}$$

These relations are important from a practical standpoint, because they allow us to determine the structure functions of both components ± 1, by using the $+1$ component over a frequency range $(-\omega_{\min}, \omega_{\max})$.

In order to perform a check on the numerical accuracy of the calculation of the structure functions, one can use the f-sum rules for the corresponding excitation

*For the residual interaction $K_{\sigma\sigma'}$, one gets

$$K_{\sigma\sigma'}(\mathbf{r}, \mathbf{r}') = \sum_l K_{\sigma\sigma'}^{(l)}(r, r') e^{il(\theta - \theta')}. \tag{8.318}$$

operators. One finds (in effective atomic units):

$$m_1^{(ss)} = \int S_{ss}(\omega)\omega d\omega = \frac{1}{2}\langle 0|[D_s,[H,D_s]]|0\rangle = \frac{N}{2},$$

$$m_1^{(aa)} = \int S_{aa}(\omega)\omega d\omega = \frac{1}{2}\langle 0|[D_a,[H,D_a]]|0\rangle = \frac{N}{2}, \qquad (8.321)$$

$$m_1^{(as)} = m_1^{(sa)} = \int S_{as}(\omega)\omega d\omega + \int S_{sa}(\omega)\omega d\omega = \langle 0|[D_a,[H,D_s]]|0\rangle = 2S_z.$$

In the transverse case, and again to exploit the circular symmetry, one considers the operators:

$$D_{\pm 1,\pm} = \sum_j r_j e^{\pm i\theta_j} \sigma_\pm^j. \qquad (8.322)$$

with

$$\sum_j x^j \sigma_\pm^j = \frac{1}{2}(D_{+1,\pm} + D_{-1,\pm}), \qquad (8.323)$$

keeping in mind that such operators, unlike the longitudinal case where states are excited without varying the third spin component (i.e. $\Delta S_z = 0$), now induce variations with $\Delta S_z = \pm 1$. With the use of such operators one then solves the integral equations (8.214) and (8.218), and computes the polarizabilities (8.216) and (8.220).

Figures 8.25–8.27 show the dipolar structure functions of the $N = 5$, 25, and 210 dots for some selected values of the magnetic field B. The full curves correspond to the density response to D_s, and the dotted curves mark the spin-density response to D_a, i.e. to S_{ss} and to S_{aa}, respectively. The dashed curves represent the single-particle structure function.

For the dot with 5 electrons the parabolic confinement potential $v_{\text{ext}}(r) = m\omega_0^2 r^2/2$ was used, with $\omega_0 = 4.28$ meV, while for the other two dots the confinement potential was the one generated by a disc of positive charge as in Section 5.6 [see Eq. (5.62)]. As will be shown later, the experimental results of Demel et al. are better reproduced for the $N = 25$ dot, using a parabolic confinement potential. This is why in the $N = 25$ case, in Fig. 8.28 we present the structure function obtained with the parabolic potential as well.

These figures show that in both the density and spin-density channels, the response at $B = 0$ is concentrated in a small energy range, either with only one peak or with several very close peaks, which exhaust most of the f-sum rule. The peak energy is lower in the spin channel than in the density one. This is due to the character of the residual interaction $K_{\sigma\sigma'}$, which is attractive in the spin channel and repulsive in the charge one, and shifts the $TDLSDA$ response with respect to the single-particle one in opposite directions.

Moreover, the residual interaction in the spin channel is weaker than it is in the density channel, where it is not only the exchange-correlation energy that
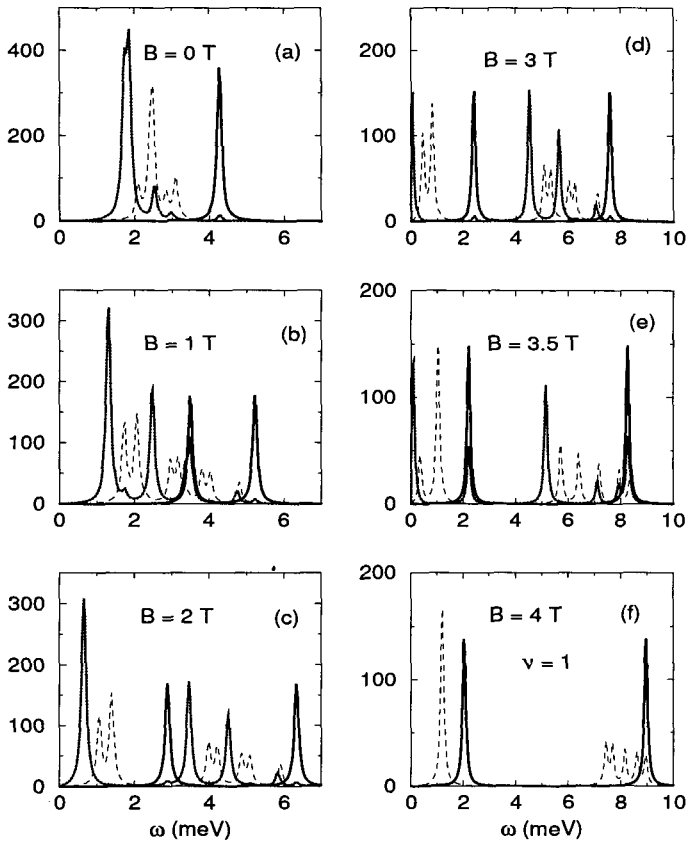
Fig. 8.25   Dipole structure function in arbitrary units of the $N = 5$ dot, as a function of frequency. The thick and dotted lines correspond to the density response to D_s, and to the spin-density response to D_a, respectively. The dashed lines represent the single-particle structure function.

contributes, but also the direct Coulomb term as well. As a result, the spin response is closer to the free response. Therefore, it is difficult to distinguish the spin longitudinal collective mode from the single-particle spectrum. In the dots with a large number of electrons, this also induces a much larger Landau damping in the spin channel than it does in the density one (Schuller et al. 1998).

At $B = 0$, as a consequence of the generalized Kohn theorem (see Section 8.10.1), and if the confinement potential is harmonic with frequency ω_0, the excitation energy of the dipole density mode is equal to ω_0 irrespective of the number of electrons in the dot. Otherwise (for other kinds of confinement potential), the excitation energy depends on N, (see e.g. Serra and Lipparini 1997 and Gudmundsson and Gerhardts 1991). In the spin channel this theorem does not hold; moreover one observes N-dependence also for parabolic confinement potentials.

When B is different from zero, the dipole mode in both channels is split into two branches, one with negative B-dispersion while the other with positive dispersion.
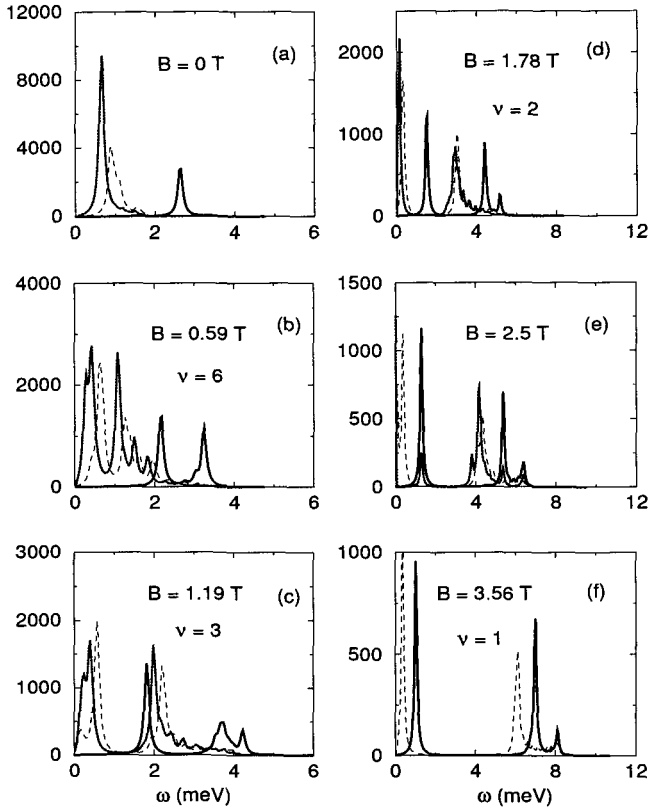
Fig. 8.26 Same as with Fig. 8.25, but for $N = 25$.

The splitting originates from the breaking of the l degeneracy of the single-particle levels, in the presence of a magnetic field. Therefore, several new phenomena occur. First, we note that for B values such that the ground state spin is not zero, the two excitation modes (i.e. density and spin) are coupled. This can be seen particularly in the dot with $N = 210$ electrons. In fact, at $B = 1.71$ T ($\nu = 6$) and 5.14 T ($\nu = 2$), the system is practically paramagnetic, having $2S_z = 2$ and 0, respectively (see Fig. 5.10 of Section 5.6). As a consequence of that, the two modes are uncoupled, as can be seen in Fig. 8.27. Contrary to these cases, at $B = 3.43$ T ($\nu = 3$) and 7 T we have $2S_z = 54$ and 74: the system possesses a large spin magnetization in the ground state, and the two modes are clearly coupled. This is shown in the same Fig. 8.27, where we can observe a separate peak in the spin response at the energy of the density mode. This effect was observed experimentally by Schuller et al. (1998). The strength of this peak increases with S_z, and when the system is completely spin-polarized the whole strength is transferred from the spin channel to the density one. On the other hand, the spin mode can be observed in the density channel with some intensity. This effect is somewhat masked because the Kohn
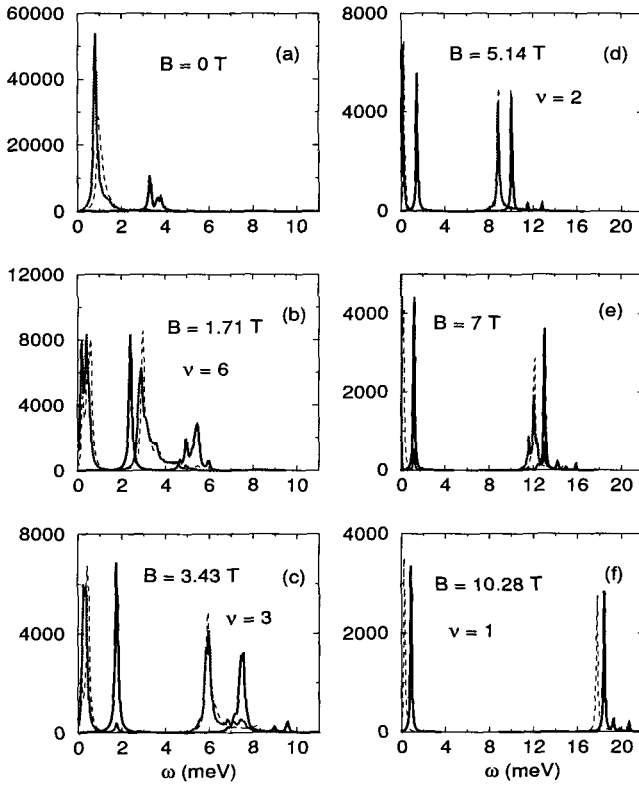
Fig. 8.27   Same as with Fig. 8.25, but for $N = 210$.

theorem forbids it for parabolic potentials, and for the disc potential it is of the order of $(2S_z/N)^2$.

The coupling between density and spin modes is especially evident in the mixed channel which is described by the density response to the spin-dipole excitation operator D_a, or by the spin response to the density dipole operator D_s. This is shown in Fig. 8.29 for the $N = 210$ quantum dot at $\nu = 3$. One clearly observes two peaks at the energy of the density mode, and two more peaks at the energy of the spin mode. This can be well understood by dividing the mixed structure function by a sum over the "spin-dipole states" $|a\rangle$, plus a sum over the "charge-dipole states" $|s\rangle$

$$S_{as}(\omega) = S_{sa}(\omega) = \sum_i \langle 0|D_s|i\rangle\langle i|D_a|0\rangle\delta(\omega - \omega_{i0})$$

$$= \sum_s \langle 0|D_s|s\rangle\langle s|D_a|0\rangle\delta(\omega - \omega_{s0})$$

$$+ \sum_a \langle 0|D_s|a\rangle\langle a|D_a|0\rangle\delta(\omega - \omega_{a0}). \qquad (8.324)$$
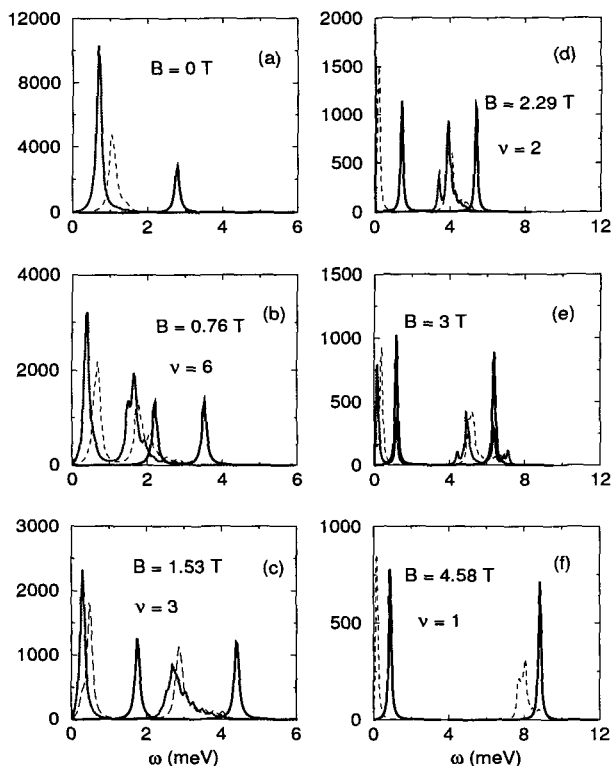
Fig. 8.28 Same as with Fig. 8.26, but using the parabolic confinement potential with $\omega_0 = 2.78$ meV, instead of the disc potential.
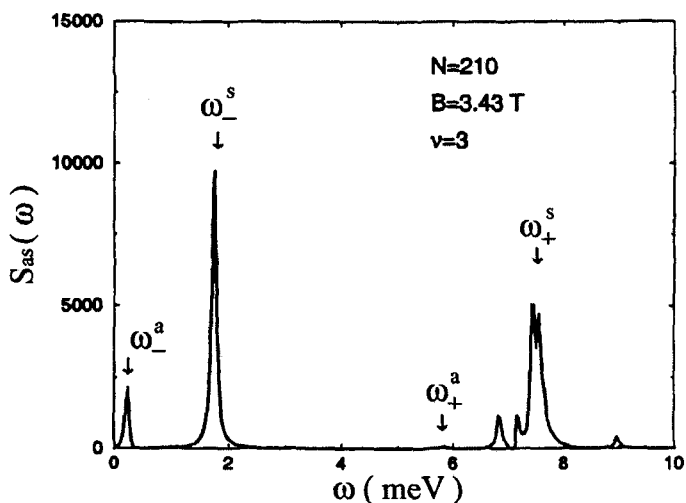
Fig. 8.29 Mixed structure function $S_{as}(\omega)$ (in effective atomic units) of the $N = 210$ dot, at $\nu = 3$.
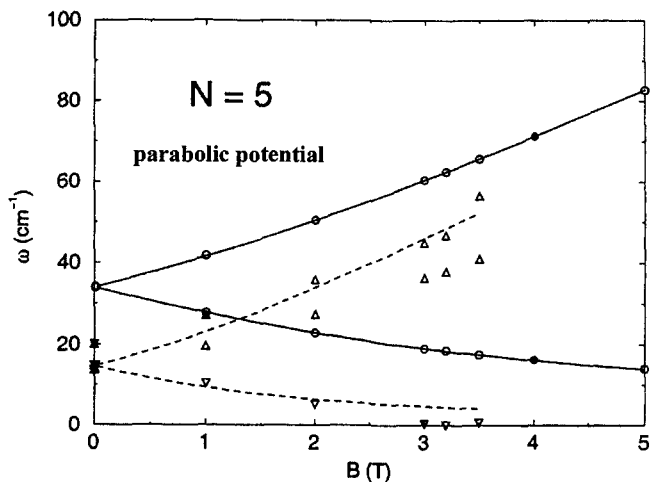
Fig. 8.30 *B*-dispersion of the major peaks of the $N = 5$ spectrum. The circles correspond to density modes, the triangles to spin modes. The lines indicate the *B*-dispersion of the vibrating potential model of Section 10.2.5, with the values fitted at $B = 0$.
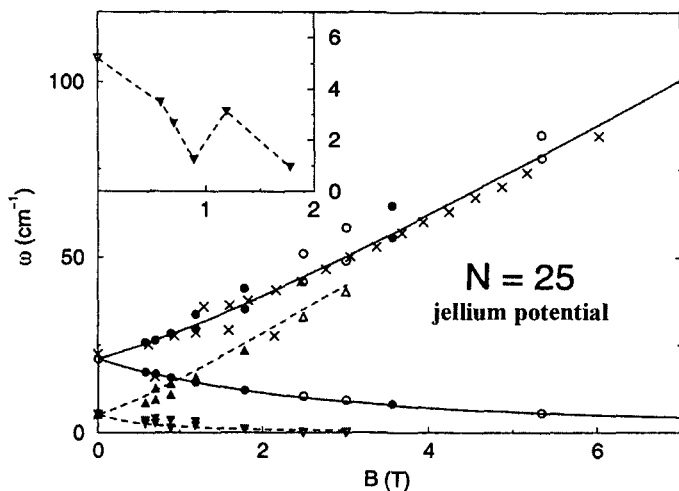
Fig. 8.31 *B*-dispersion of the major peaks of the $N = 25$ spectrum for a disc confinement potential. The circles correspond to density modes and triangles to spin modes. The crosses mark the experimental points by Demel et al. (1990). The lines represent the *B*-dispersion of the *VPM* of Section 10.2.5, with the $B = 0$ values fitted. The insert shows the negative B dispersion branch of the spin mode. From the left to right the solid symbols correspond to $\nu = 6$ to 1.

For the disc confinement potential, the matrix element $\langle 0|D_s|a\rangle$ is different from zero and there is a contribution to S_{as} from the spin modes. For a parabolic confinement potential $\langle 0|D_s|a\rangle$ vanishes, and only the density modes contribute to S_{as} through the sum over s in (8.324).
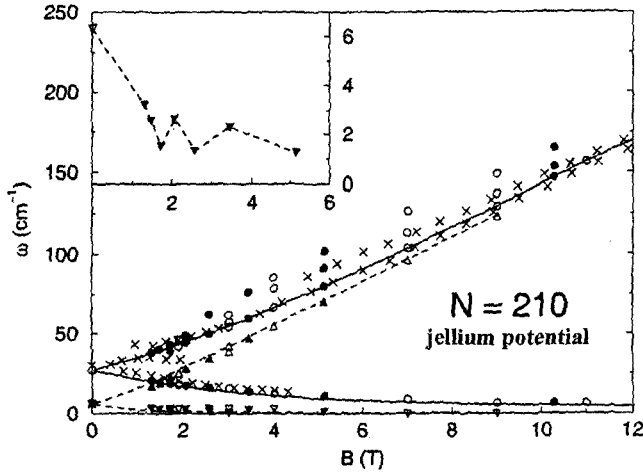
Fig. 8.32   *B*-dispersion of the major peaks of the $N = 210$ spectrum, for a disc confinement potential. The circles correspond to density modes, the triangles to spin modes. The crosses are the experimental points from Demel et al. (1990). The lines represent the *B*-dispersion of the *VPM* of Section 10.2.5, with values fitted at $B = 0$. The insert shows the negative-dispersion branch of the spin mode. From left to right the solid symbols correspond to ν values from 8 to 1.
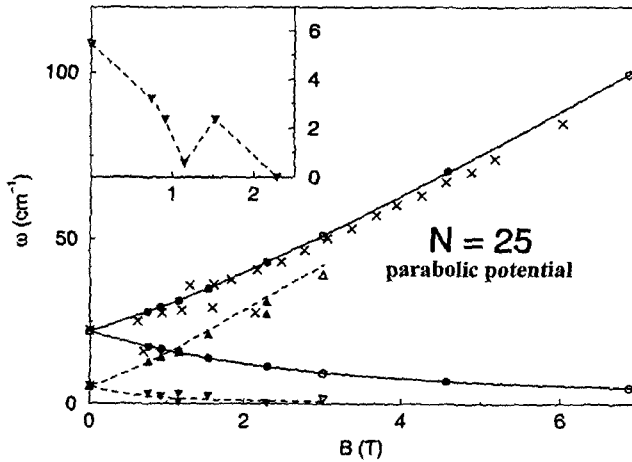
Fig. 8.33   Same as with Fig. 8.31, but using a parabolic confinement potential with $\omega_0 = 2.78$ meV in place of the disc potential.

In Figs. 8.30–8.33 we report the dispersion with B of the major peaks of the two spectra. The density modes are represented by circles, the spin modes by triangles. The full symbols correspond to integer filling factors, and the insets show the branch with negative B-dispersion of the spin mode. In the figure, also present are lines starting from the frequency at $B = 0$, and following the B-dispersion laws predicted by the vibrating potential model (*VPM*), which will be described in Section 10.2.5.

The figures evidence several interesting features that deserve discussion. As concerns the spin modes, we first note that at low B their energy is much lower than that of density modes, in agreement with the experimental findings of Schuller et al. At higher B values, the quantum dot is eventually completely spin-polarized, and the longitudinal density and spin modes coincide, as in the case of the $2D$ electron gas (Kallin and Halperin 1984). This effect is not explicitly shown by the figure. Moreover, the branch with negative B-dispersion of the spin mode exhibits a clearly oscillating behaviour with ν, similar to the one observed experimentally for the density response by Bollweg et al. (1996), which reveals that the paramagnetic configurations of the dots have spin modes which are softer than in the ferromagnetic configurations.

The $TDLSDA$ approximation predicts the existence of a spin instability when the lowest-energy branch of the spin mode goes to zero at some critical value of B, between $\nu = 1$ and 2. Such instability appears also in the static spin polarizability $\mathrm{Re}[\chi_{aa}^{(-1)}(0)]$, which becomes negative at these values of B, indicating that the ground state of the dot is no longer stable. The lack of experimental observation of collective spin states at these values of magnetic field, might be the mark of the instabilities, but it cannot be excluded that the lack of data be due to the Landau damping which, in this energy range, is particularly strong. Moreover, it might be that in this region, correlations which are not included in the $TDLSDA$ approximation, are important and quench the spin instability.

As regards the density dipole mode, the following considerations apply. For the parabolic confinement potential, Figs. 8.30 and 8.33 show that the density response follows the law

$$\omega_{\pm}^{s} = \Omega \pm \frac{\omega_c}{2},$$

where $\Omega^2 = \omega_0^2 + \omega_c^2/4$. This is so because the $TDLSDA$ approximation that we are using obeys the generalized Kohn theorem (see Section 8.10.1). For the disc confinement potential, this law is also approximately satisfied, especially by the branch with negative B-dispersion. As concerns the other branch, it is systematically fragmented, especially for the $N = 210$ dot. Comparing the calculations for the $N = 25$ dot with the experimental results of Demel et al., we may conclude that the parabolic potential works better than the disc one, in reproducing the experimental situation. On the contrary, the confinement potential of the $N = 210$ dot is not parabolic, and this originates the second high-energy branch observed in experiment. The non-harmonic character of the confinement potential was indicated as the origin of such branch in calculations of the Hartree + RPA type with $N \leq 30$ dots by Gudmundsson and Gerhardts (1991) and Ye and Zaremba (1994). The $TDLSDA$ calculations support this interpretation.

To complete the description of the $TDLSDA$ dipole response in quantum dots, we turn now to transverse spin modes. We will consider the $N = 210$ dot, which allows us to present very clear results for several ground states corresponding to

integer filling factors. This will emphasize the sensitivity of the transverse response to the applied magnetic field B, which shows itself by having large oscillations of the excitation energies as a function of B, and by a nearly-collapsed, low-energy excitation mode $x\sigma_+$ at $\nu = 2$ (Lipparini et al. 1999).

Due to the rotational invariance in spin space, the longitudinal ($\Delta S_z = 0$) and transverse ($\Delta S_z = \pm 1$) spin excitations (SDE) are degenerate at $B = 0$ if $S_z = 0$ in the ground state of the dot. When the magnetic field is not zero, rotational invariance is broken by the Zeeman term. Then, if the ground state is paramagnetic (or quasi-paramagnetic), the SDE are split in a simple way:

$$\omega_\pm^{tr} = \omega^{lon} \pm g^* \mu_0 B \,, \tag{8.325}$$

where the apex $lon(tr)$ indicates the longitudinal (transverse) character of the mode, and the $\pm$ sign corresponds to the two possible transition with the change of spin. If the ground state has a large value of S_z, i.e. a large spin magnetization, then equation (8.325) does not hold any more, and the longitudinal and transverse SDE excitations become very different due to the spin-dependence of the particle-hole residual interaction (vertex correction).

In the following we will study the structure functions corresponding to the operators

$$D_a = \sum_{i=1}^{N} x_i \sigma_i^z \quad \text{and} \quad D_\pm = \sum_{i=1}^{N} x_i \sigma_i^\pm \,,$$

that will be indicated by $x\sigma_z$, $x\sigma_+$, $x\sigma_-$, as well as of the combination $x\sigma_x = x(\sigma_+ + \sigma_-)$.

Some of the characteristics of the structure functions can be easily understood in terms of the single-particle excitations, employed to set up the corresponding correlation function [see Eqs. (8.215) and (8.219)], whose basic ingredients are the single-particle energies $\epsilon_{nl\sigma}$ and wavefunctions $\phi_{nl\sigma}(\mathbf{r})$, provided by the solution of the Kohn–Sham equations. However, the particle-hole residual interaction, which has the effect of the interaction on the excited states, can drastically change the situation as represented by the single-particle response.

Figure 8.34 shows the structure function $S(\omega)$ (full lines) corresponding to $x\sigma_x$, which was subsequently decomposed into its components $x\sigma_+$ and $x\sigma_-$, that are plotted in Figs. 8.35 and 8.36.

The corresponding single-particle responses (SPE) are represented by dashed lines; all functions are expressed in effective atomic units, and frequencies are in meV.

We will start by commenting on the results corresponding to paramagnetic ground states, in which both single-particle states with spin-up and spin-down tend to be equally populated, leading to a ground state with a low value of S_z. As a consequence, the particle-hole residual interaction $\mathcal{F}_{xc}$ (see Section 8.9.2), which is proportional to the magnetization m of the ground state is weak, and the SDE
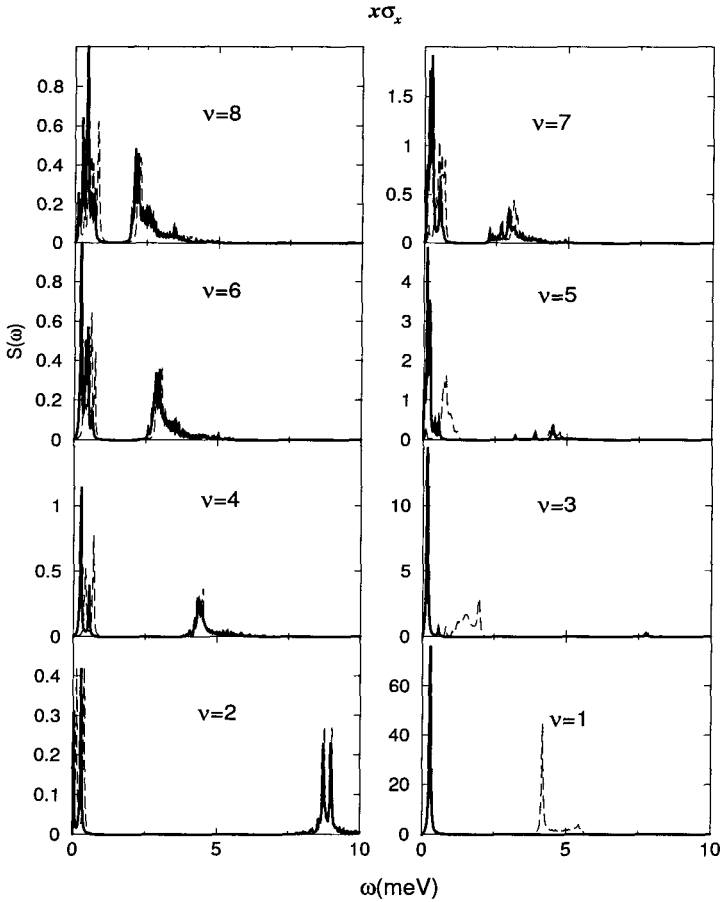
Fig. 8.34   Structure function of the N=210 dot, corresponding to $x\sigma_x$ (full lines). The dashed lines represent the single-particle structure function. $S(\omega)$ is in effective atomic units divided by 10^5.

collective excitations are very close in energy to the single-particle ones. In both the $x\sigma_+$ and $x\sigma_-$ components, the strength exhibits a structure at high energy very close to the single particle one, and a low-energy structure. For paramagnetic ground states, the low-energy excitation is *a transverse edge spin excitation* built up starting from the particle-hole pairs near to the Fermi level. These pairs can be easily identified in Fig. 5.9 (even values of ν), since they are at the intersection of the chemical potential with the Landau levels. The band structure of the single-particle levels also explains why the edge mode is more fragmented at low magnetic field values. For example, at $\nu = 8$ four particle-hole pairs (each with single-particle angular momenta completely different from the other pairs) contribute to the $x\sigma_-$ strength, while just one pair contributes at $\nu = 2$. These pairs are only weakly mutually correlated, and this results in an edge mode which is fourfold fragmented

$x\sigma_+$
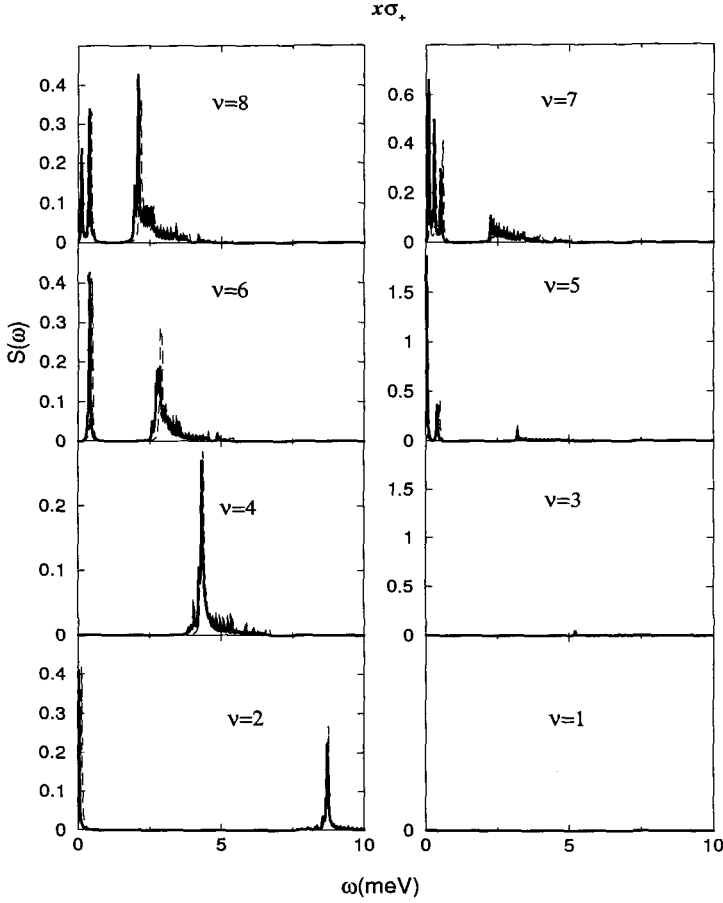
Fig. 8.35 Structure function of the $N = 210$ dot, corresponding to $x\sigma_+$ (full lines). The dashed lines represent the single-particle structure function. $S(\omega)$ is in effective atomic units divided by 10^5.

at $\nu = 8$, threefold at $\nu = 6$, and so on. This corresponds to the number of level crossings between the Fermi level and the $(M, \uparrow\downarrow)$ levels in Fig. 5.9.

In the $x\sigma_+$ case, the edge mode is less fragmented because some of the one-particle–one-hole spin-flip transitions with $\Delta S_z = +1$ are forbidden by the Pauli principle, due to our arbitrary choice of directing B along the positive z axis (recall that it must be $\Delta L_z = \pm 1$, which cannot be always simultaneously fulfilled for the spin and edge conditions). The lack of the edge state in the $\nu = 4$ case, is due to the special single-particle structure around the Fermi level at $B = 2.57$ T. This accidental occurrence is not relevant for the general discussion.

As can be seen in Fig. 8.35, when the dot is completely spin-polarized at $\nu = 1$, $x\sigma_+$ does not excite it any more due to the Pauli blocking. Also, at $\nu = 3$ ($B = 3.43$ T), its strength is very small. On the contrary, the excitation produced by $x\sigma_-$,

xσ_
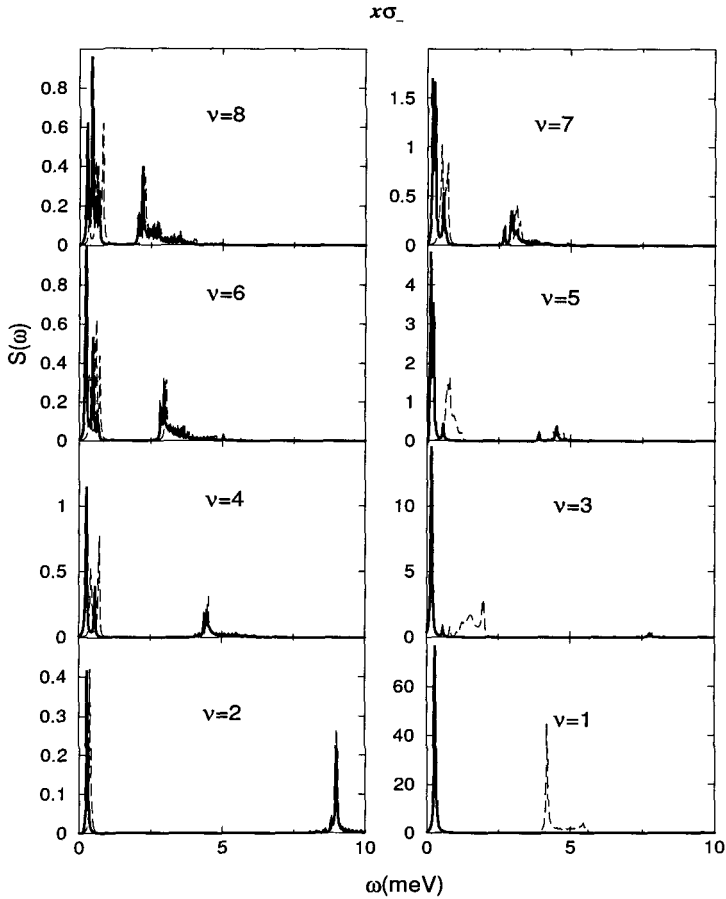
Fig. 8.36   Structure function of the $N = 210$ dot, corresponding to $x\sigma_-$ (full lines). The dashed lines represent the single-particle structure function. $S(\omega)$ is in effective atomic units divided by 10^5.

and shown in Fig. 8.36, is appreciably red-shifted with respect to the single-particle response. The difference between the two strengths represents the intensity of the residual interaction (vertex correction) due to exchange and correlation terms of the electron–electron interaction; these terms, in the time-dependent density functional theory, are the only ones to contribute to the dressing of the free particle-hole vertex in the spin channel. This effect is more pronounced at $\nu = 1$, when the system is completely magnetized.

The low-energy peak excited by $x\sigma_-$ exhausts almost all of the strength. Note that the SDE excitations in ferromagnetic (spin-polarized) ground states caused by both $x\sigma_+$ and $x\sigma_-$ are *not edge but bulk excitations*. Again, Fig. 5.9 helps us to understand this feature. For these ground states with odd filling factor ν, the Fermi level lies between the Landau levels with $(M_{max}, \uparrow)$ and $(M_{max}, \downarrow)$, the former being

occupied and the latter empty. Even though finite-size effects distort the bands at the dot edge, which is built up with single-particle high-l levels, it is evident that the low-energy transitions with a change of spin involve single-particle states whose energy difference is exactly the energy difference between the $(M_{max}, \uparrow\downarrow)$ levels. Such excitations exist in the two-dimensional electron gas as well (see previous Section). The role played by the residual interaction is evident in Fig. 8.36, if we compare, for instance, the single-particle and *TDLSDA* strengths at $\nu = 5$ and $\nu = 3$. It can be seen that the SPE energies have nothing in common with the SDE ones at low energy. Thus, the *IPM* model turns out to be completely useless for a quantitative analysis of the SDE excitations in spin-polarized quantum dots, and the situation becomes worse and worse as the polarization degree increases.

In Fig. 8.37 we show in more detail the transverse structure function at high B, excited by $x\sigma_x$ in the region $2 > \nu \geq 1$. In this range of filling factors, which correspond to $5.14 \text{ T} < B \leq 10.28 \text{ T}$, $2S_z$ increases from zero to 210 (see Fig. 5.13),
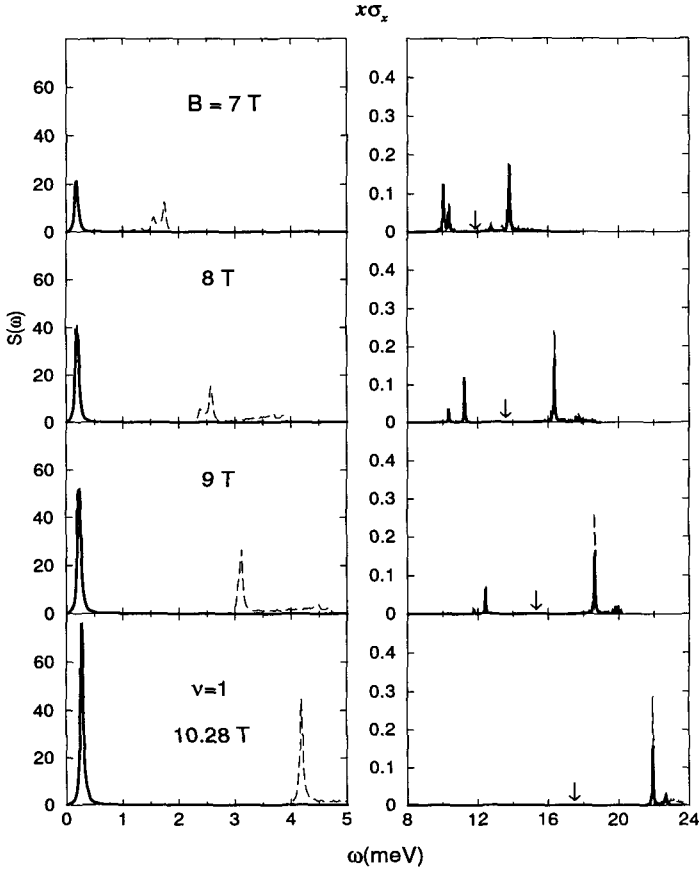
Fig. 8.37 Same as with Fig. 8.34, but for $2 > \nu \geq 1$. The vertical arrows mark the value of ω_c.

so that the strength $x\sigma_x$ practically coincides with that of $x\sigma_-$, that we already discussed. The new and interesting feature in Fig. 8.37, is the structure of the high-energy peaks. These are two orders of magnitude less intense than the low-energy ones, which saturate most of the strength. Among the high-energy peaks, the most energetic ones are excited by $x\sigma_-$, the least energetic ones by $x\sigma_+$ (note that the high-energy transitions induced by $x\sigma_+$ are blocked by the Pauli principle only when the system is completely spin-polarized). It can be shown that such high-energy peaks are not collective, and that the SPE and SDE excitations are very similar; moreover, the centroid of the peaks excited by $x\sigma_+$ and $x\sigma_-$ follows, approximately, the same B-evolution as the cyclotron frequency. The value of ω_c is marked in Fig. 8.37 by vertical arrows. When both peaks are well visible in the structure function, like e.g. at $B = 7$ T, their splitting provides a quantitative measure of the spin-dependent exchange-correlation term W_{xc}, and its measurement, when feasible, may be considered as a spectroscopic complement for the measurement of the same quantity by conductivity experiments (Usher et al. 1990), which are directly connected to the single-particle energies. In fact, since the correlation effects are negligible, such splitting is given by the *IPM* result $4W_{xc} + 2g^*\mu_0 B$ and is twice as large as the energy difference between the Landau levels $(M,\uparrow)$ and $(M,\downarrow)$ around the Fermi level [see Eq. (8.285)]. Such correspondence is well confirmed by the numerical *LSDA* calculation in the cases $B = 7$ T and 9 T, so that an explicit comparison can be established between the splitting of the *TDLSDA* states excited at high energy by $x\sigma_+$ and $x\sigma_-$, and the energy difference of the static Landau levels (see Fig. 5.17).

The high-energy peak of the longitudinal structure function lies at $\omega^{lon} \sim \omega_c$ (Serra et al. 1999, see also Fig. 8.39), and it is possible to write an expression similar to equation (8.325):

$$\omega_\pm^{tr} \sim \omega^{lon} \pm 2W_{xc}. \tag{8.326}$$

The validity of (8.326) is a consequence of the weakness of the particle-hole residual interaction in the situation where such expression holds. Note that W_{xc} is negative.

Figure 8.38 shows the longitudinal ($x\sigma_z$, dotted lines) and transverse ($x\sigma_x$, full lines) spin structure functions. It can be noticed that in the ferromagnetic states the strength is dominated by transverse modes. It can also be noted that for $\nu \geq 2$, i.e. low B, apart from fine-structure effects, the longitudinal and transverse spin responses have their main peaks at very similar energies.

The paramagnetic configuration at $\nu = 2$ ($B = 5.14$ T), shows the situation in which at zero spin the ground state produces the result that was disclosed in (8.325): the transverse modes are shifted with respect to the longitudinal ones by the Zeeman energy (note that g^* is negative). It is also interesting to note that the low-energy mode $x\sigma_+$ has practically collapsed. This hints at the existence of spin instabilities in this transverse channel, similar to the ones found for the longitudinal spin channel in the region $2 \geq \nu > 1$.

$$x\sigma_x \; ; \; x\sigma_z$$
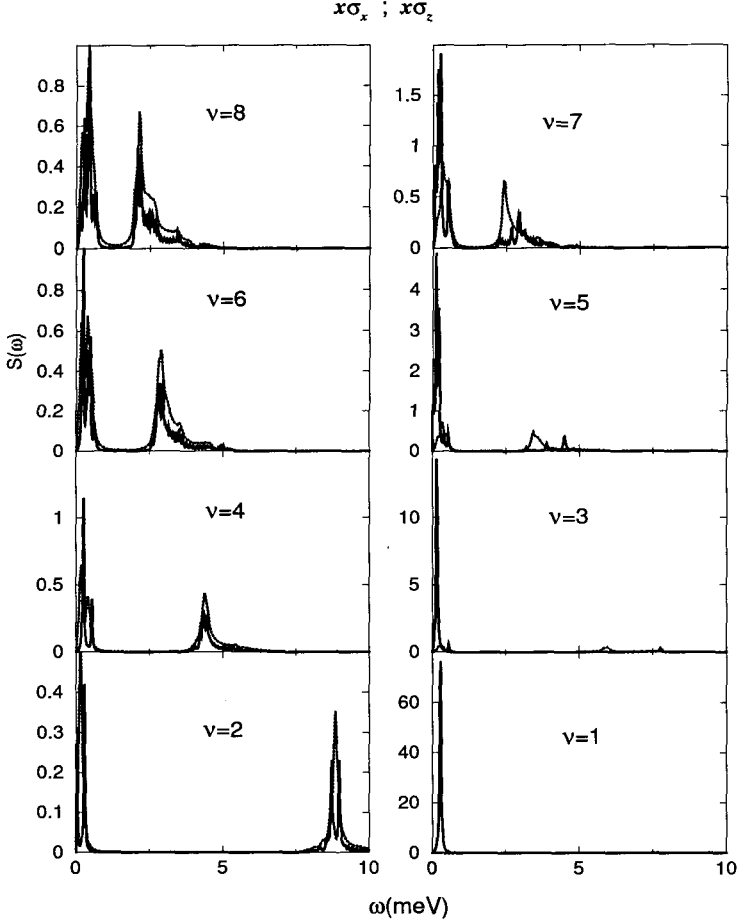
Fig. 8.38 Structure functions corresponding to $x\sigma_x$ (full lines) and to $x\sigma_z$ (dotted lines). The strengths are in effective atomic units divided by 10^5 in the transverse case, and by 5×10^4 in the longitudinal case, to make them clearly discernible.

When the system is completely spin-polarized, the longitudinal dipole strengths in the density and spin channels coincide, and among the spin modes only the transverse one makes sense.

The energies of the most intense high-energy peaks which are observed in the structure functions $x\sigma_+$ and $x\sigma_-$, are shown in Fig. 8.39 as a function of B. In the figure we also report the cyclotron frequency. The full symbols correspond to even filling factors, while the open ones correspond to odd filling factors in the range form $\nu = 10$ to $\nu = 1$. We also report (crosses) the values of the peaks of the longitudinal spin response.

In agreement with the previous discussion, we see that for even filling factors the energies of the transverse SDE are $\sim \omega_c \pm g^*\mu_0 B$, i.e. very close to ω_c (since
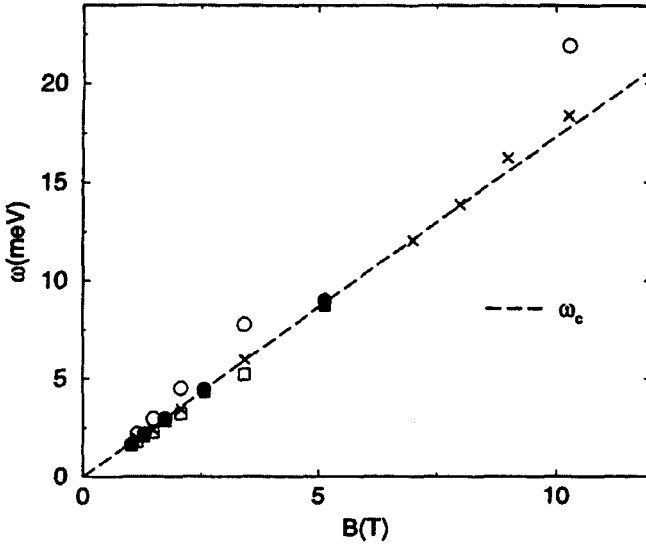
Fig. 8.39 Energies of the most intense high-energy peaks excited by $x\sigma_+$ (squares) and $x\sigma_-$ (circles), as a function of B. Solid symbols correspond to even filling factors, the open ones to odd filling factors for values of ν ranging from 10 ($B = 1.03$ T) to $\nu = 1$ ($B = 10.28$ T). Also reported in the figure are the energies of the longitudinal, high-energy spin peaks (crosses).

the Zeeman term is very small), while for odd filling factors they are quite distant from ω_c, due to the large contribution of the spin-dependent potential W_{xc}. In all cases, these peaks correspond to bulk modes since they involve one-particle–one-hole transitions made up by single-particle states belonging to different Landau levels.

In a similar fashion, Fig. 8.40 shows the energies of the most intense low-energy peaks of the structure functions $x\sigma_+$ (top) and $x\sigma_-$ (bottom). The full and open symbols have the same meaning as in Fig. 8.39. In the figure we also report the Zeeman energy $E_z = -g^*\mu_0 B > 0$. In order to evidence the zig-zag behaviour of the energies, the points corresponding to consecutive ν values were connected by a line. As we already discussed, these are edge spin modes for the paramagnetic ground states, and bulk modes for the ferromagnetic ground states.

The SDE excitation corresponding to $x\sigma_-$ is the most interesting one. In fact, this is the only transverse spin mode that shows itself at high magnetization, because the one produced by $x\sigma_+$ is blocked by the Pauli principle. For ferromagnetic states this is an undamped excitation because it is well separated from the single-particle excitations (SPE) (see Fig. 8.36). Note that the transverse SDE energy tends to the Zeeman energy E_z as B increases. When the system is completely polarized ($\nu = 1$), the energy is close to E_z, but does not coincide with it due to finite-size effects which behave like ω_c/N.

We have shown that among the SDE excitations, transverse ones are of particular relevance; in the longitudinal channel the residual interaction is very weak,
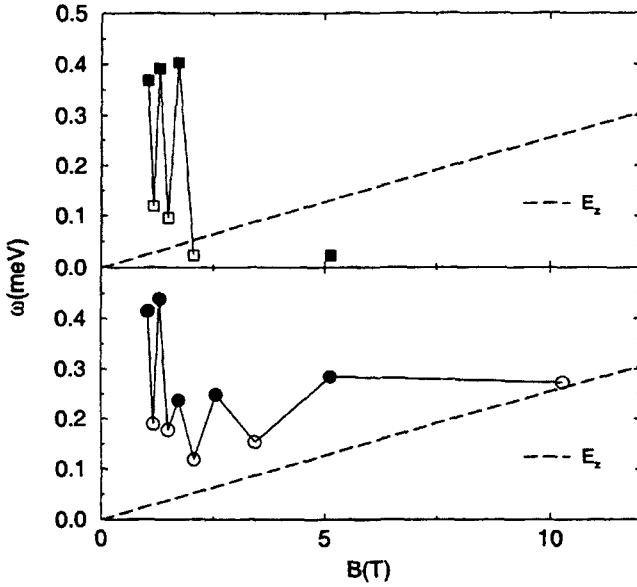
Fig. 8.40 Bottom panel: Energies of the most intense low-energy peaks excited by $x\sigma_-$ as a function of B, for the same configurations as in Fig. 8.39. In the figure we also report the Zeeman energy (dashed line). Top panel: the same as the bottom panel, but for $x\sigma_+$. Some configurations are lacking due to the Pauli blocking.

and the SDE excitations undergo Landau damping because they are very close to the SPE ones (the same happens for transverse modes at low B). In the transverse channel, when the dot has an appreciable magnetization, the SDE excitations are shifted with respect to the SPE ones by the p–h vertex correction, which originates from the electron–electron interaction. As a consequence, a very collective and dispersionless SDE excitations emerges. At large spin magnetization, Pauli exclusion principle plays a determinant role by blocking the $x\sigma_+$ component of the transverse structure function which, therefore, becomes simpler. The sensitivity of the transverse response to the applied magnetic field B is revealed by strong oscillations of the collective energies with B. Such oscillations are also a consequence of the different strength of the vertex corrections in the ferromagnetic and paramagnetic ground states.

Lastly, we note that there is a strong analogy between SDE excitations in quantum dots, and isospin excitations in nuclei with different number of neutrons N and protons Z. In nuclei the isospin polarization given by $(N - Z)/2$, is the analogue of the spin polarization of the dots. The ingredients that produce it are the Coulomb potential which is the analogue of the applied magnetic field for the dots, and the symmetry potential which is the analogue of the spin-dependent potential W_{xc}. The excitations which are the analogue of those of the SDE discussed here are induced

by the operators

$$D_a = \sum_{i=1}^{N} x_i \tau_i^z \quad \text{and} \quad D_\pm = \sum_{i=1}^{N} x_i \tau_i^\pm \,,$$

where τ indicates the isospin operator analogous to the spin operator σ. These excitations, known as giant resonances in the isospin channels, have been studied in the framework of the time-dependent *LDA* theory, based on the density functional described in Section 4.10, by Auerbach and Klein (1983).

References to Chapter 8

D. Pines and P. Nozières, The Theory of Quantum Liquids, (Benjamin, New York, 1966), Vol. I.

E. Lipparini and S. Stringari, Phys. Rep. **175**, 103 (1989).

C.F. von Weizsacker, Z. Phys. **96**, 431 (1935).

H.A. Bethe and R.F. Bacher, Rev. Mod. Phys. **8**, 82 (1936).

C. Garcia-Recio, J. Navarro, N. Van Giai and L. Salcedo, Annals of Physics **214**, 293 (1992).

I.M. Khalatninov and A.A. Abrikosov, Sov. Phys. JEPT **6**, 84 (1958).

K. Bedell and C.J. Pethick, J. Low Temp. Phys. **49**, 213 (1982).

W.R. Abel, A.C. Anderson and J.C. Wheatley, Phys. Rev. Lett. **17**, 74 (1966).

V. Yu Denisov, Sov. J. Nucl. Phys. **49**, 38 (1989).

V. Baran, M. Colonna, M. Di Toro, A. Guarnera, V.N. Kondratyev and A. Smerzi, Nucl. Phys. A **599**, C 29 (1996).

V.P. Silin, Sov. Phys. JEPT **6**, 387 (1957); **6**, 985 (1957).

L. Hedin and B.I. Lundqvist, Solid State Physics **23**, 1 (1969).

S.H. Vosko, L. Wilk and M. Nusair, Can. J. Phys. **58**, 1200 (1980).

N. Iwamoto and D. Pines, Phys. Rev. B **29**, 3924 (1984).

A. vom Felde, J. Sprosser-Prou and J. Fink, Phys. Rev. B **40**, 10181 (1989).

Y. Kwon, D.M. Ceperley and R.M. Martin, Phys. Rev. B **50**, 1684 (1994) and references therein.

T. Ando, A.B. Fowler and F. Stern, Rev. Mod. Phys. **54**, 437 (1982).

M.S.C. Luo, S.L. Chuang, S. Schmitt-Rink and A. Pinczuk, Phys. Rev. B **48**, 11086 (1993).

A. Pinczuk et al., Phys. Rev. Lett. **63**, 1633 (1989).

M.A. Eriksson, A. Pinczuk, B.S. Dennis, S.H. Simon, L.N. Pfeiffer and K.W. West, Phys. Rev. Lett. **82**, 2163 (1999).

I.S. Gradshteyn and I.M. Ryzhik, Table of Integrals, Series and Products (Academic Press, New York, 1980).

S.J. Allen, D.C. Tsui and R.A. Logan, Phys. Rev. Lett. **38**, 980 (1977).

C.C. Grimes and G. Adams, Phys. Rev. Lett. **36**, 145 (1976).

F.L. Braghin and D. Vautherin, Phys. Lett. B **333**, 289 (1994).

E.S. Hernandez, J. Navarro, A. Polls and J. Ventura, Nucl. Phys. A **597**, 1 (1996).

D.M. Brink, A. Dellafiore, M. Di Toro, Nucl. Phys. A **456**, 205 (1986).

S. Tomonaga, Prog. Theor. Phys. (Kyoto) **5**, 544 (1950).

J.M. Luttinger, J. Math. Phys. **4**, 1154 (1963).

A.R. Goi et al., Phys. Rev. Lett. **67**, 3298 (1991).

Quiang Li and S. Das Sarma, Phys. Rev. B **40**, 5860 (1989); **43**, 11768 (1991).

D. Agosti, F. Pederiva, E. Lipparini and K. Takayanagi, Phys. Rev. B **57**, 14869 (1998).

K. Huang, Statistical Mechanics, Second Edition (John Wiley and Sons, New York 1987).

R.J. Donnelly, J.A. Donnelly and R.N. Hills, J. Low. Temp. Phys. **44**, 471 (1981).

F. Dalfovo, A. Lastri, L. Pricaupenko, S. Stringari and J. Treiner, Phys. Rev. B **52**, 1193 (1995).

A.D.B. Woods and R.A. Cowley, Rep. Prog. Phys. **36**, 1135 (1973).

L.D. Landau and E.M. Lifchitz, "Fisica Statistica", Teoria dello Stato Condensato, Editori riuniti (Edizioni Mir, 1981).

P. Nozières and D. Pines, The Theory of Quantum Liquids, Superfluid Bose liquids (Addison Wesley, 1990).

N. Bogoliubov, J. Phys. (Moscow) **11**, 23 (1947).

F. Dalfovo, S. Giorgini, L. Pitaevskii and S. Stringari, Rev. Mod. Phys. **71**, 3 (1999).

E.P. Gross, Nuovo Cimento **20**, 454 1961; J. Math. Phys. **4**, 195 (1963).

L.P. Pitaevskii, Sov. Phys. JEPT **13**, 451 (1961).

M.R. Edwards et al., Phys. Rev. Lett. **77**, 1671 (1996).

P.A. Ruprecht et al., Phys. Rev. A **54**, 4178 (1996).

K.G. Singh and D.S. Rokhsa, Phys. Rev. Lett. **77**, 1667 (1996).

F. Dalfovo et al., Phys. Rev. A **56**, 3840 (1997).

B.D. Esry, Phys. Rev. A **55**, 1147 (1997).

D.A. Hutchinson and E. Zaremba, Phys. Rev. A **57**, 1280 (1997).

D.A. Hutchinson, E. Zaremba and A. Griffin, Phys. Rev. Lett. **78**, 1842 (1997).

L. You, W. Hoston and M. Lewenstein, Phys. Rev. A **55**, R1581 (1997).

D.S. Jin et al., Phys. Rev. Lett. **77**, 420 (1996).

A.L. Fetter, Ann. Phys. (N.Y.) **70**, 67 (1972).

V.N. Popov, Sov. Phys. JEPT **20**, 1185 (1965).

V.N. Popov, Functional integrals and Collective Excitations (Cambridge, University Press, Cambridge, 1987).

A. Griffin, Phys. Rev. B **53**, 9341 (1996).

G.B. Bachelet, D.M. Ceperley and M.G.B. Chiocchetti, Phys. Rev. Lett. **62**, 2088 (1989).

C. Guet and W.R. Johnson, Phys. Rev. B **45**, 11283 (1992).

E. Lipparini, Ll. Serra and K. Takayanagi, Phys. Rev. B **49**, 16733 (1994).

W. Ekardt, Phys. Rev. B **31**, 6360 (1985).

C. Yannouleas, R.A. Broglia, M. Brack and P.F. Bortignon, Phys. Rev. Lett. **63**, 255 (1989).

O. Bohigas, A.M. Lane, J. Martorell, Phys. Rep. **51**, 267 (1979).

S. Pollack, C.R.C. Wang and M.M. Kappes, J. Chem. Phys. **94**, 2496 (1991).

C. Bréchignac, Ph. Cahuzac, J. Leygnier and A. Sarfati, Phys. Rev. Lett. **70**, 2036 (1993).

Ll. Serra, G.B. Bachelet, N. Van Giai and E. Lipparini, Phys. Rev. B **48**, 14708 (1993).

S.A. Blundell and C. Guet, Z. Phys. D **28**, 81 (1993).

F. Alasia, R.A. Broglia, N. Van Giai, E. Lipparini, H.E. Roman and Ll. Serra, Phys. Rev. B **52**, 8488 (1995).

J. Borggreen, P. Chowdhury, N. Kebaïli, L. Lundsberg-Nielsen, K. Lützenkirchen, M.B. Nielsen, J. Pedersen and H.D. Rasmussen, Phys. Rev. B **48**, 17507 (1993).

C. Ellert et al., Phys. Rev. Lett. **75**, 1731 (1995).

Th Reiners et al., Phys. Rev. Lett. **75**, 1558 (1995).

K. Selby, V. Kresin, J. Masui, M. Vollmer, W.A. de Heer, A. Scheidemann and W. D. Knight, Phys. Rev. B **43**, 4565 (1991).

W.D. Knight, K. Clemenger, W.A. de Heer and W.A. Saunders, Phys. Rev. B **31**, 445 (1985).

E.K.U. Gross and W. Kohn, Adv. Quant. Chem. **21**, 255 (1990).

W.M. Alberico, A Depace, A. Drago and A. Molinari, R.N.C. **14**, 1, (1991).

G.F. Bertsch and S.F. Tsai, Phys. Rep. C **18**, 126 (1975).

K.F. Liu and G.E. Brown, Nucl. Phys. A **265**, 385 (1976).

K.F. Liu and N. Van Giai, Phys. Lett. B **65**, 23 (1976).

Ll. Serra, J. Navarro, M. Barranco and N. Van Giai, Phys. Rev. Lett. **67**, 2311 (1991).

M. Barranco et al., Phys. Rev. B **56**, 8997 (1997).

M. Casas et al., Z. Phys. D **35**, 67 (1995).

A. K. Rajagopal, Phys. Rev. B **17**, 2980 (1978).

E. Lipparini and Ll. Serra, Phys. Rev. B **57**, R6830 (1998).

E. Lipparini, M. Barranco, A. Emperador, M. Pi and Ll. Serra, Phys. Rev. B **60**, 8734 (1999).

V.P. Silin, Sov. Phys. JEPT **6**, 945 (1958); **8**, 870 (1959).

P.M. Platzman and P.A. Wolff, Phys. Rev. Lett. **18**, 280 (1967).

S. Schultz and G. Dunifer, Phys. Rev. Lett. **18**, 283 (1967).

S. Stringari and F. Dalfovo, J. Low Temp. **78**, 1 (1990).

K. von Klitzing, G. Dorda and M. Pepper, Phys. Rev. Lett. **45**, 494 (1980).

D.C. Tsui, H. Stormer and A.C. Gossard, Phys. Rev. Lett. **48**, 1559 (1982).

R. Willet, J.P. Eisenstein, H. Stormer, D.C. Tsui, A.C. Gossard and J.H. English, Phys. Rev. Lett. **59**, 1776 (1987).

K. Takayanagi and E. Lipparini, Phys. Rev. B **52**, 1738 (1995); B **54**, 8122 (1996).

H.J. Schulze, P. Schuck and N. Van Giai, Phys. Rev. B **61**, 8026 (2000).

N.F. Mott and H. Jones, Theory of Metals and Alloys (Dover, New York, 1936).

C. Schüller, K. Keller, G. Biese, E. Ulrichs, L. Rolf, C. Steinebach, D. Heitmann and K. Eberl, Phys. Rev. Lett. **80**, 2673 (1998).

C. Kallin and B. Halperin, Phys. Rev. B **30**, 5655 (1984).

A.H. MacDonald, J. Phys. C **18**, 1003 (1985).

A. Ghizzi, Tesi di Laurea in Fisica, Università di Trento, A.A. 1999-2000.

Ll. Serra, M. Barranco, A. Emperador, M. Pi and E. Lipparini, Phys. Rev. B **59**, 15290 (1999).

O. Steffens and M. Suhrke, Phys. Rev. Lett. **82**, 3891 (1999).

Ch. Sikorski and U. Merkt, Phys. Rev. Lett. **62**, 2164 (1989).

T. Demel, D. Heitmann, P. Grambow and K. Ploog, Phys. Rev. Lett. **64**, 788 (1990).

R. Strenz, U. Bockelmann, F. Hirler, G. Abstreiter, G. Böhm and G. Weimann, Phys. Rev. Lett. **73**, 3022 (1994).

C. Schüller, G. Biese, K. Keller, C. Steinebach, D. Heitmann, P. Grambow and K. Eberl, Phys. Rev. B **54**, R17304 (1996).

Ll. Serra and E. Lipparini, Europhys. Lett. **40**, 667 (1997).

V. Gudmundsson and R. R. Gerhardts, Phys. Rev. B **43**, 12098 (1991).

K. Bollweg, T. Kurth, D. Heitmann, V. Gudmundsson, E. Vasiliadou, P. Grambow and K. Eberl, Phys. Rev. Lett. **76**, 2774 (1996).

Z. L. Ye and E. Zaremba, Phys. Rev. B **50**, 17217 (1994).

A. Usher et al., Phys. Rev. B **41**, 1129 (1990).

N. Auerbach and A. Klein, Nuclear Physics A **395**, 77 (1985).

This page is intentionally left blank

Chapter 9

Dynamic Correlations and Response Function

9.1 Introduction

As we saw in the previous Chapter, the formulation of the many body problem in terms of the density response function of the system produces many very interesting results for several systems; above all, for the degenerate electron gas in a background of positive charge, which is a model of basic importance for studying many properties of metals and of systems realized recently in the laboratory, such as quantum wells, metal clusters and quantum dots. This approach is very useful, in general, for all Bosonic and Fermionic quantum liquids. With this formulation, not only is it possible to study the excitation spectrum of many body systems, but it is also possible to express in a rigorous fashion the ground state energy and the related static properties, for example, the pair correlation function and the compressibility.

In the present Chapter, we will study this formulation, and present the different approximations that have been used in the literature and compare them with one other and, whenever possible, with the results of "exact" calculations provided, e.g. by the Monte Carlo method. All the calculations are performed in the zero temperature limit.

9.2 Interaction Energy and Correlation Energy

When we evaluate the ground state energy of a many body system, we must take into account two contributions, i.e. the kinetic one and the one due to interaction:

$$E = T + E_{\text{int}} , \tag{9.1}$$

where

$$T = \langle 0 | \sum_{i=1}^{N} \frac{p_i^2}{2m} | 0 \rangle , \quad E_{\text{int}} = \frac{1}{2} g \langle 0 | \sum_{i \neq j} v(|\mathbf{r}_i - \mathbf{r}_j|) | 0 \rangle . \tag{9.2}$$

In equation (9.2), g is the coupling constant of the interaction, for example the squared charge in the case of the Coulomb interaction; in this case $v(|\mathbf{r}_i - \mathbf{r}_j|) = |\mathbf{r}_i - \mathbf{r}_j|^{-1}$. Introducing the Fourier transform $v_{\mathbf{q}}$ of $v(|\mathbf{r}_i - \mathbf{r}_j|)$, the interaction term may be rewritten as

$$E_{\text{int}} = g\langle 0| \int \frac{d\mathbf{q}}{(2\pi)^D} \frac{v_{\mathbf{q}}}{2} (\rho_{-\mathbf{q}}\rho_{\mathbf{q}} - N)|0\rangle\,, \tag{9.3}$$

where $\rho_{\mathbf{q}} = \sum_{i=1}^{N} e^{i\mathbf{q}\cdot\mathbf{r}_i}$ is the density operator. If we introduce the static form factor as defined in equations (7.71) and (7.72), we obtain

$$E_{\text{int}} = g \int \frac{d\mathbf{q}}{(2\pi)^D} \frac{v_{\mathbf{q}}}{2} \left(\int_0^\infty d\omega \, S(\mathbf{q},\omega) - N + N^2\delta_{\mathbf{q}0} \right)$$

$$= -g \int \frac{d\mathbf{q}}{(2\pi)^D} \frac{v_{\mathbf{q}}}{2} \left(N - N^2\delta_{\mathbf{q}0} + \frac{1}{\pi} \int_0^\infty d\omega \, \text{Im}\, \chi(\mathbf{q},\omega) \right)\,. \tag{9.4}$$

Starting from (9.4) it is easy to show that, using the free response functions of Section 7.7 in place of χ, we can obtain for the interaction energy of homogeneous systems the Hartree–Fock energy in the Fermion case, and the Gross–Pitaevskii mean field energy for Bosons. The direct Hartree–Fock term results from the term proportional to $N^2\delta_{\mathbf{q}0}$, and in the case of the electron gas this is canceled by the field produced by the positive background charge. We recall that

$$\delta_{\mathbf{q}0} = 1/L^D \int d\mathbf{r} e^{i\mathbf{q}\cdot\mathbf{r}}\,.$$

It is clear that any theory which, for the response function, yields an approximation beyond the free response one, will also provide a result for the interaction energy which takes into account correlations other than the statistical ones. However, dynamic correlations contribute to the kinetic energy term as well, and in order to obtain the total contribution of dynamic correlations to the ground state energy, starting from the density response function, it is necessary to proceed further with the theory. It is necessary to use a theorem, due to Pauli, which allows the kinetic energy of the system to be computed by means of the interaction energy of equation (9.4). We define

$$E_0^\alpha = \langle 0|\hat{H}^\alpha|0\rangle \tag{9.5}$$

where

$$\hat{H}^\alpha = \hat{T} + \alpha \sum_{i \neq j} v(|\mathbf{r}_i - \mathbf{r}_j|)\,, \tag{9.6}$$

so that, if the coupling constant α is set equal to g, we obtain the usual inter-particle interaction, while if it is set to zero we are back into the non-interacting system. By taking into account the normalization condition of the ground state $|0\rangle$ of the

system, we have

$$\frac{\partial E_0^\alpha}{\partial \alpha} = \langle 0 | \frac{\partial \hat{H}^\alpha}{\partial \alpha} | 0 \rangle + \langle 0 | \hat{H}^\alpha \left| \frac{\partial 0}{\partial \alpha} \right\rangle + \left\langle \frac{\partial 0}{\partial \alpha} \right| \hat{H}^\alpha | 0 \rangle$$

$$= \langle 0 | \sum_{i \neq j} v(|\mathbf{r}_i - \mathbf{r}_j|) | 0 \rangle = \frac{E_{\text{int}}}{\alpha} \,, \tag{9.7}$$

and by integrating this equation with respect to α, up to the value g, we obtain

$$\int_0^g \frac{\partial E_0^\alpha}{\partial \alpha} d\alpha = \int_0^g \frac{E_{\text{int}}}{\alpha} d\alpha = E_0(\alpha = g) - E_0(\alpha = 0) \,, \tag{9.8}$$

where

$$E_0(\alpha = 0) = \begin{cases} \dfrac{D}{D+2} N \dfrac{k_F^2}{2m} & \text{for Fermions} \\ 0 & \text{for Bosons} \end{cases} \,. \tag{9.9}$$

Equations (9.4), (9.7) and (9.8) allow us to evaluate the ground state energy of the homogeneous system, starting from the density response function, through the equation

$$E_0 = T_0 + \int_0^g \frac{E_{\text{int}}}{\alpha} d\alpha \,, \tag{9.10}$$

where T_0 is the kinetic energy of the free gas.

Knowledge of the density response function of the system, also allows us to calculate the contribution from dynamic correlations to the pair correlation function as defined in (7.74). In fact, from the relation between such quantity and the static form factor (see Section 7.5):

$$S(\mathbf{q}) = 1 + \rho \int d\mathbf{r}(g(r) - 1) e^{i\mathbf{q} \cdot \mathbf{r}} \,,$$

we obtain after taking its inverse transform

$$g(r) = 1 + \frac{1}{\rho} \int \frac{d\mathbf{q}}{(2\pi)^D} (S(\mathbf{q}) - 1) e^{-i\mathbf{q} \cdot \mathbf{r}} \,, \tag{9.11}$$

which allows the numerical calculation of $g(r)$.

9.3   The RPA Correlation Energy

In this Section, we will apply the formalism described above to the case where the density response is that obtained from the RPA theory (see Section 8.2):

$$\chi^{RPA}(q,\omega) = \frac{\chi^0(q,\omega)}{1 - g\frac{v_\mathbf{q}}{L^D}\chi^0(q,\omega)},$$

with $\chi^0(q,\omega)$ free response function of Section 7.7. Then, we obtain the following relation for the ground state energy in the RPA approximation

$$E_0^{RPA} = T_0 - \int \frac{d\mathbf{q}}{(2\pi)^D} \frac{v_\mathbf{q}}{2} \int_0^g d\alpha$$

$$\times \left(N - N^2\delta_{\mathbf{q}0} + \frac{1}{\pi}\int_0^\infty d\omega \,\mathrm{Im}\,\chi^{RPA}(\mathbf{q},\omega) \right). \quad (9.12)$$

The RPA correlation energy is subsequently obtained by subtracting from the above expression the HF energy which, as discussed previously, in the framework of the density response function, is obtained using the free response function for χ. In this way, we have for the correlation energy per particle

$$\frac{E_c^{RPA}}{N} = \frac{1}{2\pi N} \int \frac{d\mathbf{q}}{(2\pi)^D} v_\mathbf{q} \int_0^g d\alpha \int_0^\infty d\omega \, (\mathrm{Im}\,\chi^{RPA} - \mathrm{Im}\,\chi_0). \quad (9.13)$$

The RPA correlation energy has been computed for the electron gas immersed in a background of positive charge, in several dimensions, by many authors (see, for example, Pines and Nozières 1966; Jonson 1976; Agosti et al. 1998). The numerical results one obtains are in agreement with the ones derived by Gell-Mann and Brueckner (1957) in $3D$, and by Isihara and Toyoda (1977) and Rajagopal and Kimball (1977) in $2D$, using perturbation theory in the limit of high density ($r_s \ll 1$). In this limit, the leading terms in the correlation energy are a series of diagrams (ring diagrams) corresponding to the most diverging direct terms which, when summed up, lead to a rigorous and converging result. Therefore, the RPA is the proper theory for the correlation energy of the electron gas in the limit of high density. As can be seen from Table 9.1, where the RPA correlation energy is compared with the results of other theories in the case of the $2D$ electron gas (taken as an example), the RPA theory works well only at very low values of r_s. Even at $r_s = 0.5$ there is a large discrepancy between the RPA correlation energy and the one obtained from Monte Carlo calculations (Tanatar and Ceperley 1989).

The direct connection between the RPA theory as discussed in this Section, and the high-density perturbation theory, can be established by starting from the expression for the RPA correlation energy (9.13), and assuming that in

$$\chi^{RPA}(q,\omega) = \frac{\chi^0(q,\omega)}{1 - e^2\frac{v_\mathbf{q}}{L^D}\chi^0(q,\omega)},$$

the term $e^2 v_{\mathbf{q}} \chi^0 / L^D$ represents a small parameter. In this case, it is possible to write a series expansion of the type

$$\chi^{RPA} = \chi^0 \left(1 + e^2 \frac{v_{\mathbf{q}}}{L^D} \chi^0 + \left(e^2 \frac{v_{\mathbf{q}}}{L^D} \right)^2 (\chi^0)^2 + \cdots \right), \tag{9.14}$$

and verify that the terms proportional to $\text{Im}(\chi_0)^2$, $\text{Im}(\chi_0)^3$, and so on, give the ring diagrams of perturbation theory.

Finally we point out that the *RPA* correlation energy can also be calculated in finite size systems. To reach this goal one has to solve both the *RPAE* and Tamm–Dancoff *(TD)* equations, (8.138) and (8.161), respectively, taking care of all the possible *p–h* excitations up to some cut-off energy which fixes the model space of the calculation. The *RPA* correlation energy is then given by the sum

$$E_{RPAE} - E_{HF} = \frac{1}{2} \sum_\lambda (\omega_\lambda^{RPA} - \omega_\lambda^{TD}), \tag{9.15}$$

of all differences in the excitation energies between the *RPAE* and *TD* approaches [for the derivation of Eq. (9.15), see e.g. Ring and Schuck 1980]. Clearly, in the calculation of the sum (9.15), one must reach convergence of the result with the cut-off. A calculation of this kind has been done, for example, in metal clusters by Reinhard (1992).

9.3.1 The RPA correlation energy for the cold and dilute gas of Bosons and Fermions

As an example of analytic calculation of *RPA* correlations, we consider the case of a cold and dilute gas of Bosons and Fermions, for which it is possible to replace the two-body interaction by the effective interaction $v(r) = g\delta(r)$, where g is connected to the scattering length a for the low-energy scattering of the gas atoms. As was shown in Section 8.5, in the Boson case and using the following expression for the free response:

$$\chi_0^B(\mathbf{q}, \omega) = \frac{\frac{Nq^2}{m}}{\omega^2 - (\frac{q^2}{2m})^2},$$

we obtain for the *RPA* response the expression

$$\chi_{RPA}^B(\mathbf{q}, \omega) = \frac{\frac{Nq^2}{m}}{\omega^2 - \frac{\rho q^2 g}{m} - (\frac{q^2}{2m})^2}, \tag{9.16}$$

which has only one pole at energy

$$\omega_{RPA}^B = \sqrt{\frac{\rho q^2 g}{m} + \left(\frac{q^2}{2m} \right)^2} \cdot \cdot$$

The imaginary part of $\chi_{RPA}^B(\mathbf{q}, \omega)$ is, therefore, given by

$$\text{Im }\chi_{RPA}^B(\mathbf{q}, \omega) = -\frac{Nq^2}{m}\frac{\pi\delta(\omega - \omega_{RPA}^B)}{2\omega_{RPA}^B}. \tag{9.17}$$

By inserting this result in (9.12), it is easy to obtain the following result for the *RPA* energy in the ground state of a dilute Boson gas:

$$\frac{E_B^{RPA}}{N} = \frac{\rho g}{2} + \frac{1}{2\rho}\int\frac{d\mathbf{q}}{(2\pi)^3}\left[\frac{q^2}{2m}\sqrt{1 + \frac{4m\rho g}{q^2}} - \frac{q^2}{2m} - g\rho\right], \tag{9.18}$$

where (ρ is the gas density) the first term is the (Gross–Pitaevskii) mean-field energy which derives from the term proportional to $N^2\delta_{\mathbf{q}0}$ in (9.12), and the second term is the *RPA* correlation energy. By expanding the integral in the correlation term, it is possible to write

$$\frac{E_B^{RPA}}{N} = \frac{\rho g}{2} + \frac{8}{15\pi^2}gm^3\left(\frac{g\rho}{m}\right)^{3/2} - \frac{1}{2}mg^2\rho\int\frac{d\mathbf{q}}{(2\pi)^3}\frac{1}{q^2}. \tag{9.19}$$

The last term in (9.19) diverges in the limit of large q. Such ultraviolet divergence can be removed by a suitable renormalization of the bare coupling constant g which appears in the δ-like interaction, by using the ladder theory of Section 3.3. In fact, when applied to such interaction, the ladder theory produces the result $\tilde{g}$ [see Eq. (3.9)] for the renormalized coupling constant (with $V(q) = g$):

$$\tilde{g} = g\left(1 - \tilde{g}\int\frac{d\mathbf{k}}{(2\pi)^3}\frac{m}{k^2}\right), \tag{9.20}$$

which, at second order in $\tilde{g}$, yields

$$g = \tilde{g}\left(1 + \tilde{g}\int\frac{d\mathbf{k}}{(2\pi)^3}\frac{m}{k^2}\right). \tag{9.21}$$

For a dilute and cold gas $\tilde{g} = 4\pi a/m$, where a is the scattering length, and finally from equation (9.21) we get for the renormalization of the bare coupling constant

$$g = \frac{4\pi a}{m}\left(1 + \frac{4\pi a}{m}\int\frac{d\mathbf{k}}{(2\pi)^3}\frac{m}{k^2}\right), \tag{9.22}$$

which is valid to second order. The substitution of this result into (9.19), leads to the following expression for the ground-state energy per particle:

$$\frac{E_B^{RPA}}{N} = \frac{2\pi a\rho}{m}\left(1 + \frac{128}{15\sqrt{\pi}}\sqrt{a^3\rho}\right). \tag{9.23}$$

This result coincides, at lowest order, with the exact result derived by Lee, Huang and Yang (1957) by expansion in powers of $\sqrt{a^3\rho}$ of the ground state energy of a homogeneous and dilute Bose gas. A rigorous derivation of the exact energy per particle of a homogeneous and dilute Bose gas, can be found in Lieb and Yngvason

(1998). These authors also derived in a rigorous way the energy of the same gas in the two-dimensional case (Lieb and Yngvason 2000):

$$\frac{E_B^{2D}}{N} = \frac{2\pi\rho}{m} |\ln(\rho a^2)|^{-1}, \tag{9.24}$$

which holds at lowest order in ρa^2. This result had been derived previously by Schick and Hines (1971), Frankel and Mitchell (1978), and extended to finite temperature by Popov (1977) and Fisher and Hohenberg (1988).

In the case of a dilute Fermion gas, an analytic calculation of the RPA ground state energy, analogous to the one carried out for Bosons, is not possible. In fact, the Fermion free response function is much more complicated than that for Bosons, and the integrals which appear in the expression for the RPA ground state energy (9.12) are not analytical. However, we do obtain an analytical result if in (9.12) we use for χ^{RPA} the expansion (9.14) truncated at second order, and with $e^2 v_{\mathbf{q}} = g$, for the dilute Fermion gas. The result one obtains, by adding the second order exchange term (which, for the δ-like interaction, is a half of the direct one with opposite sign), then coincides with that of second-order perturbation theory (see, for example, Landau–Lifchitz 1981):

$$\frac{E_F^{3D}}{N} = \frac{3k_F^2}{10m} \left[1 + \frac{10}{9\pi} k_F a + \frac{4(11 - 2\ln 2)}{21\pi^2} (k_F a)^2 \right], \tag{9.25}$$

where k_F is the Fermi momentum and a is the scattering length for the Fermion gas. Note that, in deriving this result, and as in the Boson case, we take into account the renormalization of the bare coupling constant. Such renormalization cancels exactly the ultraviolet divergence of the correlation energy term. Expression (9.25) gives the first terms of the expansion of the energy in powers of the parameter $k_F a$ (Huang and Yang 1957). The above calculation also allows the derivation of quasiparticle properties of the dilute Fermion gas. For example, the effective mass turns out to be given by

$$\frac{m^*}{m} = 1 + \frac{8}{15\pi^2} (7\ln 2 - 1)(k_F a)^2. \tag{9.26}$$

At first, one might think that the above results for the dilute Fermion gas are valid both for repulsion and attraction among Fermions, i.e. both for positive and negative scattering lengths. However, in the case of attraction ($a < 0$) this is not true, since the ground state of the system defined in this way is unstable against the formation of pairs of particles near the Fermi surface, with momenta that are equal in magnitude and opposite in direction, and whose spins are antiparallel (Cooper pairs). In this case, the right theory to use is the BCS theory described in Section 2.7 starting from equation (2.110) with $V_{kl} = -g/V$. Therefore, the above results are to be considered valid only when the forces among Fermions are repulsive.

9.4   Theories Beyond the RPA

In general, the linear response χ of the system can always be expressed in terms of the free response function χ^0 as

$$\chi(\mathbf{q}, \omega) = \frac{\chi^0(\mathbf{q}, \omega)}{1 - \frac{v_\mathbf{q}}{L^D}(1 - G(\mathbf{q}, \omega))\chi^0(\mathbf{q}, \omega)}, \tag{9.27}$$

where $G(\mathbf{q}, \omega)$ is the so-called field factor which is to be determined through a microscopic calculation. When $G(\mathbf{q}, \omega) = G(\mathbf{q})$, one talks about static field theories. In general, G depends on ω as well, and in this case one talks about dynamic field theories. The RPA theory has $G = 0$, while the adiabatic $TDLDA$ theory is a static theory with

$$G^{TDLDA}(\mathbf{q}) = -\frac{1}{v_\mathbf{q}} \frac{\partial V_{xc}}{\partial \rho}\bigg|_{\rho = \rho_0}, \tag{9.28}$$

where V_{xc} is the exchange-correlation potential. Another static theory is the Hubbard theory (Hubbard 1957) for the electron gas, where one assumes

$$G^H(\mathbf{q}) = \frac{q^2}{2(q^2 + k_F^2)}, \qquad \text{(in } 3D), \tag{9.29}$$

and

$$G^H(\mathbf{q}) = \frac{q}{2\sqrt{q^2 + k_F^2}}, \qquad \text{(in } 2D). \tag{9.30}$$

This theory takes into account in an approximate way the exchange effects which are neglected in the RPA.

$G(\mathbf{q}, \omega)$ has been computed numerically for the $2D$ electron gas, starting from the $RPAE$ results (see Section 8.11) for $\chi(\mathbf{q}, \omega)$ of Takayanagi and Lipparini (1995) and Schulze et al. (2000), which treat the exchange exactly. At $\omega = 0$, $G(\mathbf{q}, 0)$ exhibits a linear behaviour in the low-q limit, a peak around $q = 2k_F$, and tends to $1/2$ for $q \to \infty$. This is shown in Fig. 9.1, where the $RPAE$ results for $G(\mathbf{q}, 0)$ are compared with those of other models (Pederiva et al. 1997). From this figure, one notices that for $q < 2k_F$ the $RPAE$ result is in very good agreement with the Monte Carlo (MC) results at $r_s = 1$ and $r_s = 5$, while for high momentum values one observes a substantial difference between the $RPAE$ and MC results. In fact, the Monte Carlo calculation (Moroni et al. 1992) predicts a nearly linear increase of $G(\mathbf{q}, 0)$ with q, as expected (Likos et al. 1997), while the $RPAE$ yields $G(\mathbf{q}, 0)$ tending to $1/2$ for large q. As was shown in Takayanagi and Lipparini (1996), a large part of the difference existing between $RPAE$ and MC results can be accounted for by taking into consideration electron–electron correlations due to re-scattering processes of the ladder diagrams, and then using the effective Brueckner–Hartree–Fock interaction (g matrix, see Chapter 3) instead of the bare interaction to solve the integral Dyson equation. The results of such calculation ($RPAEG$) for the static response function
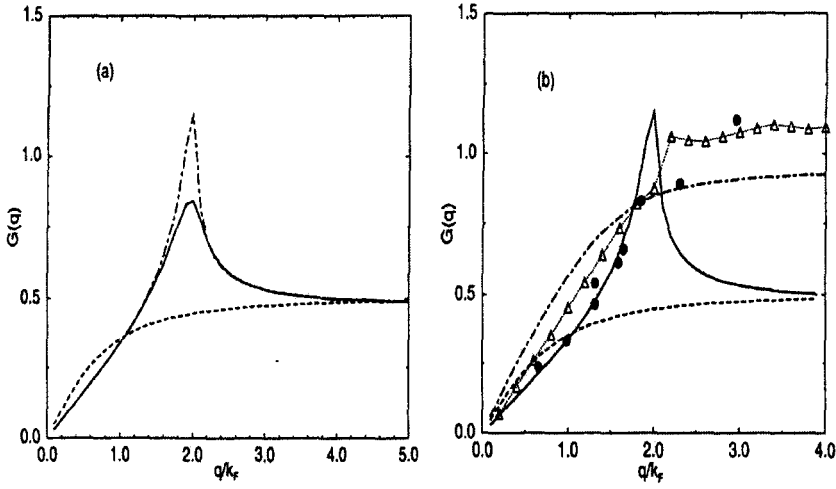
Fig. 9.1 (a) Static field factor G(q) of the $2D$ electron gas, computed in the $RPAE$ as a function of q/k_F for two different values of the density. Full curve: $r_s = 1$, dashed-dotted curve $r_s = 5$. The dashed curve is the Hubbard approximation; (b) $G(q)$ for $r_s = 5$ in different models: dashed curve: Hubbard approximation; full curve: $RPAE$; dashed-dotted curve: $STLS$ approximation; triangles: $RPAEG$; full dots: QMC results.

$\chi(q)$ are shown in Fig. 9.2, together with the results of the MC calculation. The peak at $q = 2k_F$ in $\chi(q)$ is a consequence of the similar peak in $G(\mathbf{q}, 0)$. For reasons of numerical accuracy, it is not possible to draw a definite conclusion as to the behaviour of such quantities in the neighborhood of $q = 2k_F$, and in this q region there is still some ambiguity in the determination of the static field factor.

9.5 $STLS$ Theory

The $STLS$ (Singwi, Tosi, Land and Sjolander 1968) model is based on an approximate solution of the equation of motion for the one-particle distribution function $f(\mathbf{r}, \mathbf{p}, t)$ which gives the probability of finding a particle at position $\mathbf{r}$ with momentum $\mathbf{p}$ at time t. This quantity, which is related to the spatial density of the particle $\rho(\mathbf{r}, t)$ by the relationship:

$$\rho(\mathbf{r}, t) = \int d\mathbf{p} f(\mathbf{r}, \mathbf{p}, t) \,, \tag{9.31}$$

fulfills, in the presence of an external field $v_{\text{ext}}(\mathbf{r}, t)$, the kinetic equation (see, e.g. Cohen 1962):

$$\frac{\partial}{\partial t} f(\mathbf{r}, \mathbf{p}, t) + \frac{\mathbf{p}}{m} \cdot \nabla_{\mathbf{r}} f(\mathbf{r}, \mathbf{p}, t) - \nabla_{\mathbf{r}} v_{\text{ext}}(\mathbf{r}, t) \cdot \nabla_{\mathbf{p}} f(\mathbf{r}, \mathbf{p}, t)$$

$$- \int \nabla_{\mathbf{r}} v(\mathbf{r} - \mathbf{r}') \cdot \nabla_{\mathbf{p}} f(\mathbf{r}, \mathbf{p}, \mathbf{r}'; \mathbf{p}', t) d\mathbf{r}' d\mathbf{p}' = 0 \,, \tag{9.32}$$
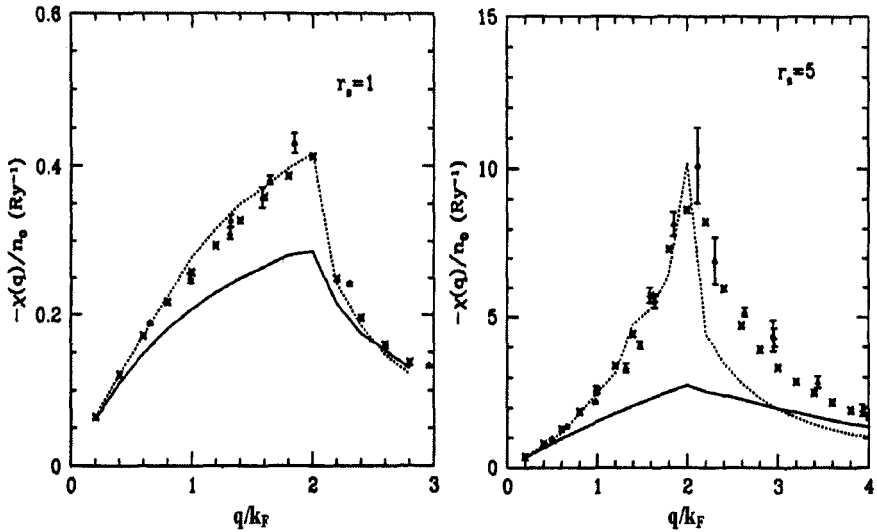
Fig. 9.2   Static linear response of the $2D$ electron gas as a function of q/k_F at $r_s = 1$ and $r_s = 5$. The full and dashed lines give the RPA and $RPAE$ results, respectively. The stars indicate the $RPAEG$ results (including the ladder correlations), and the triangles the QMC results.

where $v(\mathbf{r} - \mathbf{r}')$ is the inter-particle interaction potential, and $f(\mathbf{r}, \mathbf{p}, \mathbf{r}'; \mathbf{p}', t)$ is the two-particle distribution function. The equation for the two-particle distribution function, in turn, contains the three-particle distribution function, and so on. *STLS* truncated such infinite hierarchy of equations by the ansatz:

$$f(\mathbf{r}, \mathbf{p}, \mathbf{r}'; \mathbf{p}', t) = f(\mathbf{r}, \mathbf{p}, t)f(\mathbf{r}', \mathbf{p}', t)g(\mathbf{r} - \mathbf{r}'), \qquad (9.33)$$

where $g(\mathbf{r} - \mathbf{r}')$ is the static pair correlation function [see Eq. (7.74)]. Such ansatz, considers in an approximate fashion the short-range correlations among particles, through the function $g(\mathbf{r} - \mathbf{r}')$ that tends to 1 in the limit of large separation between particles, while for small separation it is affected by the dynamic correlations among particles due to interaction. Assuming $g(\mathbf{r} - \mathbf{r}') = 1$ for all distances, it is easy to obtain from equations (9.32) and (9.33), the result of (8.97), i.e. the semiclassical limit of the time-dependent Hartree equations which, in turn, coincide with the Landau–Vlasov equations (1.119) in the absence of collisions. If we write

$$f(\mathbf{r}, \mathbf{p}, t) = f^0(\mathbf{p}) + \delta f(\mathbf{r}, \mathbf{p}, t), \qquad (9.34)$$

where $\delta f(\mathbf{r}, \mathbf{p}, t)$ is the deviation from the equilibrium distribution function $f^0(\mathbf{p})$, induced by the (weak) external field, and if we linearize equations (9.32), we obtain an equation for $\delta f(\mathbf{r}, \mathbf{p}, t)$ which, once solved, allow us to write the response function of the system to the external field

$$v_{\text{ext}}(\mathbf{r}, t) = v_{\text{ext}}(\mathbf{q}, \omega)e^{i(\mathbf{q}\cdot\mathbf{r} - \omega t)} + c.c., \qquad (9.35)$$

in the following way:

$$\chi^{STLS}(\mathbf{q}, \omega) = \frac{\chi^0(\mathbf{q}, \omega)}{1 - \frac{g v_\mathbf{q}}{L^D}(1 - G^{STLS}(\mathbf{q}))\chi^0(\mathbf{q}, \omega)}. \tag{9.36}$$

In equation (9.36), $v_\mathbf{q}$ is the Fourier transform of the inter-particle interaction and g is the coupling constant, $\chi^0(\mathbf{q}, \omega)$ is the classical free response function, and the field factor $G^{STLS}(\mathbf{q})$ is given by

$$G^{STLS}(\mathbf{q}) = -\frac{1}{\rho_0} \int \frac{d\mathbf{q}'}{(2\pi)^D} \frac{\mathbf{q} \cdot \mathbf{q}'}{q'^2}(S(|\mathbf{q} - \mathbf{q}'|) - 1), \tag{9.37}$$

where the static form factor $S(\mathbf{q})$ is given by

$$S(\mathbf{q}) = -\frac{1}{\pi} \int_0^\infty d\omega \, \mathrm{Im} \, \chi(\mathbf{q}, \omega). \tag{9.38}$$

Equations (9.36), (9.37), together with (9.38), constitute a set of equations that are to be solved in a self-consistent way. The derivation of such a set of equations is completely classical. The application to quantum systems is carried out just by replacing the classical response function and field factor by their quantum counterparts. In this case, equation (9.36) reduces to the *RPA* response function provided we neglect field corrections, and equation (9.37) for $G^{STLS}(\mathbf{q})$, in the case of the electron gas, reproduces the Hubbard expression (9.29) and (9.30) provided one uses for $S(\mathbf{q})$ the static form factor of the Fermi gas [see Eqs. (1.100) and (1.101)]. Once the self-consistent solution for all values of the density is obtained, it is possible to derive the pair correlation function through relation (9.11) from the knowledge of the static form factor. The correlation energy in the *STLS* approximation can be derived by integrating on the coupling constant of the interaction energy per particle

$$\frac{E_\mathrm{int}(\alpha)}{N} = \frac{\alpha}{2} \int \frac{d\mathbf{q}}{(2\pi)^D} v_\mathbf{q}[S(\mathbf{q}) - 1 + N\delta_{\mathbf{q}0}]. \tag{9.39}$$

This calculation was carried out for the $3D$ electron gas by Singwi, Tosi, Land and Sjolander (1968), in $2D$ by Jonson (1976), and in quasi-one-dimensional systems by Freser and Bergensen (1980), and Camels and Gold (1995), (1997) (for these systems the term $N\delta_{\mathbf{q}0}$ is canceled by the positive background).

Several authors attempted at improving the *STLS* theory, in order to better reproduce the high-density limit ($r_s \ll 1$), and the compressibility sum rule of equations (7.67)–(7.70) and (8.274). In particular, people abandoned the ansatz (9.33), by taking into account three-body correlations in the kinetic equation (9.32), and truncating the infinite series of such equations at this order (see Ichimaru 1982). In this way, for the local field factor one obtains the expression

$$G(\mathbf{q}) = -\frac{1}{\rho_0} \int \frac{d\mathbf{q}'}{(2\pi)^D} \frac{\mathbf{q} \cdot \mathbf{q}'}{q'^2} S(\mathbf{q}')(S(|\mathbf{q} - \mathbf{q}'|) - 1), \tag{9.40}$$

by which one should then solve the triad of equations for χ, G and S. The result of such calculations appreciably improves the $STLS$ approximation.

Lastly, we mention the "Hypernetted chain" approximation (HNC), which was developed in the physics of classic liquids (van Leeuwen, Groeneveld and De Boer 1959; Morita 1960), and applied to the study of several physical systems such as the electron gas, liquid helium, and nuclear matter (Fantoni and Rosati 1972, 1975; Ripka 1979). Such theory, leads to the following result for $G(\mathbf{q})$:

$$G(\mathbf{q}) = -\frac{1}{\rho_0} \int \frac{d\mathbf{q}'}{(2\pi)^D} \frac{\mathbf{q} \cdot \mathbf{q}'}{q'^2} (S(|\mathbf{q} - \mathbf{q}'|) - 1)\{1 + [1 - G(\mathbf{q}')][S(\mathbf{q}') - 1]\}. \quad (9.41)$$

Note that the $STLS$ scheme is obtained from the above expression by putting $G(\mathbf{q}') = 1$ in the right-hand side, while the convolution formula (9.40) is obtained by assuming $G(\mathbf{q}') = 0$. The HNC approximation turns out to be the best approximation for static field theories, and is discussed in detail and compared to $STLS$ and other theoretical schemes in Chihara (1973), Choquard (1978) and Chihara and Sasaki (1979). For a review of works on HNC applied to the electron gas, see Ichimaru (1982).

9.6   Comparison of Different Theories for the Electron Gas in 2D

In this section we will compare the results of the calculations carried out in the framework of the models discussed previously, for the case of the two-dimensional electron gas, which is taken as an example of many Fermion homogeneous systems, and for which in the literature one finds a great deal of results.

In Tables 9.1 and 9.2 we show (Pederiva, Lipparini and Takayanagi 1997) the correlation energies and compressibilities per particle as a function of the Wigner–Seitz radius r_s computed by: Monte Carlo (QMC, Tanatar and Ceperley 1989), RPA, Hubbard approximation (HA), RPA with the exchange term treated in an exact way ($RPAE$, Takayanagi and Lipparini 1995), $STLS$ approximation (Jonson 1976), and $RPAE$ including ladder correlations ($RPAEG$, Takayanagi and Lipparini 1996).

TABLE 9.1

r_s	ϵ_c^{MC}	ϵ_c^{RPA}	ϵ_c^{HA}	ϵ_c^{RPAE}	ϵ_c^{STLS}	ϵ_c^{RPAEG}
0.5	−3.64	−6.28	−4.26	−3.65	−3.40	−3.92
1	−2.99	−5.40	−3.70	−3.14	−2.87	−3.11
2	−2.26	−4.42	−3.10	−2.56	−2.11	−2.54
4	−1.55	−3.43	−2.46	−1.99	−1.47	−1.50
5	−1.34	−3.10	−2.21	−1.76	−1.25	−1.15
8	−0.98	−2.56	−1.86	−1.56	−0.90	−0.89

TABLE 9.2

r_s	K_0/K^{MC}	K_0/K^{RPA}	K_0/K^{HA}	K_0/K^{RPAE}	K_0/K^{STLS}	K^{RPAEG}
0.5	0.77	0.77	0.77	0.77	0.77	0.77
1	0.54	0.54	0.54	0.54	0.54	0.54
2	0.06	0.05	0.07	0.05	0.06	0.05
4	−0.96	−1.02	−0.94	−0.98	−0.96	−0.99
5	−1.49	−1.58	−1.46	−1.51	−1.49	−1.52
8	−3.12	−3.38	−3.13	−3.11	−3.09	−3.16

From these tables, comparing the different results with Monte Carlo (which should be considered as the best possible calculation), we see that the exact treatment of Coulomb exchange in $RPAE$ greatly improves the results obtained by RPA and HA, and that inclusion of the short-range correlations as performed in $RPAEG$ and in the $STLS$ calculation, are crucial for correctly reproducing the correlation energies. This trend can also be seen in Figs. 9.3 and 9.4, where, in the $r_s = 5$ case, we compare the results of different calculations for the static form factor and the pair correlation function.

9.7 Quasiparticle Properties

In the RPA theory, and in local field theories such as the Hubbard theory and the $STLS$ model, the quasiparticle properties can be calculated in a rigorous way
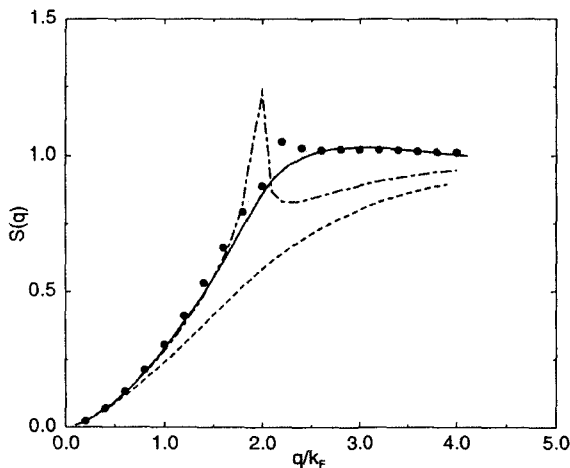
Fig. 9.3 Static form factor of the electron gas in $2D$ at $r_s = 5$. The dashed and dashed-dotted curves give the RPA and $RPAE$ results, respectively. The circles give the $RPAEG$ results (including the ladder correlations), and the full line is the QMC result.
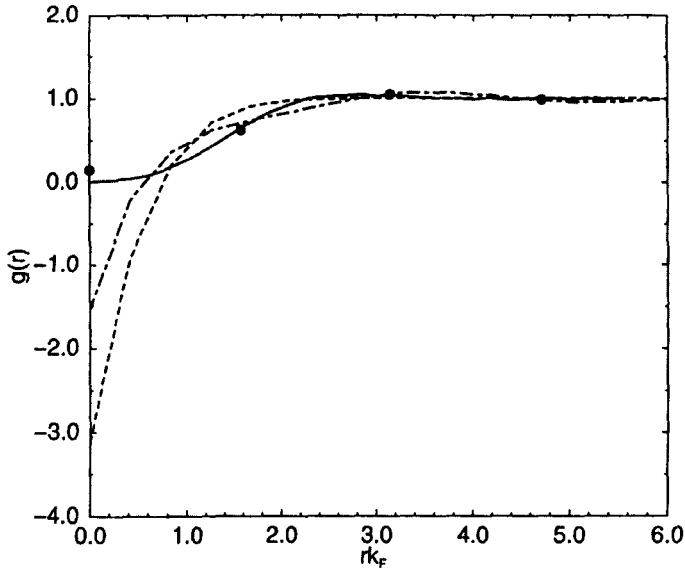
Fig. 9.4   Pair correlation function of the $2D$ electron gas at $r_s = 5$. The dashed and dotted-dashed curves give the RPA and $RPAE$ results, respectively. The circles are the $RPAEG$ results (including the ladder correlations), and the full line is the QMC result.

starting from the following expression

$$E_0 = T_0 - \int \frac{d\mathbf{q}}{(2\pi)^D} \frac{v_{\mathbf{q}}}{2} \int_0^g \frac{d\alpha}{\alpha}$$

$$\times \left(N - N^2 \delta_{\mathbf{q}0} + \frac{1}{2\pi} \int_{-\infty}^{\infty} dw \frac{\alpha \chi^0(\mathbf{q}, iw)}{1 - \frac{\alpha v_{\mathbf{q}}}{L^D}(1 - G(\mathbf{q}))\chi^0(\mathbf{q}, iw)} \right) \quad (9.42)$$

for the ground state energy, and by performing functional differentiation with respect to the occupation number $n_{\mathbf{k}}$ (Ting, Lee and Quinn 1975). Equation (9.42) can be derived from the results of Section 9.2 by means of the relation

$$\int_0^{\infty} d\omega \, \mathrm{Im} \, \chi(\mathbf{q}, \omega) = \frac{1}{2} \int_{-\infty}^{\infty} dw \, \chi(\mathbf{q}, iw) \,, \quad (9.43)$$

with $\omega = iw$, and writing χ in terms of the free response function as in (9.27). In the integral that appears in (9.42), the only terms which depends on the occupation number is the one involving the free response function χ^0 given by

$$\chi^0(\mathbf{q}, iw) = \int \frac{d\mathbf{k}}{(2\pi)^D} G_0^{ph}(\mathbf{k}, \mathbf{q}, iw) \,, \quad (9.44)$$

where $G_0^{ph}(\mathbf{k}, \mathbf{q}, iw)$ is the free p–h Green function:

$$G_0^{ph}(\mathbf{k}, \mathbf{q}, iw) = \frac{(1 - n_{\mathbf{k}+\mathbf{q}})n_{\mathbf{k}}}{iw - \varepsilon_{\mathbf{kq}} + i\eta} - \frac{(1 - n_{\mathbf{k}})n_{\mathbf{k}+\mathbf{q}}}{iw - \varepsilon_{\mathbf{kq}} - i\eta} \,, \quad (9.45)$$

with

$$\varepsilon_{\mathbf{kq}} = \frac{(\mathbf{k} + \mathbf{q})^2}{2m} - \frac{\mathbf{k}^2}{2m}.$$

Note that the local field factor $G(q)$ can also be a functional of $\alpha\chi^0$. The kinetic energy is given by $T_0 = \sum_{\mathbf{k}} n_{\mathbf{k}} \varepsilon_{\mathbf{k}}$ with $\frac{\delta T_0}{\delta n_{\mathbf{k}}} = \varepsilon_{\mathbf{k}}$, and the self-energy is given by

$$\Sigma(\mathbf{k}, ik) = \frac{\delta E_0}{\delta n_{\mathbf{k}}} - \varepsilon_{\mathbf{k}}. \tag{9.46}$$

The integrand (denote by $\mathcal{F}$) in the interaction term of equation (9.42) is a function of $\alpha\chi^0$, and the functional derivative of $\mathcal{F}$ with respect to the occupation number is written as

$$\frac{\delta \mathcal{F}}{\delta n_{\mathbf{k}}} = \frac{\delta \mathcal{F}}{\delta \chi^0} \frac{\delta \chi^0}{\delta n_{\mathbf{k}}}, \tag{9.47}$$

where

$$\frac{\delta \chi^0}{\delta n_{\mathbf{k}}} = \mathcal{G}_0(\mathbf{k} + \mathbf{q}, iw + ik) + \mathcal{G}_0(\mathbf{k} + \mathbf{q}, -iw + ik), \tag{9.48}$$

and $\mathcal{G}_0$ is the free single-particle Green function:

$$\mathcal{G}_0(\mathbf{k}, iw) = \frac{n_{\mathbf{k}}}{iw - \varepsilon_{\mathbf{k}} - i\eta} + \frac{(1 - n_{\mathbf{k}})}{iw - \varepsilon_{\mathbf{k}} + i\eta}. \tag{9.49}$$

Note that the two terms of (9.48) give the same contribution, since $\mathcal{F}$ is a symmetric function of the complex frequency iw. Moreover, the integral on the coupling constant and the functional derivative of $\mathcal{F}$ with respect to χ^0, may be arranged in the following way by introducing the variable $y = \alpha\chi^0$:

$$\int_0^g \frac{d\alpha}{\alpha} \frac{\delta \mathcal{F}(\alpha\chi^0)}{\delta \chi^0} = \frac{1}{\chi^0} \int_0^{g\chi^0} dy \frac{\delta \mathcal{F}(y)}{\delta y} = \frac{\mathcal{F}(g\chi^0)}{\chi^0}. \tag{9.50}$$

Using all these results, it is easy to obtain the following expression for the interaction self-energy:

$$\Sigma(\mathbf{k}, ik) = -g \int \frac{d\mathbf{q}}{(2\pi)^D} v_{\mathbf{q}} \frac{1}{2\pi} \int_{-\infty}^{\infty} dw \frac{\mathcal{G}_0(\mathbf{k} + \mathbf{q}, iw + ik)}{1 - \frac{gv_{\mathbf{q}}}{L^D}(1 - G(\mathbf{q}))\chi^0(\mathbf{q}, iw)}. \tag{9.51}$$

This expression may be rewritten in a more general form by introducing the screened vertex function Γ as

$$\Sigma(\mathbf{k}, ik) = -g \int \frac{d\mathbf{q}}{(2\pi)^D} v_{\mathbf{q}} \frac{1}{2\pi} \int_{-\infty}^{\infty} dw \mathcal{G}_0(\mathbf{k} + \mathbf{q}, iw + ik) \frac{\Gamma(\mathbf{q}, iw)}{\epsilon(\mathbf{q}, iw)}, \tag{9.52}$$

where

$$\Gamma(\mathbf{q}, iw) = \epsilon(\mathbf{q}, iw) f(\mathbf{q}, iw). \tag{9.53}$$

Here $\epsilon(\mathbf{q}, iw)$ is the dielectric constant as defined in equations (8.275) and (8.276), and $f(\mathbf{q}, iw)$ is the vertex function defined in Section 8.11. In general, $f(\mathbf{q}, iw)$ also depends on the variable k, and neglecting such dependence is an approximation that leads to the result

$$f(\mathbf{q}, iw) = \frac{\chi(\mathbf{q}, iw)}{\chi^0(\mathbf{q}, iw)}, \qquad (9.54)$$

and hence, for static field theories, to expression (9.51).

Starting from expression (9.51), the quasiparticle properties of the electrons in the homogeneous gas were computed, in the different static field approximations. The results of these computations are discussed in detail, e.g. in Rice (1965) and in the book of Mahan (1981). It is important to notice that the self-energy as computed in the *RPA* theory [i.e. putting $G(q) = 0$ in the above expressions] has the following important characteristic: the reciprocal effective mass does not diverge any more at the Fermi surface. Or, in other words, the divergence affecting the reciprocal mass at the Fermi surface in the *HF* theory [see Eq. (2.37)], is removed by the *RPA* theory which takes into account the dynamic electron–electron correlations.

As a general remark, in the case of electrons the quasiparticle properties are little affected by the effects due to the electron–electron interactions. Other effects, such as those due to the band structure in real metals, and to electron–phonon interactions, are more important.

The quasiparticle properties and the nonlocal effects (see next section) are of more relevance for other Fermion systems, and are discussed in detail in the review paper by Mahaux et al. (1985).

9.8   Nonlocal Effects

The local theories for the linear response function discussed above assume that the field factor $G(q, \omega)$ does not depend on frequency, but only on the transferred momentum q. Clearly, this is an approximation. In the parlance of the Landau theory for Fermi liquids, this is equivalent to assuming that the Landau parameters F_ℓ are equal to zero when $\ell \geq 1$. Only in this approximation, and in the limit of small q and ω, does the local field theories and the Landau theory coincide.

Are nonlocal effects important? The answer to this question is, in general, positive for strongly interacting liquids like, e.g. ^{3}He, where the Landau parameters F_1 and F_2 play a fundamental role in determining the frequency difference between first sound and "zero sound" (see Section 8.1). As we will see in the following, these effects are relevant also for the electron gas, when the density is low and correlations are more important.

In the parlance of density functional theory, this means that one is not allowed to neglect non-local (current) terms in the energy functional if one wants to reproduce correctly the dynamic response of the system. Current terms in the energy

functional, which have no effects on the static properties of the system, may nevertheless be crucial for the dynamic properties.

In what follows we will discuss two approaches which take account of non-local effects in the effective interaction, through the introduction of a velocity-dependent term. The effects of such term will be studied in connection with the problem of correctly reproducing the dispersion of phonon-roton collective states in superfluid ^{4}He, and of the plasmon ones in the electron gas.

The importance of nonlocal effects for obtaining such dispersions, can be easily understood by studying the moments

$$m_k(q) = \int_0^\infty d\omega \; \omega^k S(q,\omega) \tag{9.55}$$

of the dynamic structure function $S(q,\omega)$. In the case of Bosons, such function, at small ω, is determined primarily by collective modes; in Fermi systems by collective modes and one-particle–one-hole excitations; and in the region of high ω by the many-particle–many-hole excitations $(mp - mh)$. The situation is schematized in Fig. 9.5. The mean field theories discussed so far account only for single-particle and collective excitations, but not for excitations due to many-particle, and hence they provide an incomplete description of $S(q,\omega)$. This can be seen explicitly by comparing, e.g. in the case of liquid ^{3}He, the f-sum rule

$$m_1(q) = \int_0^\infty d\omega\omega S(q,\omega) = \frac{Nq^2}{2m} \,, \tag{9.56}$$

which holds for interaction potentials that do not depend on velocity (both for density and spin-density excitations), with the analogous sum rule for the spin-
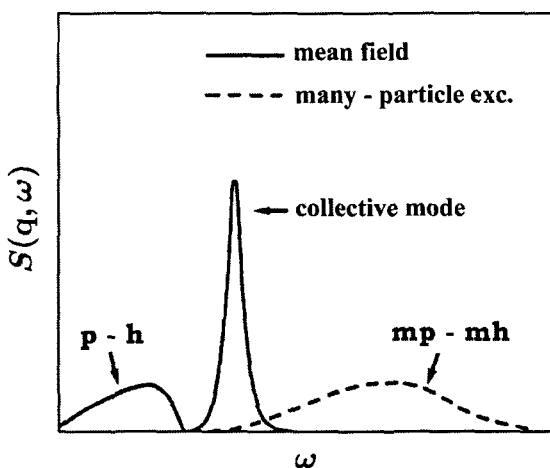
Fig. 9.5 Schematic representation of $S(q,\omega)$. For Bosons, the part corresponding to 1-particle–1-hole $(p–h)$ excitations, should be ignored.

density operator in the Landau theory [see Eq. (8.25)]:

$$m_1^a(q) = \frac{Nq^2}{2m} \frac{1 + F_1^a/3}{1 + F_1^s/3}.$$

The result of the Landau theory ($F_1^a = -0.55$, $F_1^s = 6$ for ^{3}He) is much smaller than the exact result of (9.56), and this means that the elementary excitations considered by the Landau theory do not saturate the f-sum rule even at small q. The many-particle excitations also contribute to m_1^a at small q, thanks to the factor in ω in the f-sum rule, which amplifies the contribution of such high-energy excitations. A different situation is realized in the case of the inversely energy-weighted sum rule:

$$m_{-1}(q) = \int_0^\infty d\omega \frac{S(q,\omega)}{\omega} = \frac{-\chi(q)}{2}, \tag{9.57}$$

where $\chi(q)$ is the static response of the system. Due to the factor ω^{-1} in the integral (9.57), which quenches the contribution of many-particle excitations, such sum rule is saturated at low q by the collective mode. In the case of superfluid ^{4}He, this is the case even at rather large q values, as evident from Fig. 8.8 where the experimental results for $\chi(q)$ are well reproduced by the density functional theory of Dalfovo et al. (1995), where $\chi(q)$ is given by the second functional derivative of energy in momentum space (V is the volume):

$$-\frac{N}{\chi(q)} = \frac{q^2}{4m} + \frac{\rho}{V} \int d\mathbf{r}d\mathbf{r}' \frac{\delta^2 E}{\delta\rho(\mathbf{r})\delta\rho(\mathbf{r}')} e^{i\mathbf{q}\cdot(\mathbf{r}-\mathbf{r}')}. \tag{9.58}$$

For Fermions, such as the electron gas, the static response can be computed starting from the expression

$$-\frac{V}{\chi(q)} = f_{xc}(q) - \frac{V}{\chi_{RPA}(q)} = f_{xc}(q) - \frac{V}{\chi_0(q)} + v(q), \tag{9.59}$$

where the exchange-correlation factor $f_{xc}(q)$ is connected to the local field factor $G(q)$ by

$$f_{xc}(q) = -v(q)G(q), \tag{9.60}$$

and is given by the Fourier transform of the second functional derivative of the exchange-correlation energy with respect to density:

$$f_{xc}(q) = \frac{1}{V} \int d\mathbf{r}d\mathbf{r}' \frac{\delta^2 E_{xc}}{\delta\rho(\mathbf{r})\delta\rho(\mathbf{r}')} e^{i\mathbf{q}\cdot(\mathbf{r}-\mathbf{r}')}. \tag{9.61}$$

The m_1 and m_{-1} sum rules can be used to study the dispersion of the collective modes in both Boson and Fermion systems, through their ratio:

$$\omega^2(q) = \frac{m_1(q)}{m_{-1}(q)}. \tag{9.62}$$

In the following we will study such ratio in the case of the phonon-roton density modes of superfluid ^{4}He, and of the plasmon mode of the electron gas and, in this framework, we will discuss the relevance of nonlocal effects in the energy functional.

In the case of superfluid ^{4}He, employing the exact results for m_1 and m_{-1}, (9.56) and (9.57), we obtain

$$\omega^2(q) = \frac{Nq^2}{m|\chi(q)|}, \tag{9.63}$$

which may be considered as a rigorous upper bound for the collective-mode dispersion. Note that, since the following inequality holds

$$\sqrt{\frac{m_1(q)}{m_{-1}(q)}} \le \frac{m_1(q)}{m_0(q)} = \frac{q^2}{2mS(q)}, \tag{9.64}$$

where $S(q)$ is the static structure factor, expression (9.63) is a better approximation to the exact dispersion than the more renowned Feynman approximation

$$\omega^F(q) = \frac{q^2}{2mS(q)}. \tag{9.65}$$

Using for $\chi(q)$, the result of the density functional theory of (9.58), which reproduces the experimental value up to high enough q-values, we obtain for the dispersion of the phonon-roton mode the dashed curve in Fig. 9.6. While the phonon
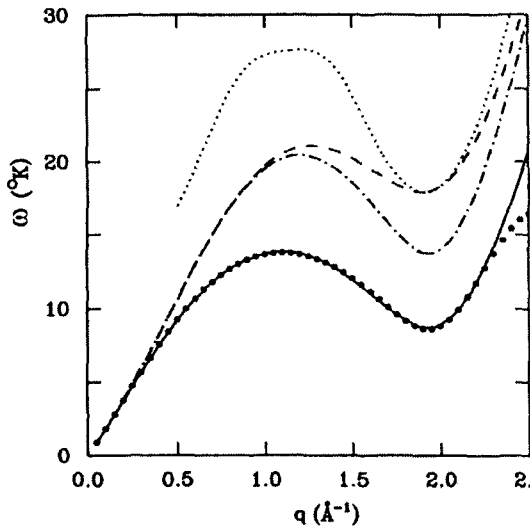
Fig. 9.6   Phonon-roton dispersion in superfluid ^{4}He. The dots are the experimental data of Donnelly et al. (1981); the dotted line is the Feynman approximation with the experimental value for the static form factor $S(q)$ (Svensson et al. 1980); the dashed line is the result of Eq. (9.63) using, for χ, the result of the static density functional; the dotted-dashed line is the result of the dynamic theory without the backflow term, while the full line includes the backflow term.

dispersion $\omega = cq$, with $c^2 = -(m\chi(0))^{-1}$, is well reproduced at low q, the roton one at higher q values is largely over-estimated. From the previous discussion, it is clear that the estimate (9.63) can be improved by including velocity-dependent terms in the energy functional, which change the energy-weighted sum rule m_1^{col} with respect to the exact result (9.56). The difference with respect to the exact result $m_1 - m_1^{\text{col}}$, is due to the contribution of many-particle excitations, which is correctly subtracted in the computation of the energy-weighted sum rule, due to the collective excitations alone. Since the many-particle excitations do not affect the inversely energy-weighted sum rule, the ratio $m_1^{\text{col}}/m_{-1}^{\text{col}}$ will turn out to be a better approximation for the exact dispersion of the collective mode of superfluid ^{4}He. Dalfovo et al. (1995) added the velocity-dependent term to the energy functional

$$E_v = -\frac{m}{4} \int d\mathbf{r} d\mathbf{r}' V_J(|\mathbf{r} - \mathbf{r}'|)\rho(\mathbf{r})\rho(\mathbf{r}')(\mathbf{v}(\mathbf{r}) - \mathbf{v}(\mathbf{r}'))^2 , \qquad (9.66)$$

where V_J is a finite-range current-current effective interaction, which plays the role of a non-local kinetic energy, and gives rise to hydrodynamic equations (see Chapter 10) with a backflow current term. From a microscopic point of view, an effective interaction with these characteristics (i.e. finite-range and velocity-dependent), emerges naturally in the Brueckner–Hartree–Fock theory described in Chapter 3 and applies to the electron gas.

The interaction (9.66) lowers the value of the energy-weighted sum rule with respect to the exact value and yields, for the homogeneous system, the result

$$m_1^{\text{col}}(q) = \frac{Nq^2}{2m}(1 - \rho(\hat{V}_J(0) - \hat{V}_J(q))) , \qquad (9.67)$$

where $\hat{V}_J(q)$ is the Fourier transform of the current-current interaction $V_J(r)$. However, it does not change the value of the static response, which is fixed by the part of the energy functional which depends on density and not on velocity. The dispersion of the phonon-roton collective mode is thus given by

$$\omega^2(q) = \frac{Nq^2}{m|\chi(q)|}(1 - \rho(\hat{V}_J(0) - \hat{V}_J(q))) . \qquad (9.68)$$

It is possible to fix $V_J(r)$ in order to reproduce both the phonon-roton dispersion and the energy-weighted sum rule as derived from neutron scattering experiments in the energy range where only the collective contribution to the sum rule is important. The results are shown in Figs. 9.6 and 9.7. The fact that the new functional does not satisfy the exact f-sum rule, clearly evidences the fact that the density functional theory does not take account of many-particle excitations, but only one-particle ones, and that in order to reproduce the dispersion of such excitations it is crucial to introduce current-current interaction terms in the functional. Note that the new current-current term in the dispersion (9.68) does not alter the hydrodynamic limit $q \to 0$, given by $\omega = cq$ with $c = (m|\chi(0)|)^{-1}$ the sound velocity. This is an important fact, ensured by Galilean invariance.
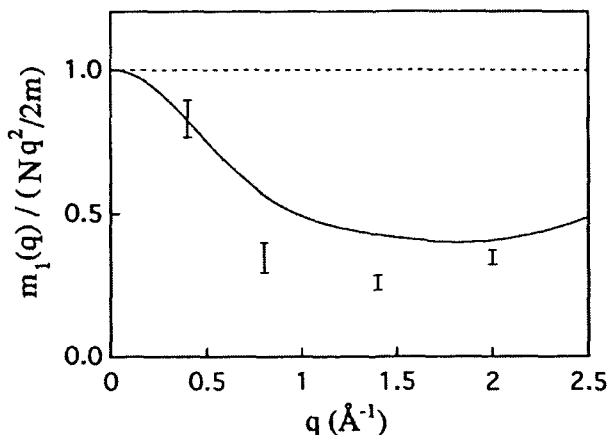
Fig. 9.7 Energy-weighted sum rule. The dashed line is the exact sum rule; the bars give the mean-field contribution to the sum rule, as measured by neutron scattering (Woods and Cowley 1973); the full line is the result of Eq. (9.67).

The current-current term is also very important for reproducing correctly the dynamics of non-homogeneous systems, such as free surfaces, thin films and helium drops. Calculations for such systems are found in Dalfovo et al. (1995).

In the case of the electron gas, the situation is similar to the above-described one, but with the further complication of one-particle–one-hole excitations which, together with the collective ones, are present in the low-energy spectrum of Fermions. The situation for the plasmon dispersion is the one already discussed in Sections 8.4 and 8.9.1, and reported in Fig. 8.3. The experimental results are obtained by inelastic electron scattering experiments on alkali metals ranging from sodium to caesium. These metals represent, in nature, the physical system closest to the interacting electron gas in $3D$, with a value of r_s varying from 4 to about 6. The local field theories predict for the α coefficient of the dispersion relation

$$E(q) = E(0) + \alpha q^2 \,,$$

values which are in serious disagreement with the experimental ones for $r_s > 4$. In the following, using the sum rules discussed above, we will show that current-interaction effects (Lipparini, Stringari and Takayanagi 1994) can improve the agreement between theory and experiment, even though other effects such as those due to the band structure of alkali metals (Aryasetiawan and Karlsson 1994; Taut and Sturm 1992), appear to be also relevant for establishing a quantitative comparison with observation.

The dependence on the transferred momentum q of the density excitation strength $|\rho_{n0}|^2 = |\langle n|\rho_q|0\rangle|^2$, of the excitation frequencies and of the sum rules, due to the possible excitations of the electron gas, can be deduced on the basis of simple arguments based on conservation laws and sum rules (Pines and Nozières

1966), and is reported in Table 9.3, in the limit of small q, with the main contributions. In this table v_F and ϵ_F are the Fermi velocity and energy, respectively, and $\omega_p = \sqrt{4\pi\rho e^2/m}$ is the plasma frequency.

TABLE 9.3

	single-particle	plasmon	many-particle
$\displaystyle\sum_n \|\langle n\|\rho_{\mathbf{q}}\|0\rangle\|^2$	q^5	$\dfrac{Nq^2}{2m\omega_p}$	q^4
ω_{n0}	qv_F	ω_p	ω_{mp}
m_{-1}	$\dfrac{4}{15}\dfrac{N\epsilon_F}{m^2\omega_p^4}q^4$	$\dfrac{Nq^2}{2m\omega_p^2}$	q^4
m_1	q^6	$\dfrac{Nq^2}{2m}$	q^4
m_3	q^8	$\dfrac{N\omega_p^2q^2}{2m}$	q^4

If, as we did in the case of superfluid helium, we neglect the contribution of many-particle (mp) excitations to the inversely energy-weighted sum rule, up to terms in q^4 we can write:

$$m_{-1} = m_{-1}^{pl} + m_{-1}^{sp} \qquad m_1 = m_1^{pl} + m_1^{mp}. \tag{9.69}$$

If then we want to calculate the plasmon dispersion through the ratio m_1^{pl}/m_{-1}^{pl}, we clearly need to subtract from the exact results for m_{-1} and m_1 the single-particle and many-particle contributions, respectively. The exact result for m_1 is given by the f-sum rule (9.56), and that for the inversely energy-weighted sum rule can be easily derived starting from equation (9.59), by performing the limit for small q and recalling the result (8.274). In this way we obtain the result, valid up to terms in q^4:

$$m_{-1} = \frac{Nq^2}{2m\omega_p}\left(1 - \frac{v^2q^2}{\omega_p^2}\right), \tag{9.70}$$

where v^2 is the sound velocity. The single-particle contribution to m_{-1} can be evaluated rigorously (Lipparini, Stringari and Takayanagi 1994) and is given by

$$m_{-1}^{sp} = \frac{4}{15}\frac{N\epsilon_F}{m^2\omega_p^4}q^4. \tag{9.71}$$

As regards the many-particle contribution to m_1, considering the exact result (9.56) as well as equation (9.69) and Table 9.3, one concludes that the corrections in q^4 due to the plasmon and many-particle excitations must cancel each other exactly. The plasmon q^4 contribution can be obtained only in non-local theories with finite-range and velocity-dependent effective interactions. One such theory is

the Brueckner–HF theory discussed in Chapter 3, in the separable approximation of equation (3.42), in which the effective interaction is given by $g^c = c(p)v(q)$. For the plasmon contribution to m_1 up to order q^4, it gives the result

$$m_1^{pl}(q) = \frac{Nq^2}{2m} - K\frac{Nq^4}{2m},$$ (9.72)

with

$$K = \frac{9}{8r_s^3}\left(v''(0)\int\left(\frac{j_1(k_Fr/2)}{k_Fr/2}\right)^2 c(r)r^4dr\right.$$

$$\left. - \frac{1}{2}c''(0)\int\left(\frac{j_1(k_Fr)}{k_Fr}\right)^2 v(r)r^4dr\right),$$ (9.73)

where $j_1(x) = 1/x(\sin x/x - \cos x)$ and $v''(0) = \frac{d^2}{dq^2}v(q)|_{q=0}$, $c''(0) = \frac{d^2}{dp^2}c(p)|_{p=0}$ and $v(r)$, $c(r)$ are the Fourier transforms of $v(q)$ and $c(p)$, respectively. The values of K, together with those of the Fermi energy and plasmon frequency, are reported in atomic units in Table 9.4 for some values of r_s.

TABLE 9.4

r_s	ϵ_F	ω_p	K	ω_{mp}
2	0.460	0.613	0.05	1.52
3	0.205	0.333	0.3	0.68
4	0.115	0.217	0.5	0.48
5	0.074	0.155	1.0	0.30
6	0.051	0.118	2.0	0.20

The plasmon dispersion can then be calculated by means of the equation:

$$E^{pl}(q) = \sqrt{\frac{m_1^{pl}}{m_{-1}^{pl}}} = \omega_p\left(1 + \frac{q^2}{2m\omega_p^2}\left(mv^2 + \frac{8}{15}\epsilon_F - Km\omega_p^2\right)\right),$$ (9.74)

obtained using the results of (9.70)–(9.72). Note that putting $K = 0$ in this equation, and expressing the sound velocity through the second derivative of the LDA exchange-correlation energy with respect to the density, one obtains the $TDLDA$ dispersion of (8.208).

From equation (9.74) we then obtain the following result for the coefficient α normalized to its RPA value $\alpha_{RPA} = \frac{3\epsilon_F}{5\omega_p}$:

$$\frac{\alpha}{\alpha_{RPA}} = \frac{5}{6\epsilon_F}\left(mv^2 + \frac{8}{15}\epsilon_F - Km\omega_p^2\right).$$ (9.75)

The predictions of such equation are plotted in Fig. 9.8. The general trend indicated by the experiments is rather well reproduced. The term in K, which is due to
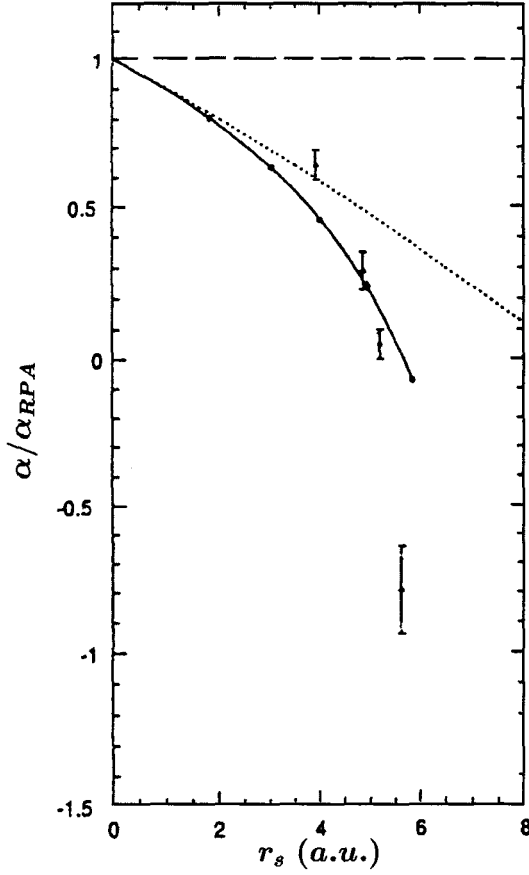
Fig. 9.8   Coefficient of the bulk plasmon dispersion, normalized to its RPA value, as a function of density. The full line is the result from equation (9.75). The dotted line gives the dispersion of local field theories. The experimental data are taken from Von Felde et al. (1989).

nonlocal effects in the effective interaction, and which accounts for the plasmon q^4 contribution to the m_1 sum rule, plays a crucial role. In fact, in the absence of such ($K = 0$) we obtain the dotted curve, which is the prediction of local field theories.

9.9   Mean Energy of Many-Particle Excitations

Using the method of sum rules, in some cases it is possible to evaluate explicitly the value of the mean energy of the many-particle excitations through the ratio

$$\omega^{mp} = \sqrt{\frac{m_3^{mp}}{m_1^{mp}}} \, , \tag{9.76}$$

where m_3^{mp} is the contribution of many-particle excitations to the sum rule weighted by the cube of energy: $m_3 = \int S(q, \omega) \omega^3 d\omega$.

In the case of the electron gas in $3D$, m_3^{mp} can be computed using the result (see Table 9.3):

$$m_3^{mp} = m_3 - m_1^{pl} (E^{pl}(q))^2 \,, \tag{9.77}$$

which holds to order q^4, where m_3 is given by (Puff 1965; Iwamoto, Krotscheck and Pines 1984):

$$m_3 = \frac{Nq^2}{2m} \left(\omega_p^2 + \frac{2q^2}{m} \left(E_{\text{kin}} + \frac{2}{15} E_{\text{pot}} \right) \right) \,, \tag{9.78}$$

and the second term in the right hand side of Eq. (9.77) is the plasmon contribution. In equation (9.78), E_{kin} and E_{pot} are the kinetic and potential energies per particle of the electron gas, whose values were computed by Monte Carlo. Using the results of the previous Section, we can then write the mean energy of the many-particle excitations:

$$\omega^{mp} = \sqrt{\frac{m_3^{mp}}{m_1^{mp}}}$$

$$= \sqrt{\frac{2}{mK} \left(\left(E_{\text{kin}} + \frac{2}{15} E_{\text{pot}} \right) - \left(\frac{1}{2} mv^2 + \frac{4}{15} \epsilon_F - Km\omega_p^2 \right) \right)}. \tag{9.79}$$

The values predicted by this expression are reported in Table 9.4. As expected, ω^{mp} is systematically larger than E^{pl} and ϵ_F.

As a second example we consider the contribution of many-particle excitations to the spin-density response function of liquid ^{3}He. The sum rule cubic in energy for the spin-density operator $\rho_q^\sigma = \sum_j e^{i\mathbf{q}\cdot\mathbf{r}_j} \sigma_j^z$ is given by

$$m_3^\sigma = N \left(\frac{q^6}{8m^3} + \frac{q^4}{m^2} E_{\text{kin}} + \frac{\rho q^2}{2m^2} \int [g(r) - g^\sigma(r) \cos qz] \nabla_z^2 V(r) d\mathbf{r} \right) , \tag{9.80}$$

where

$$g(r) = \rho^{-2} \sum_{\sigma_1, \sigma_2} \rho^{(2)}(1, 2; 1, 2) \,,$$

$$g^\sigma(r) = \rho^{-2} \sum_{\sigma_1, \sigma_2} \sigma_1 \sigma_2 \rho^{(2)}(1, 2; 1, 2) \,,$$

and $r = r_1 - r_2$, and $\rho^{(2)}(1, 2; 1, 2)$ is the diagonal two-body density matrix. $V(r)$ is the helium-helium interaction potential.

In the limit of small q, the m_3^σ sum rule becomes

$$\lim_{q \to 0} m_3^\sigma = N \frac{\rho q^2}{m^2} \int g_{+-}(r) \nabla_z^2 V(r) d\mathbf{r} \,, \tag{9.81}$$

with $g_{+-} = 1/2(g(r) - g^\sigma(r))$, and in this limit is a pure effect of correlations in the ground state (Dalfovo and Stringari 1989). In fact, the mean field theories based on RPA, time-dependent density functional theory, or the Landau theory, only account for Pauli correlations in the ground state (a Slater determinant), and hence (see Section 1.8) they predict a constant value for g_{+-} ($= 2$). Therefore, the q^2 term in m_3^σ vanishes, consistent with the result (8.26) of the Landau theory. This result evidences that in liquid ^{3}He, in the limit of small q, the m_3^σ sum rule is fully determined by many-particle effects.

The contribution of many-particle excitations to the f-sum rule can, then, be easily calculated in the same limit, through the difference

$$m_1^\sigma(mp) = m_1^\sigma - m_1^\sigma(mf) \to_{q\to 0} N\frac{\rho q^2}{m^2}\frac{1}{3}\frac{F_1^s - F_1^a}{1 + 1/3F_1^s}, \qquad (9.82)$$

where for the mean field contribution to m_1^σ ($m_1^\sigma(mf)$) in the limit of small q, we took the result of the Landau theory of (8.25). Combining the results of equations (9.81) and (9.82) into (9.76), we can finally give an estimate of the mean energy of many-particle excitations in the spin-density channel, which turns out to be $\omega^{mp} \simeq 50$ K at saturated vapor pressure.

9.10   The Polarization Potential Model

A separation between mean-field and many-particle excitations in the framework of the linear response theory, of the same type as the one discussed above, has been developed by Pines (1985) for quantum liquids, and is known in the literature as the polarization potential model. In this theory, the linear responses in the density and spin-density channels are written as

$$\chi^s(q,\omega) = \frac{\chi^{sc}(q,\omega)}{1 - (v_c(q) + f_0^s(q) + \frac{\omega^2}{q^2}f_1^s(q))\chi^{sc}(q,\omega)}, \qquad (9.83)$$

$$\chi^a(q,\omega) = \frac{\chi^{sc}(q,\omega)}{1 - (f_0^a(q) + \frac{\omega^2}{q^2}f_1^a(q))\chi^{sc}(q,\omega)}, \qquad (9.84)$$

where $v_c(q)$ is non-vanishing only for charged systems (in which case it is equal to the Fourier transform of the Coulomb field), and $\chi^{sc}(q,\omega)$ is the screened response function which describes the response of density fluctuations to the combined action of the external and induced polarization fields. $\chi^{sc}(q,\omega)$ includes contributions from both single- and many-particle excitations. If we neglect many-particle contributions then $\chi^{sc}(q,\omega) = \chi^0(q,\omega)$ (i.e. the free response) and the local mean field theories become a particular case of the Pines theory in which $f_1 = 0$.

The frequency-dependent term, which is proportional to f_1^s in (9.83), is connected to an effective mass depending on q, which characterizes the single-particle or pair excitations with momentum q, with which $\chi^{sc}(q,\omega)$ is built up. In fact, from

equation (9.83) in the large ω limit (see Section 7.3), and from the results

$$\chi^s(q,\omega) = \frac{\rho q^2}{m\omega^2}, \qquad \chi^{sc}(q,\omega) = \frac{\rho q^2}{m_q^*\omega^2},$$

which hold in this limit, we obtain

$$m_q^* = m + \rho f_1^s(q). \tag{9.85}$$

On the other hand, in the spin channel, performing the high ω limit in (9.84), we obtain for the energy-weighted sum rule:

$$m_1^a = \frac{\rho q^2}{2m^*} \frac{1}{1 - \rho f_1^a(q)/m^*}. \tag{9.86}$$

The polarization potential model reduces to the Landau theory in the limit $q \to 0$, $\omega \to 0$, provided the following identifications are made

$$f_0^s(0) = \frac{F_0^s \pi}{m^*}, \qquad f_0^a(0) = \frac{F_0^a \pi}{m^*}, \tag{9.87}$$

$$f_1^s(0) = \frac{F_1^s}{1 + F_1^s/2} \frac{m^* \pi}{k_F^2}, \qquad f_1^a(0) = \frac{F_1^a}{1 + F_1^a/2} \frac{m^* \pi}{k_F^2}, \tag{9.88}$$

in the $2D$ case, and

$$f_0^s(0) = \frac{F_0^s \pi^2}{m^* k_F}, \qquad f_0^a(0) = \frac{F_0^a \pi^2}{m^* k_F}, \tag{9.89}$$

$$f_1^s(0) = \frac{F_1^s}{1 + F_1^s/3} \frac{m^* \pi^2}{k_F^3}, \qquad f_1^a(0) = \frac{F_1^a}{1 + F_1^a/3} \frac{m^* \pi^2}{k_F^3}, \tag{9.90}$$

in the $3D$ case, and provided that in the same limit we identify $\chi^{sc}(q,\omega)$ with $\Omega_{0,0}$ and $\Lambda_{0,0}$, respectively. Here $\Omega_{0,0}$ and $\Lambda_{0,0}$ are the long-wavelength limits of the free response function in $3D$ and $2D$, to excite single-quasiparticle-quasihole states of effective mass m^* around the Fermi surface (see Section 8.1). In equations (9.87)–(9.90), the F are the usual dimensionless Landau parameters. In particular, it can be remarked that from equations (9.85)–(9.86) one obtains the usual results of the Landau theory, $m^*/m = 1 + F_1^s/2$ for the effective mass, and

$$m_1^a = \frac{\rho q^2}{2m^*}(1 + F_1^a/2), \tag{9.91}$$

for the energy-weighted sum rule in the spin channel. Comparison of equations (9.86) and (9.91) with the exact result $m_1^a = \rho q^2/2m$ shows once again that in the spin channel many-particle excitations contribute to m_1^a at order q^2.

One can notice that the adiabatic $TDLSDA$ theory that we developed in Section 8.9 can be generalized to include non-local components of the type

$$\frac{1}{2}t_1 \int (\rho\tau - j^2)d\mathbf{r} \tag{9.92}$$

in the energy functional, which yield a response that is analogous to that, of the polarization potential theory in the long-wavelength limit. In equation (9.92),

$$\tau = \left\langle \sum_i \mathbf{p}_i^2 \delta(\mathbf{r} - \mathbf{r}_i) \right\rangle$$

is the kinetic energy density, and j is the current density defined by

$$\mathbf{j}(\mathbf{r}) = 1/2 \left\langle \left(\sum_i \delta(\mathbf{r} - \mathbf{r}_i)\mathbf{p}_i + h.c. \right) \right\rangle . \qquad (9.93)$$

The form (9.92) ensures translational invariance. The coefficient t_1 is connected to $f_1^s(0)$, and hence to the Landau parameter F_s^1. For example, in $2D$ we have

$$t_1 = -\frac{1}{\rho} \frac{F_1^s/2}{1 + F_1^s/2} ,$$

as follows from the fact that the term of equation (9.92) produces an effective mass given by $m^*/m = (1 + t_1\rho)^{-1}$. The term of Eq. (9.92) gives rise (Stringari and Dalfovo 1990) to a density-current response

$$\chi_{sj} = \sum_n \left(\frac{(\rho_q)_{0n}(j_q^\dagger)_{n0}}{\omega - \omega_{n0}} - \frac{(\rho_q^\dagger)_{0n}(j_q)_{n0}}{\omega + \omega_{n0}} \right)$$

which is coupled to the density-density response χ_s by

$$\chi_s = [(v_c(q) + \mathcal{K})\chi_s + 1]\chi_s^0 - t_1\chi_{sj}\chi_{js}^0 , \qquad (9.94)$$

where $\mathcal{K}$ is the second derivative of the exchange-correlation energy with respect to the density [see Eq. (8.196)], and χ_s^0 and χ_{js}^0 are the single-particle (with effective mass) density-density and density-current responses, respectively. Using the relations (Pines and Nozières 1966):

$$\chi_{sj}^0 = \frac{m^*}{q}\omega\chi_s^0 , \qquad (9.95)$$

$$\chi_{sj} = \frac{1}{q}\omega\chi_s , \qquad (9.96)$$

that link the density-density and density-current responses, we can establish an equation of the kind (9.83) with f_0^s and f_1^s independent of q and related to $\mathcal{K}$ and t_1. An analogous calculation can be carried out in the case of the spin-density–spin-density and spin-current–spin-density responses, which leads to an equation of the kind (9.84). In this case, all the quantities that appear in the above expressions have a spin-dependence. For example, the spin current density $\mathbf{j}^\sigma$ becomes

$$\mathbf{j}^\sigma(\mathbf{r}) = 1/2 \left\langle \left(\sum_i \delta(\mathbf{r} - \mathbf{r}_i)\mathbf{p}_i\sigma_i + h.c. \right) \right\rangle \qquad (9.97)$$

and the coefficient t_1^σ of the equation analogous to (9.92) is related to the Landau parameter F_1^a. For example, in $2D$, we have

$$t_1^\sigma = -\frac{1}{\rho}\frac{F_1^a/2}{1+F_1^a/2}\,.$$

The polarization potential model has been applied, particularly, to the study of elementary excitations of ^{3}He and ^{4}He. An extensive review of the applications of such model, together with a list of the most important references, can be found in Pines (1985).

9.11 The Gross–Kohn Model

In Section 8.9 we developed the time-dependent density functional theory in the so-called adiabatic approximation, in which one assumes for the exchange and correlation functional the same static form hypothesized to calculate the properties of the ground state of the system. In general, one expects this to be a good approximation only for processes that depend very slowly on time, i.e. one implicitly assumes the adiabatic approximation. This is reflected also in the fact that the exchange-correlation kernel of equations (8.195) and (8.196) is frequency-independent. For homogeneous systems, and in the density channel, this kernel is given by

$$\lim_{q\to 0} f_{xc}^{\mathrm{hom}}(q,\omega=0) = \frac{d^2}{d\rho^2}(\rho\epsilon_{xc}(\rho)) \equiv f_0(\rho)\,, \qquad (9.98)$$

where $\epsilon_{xc}(\rho)$ is the exchange-correlation energy per particle of the homogeneous electron gas. $f_{xc}^{\mathrm{hom}}(q,\omega=0)$ was defined in (9.60) and (9.61). In general, f_{xc}^{hom} is a quantity that depends on both q and ω, and is related to the field factor $G(q,\omega)$ of (9.27) by

$$f_{xc}^{\mathrm{hom}}(q,\omega) = -v_c(q)G(q,\omega)\,. \qquad (9.99)$$

This $f_{xc}^{\mathrm{hom}}(q,\omega)$ has the following properties (see, e.g. Gross and Kohn 1990):

(1)
$$\lim_{q\to 0} f_{xc}^{\mathrm{hom}}(q,\omega=\infty) = -\frac{4}{5}\rho^{2/3}\frac{d}{d\rho}\left(\frac{\epsilon_{xc}(\rho)}{\rho^{2/3}}\right) + 6\rho^{1/3}\frac{d}{d\rho}\left(\frac{\epsilon_{xc}(\rho)}{\rho^{1/3}}\right)$$

$$\equiv f_\infty(\rho)\,. \qquad (9.100)$$

This follows from the sum rule cubic in energy.

(2)
$$f_0(\rho) < f_\infty(\rho) < 0\,. \qquad (9.101)$$

This follows from Monte Carlo calculations on $\epsilon_{xc}(\rho)$.

(3)
$$\lim_{q\to\infty} f_{xc}^{\mathrm{hom}}(q,\omega=0) = -\frac{4\pi}{q^2}(1-g(0))\,. \qquad (9.102)$$

Here $g(r)$ is the pair correlation function (Shaw 1970).

(4)
$$\lim_{q \to \infty} f_{xc}^{\text{hom}}(q, \omega \neq 0) = -\frac{2}{3} \frac{4\pi}{q^2} (1 - g(0)) .$$
(9.103)

This was shown by Niklasson (1974).

(5) $f_{xc}^{\text{hom}}(q, \omega)$ is a complex function that fulfills the symmetry relations:

$$\text{Re } f_{xc}^{\text{hom}}(q, \omega) = \text{Re } f_{xc}^{\text{hom}}(q, -\omega) ,$$
$$\text{Im } f_{xc}^{\text{hom}}(q, \omega) = -\text{Im } f_{xc}^{\text{hom}}(q, -\omega) .$$
(9.104)

Here, $f_{xc}^{\text{hom}}(q, \omega)$ is an analytic function of ω in the upper part of the complex plane and tends to a real function $f_\infty(q)$ for $\omega \to \infty$ (Kugler 1975). Hence, the function $f_{xc}^{\text{hom}}(q, \omega) - f_\infty(q)$ obeys the standard Kramers-Kronig relations. The imaginary part of $f_{xc}^{\text{hom}}(q, \omega)$ exhibits the following high-frequency behaviour

$$\lim_{\omega \to \infty} \text{Im } f_{xc}^{\text{hom}}(q, \omega) = -\frac{c}{\omega^{3/2}}$$
(9.105)

for all values of $q < \infty$ (Holas and Singwi 1989). As for c, its value in the limit of high density is known: $c = 23\pi/15$ (Holas and Singwi 1989; Glick and Long 1971). In the same limit, the real part of $f_{xc}^{\text{hom}}(q, \omega)$ behaves like (Gross and Kohn 1985):

$$\lim_{\omega \to \infty} \text{Re } f_{xc}^{\text{hom}}(q, \omega) = f_\infty(q) + \frac{c}{\omega^{3/2}} .$$
(9.106)

Since $c > 0$, the infinite-frequency value f_∞ is approached from above. Due to relation (9.101), this implies that $\text{Re } f_{xc}^{\text{hom}}(q = 0, \omega)$ cannot grow monotonically from f_0 to f_∞.

All of the above considerations hold in $3D$. Analogous results have been obtained in $2D$ by Holas and Singwi (1989) and Iwamoto (1984).

Gross and Kohn (1985) advanced a local approximation with respect to the space co-ordinates ($q = 0$) for the exchange-correlation kernel, which however includes an explicit frequency dependence. In the density channel, such approximation for the kernel of the integral equation (8.205) is written as

$$K_{ss}^{xc}(\mathbf{r}_1, \mathbf{r}_2; \omega) = \delta(\mathbf{r}_1 - \mathbf{r}_2) f_{xc}^{\text{hom}}(q = 0, \omega; \rho)|_{\rho = \rho_0(\mathbf{r})} .$$
(9.107)

The frequency dependence of $\text{Im } f_{xc}^{\text{hom}}(q = 0, \omega)$ is approximated with a Padè-like interpolation between the high and low frequency limits:

$$\text{Im } f_{xc}^{\text{hom}}(q = 0, \omega) = \frac{a(\rho)\omega}{(1 + b(\rho)\omega^2)^{5/4}} ,$$
(9.108)

where

$$a(\rho) = -c(\gamma/c)^{5/3}(f_\infty(\rho) - f_0(\rho))^{5/3} ,$$
$$b(\rho) = (\gamma/c)^{4/3}(f_\infty(\rho) - f_0(\rho))^{4/3} ,$$
(9.109)

where $\gamma = (\Gamma(1/4))^2/(4\sqrt{2\pi})$, and f_0 and f_∞ are given in (9.98) and (9.100), and $c = 23\pi/15$. For the exchange-correlation energy $\epsilon_{xc}(\rho)$, the parametrization of Vosko, Wilk and Nusair (1980) is employed. Subsequently, from the Kramers–Kronig relation, we get for the real part of $f_{xc}^{\text{hom}}(q = 0, \omega)$ the following result:

$$
\text{Re } f_{xc}^{\text{hom}}(q = 0, \omega) = f_\infty + \frac{a}{\pi s^2} \sqrt{\frac{8}{b}} \left(2E\left(\frac{1}{\sqrt{2}}\right) - \frac{1+s}{2}\Pi\left(\frac{1-s}{2}, \frac{1}{\sqrt{2}}\right) \right.
$$
$$
\left. - \frac{1-s}{2}\Pi\left(\frac{1+s}{2}, \frac{1}{\sqrt{2}}\right) \right), \tag{9.110}
$$

where E and Π are the complete second and third type elliptical integrals in the standard notation of Byrd and Friedman (1954), and $s^2 = 1 + b\omega^2$.

In Figs. 9.9 and 9.10 we show the real and imaginary parts of $f_{xc}^{\text{hom}}(q = 0, \omega)$, for the two density values corresponding to $r_s = 2$ and $r_s = 4$. From these figures, we note that frequency-dependence grows with increasing r_s. In the $r_s \to 0$ limit, we find that the difference $f_\infty(\rho) - f_0(\rho)$ goes to zero like r_s^2, and that the depth of the minimum of Im $f_{xc}^{\text{hom}}(q = 0, \omega)$ still decreases proportionally to r_s^2.

An extension of the parametrization (9.108) to the finite q case has been carried out by Dabrowski (1986), and the $2D$ case has been treated by Holas and Singwi (1989).

The Gross–Kohn theory, with the frequency-dependent parametrization described above, has been applied extensively to the calculation of the density response of a metallic surface to an uniform external electric field perpendicular to the surface itself (see e.g. Liebsch 1987; Kempa and Schaich 1988). With respect to RPA calculations, in which exchange and correlation effects are neglected, modifications are generally of the order of 10%.

Another application of the theory concerns the study of plasmon dispersion in the $3D$ and $2D$ interacting electron gas. An extensive discussion of such problem, and of the connection between $f_{xc}^{\text{hom}}(q = 0, \omega)$ and the spectrum of two-particles–two-holes excitations at lowest order in q, can be found in Bohm, Conti and Tosi (1996) and Nifosi, Conti and Tosi (1998), together with an extensive review of references on the problem.

Finally, we recall that, contrary to the adiabatic $TDLDA$, the theory of Gross and Kohn with the frequency-dependent parametrization does not fulfill the generalized Kohn theorem discussed in Section 8.10.1 (Dobson 1994) when applies to the interacting electron systems confined in an external parabolic potential. This theorem guarantees the existence of a collective state at the same frequency as the harmonic potential, which corresponds to the rigid oscillation of the many-body wavefunction around the centre of the external potential. This problem was further addressed by Vignale (1995) and by Vignale and Kohn (1996), who proposed a new theory for the exchange-correlation kernel. Such theory is described in detail by Vignale and Kohn (1997).

Another theory with the frequency-dependent parametrization, which satisfies the generalized Kohn theorem, is the one described at the end of Section 9.10 and
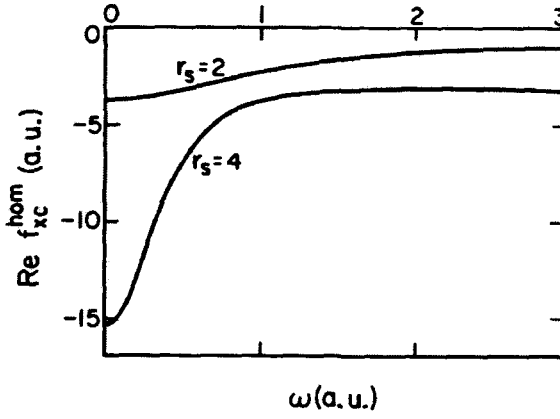
Fig. 9.9   Real part of the parametrization for $f_{xc}^{\text{hom}}(q,\omega)$.
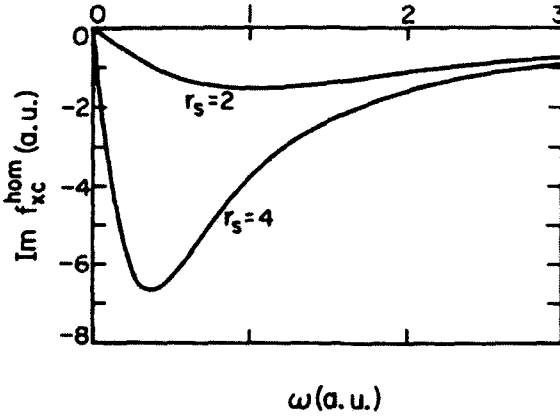
Fig. 9.10   Imaginary part of the parametrization for $f_{xc}^{\text{hom}}(q,\omega)$.

synthetically represented by the equations (9.92)–(9.96). This approach gives the result

$$f_{xc}^{\text{hom}}(q,\omega) = \mathcal{K} - \frac{m^*}{m} t_1 \frac{\omega^2}{q^2} \, .$$

9.12   The Method of Lorentz Transforms

Recently (Efros, Leideman and Orlandini 1994), a new method has been proposed for the calculation of the dynamic form factor

$$S(F,\omega) = \sum_n |\langle n|F|0\rangle|^2 \delta(\omega - (E_n - E_0)) \, .$$

This method uses the integral Lorentz transforms. It allows the calculation of $S(F,\omega)$ with no explicit knowledge of the set of excited states $|n\rangle$ (both discrete and continuous) which, in general, are very complicated.

The Lorentz transform of $S(F,\omega)$ is written as

$$\Phi(\sigma_R, \sigma_I, F) = \int_{\omega_{\min}}^{\infty} d\omega \frac{S(F,\omega)}{(\omega - \sigma_R)^2 + \sigma_I^2}. \tag{9.111}$$

Its advantage over to the direct calculation of $S(F,\omega)$ lies in the resonant form of the kernel, which allows one to solve even very complex forms of $S(F,\omega)$ by choosing sufficiently small values of σ_I.

The method goes forward in two steps. First one computes $\Phi(\sigma_R, \sigma_I, F)$ by making use of the closure relationship $\sum_n |n\rangle\langle n| = 1$:

$$\Phi(\sigma_R, \sigma_I, F) = \langle 0|F^\dagger (H - E_0 - \sigma_R - i\sigma_I)^{-1}(H - E_0 - \sigma_R + i\sigma_I)^{-1}F|0\rangle$$

$$\equiv \langle \Psi|\Psi\rangle, \tag{9.112}$$

where E_0 is the energy of the ground state of the Hamiltonian H of the system, and $|\Psi\rangle$ is determined by the equation

$$(H - E_0 - \sigma_R + i\sigma_I)|\Psi\rangle = F|0\rangle. \tag{9.113}$$

Note that due to (9.112), the norm of $|\Psi\rangle$ exists and so, contrary to the wavefunctions of states in continuum, $|\Psi\rangle$ cancels out at large distances like the wavefunctions of bounded states. This makes the solution of (9.113) much simpler than the solution of the equation for the excited states of the continuum. The solution of (9.113) is unique, since the corresponding homogeneous equation has no solution known due to the complex nature of $\sigma = -\sigma_R + i\sigma_I$.

The second step consists in inverting the Lorentz transform (9.111), to obtain the dynamic form factor. In order that the dynamic form factor is obtained with good accuracy even at rather high frequencies, one needs an ad hoc procedure that is discussed in detail in Efros, Leideman and Orlandini (1999).

So far, the Lorentz-transform method has been applied only in nuclear physics and for light nuclei up to a maximum of 6 nucleons. The results of such calculations for the photo-disintegration and inelastic electron-scattering cross sections, as well as their comparison with experimental data, can be found in Efros, Leideman and Orlandini (1997).

References to Chapter 9

D. Pines and P. Nozières, The Theory of Quantum Liquids (Benjamin, New York, 1966).

M. Jonson, J. Phys. C **9**, 3055 (1976).

D. Agosti, F. Pederiva, E. Lipparini and K. Takayanagi, Phys. Rev. B **57**, 14869 (1998).

M. Gell-Mann and K.A. Brueckner, Phys. Rev. **106**, 364 (1957).

A. Isihara and T. Toyoda, Ann. Phys. (N.Y.) **106**, 394 (1977); **114**, 497 (1978).

A.K. Rajagopal and J.C. Kimball, Phys. Rev. B **15**, 2819 (1977).

B. Tanatar and D.M. Ceperley, Phys. Rev. B **39**, 5005 (1989).

P. Ring and P. Schuck, The Nuclear Many-Body Problem (Springer Verlag, N.Y. 1980).

P.G. Reinhard, Phys. Lett. A **169**, 281 (1992).

T.D. Lee, K.W. Huang and C.N. Yang, Phys. Rev. **106**, 1135 (1957).

E.H. Lieb and J. Yngvason, Phys. Rev. Lett. **80**, 2504 (1998).

E.H. Lieb and J. Yngvason, J. Stat. Phys. **103**, 509 (2001).

M. Schick, Phys. Rev. A **3**, 1067 (1971).

D.F. Hines, N.E. Frankel and D.J. Mitchell, Phys. Lett. A **68**, 12 (1978).

V.N. Popov, Theor. and Math. Phys. **11**, 565 (1977).

D.S. Fisher and P.C. Hohenberg, Phys. Rev. B **37**, 4936 (1988).

L.D. Landau and E.M. Lifchitz, "Fisica Statistica", Teoria dello Stato Condensato (Editori Riuniti, Edizioni Mir, 1981).

K. Huang and C.N. Yang, 1957.

K. Takayanagi and E. Lipparini, Phys. Rev. B **52**, 1730 (1995).

H.J. Schulze, P. Schuck and N. Van Giai, Phys. Rev. B **61**, 8026 (2000).

F. Pederiva, E. Lipparini and K. Takayanagi, Europh. Lett. **40**, 607 (1997).

S. Moroni, D.M. Ceperley and G. Senatore, Phys. Rev. Lett. **69**, 1837 (1992).

C.N. Likos, S. Moroni and G. Senatore, Phys. Rev. B **55**, 8867 (1997).

K. Takayanagi and E. Lipparini, Phys. Rev. B **54**, 8122 (1996).

K.S. Singwi, M.P. Tosi, R.H. Land and A. Sjolander, Phys. Rev. **176**, 589 (1968).

E.G.D. Cohen, "Fundamental Problems in Statistical Mechanics" (North-Holland Publishing Co., Amsterdam, 1962).

W.L. Freser and J. Bergersen, J. Phys. C **13**, 6627 (1980).

L. Camels and A. Gold, Phys. Rev. B **52**, 10841 (1995); P**56**, 1762 (1997).

S. Ichimaru, Rev. Mod. Phys. **54**, 1017 (1982).

J.M.J. van Leeuwen, J. Groeneveld and J. De Boer, Physica **25**, 792 (1959).

T. Morita, Progr. Theor. Phys. **23**, 829 (1960).

S. Fantoni and S. Rosati, Nuovo Cimento A **10**, 145 (1972); A **25**, 593 (1975).

G. Ripka, Phys. Rep. **56**, 1 (1979).

J. Chihara, Progr. Theor. Phys. **50**, 409 (1973).

Ph. Choquard, in Strongly Coupled Plasmas, ed. by G. Kalman (Plenum, New York 1978), p. 347.

J. Chihara and K. Sasaki, Progr. Theor. Phys. **62**, 1533 (1979).

C.S. Ting, T.K. Lee and J.J. Quinn, Phys. Rev. Lett. **34**, 870 (1975).

T.M. Rice, Ann. Phys. **31**, 100 (1965).

G.D. Mahan, Many Particle Physics (Plenum Press, New York and London, 1981).

C. Mahaux, P.F. Bortignon, R.A. Broglia and C.H. Dasso, Phys. Rep. **120**, 1 (1985).

F. Dalfovo, A. Lastri, L. Pricaupenko, S. Stringari and J. Treiner, Phys. Rev. B **52**, 1193 (1995).

R.J. Donnelly, J.A. Donnelly and R.N. Hills, J. Low Temp. Phys. **44**, 471 (1981).

E.C. Svensson, V.F. Sears, A.D.B. Woods and P. Martel, Phys. Rev. **21**, 3638 (1980).

A.D.B. Woods and R.A. Cowley, Rep. Prog. Phys. **36**, 1135 (1973).

E. Lipparini, S. Stringari and K. Takayanagi, J. Phys. Cond. Matt. **6**, 2025 (1994).

F. Aryasetiawan and K. Karlsson, Phys. Rev. Lett. **73**, 1679 (1994).

M. Taut and K. Sturm, Sol. State Commun. **82**, 295 (1992).

A. vom Felde, J. Sprosser-Prou and J. Fink, Phys. Rev. B **40**, 10181 (1989).

N. Iwamoto, E. Krotscheck and D. Pines, Phys. Rev. B **29**, 3936 (1984).

R.D. Puff, Phys. Rev. A **137**, 406 (1965).

F. Dalfovo and S. Stringari, Phys. Rev. Lett. **63**, 532 (1989).

D. Pines, in Proceedings of International School of Physics (E. Fermi), Course LXXXIX, F. Bassani, F. Fumi and M. Tosi, Eds. (North Holland, Amsterdam, 1985).

S. Stringari and F. Dalfovo, J. Low Temp. Phys. **78**, 1 (1990).

E.K.U. Gross and W. Kohn, Adv. Quant. Chem. **21**, 255 (1990).

R.W. Shaw, J. Phys. C **3**, 1140.

G. Niklasson, Phys. Rev. B **10**, 3052 (1974).

A.A. Kugler, J. Stat. Phys. **12**, 35 (1975).

A. Holas and S. Singwi, Phys. Rev. B **40**, 158 (1989).

A.J. Glick and W.F. long, Phys. Rev. B **4**, 3455 (1971).

E.K.U. Gross and W. Kohn, Phys. Rev. Lett. **55**, 2850 (1985).

N. Iwamoto, Phys. Rev. A **30**, 2597 (1984); 3289 (1984).

N. Iwamoto and W. Gross, Phys. Rev. B **35**, 3003 (1987).

S.H. Vosko, L. Wilk and M. Nusair, Can. J. Phys. **58**, 1200 (1980).

P.F. Byrd and M.D. Friedman, "Handbook of Elliptical Integrals for Engineers and Physicists" (Springer-Verlag, Berlin, 1954).

B. Dabrowski, Phys. Rev. B **34**, 4989 (1986).

A. Liebsch, Phys. Rev. B **36**, 7378 (1986).

K. Kempa and W.L. Schaich, Phys. Rev. B **37**, 6711 (1988).

H. M. Bohm, S. Conti and M.P. Tosi, J. Phys. Cond. Matter **8**, 781 (1996).

R. Nifosi, S. Conti and M.P. Tosi, Phys. Rev. B **58**, 12758 (1998).

J.F. Dobson, Phys. Rev. Lett. **73**, 2244 (1994).

G. Vignale, Phys. Rev. Lett. **74**, 3233 (1995); Phys. Lett. A **209**, 206 (1995).

G. Vignale and W. Kohn, Phys. Rev. Lett. **77**, 2037 (1996).

G. Vignale and W. Kohn, in Electronic Density Functional Theory, edited by J. Dobson, M.P. Das and G. Vignale (Plenum Press, New York, 1997).

V.D. Efros, W. Leidemann and G. Orlandini, Phys. Lett. B **338**, 130 (1994); Few-Body Systems **26**, 251 (1999); Phys. Rev. Lett. **78**, 432 (1997); 4015 (1997).

This page is intentionally left blank

Chapter 10

The Hydrodynamic and Elastic Models

10.1 The Hydrodynamic Model for Bosons

A simple way to derive the hydrodynamic equations for a system of Bosons at zero temperature is to extend the formalism of (the Hartree–Fock) density functional used in the static case, to the time-dependent problem. In the time-dependent case, one assumes that the single-particle wavefunction φ relative to the Bose condensate evolves in time with a phase that breaks its time-reversal invariance, and generates velocity-dependent terms in the energy functional $E(\rho, \nabla\rho) = \int d\mathbf{r}\rho\epsilon(\rho, \nabla\rho)$. This single particle wavefunction has the form

$$\varphi(\mathbf{r}, t) = \psi(\mathbf{r}, t)e^{is(\mathbf{r},t)}, \tag{10.1}$$

where both ψ and s are real functions. With this assumption, the system density is still given by

$$\rho = N\psi^2, \tag{10.2}$$

but the kinetic energy density $\tau = N\nabla\varphi^*\nabla\varphi$ becomes

$$\tau = \frac{1}{4}\frac{(\nabla\rho)^2}{\rho} + \rho(\nabla s)^2. \tag{10.3}$$

From equation (10.3) we see that the phase s determines the velocity of the fluid through the relationship

$$\mathbf{v} = (1/m)\nabla s. \tag{10.4}$$

In the calculation of the ground state, only zero-velocity states are considered, so that the energy is a functional of density alone, and from this we derive Hartree–Fock-like equations by the variational method. On the contrary, in the dynamic case

the action of the system:

$$I = \int dt \langle \Phi | H - \mu - i\frac{\partial}{\partial t} | \Phi \rangle$$

$$= \int dt \int dr \left(\rho\epsilon(\rho, \nabla\rho) + \frac{1}{2m}\rho(\nabla s)^2 - \mu\rho + \rho\frac{\partial}{\partial t}s \right), \qquad (10.5)$$

where $\epsilon(\rho, \nabla\rho)$ is the same energy functional as in the static case, depends explicitly on velocity, and yields equations which describe the motion of the condensate. In equation (10.5), the term $\mu\rho$ ensures that the density stays normalized to the number of particles. The variation of the action integral with respect to the phase s leads to the continuity equation

$$\frac{\partial}{\partial t}\rho + \nabla(\mathbf{v}\rho) = 0, \qquad (10.6)$$

while the variation with respect to ρ leads to the following equations for s:

$$\frac{\partial}{\partial t}s + \frac{\partial}{\partial\rho}(\rho\epsilon(\rho, \nabla\rho)) - \mu + \frac{1}{2m}(\nabla s)^2 = 0. \qquad (10.7)$$

Performing the gradient of (10.7) we then obtain:

$$m\frac{\partial}{\partial t}\mathbf{v} + \nabla\left(\frac{\partial}{\partial\rho}(\rho\epsilon(\rho, \nabla\rho)) + m\frac{v^2}{2} \right) = 0. \qquad (10.8)$$

Equation (10.8) shows the irrotational nature of the superfluid motion.

For a system of N weakly interacting Bosons in a magnetic trap, equations (10.8) can be derived directly from the time-dependent Gross–Pitaevskii equations by writing the order parameter Ψ of (8.122) as

$$\Psi(\mathbf{r}, t) = \sqrt{\rho(\mathbf{r}, t)}e^{is(\mathbf{r}, t)}.$$

In this case we obtain

$$m\frac{\partial}{\partial t}\mathbf{v} + \nabla\left(v_{\text{ext}} + g\rho - \frac{1}{2m\sqrt{\rho}}\nabla^2\sqrt{\rho} + m\frac{v^2}{2} \right) = 0, \qquad (10.9)$$

which is the equation corresponding to (10.8). The continuity equation is unchanged. For a harmonic confinement field, such equations hold when the condition $Na/a_{ho} \gg 1$ is satisfied (see Dalfovo et al. 1999). In this case the frequencies which are the solutions of (8.125) tend to an asymptotic value which corresponds to the collisionless hydrodynamic limit.

Equation (10.8), once linearized, takes the form:

$$\frac{\partial^2}{\partial t^2}\delta\rho = \frac{1}{m}\nabla \cdot \left(\rho_0 \frac{\partial^2\rho\epsilon}{\partial\rho^2}\bigg|_{\rho=\rho_0} \nabla\delta\rho \right), \qquad (10.10)$$

where we have written $\rho(\mathbf{r}, t) = \rho_0(\mathbf{r}) + \delta\rho(\mathbf{r}, t)$ and ρ_0 is the density of the condensate in the ground state. Equations (10.6) and (10.10) have the classical form of the equations of hydrodynamics.

In the case of Bosons the formulation of the equations of motion using the conjugate variables ρ and s, as described above, is fully equivalent to the zero-temperature, time-dependent density functional theory. In this theory, (see also Section 8.9), starting from the action integral and from an energy functional $E(\rho, \nabla\rho)$, and performing variations with respect to the wavefunction ϕ or ϕ^* which appears in the density, one finds a Schrödinger-like equation of the form $(H - \mu)\phi = i\frac{\partial}{\partial t}\phi$, where $H = \frac{\delta E}{\delta \phi^*}$ is an effective Hamiltonian. If we linearize the equation by writing $\phi(\mathbf{r}, t) = \phi_0(\mathbf{r}) + \delta\phi(\mathbf{r}, t)$, where $\phi_0(\mathbf{r})$ is related to the ground state then the Hamiltonian H assumes the form $H = H_0 + \delta H$, where H_0 is the static Hamiltonian that determines the ground state, and δH (linear in $\delta\phi$) takes account of the variations of H induced by the collective motion of the system. The self-consistent solution of

$$(H_0 - \mu)\delta\phi + \delta H \phi_0 = i\frac{\partial}{\partial t}\delta\phi$$

is then completely equivalent to the solution of the hydrodynamic equations.

In homogeneous systems, remembering that the speed of sound is related to the compressibility K by equation (1.80) $(c^2 = 1/Km\rho_0)$, and that the compressibility is given by the expression

$$\frac{1}{K} = \rho_0^2 \frac{\partial^2 \rho\epsilon}{\partial\rho^2}\bigg|_{\rho=\rho_0},$$

we obtain

$$\frac{\partial^2}{\partial t^2}\delta\rho = \nabla \cdot (c^2 \nabla\delta\rho), \tag{10.11}$$

which immediately leads us to the phonon-like dispersion law: $\omega = cq$.

In the presence of a surface, the equations of hydrodynamics have a class of solutions different from phonons which, in the literature, are known as ripplons (see, e.g. Pricaupenko and Treiner 1994). Ripplons are characterized by the dispersion relation

$$\omega^2 = \frac{\sigma}{m\rho_0}q^3, \tag{10.12}$$

where σ is the surface tension of the quantum liquid, q is the momentum parallel to the surface, and ρ_0 is the saturation density.

10.1.1 *Backflow*

In Section 9.8 we discussed the nonlocal effects on the dynamic properties of superfluid ^{4}He, adding to the energy functional the velocity-dependent term [see

Eq. (9.66)]:

$$E_v = -\frac{m}{4} \int d\mathbf{r} d\mathbf{r}' V_J(|\mathbf{r} - \mathbf{r}'|)\rho(\mathbf{r})\rho(\mathbf{r}')(\mathbf{v}(\mathbf{r}) - \mathbf{v}(\mathbf{r}'))^2 ,$$

where V_J is an effective, finite-range current-current interaction which plays the role of a non-local kinetic energy. This term transforms the equations of hydrodynamics (10.6) and (10.7) into

$$\frac{\partial}{\partial t}\rho + \nabla \cdot \rho \left(\mathbf{v} + \int d\mathbf{r}' V_J(|\mathbf{r} - \mathbf{r}'|)\rho(\mathbf{r}')(\mathbf{v}(\mathbf{r}) - \mathbf{v}(\mathbf{r}')) \right) = 0 , \quad (10.13)$$

$$\frac{\partial}{\partial t}s + \frac{\partial}{\partial \rho}(\rho\epsilon(\rho, \nabla\rho)) - \mu$$

$$+ \frac{m}{2} \left((\mathbf{v})^2 - \int d\mathbf{r}' V_J(|\mathbf{r} - \mathbf{r}'|)\rho(\mathbf{r}')(\mathbf{v}(\mathbf{r}) - \mathbf{v}(\mathbf{r}'))^2 \right) = 0 . \quad (10.14)$$

Equation (10.13) leads to the conserved current

$$\mathbf{j}(\mathbf{r}) = \mathbf{j}_0(\mathbf{r}) + \mathbf{j}_B(\mathbf{r}) , \qquad (10.15)$$

where $\mathbf{j}_0(\mathbf{r}) = \rho\mathbf{v}$, and

$$\mathbf{j}_B(\mathbf{r}) = \rho \int d\mathbf{r}' V_J(|\mathbf{r} - \mathbf{r}'|)\rho(\mathbf{r}')(\mathbf{v}(\mathbf{r}) - \mathbf{v}(\mathbf{r}')) . \qquad (10.16)$$

$\mathbf{j}_B(\mathbf{r})$ is the "backflow" current, which depends on velocity and on the density near point $(\mathbf{r})$. It is evident that its contribution vanishes when the effects of the medium are not present $(\rho \to 0)$.

The backflow term has been used, among others, by Dalfovo et al. (1995) to study the dynamics of free surfaces and thin films of ^{4}He.

10.1.2 *Compression and surface modes of spherical drops*

Equations (10.6) and (10.10) have been applied to study drops of ^{4}He atoms, by Casas and Stringari (1990) and Barranco and Hernandez (1994), and ^{4}He films by Pricaupenko and Treiner (1994).

In the case of ^{4}He drops, that we consider here, one has both bulk excitations (compression modes) and surface excitations. For spherical drops, both kinds of excitations are classified according to their angular momentum ℓ, which plays the role of the wavevector q which characterizes homogeneous systems and free surfaces, and one looks for solutions of the hydrodynamic equations in the form:

$$\delta\rho(\mathbf{r}, t) = \rho(\mathbf{r}, t) - \rho_0(\mathbf{r}) = \delta\rho(r, t)y_{\ell m}(\theta, \phi) . \qquad (10.17)$$

Surface excitations exist only for $\ell > 1$. In fact, the monopole excitation with $\ell = 0$ exists only as compression mode, and the surface mode with $\ell = 1$ corresponds to a

rigid translation of the cluster which, due to translational invariance of the system, takes place at zero energy.

For very large drops, so that we can assume that the number N of atoms in the drop is large, the compression modes can be obtained by solving equation (10.11) in a sphere of homogeneous liquid ($\rho = const$) having radius $R_0 = r_0 N^{1/3}$. In this case, equation (10.11) has the solution

$$\delta\rho(\mathbf{r}, t) = \text{constant} \cdot j_\ell(qr)y_{\ell m}(\theta, \phi)e^{-i\omega t}, \qquad (10.18)$$

where $j_\ell(qr)$ is the spherical Bessel function and the frequency ω is given by the usual dispersion relation

$$\omega = cq,$$

where q is determined by the boundary condition that the pressure produced by the density variation is zero at the sphere surface [see Eq. (4.72)]:

$$\delta P(r = R_0) = \frac{1}{\rho K}\delta\rho(r = R_0) = 0. \qquad (10.19)$$

Such condition leads to the relationship

$$j_\ell(qR_0) = 0, \qquad (10.20)$$

and hence to the values $qR_0 = 3.14, 4.49, 5.76$ for the lowest-energy modes with $\ell = 1, 2, 3$, respectively. In the case of $\ell = 0$, the lowest-energy solution is obtained for $qR_0 = \pi$, and the compression monopole mode has an energy

$$\omega_{\ell=0} = \frac{\pi}{r_0}cN^{-1/3} = 25.6N^{-1/3}\,^\circ\text{K}, \qquad (10.21)$$

where for r_0 and c we used the values of Section 4.9. Note that this formulation completely neglects surface and finite-size effects, and as such it can be applied only to clusters with a really large number of atoms ($N \geq 500$). For smaller clusters, one needs to solve directly the differential equations of hydrodynamics.

The surface vibrations of the helium drop can be described by a set of normal coordinates $\alpha_{\ell m}$ of the system in the space of angular momentum, which are obtained by expanding the surface in spherical harmonics (Bohr and Mottelson 1975):

$$R(\theta, \phi) = R_0 \left(1 + \sum_{\ell m} \alpha_{\ell m}y^*_{\ell m}(\theta, \phi)\right) \qquad (10.22)$$

where R_0 is the radius at equilibrium, and $R(\theta, \phi)$ is the distance between the surface and the origin. Volume conservation implies the relation

$$\alpha_0 = -\frac{1}{4\pi}\sum_{\ell m} |\alpha_{\ell m}|^2, \qquad (10.23)$$

which holds at leading order. Furthermore, from equation (10.22) it is easy to verify what was mentioned above, i.e. that the term with $\ell = 0$ represents a compression

without change of shape, and the one with $\ell = 1$ is a translation of the whole system. Therefore, the surface vibrations of lowest order are the quadrupole one.

In the limit of small oscillations it is possible to use a Lagrangian formulation:

$$L = \frac{1}{2} \sum_{\ell m} (D_\ell \dot{\alpha}^*_{\ell m} \dot{\alpha}_{\ell m} - C_\ell \alpha^*_{\ell m} \alpha_{\ell m}) \,, \qquad (10.24)$$

which allows us to derive the equations of motion of the surface oscillations:

$$D_\ell \ddot{\alpha}_{\ell m} + C_\ell \alpha_{\ell m} = 0 \,, \qquad (10.25)$$

where D_ℓ and C_ℓ are the mass parameter and the restoring force parameter of the oscillation, respectively. The equation for the oscillation frequencies is given by

$$\omega_\ell^{sup} = \sqrt{\frac{C_\ell}{D_\ell}} \,. \qquad (10.26)$$

The parameter C_ℓ of the restoring force of surface oscillations in a helium drop described by the mass formula (4.83) is computed starting from the variation of surface energy

$$\delta E = \frac{1}{2} \sum_{\ell m} C_\ell |\alpha_{\ell m}|^2 = \sigma \delta S \,, \qquad (10.27)$$

where δS is the surface variation, and σ $(a_s = 4\pi r_0^2 \sigma)$ is the surface tension of the drop. By means of standard techniques described by Bohr and Mottelson (1975) to evaluate δS as a function of the deformation coefficients $\alpha_{\ell m}$, one obtains

$$C_\ell = (\ell - 1)(\ell + 2) R_0^2 \sigma \,. \qquad (10.28)$$

In order to calculate the mass parameter D_ℓ, one needs to make an assumption as to the kind of flux associated to the surface oscillations. For uncompressible and irrotational fluid, for which the velocity field is the gradient of a potential $f(\mathbf{r})$: $\mathbf{v}(\mathbf{r}) = -\nabla f(\mathbf{r})$, the continuity equation (10.6) demands that the potential fulfills the Laplace equation $\nabla^2 f(\mathbf{r}) = 0$, with solution

$$f(\mathbf{r}) = \sum_{\ell m} a_\ell r^\ell y^*_{\ell m}(\theta, \phi) \,. \qquad (10.29)$$

The coefficients a_ℓ and D_ℓ are connected by the surface boundary condition, which requires that on the surface the radial component of the velocity be equal to the radial velocity of surface displacement. For small displacements of the surface, such boundary condition requires

$$-\frac{\partial}{\partial r} f(r = R_0) = \frac{dR}{dt} \,, \qquad (10.30)$$

from which it follows

$$a_\ell = \frac{R_0^{2-\ell}}{\ell} \dot{\alpha}_{\ell m} \,. \qquad (10.31)$$

Then, the kinetic energy of the fluid relative to the surface deformations becomes

$$T = \frac{1}{2} M \rho_0 \int \mathbf{v}^2(\mathbf{r}) d\mathbf{r} = \frac{1}{2} M \rho_0 \sum_{\ell m} \frac{R_0^5}{\ell} \dot{\alpha}_{\ell m}^* \dot{\alpha}_{\ell m}, \tag{10.32}$$

and at last, comparison with (10.24) yields the result

$$D_\ell = \frac{1}{\ell} M \rho_0 R_0^5, \tag{10.33}$$

where M is the mass of a helium atom, and $\rho_0 = 3/(4\pi r_0^3)$.

Therefore, the frequencies of the surface modes of the drop are given by

$$\omega_\ell^{sup} = \sqrt{\frac{\ell(\ell-1)(\ell+2)}{3} \frac{a_s}{Mr_0^2}} N^{-\frac{1}{2}}. \tag{10.34}$$

Using the values of Section 4.9 for a_s and r_0, we obtain for the energy of the quadrupole mode, which is the lowest-energy surface mode, the estimate $\omega_{\ell=2}^{sup} = 10.5 \, N^{-\frac{1}{2}} \, ^\circ$K. Comparing such estimate with that for the energy of the monopole compression mode of (10.21), we see that the quadrupole surface mode has a different dependence on the number of particles, and it always lies at lower energy. Therefore, it is believed that this is the lowest-energy elementary excitation of spherical ^{4}He drops. Note that, apart from the drops with a small number of atoms ($N \leq 100$), there are many surface modes at lower energy than the monopole compression mode. For example, for $N = 1000$ we have $\omega_{\ell=0} = 2.56 \, ^\circ$K and $\omega_\ell^{sup} = 0.33, 065, 1.00, 1.40, 1.83, 2.29$ and $2.79 \, ^\circ$K, for $\ell = 2, 3, 4, 5, 6, 7$ and 8, respectively.

Assuming that in a helium drop only surface vibrations are thermally excited, and using the result (10.34), Brink and Stringari (1990) evaluated the density of states $\omega(E)$ of helium clusters starting from the relation

$$Z(\beta) = \int dE \omega(E) e^{-\beta E}, \tag{10.35}$$

where Z is the partition function, which is computed by assuming that the surface vibrations are thermally excited with a phonon-like population:

$$\ln Z(\beta) = -\sum_\ell \ln(1 - e^{-\beta \omega_\ell}). \tag{10.36}$$

The result for the density of states was then used to compute the evaporation rate of helium drops using the Weisskopf formula (Weisskopf 1937).

10.1.3 Compression and surface modes of a Bose gas in a magnetic trap

Starting from (10.9), it is also possible to derive an equation similar to (10.11) for a cold and dilute Boson gas in a magnetic trap, for which the non-superfluid component of the system is negligible, when the repulsive interaction among atoms

is strong enough to push them outwards, thus producing a very flat density. In this case, it is safe to ignore the kinetic pressure term $\nabla^2\sqrt{\rho}/2m\sqrt{\rho}$ in (10.9), giving:

$$m\frac{\partial}{\partial t}\mathbf{v} + \nabla\left(v_{\text{ext}} + g\rho + m\frac{v^2}{2}\right) = 0,\tag{10.37}$$

and thus, after linearization, an equation of the form (10.11), with $mc^2(r) = \mu - v_{\text{ext}}$. Taking for v_{ext} a harmonic potential, we have

$$m\frac{\partial^2}{\partial t^2}\delta\rho = \nabla\cdot\left(\left(\mu - \frac{m}{2}\omega_{ho}^2 r^2\right)\nabla\delta\rho\right).\tag{10.38}$$

Note that the stationary solution ($\mathbf{v} = 0$) of equation (10.37) coincides with the Thomas–Fermi density (4.21).

The solutions of (10.38) that have a wavelength much smaller than the system size (and frequency much higher than the frequency ω_{ho} of the trap) propagate like sound waves. On the other hand, those with lower frequency (of the same order as ω_{ho}) involve the motion of the whole system (Baym and Pethick 1996), and coincide with the lowest-energy solutions of the Gross–Pitaevskii equations (8.125). For a spherical trap, such solutions (Stringari 1996b) are defined in the interval $0 \le r \le R$, where R is the r-value at which the density (4.21) vanishes: $\mu = m\omega_{ho}^2 R^2/2$. Using for μ the value (4.22), we find $R = a_{ho}(15Na/a_{ho})^{1/5}$. They have the form

$$\delta\rho(\mathbf{r}, t) = \text{const} P_\ell^{(2n_r)}(r/R)r^\ell y_{\ell m}(\theta, \phi)e^{-i\omega t},\tag{10.39}$$

where $P_\ell^{(2n_r)}$ are polynomials of degree $2n_r$, with only even powers. The frequencies of the excitation modes are given by

$$\omega(n_r, \ell) = \omega_{ho}(2n_r^2 + 2n_r\ell + 3n_r + \ell)^{1/2},\tag{10.40}$$

and turn out to be different from the ones predicted for the system without interaction:

$$\omega(n_r, \ell) = \omega_{ho}(2n_r + \ell).\tag{10.41}$$

The surface modes are characterized by $n_r = 0$. The dipole mode ($n_r = 0, \ell = 1$) is located at the correct energy ω_{ho}, in agreement with the generalized Kohn theorem. The remaining surface modes ($n_r = 0, \ell$) are predicted at energy $\omega = \sqrt{\ell}\omega_{ho}$, which is systematically lower than the harmonic oscillator result $\ell\omega_{ho}$.

The compression mode ($n_r \ne 0$) at lowest energy is the monopole mode ($n_r = 1, \ell = 0$). Characterized by the energy $\sqrt{5}\omega_{ho}$, it is higher than the corresponding one for the non-interacting system, $2\omega_{ho}$.

For fixed N, the results of the hydrodynamic model become less and less accurate as n_r and ℓ increase because the oscillation wavelength becomes smaller and smaller, and it is no longer possible to ignore the kinetic energy term in the hydrodynamic equations.

The above results can be easily generalized to the case of non-spherical traps (Stringari 1996b).

It is important to remark that in the case of homogeneous dilute and cold gases in $3D$ the equations of hydrodynamics are fully equivalent to the time-dependent Gross–Pitaevskii equations, since in $3D$ the Bose–Einstein condensation and hydrodynamics are equivalent. The same is not the case for lower dimensional systems where the Hohenberg, Mermin and Wagner (Mermin and Wagner 1966; Hohenberg 1967; Mermin 1968) theorem holds, which rules out BEC at finite temperature, and in $1D$ also at zero temperature (Stringari and Pitaevskii 1991). For these systems the BEC and the hydrodynamics do not coincide, and the equations of hydrodynamics are more general than those of mean-field theories. In order to solve the equations of hydrodynamics, the state equation of the system is necessary. In the case of cold dilute gases where the interaction is δ-like, such equation, in general, is known.

10.1.4 *Moment of inertia and the scissors mode of a Bose gas in a magnetic trap*

In this Section, starting from (10.6) and (10.37), we will calculate the moment of inertia of a cold and dilute Bose gas, in the Thomas–Fermi limit, in a trap that rotates with angular velocity Ω directed along the z axis. We will consider harmonic external fields of the type

$$V_{\text{ext}} = \sum_{i=1}^{N} \frac{m}{2}(\omega_x^2 x_i^2 + \omega_y^2 y_i^2 + \omega_z^2 z_i^2)\,, \qquad (10.42)$$

with an asymmetry $(\omega_x \neq \omega_y)$ on the rotating plane.

The moment of inertia characterizes the system response to the rotation field $-\Omega L_z$, and is defined by the ratio

$$\Theta = \frac{\langle L_z \rangle}{\Omega}\,, \qquad (10.43)$$

between the angular momentum $\langle L_z \rangle$ induced by the rotation (along z) and the angular velocity Ω. In equation (10.43), the mean is over the state perturbed by the rotation.

In the rotating reference the equations of hydrodynamics become

$$\frac{\partial}{\partial t}\rho + \nabla(\rho(\mathbf{v} - \mathbf{\Omega} \times \mathbf{r})) = 0\,, \qquad (10.44)$$

$$m\frac{\partial}{\partial t}\mathbf{v} + \nabla\left(v_{\text{ext}} + g\rho + m\frac{v^2}{2} - m\mathbf{v} \cdot (\mathbf{\Omega} \times \mathbf{r})\right) = 0\,, \qquad (10.45)$$

and have the stationary solution (Zambelli and Stringari 2001):

$$\mathbf{v} = \Omega \frac{\langle x^2 - y^2 \rangle}{\langle x^2 + y^2 \rangle} \nabla(xy). \tag{10.46}$$

Then, the angular momentum induced by the rotation along z is given by

$$\langle L_z \rangle = mN\Omega \frac{\langle x^2 - y^2 \rangle^2}{\langle x^2 + y^2 \rangle},$$

and the moment of inertia by the irrotational value

$$\Theta = \left(\frac{\langle x^2 - y^2 \rangle}{\langle x^2 + y^2 \rangle} \right)^2 \Theta_{rig}, \tag{10.47}$$

where $\Theta_{rig} = mN\langle x^2 + y^2 \rangle$ is the rigid value of the moment of inertia. Equation (10.47) clearly shows that in a superfluid the value of the moment of inertia is smaller than the rigid value (the irrotational and rigid values coincide only for very deformed systems with $\langle x^2 \rangle \gg \langle y^2 \rangle$). In the limit of small rotational velocity Ω, the moment of inertia (10.47) can be rewritten as

$$\Theta = \left(\frac{\omega_x^2 - \omega_y^2}{\omega_x^2 + \omega_y^2} \right)^2 \Theta_{rig}. \tag{10.48}$$

This result is attained by putting in (10.47) the values of the mean square radii predicted by the Thomas–Fermi approximation of Section 4.3.2, which scale like $1/\omega^2$. We recall again that the Thomas–Fermi approximation is obtained from (10.45) by setting $\mathbf{v} = 0$ and $\Omega = 0$.

It is interesting to note that the prediction (10.48) for Θ can be obtained in a different way that makes use of perturbation theory. In fact, in the limit of small Ω, the moment of inertia can be evaluated by treating the rotational field $-\Omega L_z$ as a small perturbation to the Hamiltonian

$$H = \sum_{i=1}^{N} \left[\frac{p_i^2}{2m} + \frac{m}{2}(\omega_x^2 x_i^2 + \omega_y^2 y_i^2 + \omega_z^2 z_i^2) \right] + \sum_{i<j} V(\mathbf{r}_i - \mathbf{r}_j), \tag{10.49}$$

and we obtain the result (Radomski 1976; Stringari and Lipparini 1980)

$$\Theta = 2 \sum_n \frac{|\langle n|L_z|0\rangle|^2}{E_n - E_0}, \tag{10.50}$$

where n and E_n are the eigenstates and eigenvalues of the unperturbed Hamiltonian (10.49). Equation (10.50) shows that the moment of inertia is related to the moment $m_{-1}(L_z)$ of the excitation strength

$$S(L_z, \omega) = \sum_n |\langle n|L_z|0\rangle|^2 \delta(\omega - (E_n - E_0))$$

of the angular momentum

$$L_z = \sum_{i=1}^{N} (x_i p_i^y - y_i p_i^x)$$

(see Section 7.3) through the relation

$$\Theta = 2m_{-1}(L_z).$$ (10.51)

The angular momentum excites the system because of the asymmetric external potential, which breaks rotational invariance of Hamiltonian (10.49), and does not commute with L_z, yielding the result

$$[H, L_z] = -im(\omega_x^2 - \omega_y^2)Q,$$ (10.52)

where

$$Q = \sum_{i=1}^{N} x_i y_i$$

is the relevant quadrupole operator. Equation (10.52) shows that the degrees of freedom associated with the angular-momentum and quadrupole variables are coupled by the deformation of the confinement potential, and that the moment $m_1(L_z)$ does not depend on the interaction and is given by

$$m_1(L_z) = \frac{1}{2}\langle|[L_z, [H, L_z]]|\rangle = m\frac{N}{2}(\omega_x^2 - \omega_y^2)\langle y^2 - x^2\rangle.$$ (10.53)

Furthermore, noting that the rigid value of the moment of inertia can be related to the $m_1(Q)$ sum rule for the quadrupole operator, and using the identity

$$\sum_{i=1}^{N} x_i^2 y_i^2 = [Q, [H, Q]],$$ (10.54)

it is simple to derive from equations (10.51), (10.52) and (10.54) the result

$$\frac{\Theta}{\Theta_{rig}} = (\omega_x^2 - \omega_y^2)\frac{m_{-3}(Q)}{m_1(Q)}.$$ (10.55)

This shows that the moment of inertia of the system can be obtained by measuring the quadrupole excitations of the system itself.

The results (10.51)–(10.55) are exact results for Hamiltonian (10.49). They hold for any value of N, and for both Bose and Fermi systems.

In the case of Bose systems with repulsive interaction strong enough that the Thomas–Fermi approximation holds, and that it is possible to write the equations of hydrodynamics, the quadrupole and angular-momentum operators excite only one state at energy

$$\omega_{HD} = \sqrt{\omega_x^2 + \omega_y^2}.$$ (10.56)

This result generalizes for the case of an asymmetric trap the one obtained in Section 10.1.3 (i.e. $\sqrt{2}\omega_{ho}$) for the quadrupole mode of the system in a spherical trap. Using the result (10.56), together with equations (10.53) or (10.54), it is then possible to evaluate the moments $m_{-1}(L_z)$ and $m_{-3}(Q)$, $m_1(Q)$, and derive [either from Eqs. (10.51) or (10.55)] the value of Θ, which is equal to the one we already found (10.48) by direct solution of the equations of hydrodynamics.

The method just described for the calculation of Θ is very interesting because it evidences how important the dynamics is in determining the moment of inertia of the system. A further step towards the understanding of the problem can be made by studying the non-interacting system whose Hamiltonian is given by

$$H_0 = \sum_{i=1}^{N} \left[\frac{p_i^2}{2m} + \frac{m}{2}(\omega_x^2 x_i^2 + \omega_y^2 y_i^2 + \omega_z^2 z_i^2) \right].$$

In this model, it is easy to verify that the angular-momentum and quadrupole operators excite two modes at frequencies

$$\omega_\pm = \omega_x \pm \omega_y, \tag{10.57}$$

whose strengths are given by the formulae

$$|\langle \omega_\pm | L_z | 0 \rangle|^2 = \frac{Nm}{4\omega_x\omega_y}\omega_\mp^2(\omega_y\langle y^2 \rangle \pm \omega_x\langle x^2 \rangle), \tag{10.58}$$

and

$$|\langle \omega_\pm | Q | 0 \rangle|^2 = \frac{N}{4m\omega_x\omega_y}(\omega_y\langle y^2 \rangle \pm \omega_x\langle x^2 \rangle). \tag{10.59}$$

Using these results in (10.51) or (10.55), we obtain for θ the value

$$\Theta = \frac{mN}{\omega_x^2 - \omega_y^2}[(\omega_x^2 + \omega_y^2)\langle y^2 - x^2 \rangle + 2(\omega_y^2\langle y^2 \rangle - \omega_x^2\langle x^2 \rangle)]. \tag{10.60}$$

The results (10.57)–(10.60) are exact for the non-interacting Hamiltonian H_0. They hold for any value of N, and for both Bose and Fermi systems.

In the case of Bosons at zero temperature, when only the state $(n_x, n_y, n_z) = (0, 0, 0)$ is occupied, we have $\langle x^2 \rangle = 1/2m\omega_x$ and $\langle y^2 \rangle = 1/2m\omega_y$, and we obtain $|\langle \omega_- | L_z | 0 \rangle|^2 = 0$ and $|\langle \omega_- | Q | 0 \rangle|^2 = 0$, i.e. only the resonance at energy

$$\omega_+ = \omega_x + \omega_y \tag{10.61}$$

is excited. In this case the moment of inertia takes on the value

$$\Theta = \left(\frac{\omega_x - \omega_y}{\omega_x + \omega_y} \right)^2 \Theta_{rig}. \tag{10.62}$$

The results (10.61) and (10.62) correspond to the results (10.56) and (10.48), respectively, of the hydrodynamic model. The differences are due to the interaction. However, the physics is the same, in the sense that to the unique excited state

corresponds a moment of inertia which, in the spherical case, tends to zero in proportional to the square of deformation, thereby evidencing the superfluidity of the condensate.

However, the non-interacting model shows that there are two states that can be excited by quadrupole and angular-momentum operators: ω_+ and ω_-. In the Fermion case, these two resonances are always present in the system, and the state of higher energy is of quadrupole type, in the sense that it acquires much more quadrupole strength as compared to that of the orbital-angular-momentum, while the lower-energy state is orbital-angular-momentum type since it acquires more angular-momentum strength than quadrupole strength. The state ω_- is known in the literature as the scissor mode and has been observed (Bohle et al. 1984), and theoretically predicted (Lo Iudice and Palumbo 1978; Lipparini and Stringari 1983, 1989; Iachello 1984; Nojarov, Bochnacki and Faessler 1986) for the first time in atomic nuclei. Its existence has also been predicted for metal clusters (Lipparini and Stringari 1989b; Nesterenko et al. 1999) and quantum dots (Serra, Puente and Lipparini 1999). It has also been predicted (D. Guery-Odelin and Stringari 1999; Zambelli and Stringari 2001) and subsequently measured (Maragò et al. 2000) in Bose condensates. The scissor mode in Fermions will be considered in forthcoming Sections. In general, it can be said that its existence strongly affects the value of the moment of inertia of the system, as we will show in this Section for Bosons.

In the case of a Boson gas in a magnetic trap, the scissor mode exists only at temperatures higher than the critical temperature T_c. In fact, at these temperatures the situation changes drastically. The system becomes much less dense and, as a first approximation, the interaction can be neglected, and we pass from a hydrodynamic regime with only one excited state at energy (10.56), to a non-interacting regime with two excited states at energies (10.57), and with a moment of inertia given by expression (10.60). To evaluate the quadratic radii $\langle x^2 \rangle$ and $\langle y^2 \rangle$, Stringari (1996) used the so-called macroscopic limit in which one separates the contribution of the condensate from those of the excited states. Such limit is appropriate for temperatures KT much higher than the energies ω_x, ω_y, ω_z of the confinement potential, and leads to the result (1.66) for the depletion of the condensate. One finds that

$$N\langle x^2 \rangle = N_0(T)\frac{1}{2m\omega_x} + [N - N_0(T)]\frac{KT}{3m\omega_x^2}\frac{Q(3)}{Q(2)}, \qquad (10.63)$$

where

$$Q(c) = \int_0^\infty [s^c/(e^s - 1)]ds,$$

and similarly for $\langle y^2 \rangle$. The first term of equation (10.63) is the contribution to $\langle x^2 \rangle$ originating from the particles in the condensate, and scales as $1/\omega_x$. The second term is the contribution from the particles out of the condensate, and scales as $1/\omega_x^2$. Inserting result (10.63) into the expression (10.60) for the moment of inertia,

we find

$$\Theta = \epsilon_0^2 m \langle x^2 + y^2 \rangle_0 N_0(T) + m \langle x^2 + y^2 \rangle_{nc} [N - N_0(T)], \qquad (10.64)$$

where the indices at $\langle \ \rangle_0$ and $\langle \ \rangle_{nc}$ mean average over the condensate and non-condensate components, respectively, while ϵ_0 is the deformation parameter of the density of the condensate:

$$\epsilon_0 = \frac{\langle x^2 - y^2 \rangle_0}{\langle x^2 + y^2 \rangle_0}. \qquad (10.65)$$

ϵ_0 can also be written as $\epsilon_0 = (\omega_y - \omega_x)/(\omega_y + \omega_x)$. Equation (10.64) shows that for temperatures higher than the critical temperature T_c, where $N_0 = 0$, the moment of inertia takes the rigid (classical) value, while at $T = 0$, when all atoms are in the condensate, it takes the irrotational value. These results have been confirmed experimentally by Maragò et al. (2000), who studied the oscillations of a Boson gas in a magnetic trap, as excited by a sudden rotation of the confinement potential. At temperatures lower than the critical temperature, the condensate oscillates with only one frequency, which is in very good agreement with the hydrodynamic prediction (10.56). Moreover, it is possible to extract from the signal (Zambelli and Stringari 2001) a value of the moment of inertia $\Theta/\Theta_{rig} = 0.6$, which shows the superfluid nature of the system. At temperatures higher than the critical temperature, the same experiment evidences oscillations of the system at the two frequencies (10.57), and from the signal we derive a value of the moment of inertia equal to the rigid one.

10.1.5   *Vortices in the Bose gas in a magnetic trap*

In nonlinear regime, when the angular velocity of rotation Ω of the system becomes large, the term $-\Omega L_z$ may favor the creation of a vortex in the system. A vortex quantized along the z axis can be described by writing the order parameter in the form

$$\Psi(\mathbf{r}) = \Psi_v(r_\perp, z) e^{ik\psi}, \qquad (10.66)$$

where ψ is the angle around the z axis, k is an integer number, and $\Psi_v(r_\perp, z) = \sqrt{\rho(r_\perp, z)}$. The state of a vortex has a tangential velocity

$$v = \frac{\hbar}{mr_\perp} k. \qquad (10.67)$$

The number k is the quantum circulation, and the angular momentum along z is given by $\hbar N k$. The equation for $\Psi_v(r_\perp, z)$ is derived from the Gross–Pitaevskii equation (8.123), and includes a centrifugal-energy term which pushes the atoms
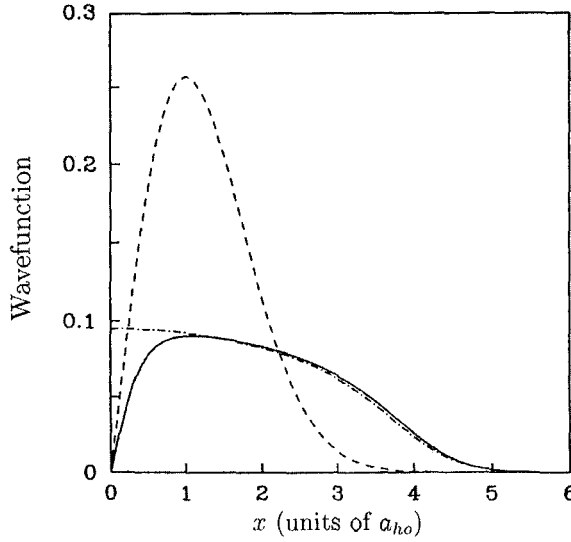
Fig. 10.1 Condensate with a vortex quantized along the z axis. The order parameter $\Psi_v(x,0,0)$ is plotted for a gas of 10^4 Rubidium atoms in a spherical trap with $a_{ho} = 0.791\ \mu m$. The dashed-dotted line is the solution without vortex; the full line is the profile of the solution of Eq. (10.68) with a vertex; the dashed line is the non-interacting solution of Eq. (10.69).

away from the rotation axis:

$$\left[-\frac{\hbar^2 \nabla^2}{2m} + \frac{\hbar^2 k^2}{2mr_\perp^2} + \frac{m}{2}(\omega_\perp r_\perp^2 + \omega_z^2 z^2) + g\Psi_v^2(r_\perp, z) \right] \Psi_v(r_\perp, z)$$

$$= \mu\Psi_v(r_\perp, z). \tag{10.68}$$

Due to such centrifugal term, the solution of equation (10.68) for $k \neq 0$ must vanish on the z axis. The solution $\Psi_v(x,0,0)$ of this equation (Dalfovo et al. 1999) for a gas of 10^4 Rubidium atoms in a spherical trap with $a_{ho} = 0.791\ \mu m$ and for $k = 1$, is plotted in Fig. 10.1, together with the solution without interaction. The latter is analytic and given by:

$$\Psi_v(r_\perp, z) \propto r_\perp e^{-\frac{m}{2\hbar}(\omega_\perp r_\perp^2 + \omega_z^2 z^2)}. \tag{10.69}$$

Thus, in the non-interacting case the vortex state is obtained by putting all atoms in the single-particle state with $m = 1$. Therefore, its energy is $N\hbar\omega_\perp$, plus the energy of the ground state. From the figure, it can be seen that the (repulsive) interaction significantly reduces the density as compared to the non-interacting case. The difference between the energy of the vortex state and that of the ground state, allows us to calculate the critical frequency needed to create a vortex. In fact, in a system rotating at angular frequency Ω, the energy of the system is $E - \Omega L_z$, where E and L_z are defined in the laboratory frame. For small Ω the energy is minimum without vortex. If Ω is large enough, the vortex state becomes favored because of

the term $-\Omega L_z$. The critical frequency turns out to be

$$\Omega_c = (\hbar k)^{-1}[(E/N)_k - (E/N)_0],\tag{10.70}$$

where E_k is the energy of the system with a vortex having angular momentum $\hbar N k$. Lundh, Pethick and Smith (1997) found for large N the following analytic expression for Ω_c:

$$\Omega_c = \frac{5\hbar}{2mR_\perp^2}\ln\frac{0.671R_\perp}{\xi},\tag{10.71}$$

where $R_\perp$ is the Thomas–Fermi radius of the density in the xy plane, which is perpendicular to the vortex line, and $\xi = (8\pi\rho a)^{-1/2}$ (with ρ central density of the gas with no vortex) is the healing length. The critical frequency turns out to be a fraction of the oscillator frequency, and shows a decreasing behaviour as a function of the number of atoms N.

The vortices in condensates have been generated and studied in several experiments (Matthews et al. 1999; Madison et al. 2000; Anderson et al. 2000). One of the most important effects of vortices is to change the frequencies of the collective modes of the condensate, and this can be measured with high precision. This can be easily seen by studying, for example, the m_2^- sum rule of equation (7.39) for the exact Hamiltonian of the system

$$H = \sum_{i=1}^{N}\left[\frac{p_i^2}{2m} + \frac{m}{2}(\omega_\perp r_\perp^2 + \omega_z^2 z^2)_i\right] + g\sum_{i<j}\delta(\mathbf{r}_i - \mathbf{r}_j),$$

and for the quadrupole operators

$$F = \sum_j (xz - izy)_j$$

and

$$G^\dagger = F^\dagger = \sum_j (xz + izy)_j.$$

One obtains the result

$$m_2^- = \frac{\hbar^3}{m^2}\langle L_z\rangle = \frac{\hbar^4}{m^2}Nk,\tag{10.72}$$

which shows that this sum rule is different from zero only in the presence of vortices. Zambelli and Stringari (1998) used the sum-rule approach to study the splitting of the oscillation frequencies of the quadrupole mode due to the presence of vortices in the condensate. Fetter and Svidzinsky (1998) studied the same problem using the hydrodynamic model. The same authors wrote a review paper (Fetter and Svidzinsky 2001) on the vortices in condensates in a magnetic trap.

10.2   The Fluidodynamic and Hydrodynamic Model for Fermions

Hydrodynamic equations for Fermions can be derived along the same line as done for the Bose systems by assuming that:

(i) All the single-particle orbitals evolve in time with a common complex phase as follows

$$\varphi_i(\mathbf{r}, t) = \psi_i(\mathbf{r}, t) e^{is(\mathbf{r}, t)} , \tag{10.73}$$

where both $\psi_i(\mathbf{r}, t)$ and $s(\mathbf{r}, t)$ are real functions;

(ii) The energy functional that describes the system is a functional $E = E(\rho)$ of the density ρ alone. This assumption implies the Thomas–Fermi approximation (4.14) for the kinetic energy density in $3D$, or the equivalent in $2D$:

$$\tau_{2D}(\rho) = \frac{\pi}{2m} \rho^2 . \tag{10.74}$$

Terms depending on the density derivatives can be added to the expression of $\tau(\rho)$ when necessary.

Then, the equations one derives are identical to equations (10.6)–(10.8). More-over, such equations can be easily generalized (Puente, Casas and Serra 2000) to include cases in which the (up and down) spin densities do not oscillate in phase, e.g. for the spin modes, or in which it is the isospin densities which do not oscillate in phase, as in nuclei.

Recently, these equations have been solved in the cases of metal clusters (Domps, Reinhard and Suraud 1998) and of quantum dots (Puente, Casas and Serra 2000),
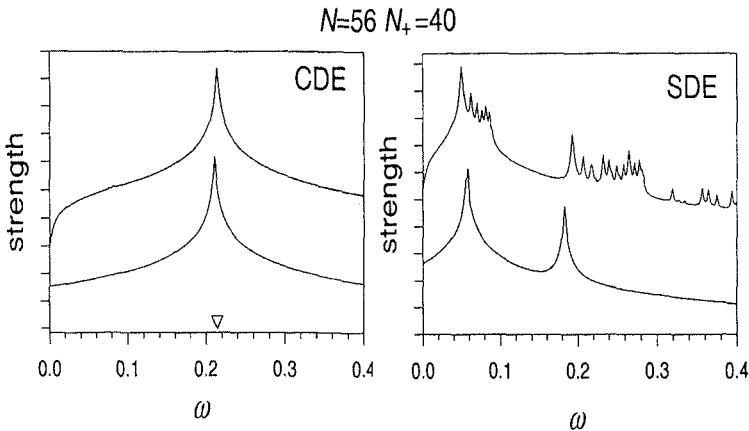
Fig. 10.2   Dipole excitation spectrum, in arbitrary logarithmic units, for density and spin-density excitations in a parabolic quantum dot with 56 electrons. The upper curve corresponds to the microscopic calculation in the *RPA* approximation, the lower one to the hydrodynamic calculation. In the CDE spectrum the triangle indicates the value of the frequency of the parabolic potential, ω_0. The Kohn theorem is evidently satisfied.

in order to study the (dipole) excitations with $\ell = 1$. In Fig. 10.2 we compare the results of such calculations for quantum dots, with microscopic calculations based on the RPA approximation. This comparison shows that in the case of dipolar excitations the hydrodynamic model works very well.

In general, the hydrodynamic model is expected to work well also in the monopole case ($\ell = 0$, compression mode), but not for all other excitation modes with $\ell > 1$. In fact, it is well known (Bertsch 1974, 1975) that Fermion can vibrate like an elastic medium. Such vibrations are characterized by the presence of non-diagonal terms in the stress tensor, which are absent in the hydrodynamic model. The presence of these components can be traced back microscopically to a typical quantum effect exhibited by the Fermi systems, viz. deformations of the Fermi surface characterized by higher than multipolarity 1 in momentum space during collective motion. Such deformations affect significantly the frequencies of elementary excitations of Fermi systems with multipolarity higher than 1. Typical elastic modes of the Fermi systems are the quadrupole mode and the scissor mode. The elastic component of the quadrupole mode for example, can also be verified in a simple way by considering a harmonic oscillator model, where the quadrupole excitation operator $Q = \sum_i r^2 Y_{2m}$ induces single-particle transitions with both $\Delta N = 0$ and $\Delta N = 2$. The excitations with $\Delta N = 0$ are the microscopic counterpart of the surface vibrations of the drop model discussed in Section 10.1.2 while those with $\Delta N = 2$ characterize a new class of excitations with no analogue in Bose systems. The restoring force related to these excitations is a pure elastic effect and is fixed by the Fermi energy, rather than by compressibility, and thus these modes are different from the compression modes discussed in Section 10.1.2.

The distortions of the Fermi surface with higher than multipolarity 1 are important in the bulk as well; for example, they are responsible for the difference between zero sound and first sound in ^{3}He.

In the following we will present the main characteristics of elastic vibrations of Fermi systems, using the generalized scaling model. The hydrodynamic model is obtained from the latter by just ignoring the terms related to the deformation of the Fermi surface in the derivation of the equations of motion. Moreover the generalized scaling model was developed in nuclear physics (Bertsch 1974, 1975; Brink and Leonardi 1976; Stringari 1977, 1983; Wong and McDonald 1977; Holzwart and Eckardt 1978, 1979; Lipparini and Stringari 1989) and in the study of metal clusters (Lipparini 1989; Lipparini and Stringari 1991).

In this model, one derives fluidodynamic equations of motion, looking for solutions of the time-dependent equations in the form of the following unitary transformation:

$$|\Psi\rangle = e^{im\sum_i \xi(\mathbf{r}_i, t) t_i} e^{i\frac{1}{2}\sum_i (\mathbf{u}(\mathbf{r}_i, t) \cdot \mathbf{p}_i + \mathbf{p}_i \cdot \mathbf{u}(\mathbf{r}_i, t)) t_i} |0\rangle \qquad (10.75)$$

which is applied to the ground state $|0\rangle$. In equation (10.75), $\mathbf{p}_i$ is the momentum operator which acts on the i-th particle, $\xi(\mathbf{r}, t)$ is interpreted as a velocity potential,

while $\mathbf{u}(\mathbf{r}, t)$ is the displacement field. t_i is equal to 1 for density excitations, and equal to the third component of the spin operator σ_z in the case of the spin-density excitations (i.e. 1 for Fermions with spin up, and -1 for Fermions with spin down), or to the third component of the isospin operator τ_z in the case of isospin-density excitations (i.e., 1 for neutrons and -1 for protons). If $|0\rangle$ is a Slater determinant then the state $|\Psi\rangle$ is a Slater determinant as well. The term in ξ introduces components which break the invariance under time-reversal in $|\Psi\rangle$, without affecting the density.

The transition density associated with the transformation (10.75) is given by

$$\rho_{tr}(\mathbf{r}, t) = \langle\Psi|\sum_i \delta(\mathbf{r} - \mathbf{r}_i)t_i|\Psi\rangle - \langle 0|\sum_i \delta(\mathbf{r} - \mathbf{r}_i)t_i|0\rangle$$

$$= \nabla(\mathbf{u}(\mathbf{r}, t)\rho_0(\mathbf{r})), \qquad (10.76)$$

where $\rho_0(\mathbf{r})$ is the ground state density. The velocity field is expressed through ξ as

$$\mathbf{v}(\mathbf{r}, t) = \frac{1}{\rho_0(\mathbf{r})}\langle\Psi|\frac{1}{2m}\sum_i(\delta(\mathbf{r} - \mathbf{r}_i)\mathbf{p}_i + h.c.)t_i|\Psi\rangle = \nabla\xi(\mathbf{r}, t), \qquad (10.77)$$

and is irrotational.

The fluidodynamic equations of motion can be derived using the variational principle as applied to the action integral: $\delta I = 0$, with

$$I = \int dt\langle\Psi|i\frac{\partial}{\partial t} - H|\Psi\rangle.$$

As we saw in Chapter 8, this method reproduces the $TDHF$ or $TDLDA$ equations if $|\Psi\rangle$ is the most general Slater determinant. As a result, using expression (10.75) for $|\Psi\rangle$, where $|0\rangle$ is a Slater determinant, we will derive approximate solutions of the $TDHF$ ($TDLDA$) theory. Moreover, we will study small oscillations around the ground state so that the found solution can be considered as an approximation of the RPA theory.

Keeping only terms quadratic in ξ and $\mathbf{u}$, and neglecting the total derivatives which do not appear in the equations of motion, we find:

$$\langle\Psi|i\frac{\partial}{\partial t}|\Psi\rangle = m\int \mathbf{u} \cdot \dot{\mathbf{v}}\rho_0 d\mathbf{r}, \qquad (10.78)$$

and

$$\langle\Psi|H|\Psi\rangle = \langle 0|H|0\rangle + E(\mathbf{u}) + T(\xi), \qquad (10.79)$$

where we have introduced the collective potential energy

$$E(\mathbf{u}) = \langle 0|e^{-i\frac{1}{2}\sum_i(\mathbf{u}\cdot\mathbf{p}_i + h.c.)t_i}He^{i\frac{1}{2}\sum_i(\mathbf{u}\cdot\mathbf{p}_i + h.c.)t_i}|0\rangle - \langle 0|H|0\rangle$$

$$= \frac{1}{2}\langle 0|\frac{1}{2}\left[\sum_i(\mathbf{u}\cdot\mathbf{p}_i + h.c.)t_i, \left[H, \frac{1}{2}\sum_i(\mathbf{u}\cdot\mathbf{p}_i + h.c.)t_i\right]\right]|0\rangle \qquad (10.80)$$

and the collective kinetic energy

$$T(\xi) = \langle 0|e^{-im\sum_i \xi t_i} H e^{im\sum_i \xi t_i}|0\rangle - \langle 0|H|0\rangle$$

$$= \frac{1}{2}m^2\langle 0|\left[\sum_i \xi t_i, \left[H, \sum_i \xi t_i\right]\right]|0\rangle. \qquad (10.81)$$

Note that the terms linear in **u** and ξ vanish due to the property of the ground state $\langle 0|[H, F]|0\rangle = 0$. Assuming that the interaction term in Hamiltonian H commutes with the local and scalar operator in spin (isospin) space $\sum_i \xi_i$, and that it contributes to the commutator with the vector operator (in spin or isospin space) $\sum_i \xi t_i$, through the term [in $k_v(\rho_0)$] which depends on density, we obtain the following result for $T(\xi)$:

$$T(\xi) = \frac{1}{2m}\int v^2 \rho_0 d\mathbf{r} \qquad \text{(scalar)}$$

$$(10.82)$$

$$T(\xi) = \frac{1}{2m}\int v^2(1 + k_v(\rho_0))\rho_0 d\mathbf{r} \qquad \text{(vector)}.$$

The term $k_v(\rho_0)$ originates from possible non-local components of the interaction such as the terms in a and a_1 of equation (4.95). In the case of the functional (4.95), we obtain $k_v(\rho_0) = 2m(a - a_1)\rho_0$. Note that for the local density functionals such as those which lead to the Kohn–Sham equations (4.44), we have $k_v = 0$.

Equation (10.82) shows that the collective kinetic energy depends on the scalar potential ξ only through the velocity field $\mathbf{v} = \nabla\xi$.

The equations of motion can subsequently be derived after performing the variation with respect to the displacement field **u** and the velocity field **v**:

$$\frac{\delta I}{\delta \mathbf{u}} = 0, \qquad \frac{\delta I}{\delta \mathbf{v}} = 0. \qquad (10.83)$$

For the scalar (s) and vector (v) modes, we find

$$\frac{\delta E_s}{\delta \mathbf{u}} = m\dot{\mathbf{v}}\rho_0, \quad \dot{\mathbf{u}} = -\mathbf{v}, \qquad (10.84)$$

and

$$\frac{\delta E_v}{\delta \mathbf{u}} = m\dot{\mathbf{v}}\rho_0, \quad \dot{\mathbf{u}} = -\mathbf{v}(1 + k_v(\rho_0)), \qquad (10.85)$$

respectively. Looking for solutions of the kind $\mathbf{u}(rt) = \mathbf{u}(r)U(t)$ which oscillating at frequency ω, we arrive at the fluidodynamic equations of motion

$$\frac{\delta E_s}{\delta \mathbf{u(r)}} = m\omega^2\mathbf{u(r)}\rho_0(\mathbf{r}), \qquad (10.86)$$

for the case of scalar excitations in spin (isospin) space, and

$$\frac{\delta E_v}{\delta \mathbf{u(r)}} = \frac{1}{1 + k_v(\rho_0)}m\omega^2\mathbf{u(r)}\rho_0(\mathbf{r}), \qquad (10.87)$$

for vector excitations in spin (isospin) space.

Furthermore, from (10.76), (10.84) and (10.85) it is possible to derive the continuity equations for the density $\rho = \rho_\uparrow + \rho_\downarrow$ ($\rho = \rho_n + \rho_p$, $n \equiv neutron$ and $p \equiv proton$), in the scalar case, and for the density $\rho_v = \rho_\uparrow - \rho_\downarrow$ ($\rho_v = \rho_n - \rho_p$) in the vector case (note that in Chapter 4, we indicated ρ_v as m in the case of spin density, and as ρ_1 in the case of the isovector density of nuclear physics).

Starting from a non-polarized system, i.e. one with $\rho_\uparrow^0 = \rho_\downarrow^0$ ($\rho_n^0 = \rho_p^0$), we obtain

$$\frac{\partial \rho}{\partial t} + \nabla(\mathbf{v}\rho_0) = 0\,, \tag{10.88}$$

for the scalar case, and

$$\frac{\partial \rho_v}{\partial t} + \nabla(\mathbf{v}(1 + k_v(\rho_0))\rho_0) = 0\,, \tag{10.89}$$

for the vector case.

In order to solve the fluidodynamic equations (10.86) and (10.87), it is necessary to specify the energy functional $E = \langle \Psi | H | \Psi \rangle$ and subsequently compute the collective potential energy $E(\mathbf{u})$ of equation (10.80). Starting from energy functionals such as those we used in Chapter 4 to compute $E(\mathbf{u})$, one needs to know the variations $\delta\rho$, $\delta\rho_v$ and $\delta\tau$, up to terms quadratic in $\mathbf{u}$, which are induced by the transformation (10.75). The general expressions of these variations, in both the scalar and vector cases, can be found in the paper by Stringari (1983), where the formalism of generalized scaling is applied to the study of collective modes (both compression and elastic ones) of nuclear physics. In the following, for the sake of simplicity, we will limit ourselves to treating the very interesting case of zero-divergence excitations, i.e. those characterized by

$$\nabla \cdot \mathbf{u} = 0\,. \tag{10.90}$$

These excitation modes can be obtained by taking

$$\mathbf{u} = \frac{1}{m_v}\nabla f\,, \tag{10.91}$$

where f characterizes the multipolar excitation operator

$$F = \sum_{i=1}^{N} f(\mathbf{r}_i)t_i = \sum_{i=1}^{N} r_i^\ell Y_{\ell,m}(\Omega_i)t_i\,.$$

Note that $m_v = m$ in the scalar case, and $m_v = m/(1 + k_v)$ in the vector case and for non-local interactions.

The choice (10.91) automatically leads to zero-divergence excitations with

$$\rho_{tr} = \frac{1}{m_v}\nabla f \cdot \nabla \rho_0\,,$$

because $\Delta r^\ell Y_{\ell,m} = 0$, and to the irrotational velocity fields

$$\mathbf{v} = -\dot{U}\mathbf{u} = -\dot{U}\frac{1}{m_v}\nabla f\,.$$

For zero-divergence excitations, the changes induced by transformation (10.75) on the densities ρ and ρ_v, and in the kinetic-energy density τ, are given by:

$$\delta\rho = u_k\nabla_k\rho_0 + \frac{1}{2}u_k\nabla_k u_l\nabla_l\rho_0, \qquad \delta\rho_v = 0\,,$$

$$\delta\tau = u_k\nabla_k\tau_0 + \frac{1}{2}u_k\nabla_k u_l\nabla_l\tau_0 + \frac{1}{6}(\nabla_k u_l + \nabla_l u_k)^2\tau_0\,, \tag{10.92}$$

for scalar excitations $(t_i = 1)$, and by

$$\delta\rho = \frac{1}{2}u_k\nabla_k u_l\nabla_l\rho_0\,, \quad \delta\rho_v = u_k\nabla_k\rho_0\,,$$

$$\delta\tau = \frac{1}{2}u_k\nabla_k u_l\nabla_l\tau_0 + \frac{1}{6}(\nabla_k u_l + \nabla_l u_k)^2\tau_0\,, \tag{10.93}$$

for vector excitations $(t_i = \sigma_i^z$ or $\tau_i^z)$.

From these expression, we see that the density-variations of the zero divergence excitation modes have surface terms which are proportional to the derivatives of the density ρ_0 and the kinetic energy density τ_0 of the ground state, as well as bulk terms (which appear only in the kinetic energy variation) in which the derivatives act only on the displacement fields. In homogeneous systems, the collective potential energy gets contribution only from the variation of kinetic energy, and the corresponding excitation modes are of the elastic type. In fact, in this case we find

$$E(\mathbf{u}) = \frac{1}{10}\epsilon_F\int\left(\sum_{k,l}(\nabla_k u_l + \nabla_l u_k)^2\right)\rho_0 d\mathbf{r}\,, \tag{10.94}$$

which holds both for the scalar and vector case, and is non-vanishing only for $\ell \geq 2$. The collective potential energy (10.94) has the same form as the transverse force contribution to the energy of an elastic medium with elastic Lamè constant given by $2/5\epsilon_F\rho_0$ (where ϵ_F is the Fermi energy). Therefore, the Fermi energy is the main ingredient of the restoring force of the elastic-like oscillation modes.

On the contrary, the compression modes are modes of hydrodynamic nature, and characterized by the fact that the divergence of $\mathbf{u}$ is different from zero. Therefore, in order to derive the hydrodynamic model from the equations of generalized scaling, it is necessary to consider the most general transformations which lead to transition densities such as (10.76). For a detailed discussion of this derivation, see Stringari (1983). Here we limit ourselves to remarking that, unlike the general case, the hydrodynamic model assumes the Thomas–Fermi relation $[\tau = (3/5)(3\pi^2/2)^{2/3}\rho^{5/3}$, in $3D]$ as a functional relation for the kinetic energy density τ, and subsequently calculates the variations of τ starting from the variations of the density ρ. In this

way, one neglects the distortions caused by the transformation (10.75) on the Fermi sphere (Jennings 1980), which are responsible for the elastic contribution. For these compression modes, the main ingredient that appears in the restoring force $E(\mathbf{u})$ of the oscillation is not the Fermi energy. Rather it is the compressibility for the case of scalar excitations, the symmetry energy of nuclear matter for the vector isospin excitations, and the magnetization energy for the spin-density excitations.

In non-homogeneous systems, we have $\nabla\rho_0 \neq 0$ and $\nabla\tau_0 \neq 0$, and hence one will obtain collective potential energies which include both surface and elastic contributions. The surface terms are the only ones that remain in the dipolar case with $\ell = 1$. Therefore, the zero-divergence dipolar mode is purely a surface mode. It characterizes the giant resonances of nuclei, as well as the plasmon modes of confined and finite electron systems, such as metal clusters and quantum dots.

The choice (10.90) is particularly suited for studying very narrow resonances of finite systems, which exhaust most of the excitation strength. In fact, the transition density $\rho_{tr} = \nabla f \cdot \nabla\rho_0/m_v$ and the irrotational velocity fields $\mathbf{v} = -\dot{U}\mathbf{u} = -\dot{U}(1/m_v)\nabla f$ can be obtained microscopically by assuming that a single collective state exhausts the mixed sum rules for the density operator

$$\hat{\rho} = \sum_{i=1}^{N} \delta(\mathbf{r} - \mathbf{r}_i)t_i \,,$$

and for the current operator $\hat{\mathbf{J}} = (1/2m)\sum_{i=1}^{N}(\mathbf{p}_i\delta(\mathbf{r} - \mathbf{r}_i) + h.c.)t_i$, namely

$$\sum_n \omega_{n0}\langle 0|F|n\rangle\langle n|\hat{\rho}|0\rangle = \frac{1}{2}\langle 0|[F,[H,\hat{\rho}]]|0\rangle = -\frac{1}{2m_v}\nabla f \cdot \nabla\rho_0 \,, \qquad (10.95)$$

and

$$\sum_n (\langle 0|F|n\rangle\langle n|\hat{\mathbf{J}}|0\rangle - \langle 0|\hat{\mathbf{J}}|n\rangle\langle n|F|0\rangle) = \frac{1}{2}\langle 0|[F,\hat{\mathbf{J}}]|0\rangle = -\frac{i}{2m_v}\rho_0\nabla f \,, \qquad (10.96)$$

where we recall that $m_v = m$ for scalar excitations ($t_i = 1$), and $m_v = m/(1+k_v)$ for vector excitations ($t_i = \sigma_i^z$ or $t_i = \tau_i^z$) and interactions with non-local components.

In this case, the collective energy

$$E_{coll} = \frac{1}{2}\dot{U}^2 \int u^2(\mathbf{r})\rho_0 \, d\mathbf{r} + \frac{1}{2}K(\mathbf{u})U^2 \,, \qquad (10.97)$$

with the restoring constant K given by $K(\mathbf{u}) = 2E(\mathbf{u})$ determines the energy of the one and only collective mode through the expression

$$\omega = \sqrt{\frac{K}{M}} = \sqrt{\frac{2E(\mathbf{u})}{\int(\frac{1}{m_v}\nabla f)^2\rho_0 d\mathbf{r}}} \,. \qquad (10.98)$$

This energy can be interpreted as the ratio $\sqrt{m_3/m_1}$ between the sum rule cubic in energy m_3 and the f-sum rule m_1 of (7.30). In fact, for the excitation operator

$$F = \sum_{i=1}^{N} f(\mathbf{r}_i) t_i = \sum_{i=1}^{N} r_i^{\ell} Y_{\ell,m}(\Omega_i) t_i \,,$$

the following commutation rule holds

$$[H, F] = -\frac{1}{2} \sum_{i=1}^{N} \frac{1}{m_v} (\nabla f \cdot \nabla + \nabla \cdot \nabla f)_i t_i = -\frac{1}{2} \sum_{i=1}^{N} (\mathbf{u} \cdot \nabla + \nabla \cdot \mathbf{u})_i t_i \quad (10.99)$$

so that the transformation $e^{i\frac{1}{2} U(t) \sum_i (\mathbf{u}(\mathbf{r}_i) \cdot \mathbf{p}_i + \mathbf{p}_i \cdot \mathbf{u}(\mathbf{r}_i)) t_i} |0\rangle$ of equation (10.75), can be rewritten as $e^{-U(t)[H,F]} |0\rangle$. The collective potential energy (10.80) then becomes

$$E(\mathbf{u}) = 1/2 \langle 0 | [[[F, H], H], [H, F]] | 0 \rangle \,,$$

and coincides with the sum rule cubic in energy m_3. The f-sum rule for the operator F can be easily computed and leads to the result

$$m_1 = \frac{1}{2} \langle 0 | [F, [H, F]] | 0 \rangle = \frac{1}{2} \int \left(\frac{1}{m_v} \nabla f \right)^2 \rho_0 dr \,, \quad (10.100)$$

and hence to

$$\frac{K}{M} = \frac{m_3}{m_1} \quad (10.101)$$

by comparison with (10.98).

As regards the connection with the sum rules, in general it can be said that both the elastic and the hydrodynamic models well reproduce the f-sum rule m_1; moreover, the elastic model correctly reproduces the sum rule cubic in energy which, however, is not reproduced by the hydrodynamic model. On the contrary, the inversely energy-weighed sum rule, which is related to the static polarizability of the system, is better reproduced by the hydrodynamic model. The latter result stems from the Landau theory of Fermi liquids, which shows that the spherical shape of the Fermi sphere is preserved in the presence of a static external field, and as a consequence the linear response is correctly predicted by the hydrodynamic model in the static limit. As was discussed in Section 8.1, the first sound is a compression mode of hydrodynamic nature, whose frequency is well reproduced by the ratio m_1/m_{-1}, while the zero sound at higher frequency is a mode of elastic nature, in which the distortion of the Fermi sphere plays a crucial role, and whose frequency is well reproduced by the ratio m_3/m_1. In the following, we will analyze in detail the frequencies of some collective surface and elastic modes by using the m_3/m_1 ratio.

10.2.1 Dipolar modes in metal clusters

In metal clusters described by the Hamiltonian (2.22), the zero-divergence dipolar mode with $\ell = 1$ and $m = 0$ is naturally excited by the operator $F = \sum_i z_i t_i$, where z_i is the z component of the position operator of the i-th electron. Therefore, we have $f(\mathbf{r}) = z$ and $\mathbf{u} = \nabla z$, and the transformation that determines the restoring force (10.80) of the collective mode becomes

$$e^{U(t) \sum_{i=1}^{N} \nabla_z^i t_i} |0\rangle . \tag{10.102}$$

Physically this transformation corresponds in the scalar case ($t_i = 1$) to a rigid shift of the whole electron cloud, and in the vector case ($t_i = \sigma_i^z$) to a rigid shift of the cloud of electrons with spin up in opposite direction with respect to the electrons with spin down.

In the scalar case, due to translational invariance, the only term of Hamiltonian (2.22) which contributes to the collective potential energy, and thus to m_3, is the confinement potential of the ions, which breaks such invariance through the inter-action term $\int V_+(\mathbf{r})\rho(\mathbf{r})d(\mathbf{r})$ with the electrons. The second-order variation in $\mathbf{u}$ of such energy is due to the second-order variation of the electron density, which is given by $1/2\nabla_z^2\rho_0$ [see Eq. (10.92)]. Therefore, we obtain

$$E_s(\mathbf{u}) = m_3^s = \frac{1}{2} \int V_+(\mathbf{r})\nabla_z^2\rho_0(\mathbf{r}) \, d\mathbf{r} . \tag{10.103}$$

Performing an integration by parts and using the Poisson equation $\nabla^2 V_+ = 4\pi\rho_I$, where ρ_I is the ion charge-density distribution, we obtain (Brack 1989):

$$E_s(\mathbf{u}) = m_3^s = \frac{1}{2} \int \rho_I(\mathbf{r})\rho_0(\mathbf{r})d\mathbf{r} . \tag{10.104}$$

For a jellium sphere [see Eq. (2.21)], we then have

$$E(\mathbf{u}) = m_3^s = \frac{1}{2}\rho_{bulk} \int_0^R \rho_0(\mathbf{r})dr = \frac{1}{2}\rho_{bulk}N_{in} , \tag{10.105}$$

where N_{in} is the number of electrons inside the jellium sphere of radius R. The m_1 sum rule is model independent and, in both the scalar and vector models, it is given by [see Eq. (10.100)]

$$m_1 = \frac{N}{2} , \tag{10.106}$$

where N is the total number of electrons. Therefore, the energy of the scalar plasmon mode is given by

$$\omega_s = \sqrt{\frac{m_3^s}{m_1}} = \frac{\omega_p}{\sqrt{3}}\sqrt{\frac{N_{in}}{N}} , \tag{10.107}$$

where we have introduced the plasma frequency $\omega_p = \sqrt{4\pi\rho_{bulk}}$ which gives the plasmon energy in metals. As can be seen, the finite-size effects are relevant, and
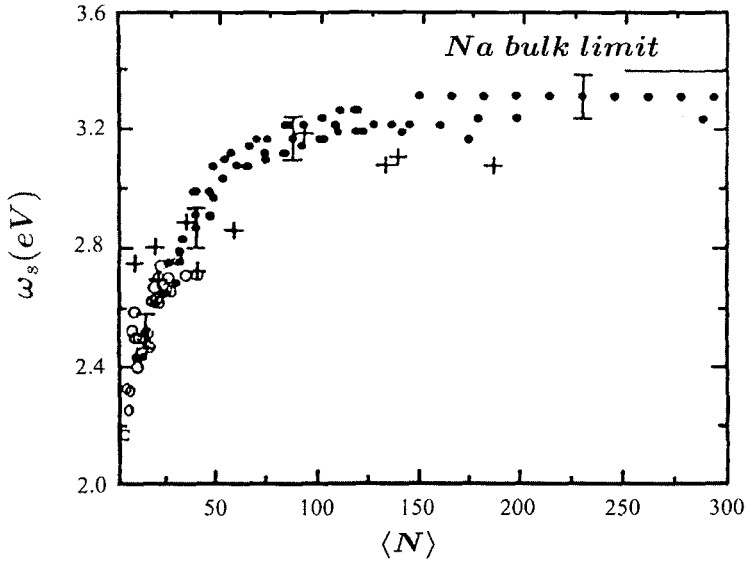
Fig. 10.3 Plasmon resonance frequency as a function of the average number of atoms, $\langle N \rangle$, in sodium clusters. The experimental data of Knight et al. (1985) (full circles) are compared with the result of Eq. (10.107) (open circles), and with the calculations of Beck (1984) (crosses).

strongly reduce the energy of the plasmon mode in metal clusters with respect to the bulk frequency. The expression (10.107) reproduces quite well the systematic variation with N in the experimental data of Knight et al. (1985) for the plasma resonance in Sodium clusters, as shown in Fig. 10.3.

In the vector case, the calculation of m_3 is somewhat more complex because the interaction contributes to the sum rule. One finds

$$E_v(\mathbf{u}) = m_3^v = \frac{1}{2}\langle 0| \left[\sum_{i=1}^{N} \nabla_z^i \sigma_i^z, \left[\sum_{i=k}^{N} \nabla_z^k \sigma_k^z, H\right]\right] |0\rangle,\qquad (10.108)$$

and expanding the commutator

$$m_3^v = \frac{2\pi}{3}\langle 0| \sum_{i=1}^{N} \rho_I(\mathbf{r}_i) - \sum_{i<j=1}^{N} \delta(r_{ij})(\sigma_i^z - \sigma_j^z)^2 |0\rangle,\qquad (10.109)$$

where, again, we have used the Poisson equation for the ion charge distribution, and the property $\nabla^2(1/r) = -4\pi\delta(r)$. Therefore, the final result for m_3^v is

$$m_3^v = \frac{2\pi}{3}\int (\rho_I(\mathbf{r})\rho_0(\mathbf{r}) - \rho_0(\mathbf{r})^2)d\mathbf{r}.\qquad (10.110)$$

An estimate of m_3^v can be carried out using the Wood-Saxon density: $\rho_0 = \rho_b(1 + \exp((r - R)/a))^{-1}$ for ρ_0, and that of a jellium for $\rho_I(\mathbf{r})$. In this way we get

$$m_3^v \simeq 2\pi N \rho_b \frac{a}{R}, \tag{10.111}$$

and using the result (10.106) for m_1:

$$\omega_v = \sqrt{\frac{m_3^v}{m_1}} = \omega_p \sqrt{\frac{a}{R}}, \tag{10.112}$$

which shows that the vector dipole mode is a pure surface mode whose energy is always lower than that of the scalar mode. Vector surface modes of this kind have been measured in the case of quantum dots (Schuller et al. 1998).

10.2.2 The scalar quadrupole mode in confined systems

In what follows, we shall calculate the frequency of the scalar quadrupole mode, which is excited by the operator

$$Q = \sum_{i=1}^{N} r_i^2 Y_{2m}, $$

for a system whose local energy functional is of the same type as in (4.27):

$$E(\rho) = T + \int d\mathbf{r} \rho(r) \left[V_{\text{conf}}(r) + \frac{1}{2} U(r) \right] + E_V(\rho), \tag{10.113}$$

where $U(r)$ is the Hartree potential, V_{conf} is the potential of the positive-charge distribution generated by the ions, and $E_V(\rho)$ is the exchange-correlation energy. However, the functional can also describe the Boson gas in a magnetic trap by taking for V_{conf} a harmonic oscillator potential, $U = 0$ and

$$E_V(\rho) = (1/2)g \int d\mathbf{r} \rho^2(r), $$

as well as other Fermionic systems.

The energy change connected with the transformation $e^{-U(t)[H,Q]}|0\rangle$, can be easily computed, and one finds a very simple expression for $m_3(Q)$ (Bohigas, Lane and Martorell 1979):

$$m_3(Q) = \frac{5}{\pi m^2}(E_{\text{kin}} + E_X). \tag{10.114}$$

In the above equation, E_{kin} is the expectation value of the kinetic energy operator in the ground state. E_X caters for other forms of energy. It is equal to $-E_C/5 + E_{\text{conf}}$ for charged systems (where E_C is the direct electron–electron Coulomb energy). It is the confinement energy of the harmonic oscillator in the case the Boson gas in a parabolic magnetic trap, and is zero for the other systems such as nuclei.

The m_1 sum rule for the quadrupole operator is then given by:

$$m_1(Q) = \frac{5}{4\pi m}N\langle r^2\rangle\,,\qquad (10.115)$$

where

$$\langle r^2\rangle = 1/N \int r^2 \rho_0 d\mathbf{r}$$

is the mean square radius of the system. Therefore, the frequency of the quadrupole scalar model in the elastic model is given by

$$\omega_Q = \sqrt{\frac{m_3(Q)}{m_1(Q)}} = \sqrt{\frac{4(E_{\text{kin}} + E_X)}{mN\langle r^2\rangle}}\,.\qquad (10.116)$$

In the non-interacting system one has $E(X) = E_{\text{conf}}$ and $E_{\text{kin}} = E_{\text{conf}}$ from the virial theorem, and equation (10.116) yields the result $\omega_Q = \sqrt{8E_{\text{conf}}/mN\langle r^2\rangle}$ which, in the case of parabolic confinement, becomes the result of the harmonic oscillator $\omega_Q = 2\omega_{ho}$. For a Boson gas in a magnetic trap, and in the Thomas–Fermi limit $Na/a_{ho} \gg 1$ where the kinetic energy term is negligible, one then obtains $\omega_Q = \sqrt{2}\omega_{ho}$. For negative a, when the kinetic energy term is greater than E_{conf}, there is an increase of the quadrupole frequency with respect to that of the harmonic oscillator. Furthermore, for a charged system with a jellium confinement, neglecting the electron spill-out, we have $E(X) = (9/50)e^2(N^2/R)$. Finally, in the nuclear case (where $V_{\text{conf}} = E_{\text{conf}} = 0$), we obtain $\omega_Q = \sqrt{4E_{\text{kin}}/mN\langle r^2\rangle}$. All of these results turn out to be very close to the numerical solutions of the *RPA* equations of the respective systems.

10.2.3 *The scissors mode in Fermi systems*

A good example of elastic behaviour in Fermi systems is the scissor mode in systems with non-zero deformation. We have previously discussed such mode for the Boson gas in an unsymmetrical magnetic trap.

A macroscopic example of such state is provided by the following form of the displacement field relative to the electron motion in the case of metal clusters or of quantum dots, and to nucleons in the case of atomic nuclei (Lipparini and Stringari 1989, 1991; Serra, Puente and Lipparini 1999):

$$\mathbf{u} = \hat{\omega} \times \mathbf{r} + \delta\nabla(yz)\,,\qquad (10.117)$$

which satisfies the condition $\nabla \cdot \mathbf{u} = 0$. In equation (10.117), $\hat{\omega}$ is the unit vector in the x direction (the system is assumed to be axially deformed along z), and $\delta = (3/2)(R_z^2 - R_y^2)/(R_z^2 + 2R_y^2)$ in 3D, while $\delta = (R_z^2 - R_y^2)/(R_z^2 + R_y^2)$ in 2D (where the Fermion motion is in the yz plane). This δ is the deformation of the density profile, which is assumed to have spheroidal shape: $\rho_0 = \rho_0(x^2/R_x^2 + y^2/R_y^2 + z^2/R_z^2)$ in 3D

(a) **(b)**
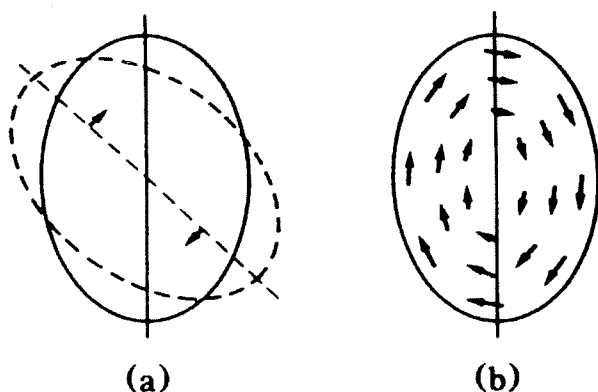
Fig. 10.4 Displacement field for the rotational state $M1$ at low energy. Figure 10.4(a) corresponds to a rigid rotation (scissor mode) of the Fermions with respect to the confinement field. Figure 10.4(b) corresponds to a rotation within a rigid surface.

(here R_z and $R_x = R_y$ are the radii parallel and perpendicular to the symmetry axis, respectively).

The term $\hat{\omega} \times \mathbf{r}$ of equation (10.117), in the scalar case and for metal clusters and quantum dots, corresponds to a rigid rotation of the electrons with respect to the distribution of positive charge which is motionless. In the vector case $(t_i = \tau_i^z)$, and for nuclei, it corresponds to a rigid, counter-phase rotation of protons and neutrons, as follows from transformation (10.80), which becomes

$$e^{U(t)\sum_{i=1}^{N} l_i^x t_i}|0\rangle,\tag{10.118}$$

where l_i^x is the x component of the orbital angular momentum of the i-th Fermion (scissor mode, see Fig. 10.4(a)). If we were to include only this term in the Fermion motion, the electrons would feel a restoring force whose origin would be the Coulomb interaction with the ions, as happens in the dipole case, and the nucleons would be subjected to the force resulting from the neutron–proton interaction (symmetry term, proportional to $\rho_v^2 = (\rho_n - \rho_p)^2$). However, the Coulomb and symmetry energy cost is minimized by including the quadrupole term $\nabla(yz)$ in the displacement field. This can be seen easily by noting that the density change $\delta\rho$ and $\delta\rho_v$ given in both cases by $\nabla \cdot (\mathbf{u}\rho_0)$ [see Eq. (10.76)], becomes zero under (10.117) because $\mathbf{u} \cdot \nabla\rho_0 = 0$ in the spheroidal model. The resulting motion is shown in Fig. 10.4(b): there is a rotation within a spheroid with rigid surface (in the nuclear case, the rotations of neutrons and protons have opposite phases) with a velocity field such that

$$\mathbf{v} \cdot \mathbf{n}|_{\text{surface}} = 0.\tag{10.119}$$

The relevant restoring force that originates during this motion is not derived from the electron–ion or neutron–proton interaction energy, but rather from the kinetic energy, and is produced by the quadrupolar component $\nabla(yz)$ of the velocity

field which gives rise to a distortion of the Fermi sphere and to a collective potential energy of the type (10.94). The frequency of the resulting elastic mode is given by $\omega_{M1} = (K/M)^{1/2}$ where $K = 2E(\mathbf{u})$, with $E(\mathbf{u})$ given by equation (10.94), and $M = m \int \rho \mathbf{u}^2 d\mathbf{r}$ which in the limit of small deformations coincides with the rigid value of the moment of inertia θ of the rotational motion. In this limit, one finds:

$$\omega_{M1} = \delta \sqrt{\frac{4\epsilon_F}{mr_s^2}} N^{-1/3}, \quad \langle r \rangle^2 = \frac{3}{5} r_s^2 N^{2/3}, \tag{10.120}$$

in $3D$, and

$$\omega_{M1} = \delta \sqrt{\frac{16\epsilon_F}{3mr_s^2}} N^{-1/2}, \quad \langle r \rangle^2 = r_s^2 N/2, \tag{10.121}$$

in $2D$. The elastic mode, whose frequency is given by the above expressions, is a low-energy mode with respect to the quadrupole mode we studied in the previous Section, which goes to zero linearly with the deformation, and is the analogue of the low-energy mode of (10.57) for the Boson gas in a magnetic trap.

For sodium clusters ($r_s = 4$ a.u., $\epsilon_F = 3.1$ eV), $\omega_{M1} = \delta$ 4.6 $N^{-1/3}$ eV, which for N in the range 10–100 and for typical deformations $\delta = 0.2 - 0.4$, gives $\omega_{M1} = 0.2 - 0.6$ eV. This value should be compared with the dipolar plasmon frequency $\omega_s = 3.4$ eV. The scissor state lies below the threshold for particle emission, and is excited by the orbital angular momentum operator, with a strength given by

$$BM1 = \sum_k |\langle 0| \sum_{i=1}^{N} l_i^k |M1 \rangle|^2 = \frac{4}{5} \mu_0^2 \delta \sqrt{\epsilon_F r_s^2} N^{4/3}, \tag{10.122}$$

where $\mu_0 = e\hbar/2mc$ is the Bohr magneton.

For quantum dots, the scissor mode has been studied microscopically by solving the time-dependent Kohn–Sham equations, with different initial conditions corresponding to a pure rotation, a pure quadrupole distortion, and to a combination of the two. The results relative to the time-evolution of an elliptic quantum dot with 20 electrons, $r_s = 1.51$ (effective a.u.) and $\delta = 0.28$, are shown in Fig. 10.5 (Serra, Puente and Lipparini 1999). From this figure, we see that two states are excited: the scissor mode at low energy, and the scalar quadrupole mode at high energy. The elastic macroscopic model reproduces the energies of the microscopic calculation to a very good extent.

Experimental evidence is still lacking for the existence of such excitation modes for both the metal clusters and quantum dots. On the other hand, there are many experimental results in the nuclear case, where the existence of the scissor mode has been verified in a systematic way in deformed nuclei (Bohle et al. 1984). A recent experimental analysis (Enders et al. 1999) showed that the energies of the low-energy mode, as well as the excitation strength M1, are well reproduced using the moment of inertia and the gyromagnetic factors of the rotational band of the
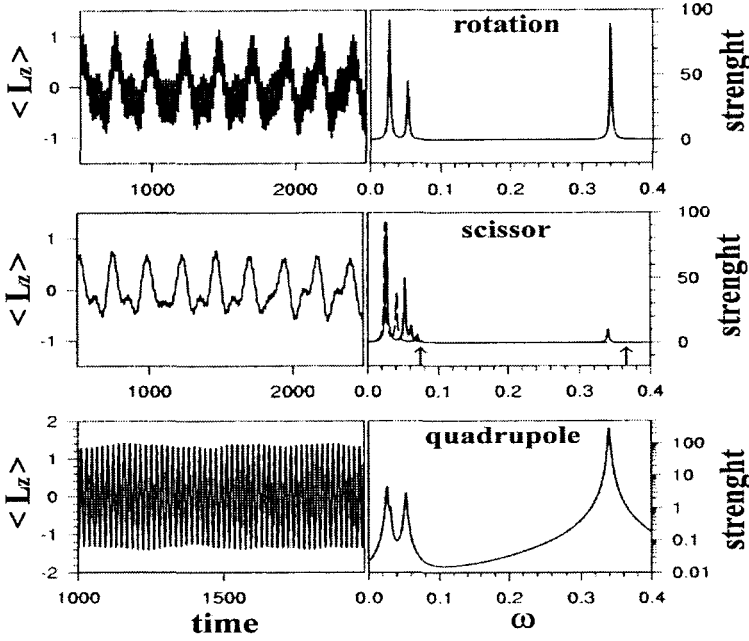
Fig. 10.5 Time evolution of an elliptic dot with 20 electrons, with three different kinds of initial conditions: pure rotation, pure quadrupolar distortion (quadrupole), and a combination of the two (scissor). The left-hand panels show the M1 signal as a function of time, while the right-hand ones show the corresponding excitation strengths in arbitrary units. The midde right-hand panel also shows the strength without interaction effects (dashed line) as well as the predictions of the elastic model for the scissor and quadrupole modes (arrows).

ground state. Such values of the moment of inertia are smaller than the rigid value, and so the analysis shows that only some of the nucleons participate in the rotational motion.

10.2.4 *The moment of inertia of quantum dots*

The quantum evaluation of the moment of inertia of a Fermion system, like electrons confined in an elliptic quantum dot, is not a trivial task and requires, for example in the framework of the density functional theory, the solution of the Kohn–Sham equations with an angular-momentum constraint (Serra, Puente and Lipparini 2002):

$$[h_\sigma(\rho, m) - \Omega\ell_z]\varphi_\sigma(\mathbf{r}; \Omega) = \epsilon_\sigma(\Omega)\varphi_\sigma(\mathbf{r}; \Omega), \qquad (10.123)$$

where ℓ_z is the z component of the orbital angular momentum of the individual electron, $\sigma = \uparrow, \downarrow$ is the spin label, and the densities and magnetization are given, respectively, by $\rho = \rho_\uparrow + \rho_\downarrow$ and $m = \rho_\uparrow - \rho_\downarrow$, where

$$\rho_\sigma = \sum_i |\varphi_{i\sigma}(\mathbf{r}; \Omega)|^2.$$

Besides the kinetic energy term, the single-particle Hamiltonian h_σ in (10.123) includes the confinement potential

$$v_{\text{conf}}(\mathbf{r}) = 1/2(\omega_x^2 x^2 + \omega_y^2 y^2)\,,$$

the Hartree potential

$$v^H(\mathbf{r}) = \int d\mathbf{r}' \rho(\mathbf{r}')/|\mathbf{r} - \mathbf{r}'|\,,$$

and the exchange-correlation potential

$$v_\sigma^{xc}(\mathbf{r}) = \partial \mathcal{E}_{xc}(\rho, m)/\partial \rho_\sigma\,.$$

The Kohn–Sham equations can be solved by subdividing the x-y plane into a discrete uniform grid of points, and subsequently using the methods described in detail, for example, by Puente and Serra (1999). The moment of inertia is then computed using (10.43), where the average is taken on the Slater determinant constructed by means of the solutions $\varphi_\sigma(\mathbf{r}; \Omega)$ of equation (10.123). The results are plotted in Fig. 10.6, together with those of the non-interacting model given by (10.60), as a function of the deformation $\beta = \omega_y/\omega_x$. The average parameter of the harmonic oscillator, i.e. $\omega_0 = (\omega_x + \omega_y)/2$, is determined by $\omega_0^2 = 1/r_s^3 \sqrt{N}$. In these figures, we note that there are some small oscillations at large values of the deformation, which are due to deformation shell effects; there are also some large oscillations at small values of the
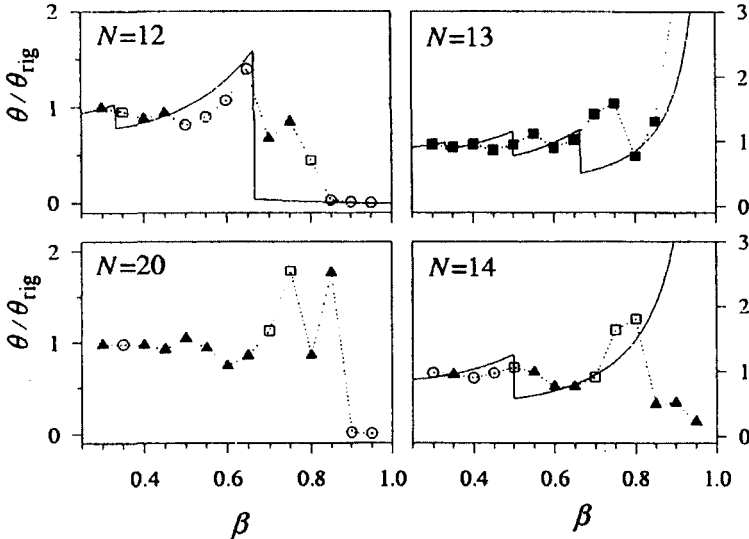
Fig. 10.6   Results for the θ/θ_{rig} ratio in elliptic quantum dots, with different numbers of electrons (N), as a function of the deformation parameter β, and for $r_s = 1.5$. Full lines are the results of the harmonic oscillator without interaction, the symbols are the $LSDA$ results. Different symbols refer to different values of the total ground-state spin: open circle ($S_z = 0$), open square (0 with spin wave), full square (1/2), full triangle (1).

deformation (β close to unity) in the closed-shell dots (12,20), and some divergences in the open-shell dots (13,14), that are cured by the interaction only for $N = 14$. The large oscillations at small deformation are related to the emergence, with the deformation, of spin waves in the ground state, while the divergences reflect the vanishing of the excited-state energies in the denominator of (10.50) for the open-shell dots, which in some cases are not cured by the interaction. These effects might be investigated experimentally by studying the diamagnetic susceptibility of the dot which is given by (see Section 7.6):

$$\chi_D = -\frac{e^2}{4m^2c^2}\Theta_{rig}\left(1 - \frac{\Theta}{\Theta_{rig}}\right).$$
(10.124)

Another possibility of studying the moment of inertia of Fermion systems, is provided by its connection with the excitation, and in particular with the scissor mode. In Fig. 10.7 we show the evolution of the strength M1 with the deformation for $N = 13$ and 20. The orbital strength M1 is clearly separated into two regions; a high-energy one, related to the quadrupole, and a low-energy one related to the scissor mode. For intermediate values of deformation ($0.5 < \beta < 0.7$), the strength is shared by the two coexisting modes, while at high and low deformations it is practically exhausted by only one mode. For large deformations the quadrupole mode survives, while for $\beta \to 1$ the dominant mode depends on θ. For systems
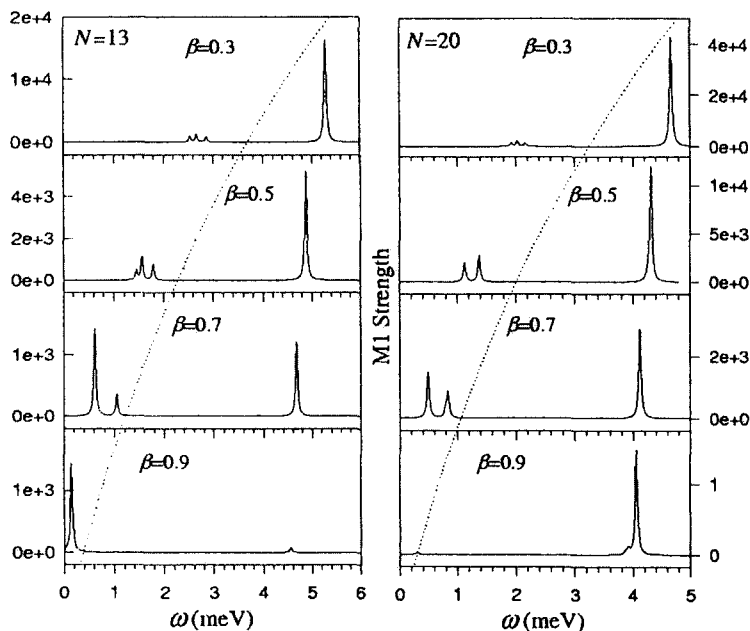
Fig. 10.7 Evolution of the strengths M1 with the deformation for $r_s = 1.5$, $N = 13, 20$. The dashed lines, at the intersection with the base line of each spectrum, indicate the energy ω_- in the harmonic oscillator model, while ω_+ is 6.8 meV for $N = 13$, and 6.1 meV for $N = 20$.
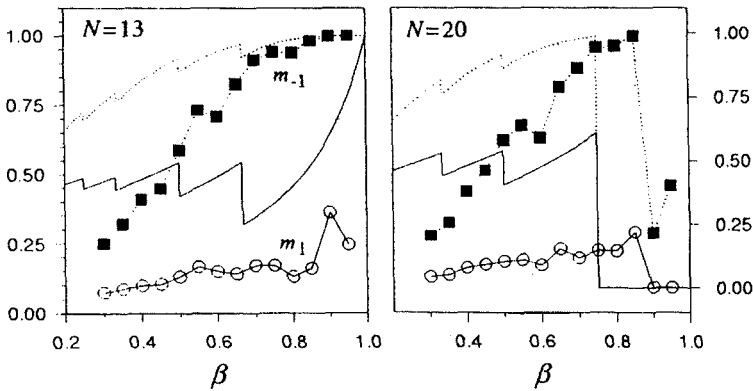
Fig. 10.8 Fractional contribution of the scissor mode to the $m_1(L_z)$ sum rule in the harmonic oscillator model (full line), and in the $LSDA$ theory (open circles connected by a full line). Also shown is the contribution to $m_{-1}(L_z)$ in the harmonic oscillator (dotted line) and in $LSDA$ (full squares connected by a dotted line).

with divergent moment of inertia, the dominant mode is the scissor mode, while for vanishing moment of inertia the dominant mode is the quadrupole one. The figure also shows that the interaction lowers the energy of the scissor mode when compared to the prediction of the harmonic oscillator (10.57). The fractional contribution of the scissor mode to $m_{-1} = \theta/2$ and to the energy-weighed sum rule (10.53) is shown in Fig. 10.8. This figure shows quantitatively the contribution of the scissor mode to the moment of inertia in the $LSDA$ theory (squares), and in the harmonic oscillator (dotted line). At large deformations, we observe an appreciable decrease of such contribution due to interaction.

10.2.5   *The vibrating potential model*

As discussed several times, the study of collective vibration modes such as the surface and elastic ones which were described previously by using sum-rule techniques, is carried out in a natural way within the framework of time-dependent, self-consistent theories such as the $TDLDA$ theory of Section 8.9. These methods, are based on the study of the variations of the average one-body potential, induced by a density oscillation. These average-potential variations produce excited states of the system, and one obtains a self-sustained collective mode, if the induced density-variations are equal to the ones required to generate the oscillatory potential.

In the present Section we will study an approximate solution of the problem, which corresponds to a first iteration of the fully self-consistent calculation. This method is known as the vibrating potential model (Rowe 1970), and in homogeneous systems (where the translational invariance determines the pattern of density oscillations) leads to the exact solution (see Sections 8.2 and 8.9). In finite systems (i.e. nuclei, quantum dots, etc.) this method provides a useful and simple

approximation, and it has been widely used (Bohr and Mottelson 1975; Lipparini and Stringari 1991; Serra et al. 1999; Nesterenko et al. 1999).

For simplicity, we will limit ourselves to studying scalar excited states. The generalization to vector states is very simple.

The basic ingredients of the model are:

(i) A local functional of the scalar density ρ of the form

$$E(\rho, \tau) = \frac{1}{2m} \int \tau d\mathbf{r} + \int v(\rho) d\mathbf{r} + \frac{1}{2} \int \rho(\mathbf{r}) \rho(\mathbf{r}') v(|\mathbf{r} - \mathbf{r}'|) d\mathbf{r} d\mathbf{r}', \quad (10.125)$$

where

$$\rho(\mathbf{r}) = \sum_i |\varphi_i(\mathbf{r})|^2 \quad \text{and} \quad \tau(\mathbf{r}) = \sum_i |\nabla \varphi_i(\mathbf{r})|^2,$$

and the function $v(\rho)$ includes contributions from both the external potential, and the exchange-correlation one.

(ii) The density-variations $\delta\rho(\mathbf{r}, t) = \alpha(t)\nabla(\rho_0(\mathbf{r})\nabla f(\mathbf{r}))$, equal to those of the generalized scaling of (10.76) with $\mathbf{u}(\mathbf{r}, t) = \alpha(t)\nabla f(\mathbf{r})$, where $\alpha(t)$ gives the oscillation amplitudes and $f(\mathbf{r})$ is the multipole operator which excites the collective mode.

The one-body Hamiltonian used to describe the collective vibrations is given by

$$H\varphi_i(\mathbf{r}) = \frac{\delta E}{\delta \varphi_i^*(\mathbf{r})} = \left(\frac{-\nabla^2}{2m} + V(\mathbf{r}, t) \right) \varphi_i(\mathbf{r}), \quad (10.126)$$

where

$$V(\mathbf{r}, t) = \frac{\partial v(\rho)}{\partial \rho} + \int \rho(\mathbf{r}') v(|\mathbf{r} - \mathbf{r}'|) d\mathbf{r}'. \quad (10.127)$$

In $H(\mathbf{r}, t)$, we can separate a static part (i.e. the one-body Hamiltonian relative to the static ground state):

$$H^0 = \frac{-\nabla^2}{2m} + \left(\frac{\partial v(\rho)}{\partial \rho} \right)_{\rho = \rho_0} + \int \rho_0(\mathbf{r}') v(|\mathbf{r} - \mathbf{r}'|) d\mathbf{r}', \quad (10.128)$$

and a dynamic time-dependent part which stems from density changes that occur during the collective motions:

$$\delta H = \delta V(\mathbf{r}, t) = \left. \frac{\partial V}{\partial \rho} \right|_{\rho = \rho_0} \delta\rho(\mathbf{r}, t)$$

$$= \left. \frac{\partial^2 v(\rho)}{\partial \rho^2} \right|_{\rho = \rho_0} \delta\rho(\mathbf{r}, t) + \int \delta\rho(\mathbf{r}', t) v(|\mathbf{r} - \mathbf{r}'|) d\mathbf{r}'. \quad (10.129)$$

If we introduce in (10.129) the density variations of the generalized scaling, we obtain

$$\delta H = \alpha(t)\left[\left.\frac{\partial^2 v(\rho)}{\partial\rho^2}\right|_{\rho=\rho_0}\nabla(\rho_0(\mathbf{r})\nabla f(\mathbf{r}))\right.$$

$$\left. + \int \nabla(\rho_0(\mathbf{r}')\nabla f(\mathbf{r}'))v(|\mathbf{r}-\mathbf{r}'|)d\mathbf{r}'\right].\qquad(10.130)$$

For excitation operators of the form $f = r^\ell Y_{\ell,m}$, for which $\nabla^2 f = 0$, we obtain

$$\delta H = \alpha(t)\left[\nabla V_0\cdot\nabla f + \int \nabla\rho_0(\mathbf{r}')\cdot\nabla f(\mathbf{r}'))v(|\mathbf{r}-\mathbf{r}'|)d\mathbf{r}'\right],\qquad(10.131)$$

where $V_0 = \left.\frac{\partial v(\rho)}{\partial\rho}\right|_{\rho=\rho_0}$. Defining the operator

$$\hat{Q} = \sum_{i=1}^{N}Q(r_i) = \sum_{i=1}^{N}\left(\nabla V_0\cdot\nabla f + \int \nabla\rho_0(\mathbf{r}')\cdot\nabla f(\mathbf{r}'))v(|\mathbf{r}-\mathbf{r}'|)d\mathbf{r}'\right)_i,\qquad(10.132)$$

it is then possible to write

$$\sum_{i=1}^{N}\delta H(r_i) = \alpha(t)\hat{Q}.\qquad(10.133)$$

Finally, using the result

$$Q(t) = \int Q(r)\delta\rho(\mathbf{r},t)d\mathbf{r} = \alpha(t)\int \nabla Q\cdot\nabla f\rho_0 d\mathbf{r},\qquad(10.134)$$

it is possible to write the time-dependent dynamic term in separable form:

$$\sum_{i=1}^{N}\delta H(r_i) = -kQ(t)\hat{Q},\qquad(10.135)$$

with

$$\frac{1}{k} = \int \nabla Q\cdot\nabla f\rho_0.\qquad(10.136)$$

The solution of the linearized time-dependent equations in an oscillating external field

$$\sum_{i=1}^{N}(H_0(r_i) + \delta H(r_i) + \lambda(Q(r_i)e^{i\omega t} + h.c.))|\Psi(t)\rangle = i\frac{\partial}{\partial t}|\Psi(t)\rangle,\qquad(10.137)$$

with $H_0(r_i)$ and $\delta H(r_i)$ given by equations (10.128) and (10.135), respectively, can be reduced (Lipparini and Stringari 1981) to the solution of the dispersion relation

$$2\sum_{k}\epsilon_k\frac{|\langle 0|\hat{Q}|k\rangle|^2}{\epsilon_k^2-\omega^2} = \frac{1}{k},\qquad(10.138)$$

where ϵ_k and $|k\rangle$ are the eigenvalues and eigenfunctions of the static Hamiltonian (10.128).

The oscillatory potential (10.135) can also be derived starting from a separable, effective two-body interaction (Bohr and Mottelson 1975; Rowe 1970) of the form

$$V = \frac{1}{2}k\sum_{i,j} Q(r_i)Q(r_j)\,. \tag{10.139}$$

In this case, the analysis of the present Section is equivalent to studying the effects of RPA correlations in the many body system, as produced by such separable interaction.

As an example of the application of the vibrating potential model (VPM), let us consider the case of quadrupole excitations in metal clusters.

For these systems, simple and significant solutions of the VPM are obtained by assuming:

(i) A complete screening between the Coulomb potential produced by the electron–electron interaction (direct term) and that of the jellium of positive charge (produced by the jellium density ρ_j), so that the static Hamiltonian becomes

$$\sum_{i=1}^{N} H^0(r_i) = \sum_{i=1}^{N} \left(\frac{-\nabla_i^2}{2m} + v_{xc}(\rho_0(r_i)) + \int \frac{(\rho_0(\mathbf{r}') - \rho_j(\mathbf{r}'))}{|\mathbf{r}_i - \mathbf{r}'|}d\mathbf{r}' \right)$$

$$\simeq \sum_{i=1}^{N} \left(\frac{-\nabla_i^2}{2m} + V_0(r_i) \right)\,. \tag{10.140}$$

(ii) A harmonic-oscillator-like exchange-correlation one-body potential, i.e.

$$V_0(r_i) = \frac{1}{2}\omega_0^2 r_i^2\,, \tag{10.141}$$

where the harmonic oscillator parameter ω_0 is given by the relation

$$\omega_0 = \sqrt{\frac{2\epsilon_F}{mr_s^2}}N^{-1/3}\,, \tag{10.142}$$

which is obtained by equating the kinetic energy per particle as given by the harmonic oscillator model with that of the Fermi gas, and by approximating $\langle r^2 \rangle$ as $(3/5)r_s^2 N^{2/3}$.

For the quadrupole excitations we then have $f = yz$ and $Q(r) = (2\omega_0^2 - \frac{2}{5}\omega_p^2)yz$, where, in order to obtain the expression for Q, we have made use of the relations

$$\int \frac{\nabla_{z'}\rho_0(\mathbf{r}')}{|\mathbf{r} - \mathbf{r}'|}d\mathbf{r}' = \nabla_z \int \frac{\rho_0(\mathbf{r}')}{|\mathbf{r} - \mathbf{r}'|}d\mathbf{r}'\,, \tag{10.143}$$

and

$$\int \frac{z' \rho_0(\mathbf{r}')}{|\mathbf{r} - \mathbf{r}'|} d\mathbf{r}' = z \int \frac{\rho_0(\mathbf{r}')}{|\mathbf{r} - \mathbf{r}'|} d\mathbf{r}' - \nabla_z \int \rho_0(\mathbf{r}') |\mathbf{r} - \mathbf{r}'| d\mathbf{r}' , \qquad (10.144)$$

as well as the results

$$\int \frac{\rho_0(\mathbf{r}')}{|\mathbf{r} - \mathbf{r}'|} d\mathbf{r}' = -\frac{1}{2} \frac{N}{R^3} r^2 ,$$

$$\int \rho_0(\mathbf{r}') |\mathbf{r} - \mathbf{r}'| d\mathbf{r}' = NR \left(\frac{3}{4} + \frac{1}{2} \frac{r^2}{R^2} - \frac{1}{20} \frac{r^4}{R^4} \right) , \qquad (10.145)$$

which hold for a uniform distribution $\rho_0(r)$. Moreover, one has

$$\frac{1}{k} = \frac{2}{3} N \left(2\omega_0^2 - \frac{2}{5} \omega_p^2 \right) \langle r^2 \rangle , \qquad \left| \langle 0 | \sum_{i=1}^{N} y_i z_i | k \rangle \right|^2 = \frac{N \langle r^2 \rangle}{6\omega_0} . \qquad (10.146)$$

Using these results, and considering that only one state at energy $2\omega_0$ contributes to the sum of (10.138), we obtain the solution for the dispersion relation

$$\omega_Q = \sqrt{2\omega_0^2 + \frac{2}{5} \omega_p^2} . \qquad (10.147)$$

The frequency (10.147) coincides with the result (10.116) provided we use $E(X) = (9/50)e^2(N^2/R)$, $\langle r^2 \rangle = 3/5NR^2$ and equation (10.142). Moreover, it coincides with the classical plasma frequency for the quadrupole, i.e. $\omega_Q^{cl} = \sqrt{2/5}\omega_p$, if we neglect the term in $2\omega_0$ which is produced by the quantum distortion of the Fermi sphere. Therefore, we see that, although the simplified RPA model lacks the finite-dimension effects due to electron spill-out outside the jellium radius [total screening assumption (10.140)], yet it contains quantum effects that can be appreciable. Such effects in deformed systems give rise, for example, to the low-energy scissor state which has no classical analogue. The scissor state is easily obtained in the VPM model using the above results for the quadrupole case, and taking into account the fact that in the deformed case two single-particle levels contribute to the sum of (10.138), with energies $\epsilon_0 = \omega_y - \omega_z = \delta\omega_0$ and $\epsilon_2 = \omega_y + \omega_z = 2\omega_0$, with the respective matrix elements

$$\left| \langle 0 | \sum_{i=1}^{N} y_i z_i | \epsilon_0 \rangle \right|^2 = \frac{N \langle r^2 \rangle}{12\omega_0} \delta , \qquad \left| \langle 0 | \sum_{i=1}^{N} y_i z_i | \epsilon_2 \rangle \right|^2 = \frac{N \langle r^2 \rangle}{6\omega_0} , \qquad (10.148)$$

and where we have considered only the contributions of the lowest order in the deformation δ.

Then, from the dispersion relation (10.138), we have two solutions. The higher-energy one is the quadrupole plasmon excitation of (10.147), while the lower-energy one has a frequency given by

$$\omega_{M1} = \sqrt{2}\omega_0\delta \left(1 + 5\frac{\omega_0^2}{\omega_p^2}\right)^{-1/2} . \tag{10.149}$$

This solution coincides with that of the scissor mode in (10.120), as readily seen using expression (10.142) for ω_0 and neglecting the correction $5\omega_0^2/\omega_p^2$.

10.3 The Surface Vibrations of Charged Systems in 2D and 3D

In this Section we will study the surface vibrations of a drop of charged Fermions, using the techniques developed in Section 10.1.2 for helium drops. The valence electrons of alkali metal clusters, and the two-dimensional electron gas confined in a quantum dot under a magnetic field are the examples of charged quantum fluid that we shall consider.

10.3.1 *Surface vibrations of charged metal clusters*

In the following, we will describe metal clusters by means of the jellium model, in which the total cluster energy is dominated by the electronic energy, and the equilibrium shape of the system corresponds to the minimum electronic energy. The positive ions have the role of screening the electrostatic potential of the valence electrons and the shape of the positive charge background is assumed to conform to that of the electrons.

For such clusters, when the system is neutral, the total energy is well represented by formula of the liquid-drop model:

$$E(N) = a_v N + a_s N^{2/3} , \tag{10.150}$$

where a_v is the mean total energy per electron in the infinite jellium, and $a_s = 4\pi r_s^2 \sigma$ is the surface energy connected to the surface tension of a semi-infinite jellium. In the case of sodium clusters, we have $r_s = 3.93$, $a_v = -2.1$ eV and $a_s = 0.57$ eV (Perdew 1988).

Therefore, the frequencies of the surface modes of the neutral jellium drop are given by the same expression as in the case of the Helium drop:

$$\omega_\ell^{\text{sup}} = \sqrt{\frac{\ell(\ell-1)(\ell+2)}{3} \frac{a_s}{M r_s^2}} N^{-\frac{1}{2}} .$$

Since all of the cluster mass is concentrated on the positive ions, the cluster vibrations in the jellium model are due to the shape changes of positive charge background, so that the masses that appear in such formula are the ionic masses.

If we use for a_s and r_s the above values suitable for sodium, we obtain for the energy of the quadrupole mode the estimate $\omega_{\ell=2}^{\text{sup}} = 0.01$ eV, i.e. a value that is smaller than the plasmon excitation energies by a factor of 100. The coupling between the quadrupolar surface vibrations and the plasma modes was studied by Bertsch and Tomanek (1989) and Pacheco and Broglia (1989), and accounts for the broadening of the excited states as observed in photoemission experiments.

When the cluster is charged, the Coulomb repulsion due to the extra charge contrasts the effect of the surface tension which tends to restore the system to the original shape, and may lead to its instability. Producing a critical deformation that leads to a fission process may require a rather small amount of energy. The electrostatic energy change connected with the surface deformation of the drop has been evaluated by Lipparini and Vitturi (1990), and the calculation proceeds as follows. One starts from the usual expression

$$E_{Coul} = \frac{1}{2} \int \frac{(\rho - \rho_I)_{\mathbf{r}}(\rho - \rho_I)_{\mathbf{r}'}}{|\mathbf{r} - \mathbf{r}'|} d\mathbf{r} d\mathbf{r}' , \qquad (10.151)$$

for the electrostatic energy. The electronic and ionic densities, ρ and ρ_I, are written as

$$\rho(r,\theta,\phi) = \rho_0 S(R^e(\theta,\phi) - r), \qquad \rho_I(r,\theta,\phi) = \rho_I S(R(\theta,\phi) - r) , \qquad (10.152)$$

where both $R^e(\theta,\phi)$ and $R(\theta,\phi)$ have the form (10.22), and S is the step function. Due to the conducting nature of the metal clusters, the extra charge Z is distributed on the surface, the central densities may be assumed identical, and the ratio of the equilibrium radii R_0^e and R_0 is given by

$$\frac{R_0^e}{R_0} = \left(1 - \frac{Z}{N}\right)^{1/3} . \qquad (10.153)$$

In order that this distribution of extra surface charge is conserved even when the surface is deformed, one further assumes the same form for the electron and ion densities, i.e. equal deformation parameters $\alpha_{\ell,m}$ with $\ell > 1$ for the two distributions. For small deformations $|R(\theta,\phi) - R_0| \ll R_0$, it is possible to use the expansion

$$\rho(r,\theta,\phi) = \rho_0 \bigg(S(R_0 - r) + (R(\theta,\phi) - R_0)\delta(R_0 - r)$$

$$- \frac{1}{2}(R(\theta,\phi) - R_0)^2 \delta'(R_0 - r) + \cdots \bigg) \qquad (10.154)$$

for both the densities (10.152). This yields ($Z/N \ll 1$):

$$E_{Coul} = \frac{Z^2}{2R_0} - \frac{1}{2}\frac{Z^2}{4\pi R_0} \sum_{\ell m} \frac{\ell^2 + 3\ell - 5}{2\ell + 1} |\alpha_{\ell m}|^2 , \qquad (10.155)$$

where the first term is the spherical contribution to the electrostatic energy due to the extra charge Z, and the second one gives the energy variation caused by the

deformation of the surface. Therefore, the contribution of the Coulomb energy to the restoring force is ($\ell > 1$):

$$(C_\ell)_{Coul} = -\frac{Z^2}{4\pi R_0}\frac{\ell^2 + 3\ell - 5}{2\ell + 1}.$$ (10.156)

From equations (10.28) and (10.156), we get

$$C_\ell = (C_\ell)_{surf} + (C_\ell)_{Coul}$$

$$= \frac{1}{4\pi}(\ell - 1)(\ell + 2)a_s N^{2/3} - \frac{Z^2}{4\pi r_s}\frac{\ell^2 + 3\ell - 5}{2\ell + 1}N^{-1/3}$$ (10.157)

for the total restoring force. As mentioned, we see that the Coulomb repulsion contrasts the effect of surface tension, and leads to instability for large values of Z^2/N. Instability against the lowest-energy quadrupole mode ($\ell = 2$) sets on for a critical value of Z^2/N given by

$$\left(\frac{Z^2}{N}\right)_{crit} = 4r_s a_s.$$ (10.158)

Using the values $r_s = 4$ and $a_s = 0.57$ eV, which are the relevant parameters for sodium clusters, we can predict that for the number of atoms N larger than 3.1 Z^2, ionized clusters with charge Z are stable against fission processes. Such prediction, which overlooks other possible fragmentation channels, such as monomer emission which is privileged for small Z (Perdew 1988; Baladron 1989), is not too far from experimental results, in which fission processes are induced through reactions with photons. An exhaustive study of fission processes in metal clusters, including both theoretical and experimental aspects, is found in the review paper of Naher et al. (1997).

10.3.2 *Edge vibrations of quantum dots*

In this Section we will consider a drop of uncompressible liquid in two dimensions, and develop the formalism of the edge vibrations of the drop, analogous to what was done previously in three-dimensional systems (Giovanazzi 1993). Unlike the previous Section, where we studied the problem of instability due to excess charge in a three-dimensional drop and assumed that the shape of the jellium conforms to that of the electrons, here we consider the surface vibrations of the electron drop in a rigid confinement field. Such electronic surface vibrations correspond to the low-energy excited states that were studied in Section 8.13.2 in a microscopic fashion and as a function of an external magnetic field acting on the quantum dot.

In analogy of what we did in Section 10.1.2, we may describe the edge vibrations of the two-dimensional drop by a set of normal co-ordinates α_{ℓ_0} of the system, in angular momentum space, by expanding the distance $R(\theta)$ of the edge from the

origin in terms of the functions $e^{i\ell_0\theta}$:

$$R(\theta) = R_0 \left(1 + \sum_{\ell_0} \alpha_{\ell_0} e^{i\ell_0\theta}\right), \tag{10.159}$$

where R_0 is the equilibrium radius and the sum runs over the (positive and negative) integers ℓ_0. Like in the $3D$ case, the term with $\ell_0 = 0$ represents a compression without change of shape, and the one with $\ell_0 = 1$ represents a translation of the whole system. The mode relative to α_2 is the first one that implies a shape-change in the drop, and is the quadrupole mode.

The density variations are limited to changes in the drop profile. If $\rho(r,\theta) = \rho_0 S(R(\theta) - r)$, we have

$$\rho(r,\theta) = \rho_0 \bigg(S(R_0 - r) + (R(\theta) - R_0)\delta(R_0 - r)$$

$$-\frac{1}{2}(R(\theta) - R_0)^2\delta'(R_0 - r) + \cdots \bigg). \tag{10.160}$$

Surface conservation implies the relation

$$\alpha_0 = -\frac{1}{2}\sum_{\ell_0} |\alpha_{\ell_0}|^2. \tag{10.161}$$

In the limit of small oscillations, a Lagrangian formulation is possible, which allows us to derive the equations of motion of the edge oscillations in the presence of a magnetic field:

$$L = \frac{1}{2}\sum_{\ell_0} \left(D_{\ell_0}\dot{\alpha}_{\ell_0}^*\dot{\alpha}_{\ell_0} - \frac{i}{2}D_{\ell_0}\omega_c\frac{|\ell_0|}{\ell_0}(\dot{\alpha}_{\ell_0}^*\alpha_{\ell_0} - \alpha_{\ell_0}^*\dot{\alpha}_{\ell_0}) - C_{\ell_0}\alpha_{\ell_0}^*\alpha_{\ell_0} \right), \tag{10.162}$$

where the term proportional to the cyclotron frequency $\omega_c = eB/mc$ accounts for the external magnetic field applied in a direction perpendicular to the drop plane, which gives rise to a Lorentz force $-e/c\mathbf{v} \times \mathbf{B}$, with $\mathbf{v}$ the velocity of the drop edge. The equations of motion have the form

$$D_{\ell_0}\ddot{\alpha}_{\ell_0} - iD\ell_0\omega_c\frac{|\ell_0|}{\ell_0}\dot{\alpha}_{\ell_0} + C_{\ell_0}\alpha_{\ell_0} = 0, \tag{10.163}$$

where D_ℓ and C_ℓ are the mass parameter and the restoring-force parameter of the oscillation, respectively. The equation for the oscillation frequency is given by

$$\omega_{\ell_0}\left(\omega_{\ell_0} + \omega_c\frac{|\ell_0|}{\ell_0}\right) = \frac{C_{\ell_0}}{D_{\ell_0}}. \tag{10.164}$$

If $\omega_{\ell_0} \ll \omega_c$, the lowest frequency is given by

$$\omega_{\ell_0} = \frac{\ell_0 C_{\ell_0}}{\omega_c|\ell_0|D_{\ell_0}}. \tag{10.165}$$

For the calculation of the mass parameter D_{ℓ_0}, we will assume (like in $3D$) that the flux is uncompressible (at constant density) and irrotational, so that the velocity field is written as the gradient of some potential $\chi(\mathbf{r})$:

$$\mathbf{v}(\mathbf{r}) = -\nabla\chi(\mathbf{r}) .$$

Then, the continuity equation (10.6) implies that the potential satisfies the Laplace equation $\nabla^2\chi(\mathbf{r}) = 0$, with solution

$$\chi(\mathbf{r}) = \sum_{\ell_0} a_{\ell_0} r^{\ell_0} e^{i\ell_0\theta} . \tag{10.166}$$

The coefficients a_{ℓ_0} and α_{ℓ_0} are connected by the boundary condition on the edge, which demands that on the edge itself the radial component of velocity be equal to the radial velocity at which the edge moves. For small edge displacements, such boundary condition requires

$$-\frac{\partial}{\partial r}\chi = \frac{dR}{dt} ,$$

as computed in $r = R_0$, from which it follows that

$$a_{\ell_0} = \frac{R_0^{2-\ell_0}}{|\ell_0|}\dot{\alpha}_{\ell_0} . \tag{10.167}$$

Then, the kinetic energy of the fluid due to the edge deformations becomes

$$T = \frac{1}{2}m\rho_0 \int \mathbf{v}^2(\mathbf{r})d\mathbf{r} = \sum_{\ell_0} M\frac{R_0^2}{|\ell_0|}\dot{\alpha}^*_{\ell_0}\dot{\alpha}_{\ell_0} , \tag{10.168}$$

and comparison with (10.162) finally yields the result

$$D_{\ell_0} = \frac{2}{|\ell_0|}MR_0^2 , \tag{10.169}$$

where $M = mN$ is the total mass of the electron drop.

The parameter C_{ℓ_0} of the restoring force of the edge oscillations on the drop, is computed starting from the Coulomb energy variations which are connected with the electron density variation. First of all, let us consider the interaction term with the jellium:

$$\delta E_{je} = \int \delta\rho(r,\theta)V_+(r)d\mathbf{r} = -\frac{1}{2}R_0^2 \sum_{\ell_0} |\alpha_{\ell_0}|^2 \int (\partial_r^2\rho(r))V_+(r)dr , \tag{10.170}$$

where $\partial_r\rho(r)$ is the radial derivative of the static density of the electron drop, and V_+ is the Coulomb potential generated by the jellium density $\rho_0 S(R_0 - r)$. It is immediate to show that the integral in (10.170) can be related to the electric field

$\mathcal{E}(R_0)$ produced by the electrons on the jellium edge, so that

$$\delta E_{je} = \pi \rho_0 R_0^3 \mathcal{E}(R_0) \sum_{\ell_0} |\alpha_{\ell_0}|^2 \,. \tag{10.171}$$

For large values of the electron number N, one finds $\mathcal{E}(R_0) = \rho_0 \ln(\beta N)$ with $\beta = 16.4$ (Giovanazzi, Pitaevskii and Stringari 1994). We remark that $\mathcal{E}(r)$ was studied numerically in a dot in Section 5.6.

Let us consider now the variations of the electron–electron Coulomb interaction energy:

$$\delta E_{ee} = \int \delta\rho(r,\theta) \frac{1}{|r-r'|} \rho(r') \mathbf{dr}\mathbf{dr'} + \frac{1}{2} \int \delta\rho(r,\theta) \frac{1}{|r-r'|} \delta\rho(r',\theta') \mathbf{dr}\mathbf{dr'} \,. \tag{10.172}$$

This quantity becomes

$$\delta E_{ee} = \frac{1}{2} R_0^2 \sum_{\ell_0} |\alpha_{\ell_0}|^2 \int \partial_r \rho(r) \frac{\cos(\ell_0(\theta-\theta')) - \cos(\theta-\theta')}{|r-r'|} \partial_{r'} \rho(r') \mathbf{dr}\mathbf{dr'} \tag{10.173}$$

and, in the limit of large N ($N \gg \ell_0$):

$$\delta E_{ee} = -4\pi R_0^3 \rho_0^2 \sum_{\ell_0} |\alpha_{\ell_0}|^2 \sum_{k=2}^{\ell_0} \frac{1}{2k-1} \,, \tag{10.174}$$

where we have used

$$\int_0^{2\pi} \frac{\cos(\ell_0\theta) - \cos\theta}{\sqrt{1-\cos\theta}} = -4\sqrt{2} \sum_{k=2}^{\ell_0} \frac{1}{2k-1} \,, \tag{10.175}$$

which holds for $\ell_0 > 1$ (for $\ell_0 = 1$, $\delta E_{ee} = 0$). Furthermore, we have

$$\sum_{k=2}^{\ell_0} \frac{1}{2k-1} = \frac{1}{2}(\ln(\ell_0) + C + \ln 4 - 2) = \frac{1}{2}\ln(\gamma\ell_0) \,,$$

where $C = 0.577215$ is the Euler constant, and therefore $\gamma = 0.96417$.

Finally, by combining the above results we find

$$C_{\ell_0} = C_{\ell_0}^{je} + C_{\ell_0}^{ee} = 4\pi R_0^3 \rho_0^2 \ln(\sqrt{\beta N}) - 4\pi R_0^3 \rho_0^2 \ln(\gamma\ell_0)$$

$$= 4\pi R_0^3 \rho_0^2 \ln\left(\frac{\sqrt{\beta N}}{\gamma\ell_0}\right) \tag{10.176}$$

which holds for $\ell_0 > 1$ and large N. In the dipolar case $C_1^{ee} = 0$, thus

$$C_1^{je} = 2\pi R_0^3 \rho_0 \mathcal{E}(R_0) \,. \tag{10.177}$$

Using the results of equations (10.164) and (10.169), we then find for the edge frequency

$$\omega_{\ell_0}\left(\omega_{\ell_0} + \omega_c \frac{\ell_0}{|\ell_0|}\right) = \frac{2\ell_0\rho_0}{mR_0} \ln\left(\frac{\sqrt{\beta}N}{\gamma\ell_0}\right), \qquad (10.178)$$

for $\ell_0 > 1$ and large N, and

$$\omega_1(\omega_1 \pm \omega_c) = \frac{\mathcal{E}(R_0)}{mR_0}, \qquad (10.179)$$

for $\ell_0 = 1$. Note that for parabolic confinement, the procedure that led us to (10.179) gives exactly the result $\omega_\pm = \sqrt{\omega_0^2 + \omega_c^2/4} \pm \omega_c/2$ of the generalized Kohn theorem of Section 8.10.1.

As an application of (10.178), we compute the frequency of the lowest energy solution in the case where the magnetic field is such that the filling factor is 1. In this case the electron density for large N is given by $\rho_0 = (2\pi l^2)^{-1}$ within the circle of radius $R_0 = l\sqrt{2N}$, where $l = (\hbar c/eB)^{1/2}$ is the magnetic length. For large values of ℓ_0, it is natural to bring in the parametrization $\ell_0 = qR_0 = ql\sqrt{2N}$, which follows from the condition that the oscillatory mode is stationary; this condition requires that an integer number ℓ_0 of wavelengths fits in the length of the edge. In this way we obtain the dispersion relation

$$\omega_q = \frac{q}{\pi}\ln\frac{q_0}{q}, \qquad (10.180)$$

where $q_0 = \sqrt{\beta}/(\sqrt{2}\gamma l) = 3.0/l$. Such relation holds in the limit where $N \gg \ell_0$, i.e. large wavelength limit: $ql \ll 1$. The $q\ln(1/q)$ dependence is typical of the long-range Coulomb interaction and for jellium confinement, and has been derived by many authors (Volkov and Mikhailov 1985; Wen 1991; Giovanazzi, Pitaevskii and Stringari 1994).

It is interesting to note that for a neutral drop with short-range interaction among its constituents, the dispersion relation is completely different from equation (10.180). This can be seen by calculating the parameter C_{ℓ_0} on the restoring force of the edge oscillations on the drop, starting from the variation of the edge energy

$$\delta E = \frac{1}{2}\sum_{\ell_0} C_{\ell_0}|\alpha_{\ell_0}|^2 = \lambda\delta L, \qquad (10.181)$$

where δL is the edge-length variation and λ is analogous to surface tension in $3D$. This restoring force is typical of short-range-interaction systems, such as the nucleon drop. However it is also typical of electron systems under an intense magnetic field, which can lead to a fractional regime; in fact, in this case short-range interactions produce eigenfunctions which coincide with the Laughlin wavefunctions of the fractional regime.

Using

$$\delta L = \int_0^{2\pi} d\theta (R^2(\theta) + (\partial_\theta R(\theta))^2)^{1/2} - 2\pi R_0, \qquad (10.182)$$

and expanding the square root, we obtain in the limit of small oscillations (where the derivative with respect to θ is small):

$$\delta E = \lambda \int_0^{2\pi} d\theta \left(R(\theta) - R_0 + \frac{1}{2R_0}(\partial_\theta R(\theta))^2 \right) = \lambda\pi R_0 \sum_{\ell_0}(\ell_0^2 - 1)|\alpha_{\ell_0}|^2, \quad (10.183)$$

from which we derive the force parameter:

$$C_{\ell_0} = 2\lambda\pi R_0(\ell_0^2 - 1). \qquad (10.184)$$

Therefore, the frequencies of the edge modes on the drop are given by

$$\omega_{\ell_0} = \frac{1}{\omega_c}\frac{\lambda\pi}{mNR_0}\ell_0(\ell_0^2 - 1). \qquad (10.185)$$

Moreover, if we put $\ell_0 = qR_0$ we obtain

$$\omega_q = \frac{\lambda q^3}{m\omega_c\rho_0}, \qquad (10.186)$$

whose q-dependence is completely different from that of (10.180).

References to Chapter 10

F. Dalfovo, S. Giorgini, L. Pitaevskii and S. Stringari, Rev. Mod. Phys. **71**, 3 1999.

L. Pricaupenko and J. Treiner, J. Low Temp. Phys. **96**, 19 (1994).

F. Dalfovo, A. Lastri, L. Pricaupenko, S. Stringari and J. Treiner, Phys. Rev. B **52**, 1193 (1995).

M. Casas and S. Stringari, J. Chem. Phys. **87**, 5021 (1990).

M. Barranco and E.S. Hernandez, Phys. Rev. B **49**, 12078 (1994).

A. Bohr and B. Mottelson, Nuclear Structure, (Benjamin, New York, 1975), Vol. 2.

D.M. Brink and S. Stringari, Z. Phys. D **15**, 257 (1990).

V. Weisskopf, Phys. Rev. **52**, 295 (1937).

G. Baym and C. Pethick, Phys. Rev. Lett. **76**, 6 (1996).

S. Stringari, Phys. Rev. Lett. **77**, 2360 (1996b).

P.C. Hohenberg, Phys. Rev. **158**, 383 (1967).

N.D. Mermin and H. Wagner, Phys. Rev. Lett. **17**, 1133 (1966).

N.D. Mermin, Phys. Rev. **176**, 250 (1968).

L. Pitaevskii and S. Stringari, J. Low Temp. Phys. **85**, 377 (1991).

F. Zambelli and S. Stringari, Phys. Rev. A **63**, 1 (2001).

M. Radomski, Phys. Rev. C **14**, 1704 (1976).

S. Stringari and E. Lipparini, Phys. Rev. C **22**, 884 (1980).

D. Bohle et al., Phys. Lett. B **137**, 27 (1984).

N. Lo Iudice and F. Palumbo, Phys. Rev. Lett. **41**, 1532 (1978).

E. Lipparini and S. Stringari, Phys. Lett. B **130**, 139 (1983).

E. Lipparini and S. Stringari, Phys. Rep. **175**, 103 (1989).

F. Iachello, Phys. Rev. Lett. **53**, 1927 (1984).

R. Nojarov, Z. Bochnacki and A. Faessler, Z. Phys. A 324, 289 (1986).

E. Lipparini and S. Stringari, Phys. Rev. Lett. **63**, 570 (1989b).

V.O. Nesterenko et al., Phys. Rev. Lett. **83**, 57 (1999).

Ll. Serra, A. Puente and E. Lipparini, Phys. Rev. B **60**, R13966 (1999).

D. Guery-Odelin and S. Stringari, Phys. Rev. Lett. **83**, 4452 (1999).

O.M. Maragò et al., Phys. Rev. Lett. **84**, 2056 (2000).

S. Stringari, Phys. Rev. Lett. **76**, 1405 (1996).

E. Lund, C.J. Pethick and H. Smith, Phys. Rev. A **55**, 2126 (1997).

M.R. Matthews et al., Phys. Rev. Lett. **83**, 2498 (1999).

K.W. Madison et al., Phys. Rev. Lett. **84**, 806 (2000).

B.P. Anderson et al., Phys. Rev. Lett. **85**, 2857 (2000).

F. Zambelli and S. Stringari, Phys. Rev. Lett. **81**, 1754 (1998).

A.A. Svidzinsky and A.L. Fetter, Phys. Rev. A **58**, 3168 (1998).

A.L. Fetter and A.A. Svidzinsky, J. Phys. Cond. Matt. **13**, R135 (2001).

A. Puente, M. Casas and Ll. Serra, Physica E **8**, 387 (2000).

A. Domps, P.G. Reinhard and E. Suraud, Phys. Rev. Lett. **80**, 5520 (1998).

G.F. Bertsch, Ann. Phys. **86**, 138 (1974); Nucl. Phys. A **249**, 253 (1975).

D.M. Brink and R. Leonardi, Nucl. Phys. A **258**, 285 (1976).

S. Stringari, Nucl. Phys. A **279**, 454 (1977); Ann. Phys. **151**, 35 (1983).

C.Y. Wong and J. MacDonald, Phys. Rev. C **16**, 1196 (1977).

G. Holzwarth and G. Eckart, Z. Phys. A **284**, 291 (1978); Nucl. Phys. A **325**, 1 (1979).

E. Lipparini and S. Stringari, Phys. Rep. **175**, 103 (1989).

E. Lipparini: Lecture notes for the Workshop Metal Clusters. Villa Monastero, Varenna, September 1989 (unpublished).

E. Lipparini and S. Stringari, Z. Phys. D **18**, 193 (1991).

B.K. Jennings, Phys. Lett. B **96**, 1 (1980).

M. Brack, Phys. Rev. B **39**, 3533 (1989).

W.D. Knight et al., Phys. Rev. B **31**, 2539 (1985).

D.E. Beck, Phys. Rev. B **30**, 6935 (1984).

C. Schuller et al., Phys. Rev. Lett. **80**, 2673 (1998).

O. Bohigas, A.M. Lane and J. Martorell, Phys. Rep. **51**, 267 (1979).

J. Enders et al., Phys. Rev. C **59**, R1851 (1999).

D.J. Rowe, Nuclear Collective Motion (Methuen, London, 1970).

Ll. Serra et al., Phys. Rev. B **59**, 15290 (1999).

J.P. Perdew, Phys. Rev. B **37**, 6175 (1988).

G.F. Bertsch and D. Tomanek, Phys. Rev. B **40**, 2749 (1989).

J.M. Pacheco and R.A. Broglia, Phys. Rev. Lett. **62**, 1400 (1989).

E. Lipparini and A. Vitturi, Z. Phys. D **17**, 57 (1990).

C. Baladron et al., Z. Phys. D **11**, 323 (1989).

V. Naher et al., Phys. Rep. **285**, 245 (1997).

S. Giovanazzi, Eccitazioni di bordo nell'effetto Hall quantistico, Tesi di Laurea, 1993 (unpublished).

S. Giovanazzi, L. Pitaevskii and S. Stringari, Phys. Rev. Lett. **72**, 3230 (1994).

X.G. Wen, Phys. Rev. B **44**, 5708 (1991).

V.A. Volkov and S.A. Mikhailov, JEPT Lett. **42**, 556 (1985).

This page is intentionally left blank

Index

Modern Many-Particle Physics

Atomic Gases, Quantum Dots and Quantum Fluids

An important part of this book is devoted to the description of homogenous systems, such as electron gas in different dimensions, the quantum well in an intense magnetic field, liquid helium and nuclear matter. However, the most relevant part is dedicated to the study of finite systems: metallic clusters, quantum dots, the condensate of cold and dilute atoms in magnetic traps, helium drops and nuclei. The book focuses on methods of getting good numerical approximations to energies and linear response based on approximations to first-principles Hamiltonians. These methods are illustrated and applied to Bose and Fermi systems at zero and finite temperature.

Modern Many-Particle Physics is directed towards students who have taken a conventional course in quantum mechanics and possess a basic understanding of condensed matter phenomena.